frontiers | Research Topics

Cuproptosis and tumor

Edited by
Lin-Lin Bu, Bing Liu, Guojun Chen and Chun Xu

Coordinated by
Jiannan Liu

Published in
Frontiers in Immunology
Frontiers in Cell and Developmental Biology
Frontiers in Oncology

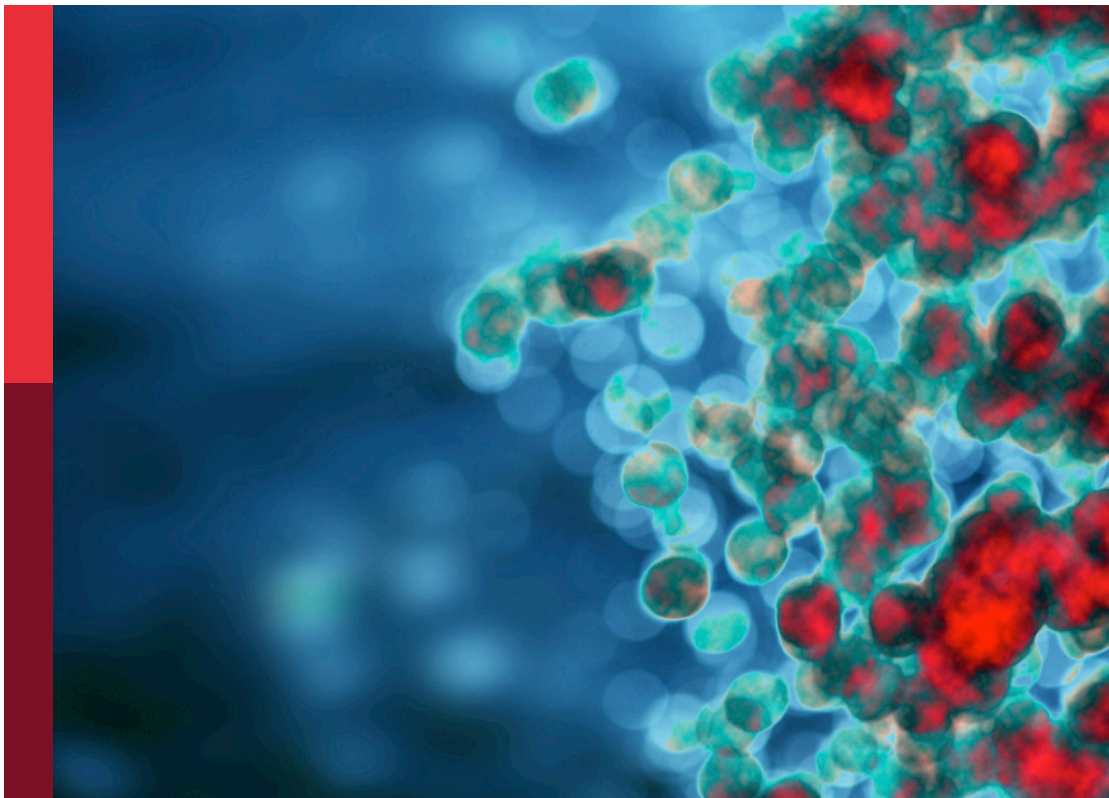

ISSN 1664-8714
ISBN 978-2-8325-4089-3
DOI 10.3389/978-2-8325-4089-3

About Frontiers

Frontiers is more than just an open access publisher of scholarly articles: it is a pioneering approach to the world of academia, radically improving the way scholarly research is managed. The grand vision of Frontiers is a world where all people have an equal opportunity to seek, share and generate knowledge. Frontiers provides immediate and permanent online open access to all its publications, but this alone is not enough to realize our grand goals.

Frontiers journal series

The Frontiers journal series is a multi-tier and interdisciplinary set of open-access, online journals, promising a paradigm shift from the current review, selection and dissemination processes in academic publishing. All Frontiers journals are driven by researchers for researchers; therefore, they constitute a service to the scholarly community. At the same time, the *Frontiers journal series* operates on a revolutionary invention, the tiered publishing system, initially addressing specific communities of scholars, and gradually climbing up to broader public understanding, thus serving the interests of the lay society, too.

Dedication to quality

Each Frontiers article is a landmark of the highest quality, thanks to genuinely collaborative interactions between authors and review editors, who include some of the world's best academicians. Research must be certified by peers before entering a stream of knowledge that may eventually reach the public - and shape society; therefore, Frontiers only applies the most rigorous and unbiased reviews. Frontiers revolutionizes research publishing by freely delivering the most outstanding research, evaluated with no bias from both the academic and social point of view. By applying the most advanced information technologies, Frontiers is catapulting scholarly publishing into a new generation.

What are Frontiers Research Topics?

Frontiers Research Topics are very popular trademarks of the *Frontiers journals series*: they are collections of at least ten articles, all centered on a particular subject. With their unique mix of varied contributions from Original Research to Review Articles, Frontiers Research Topics unify the most influential researchers, the latest key findings and historical advances in a hot research area.

Find out more on how to host your own Frontiers Research Topic or contribute to one as an author by contacting the Frontiers editorial office: frontiersin.org/about/contact

Cuproptosis and tumor

Topic editors
Lin-Lin Bu — Wuhan University, China
Bing Liu — Wuhan University, China
Guojun Chen — McGill University, Canada
Chun Xu — The University of Queensland, Australia

Topic Coordinator
Jiannan Liu — Shanghai Jiao Tong University, China

Citation
Bu, L.-L., Liu, B., Chen, G., Xu, C., Liu, J., eds. (2023). *Cuproptosis and tumor*. Lausanne: Frontiers Media SA. doi: 10.3389/978-2-8325-4089-3

Table of contents

frontiers | Frontiers in Cell and Developmental Biology

TYPE Editorial
PUBLISHED 24 November 2023
DOI 10.3389/fcell.2023.1307501

OPEN ACCESS

EDITED AND REVIEWED BY
Shyamala Maheswaran,
Harvard Medical School, United States

*CORRESPONDENCE
Bing Liu,
liubing9909@whu.edu.cn
Jian-Nan Liu,
laurence_ljn@163.com
Guo-Jun Chen,
guojun.chen@mcgill.ca
Chun Xu,
chun.xu@uq.edu.au
Lin-Lin Bu,
lin-lin.bu@whu.edu.cn

RECEIVED 04 October 2023
ACCEPTED 14 November 2023
PUBLISHED 24 November 2023

CITATION
Liu B, Liu J-N, Chen G-J, Xu C and Bu L-L (2023), Editorial: Cuproptosis and tumor. *Front. Cell Dev. Biol.* 11:1307501. doi: 10.3389/fcell.2023.1307501

Editorial: Cuproptosis and tumor

Bing Liu[1,2]*, Jian-Nan Liu[3]*, Guo-Jun Chen[4]*, Chun Xu[5]* and Lin-Lin Bu[1,2]*

[1]State Key Laboratory of Oral and Maxillofacial Reconstruction and Regeneration, Key Laboratory of Oral Biomedicine Ministry of Education, Hubei Key Laboratory of Stomatology, School and Hospital of Stomatology, Wuhan University, Wuhan, Hubei, China, [2]Department of Oral and Maxillofacial—Head Neck Oncology, School and Hospital of Stomatology, Wuhan University, Wuhan, Hubei, China, [3]Department of Oral Maxillofacial—Head and Neck Oncology, Shanghai Ninth People's Hospital Affiliated to Shanghai Jiao Tong University School of Medicine, Shanghai, China, [4]Department of Biomedical Engineering and Rosalind and Morris Goodman Cancer Institute, McGill University, Montreal, QC, Canada, [5]School of Dentistry, The University of Queensland, Brisbane, QLD, Australia

KEYWORDS

cell death, cuproptosis, molecular mechanism of cuproptosis, tumor, drug delivery system

Editorial on the Research Topic
Cuproptosis and tumor

As a trace element, copper is widely involved in the physiological activities of cells and plays an important role. Accumulation of copper in cells can induce oxidative stress and disrupt cellular function, thus copper homeostasis in cells is strictly regulated. Cuproptosis is a new type of programmed cell death induced by copper and is different from other types such as apoptosis, pyroptosis, and ferroptosis (Tsvetkov, et al., 2022). Copper ions bind to lipoacyl proteins during the tricarboxylic acid (TCA) cycle, leading to abnormal oligomerization of lipoacyl protein (Li, et al., 2022). In addition, the level of iron-sulfur cluster proteins can be reduced by copper ions, resulting in toxic stress reactions in proteins and leading to cell death. Cuproptosis impacts the pathogenesis of various diseases, including hepatolenticular degeneration, neurodegenerative diseases, and cancer (Wang, et al., 2023). Therefore, targeting cuprotosis may become a potential treatment method for various diseases and has attracted widespread attention.

This Research Topic focuses on the molecular mechanism of cuprotosis in the development of tumors and the potential therapeutic approach to targeting cuprotosis. Based on the significant impact of cuproptosis in the pathogenesis of colorectal cancer, Li et al. identified potential cuprotosis-related genes (CRGs) and developed a new predictive model using LASSO regression and multivariate Cox stepwise regression in the TCGA dataset, which evaluates the immune characteristics of colorectal cancer patients while predicting their prognosis. In addition, Wang et al. comprehensively analyzed the relationship between CRG and TME in colon adenocarcinoma (COAD), constructed a CRG risk scoring system, and accurately predicted the survival rate of COAD patients. The CRG risk scoring systems have provided clinical doctors with new insights to develop more effective and personalized treatment strategies. Fan et al. designed a new nomograph containing CRG scores and clinical characteristics, which can predict the 3-year, 5-year, and 7-year recurrence risk of ER + breast cancer. Liu et al. revealed the potential impact on the overall survival period, immune invasion, drug sensitivity, and metabolic spectrum of breast cancer through CRG. Similarly, scholars have also explored the prognostic value of CRG in prostate adenocarcinoma, lung adenocarcinoma, and gastric cancer.

The impact of cuproptosis on the occurrence and development of hepatocellular carcinoma, as well as its potential targets and prognostic value, seems to have aroused great interest. For example, Shao et al. and Shi et al. developed scoring models based on CRG to predict the prognosis of hepatocellular carcinoma and revealed the potential synergistic effect of novel immunotherapies such as TIGHT, CD274, and LAG-3 on cuproptosis. Cao et al. explained the characteristics of cuproptosis in hepatocellular carcinoma through single-cell sequencing and genetic multiomics and identified that BEX1 may be a key hub gene mediating cuproptosis in hepatocellular carcinoma and serve as a potential therapeutic target. Wang et al. explained the potential role of targeted cuproptosis in targeted immune microenvironment therapy for hepatocellular carcinoma and proposed that CRG can serve as a biomarker for immune checkpoint inhibitor therapy.

Although this Research Topic has collected many interesting and valuable research results, the relationship between cuproptosis and tumors still needs to be further explored. A deeper understanding of the role of cuproptosis in different tumor mechanisms should be explored, which may include aspects such as cell death, energy metabolism, and tumor immunity (Chen, et al., 2022). In addition, the role of targeted cuproptosis in tumor treatment should also be taken seriously. Recent studies have shown that inducing abnormal programmed cell death may be a potential method for treating and preventing tumor diseases. Therefore, targeting cuproptosis to increase the level of cuproptosis in tumor cells provides a new approach for tumor treatment. Cuproptosis, as an immunogenic death (ICD), can promote the release of tumor antigens, increase antigen presentation levels, promote T cell activation, and enhance anti-tumor immunity (Xie, et al., 2023). Therefore, targeting cuproptosis as a supplement to immunotherapy or an adjuvant therapy to improve the effectiveness of immunotherapy has enormous potential application value. The combination of cuproptosis with other therapies such as chemotherapy, radiotherapy, and photodynamic therapy has also received attention (Li, et al., 2023). Currently, drug delivery systems have received a lot of attention. The drug delivery system can accurately deliver drugs that induce cuproptosis to the tumor microenvironment. While improving the level of cuproptosis in tumor cells, it can reduce the systemic toxicity and side effects of drugs, thereby improving the survival period and quality of life of tumor patients. This will be the focus of future research.

Author contributions

BL: Writing–review and editing, Writing–original draft. J-NL: Writing–review and editing. G-JC: Writing–review and editing. CX: Writing–review and editing. L-LB: Writing–original draft, Writing–review and editing.

Funding

The author(s) declare financial support was received for the research, authorship, and/or publication of this article. This study was supported by the Postdoctoral Science Foundation of China (2018M630883 and 2019T120688), the Hubei Province Chinese Medicine Research Project (ZY 2023Q015), the Natural Science Foundation of Hubei Province (2023AFB665), Wuhan Young Medical Talents Training Project to L-LB, and Medical Young Talents Program of Hubei Province.

Acknowledgments

We thank all contributing authors and reviewers for their work and dedication to this Research Topic.

Conflict of interest

The authors declare that the research was conducted in the absence of any commercial or financial relationships that could be construed as a potential conflict of interest.

The author(s) declared that they were an editorial board member of Frontiers, at the time of submission. This had no impact on the peer review process and the final decision.

Publisher's note

References

Chen, L., Min, J., and Wang, F. (2022). Copper homeostasis and cuproptosis in health and disease. *Signal Transduct. Target Ther.* 7, 378. doi:10.1038/s41392-022-01229-y

Li, S. R., Bu, L. L., and Cai, L. (2022). Cuproptosis: lipoylated TCA cycle proteins-mediated novel cell death pathway. *Signal Transduct. Target Ther.* 7, 158. doi:10.1038/s41392-022-01014-x

Li, Z. Z., He, J. Y., Wu, Q., Liu, B., and Bu, L. L. (2023). Recent advances in targeting myeloid-derived suppressor cells and their applications to radiotherapy. *Int. Rev. Cell Mol. Biol.* 378, 233–264. doi:10.1016/bs.ircmb.2023.03.007

Tsvetkov, P., Coy, S., Petrova, B., Dreishpoon, M., Verma, A., Abdusamad, M., et al. (2022). Copper induces cell death by targeting lipoylated TCA cycle proteins. *Science* 375, 1254–1261. doi:10.1126/science.abf0529

Wang, Q., Sun, J., Chen, T., Song, S., Hou, Y., Feng, L., et al. (2023). Ferroptosis, pyroptosis, and cuproptosis in alzheimer's disease. *ACS Chem. Neurosci.* 14, 3564–3587. doi:10.1021/acschemneuro.3c00343

Xie, J., Yang, Y., Gao, Y., and He, J. (2023). Cuproptosis: mechanisms and links with cancers. *Mol. Cancer* 22, 46. doi:10.1186/s12943-023-01732-y

frontiers | Frontiers in Oncology

TYPE Original Research
PUBLISHED 17 March 2023
DOI 10.3389/fonc.2023.1145446

OPEN ACCESS

EDITED BY
Chun Xu,
The University of Queensland, Australia

REVIEWED BY
Lichao Liu,
University of Tennessee, United States
Sara Malih,
University of Wisconsin-Madison,
United States

*CORRESPONDENCE
Yunwei Han
530018842@qq.com

SPECIALTY SECTION
This article was submitted to Gastrointestinal Cancers: Gastric and Esophageal Cancers, a section of the journal Frontiers in Oncology

RECEIVED 16 January 2023
ACCEPTED 06 March 2023
PUBLISHED 17 March 2023

CITATION
Jiang L, Liao J and Han Y (2023) Study on the role and pharmacology of cuproptosis in gastric cancer.
Front. Oncol. 13:1145446.
doi: 10.3389/fonc.2023.1145446

Study on the role and pharmacology of cuproptosis in gastric cancer

Lin Jiang[1,2], Junzuo Liao[3] and Yunwei Han[1,4]*

[1]Department of Oncology, The First Affiliated Hospital of Jinan University, Guangzhou, China, [2]Department of Oncology, The Second Affiliated Hospital of North Sichuan Medical College, Nanchong, Sichuan, China, [3]Department of General Surgery, Affiliated Hospital of North Sichuan Medical College, Nanchong, Sichuan, China, [4]Department of Oncology, The Affiliated Hospital of Southwest Medical University, Luzhou, Sichuan, China

Objective: Gastric cancer has a poor prognosis and high mortality. Cuproptosis, a novel programmed cell death, is rarely studied in gastric cancer. Studying the mechanism of cuproptosis in gastric cancer is conducive to the development of new drugs, improving the prognosis of patients and reducing the burden of disease.

Methods: The TCGA database was used to obtain transcriptome data from gastric cancer tissues and adjacent tissues. GSE66229 was used for external verification. Overlapping genes were obtained by crossing the genes obtained by differential analysis with those related to copper death. Eight characteristic genes were obtained by three dimensionality reduction methods: lasso, SVM, and random forest. ROC and nomogram were used to estimate the diagnostic efficacy of characteristic genes. The CIBERSORT method was used to assess immune infiltration. ConsensusClusterPlus was used for subtype classification. Discovery Studio software conducts molecular docking between drugs and target proteins.

Results: We have established the early diagnosis model of eight characteristic genes (ENTPD3, PDZD4, CNN1, GTPBP4, FPGS, UTP25, CENPW, and FAM111A) for gastric cancer. The results are validated by internal and external data, and the predictive power is good. The subtype classification and immune type analysis of gastric cancer samples were performed based on the consensus clustering method. We identified C2 as an immune subtype and C1 as a non-immune subtype. Small molecule drug targeting based on genes associated with cuproptosis predicts potential therapeutics for gastric cancer. Molecular docking revealed multiple forces between Dasatinib and CNN1.

Conclusion: The candidate drug Dasatinib may be effective in treating gastric cancer by affecting the expression of the cuproptosis signature gene.

KEYWORDS

gastric cancer, cuproptosis, Diagnostic model, molecular docking, cancer

1 Introduction

Gastric cancer is one of the most common malignant tumors in the world, with the third highest mortality rate from cancer. In 2020, the number of new cases of stomach cancer in the world exceeded 1 million, and 769,000 people died from stomach cancer (1). East Asia is the concentrated area of the increasing gastric cancer cases in the world, and our country is the increasing main country in East Asia (2). The National Cancer Center reports that gastric cancer ranks second place in the incidence rate of malignant tumors and third in the mortality rate, posing a serious threat to the health of residents (3). The development of gastric cancer is a complex evolutionary process involving many factors and genes (4). Helicobacter pylori infection is the most important risk factor for gastric cancer. In addition, excessive consumption of preserved foods, alcohol consumption, and smoking are also risk factors for an increased risk of gastric cancer (5, 6). The molecular mechanism of gastric cancer is not fully understood. Current studies suggest that gastric mucosal epithelial cells undergo gene mutations under the influence of a number of complex factors, which then activate proto-oncogenes or silence tumor suppressor genes, thereby disrupting the balance between cell proliferation and apoptosis, and ultimately leading to the development of gastric cancer (7, 8). According to Lauren's classification, gastric cancer is mainly an intestinal type (9). The occurrence of intestinal gastric cancer is a multi-step cascade reaction: non-atrophic gastritis-multifocal atrophic gastritis with metaplasia-intestinal metaplasia-intraepithelial neoplasia-early gastric cancer-invasive advanced gastric cancer (10). Most of the previous studies have focused on advanced gastric cancer, while there are relatively few studies on abnormal molecular expression in early gastric cancer. The treatment and prognosis of gastric cancer are closely related to the timing of diagnosis. The 5-year survival rate of early gastric cancer patients after eradication is more than 90%, while the 5-year survival rate of advanced gastric cancer patients after eradication is less than 30% (11). In recent years, with the gradual enhancement of people's health awareness and the continuous progress of medical technology, the diagnosis rate of early gastric cancer has been greatly improved. The molecular mechanism of early gastric cancer is a hot topic in translational medicine in recent years.

With the rapid development of life sciences, studies on genomics, transcriptomics, proteomics, and metabolomics are emerging in an endless stream, which making it possible to analyze the molecular map of different stages of cancer transformation of gastric cancer from multiple dimensions, facilitating the monitoring of the occurrence, metastasis and drug resistance of gastric cancer. Futawatari et al. found that KK-LC-1 was abnormally highly expressed in early gastric cancer tissues, which could be used as a tumor marker for the diagnosis of early gastric cancer (12). Through genome-wide expression profiling microarray analysis, Zhang et al. found that the expression levels of GRIN2D and BRCAl in early gastric cancer and intraepithelial neoplasia were much higher than those in paired normal gastric mucosa, while the expression levels of BCL2L11, RET, and ALB were lower (13). Therefore, if the genes that regulate the changes in the progression of early gastric cancer can be screened and the specific mechanism of action can be clarified, it will be of great importance in the search for new targets of gastric cancer from the source.

Copper is an essential nutrient whose REDOX properties make it both beneficial and toxic to cells (14). Due to the high demand for copper as a metallic nutrient in tumor growth and metastasis, copper-related diagnostic methods are well suited for tumors (14). The traditional view of copper as merely a cofactor of active site metabolism has been challenged. A recent study has shown that intracellular copper induces a novel form of regulatory cell death (RCD), which differs from traditional cell death and has been termed "cuproptosis" (15). Cuproptosis is a type of programmed cell death that is distinct from apoptosis and may offer provide new hope for the treatment of gastric cancer. Although scientists have identified a number of genes and proteins that regulate cuproptosis, including FDX1, LIAS, DLAT, and CNN1, among others (15). However, the mechanism of action of these cuproptosis-related genes (CRGs) in gastric cancer remains unclear. Little is also known about the role of CRGs in diagnosis and the tumor microenvironment. Recent studies have reported that cuproptosis is closely related to cancer progression (15). There is increasing evidence that cuproptosis-associated long non-coding RNAs can be used as biomarkers for the prognosis of gastric cancer (16–18). However, the study on cuproptosis-related genes in early diagnosis and treatment of gastric cancer has not been reported. Therefore, in-depth understanding of the characteristics of TME immune cell infiltration mediated by many CRGs will help researchers better understand the potential mechanism of gastric cancer, predict the immune treatment response, and develop new safe and efficient targeted drugs.

2 Materials and methods

2.1 Microarray data set and difference analysis

Microarray datasets from gastric cancer patients and adjacent tissues were obtained from the TCGA database. The limma package in R was then used to identify and standardize differentially expressed genes (DEGs) by comparing the gene expression levels of gastric cancer patients and adjacent tissues (19). $P < 0.05$ and $|\log FC| > 1$ were used to define the standard of DEG. The ACRG (Asian Cancer Research Group) dataset GSE66229 was used for external validation.

2.2 Analysis of cuproptosis and immune-related genes

From a genome-wide CRISPR-Cas9 dysfunction test reported in the previous literature (15), a total of 347 potential copper-associated genes were identified (FDR<0.05). The list of 1793 immune-related genes were obtained from the Immunology Database and Analysis Portal (ImmPort; https://www.immport.org/home).

2.3 Functional annotation and pathway enrichment analysis

ClusterProfiler packages are used for functional analysis of biological functions, including Gene Ontology (GO) and the Kyoto

Encyclopedia of Genes and Genomes (KEGG). *P* values are adjusted using the Benjamini-Hochberg method or FDR for multiple testing corrections. The threshold is set to FDR<0.05. The GO category includes biological processes (BP), molecular functions (MF), and cellular components (CC). GENEMANIA (http://genemania.org/search/) was used to build a gene-interaction network for DEGs to evaluate the function of these genes.

2.4 Selection of characteristic genes

Three machine learning algorithms, LASSO, Random Forest, and SVM-RFE, were used to screen the trait genes. LASSO is a dimensionality reduction method that has been shown to be superior to regression analysis in evaluating high-dimensional data. The LASSO analysis was performed using the steering/penalty parameters with 10x cross-validation *via* the glmnet package. Recursive Feature Elimination (RFE) of the Random Forest algorithm is a supervised machine learning method for sequencing genes associated with atherosclerotic plaque progression and immunity. The predicted performance was estimated by ten-fold cross-validation. SVM-RFE is superior to linear discriminant analysis (LDA) and means square error (MSE) methods in selecting correlation features and removing redundant features. SVM-RFE was applied to feature selection by ten-fold cross-validation. The receiver operating characteristic (ROC) curve and area under the curve (AUC) were used to estimate the diagnostic effectiveness.

2.5 Establishment of a line graph

The rms package was used to incorporate characteristic genes to create a column map. Calibration curves are used to assess the accuracy of a column plot. The clinical practicability of the line map was assessed by decision curve analysis.

2.6 Estimation of immune cell infiltration in gastric cancer

The CIBERSORT algorithm was used to estimate the proportion of immune cell infiltration in gastric cancer samples. Estimates of immune cell infiltration with $P<0.05$ were used for further analysis.

2.7 Consensus cluster analysis

Based on the expression profile of gastric cancer and cuproptosis-associated genes, the number of unsupervised categories in gastric cancer was quantitatively estimated by the ConsensusClusterPlus software package (50 iterations and 80% resampling rate) using the consensus clustering method (20). The consensus matrix graph, consensus cumulative distribution function (CDF) graph, the relative change in area under the CDF curve, and tracking graph were used to find the optimal clustering number. Principal component analysis (PCA) was used to define differences in the expression of gastric cancer and cuproptosis-related genes between the two subtypes. The PCA plot was generated using the ggplot2 package.

2.8 Small molecule drug prediction

We used the three characteristic genes selected by a gene-set enrichment network tool Enrichr based on the Drug Characterization Database (DSigDB) to predict potential drugs. DSigDB is a free Web-based repository of information on GSEA drugs and their target genes. DSigDB currently contains a total of 22,527 genomes, including 17,389 drugs and 19,531 genes. $P<0.05$ was used as the statistical criterion to identify drugs that were significantly associated with target genes.

2.9 Molecular docking

For molecular docking, Dasatinib was selected as the receptor target in this study. The 3D crystal structures of these receptors were downloaded from the RCSB Protein database (http://www.rscb.org/pdb/). PubChem ligand from the national library of medicine (https://pubchem.ncbi.nlm.nih) to download and save the data file format for the space (SDF). The Automatic Docking Tool version 1.5.6 was used to prepare protein ligand complexes for docking and for 2D and 3D visualization of protein ligand complexes, operated using the Discovery Studio Visualization tool 2016.

3 Results

3.1 Microarray data sets and difference analysis

The mRNA expression profile of gastric cancer was retrieved based on the TCGA database, and 375 cancer tissues and 32 para-carcinoma tissues were obtained. The limma package in R was used for the identification and standardization of differentially expressed genes (DEG). The threshold was set as $P < 0.05$ and $|\log FC| > 1$, and 2951 differentially expressed genes were obtained. There were 2,532 up-regulated genes and 419 down-regulated genes. The DEGs data is visualized as A volcano map (Figure 1A) and the first 50 DEGs are shown in a heat map (Figure 1B). The basic information is in the supplementary documents.

3.2 Analysis of cuproptosis-related genes

347 cuproptosis genes were collected according to relevant literature. Intersecting with DEGs, 66 overlapping genes (OG) were obtained (Figure 1C).

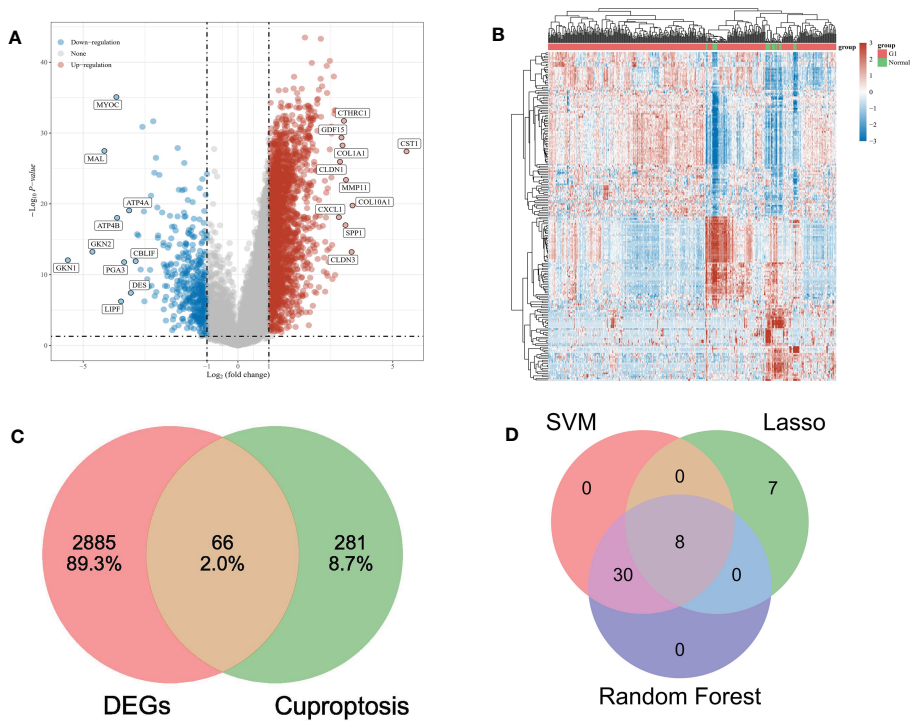

FIGURE 1
(A) The volcano map depicts the RNA expression levels of differential genes between gastric and paracancer tissues. **(B)** Heat maps showing differentially expressed genes between the above groups. **(C)** VENN diagrams show the intersection of differential genes and cuproptosis-related genes. **(D)** VENN diagram shows the intersection of three feature genes screened by machine learning.

3.3 GO term and KEGG pathway enrichment analysis of OG

GO analysis shows that the biological process (BP) of OG mainly focuses on the cellular nitrogen compound biological process, macroporous biological process, and cellular macroporous biological process (Figure 2A). The main cell components (CC) include intelligent non membrane-bound organelle, on-membrane-bounded organelle, and nuclear part (Figure 2B). Molecular function (MF) includes nuclear acid binding, RNA binding, and purine ribonuclease triphosphate binding (Figure 2C). Genes are mainly involved in the KEGG pathway of Aminoacyl tRNA biosynthesis, Cell cycle and Ribome (Figure 2D).

3.4 Analysis of protein interaction network of OGs

Based on the string website, we obtained the protein interaction network of the OG gene set. The software Cytoscape was used to present the results. The larger the circular area of the gene, the higher the degree score and the greater the importance. This shows that the element gene of the central circle is very important (Figure 3A). In addition, based on GeneMANIA's functional annotation model, a co-expression network was established to describe the genetic interaction of 66 OGs and their co-expressed genes (Figure 3B). Multiple attributes based on relationship (57.28% co-expression), (17.78% physical interaction), (10.91% prediction), (9.27% genetic interaction), (4.55% co-location). Of the 66 OGs, 13 were highly correlated with mitochondrial gene expression (adj. *P*=3.87E-9), and 11 were highly correlated with mitochondrial translation reaction (adj. *P*=5.28E-8) (Figure 3B).

3.5 Select characteristic genes through LASSO, random forest, and SVM-RFE algorithm

Three algorithms are used to select feature genes. For the LASSO algorithm, after ten cross-validation, we selected the minimum standard for constructing LASSO classifier, because the accuracy of comparison is higher, and 15 characteristic genes were identified (Figure 4A). For the random forest algorithm, 38 characteristic genes were identified (Figure 4B). For the SVM-RFE algorithm, 38 characteristic genes were also identified (Figures 4C, D). After cross-validation, eight characteristic genes (ENTPD3, PDZD4, CNN1, GTPBP4, FPGS, UTP25, CENPW, and FAM111A) shared by LASSO, Random Forest, and SVM-RFE algorithm were finally determined (Figure 1D).

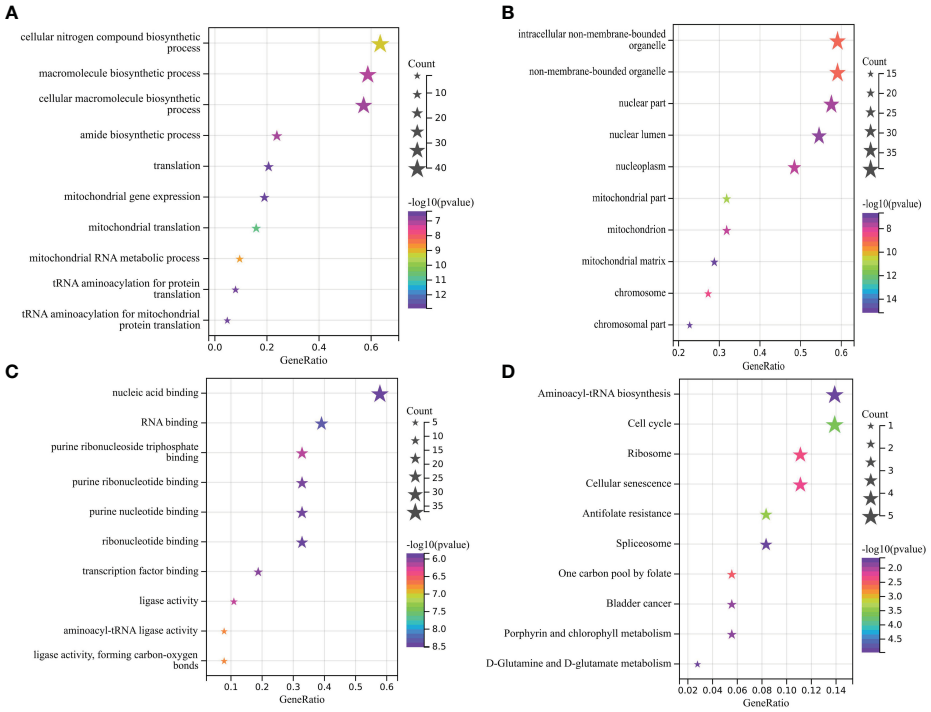

FIGURE 2
(A-C) Main BP, CC, and MF of overlapping gene enrichment. **(D)** Major KEGG pathways for the enrichment of the above overlapping genes.

3.6 Diagnostic efficacy and external validation of characteristic genes in predicting gastric cancer

Correlation analysis shows that there is a strong correlation between the eight characteristic genes (Figure 5A). When the eight characteristic genes (ENTPD3, PDZD4, CNN1, GTPBP4, FPGS, UTP25, CENPW, and FAM111A) are all fitted into one variable, the AUC of the ROC curve is 0.996, indicating a good diagnostic efficiency for gastric cancer (Figures 5B, C). We also estimated the diagnostic performance of each characteristic gene in predicting gastric cancer in the GSE126307 cohort. The AUC values of area under the ROC curve of 8 characteristic genes are very good, which proves that these characteristic genes can estimate the occurrence of gastric cancer. The expression of the characteristic genes was verified in the external data set. In the GSE66,229 dataset, the AUC value of the area under the ROC curve of eight characteristic genes (ENTPD3, PDZD4, CNN1, GTPBP4, FPGS, UTP25, CENPW, and FAM111A) is also high. When fitting together, the AUC of the ROC curve is 0.992, which shows that they can distinguish gastric cancer from healthy controls (Figures 5D, E). Therefore, the signature genes have excellent diagnostic performance in predicting the occurrence of gastric cancer.

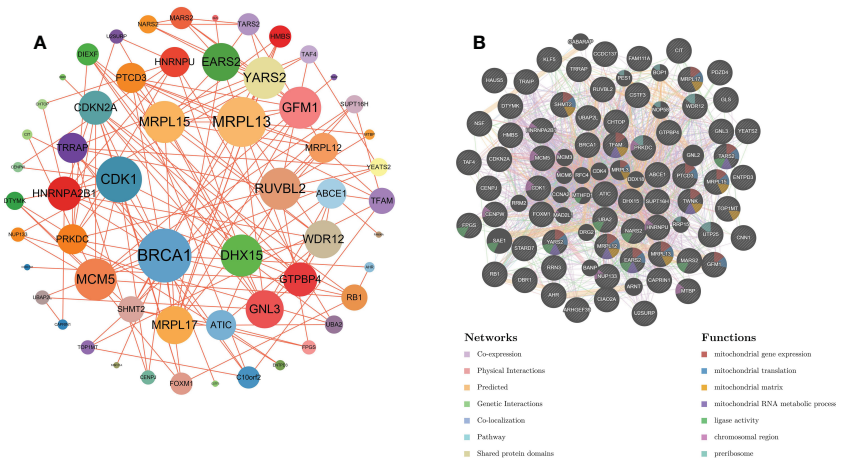

FIGURE 3
(A) PPI network of overlapping genes. **(B)** The GeneMANIA database was used to analyze the gene-gene interaction network of OG. Each node represents a gene. The node color represents the possible function of the corresponding gene.

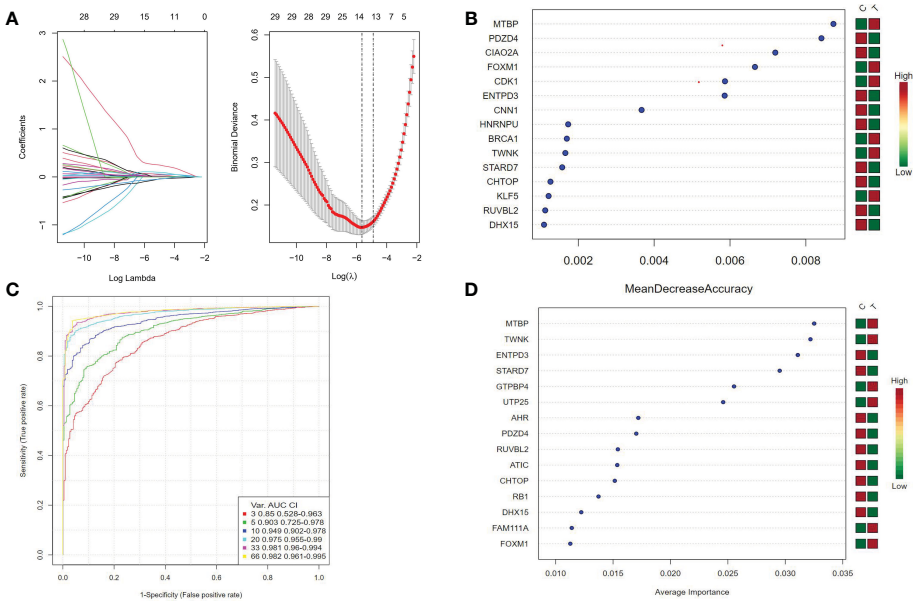

FIGURE 4
(A) Ten cross-validation of tuning parameter selection in the LASSO model. Each curve corresponds to a gene. LASSO coefficient analysis. The vertical solid line represents the partial likelihood deviation SE. The vertical dotted line is drawn at the best lambda. **(B)** Random forest algorithm for feature selection. **(C, D)** SVM-RFE algorithm for feature selection.

3.7 Establishment of characteristic gene nomogram

In the nomogram, each characteristic gene corresponds to a score, and the total score is obtained by adding the scores of all the characteristic genes. The total score corresponds to different risks of gastric cancer (Figure 6A). The calibration curve, risk comparison, and clinical decision curve show that a nomogram can accurately predict the occurrence of gastric cancer (Figures 6B–D).

3.8 Analysis of immune cell infiltration and correlation in gastric cancer

The proportion of immune cells in gastric cancer tissue samples and adjacent tissues is different. Compared with adjacent tissues, the proportion of B cell plasma, T cell CD4+memory resetting, Monocyte, and mast cell activated in the cancer group is relatively high, while the proportion of T cell CD4+memory activated, T cell follicular helper, T cell regulatory (Tregs), Macrophage M0,

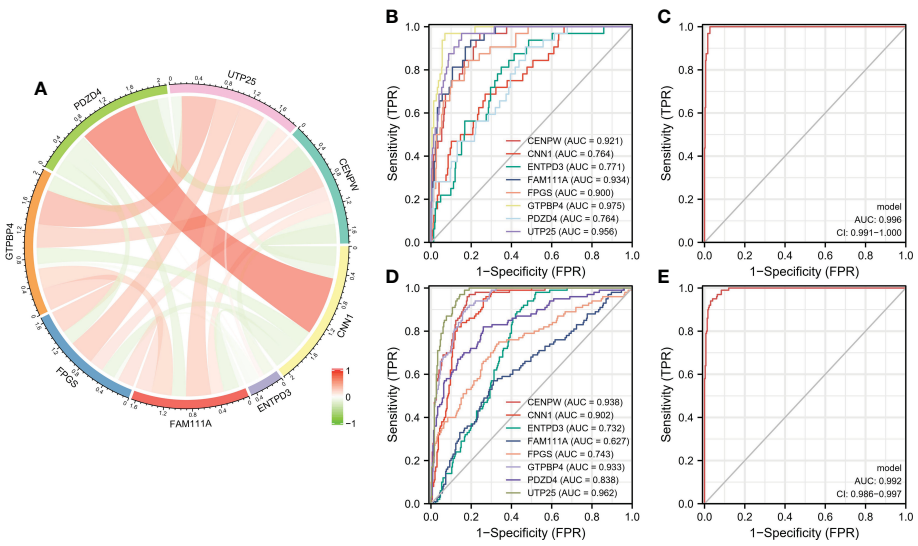

FIGURE 5
(A) Circle chart of characteristic gene correlation analysis. **(B, C)** ROC curve for estimating the diagnostic performance of characteristic genes. **(D, E)** ROC curve of externally verified characteristic genes.

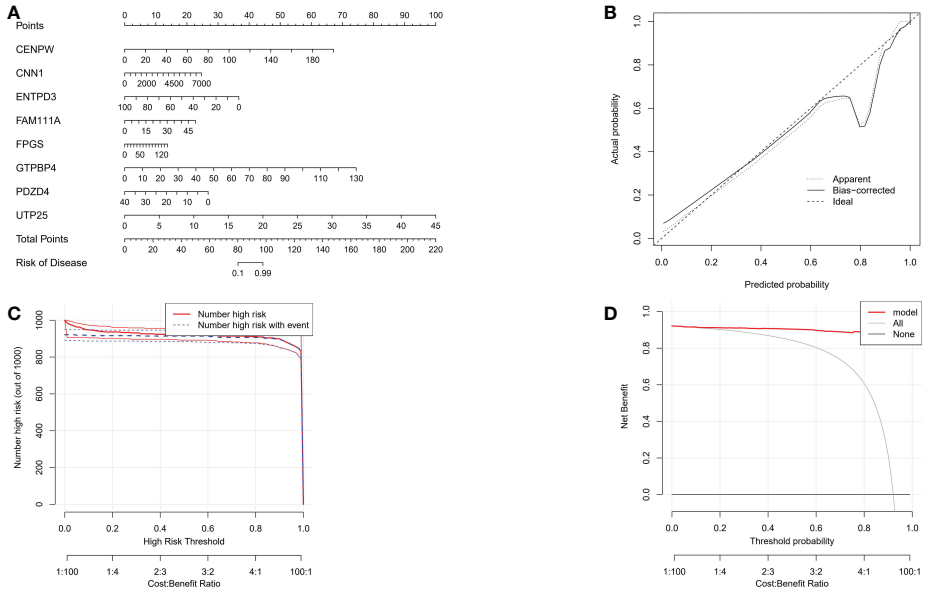

FIGURE 6
(A) The nomogram of integrated characteristic genes was established to predict the occurrence of gastric cancer. In the nomogram, each variable corresponds to a score, and the total score can be calculated by adding the scores of all variables. **(B)** Prediction accuracy of calibration curve estimation nomogram. **(C)** Risk comparison curve of nomograph. **(D)** Clinical decision curve of the nomogram.

Macrophage M1, and mast cell resetting is relatively low (Figures 7A, B). Correlation analysis showed that there was a strong correlation between the eight characteristic genes and immune cells. It shows that the cuproptosis gene may influence the degree of immune invasion of gastric cancer (Figure 8).

3.9 Construction of two subtypes of copper dead gastric cancer based on gastric cancer and cuproptosis-related genes

Using the consensus clustering method, gastric cancer was clustered according to the expression profiles of 66 gastric cancer and cuproptosis-related genes. The optimal number of subtypes is 2, as determined by the consensus matrix, the CDF chart, the relative change of area under the CDF curve, and tracking chart (Figures 9A–D). We noticed that most immune-related genes were significantly up-regulated in subtype C2 compared with subtype C1 (Figure 9E). We identified C2 as an immune subtype and C1 as a nonimmune subtype.

3.10 Prediction and molecular docking of targeted drugs for gastric cancer

Further, we screened the candidate drugs that may be used to treat gastric cancer. We consider the eight selected characteristic genes as drug targets and use the online network tool Enrichr based on DSigDB for drug target enrichment analysis. The results show that the top ten drugs may be potential drugs for the treatment of gastric cancer patients (Table 1). To verify the above results, we performed molecular docking between small molecule drugs and target genes, and the results showed that there are multiple forces between Dasatinib and CNN1. For example, multiple forces including hydrogen bonds can be formed (Figure 10). The above results indicate that candidate drugs may achieve the effect of treating gastric cancer by influencing the expression of characteristic genes.

4 Discussion

We established a diagnostic model of cuproptosis for gastric cancer based on machine learning and other methods, predicted potential therapeutic drugs based on cuproptosis-related genes, and finally performed a virtual combination of molecular docking space structure for therapeutic drugs. The mRNA expression profiles of gastric cancer were obtained from the TCGA database, and 375 cases of cancer tissues and 32 cases of para-carcinoma tissues were obtained. We identified 2,951 differential genes in the cancer tissue compared to the adjacent tissue. There were 2,532 up-regulated genes and 419 down-regulated genes. Based on three machine learning algorithms, we selected eight signature genes (ENTPD3, PDZD4, CNN1, GTPBP4, FPGS, UTP25, CENPW, and FAM111A). Both internal and external dataset validation and histogram results indicate that these signature genes can accurately predict the progression of gastric cancer. There is limited evidence to support the role of signature genes in gastric cancer. GTPBP4 is highly expressed in gastric cancer tissues, which promotes the progression of gastric cancer progression and may interact with the p53 signaling pathway (21). Low FPGS expression is an independent predictor of poor prognosis in stage II/III gastric cancer patients receiving adjuvant chemotherapy after S-1 surgery

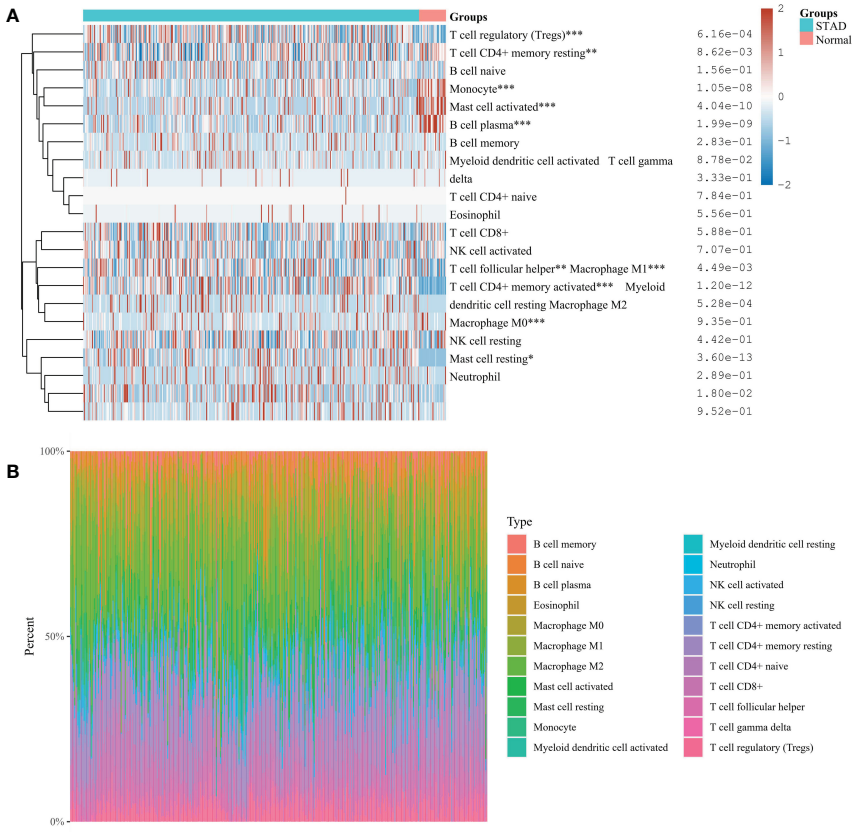

FIGURE 7
(A) Immunocyte score heat map *P< 0.05, **P < 0.01, ***P < 0.001. **(B)** The percentage abundance of tumor-infiltrating immune cells in each sample. Different colors represent different types of immune cells, the abscissa represents the sample, and the ordinate represents the percentage of immune cells in a single sample.

(22). However, the relationship between the other 6 characteristic genes and gastric cancer has not been reported.

Cuproptosis is a novel form of programmed cell death associated with copper accumulation, protein lipidation, and mitochondrial respiration (15). Cuproptosis is molecularly distinct from other forms of cell death, such as apoptosis, necrosis, autophagy, and iron death. Copper binding leads to a dangerous increase in lipid-acylated TCA circulating protein function. Excess copper increases lipid-acylated protein aggregation and Fe-S cluster protein instability, leading to protein toxic stress and cell death. As key regulators of cuproptosis, FDX1, and protein-lipid acylation play an important role in this process. Copper ionophores are extremely sensitive to cells that use mitochondrial respiration, which can be explained by their large number of lipid-acylated TCA enzymes. Tumor cells have abnormal mitochondrial metabolism due to the loss of active oncogenes and tumor suppressor genes (23). Aerobic glycolysis is widely observed in activated immune cells in the tumor microenvironment (TME) to support biosynthetic requirements (24). TME is now recognized to play a key role in carcinogenic effects and cancer development. The immune microenvironment is closely linked to the development of tumors (25, 26). It is composed of different types of immune cells and stromal cells that can provide nutritional support to tumor cells. The trace element copper has been reported to play an important role in both cellular and humoral immunity (27, 28), manipulating various immune cells to activate and maintain the immune system (29). In this study, we identified two subtypes C1 and C2 based on cuproptosis. Most immune-related genes were significantly upregulated in the C2 subtype compared to the C1 subtype. We identified C2 as an immune subtype and C1 as a non-immune subtype. The new classification of immune subtypes is helpful for the individualized classification and

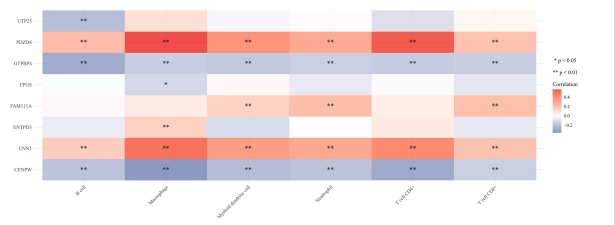

FIGURE 8
Correlation between eight characteristic genes and immune cells. *P<0.05, **P<0.01.

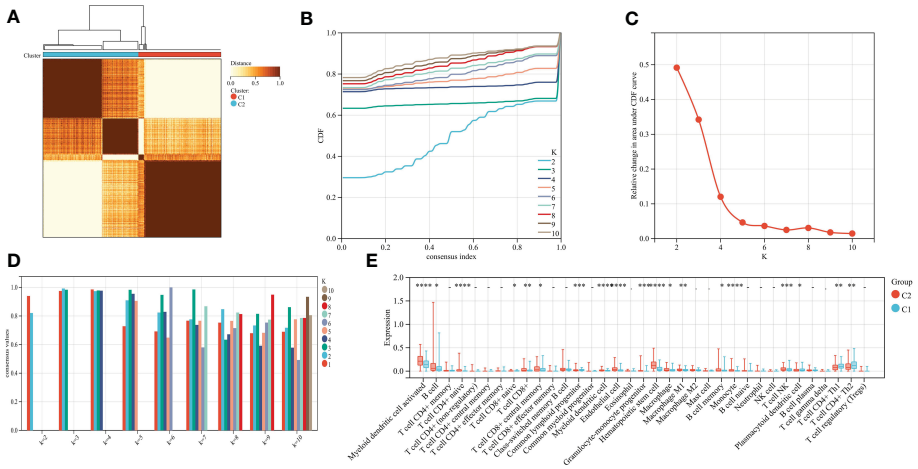

FIGURE 9
(A) Consensus matrix heat map when k=2. **(B)** Consensus CDF when k=2-9. **(C)** The relative change of area under the CDF curve. **(D)** When k=2-9, the tracking chart of sample classification is displayed. **(E)** Histogram of distribution of immune cells in subtype grouping.

medication guidance of gastric cancer patients. For small molecule drug screening, we have a list of the top 10 predictors. Numerous studies have confirmed that pemetrexed is a safe and effective drug for the treatment of metastatic gastric cancer (30–32). As a histone deacetylase (HDAC) inhibitor, Vorinostat can be used in combination with capecitabine plus cisplatin (XP) as a therapeutic agent in patients with gastric cancer (33). Dasatinib, which targets a variety of cancer kinases has strong antitumor activity and has been approved for the treatment of leukemia (34). There is increasing evidence that Dasatinib is also effective in gastric cancer (35, 36). Molecular docking showed that Dasatinib could form various forces with CNN1, including hydrogen bonding. The results indicated that candidate drugs may be effective in the treatment of gastric cancer by influencing the expression of characteristic genes. The specific mechanism needs to be further explored. In the future, we plan to establish SD rat gastric cancer

TABLE 1 Complete basic information was obtained from 261 follow-up data.

Characteristics	Cases
Gender	
Male	181
Female	80
Age at surgery	
<58	121
≥58	140
Tumor size	
<5 cm	131
≥5 cm	130
Histological type	
Diffuse	75
Intestinal	186
T classification	
T1–2	39
T3–4	222
TNM stage	
I + II	48
III + IV	213
Lymph node metastasis	
Present	216
Absent	45

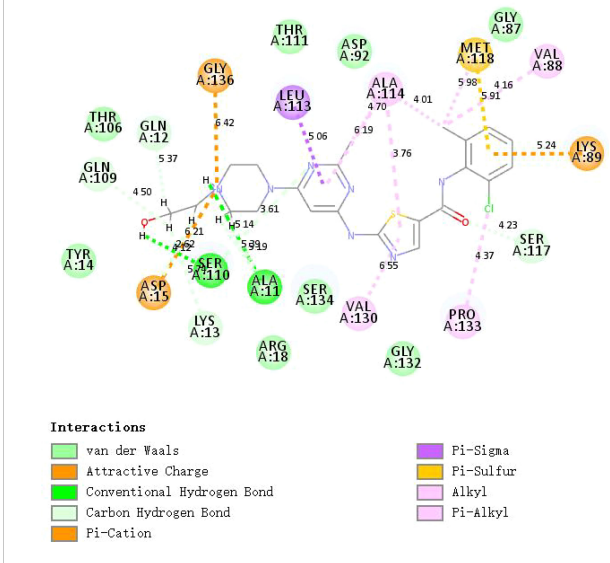

FIGURE 10
The 2D image shows the docking complex of Dashatinib and CNN1.

model and primary gastric cancer cell model *in vitro*, and use Dasatinib, siRNA and other intervention measures, combined with CCK-8, Western Blot, Scratch assay, immunofluorescence and immunocoprecipitate and other experimental technologies, to explore related molecular mechanisms from multiple perspectives and in all aspects. This will contribute to the development of new targeted therapeutic drugs in molecular pharmacology and help front-line clinical workers to better treat gastric cancer patients. Improve the prognosis of patients, improve life treatment, reduce the burden of family.

This study also has some shortcomings: Firstly, in the gastric cancer samples in the TCGA database selected for this study, the para-carcinoma tissues were not well matched to the cancer tissues, which could lead to false positive results. However, the subsequent validation of external datasets further confirms the reliability of the results. Second, the selected therapeutic drugs in this study were only predicted only by molecular docking without experimental verification. Subsequent *in vivo* and *in vitro* experiments will be carried out to further investigate the relevant molecular mechanisms.

5 Conclusion

Eight specific cuproptosis gene diagnostic models and targeted drugs have been identified in gastric cancer, which may contribute to early diagnosis and individualized immunotherapy strategies for gastric cancer patients.

Data availability statement

The original contributions presented in the study are included in the article/supplementary material. Further inquiries can be directed to the corresponding author.

Author contributions

LJ conceived and directed the project and wrote the manuscript. JL performed data bioinformatics analyses. YH helped with part of English checking. All authors contributed to the article and approved the submitted version.

Funding

This research was supported by Nanchong Municipal Science and Technology Strategic Cooperation Special Project 2020 (20SXQT0086) and Sichuan Provincial Health Commission Scientific Research Project - Universal Application Project (17PJ593).

Acknowledgments

I would like to sincerely thank all the authors of this article. Thank them for all their efforts and help.

Conflict of interest

The authors declare that the research was conducted in the absence of any commercial or financial relationships that could be construed as a potential conflict of interest.

Publisher's note

References

1. Sung H, Ferlay J, Siegel RL, Laversanne M, Soerjomataram I, Jemal A, et al. Global cancer statistics 2020: GLOBOCAN estimates of incidence and mortality worldwide for 36 cancers in 185 countries. *CA Cancer J Clin* (2021) 71(3):209–49. doi: 10.3322/caac.21660

2. Collaborators, G. B. D. O. C. The global, regional, and national burden of oesophageal cancer and its attributable risk factors in 195 countries and territories, 1990-2017: A systematic analysis for the global burden of disease study 2017. *Lancet Gastroenterol Hepatol* (2020) 5(6):582–97. doi: 10.1016/S2468-1253(20)30007-8

3. Yan H, Liu X, Yin L, Han H, Jin Y, Zhu X, et al. Effects of endoscopic therapy and surgical resection on long-term survival outcomes in patients with duodenal gastrointestinal stromal tumors: A surveillance, epidemiology, and end result program analysis. *Surg Endosc* (2022) 36(11):8030–8. doi: 10.1007/s00464-022-09231-9

4. Nadauld LD, Ford JM. Molecular profiling of gastric cancer: toward personalized cancer medicine. *J Clin Oncol* (2013) 31(7):838–9. doi: 10.1200/JCO.2012.47.1714

5. Buiatti E, Cipriani F. [Etiological epidemiology of gastric tumors]. *Ann Ist Super Sanita* (1996) 32(4):557–71.

6. Key T. Micronutrients and cancer aetiology: the epidemiological evidence. *Proc Nutr Soc* (1994) 53(3):605–14. doi: 10.1079/PNS19940069

7. Gao C, Liu H, Zhao Y, Miao X, Zheng H. Is there a relationship between neural EGFL like 1 (NELL1) promoter hypermethylation and prognosis of gastric cancer? *Med Hypotheses* (2021) 158:110723. doi: 10.1016/j.mehy.2021.110723

8. Lakshmi Ch NP, Sivagnanam A, Raja S, Mahalingam S. Molecular basis for RASSF10/NPM/RNF2 feedback cascade-mediated regulation of gastric cancer cell proliferation. *J Biol Chem* (2021) 297(2):100935. doi: 10.1016/j.jbc.2021.100935

9. Lauren P. The two histological main types of gastric carcinoma: Diffuse and so-called intestinal-type carcinoma. an attempt at a histo-clinical classification. *Acta Pathol Microbiol Scand* (1965) 64:31–49. doi: 10.1111/apm.1965.64.1.31

10. Correa P, Piazuelo MB. The gastric precancerous cascade. *J Dig Dis* (2012) 13 (1):2–9. doi: 10.1111/j.1751-2980.2011.00550.x

11. Nishida T, Sugimoto A, Tomita R, Higaki Y, Osugi N, Takahashi K, et al. Impact of time from diagnosis to chemotherapy in advanced gastric cancer: A propensity score matching study to balance prognostic factors. *World J Gastrointest Oncol* (2019) 11 (1):28–38. doi: 10.4251/wjgo.v11.i1.28

12. Futawatari N, Fukuyama T, Yamamura R, Shida A, Takahashi Y, Nishi Y, et al. Early gastric cancer frequently has high expression of KK-LC-1, a cancer-testis antigen. *World J Gastroenterol* (2017) 23(46):8200–6. doi: 10.3748/wjg.v23.i46.8200

13. Zhang Y, Wu X, Zhang C, Wang J, Fei G, Di X, et al. Dissecting expression profiles of gastric precancerous lesions and early gastric cancer to explore crucial molecules in intestinal-type gastric cancer tumorigenesis. *J Pathol* (2020) 251(2):135–46. doi: 10.1002/path.5434

14. Ge EJ, Bush AI, Casini A, Cobine PA, Cross JR, DeNicola GM, et al. Connecting copper and cancer: From transition metal signalling to metalloplasia. *Nat Rev Cancer* (2022) 22(2):102–13. doi: 10.1038/s41568-021-00417-2

15. Tsvetkov P, Coy S, Petrova B, Dreishpoon M, Verma A, Abdusamad M, et al. Copper induces cell death by targeting lipoylated TCA cycle proteins. *Science* (2022) 375(6586):1254–61. doi: 10.1126/science.abf0529

16. Wang Y, Liu K, Shen K, Xiao J, Zhou X, Cheng Q, et al. A novel risk model construction and immune landscape analysis of gastric cancer based on cuproptosis-related long noncoding RNAs. *Front Oncol* (2022) 12:1015235. doi: 10.3389/fonc.2022.1015235

17. Song X, Hou L, Zhao Y, Guan Q, Li Z. Metal-dependent programmed cell death-related lncRNA prognostic signatures and natural drug sensitivity prediction for gastric cancer. *Front Pharmacol* (2022) 13:1039499. doi: 10.3389/fphar.2022.1039499

18. Feng A, He L, Chen T, Xu M. A novel cuproptosis-related lncRNA nomogram to improve the prognosis prediction of gastric cancer. *Front Oncol* (2022) 12:957966. doi: 10.3389/fonc.2022.957966

19. Liu J, Zhou S, Li S, Jiang Y, Wan Y, Ma X, et al. Eleven genes associated with progression and prognosis of endometrial cancer (EC) identified by comprehensive bioinformatics analysis. *Cancer Cell Int* (2019) 19:136. doi: 10.1186/s12935-019-0859-1

20. Wilkerson MD, Hayes DN. ConsensusClusterPlus: A class discovery tool with confidence assessments and item tracking. *Bioinformatics* (2010) 26(12):1572–3. doi: 10.1093/bioinformatics/btq170

21. Li L, Pang X, Zhu Z, Lu L, Yang J, Cao J, et al. GTPBP4 promotes gastric cancer progression via regulating P53 activity. *Cell Physiol Biochem* (2018) 45(2):667–76. doi: 10.1159/000487160

22. Maezawa Y, Sakamaki K, Oue N, Kimura Y, Hashimoto I, Hara K, et al. High gamma-glutamyl hydrolase and low folylpolyglutamate synthetase expression as prognostic biomarkers in patients with locally advanced gastric cancer who were administrated postoperative adjuvant chemotherapy with s-1. *J Cancer Res Clin Oncol* (2020) 146(1):75–86. doi: 10.1007/s00432-019-03087-8

23. Boese AC, Kang S. Mitochondrial metabolism-mediated redox regulation in cancer progression. *Redox Biol* (2021) 42:101870. doi: 10.1016/j.redox.2021.101870

24. Reinfeld BI, Madden MZ, Wolf MM, Chytil A, Bader JE, Patterson AR, et al. Cell-programmed nutrient partitioning in the tumour microenvironment. *Nature* (2021) 593(7858):282–8. doi: 10.1038/s41586-021-03442-1

25. Xu C, Sui S, Shang Y, Yu Z, Han J, Zhang G, et al. The landscape of immune cell infiltration and its clinical implications of pancreatic ductal adenocarcinoma. *J Adv Res* (2020) 24:139–48. doi: 10.1016/j.jare.2020.03.009

26. Edlund K, Madjar K, Mattsson JSM, Djureinovic D, Lindskog C, Brunnstrom H, et al. Prognostic impact of tumor cell programmed death ligand 1 expression and immune cell infiltration in NSCLC. *J Thorac Oncol* (2019) 14(4):628–40. doi: 10.1016/j.jtho.2018.12.022

27. Djoko KY, Ong CL, Walker MJ, McEwan AG. The role of copper and zinc toxicity in innate immune defense against bacterial pathogens. *J Biol Chem* (2015) 290 (31):18954–61. doi: 10.1074/jbc.R115.647099

28. Hackler J, Heller RA, Sun Q, Schwarzer M, Diegmann J, Bachmann M, et al. Relation of serum copper status to survival in COVID-19. *Nutrients* (2021) 13(6):1898. doi: 10.3390/nu13061898

29. Su Y, Zhang X, Li S, Xie W, Guo J. Emerging roles of the copper-CTR1 axis in tumorigenesis. *Mol Cancer Res* (2022) 20(9):1339–53. doi: 10.1158/1541-7786.MCR-22-0056

30. Bajetta E, Celio L, Buzzoni R, Ferrari L, Marchiano A, Martinetti A, et al. Phase II study of pemetrexed disodium (Alimta) administered with oral folic acid in patients with advanced gastric cancer. *Ann Oncol* (2003) 14(10):1543–8. doi: 10.1093/annonc/mdg406

31. Kim YH, Chung HC, Kang WK, Park SR, Kim CS, Kim TY, et al. Pemetrexed and cisplatin in patients with advanced gastric cancer: A Korean cancer study group multicenter phase II study. *Cancer Chemother Pharmacol* (2008) 62(2):263–70. doi: 10.1007/s00280-007-0600-y

32. Celio L, Sternberg CN, Labianca R, La Torre I, Amoroso V, Barone C, et al. Pemetrexed in combination with oxaliplatin as a first-line therapy for advanced gastric cancer: A multi-institutional phase II study. *Ann Oncol* (2009) 20(6):1062–7. doi: 10.1093/annonc/mdn766

33. Yoo C, Ryu MH, Na YS, Ryoo BY, Lee CW, Kang YK. Vorinostat in combination with capecitabine plus cisplatin as a first-line chemotherapy for patients with metastatic or unresectable gastric cancer: Phase II study and biomarker analysis. *Br J Cancer* (2016) 114(11):1185–90. doi: 10.1038/bjc.2016.125

34. Shen H, Hu X, Yang X, Chen J, Fu Y, He H, et al. Inhibition of BRD4 enhanced the tumor suppression effect of dasatinib in gastric cancer. *Med Oncol* (2022) 40(1):9. doi: 10.1007/s12032-022-01831-8

35. Shi M, Lou B, Ji J, Shi H, Zhou C, Yu Y, et al. Synergistic antitumor effects of dasatinib and oxaliplatin in gastric cancer cells. *Cancer Chemother Pharmacol* (2013) 72 (1):35–44. doi: 10.1007/s00280-013-2166-1

36. Choi KM, Cho E, Bang G, Lee SJ, Kim B, Kim JH, et al. Activity-based protein profiling reveals potential dasatinib targets in gastric cancer. *Int J Mol Sci* (2020) 21 (23):9276. doi: 10.3390/ijms21239276

frontiers | Frontiers in Immunology

TYPE Original Research
PUBLISHED 30 March 2023
DOI 10.3389/fimmu.2023.1146411

OPEN ACCESS

EDITED BY
Lin-Lin Bu,
Wuhan University, China

REVIEWED BY
Kosuke Kawaguchi,
Kyoto University, Japan
Shucai Xie,
Department of Critical Care Medicine,
Central South University, China

*CORRESPONDENCE
Lichuan Wu
richard_wu@gxu.edu.cn
Jinrui Wei
weijr@gxtcmu.edu.cn

†These authors have contributed equally to this work

SPECIALTY SECTION
This article was submitted to Cancer Immunity and Immunotherapy, a section of the journal Frontiers in Immunology

RECEIVED 17 January 2023
ACCEPTED 20 March 2023
PUBLISHED 30 March 2023

CITATION
Liu R, Liu Y, Zhang F, Wei J and Wu L (2023) A cuproptosis random forest cox score model-based evaluation of prognosis, mutation characterization, immune infiltration, and drug sensitivity in hepatocellular carcinoma. *Front. Immunol.* 14:1146411. doi: 10.3389/fimmu.2023.1146411

A cuproptosis random forest cox score model-based evaluation of prognosis, mutation characterization, immune infiltration, and drug sensitivity in hepatocellular carcinoma

Ruiqi Liu[1†], Yingyi Liu[1†], Fengyue Zhang[1], Jinrui Wei[2*] and Lichuan Wu[1*]

[1]School of Medicine, Guangxi University, Nanning, China, [2]Guangxi Scientific Research Center of Traditional Chinese Medicine, Guangxi University of Chinese Medicine, Nanning, Guangxi, China

Background: Hepatocellular carcinoma is the third most deadly malignant tumor in the world with a poor prognosis. Although immunotherapy represents a promising therapeutic approach for HCC, the overall response rate of HCC patients to immunotherapy is less than 30%. Therefore, it is of great significance to explore prognostic factors and investigate the associated tumor immune microenvironment features.

Methods: By analyzing RNA-seq data of the TCGA-LIHC cohort, the set of cuproptosis related genes was extracted *via* correlation analysis as a generalization feature. Then, a random forest cox prognostic model was constructed and the cuproptosis random forest cox score was built by random forest feature filtering and univariate multivariate cox regression analysis. Subsequently, the prognosis prediction of CRFCS was evaluated *via* analyzing data of independent cohorts from GEO and ICGC by using KM and ROC methods. Moreover, mutation characterization, immune cell infiltration, immune evasion, and drug sensitivity of CRFCS in HCC were assessed.

Results: A cuproptosis random forest cox score was built based on a generalization feature of four cuproptosis related genes. Patients in the high CRFCS group exhibited a lower overall survival. Univariate multivariate Cox regression analysis validated CRFCS as an independent prognostic indicator. ROC analysis revealed that CRFCS was a good predictor of HCC (AUC =0.82). Mutation analysis manifested that microsatellite instability (MSI) was significantly increased in the high CRFCS group. Meanwhile, tumor microenvironment analysis showed that the high CRFCS group displayed much more immune cell infiltration compared with the low CRFCS group. The immune escape assessment analysis demonstrated that the high CRFCS group displayed a

decreased TIDE score indicating a lower immune escape probability in the high CRFCS group compared with the low CRFCS group. Interestingly, immune checkpoints were highly expressed in the high CRFCS group. Drug sensitivity analysis revealed that HCC patients from the high CRFCS group had a lower IC_{50} of sorafenib than that from the low CRFCS group.

Conclusions: In this study, we constructed a cuproptosis random forest cox score (CRFCS) model. CRFCS was revealed to be a potential independent prognostic indicator of HCC and high CRFCS samples showed a poor prognosis. Interestingly, CRFCS were correlated with TME characteristics as well as clinical treatment efficacy. Importantly, compared with the low CRFCS group, the high CRFCS group may benefit from immunotherapy and sorafenib treatment.

KEYWORDS

cuproptosis, hepatocellular carcinoma, prognostic signature, immunotherapy, tumor microenvironment

1 Introduction

Liver cancer remains one of the most lethal cancers, with 830,000 deaths worldwide in 2020, accounting for 8.3% of cancer related deaths (1). Hepatocellular carcinoma (HCC) is the most frequent of all primary liver cancers, comprising 75-85% of cases (2). Due to the lack of diagnostic marker, most of the HCC patients are diagnosed at advanced stages with a poor prognosis (3). Therapies such as traditional cytotoxic drugs are rarely effective. Over the last decade, sorafenib and lenvatinib are the only systemic drugs that have been proven to be clinically effective in the therapy of part of the advanced HCC patients (4). Therefore, it is crucial to find valid prognostic models as well as treatment strategies.

Immune checkpoint inhibitor (ICIs) therapy is one of the fastest-developing immunotherapy strategies, which effectively breaks the dilemma of cancer treatment, especially in advanced cancer. However, the efficacy of immunotherapy varies widely among patients (5). HCC is intimately correlated with inflammation and has a complicated tumor microenvironment (TME) (6). Immune checkpoint therapy is being used for HCC treatment recently. The sensitivity of immunotherapy in HCC varies significantly due to the heterogeneity and complexity of the TME (7). Revealing the potential TME characteristics of HCC patients is hence crucial for predicting the efficacy of immunotherapy.

Copper (Cu) is a required element for human health. Disturbance of intracellular coppers is associated with diverse pathologies (8). Previous studies have demonstrated that Cu levels are significantly increased in tumor tissues and cancer patients derived serum (9–12). The elevated levels of Cu are reported to be involved in tumor cell proliferation, angiogenesis, and metastasis (13, 14). Cu may also increase the incidence of HCC in Wilson's disease patients (15). Both copper chelators and copper ionophores have been exploited as antitumor drugs and tested in clinical trials (16–18). Besides, Cu homeostasis is essential for maintaining normal immune function (19–21) and elevated Cu levels in tumor cells contribute to immune escape by enhancing PD-L1 expression (22). These findings suggest that Cu plays an important role in tumorigenesis and TME shaping. The Cu metabolism is recognized as a unique vulnerability in cancer (23) and targeting Cu metabolism might be an alternative strategy for cancer treatment (24). Recently, a novel Cu induced programmed cell death termed cuproptosis was revealed which occurs by targeting lipoylated TCA cycle proteins (25). Previous studies have shown that cuproptosis-related signature and genes are closely related to TME in colorectal cancer (26), breast cancer (27), lung cancer (28), bladder cancer (29), kidney renal clear cancer (30), and so forth. However, the relationships between cuproptosis-related genes and prognosis, immune microenvironment, and drug sensitivity of liver cancer has not been fully elucidated.

In this study, cuproptosis-related gene sets were derived by correlation analysis as generalization features. Then a random forest Cox prognostic model was constructed, and the cuproptosis random forest Cox score (CRFCS) was built by random forest feature filtering and univariate multivariate Cox regression. The HCC patients were clustered according to CRFCS and investigated in terms of prognosis analysis, mutational characteristics, tumor microenvironment, prediction of immune evasion, immune checkpoint, and drug sensitivity.

2 Materials and methods

2.1 Data acquisition and processing

The mRNA expression data, somatic mutation data, and corresponding clinical information of HCC were downloaded from

the TCGA database *via* the R package "TCGAbiolinks". The clinical and mRNA expression data of GSE116174 and ICGC-LIHC-US cohorts were downloaded from the GEO database (https://www.ncbi.nlm.nih.gov/geo/) and the ICGC database (https://dcc.icgc.org/projects/), respectively. Then, the mRNA data were converted to TPM format and normalized by log2 transformation.

2.2 Development of cuproptosis random forest cox score (CRFCS)

The cuproptosis-associated gene set was derived as a generalization feature by correlation analysis based on the TCGA-LIHC cohort. We used the method "rfsrc" in the R package "randomForestSRC" to construct a random forest model and selected features. The Cox regression was constructed based on the mentioned characteristics, and Regression coefficients were obtained by the "coxph" method in the "survival" package. The Cuproptosis Random Forest Cox Score (CRFCS) was established by the following formula:

$$Score = \sum E_i r_i$$

Where E_i is the expression of feature gene i, and r_i is the characteristic co-efficient of feature gene i.

2.3 Survival analysis

Kaplan-Meier (K-M) survival analysis and visualization were conducted with the "survival" and "survminer" packages. The time-related receiver operating characteristic curve (time ROC) was performed by the R package "pROC" to evaluate the prediction performance of CRFCS in the training and test sets.

2.4 Processing and analysis of mutation profile

The analysis and visualization of mutation profile were performed by the "maftools" package. We plotted the mutation waterfall by the method "oncoplot". After removing the loci falling into the CNV region, the Mutant-Allele Tumor Heterogeneity (MATH) score of the samples was calculated by the "inferHeterogeneity" method (31). MSI scores were calculated by the "MSIsensor" method (32).

2.5 TME cell infiltration assessment

The immune cell infiltration was estimated by both ssGSEA and CIBERSORT algorithms. For the ssGSEA method, we used the TME-infiltrating gene set from Charoentong et al., which includes 28 immune cell types (33). We evaluated the enrichment fraction of each sample in the cohort *via* the ssGSEA method to characterize the immune cell invasion in each sample. The CIBERSORT algorithm worked in conjunction with the immune infiltration signature matrix LM22 to evaluate the invasion of various immune cells in the samples. In the case of stromal cells, we estimated the stromal cell infiltration by evaluating the expression of markers for each stromal cell.

2.6 Immune evasion prediction

The Tumor Immune Dysfunction and Exclusion (TIDE) algorithm is used to assess the immune evasion mechanism of tumors (34). The effect of both T-cell dysfunction and T-cell exclusion mechanisms on immune evasion was evaluated separately by the TIDE algorithm and the TIDE score was used to predict the degree of immune evasion of the samples.

2.7 Drugs sensitivity prediction

The IC_{50} values of the drugs in the training set samples were evaluated by the "pRRopheticPredict" method of the R package "pRRophetic", with the dataset "cgp2016". We calculated the correlation between IC_{50} values and CRFCS subgroups to investigate the association between CRFCS and drug sensitivity.

2.8 Statistical analysis

The analysis and visualization of the data were performed in R (version 4.1.1). The Wilcoxon test was used to compare the data between the two groups. Charts were mainly visualized by the " ggplot2 " package. The p-value<0.05 was regarded as statistically significant (*p<0.05; **p<0.01; ***p<0.001; ****p<0.0001).

3 Results

3.1 The expressions and prognosis analysis of cuproptosis-related genes in HCC

We initially evaluated the expressions of ten genes in HCC which were reported to be crucial regulators of cuproptosis (25). It was noticed that among these ten genes, all of them except FDX1 were significantly highly expressed in HCC (Figure 1A), indicating that the cuproptosis process might be associated with HCC. To further explore the prognosis of cuproptosis genes in HCC, we performed a correlation analysis between cuproptosis gene expression and HCC patients' survival (OS) (Figure 1B). The results displayed that genes DLAT (HR =1.71, p =0.003), PDHA1 (HR =1.42, p =0.046), GLS (HR =1.49, p =0.023), and CDKN2A (HR =1.78, p =0.001) had prominent prognostic significance in HCC, and patients with high expression of these four genes exhibited shorter survival (Figures 1C–F).

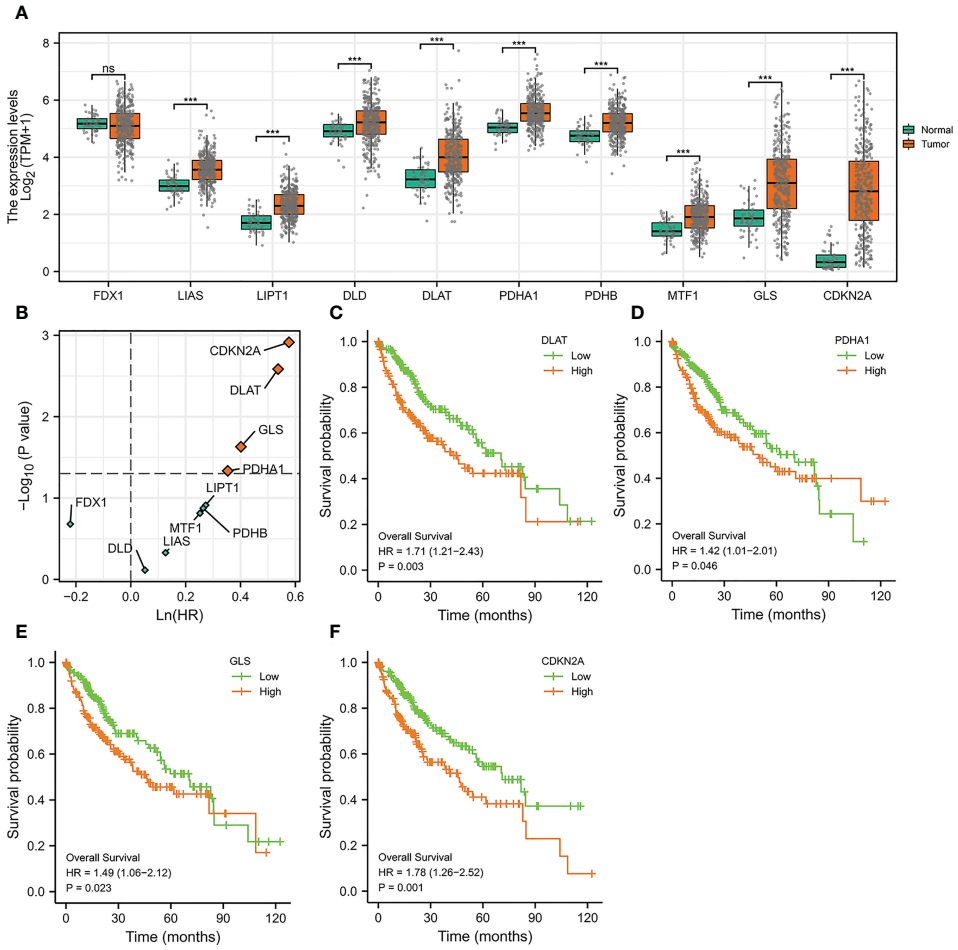

FIGURE 1
The Expressions and Prognosis Analysis of Cuproptosis-Related Genes in HCC. **(A)** Differential expression of cuproptosis-related genes in the TCGA-LIHC cohort. (***p<0.001; ns stands for not significant) **(B)** Correlation between cuproptosis-related gene expression and survival data (OS) of HCC patients. The horizontal dotted line stands for p=0.05. The vertical dotted line represents HR=1. **(C–F)** Kaplan-Meier curves of DLAT **(C)**, PDHA1 **(D)**, GLS **(E)**, and CDKN2A **(F)**.

3.2 Construction of cuproptosis random forest cox score (CRFCS) model

Given that cuproptosis may be involved in the progression of HCC, a more robust prognostic model was constructed using the above-mentioned cuproptosis genes with prominent prognostic significance (DLAT, PDHA1, GLS, and CDKN2A). First and foremost, correlation analysis of the above genes was initially conducted *via* analyzing data from TCGA-LIHC cohort to enhance the generalization ability of the model. For each cuproptosis gene listed above, the top 25 expression-related genes were identified as generalized features based on correlation coefficients. For the gene sets after the generalization of features, GO/KEGG analysis was performed to ensure that the characteristics were not distorted by generalization. The results indicated that the gene set after features generalization remained associated with key pathways of cuproptosis, such as the TCA cycle (Figures 2A, B). Training the gene set as input of the random forest model, the out-of-bag error of the model stabilized when the number of trees was approximately around 1000 (Figure 2C). The random forest model derived the variable importance (VIMP) ranking of the input features (Figure 2D). We selected the top 20% of the ranked features to be involved in the construction of the Cox model. Excluding the features not significant in the univariate Cox test, 17 features were obtained and model scores were established according to the steps in Materials and Methods (Figure 2E).

3.3 Prognosis prediction of CRFCS

To evaluate the accuracy of the model's predictions, we validated CRFCS in the training set TCGA-LIHC and the external validation set ICGC-LIHC-US and GSE116174. We divided the samples of each set into high and low score groups by the median of CRFCS. In the TCGA-LIHC set, the contemporaneous surviving rate of the high CRFCS subgroup samples was much lower than that of the low CRFCS subgroup. The HR for the CRFCS subgroups was 2.86 (1.96-4.16), with a p-value less than 0.001 (Figure 3A). Likewise, the survival of the high CRFCS subgroup samples was shorter in both validation cohorts. In the ICGC-LIHC-US cohort,

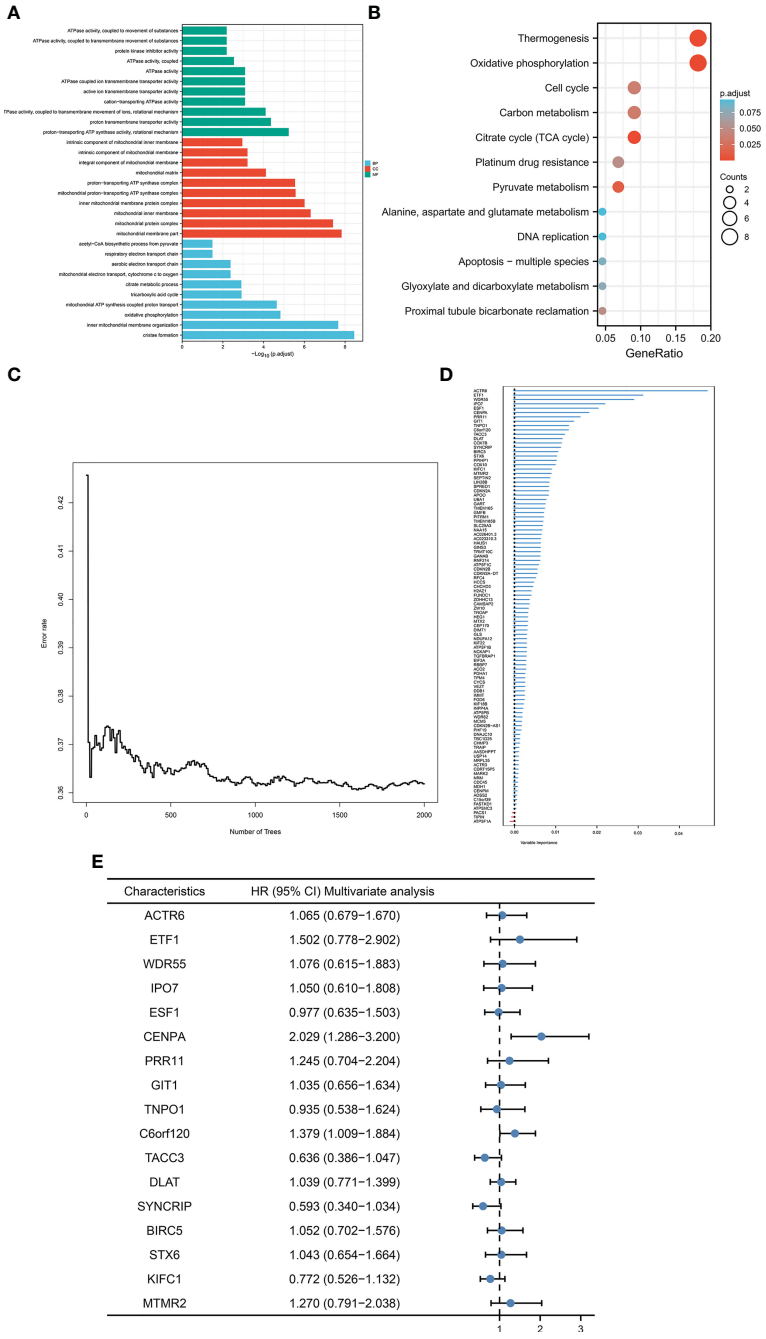

FIGURE 2
Construction of CRFCS. **(A, B)** GO **(A)** and KEGG **(B)** enrichment analysis of gene sets after generalizing features. **(C)** Trend of out-of-bag error (oob) of random forest model with the number of trees (nTree). **(D)** Ranking of variable importance (VIMP) of features. **(E)** Multivariate cox test of feature genes.

the HR of the CRFCS subgroup was 2.69 (1.65-4.38) with a p-value less than 0.001 (Figure 3B) while the HR value was 2.78 (1.24-6.23) with a p-value of 0.013 in the GSE116174 cohort (Figure 3C). Subsequently, ROC analysis was performed to evaluate the diagnostic potency of CRFCS in HCC. The results demonstrated that CRFCS was a strong predictor in both training and validation cohorts (Figures 3D–F). The AUC values for predicting OS were 0.820 at 1 year, 0.727 at 3 years, and 0.670 at 5 years in the TCGA-LIHC training cohort (Figure 3D). While AUC values for predicting OS were 0.720 at 1 year, 0.671 at 3 years, and 0.664 at 5 years in the ICGC-LIHC-US cohort (Figure 3E) and 0.727 at 1 year, 0.665 at 3 years, and 0.713 at 5 years in the GSE116174 cohort (Figure 3F). Also, we performed univariate and multivariate Cox analyses of CRFCS in order to examine the potential of CRFCS as an OS-independent prognostic factor for HCC. The results showed a hazard ratio of 2.708 (2.087-3.514) for CRFCS in the univariate analysis with a p-value less than 0.001 (Figure 3G). In the multifactorial analysis, the hazard ratio was 2.437 (1.825-3.254)

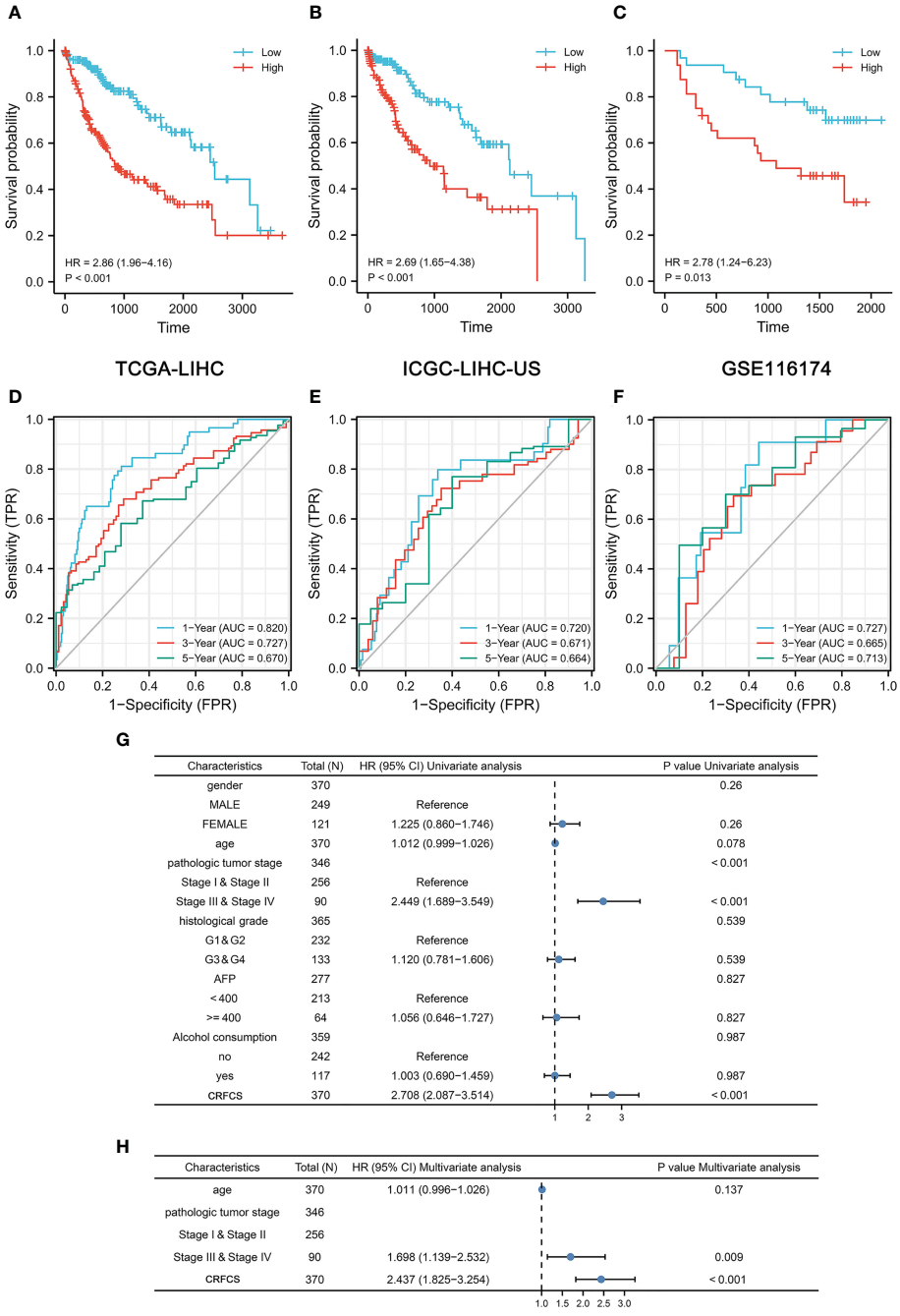

FIGURE 3
Prognosis prediction of CRFCS. **(A, C)** Kaplan-Meier curves of CRFCS subgroups for the training cohort TCGA-LIHC **(A)**, the external validation cohorts ICGC-LIHC-US **(B)**, and GSE116174 **(C)**. **(D–F)** AUC curves for the prediction of overall survival (OS) by CRFCS in samples of TCGA-LIHC **(D)**, ICGC-LIHC-US **(E)**, and GSE116174 **(F)**. **(G, H)** Univariate **(G)** and multivariate analysis **(H)** of CRFCS.

with a p-value less than 0.001 (Figure 3H). These results implied that CRFCS was a potential independent predictor of HCC.

3.4 CRFCS and mutation features

Mutational features are an integral part of the cancer process landscape. We investigated the mutational characteristics of the CRFCS subgroup of HCC. The top 3 high-frequency mutated genes in the high-CRFCS subgroup were TP53 (29%), TTN (24%), and CTNNB1 (20%) (Figure 4A) while CTNNB1 (31%), TNN (23%), and ALB (15%) were identified as the top 3 mutated genes in the low CRFCS subgroup (Figure 4B). We also found that Microsatellite Instability (MSI) score was significantly higher in the high CRFCS subgroup than in the low CRFCS group ($p<0.001$) (Figure 4C). Then, we evaluated the MATH scores which were

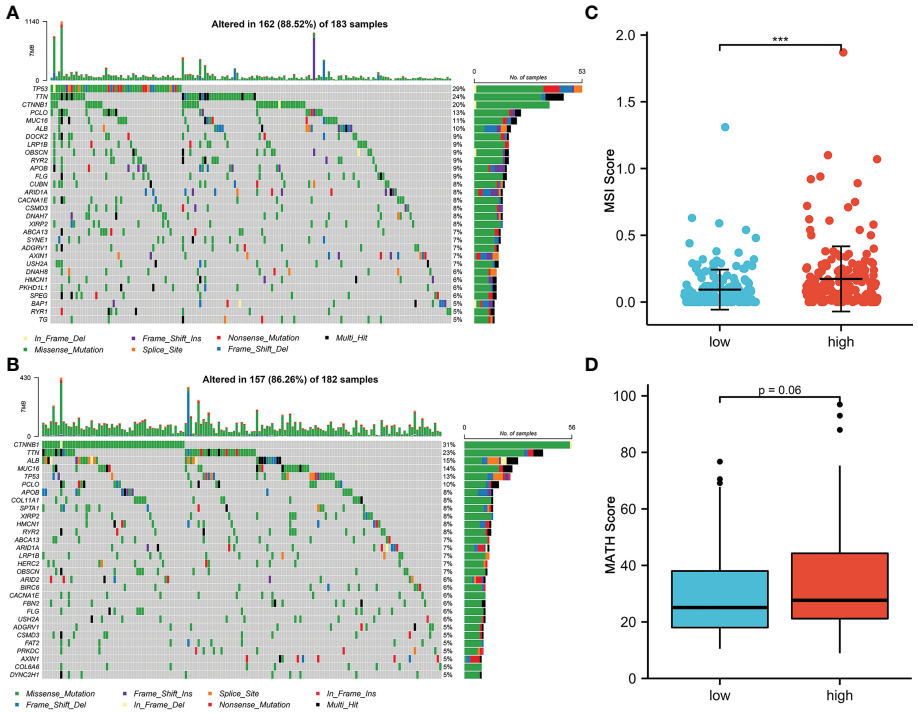

FIGURE 4
CRFCS and mutation characteristics. **(A, B)** Mutation oncoplots of high CRFCS group **(A)** and low CRFCS group **(B)**, including genes with top 30 mutation frequency. **(C)** Differences in MSI scores between high and low CRFCS subgroups. *** stands for p<0.001. **(D)** Differences in MATH scores between CRFCS subgroups.

positively correlated with tumor heterogeneity. The results revealed that the MATH scores between the two groups were not significant (Figure 4D).

3.5 CRFCS and TME

Immunotherapy is vital for the treatment of patients with advanced cancer and TME features are essential indicators of the efficacy of immune checkpoint inhibitors (ICIs). The level of various immune-related cellular infiltrates in TCGA-LIHC cohort samples was assessed by the ssGSEA method (Figures 5A, B). The results displayed a positive correlation between the CRFCS and the level of some anti-tumor immune cell infiltration, such as activated CD4 T cells (p<0.0001), activated dendritic cells (p =0.0142), central memory CD4 T cells (p<0.0001), central memory CD8 T cells (p =0.0025), and effector memory CD4 T cell (p<0.0001). Similarly, infiltrations of pro-tumor immune cells including regulatory T cells (p<0.0001), type 2 T helper cells (p<0.0001), immature dendritic cells (p =0.0239), and MDSC (p =0.0173) were also positively correlated with CRFCS. In addition, some neutral immune infiltrates such as eosinophil (p<0.0001) and mast cell (p =0.0189) were negatively related to CRFCS. We also evaluated the immune infiltration of the samples with the CIBERSORT algorithm (Figure 5C). Higher infiltration levels of T cells CD4 memory activated (p<0.001), T cells follicular helper (p<0.01), T cells regulatory (Tregs) (p<0.01), Macrophages M0 (p<0.001) and dendritic cells resting (p<0.01) were observed in the high CRFCS subgroup. In contrast, B cells naïve (p<0.05), T cells CD4 memory resting (p<0.05), NK cells activated (p<0.05), monocytes (p<0.05) and mast cells resting (p<0.001) had higher levels in the low CRFCS subgroup. Considering both methods together, the infiltration levels of activated CD4 T cells and regulatory T cells were significantly higher in the high-CRFCS subgroup, while the infiltration level of Mast cells resting was lower. Infiltration of stromal cells is also an integral part of TME. We also assessed the levels of stromal cell-related markers in the TCGA-LIHC cohort samples. The analysis showed that the levels of most markers of diverse stromal cells including CAF, EC, MSC, TAM, M1, and M2 in the samples were positively correlated with CRFCS (Figure 5D). Regulatory T cells was reported to suppress the immune response and promote tumorigenic immune escape (35). We then assessed the extent of immune escape between high and low CRFCS subgroups by the TIDE algorithm and the results showed that the high CRFCS group displayed a decreased TIDE score compared with the low CRFCS group (Figure 5E), indicating that samples with high CRFCS had lower levels of immune escape.

3.6 CRFCS and drug-sensitivity

Next, we assessed the drug-sensitivity of CRFCS in HCC by applying the R package of "pRRophetic". By analyzing data from TCGA, we found that the high CRFCS group had a lower IC_{50} of

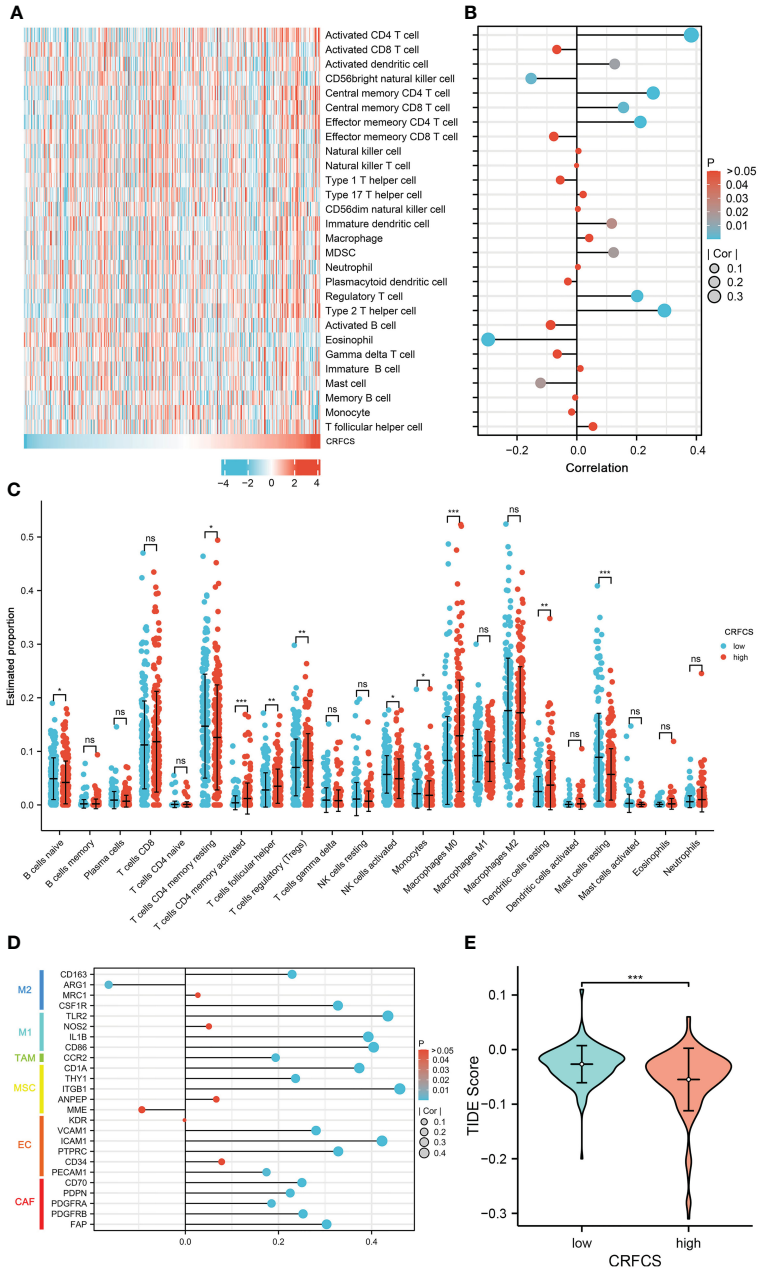

FIGURE 5
CRFCS and immune infiltration. **(A)** Heat map of ssGSEA score of various immune cells in high and low CRFCS groups via analyzing TCGA-LIHC cohort data. **(B)** The correlations between immune score and CRFCS. **(C)** Immune infiltration landscape of TCGA-LIHC cohort samples assessed by the CIBERSORT algorithm. **(D)** Correlation of stromal cell-associated markers with CRFCS. **(E)** The level of immune escape between high and low CRFCS subgroups was assessed by the TIDE algorithm. (*p<0.05; **p<0.01; ***p<0.001; ns stands for not significant).

sorafenib compared with the low CRFCS group (Figure 6A). To verify these results, an external data from ICGC-LIHC-US was analyzed which confirmed that the high CRFCS group are more sensitive to sorafenib (Figure 6B). Immunotherapy delivers more opportunities to patients with advanced HCC (36). It is well recognized that TME characteristic can significantly influence the outcome of immunotherapy (37). TME is classified into three subtypes: immune-desert, immune-inflamed, and immune-excluded. The immune-inflamed type which is highly expressed with immune checkpoint such as PD1 and PD-L1 is considered to be very sensitive to immunotherapy (38). Therefore, we evaluated the expression profile of immune checkpoint in CRFCS. Our results displayed that the immune checkpoints including PD-L1, PD1, TIGIT, TIM3, and CTLA4 were significantly highly expressed in the high CRFCS group compared with the low CRFCS group in both TCGA and ICGC HCC cohorts (Figures 6C, D). These results suggested that high CRFCS group might be more responsive to immunotherapy.

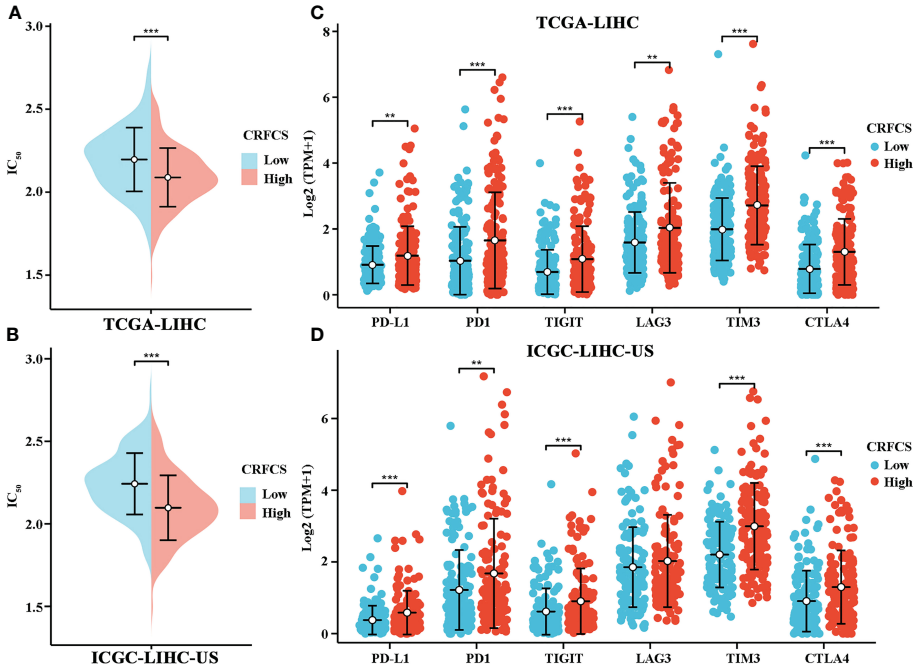

FIGURE 6
CRFCS and drug sensitivity. **(A, B)** Drug sensitivity of sorafenib in high and low CRFCS subgroups via analyzing data from TCGA cohort **(A)** and ICGC-LIHC **(B)**. **(C, D)** Differential expression of immune checkpoints between high and low CRFCS subgroups via analyzing data from TCGA cohort **(C)** and ICGC-LIHC **(D)**. (**p<0.01; ***p<0.001).

4 Discussion

Cuproptosis, a recently discovered new programmed cell death induced by excessive accumulation of intracellular Cu, is distinct from known cell death forms including apoptosis, pyroptosis, ferroptosis, necrosis. To dissect the specific regulators of cuproprosis, Tsvetkov et al. used genome-wide CRISPR/Cas9 screens and identify ten crucial cuproptosis-specific genes including FDX1, LIAS, LIPT1, DLD, DLAT, PDHA1, PDHB, MTF1, GLS, and CDKN2A (25). These ten genes are closely associated with HCC progression and TME. Zhang et al. identified FDX1 as an immunotherapy predictor of HCC (39). Yan et al. discovered that inhibition of LIPT1 restrained HCC cell proliferation and invasion (40). Zhou et al. found that overexpression of DLAT increased HCC cell growth and invasion and may facilitate cancer cell evade immune system (41). Sun et al. reported that activation of PDHA1 suppressed the Warburg effect and promoted HCC apoptosis (42). Yang et al. demonstrated that knockdown PDHB induced metabolic reprogramming of the tricarboxylic acid (TCA) cycle leading to glutamine depletion and inhibition of HCC cell proliferation (43). Yang et al. reported that over-expression of MTF1 contributed to the proliferation of HCC cells (44). Dong et al. found that GLS1 promoted HCC cell proliferation *via* activating AKT/GSK3β/Cyclin D1 pathway (45). Xu et al. revealed that upregulation of CDKN2A significantly inhibited ACTR5 induced HCC cell proliferation (46). Considering the role of these ten crucial cuproptosis-specific genes in HCC, constructing a model based on these ten genes might provide potential insights for evaluation the TME and immunotherapy efficacy of HCC.

Since the discovery of cuproptosis, the role of cuptoptosis in liver cancer prognosis and TME has been gradually evaluated. Previous studies mainly explored this issue by constructing Lasso cox model, which directly entered the target genes as model inputs (47–53). The Lasso model is applied to analyze multicollinearity data (54). Usually, nonlinear data might be generated when performing log normalization of the expression matrix. From this perspective, the lasso cox model might not be the ideal strategy. The random forest model is a set of binary trees constructed with recursive partitioning (RPART), which enables the random forest to handle nonlinear data due to the combination of trees (55). Therefore, the random forest model with nonlinear data as the application object is more suitable. Meanwhile, the random forest model is better at learning potential crossover features consisting of multidimensional features (56) and shows strong robustness when applied to large feature sets (57). These reasons led us to use the random forest model to construct the prognostic model. In addition, considering that there might be noise differences between individual data of each sample, some features may be lost due to the presence of data noise if the target genes are considered only, we trained the model using gene clusters related to cuproptosis genes as model inputs to generalize the features. We generalize the features by acquiring highly correlated genes of crucial cuproptosis genes when constructing the model so that the model could learn as much information as possible about the implicit features in the data. This makes the output of the model

smoother and less susceptible to fluctuations caused by noise in the data, thus improving the robustness of the model. The generalized input data combined with the random forest model can better learn the potential cross features in the data.

Microsatellite instability (MSI) is closely correlated with tumor immunotherapy efficacy. High MSI (MSI-H) in tumor samples usually cause additional mutant antigens and sensitize patient to immunotherapy (58). However, MSI-H also tends to increase tumor heterogeneity, which in turn results in poorer immunotherapy efficacy (59). In the present study, the mutation landscape of CRFCS subgroups was investigated which showed that the MSI scores were significantly higher in the high-CRFCS subgroup sample than in the low-CRFCS group while no significant difference between high and low CRFCS subgroups was observed in the tumor heterogeneity score MATH (Figure 4). These results suggested that high CRFCS subgroups may have better immunotherapeutic efficacy. Besides, studies exist demonstrated that tumor patients with high expression of immune checkpoints are more sensitive to immunotherapy (38). We evaluated the expression of immune checkpoints in high and low CRFCS group. Our results showed that the immune checkpoints including PD-L1, PD1, TIGIT, TIM3, and CTLA4 were remarkably highly expressed in the high CRFCS group compared with the low CRFCS group (Figures 6C, D). In addition, evidence displayed that Treg cells cause immune escape through several mechanisms, which in turn impede the anti-tumor immune response (60). To estimate the tumor immune escape effect between the CRFCS subgroups, we calculated the TIDE scores of the samples. The results showed that the high-CRFCS subgroup had significantly lower TIDE scores (Figure 5E), indicating that samples of the high-CRFCS subgroup had a lower probability of immune escape and were less prone to be resistant to immunotherapy. Combining the results above, it might be inferred that the high CRFCS group might be more suitable to receive immunotherapy than the low CRFCS group.

Although a cuproptosis related model termed CRFCS was successfully constructed to evaluate prognosis and TME characteristic in HCC, some limitations should not be neglected. First, cuproptosis was discovered in 2022, only several genes were confirmed as crucial cuproptosis-specific genes, more genes need to be identified to provide systematic and comprehensive understanding of cuproptosis. Second, our study was performed based on integrative bioinformatic analysis, it would be more valid to carry out functional experiments *in vitro* and *in vivo*. Finally, the data involved in this study were retrieved from public dataset, it would be better to use large-scale of local datasets to verify our findings.

5 Conclusions

In aggregate, we constructed a cuproptosis random forest cox score (CRFCS) model. CRFCS was identified to be an independent prognostic indicator of HCC and high CRFCS samples showed a poor prognosis. Interestingly, CRFCS were correlated with TME characteristics as well as clinical treatment efficacy. Patients with high CRFCS had a better clinical prognosis for immunotherapy and sorafenib.

Data availability statement

The datasets presented in this study can be found in online repositories. The names of the repository/repositories and accession number (s) can be found below: https://portal.gdc.cancer.gov/, TCGA-LIHC; https://www.ncbi.nlm.nih.gov/geo/, GSE116174; https://dcc.icgc.org/projects/, ICGC-LIHC-US.

Author contributions

LW and JW designed and planned the study concept. RL, YL, and FZ performed experiments and analyzed data. RL and LW drafted the manuscript. All authors contributed to the article and approved the submitted version.

Funding

This work was supported by the National Natural Science Foundation of China (82260715), the Guangxi Natural Science Foundation (2017GXNSFBA198240, 2018GXNSFAA050055, and 2021GXNSFAA075038), Youth Fund Project of Natural Science Research Project of Guangxi University of Traditional Chinese Medicine (No. 2016QN007), and Guangxi Collaborative Innovation Center for Research on Functional Ingredients of Agricultural Residues (No. CICAR2016-P6).

Acknowledgments

This is a short text to acknowledge the contributions of specific colleagues, institutions, or agencies that aided the efforts of the authors.

Conflict of interest

The authors declare that the research was conducted in the absence of any commercial or financial relationships that could be construed as a potential conflict of interest.

Publisher's note

References

1. Sung H, Ferlay J, Siegel RL, Laversanne M, Soerjomataram I, Jemal A, et al. Global cancer statistics 2020: GLOBOCAN estimates of incidence and mortality worldwide for 36 cancers in 185 countries. *CA Cancer J Clin* (2021) 71(3):209–49. doi: 10.3322/caac.21660

2. Bray F, Ferlay J, Soerjomataram I, Siegel RL, Torre LA, Jemal A. Global cancer statistics 2018: GLOBOCAN estimates of incidence and mortality worldwide for 36 cancers in 185 countries. *CA Cancer J Clin* (2018) 68(6):394–424. doi: 10.3322/caac.21492

3. Sim HW, Knox J. Hepatocellular carcinoma in the era of immunotherapy. *Curr Probl Cancer* (2018) 42(1):40–8. doi: 10.1016/j.currproblcancer.2017.10.007

4. Kudo M, Finn RS, Qin S, Han KH, Ikeda K, Piscaglia F, et al. Lenvatinib versus sorafenib in first-line treatment of patients with unresectable hepatocellular carcinoma: a randomised phase 3 non-inferiority trial. *Lancet* (2018) 391(10126):1163–73. doi: 10.1016/S0140-6736(18)30207-1

5. Topalian SL, Hodi FS, Brahmer JR, Gettinger SN, Smith DC, McDermott DF, et al. Safety, activity, and immune correlates of anti-PD-1 antibody in cancer. *N Engl J Med* (2012) 366(26):2443–54. doi: 10.1056/NEJMoa1200690

6. Nishida N, Kudo M. Immunological microenvironment of hepatocellular carcinoma and its clinical implication. *Oncology* (2017) 92 Suppl 1:40–9. doi: 10.1159/000451015

7. Kurebayashi Y, Ojima H, Tsujikawa H, Kubota N, Maehara J, Abe Y, et al. Landscape of immune microenvironment in hepatocellular carcinoma and its additional impact on histological and molecular classification. *Hepatology* (2018) 68(3):1025–41. doi: 10.1002/hep.29904

8. Chen L, Min J, Wang F. Copper homeostasis and cuproptosis in health and disease. *Signal Transduct Target Ther* (2022) 7(1):378. doi: 10.1038/s41392-022-01229-y

9. Baltaci AK, Dundar TK, Aksoy F, Mogulkoc R. Changes in the serum levels of trace elements before and after the operation in thyroid cancer patients. *Biol Trace Elem Res* (2017) 175(1):57–64. doi: 10.1007/s12011-016-0768-2

10. Stepien M, Jenab M, Freisling H, Becker NP, Czuban M, Tjønneland A, et al. Pre-diagnostic copper and zinc biomarkers and colorectal cancer risk in the European prospective investigation into cancer and nutrition cohort. *Carcinogenesis* (2017) 38(7):699–707. doi: 10.1093/carcin/bgx051

11. Zhang X, Yang Q. Association between serum copper levels and lung cancer risk: A meta-analysis. *J Int Med Res* (2018) 46(12):4863–73. doi: 10.1177/0300060518798507

12. Saleh SAK, Adly HM, Abdelkhaliq AA, Nassir AM. Serum levels of selenium, zinc, copper, manganese, and iron in prostate cancer patients. *Curr Urol* (2020) 14(1):44–9. doi: 10.1159/000499261

13. Ge EJ, Bush AI, Casini A, Cobine PA, Cross JR, DeNicola GM, et al. Connecting copper and cancer: from transition metal signalling to metalloplasia. *Nat Rev Cancer* (2022) 22(2):102–13. doi: 10.1038/s41568-021-00417-2

14. Li Y. Copper homeostasis: Emerging target for cancer treatment. *IUBMB Life* (2020) 72(9):1900–8. doi: 10.1002/iub.2341

15. Vanderwerf SM, Cooper MJ, Stetsenko IV, Lutsenko S. Copper specifically regulates intracellular phosphorylation of the wilson's disease protein, a human copper-transporting ATPase. *J Biol Chem* (2001) 276(39):36289–94. doi: 10.1074/jbc.M102055200

16. Tsang T, Posimo JM, Gudiel AA, Cicchini M, Feldser DM, Brady DC. Copper is an essential regulator of the autophagic kinases ULK1/2 to drive lung adenocarcinoma. *Nat Cell Biol* (2020) 22(4):412–24. doi: 10.1038/s41556-020-0481-4

17. Cui L, Gouw AM, LaGory EL, Guo S, Attarwala N, Tang Y, et al. Mitochondrial copper depletion suppresses triple-negative breast cancer in mice. *Nat Biotechnol* (2021) 39(3):357–67. doi: 10.1038/s41587-020-0707-9

18. Brady DC, Crowe MS, Greenberg DN, Counter CM. Copper chelation inhibits BRAFV600E-driven melanomagenesis and counters resistance to BRAFV600E and MEK1/2 inhibitors. *Cancer Res* (2017) 77(22):6240–52. doi: 10.1158/0008-5472.CAN-16-1190

19. O'Dell BL. Interleukin-2 production is altered by copper deficiency. *Nutr Rev* (1993) 51(10):307–9. doi: 10.1111/j.1753-4887.1993.tb03062.x

20. Prohaska JR, Lukasewycz OA. Copper deficiency suppresses the immune response of mice. *Science* (1981) 213(4507):559–61. doi: 10.1126/science.7244654

21. Jones DG. Effects of dietary copper depletion on acute and delayed inflammatory responses in mice. *Res Vet Sci* (1984) 37(2):205–10. doi: 10.1016/S0034-5288(18)31906-4

22. Voli F, Valli E, Lerra L, Kimpton K, Saletta F, Giorgi FM, et al. Intratumoral copper modulates PD-L1 expression and influences tumor immune evasion. *Cancer Res* (2020) 80(19):4129–44. doi: 10.1158/0008-5472.CAN-20-0471

23. Shanbhag VC, Gudekar N, Jasmer K, Papageorgiou C, Singh K, Petris MJ. Copper metabolism as a unique vulnerability in cancer. *Biochim Biophys Acta Mol Cell Res* (2021) 1868(2):118893. doi: 10.1016/j.bbamcr.2020.118893

24. Denoyer D, Masaldan S, La Fontaine S, Cater MA. Targeting copper in cancer therapy: 'Copper that cancer'. *Metallomics* (2015) 7(11):1459–76. doi: 10.1039/c5mt00149h

25. Tsvetkov P, Coy S, Petrova B, Dreishpoon M, Verma A, Abdusamad M, et al. Copper induces cell death by targeting lipoylated TCA cycle proteins. *Science* (2022) 375(6586):1254–61. doi: 10.1126/science.abf0529

26. Zhu Z, Zhao Q, Song W, Weng J, Li S, Guo T, et al. A novel cuproptosis-related molecular pattern and its tumor microenvironment characterization in colorectal cancer. *Front Immunol* (2022) 13:940774. doi: 10.3389/fimmu.2022.940774

27. Li W, Zhang X, Chen Y, Pang D. Identification of cuproptosis-related patterns and construction of a scoring system for predicting prognosis, tumor microenvironment-infiltration characteristics, and immunotherapy efficacy in breast cancer. *Front Oncol* (2022) 12:966511. doi: 10.3389/fonc.2022.966511

28. Shen Y, Li D, Liang Q, Yang M, Pan Y, Li H. Cross-talk between cuproptosis and ferroptosis regulators defines the tumor microenvironment for the prediction of prognosis and therapies in lung adenocarcinoma. *Front Immunol* (2023) 13:1029092. doi: 10.3389/fimmu.2022.1029092

29. Song Q, Zhou R, Shu F, Fu W. Cuproptosis scoring system to predict the clinical outcome and immune response in bladder cancer. *Front Immunol* (2022) 13:958368. doi: 10.3389/fimmu.2022.958368

30. Cai Z, He Y, Yu Z, Hu J, Xiao Z, Zu X, et al. Cuproptosis-related modification patterns depict the tumor microenvironment, precision immunotherapy, and prognosis of kidney renal clear cell carcinoma. *Front Immunol* (2022) 13:933241. doi: 10.3389/fimmu.2022.933241

31. Mroz EA, Rocco JW. MATH, a novel measure of intratumor genetic heterogeneity, is high in poor-outcome classes of head and neck squamous cell carcinoma. *Oral Oncol* (2013) 49(3):211–5. doi: 10.1016/j.oraloncology.2012.09.007

32. Niu B, Ye K, Zhang Q, Lu C, Xie M, McLellan MD, et al. MSIsensor: microsatellite instability detection using paired tumor-normal sequence data. *Bioinformatics* (2014) 30(7):1015–6. doi: 10.1093/bioinformatics/btt755

33. Charoentong P, Finotello F, Angelova M, Mayer C, Efremova M, Rieder D, et al. Pan-cancer immunogenomic analyses reveal genotype-immunophenotype relationships and predictors of response to checkpoint blockade. *Cell Rep* (2017) 18(1):248–62. doi: 10.1016/j.celrep.2016.12.019

34. Jiang P, Gu S, Pan D, Fu J, Sahu A, Hu X, et al. Signatures of T cell dysfunction and exclusion predict cancer immunotherapy response. *Nat Med* (2018) 24(10):1550–8. doi: 10.1038/s41591-018-0136-1

35. Yin Y, Cai X, Chen X, Liang H, Zhang Y, Li J, et al. Tumor-secreted miR-214 induces regulatory T cells: A major link between immune evasion and tumor growth. *Cell Res* (2014) 24(10):1164–80. doi: 10.1038/cr.2014.121

36. Hato T, Goyal L, Greten TF, Duda DG, Zhu AX. Immune checkpoint blockade in hepatocellular carcinoma: Current progress and future directions. *Hepatology* (2014) 60(5):1776–82. doi: 10.1002/hep.27246

37. Pardoll DM. The blockade of immune checkpoints in cancer immunotherapy. *Nat Rev Cancer* (2012) 12(4):252–64. doi: 10.1038/nrc3239

38. Doroshow DB, Bhalla S, Beasley MB, Sholl LM, Kerr KM, Gnjatic S, et al. PD-L1 as a biomarker of response to immune-checkpoint inhibitors. *Nat Rev Clin Oncol* (2021) 18(6):345–62. doi: 10.1038/s41571-021-00473-5

39. Zhang C, Zeng Y, Guo X, Shen H, Zhang J, Wang K, et al. Pan-cancer analyses confirmed the cuproptosis-related gene FDX1 as an immunotherapy predictor and prognostic biomarker. *Front Genet* (2022) 13:923737. doi: 10.3389/fgene.2022.923737

40. Yan C, Niu Y, Ma L, Tian L, Ma J. System analysis based on the cuproptosis-related genes identifies LIPT1 as a novel therapy target for liver hepatocellular carcinoma. *J Transl Med* (2022) 20(1):452. doi: 10.1186/s12967-022-03630-1

41. Zhou Y, Gu H, Shao B, Zhang S, Pall H, Peixoto RD, et al. Glycolysis-related gene dihydrolipoamide acetyltransferase promotes poor prognosis in hepatocellular carcinoma through the wnt/β-catenin and PI3K/Akt signaling pathways. *Ann Transl Med* (2022) 10(22):1240. doi: 10.21037/atm-22-5272

42. Sun J, Li J, Guo Z, Sun L, Juan C, Zhou Y, et al. Overexpression of pyruvate dehydrogenase E1α subunit inhibits warburg effect and induces cell apoptosis through mitochondria-mediated pathway in hepatocellular carcinoma. *Oncol Res* (2019) 27(4):407–14. doi: 10.3727/096504018X15180451872087

43. Yang C, Lee D, Zhang MS, Tse AP, Wei L, Bao MH, et al. Genome-wide CRISPR/Cas9 library screening revealed dietary restriction of glutamine in combination with inhibition of pyruvate metabolism as effective liver cancer treatment. *Adv Sci (Weinh)* (2022) 9(34):e2202104. doi: 10.1002/advs.202202104

44. Yang Y, Qian Cai Q, Sheng Fu L, Wei Dong Y, Fan F, Zhong Wu X. Reduced N6-methyladenosine mediated by METTL3 acetylation promotes MTF1 expression and hepatocellular carcinoma cell growth. *Chem Biodivers* (2022) 19(11):e202200333. doi: 10.1002/cbdv.202200333

45. Xi J, Sun Y, Zhang M, Fa Z, Wan Y, Min Z, et al. GLS1 promotes proliferation in hepatocellular carcinoma cells *via* AKT/GSK3β/CyclinD1 pathway. *Exp Cell Res* (2019) 381(1):1–9. doi: 10.1016/j.yexcr.2019.04.005

46. Xu X, Chan AKN, Li M, Liu Q, Mattson N, Pangeni Pokharel S, et al. ACTR5 controls CDKN2A and tumor progression in an INO80-independent manner. *Sci Adv* (2022) 8(51):eadc8911. doi: 10.1126/sciadv.adc8911

47. Liu Z, Qi Y, Wang H, Zhang Q, Wu Z, Wu W. Risk model of hepatocellular carcinoma based on cuproptosis-related genes. *Front Genet* (2022) 13:1000652. doi: 10.3389/fgene.2022.1000652

48. Xie Y, Zhang W, Sun J, Sun L, Meng F, Yu H. A novel cuproptosis-related immune checkpoint gene signature identification and experimental validation in hepatocellular carcinoma. *Sci Rep* (2022) 12(1):18514. doi: 10.1038/s41598-022-22962-y

49. Zhang G, Sun J, Zhang X. A novel cuproptosis-related LncRNA signature to predict prognosis in hepatocellular carcinoma. *Sci Rep* (2022) 12(1):11325. doi: 10.1038/s41598-022-15251-1

50. Wang G, Xiao R, Zhao S, Sun L, Guo J, Li W, et al. Cuproptosis regulator-mediated patterns associated with immune infilltration features and construction of cuproptosis-related signatures to guide immunotherapy. *Front Immunol* (2022) 13:945516. doi: 10.3389/fimmu.2022.945516

51. Cong T, Luo Y, Liu Y, Yang C, Yang H, Li Y, et al. Cuproptosis-related immune checkpoint gene signature: Prediction of prognosis and immune response for hepatocellular carcinoma. *Front Genet* (2022) 13:1000997. doi: 10.3389/fgene.2022.1000997

52. Zhang Z, Zeng X, Wu Y, Liu Y, Zhang X, Song Z. Cuproptosis-related risk score predicts prognosis and characterizes the tumor microenvironment in hepatocellular carcinoma. *Front Immunol* (2022) 13:925618. doi: 10.3389/fimmu.2022.925618

53. Zhou Z, Zhou Y, Liu D, Yang Q, Tang M, Liu W. Prognostic and immune correlation evaluation of a novel cuproptosis-related genes signature in hepatocellular carcinoma. *Front Pharmacol* (2022) 13:1074123. doi: 10.3389/fphar.2022.1074123

54. Tibshirani R. Regression shrinkage and selection *Via* the lasso. *J R Stat Society: Ser B (Methodological)* (1996) 58:267–88. doi: 10.1111/j.2517-6161.1996.tb02080.x

55. Breiman L. Random forests. *Mach Learn* (2001) 45(1):5–32. doi: 10.1023/A:1010933404324

56. Díaz-Uriarte R, Alvarez de Andrés S. Gene selection and classification of microarray data using random forest. *BMC Bioinf* (2006) 7:3. doi: 10.1186/1471-2105-7-3

57. Hua J, Xiong Z, Lowey J, Suh E, Dougherty ER. Optimal number of features as a function of sample size for various classification rules. *Bioinformatics* (2005) 21 (8):1509–15. doi: 10.1093/bioinformatics/bti171

58. Le DT, Durham JN, Smith KN, Wang H, Bartlett BR, Aulakh LK, et al. Mismatch repair deficiency predicts response of solid tumors to PD-1 blockade. *Science* (2017) 357(6349):409–13. doi: 10.1126/science.aan6733

59. Trinh A, Polyak K. Tumor neoantigens: When too much of a good thing is bad. *Cancer Cell* (2019) 36(5):466–7. doi: 10.1016/j.ccell.2019.10.009

60. Nishikawa H, Koyama S. Mechanisms of regulatory T cell infiltration in tumors: implications for innovative immune precision therapies. *J Immunother Cancer* (2021) 9 (7):e002591. doi: 10.1136/jitc-2021-002591

frontiers | Frontiers in Immunology

TYPE Original Research
PUBLISHED 20 April 2023
DOI 10.3389/fimmu.2023.1123231

OPEN ACCESS

EDITED BY
Lin-Lin Bu,
Wuhan University, China

REVIEWED BY
JItendra Kumar,
University of Delhi, India
Zhengrong Yuan,
Beijing Forestry University, China
Sarun Juengpanich,
Zhejiang University, China

*CORRESPONDENCE
Jie Tian
vaseline2001@hotmail.com
Weifeng Yu
ywf808@yeah.net
Huigang Shu
shuhuigang@126.com

†These authors have contributed equally to this work

SPECIALTY SECTION
This article was submitted to Cancer Immunity and Immunotherapy, a section of the journal Frontiers in Immunology

RECEIVED 13 December 2022
ACCEPTED 31 March 2023
PUBLISHED 20 April 2023

CITATION
Wang X, Chen D, Shi Y, Luo J, Zhang Y, Yuan X, Zhang C, Shu H, Yu W and Tian J (2023) Copper and cuproptosis-related genes in hepatocellular carcinoma: therapeutic biomarkers targeting tumor immune microenvironment and immune checkpoints. *Front. Immunol.* 14:1123231. doi: 10.3389/fimmu.2023.1123231

Copper and cuproptosis-related genes in hepatocellular carcinoma: therapeutic biomarkers targeting tumor immune microenvironment and immune checkpoints

Xiaoqiang Wang[1†], Dongfang Chen[2†], Yumiao Shi[1], Jiamei Luo[1], Yiqi Zhang[1], Xiaohong Yuan[3], Chaojin Zhang[1], Huigang Shu[1*], Weifeng Yu[1*] and Jie Tian[1*]

[1]Department of Anesthesiology, Renji Hospital, Shanghai Jiaotong University School of Medicine, Shanghai, China, [2]Department of Anesthesiology, Shanghai Fifth People's Hospital, Fudan University, Shanghai, China, [3]Zhejiang Cancer Hospital, Institute of Basic Medicine and Cancer (IBMC), Chinese Academy of Sciences, Hangzhou, China

Background: Hepatocellular carcinoma (HCC), one of the most common cancers worldwide, exhibits high immune heterogeneity and mortality. Emerging studies suggest that copper (Cu) plays a key role in cell survival. However, the relationship between Cu and tumor development remains unclear.

Methods: We investigated the effects of Cu and cuproptosis-related genes (CRGs) in patients with HCC in the TCGA-LIHC (The Cancer Genome Atlas-Liver cancer, *n* = 347) and ICGC-LIRI-JP (International Cancer Genome Consortium-Liver Cancer-Riken-Japan, *n* = 203) datasets. Prognostic genes were identified by survival analysis, and a least absolute shrinkage and selection operator (Lasso) regression model was constructed using the prognostic genes in the two datasets. Additionally, we analyzed differentially expressed genes and signal pathway enrichment. We also evaluated the effects of CRGs on tumor immune cell infiltration and their co-expression with immune checkpoint genes (ICGs) and performed validation in different tumor immune microenvironments (TIMs). Finally, we performed validation using clinical samples and predicted the prognosis of patients with HCC using a nomogram.

Results: A total of 59 CRGs were included for analysis, and 15 genes that significantly influenced the survival of patients in the two datasets were identified. Patients were grouped by risk scores, and pathway enrichment analysis suggested that immune-related pathways were substantially enriched in both datasets. Tumor immune cell infiltration analysis and clinical validation revealed that PRNP (Prion protein), SNCA (Synuclein alpha), and COX17

(Cytochrome c oxidase copper chaperone COX17) may be closely correlated with immune cell infiltration and ICG expression. A nomogram was constructed to predict the prognosis of patients with HCC using patients' characteristics and risk scores.

Conclusion: CRGs may regulate the development of HCC by targeting the TIM and ICGs. CRGs such as PRNP, SNCA, and COX17 could be promising targets for HCC immune therapy in the future.

KEYWORDS

copper, cuproptosis, hepatocellular carcinoma, immune checkpoints, tumor immune microenvironment

1 Background

Cancer is one of the leading causes of death worldwide and places a heavy burden on global health (1). According to statistical reports, hepatocellular carcinoma (HCC) is currently the third most common cancer worldwide. Moreover, based on related reports, >45% of new HCC cases and related deaths occurred in China (2–4). Although there have been advances in HCC therapy in recent years, the high heterogeneity and lack of accurate early diagnostic biomarkers have resulted in the poor prognosis of patients with HCC (5).

For patients with advanced HCC, immunotherapy has emerged as a prospective therapeutic approach through the targeting of programmed cell death protein 1 (PD-1)/programmed cell death ligand 1 (PD-L1) and cytotoxic T lymphocyte antigen 4 (CTLA4) (6). Studies have suggested that the objective response rates of anti-PD-1 treatment (including nivolumab, pembrolizumab, and camrelizumab) increased to about 15%–20% for patients with HCC that were pretreated with sorafenib (7–9). However, drugs targeting PD-1 and PD-L1 benefit few patients with HCC, as most patients have poor responses to immune checkpoint inhibitors (ICIs) (10). This may be attributed to the intrinsically high heterogeneity and immune suppression microenvironment of HCC (10, 11). Previous studies demonstrated that a large number of suppressive immune cells, such as tumor-associated macrophages (TAMs), myeloid-derived suppressor cells (MDSCs), and regulatory T cells (Tregs), were recruited to the tumor microenvironment of HCC, resulting in immune cell dysfunction and immune surveillance escape (12, 13). Therefore, exploring effective targets to improve HCC patients' response to ICIs is important.

Copper (Cu) is an endogenous metal essential for all living organisms and participates in various biological functions, such as mitochondrial respiration, iron uptake, redox reactions, glucose regulation, and cholesterol metabolism (14, 15). However, excessive accumulation of Cu induces oxidative stress, cytotoxicity, or even cuproptosis. The latter is a type of cell death that is regulated by Cu and mitochondrial respiration, which has been recently discovered (16). Furthermore, the dysfunction of Cu homeostasis can lead to severe disorders such as Wilson's and Menke's diseases (17). Therefore, intracellular Cu concentrations are typically strictly maintained at extraordinarily low levels *via* complex homeostatic mechanisms. Exploring the mechanisms underlying Cu homeostasis dysfunction and imbalanced cuproptosis may aid in the identification of novel therapeutic targets for various diseases.

A previous study has shown a significant increase in Cu levels in patients with cancer compared with healthy individuals (18). For instance, a meta-analysis including 36 studies revealed significantly upregulated serum Cu levels in patients with breast cancer compared with healthy controls (19). Furthermore, some studies have demonstrated the effective antitumor effects of Cu ionophores such as elesclomol (16, 20, 21). Some studies have also found associations among cuproptosis, tumor development, and response to ICIs (22, 23). For instance, Luo et al. (24) found that cuproptosis could regulate the response of acute myeloid leukemia cells to the immune system. Xiong et al. (25) suggested that cuproptosis may be regulated by p53, a crucial tumor suppressor and metabolic regulator. Thus, targeting cuproptosis may be a promising strategy for HCC immunotherapy.

Studies on the role of Cu and cuproptosis-related genes (CRGs) in HCC are lacking. Herein, we systematically analyzed the functions and effects of CRGs on the survival of patients with HCC based on two public HCC datasets. We aimed to identify the critical CRGs that significantly influence the overall survival (OS) of patients with HCC and to construct a useful nomogram to predict the prognosis of patients. Moreover, we investigated the

Abbreviations: HCC, hepatocellular carcinoma; Cu, copper; CRGs, cuproptosis-related genes; DEGs, differentially expressed genes; PD-1, programmed cell death protein 1; PD-L1, programmed cell death ligand 1; CTLA4, cytotoxic T lymphocyte antigen 4; ICIs, immune checkpoint inhibitors; TIM, tumor immune microenvironment; IHC, immunohistochemical; TAMs, tumor-associated macrophages; MDSCs, myeloid-derived suppressor cells; Tregs, regulatory T cells; OS, overall survival; Lasso, least absolute shrinkage and selection operator; ICGs, immune checkpoint genes; TCGA-LIHC, The Cancer Genome Atlas Liver Hepatocellular Carcinoma; ICGC, International Cancer Genome Consortium; GO, Gene Ontology; GSEA, Gene Set Enrichment Analysis; KEGG, Kyoto Encyclopedia of Genes and Genomes; MRS, myeloid response score; ROC, receiver operating characteristic; AUC, area under the curve; CI, confidence interval; HR, hazard ratio.

relationships among CRGs, tumor immune cell infiltration, and immune checkpoint genes (ICGs) to detect potential HCC biomarkers targeting the tumor immune microenvironment (TIM).

2 Methods

2.1 Data acquisition and CRG list

The total transcriptome RNA sequencing (RNA-seq) data and clinical information of patients with HCC were obtained and downloaded from The Cancer Genome Atlas Liver Hepatocellular Carcinoma (TCGA-LIHC) dataset (https://tcga-data.nci.nih.gov/tcga/), the International Cancer Genome Consortium (ICGC) portal (https://dcc.icgc.org/projects/LIRI-JP), and GEO datasets (https://www.ncbi.nlm.nih.gov/). The list of CRGs and their and functions were obtained from the Gene Ontology (GO) resource (http://geneontology.org/) and a published paper (16). The full list of CRGs is provided in Supplementary Table 1.

2.2 Survival analysis

The effects of CRGs on the OS of patients with HCC were validated using survival analysis. Patients were categorized into the low-expression (L) and high-expression (H) groups, and the median gene expression level was chosen as the cutoff value. Similarly, survival analysis of the risk scores obtained from the least absolute shrinkage and selection operator (Lasso) regression model was performed, and patients were assigned to the low-risk or high-risk group based on their risk scores. The cutoff value for grouping was the median risk score. The survival analysis was performed using the "survminer" R package.

2.3 Construction of the Lasso regression model

Prognostic genes with a *P*-value of <0.05 in the survival analysis in the two datasets were used to construct the model. A Lasso regression model (26) for predicting the prognosis of patients with HCC was constructed using the prognostic genes in the two datasets using the "glmnet" R package. A 10-fold cross-validation method was used to optimize the model. The risk score predicting the OS was calculated for every patient using the following formula: risk score = (gene A expression × a) + (gene B expression × b) … + (gene N expression × n), where a, b, and n represent regression coefficients.

2.4 Validation and effectiveness of the prognostic model

To validate the model's effectiveness, survival and time-dependent receiver operating characteristic (ROC) curve analyses were performed based on the survival time, survival status, and risk scores of patients with HCC using the "survminer" and "pROC" R packages. Relationships among the risk scores, OS, survival status, and gene expression of selected CRGs were analyzed using the online bioinformatic analysis tool Sangerbox 3.0 (http://vip.sangerbox.com/home.html).

2.5 Differentially expressed gene analysis

Patients were grouped according to risk scores, and DEGs were identified using the "limma" R package. Briefly, genes with a false discovery rate (FDR) of <0.05 and fold change of >1.5 between the two groups were identified as DEGs. DEGs were visualized with a volcano plot and generated using Sangerbox 3.0 (http://vip.sangerbox.com/home.html).

2.6 Functional enrichment analysis

DEGs were used for multiple functional enrichment analyses including Gene Set Enrichment Analysis (GSEA) and Kyoto Encyclopedia of Genes and Genome (KEGG) pathway and Gene Ontology-Biological Process (GO-BP) enrichment analyses using the "clusterProfiler (version 3.14.3)" R package (27) and GSEA software (version 3.0, http://software.broadinstitute.org/gsea/index.jsp). The minimum and maximum number of genes in the cluster were 5 and 5000, respectively. Pathways with a *P*-value of <0.05 and FDR of <0.05 were considered statistically different.

Immune-related pathway enrichment (GO-immune system process) was analyzed using the Cytoscape software and ClueGO application (https://cytoscape.org/).

2.7 Tumor immune cell infiltration analysis

Tumor immune cell infiltration levels were evaluated using the TIMER method (28) and the "IOBR" R package in the TCGA database (29). Relationships between gene expression levels and immune cell infiltration levels were calculated using the "psych (version 2.1.6)" R package. Moreover, ESTIMATE analysis (https://bioinformatics.mdanderson.org/estimate/, including ESTIMATE score, stromal score, and immune score) was performed to visualize the correlations between screened CRGs and TME in the TCGA database. These analyses were performed using the open-source online tool Sangerbox 3.0 (http://vip.sangerbox.com/home.html).

2.8 Expression of ICGs and correlations with CRGs in HCC

The expression levels of *PDCD1* (the gene coding PD-1), *CD274* (the gene coding PD-L1), and *CTLA4* in normal and HCC liver tissues were analyzed using data obtained from UALCAN (http://ualcan.path.uab.edu/analysis.html) (30). Additionally, co-expression analysis between ICGs and CRGs in HCC was performed using data obtained from cBioportal (https://www.cbioportal.org/) and the Firehose Legacy dataset (31).

2.9 Myeloid response score and different immune subtypes in HCC

The myeloid response score (MRS) model was used as a reference to distinguish between the immune subtypes in HCC (32). RNA-seq data of patients with HCC with different MRSs was obtained and analyzed using data obtained from the GSE134921 dataset. Expression levels of critical CRGs were compared between the high-MRS and low-MRS groups.

2.10 Construction of a prognostic nomogram for HCC

To provide a reliable and quantifiable method to predict the prognosis of patients with HCC, a novel nomogram was constructed by integrating risk score, age, sex, race, TNM (tumor, nodes, metastases) stage, and tumor grade into a Cox regression model using the "rms" R package.

2.11 Recruitment of patients with HCC and collection of clinical HCC samples

An observational study was conducted at the Renji Hospital, Shanghai Jiaotong University School of Medicine, and Eastern Hepatobiliary Surgery Hospital, the Third Affiliated Hospital of Naval Medical University. This study was approved by the Renji Hospital Ethics Committee (KY2020-185). The study complied with the Declaration of Helsinki and the Consolidated Standards of Reporting Trials (CONSORT) statement. Patients aged ≥18 years, those with primary HCC, and those who received HCC excision surgery were included in the study. Patients were excluded if they suffered from multiple metastases, had other additional types of cancer, or had missing clinical data. HCC samples were collected in the operation room immediately after excision and stored at −80° C. All samples were confirmed as HCC by pathological diagnosis after surgery.

2.12 Expression levels of ICGs and CRGs in HCC samples

Gene expression levels of ICGs (*PDCD1*, *CD274*, and *CTLA4*) and CRGs (*PRNP*, *SNCA*, *COX17*, *ATP7A*, *ATP13A2*, and *F5*) were analyzed in human HCC samples. Total RNA was extracted from the HCC samples using the EZ-press RNA Purification Kit (EZ Bioscience, USA) according to the manufacturers' protocol. The primers of genes are listed in Supplementary Table 2. Linear correlations between the gene expression levels of ICGs and CRGs were analyzed.

2.13 Immunohistochemical staining of ICGs and CRGs in HCC samples

To determine the protein expression levels of ICGs and CRGs in HCC samples, IHC staining of PD-1 (Servicebio, cat: GB11338-1), PD-L1 (Servicebio, cat: GB11339A), PRNP (Abclonal, cat: A18058), SNCA (Abclonal, cat: A20407), and COX17 (SANTA Cruz, cat: sc-100521) was performed.

2.14 Statistical analyses

Statistical analyses were performed using IBM SPSS Statistics 23.0 (SPSS Inc., Armonk, NY, USA). Differences in the survival analysis were compared by log-rank t-test with a 95% confidence interval. ROC curves were plotted and area under the curve (AUC) values were calculated to assess the discrimination strength of the model. Linear correlations were assessed using Spearman's or Pearson's correlation tests, and the correlation coefficient "r" was calculated. All statistical tests were two sided. A *P*-value of <0.05 was considered statistically significant.

3 Results

The study design flow chart and validation process is presented in Supplementary Figure 1. A total of 59 out of 62 CRGs were analyzed in the two datasets because the expression data of three CRGs (*MT1HL1*, *MT-CO1*, and *MT-CO2*) was missing from the raw data. From the TCGA-LIHC and ICGC-LIRI-JP datasets, 347 and 203 patients with HCC were examined, respectively.

3.1 Screening of prognostic genes in the TCGA-LIHC and ICGC-LIRI-JP datasets

Survival analysis was performed on 59 CRGs in the TCGA-LIHC dataset and 10 prognostic genes (*ATP13A2*, *ATP7A*, *COX17*, *DBH*, *F5*, *PRNP*, *SLC31A1*, *SNCA*, *STEAP4*, and *TFRC*) that were significantly correlated with the OS of patients were identified (Figure 1A). Among these 10 critical genes, *ATP13A2*, *ATP7A*, *PRNP*, *SNCA*, and *TFRC* were unfavorable for patient OS, whereas *COX17*, *DBH*, *F5*, *SLC31A1*, and *STEAP4* were favorable for patients' prognosis (Figure 1B). Similarly, seven genes (*ABCB6*, *ALB*, *BECN1*, *CP*, *DAXX*, *SLC31A1*, and *STEAP4*) were found to significantly influence the OS of patients in the ICGC-LIRI-JP dataset, and higher expression levels of *ABCB6*, *BECN1*, and *DAXX* were associated with worse OS, whereas those of *ALB*, *CP*, *SLC31A1*, and *STEAP4* were associated with better prognosis for patients with HCC (Figures 1C, D). Altogether, 15 prognostic genes were identified in the two datasets (Figure 1E).

10.3389/fimmu.2023.1123231

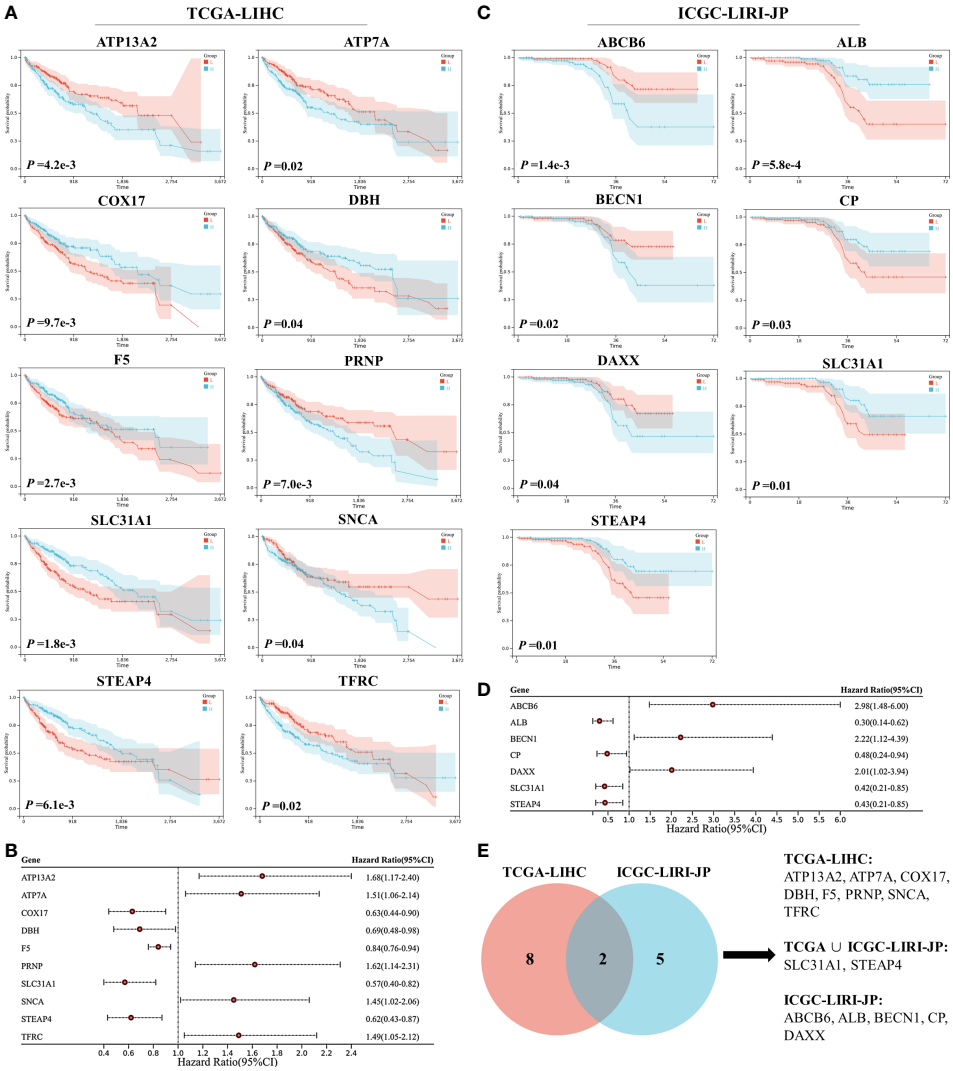

FIGURE 1
Survival analyses of cuproptosis-related genes (CRGs) for patients with hepatocellular carcinoma (HCC) in the TCGA-LIHC and ICGC-LIRI-JP datasets. **(A)** Survival analyses of CRGs for patients with HCC in the TCGA-LIHC dataset. **(B)** Forest plot of prognostic genes in the TCGA-LIHC dataset. **(C)** Survival analyses of CRGs for patients with HCC in the ICGC-LIRI-JP dataset. **(D)** Forest plot of prognostic genes in the ICGC-LIRI-JP dataset. **(E)** Venn diagram of prognostic genes in the two datasets.

3.2 Lasso model construction and validation

A Lasso regression model was constructed using the 15 prognostic genes identified above. Eight genes were successfully included in the model from the TCGA-LIHC dataset; the formula used was follows: risk score = 0.158 × ATP13A2 + 0.070 × ATP7A – 0.173 × COX17 – 0.050 × DBH – 0. 004 × F5 + 0.054 × SNCA – 0.089 × STEAP4 + 0.087 × ABCB6 (Figures 2A, B). Patients were assigned to the low-risk or high-risk group based on the median of all the risk scores. Survival analysis revealed that patients in the high-risk group showed reduced survival years compared with patients in the low-risk group, with the hazard ratio reaching 2.40 (Figure 2C). The heatmap also demonstrated that more deaths were observed in the high-risk group (Figure 2D). ROC curve analysis revealed moderate predictive efficacy, with the AUC for 1-year survival prediction reaching 0.75 (Figure 2E). Similar model construction was conducted for the ICGC-LIRI-JP dataset, and four critical genes (*ALB*, *CP*, *SLC31A1*, and *STEAP4*) were included in the model (Figures 2F, G). Survival analysis and heatmaps revealed significantly increased survival years and fewer patient deaths in the low-risk group compared with the high-risk group (Figures 2H, I). The AUC for 1-year and 2-year survival prediction reached 0.77 and 0.81 respectively, suggesting good predictive effects of the model (Figure 2J).

3.3 DEG validation and potential immune-related pathway enrichment

DEGs between the two groups divided by the median risk score in the ICGC-LIRI-JP dataset were identified and are shown in

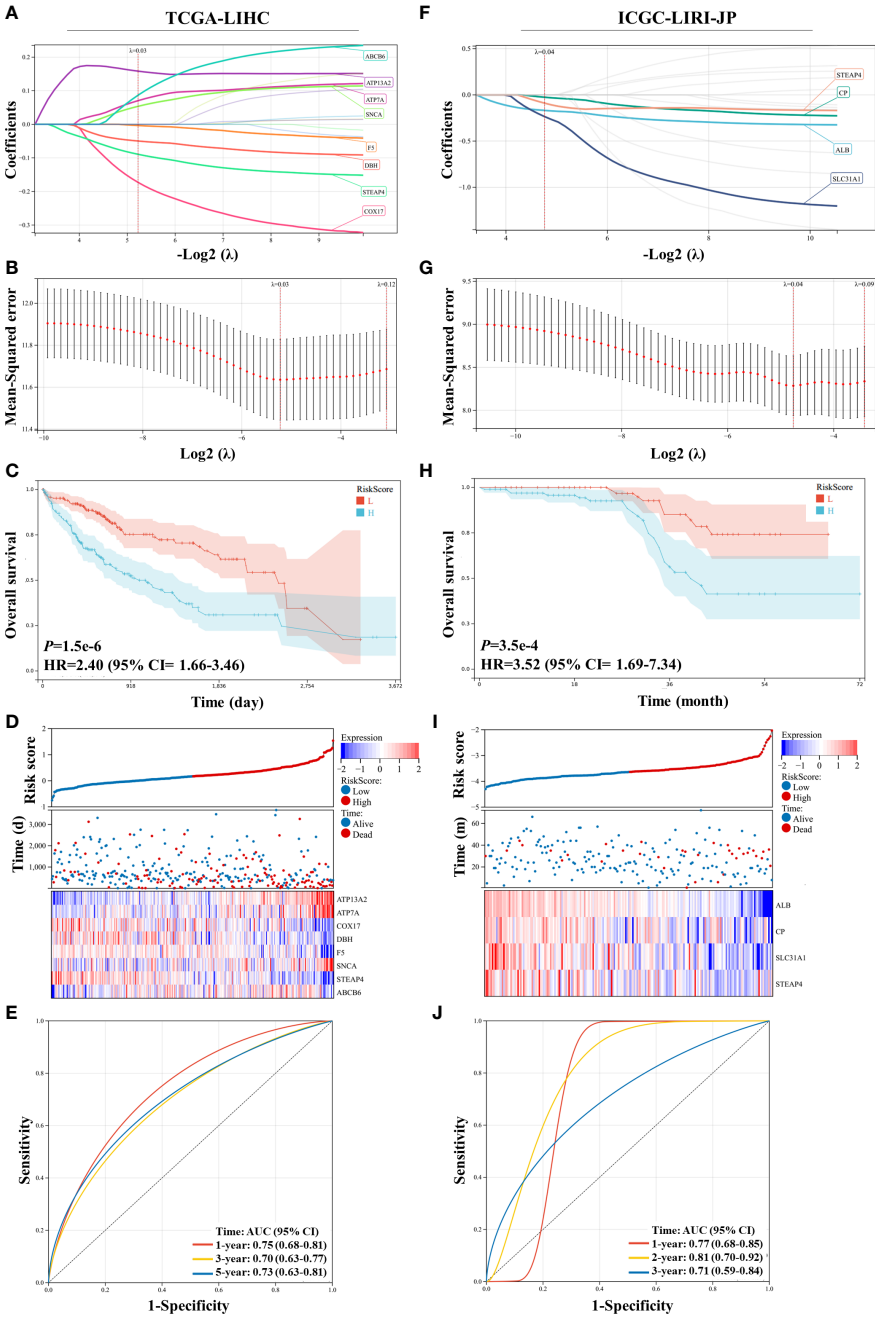

FIGURE 2
Construction and validation of the least absolute shrinkage and selection operator (Lasso) model in the TCGA-LIHC and ICGC-LIRI-JP datasets. **(A, B)** The Lasso regression model was constructed using 15 prognostic genes in the TCGA-LIHC dataset, and eight genes were successfully included in the model. **(C)** Kaplan–Meier survival analysis of patients with hepatocellular carcinoma (HCC) grouped by risk scores in the TCGA-LIHC dataset. **(D)** Distribution of the risk scores, survival status, and expression of eight critical predictive genes. **(E)** Receiver operating characteristic (ROC) curve of risk scores in the TCGA-LIHC dataset. **(F, G)** The Lasso regression model was constructed using 15 prognostic genes in the ICGC-LIRI-JP dataset, and four genes were successfully included in the model. **(H)** Kaplan–Meier survival analysis of patients with HCC grouped by risk scores in the ICGC-LIRI-JP dataset. **(I)** Distribution of the risk scores, survival status, and expression of four critical predictive genes. **(J)** ROC curve of risk scores in the ICGC-LIRI-JP dataset.

Figure 3A. A total of 317 upregulated and 113 downregulated DEGs were identified. GSEA showed that immune-related pathways, including complement activation and complement activation alternative pathway, were significantly different between the two groups. Additionally, complement activation-related genes were downregulated in the high-risk group compared with the low-risk group (Supplementary Figure 2). KEGG and GO-BP pathway enrichment analyses revealed considerable changes in immune-related pathways, including complement-related signal pathways, humoral immune response, and response to xenobiotic stimulus (Figures 3B–D). In the TCGA-LIHC dataset, 812 upregulated DEGs and 1333 downregulated DEGs were identified (Figure 3E). GSEA

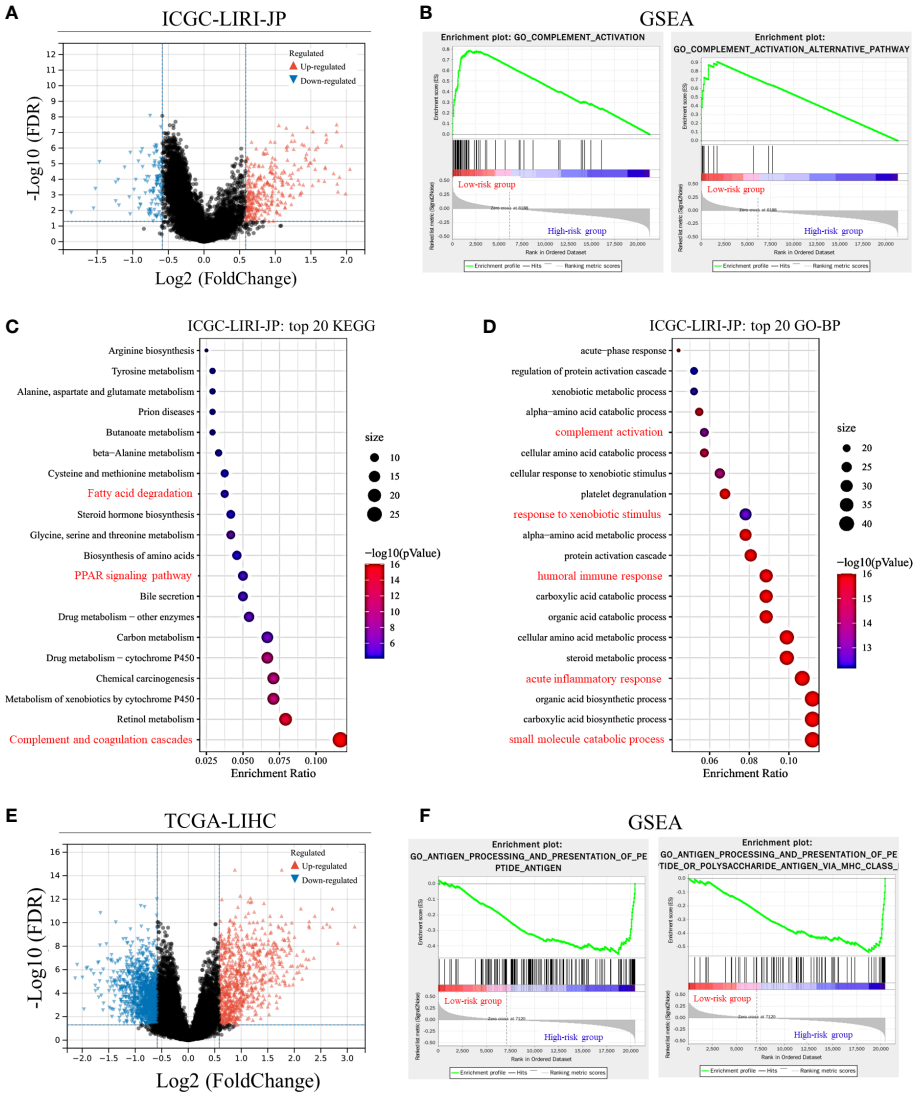

FIGURE 3
Differentially expressed gene (DEG) validation and potential pathway enrichment analysis. **(A)** Volcano plot of DEGs in the ICGC-LIRI-JP dataset. **(B)** Gene Set Enrichment Analysis (GSEA) of immune-related pathways in the ICGC-LIRI-JP dataset. **(C, D)** Top 20 enriched Kyoto Encyclopedia of Genes and Genomes (KEGG) pathways and Gene Ontology-biological process (GO-BP) pathways in the ICGC-LIRI-JP dataset. **(E)** Volcano plot of DEGs in the TCGA-LIHC dataset. **(F)** GSEA of immune-related pathways in the TCGA-LIHC dataset.

revealed that immune-related pathways, such as antigen processing and presentation pathways, were enriched in the TCGA-LIHC dataset (Figure 3F). KEGG pathway enrichment analysis showed that the complement and coagulation cascade pathways were significantly enriched (Supplementary Figure 3), suggesting potential associations between Cu homeostasis and immune function. Interestingly, metabolic pathways, such as small molecule catabolic processes and fatty acid metabolism, were also significantly enriched in both datasets, suggesting that CRGs play a role in cell metabolism (Figures 3C, D and Supplementary Figure 3) (33).

We further visualized the enrichment of GO-immune system process pathways using DEGs from the two datasets (Figure 4). Following enrichment, immune-related signal pathways were found to be considerably altered between the two groups. In the TCGA-LIHC dataset, DEGs were enriched mainly in the immune response-regulatory signaling pathway (66.7%), complement activation (11.1%), complement activation alternative pathway (11.1%), and hemopoiesis (11.1%) (Figure 4A). In the ICGC-LIRI-JP dataset, regulation of humoral immune response (66.7%), complement activation-lectin pathway (11.1%), antimicrobial humoral response (11.1%), and regulation of neutrophil-mediated cytotoxicity (11.1%) were significantly enriched (Figure 4B). These findings indicate the potential role of CRGs in immune function/response regulation in HCC.

3.4 Correlations between CRGs and tumor immune cell infiltration

Correlations between 11 prognostic genes screened by Lasso models in the two datasets and tumor immune cell infiltration levels

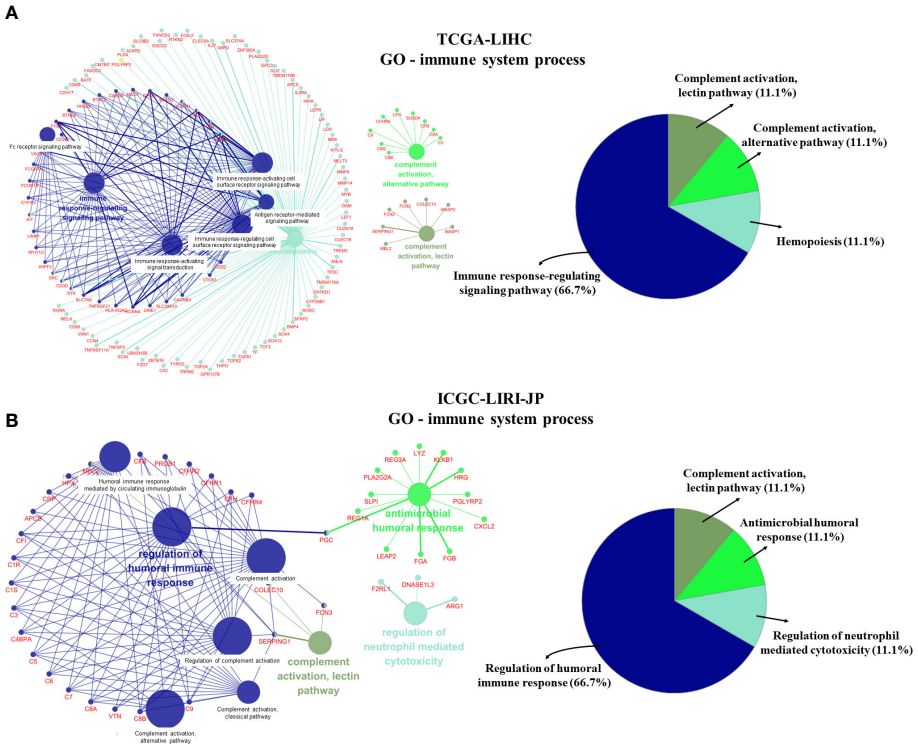

FIGURE 4
GO-immune system process pathway enrichment using differentially expressed genes (DEGs). **(A)** GO-immune system process pathway enrichment in the TCGA-LIHC dataset. **(B)** GO-immune system process pathway enrichment in the ICGC-LIRI-JP dataset.

were analyzed using the TIMER method. Six CRGs that were significantly correlated with tumor immune cell infiltration levels were identified (Figure 5). Interestingly, *ATP7A*, *ATP13A2*, and *SNCA*, which were all unfavorable for the OS of patients (Figure 1), were found to be positively correlated with multiple types of immune cell infiltration in HCC, whereas *COX17*, *F5*, and *ALB*, which were all favorable for the OS of patients, were negatively correlated with immune cell infiltration in HCC. Furthermore, we performed ESTIMATE analysis (including ESTIMATE score, stromal score, and immune score) to picture the correlations between the screened CRGs and tumor microenvironment (Supplementary Table 3). *ATP7A*, *ATP13A2*, *PRNP*, and *SNCA* were found to be positively correlated with the three scores, whereas *COX17* and *F5* were found to be negatively correlated with the three scores. No significant correlations were found between *ALB* and the three scores.

3.5 Correlations between CRGs and ICGs

A previous study has indicated that intratumoral Cu and CRGs modulate the expression of ICGs (34). ICGs are widely expressed in diverse cancer cells, including HCC, and regulate tumor development (35, 36). Therefore, we compared expression levels of ICGs between normal and HCC liver tissues. Three ICGs were expressed in HCC, and the gene expression levels of *PDCD1* and *CTLA4* were substantially increased in HCC samples compared with normal liver tissue (Figure 6A). By grouping patients based on the median risk score, similar changes were observed in that the expression levels of *PDCD1* and *CTLA4* were significantly higher in the high-risk group than in the low-risk group (Figure 6B). These findings indicate that higher expression levels of ICGs may be correlated with worse prognosis in patients with HCC.

We assessed the co-expression between CRGs and ICGs at the mRNA level in HCC (Figure 6C). Notably, *ATP7A*, *ATP13A2*, *SNCA*, and *PRNP* (unfavorable for the OS of patients with HCC) were significantly positively correlated with the expression of ICGs. However, a negative correlation was observed between ICGs and *COX17* or *F5* (favorable for the OS of patients with HCC). Collectively, these results further suggest that CRGs participate in the regulation of ICG expression and tumor immune escape.

3.6 Validation of critical CRGs in different immune subtypes of HCC

Recently, Wu et al. developed and validated a simple scoring model named MRS to distinguish between the different immune subtypes of HCC (32). A higher MRS usually represents a significantly immunosuppressive tumor microenvironment in HCC (Figure 7A). We validated our findings regarding the relationship between CRGs and the TIM using related sequencing data (GSE134921) (32). The expression of CRGs including *ATP7A*, *PRNP*, and *SNCA*, which were unfavorable for the prognosis of

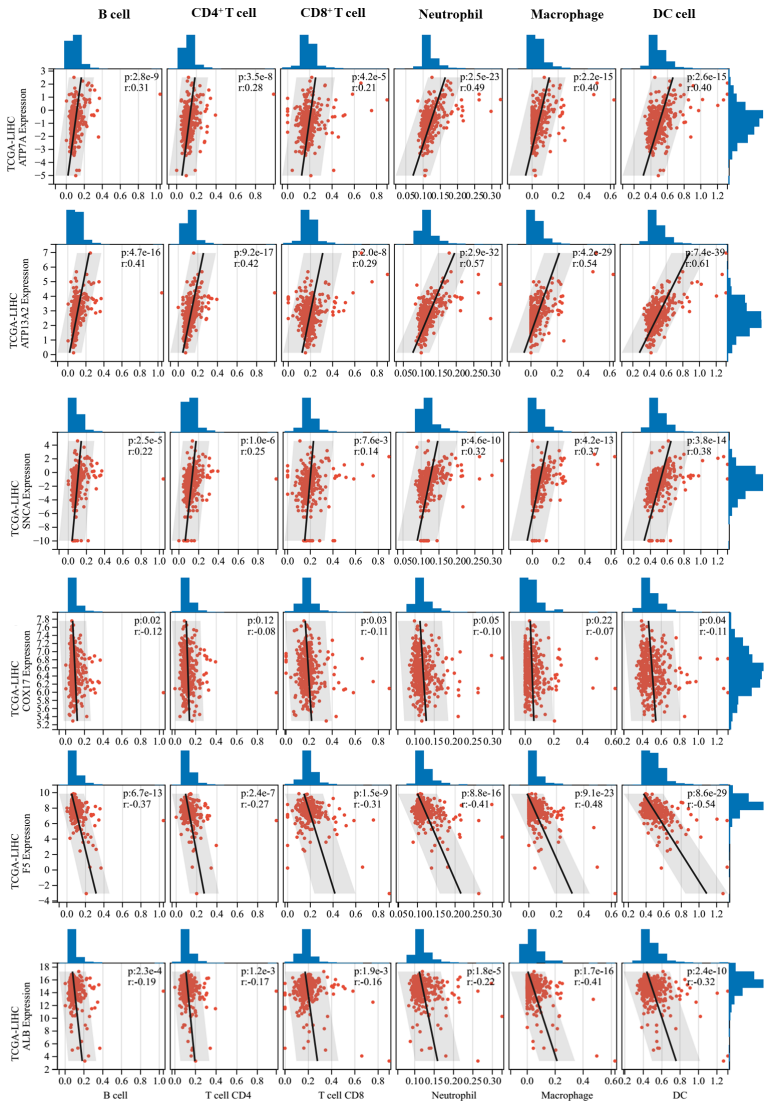

FIGURE 5
Correlations between critical cuproptosis-related genes (CRGs) and tumor immune cell infiltration. ATP7A, ATP13A2, and SNCA were positively correlated with multiple types of immune cell infiltration in hepatocellular carcinoma (HCC), while COX17, F5, and ALB were negatively correlated with immune cell infiltration in HCC.

patients with HCC, was significantly increased in the high-MRS group (Figure 7A). In contrast, the expression of *DBH* and *F5*, which were favorable for the prognosis of patients with HCC, was reduced in the high-MRS group. It was found that *CD274* and *CTLA4* were remarkably upregulated in the high-MRS group. All the abovementioned results suggest close relationships among CRGs, TIM, and immune checkpoints in HCC.

Differential signaling pathways were analyzed and compared between the low-MRS and high-MRS groups (Figure 7B). Interestingly, the results of this analysis were surprisingly similar to those of the pathway enrichment analyses of the low-risk and high-risk groups (Figure 4C and Supplementary Figure 3), suggesting good comparability between the MRS and risk scoring systems. The risk score based on CRGs may discriminate immune subtypes in HCC. Similarly, metabolic pathways such as small molecule catabolic process and fatty acid metabolism were also enriched, suggesting that cell metabolism is associated with TIM regulation in HCC (Figure 7B).

3.7 Validation of significant correlations among CRGs, TIM, and ICGs in the Renji cohort

Based on correlations analyses between CRGs and ICGs (Figure 8 and Supplementary Figure 4), we selected three CRGs (*PRNP* and *SNCA* [unfavorable for prognosis] and *COX17* [favorable for prognosis]) that had more significant correlations with ICGs than other CRGs for further validation in HCC samples; the clinical characteristics of patients are shown in Table 1. Linear regression analyses of gene expression levels revealed a significantly positive correlation between *PRNP* and ICGs, with the R-value

10.3389/fimmu.2023.1123231

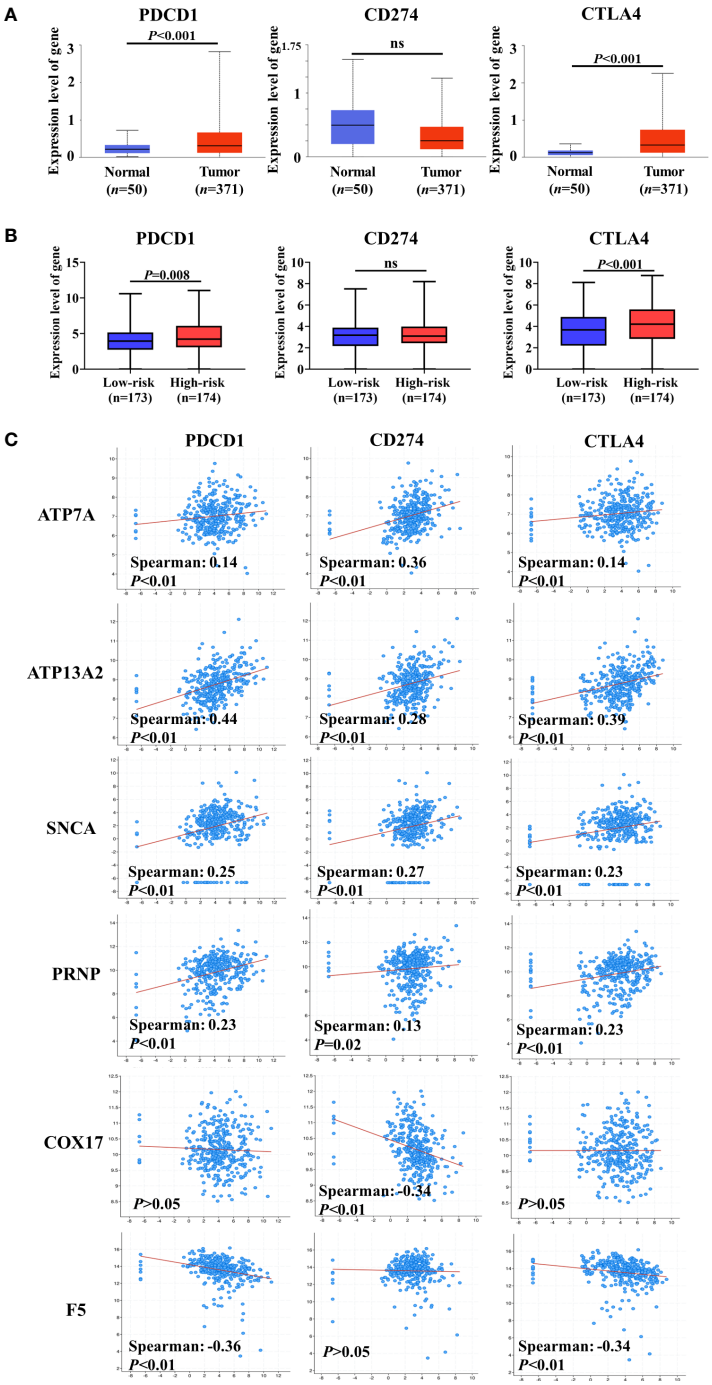

FIGURE 6
Co-expression analysis of cuproptosis-related genes (CRGs) and immune checkpoint genes (ICGs). **(A)** Expression levels of ICGs between normal liver tissue and hepatocellular carcinoma (HCC). **(B)** Differences in the expression of ICGs between low-risk and high-risk groups. **(C)** Co-expression analysis of CRGs and ICGs. ATP7A, ATP13A2, and SNCA were significantly positively correlated with the expression of ICGs, and a negative correlation between ICGs and COX17 or F5 was observed. ns, no significance.

reaching 0.94 and 0.51 for CD274 and CTLA4, respectively (Figure 8A). This strongly suggests that *PRNP* plays a key role in the regulation of ICGs in HCC. Positive correlations were observed between *SNCA* and *PDCD1*/*CTLA4*. However, a negative correlation was observed between *COX17* and *CD274*, with the R-value reaching −0.52 (Figure 8A). Moreover, IHC analysis of HCC samples revealed similar results (Figure 8B).

Correlations between CRGs and immune cell markers were observed in HCC samples (Supplementary Figure 5). Linear regression analyses of gene expression levels suggested that *PRNP* be closely associated with multiple types of immune cells in HCC (Supplementary Figure 5A). In summary, the validations in HCC samples further verified the findings obtained from the comprehensive bioinformatic analyses.

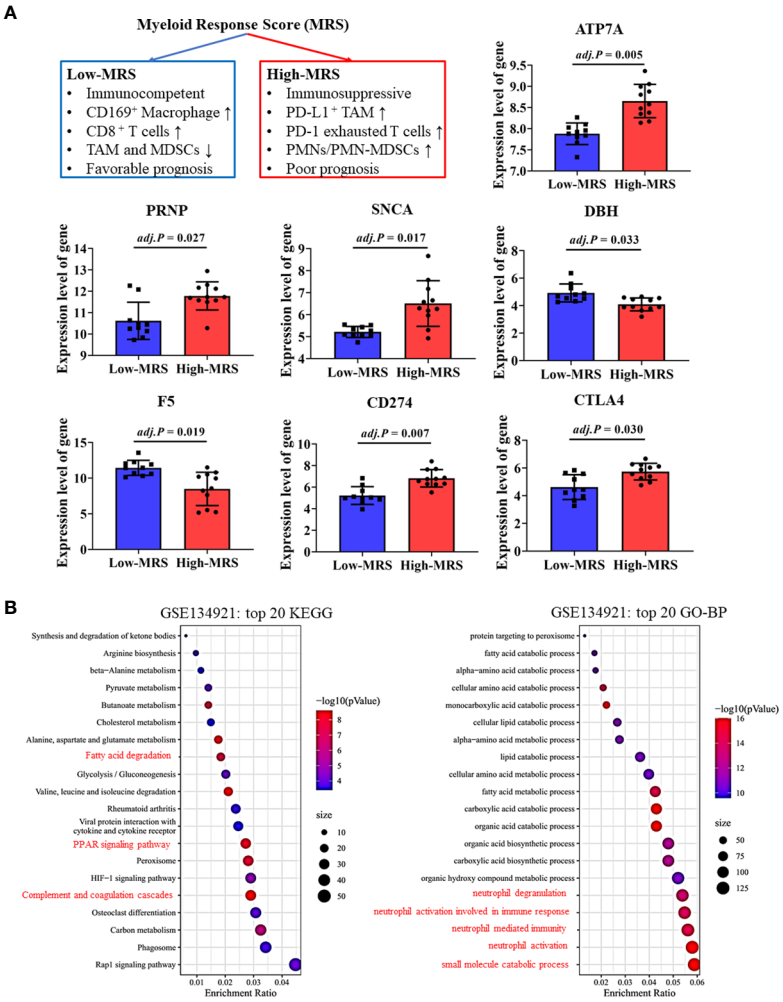

FIGURE 7
Validation of cuproptosis-related genes (CRGs) and immune checkpoint gene (ICG) expression in different immune subtypes of hepatocellular carcinoma (HCC). **(A)** Expression levels of critical CRGs and ICGs between the low-myeloid response score (MRS) group and high-MRS group. **(B)** Differential signal pathway analysis between the low- and high-MRS groups.

3.8 Nomogram construction for HCC based on CRGs

Finally, a novel prognostic nomogram to predict the survival of patients with HCC was constructed by integrating risk score, age, sex, race, TNM stage, and tumor grade. Both risk score and TNM stage significantly influenced the survival of patients (both $P < 0.05$), and the risk score had a greater influence than the TNM stage (Figure 9A). Moreover, the calibration plots and ROC curves suggested that the model could reliably predict the OS of patients with HCC (Figures 9B, C).

4 Discussion

As a critical bioinorganic element, Cu plays important roles in various biological processes in vertebrates (15, 37), and Cu homeostasis is tightly regulated within the body. However, elevated serum and tumor levels of Cu are common in many cancers, and studies have shown that Cu plays critical roles in tumor growth and immune resistance (18, 34, 38, 39). Recently, the mechanism of Cu in regulating HCC development has become a topic of interest (40–42). For instance, a newly published study showed that elevated intracellular levels of Cu promoted the radioresistance of HCC cells, and novel treatment strategies can recover the sensitivity to radiotherapy by disrupting Cu–Fe homeostasis in HCC cells (42). Davis et al. found that the expression of Cu transporter genes was significantly altered in HCC; by limiting Cu homeostasis, the growth of HCC cell lines could be inhibited (40). Therefore, exploring the relationships among Cu metabolism, cuproptosis, and tumor immune response may provide novel insights on cancer therapy.

In our study, we systematically analyzed 59 genes involved in Cu metabolism and cuproptosis in patients with HCC from two public datasets. Results suggested that 15 CRGs significantly influenced the prognosis of patients. Furthermore, we successfully constructed a Lasso model and nomogram to predict the risk of death for patients with HCC based on the screened CRGs and 11 critical genes that were

10.3389/fimmu.2023.1123231

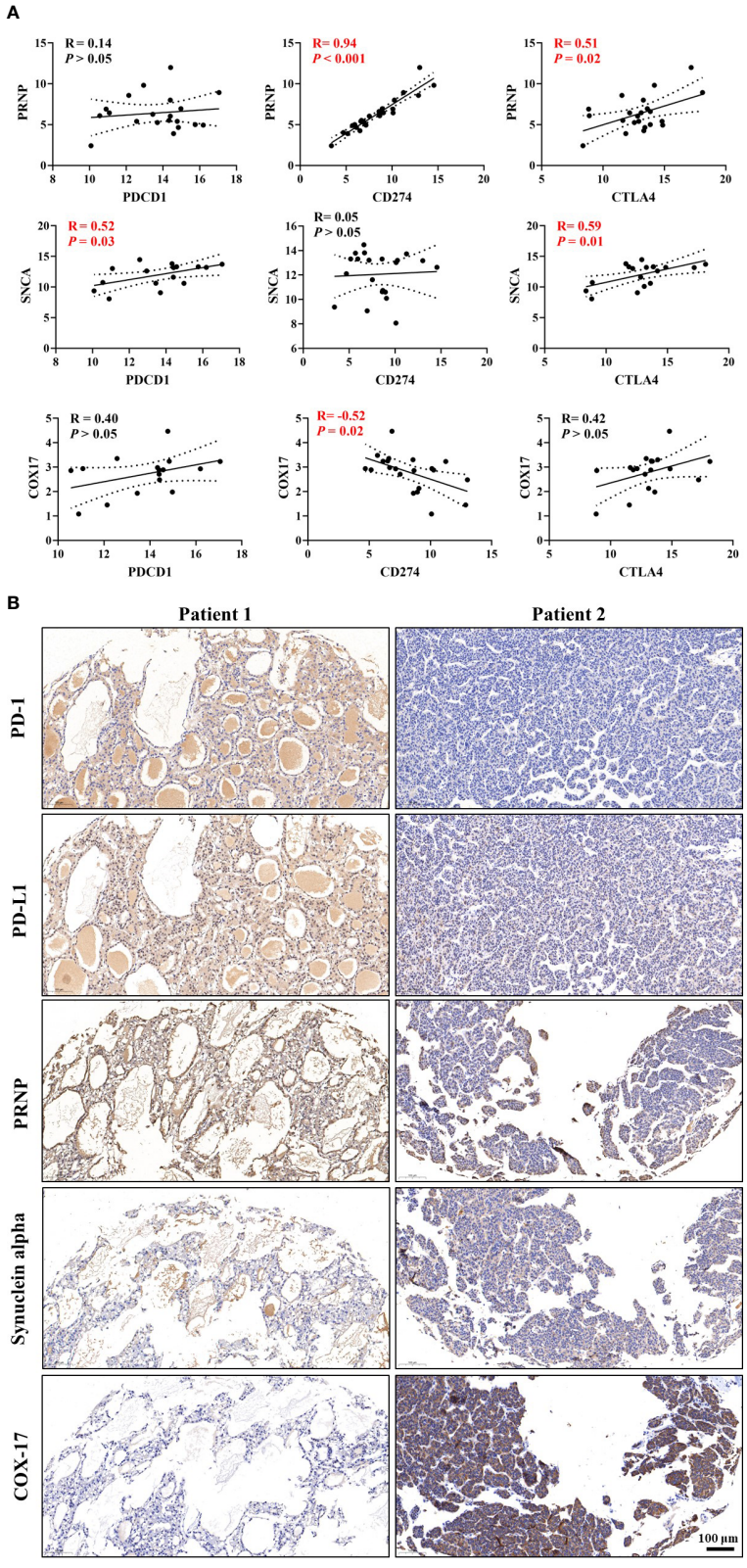

FIGURE 8
Validation of correlations among cuproptosis-related genes (CRGs), tumor immune microenvironment (TIM), and immune checkpoint genes (ICGs) in the Renji cohort. **(A)** Correlation analyses between CRGs and ICGs. **(B)** Immunohistochemical (IHC) staining of CRGs and ICGs in hepatocellular carcinoma (HCC) samples.

TABLE 1 Clinical characteristics of patients with HCC.

Characteristics	*n* = 25
Gender (male/female)	24/1
Age (year)	53.28 (11.05)
Height (cm)	170.43 (5.96)
Weight (kg)	68.10 (9.44)
ASA stage (I/II)	7/18
Child-Pugh stage (A/B)	13/12
Hypertension (Yes/No)	10/15
Diabetes (Yes/No)	2/23
Drinking (Yes/No)	5/20
Viral hepatitis (Yes/No)	24/1
Cirrhosis (Yes/No)	20/5
Tumor size (cm)	4.92 (2.53)
Operation time (hour)	2.80 (0.90)
Bleeding (ml)	295.45 (164.69)
Urine (ml)	413.64 (190.98)
Liquid transfusion	
Crystalloid fluid (ml)	1285.71 (373.21)
Colloid fluid (ml)	739.05 (375.53)
ALT (U/L)	36.64 (34.48)
AST (U/L)	35.05 (26.63)
Hb (g/L)	143.39 (16.43)
PLT (10^9/L)	175.04 (86.76)
TBiL (μmol/L)	14.35 (5.76)
ALB (g/L)	42.98 (3.96)
Cr (μmol/L)	70.57 (13.15)
INR	1.02 (0.12)

Variables are shown as "mean (SD)". ASA, American Society of Anesthesiologists; ALT, alanine transaminase; AST, aspartate aminotransferase; Hb, hemoglobin; PLT, platelets; TBiL, total bilirubin; ALB, albumin; Cr, creatine; INR, international normalized ratio.

identified using the Lasso model. HCC samples were validated and potential targets that are closely associated with ICGs and immune cells, such as *PRNP*, *SNCA*, and *COX17*, were identified. Collectively, these findings confirm the key roles of CRGs in mediating tumor development, and this prediction model could help clinicians predict the prognosis of patients with HCC more easily.

The role of Cu in regulating tumor immune function and immune checkpoints has rarely been explored. In 1981, a study reported that mice fed a Cu-deficient diet made significantly fewer antibody-producing cells and had an impaired immune system (43). Another study revealed that endogenous Cu was involved in the mediation of inflammatory responses (44). In 2020, Voli et al. reported that intratumoral Cu modulated PD-L1 expression, tumor immune cell infiltration, and immune escape in neuroblastoma. However, to the best of our knowledge, studies regarding Cu metabolism and immune function in HCC are lacking. Considering this, we focused our analyses on understanding the mechanisms underlying the effects of CRGs on immune-related pathways. By performing multiple function enrichment analyses, we identified that the immune-related pathways were significantly enriched, such as complement activation-related pathways, humoral immune response, and immune response-regulating signaling pathways. Furthermore, tumor immune cell infiltration analysis showed that *ATP7A*, *ATP13A2*, and *SNCA*, which were unfavorable for the OS of patients with HCC, were positively correlated with multiple types of immune cell infiltration, whereas *COX17*, *F5*, and *ALB*, which were favorable for the OS of patients with HCC, were negatively correlated with immune cell infiltration in HCC. These results could be explained by the complexity and heterogeneity of immune contexture in HCC. Higher levels of immune cell infiltration may be associated with worse prognosis of patients with HCC owing to the accumulation of numerous suppressive immune cells, such as TAMs, exhausted T cells, and MDSCs. For instance, Wu et al. validated a simple myeloid signature known as MRS for HCC and discriminated HCC immune subtypes as immunocompetent, immunodeficient, and immunosuppressive subtypes (32). They found that the infiltration level of $CD8^+$ T cells was comparable in the immunocompetent and immunosuppressive subtypes, while most T cells were PD-1^{high} exhausted T cells in the immunosuppressive subtypes, suggesting the presence of a highly immunosuppressive tumor microenvironment in patients with HCC with a high MRS.

Immune checkpoints play critical roles in regulating immune cell function and tumor immune cell infiltration, and ICI therapy has revolutionized the treatment of advanced malignancies and other diseases in recent years (45, 46). For example, Wang et al. found that increased PD-L1 expression in human neutrophils delays cellular apoptosis by triggering PI3K-dependent AKT phosphorylation, thereby promoting lung injury and increasing mortality during clinical and experimental sepsis (45). Additionally, ICIs targeting PD-1, PD-L1, or CTLA4 have enabled the possibility of long-term survival in patients with tumors such as melanoma, HCC, breast cancer, and colorectal cancer (47, 48). Previous studies demonstrated that tumor cell-intrinsic ICGs regulated tumor development (34, 49, 50). Therefore, correlations between CRGs and ICGs at the mRNA level were investigated and discussed in our study. Among the 15 critical prognostic genes, *ATP7A*, *ATP13A2*, *SNCA*, and *PRNP* were significantly positively correlated with the expression of ICGs, whereas *COX17* and *F5* were negatively correlated with the expression of ICGs. These results were consistent with those of the survival analysis in the two datasets, suggesting that CRGs influence tumor immune escape by regulating the expression of ICGs. Furthermore, based on the co-expression analysis between CRGs and ICGs, we hypothesized that infiltrated immune cells may be disabled by the high levels of immune checkpoints in tumor cells.

The meaningful findings of our study are as follows: 1) We found potential associations between CRGs and immune function regulation in HCC. Furthermore, we found that CRGs were correlated with the expression of PD-1, PD-L1, and CTLA4, which implies possible effects on regulating the immune escape

10.3389/fimmu.2023.1123231

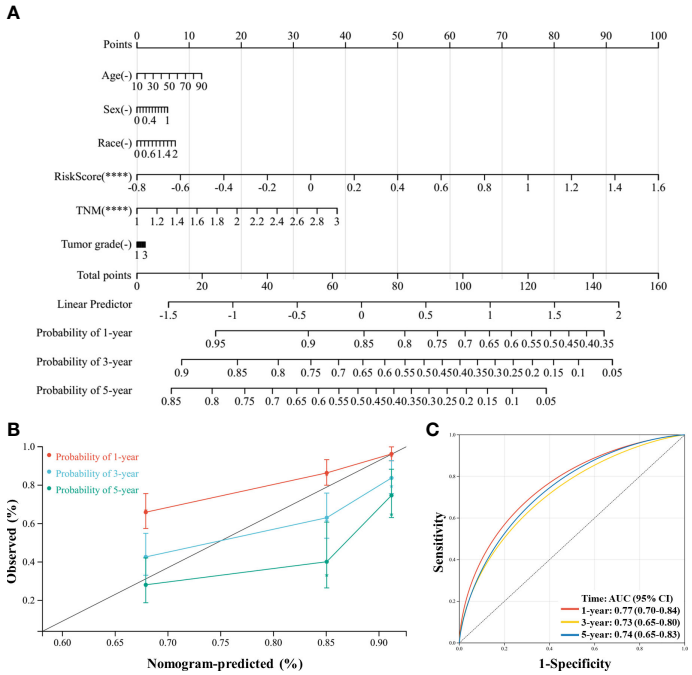

FIGURE 9
A nomogram was constructed to predict the probability of the 1-year, 3-year, and 5-year overall survival (OS) in patients with hepatocellular carcinoma (HCC). **(A)** The nomogram was constructed based on six factors, and the results suggest that the risk score and TNM (tumor, nodes, metastases) stage significantly affected the OS of patients with HCC. For the factor sex, 0 represents male and 1 represents female; for the factor race, 0 represents white, 1 represents Asian, and 2 represents others; for TNM, 1 represents stage I, 2 represents stage II, and 3 represents stages III and IV. **(B)** Calibration plots of the nomogram for the 1-year, 3-year, and 5-year OS. **(C)**, Receiver operating characteristic (ROC) curve of the nomogram prediction model. ****$P < 0.0001$.

and TIM, and may be promising targets to improve the efficacy of immunotherapy in HCC. To target these potential genes may cooperate with ICIs to suppress tumor growth. 2) We identified critical CRGs that significantly influence the survival of patients with HCC. We constructed a useful tool to predict the risk of death for patients with HCC based on the prognostic genes identified. 3) We analyzed the effect of cuproptosis on HCC and found that some CRGs, such as *ATP7A* and *SLC31A1*, significantly affected the OS of patients with HCC, suggesting that cuproptosis is involved in HCC progression. Moreover, cuproptosis may provide new research directions and targets for HCC clinical treatments, similar to ferroptosis. Finally, our study revealed complex functions of Cu in regulating the TIM, immune cell infiltration, and ICG expression.

Limitations of the present study are worth noting. First, *in vivo* or *in vitro* experiments are required to validate the enrichment of immune-related signaling pathways observed in the GSEA and KEGG pathway enrichment analysis. Nevertheless, some validations were performed on HCC samples in our study, and this provides a meaningful direction for scientists to further investigate the relationship between Cu metabolism and tumor immune response in HCC. Second, it was unclear whether immune escape and immune therapy resistance could be reversed by targeting the critical CRGs, although correlations were identified at the mRNA level among CRGs, tumor immune cell infiltration, and immune checkpoints. Third, multicenter clinical trials with large sample sizes are required to validate and improve our prognostic model.

5 Conclusion

Our study provides meaningful insight into the key roles of CRGs in the development of HCC. Functional enrichment and pathway analysis suggest a close relationship between CRGs and immune-related pathways in HCC. Critical CRGs, particularly *PRNP*, *SNCA*, and *COX17*, may influence the infiltration of multiple immune cells in HCC, and significant correlations with the expression of *PD-1*, *PD-L1*, and *CTLA4* were also observed. Collectively, CRGs could be promising therapeutic targets for HCC by regulating the TIM and immune checkpoints.

Data availability statement

The original contributions presented in the study are included in the article/Supplementary Material. Further inquiries can be directed to the corresponding authors.

Ethics statement

This study was approved by the Renji Hospital Ethics Committee (KY2020-185). The patients/participants provided their written informed consent to participate in this study.

Author contributions

conceptualization, JT, WY, and HS; methodology, XW and JT; software, XW, DC, and YS; validation, JL and YZ; formal analysis, XW and XY; investigation, JT; resources, XW, C.Z., and JT; data curation, XW and HS; writing—original draft preparation, XW and JT; writing—review and editing, WY and JT; supervision, WY and JT; funding acquisition, DC, XY, WY, and JT. All authors contributed to the article and approved the submitted version.

Funding

This work was supported by the National Natural Science Foundation of China (No. 82171177 to JT and No. 32030043 and 81971223 to WY); the Clinical Research Plan of SHDC (No. SHDC2020CR4062 to JT); The Shanghai Pudong New Area Municipal Commission of Health and Family Planning Funding (PWZxq2017-06 to WY); the Shanghai Municipal Key Clinical Specialty (shslczdzk03601 to WY); the Shanghai Engineering Research Center of Peri-operative Organ Support and Function Preservation (No. 20DZ2254200); the Shanghai Municipal Education Commission (No. 2019-01-07-00-01-E00074); the Minhang District Natural Science Research Project (No. 2022MHZ037 to DC); and the Zhejiang Medical Health Science and Technology Project (No. 2021RC047 to XY).

Conflict of interest

The authors declare that the research was conducted in the absence of any commercial or financial relationships that could be construed as a potential conflict of interest.

Publisher's note

Supplementary material

The Supplementary Material for this article can be found online at: https://www.frontiersin.org/articles/10.3389/fimmu.2023.1123231/full#supplementary-material

SUPPLEMENTARY FIGURE 1
Study design flow chart and validation process.

SUPPLEMENTARY FIGURE 2
Comparison of the expression levels of complement activation-related genes between the two groups in the ICGC-LIRI-JP dataset.

SUPPLEMENTARY FIGURE 3
Differential pathway analysis in the TCGA-LIHC dataset grouped by risk score. **(A)** Top 20 KEGG differential pathways between two groups. **(B)** Top 20 GO-BP differential pathways between two groups.

SUPPLEMENTARY FIGURE 4
Correlation analysis between cuproptosis-related genes (CRGs) and immune checkpoint genes (ICGs). **(A)** Correlation analysis between ATP7A and ICGs. **(B)** Correlation analysis between ATP13A2 and ICGs. **(C)** Correlation analysis between F5 and ICGs.

SUPPLEMENTARY FIGURE 5
Correlation analysis between cuproptosis-related genes (CRGs) and immune cell markers. **(A)** Correlation analysis between PRNP and immune cell markers. **(B)** Correlation analysis between SNCA and immune cell markers. **(C)** Correlation analysis between COX17 and immune cell markers.

References

1. Bray F, Laversanne M, Weiderpass E, Soerjomataram I. The ever-increasing importance of cancer as a leading cause of premature death worldwide. *Cancer* (2021) 127(16):3029–30. doi: 10.1002/cncr.33587

2. Xiao J, Wang F, Wong NK, He J, Zhang R, Sun R, et al. Global liver disease burdens and research trends: analysis from a Chinese perspective. *J Hepatol* (2019) 71:212–21. doi: 10.1016/j.jhep.2019.03.004

3. Sarin SK, Kumar M, Eslam M, George J, Al Mahtab M, Akbar SMF, et al. Liver diseases in the Asia-pacific region: a lancet gastroenterology & hepatology commission. *Lancet Gastroenterol Hepatol* (2020) 5:167–228. doi: 10.1016/S2468-1253(19)30342-5

4. Xia C, Dong X, Li H, Cao M, Sun D, He S, et al. Cancer statistics in China and united states, 2022: profiles, trends, and determinants. *Chin Med J (Engl)* (2022) 135:584–90. doi: 10.1097/CM9.0000000000002108

5. Qing X, Xu W, Zong J, Du X, Peng H, Zhang Y. Emerging treatment modalities for systemic therapy in hepatocellular carcinoma. *Biomark Res* (2021) 9(1):64. doi: 10.1186/s40364-021-00319-3

6. Foerster F, Gairing SJ, Ilyas SI, Galle PR. Emerging immunotherapy for HCC: a guide for hepatologists. *Hepatology* (2022) 75(6):1604–26. doi: 10.1002/hep.32447

7. Qin S, Ren Z, Meng Z, Chen Z, Chai X, Xiong J, et al. Camrelizumab in patients with previously treated advanced hepatocellular carcinoma: a multicentre, open-label, parallel-group, randomised, phase 2 trial. *Lancet Oncol* (2020) 21(4):571–80. doi: 10.1016/S1470-2045(20)30011-5

8. Finn RS, Ryoo BY, Merle P, Kudo M, Bouattour M, Lim HY, et al. Pembrolizumab as second-line therapy in patients with advanced hepatocellular carcinoma in KEYNOTE-240: a randomized, double-blind, phase III trial. *J Clin Oncol* (2020) 38(3):193–202. doi: 10.1200/JCO.19.01307

9. Zhu AX, Finn RS, Edeline J, Cattan S, Ogasawara S, Palmer D, et al. Pembrolizumab in patients with advanced hepatocellular carcinoma previously treated with sorafenib (KEYNOTE-224): a non-randomised, open-label phase 2 trial. *Lancet Oncol* (2018) 19(7):940–52. doi: 10.1016/S1470-2045(18)30351-6

10. Xing R, Gao J, Cui Q, Wang Q. Strategies to improve the antitumor effect of immunotherapy for hepatocellular carcinoma. *Front Immunol* (2021) 12:783236. doi: 10.3389/fimmu.2021.783236

11. Ringelhan M, Pfister D, O'Connor T, Pikarsky E, Heikenwalder M. The immunology of hepatocellular carcinoma. *Nat Immunol* (2018) 19(3):222–32. doi: 10.1038/s41590-018-0044-z

12. Jenne CN, Kubes P. Immune surveillance by the liver. *Nat Immunol* (2013) 14 (10):996–1006. doi: 10.1038/ni.2691

13. Cariani E, Missale G. Immune landscape of hepatocellular carcinoma microenvironment: implications for prognosis and therapeutic applications. *Liver Int* (2019) 39(9):1608–21. doi: 10.1111/liv.14192

14. Denoyer D, Masaldan S, La Fontaine S, Cater MA. Targeting copper in cancer therapy: 'Copper that cancer'. *Metallomics* (2015) 7(11):1459–76. doi: 10.1039/C5MT00149H

15. Li Y. Copper homeostasis: emerging target for cancer treatment. *IUBMB Life* (2020) 72(9):1900–8. doi: 10.1002/iub.2341

16. Tsvetkov P, Coy S, Petrova B, Dreishpoon M, Verma A, Abdusamad M, et al. Copper induces cell death by targeting lipoylated TCA cycle proteins. *Science* (2022) 375(6586):1254–61. doi: 10.1126/science.abf0529

17. Shribman S, Marjot T, Sharif A, Vimalesvaran S, Ala A, Alexander G, et al. Investigation and management of wilson's disease: a practical guide from the British

association for the study of the liver. *Lancet Gastroenterol Hepatol* (2022) 7(6):560–75. doi: 10.1016/S2468-1253(22)00004-8

18. Babak MV, Ahn D. Modulation of intracellular copper levels as the mechanism of action of anticancer copper complexes: clinical relevance. *Biomedicines* (2021) 9 (8):852. doi: 10.3390/biomedicines9080852

19. Feng Y, Zeng JW, Ma Q, Zhang S, Tang J, Feng JF. Serum copper and zinc levels in breast cancer: a meta-analysis. *J Trace Elem Med Biol* (2020) 62:126629. doi: 10.1016/j.jtemb.2020.126629

20. Kirshner JR, He S, Balasubramanyam V, Kepros J, Yang CY, Zhang M, et al. Elesclomol induces cancer cell apoptosis through oxidative stress. *Mol Cancer Ther* (2008) 7(8):2319–27. doi: 10.1158/1535-7163.MCT-08-0298

21. Zhong X, Dai X, Wang Y, Wang H, Qian H, Wang X. Copper-based nanomaterials for cancer theranostics. *Wiley Interdiscip Rev Nanomed Nanobiotechnol* (2022) 14(4):e1797. doi: 10.1002/wnan.1797

22. Xie J, Yang Y, Gao Y, He J. Cuproptosis: mechanisms and links with cancers. *Mol Cancer* (2023) 22(1):46. doi: 10.1186/s12943-023-01732-y

23. Liu Q, Li R, Wu H, Liang Z. A novel cuproptosis-related gene model predicts outcomes and treatment responses in pancreatic adenocarcinoma. *BMC Cancer* (2023) 23(1):226. doi: 10.1186/s12885-023-10678-9

24. Luo D, Liu S, Luo J, Chen H, He Z, Gao Z, et al. Characterization of cuproptosis identified immune microenvironment and prognosis in acute myeloid leukemia. *Clin Transl Oncol* (2023). doi: 10.1007/s12094-023-03118-4

25. Xiong C, Ling H, Hao Q, Zhou X. Cuproptosis: p53-regulated metabolic cell death? *Cell Death Differ* (2023) 30(4):876–84. doi: 10.1038/s41418-023-01125-0

26. Alhamzawi R, Ali HTM. The Bayesian adaptive lasso regression. *Math Biosci* (2018) 303:75–82. doi: 10.1016/j.mbs.2018.06.004

27. Mi H, Muruganujan A, Ebert D, Huang X, Thomas PD. PANTHER version 14: more genomes, a new PANTHER GO-slim and improvements in enrichment analysis tools. *Nucleic Acids Res* (2019) 47(D1):D419–26-d26. doi: 10.1093/nar/gky1038

28. Li T, Fan J, Wang B, Traugh N, Chen Q, Liu JS, et al. TIMER: a web server for comprehensive analysis of tumor-infiltrating immune cells. *Cancer Res* (2017) 77(21): e108–10. doi: 10.1158/1538-7445.AM2017-108

29. Zeng D, Ye Z, Shen R, Yu G, Wu J, Xiong Y, et al. IOBR: multi-omics immuno-oncology biological research to decode tumor microenvironment and signatures. *Front Immunol* (2021) 12:687975. doi: 10.3389/fimmu.2021.687975

30. Chandrashekar DS, Bashel B, Balasubramanya SAH, Creighton CJ, Ponce-Rodriguez I, Chakravarthi BVSK, et al. UALCAN: a portal for facilitating tumor subgroup gene expression and survival analyses. *Neoplasia* (2017) 19(8):649–58. doi: 10.1016/j.neo.2017.05.002

31. Cerami E, Gao J, Dogrusoz U, Gross BE, Sumer SO, Aksoy BA, et al. The cBio cancer genomics portal: an open platform for exploring multidimensional cancer genomics data. *Cancer Discov* (2012) 2(5):401–4. doi: 10.1158/2159-8290.CD-12-0095

32. Wu C, Lin J, Weng Y, Zeng DN, Xu J, Luo S, et al. Myeloid signature reveals immune contexture and predicts the prognosis of hepatocellular carcinoma. *J Clin Invest* (2020) 130(9):4679–93. doi: 10.1172/JCI135048

33. Ruiz LM, Libedinsky A, Elorza AA. Role of copper on mitochondrial function and metabolism. *Front Mol Biosci* (2021) 8:711227. doi: 10.3389/fmolb.2021.711227

34. Voli F, Valli E, Lerra L, Kimpton K, Saletta F, Giorgi FM, et al. Intratumoral copper modulates PD-L1 expression and influences tumor immune evasion. *Cancer Res* (2020) 80(19):4129–44. doi: 10.1158/0008-5472.CAN-20-0471

35. Li H, Li X, Liu S, Guo L, Zhang B, Zhang J, et al. Programmed cell death-1 (PD-1) checkpoint blockade in combination with a mammalian target of rapamycin inhibitor restrains hepatocellular carcinoma growth induced by hepatoma cell-intrinsic PD-1. *Hepatology* (2017) 66(6):1920–33. doi: 10.1002/hep.29360

36. Zheng H, Ning Y, Zhan Y, Liu S, Wen Q, Fan S. New insights into the important roles of tumor cell-intrinsic PD-1. *Int J Biol Sci* (2021) 17(10):2537–47. doi: 10.7150/ijbs.60114

37. Lutsenko S. Human copper homeostasis: a network of interconnected pathways. *Curr Opin Chem Biol* (2010) 14(2):211–7. doi: 10.1016/j.cbpa.2010.01.003

38. Shanbhag VC, Gudekar N, Jasmer K, Papageorgiou C, Singh K, Petris MJ. Copper metabolism as a unique vulnerability in cancer. *Biochim Biophys Acta Mol Cell Res* (2021) 1868(2):118893. doi: 10.1016/j.bbamcr.2020.118893

39. Zhang C, Cheng R, Ding J, Li X, Niu H, Li X. Serum copper and zinc levels and colorectal cancer in adults: findings from the national health and nutrition examination 2011-2016. *Biol Trace Elem Res* (2022) 200(5):2033–9. doi: 10.1007/s12011-021-02826-8

40. Davis CI, Gu X, Kiefer RM, Ralle M, Gade TP, Brady DC. Altered copper homeostasis underlies sensitivity of hepatocellular carcinoma to copper chelation. *Metallomics* (2020) 12(12):1995–2008. doi: 10.1039/d0mt00156b

41. Stepien M, Hughes DJ, Hybsier S, Bamia C, Tjønneland A, Overvad K, et al. Circulating copper and zinc levels and risk of hepatobiliary cancers in europeans. *Br J Cancer* (2017) 116(5):688–96. doi: 10.1038/bjc.2017.1

42. Yang M, Wu X, Hu J, Wang Y, Wang Y, Zhang L, et al. COMMD10 inhibits HIF1α/CP loop to enhance ferroptosis and radiosensitivity by disrupting Cu-fe balance in hepatocellular carcinoma. *J Hepatol* (2022) 76(5):1138–50. doi: 10.1016/j.jhep.2022.01.009

43. Prohaska JR, Lukasewycz OA. Copper deficiency suppresses the immune response of mice. *Science* (1981) 213(4507):559–61. doi: 10.1126/science.7244654

44. Jones DG. Effects of dietary copper depletion on acute and delayed inflammatory responses in mice. *Res Vet Sci* (1984) 37(2):205–10. doi: 10.1016/S0034-5288(18)31906-4

45. Wang JF, Wang YP, Xie J, Zhao ZZ, Gupta S, Guo Y, et al. Upregulated PD-L1 delays human neutrophil apoptosis and promotes lung injury in an experimental mouse model of sepsis. *Blood* (2021) 138(9):806–10. doi: 10.1182/blood.2020009417

46. Sharma P, Siddiqui BA, Anandhan S, Yadav SS, Subudhi SK, Gao J, et al. The next decade of immune checkpoint therapy. *Cancer Discov* (2021) 11(4):838–57. doi: 10.1158/2159-8290.CD-20-1680

47. Johnson DB, Nebhan CA, Moslehi JJ, Balko JM. Immune-checkpoint inhibitors: long-term implications of toxicity. *Nat Rev Clin Oncol* (2022) 19(4):254–67. doi: 10.1038/s41571-022-00600-w

48. Llovet JM, Castet F, Heikenwalder M, Maini MK, Mazzaferro V, Pinato DJ, et al. Immunotherapies for hepatocellular carcinoma. *Nat Rev Clin Oncol* (2022) 19(3):151–72. doi: 10.1038/s41571-021-00573-2

49. Ieranò C, Righelli D, D'Alterio C, Napolitano M, Portella L, Rea G, et al. In PD-1 + human colon cancer cells NIVOLUMAB promotes survival and could protect tumor cells from conventional therapies. *J Immunother Cancer* (2022) 10(3):e004032. doi: 10.1136/jitc-2021-004032

50. Wang X, Yang X, Zhang C, Wang Y, Cheng T, Duan L, et al. Tumor cell-intrinsic PD-1 receptor is a tumor suppressor and mediates resistance to PD-1 blockade therapy. *Proc Natl Acad Sci USA* (2020) 117:6640–50. doi: 10.1073/pnas.1921445117

frontiers | Frontiers in Immunology

TYPE General Commentary
PUBLISHED 25 August 2023
DOI 10.3389/fimmu.2023.1265565

OPEN ACCESS

EDITED BY
Lin-Lin Bu,
Wuhan University, China

REVIEWED BY
Haiyang Wu,
Tianjin Medical University, China

*CORRESPONDENCE
Yi Sun
sunyimedicine@163.com

RECEIVED 23 July 2023
ACCEPTED 14 August 2023
PUBLISHED 25 August 2023

CITATION
Xu F, Cai D, Yang Z, Yin J and Sun Y (2023) Commentary: Copper and cuproptosis-related genes in hepatocellular carcinoma: therapeutic biomarkers targeting tumor immune microenvironment and immune checkpoints.
Front. Immunol. 14:1265565.
doi: 10.3389/fimmu.2023.1265565

Commentary: Copper and cuproptosis-related genes in hepatocellular carcinoma: therapeutic biomarkers targeting tumor immune microenvironment and immune checkpoints

Fangshi Xu[1], Danrui Cai[2], Zheng Yang[1], Jian Yin[1] and Yi Sun[1]*

[1]Department of Urology, Shaanxi Provincial People's Hospital, Xi'an, Shaanxi, China, [2]Department of Ophthalmology, Second Affiliated Hospital of Xi'an Jiaotong University, Xi'an, Shaanxi, China

KEYWORDS

cuproptosis, cancer, pathogenesis, bioinformatics, signature

A Commentary on

Copper and cuproptosis-related genes in hepatocellular carcinoma: therapeutic biomarkers targeting tumor immune microenvironment and immune checkpoints

by Wang X, Chen D, Shi Y, Luo J, Zhang Y, Yuan X, Zhang C, Shu H, Yu W and Tian J (2023). *Front. Immunol.* 14:1123231. doi: 10.3389/fimmu.2023.1123231

Introduction

Since P Tsvetkov et al. have first coined "cuproptosis" in 2022, this novel pattern of programmed cell death (PCD) greatly expands our horizons of human diseases (1). Mechanistically, FDX1-mediated protein lipoylation and copper-mediated toxic gain drive the onset of cuproptosis (1). As shown in Figure 1, FDX1, as a metal reductase, is responsible for reducing Cu^{2+} to its more toxic form Cu^{1+}. Next, protein lipoylation is triggered with the aid of FDX1 and six regulators in the lipoic acid pathway. Due to the fact that protein lipoylation is only observed in four enzymes (DBT, DLST, GCSH, and DLAT), all of which participate in the tricarboxylic acid cycle (TCA), the cuproptosis process is subjected to mitochondrial respiration. In the effector phase, copper directly binds to lipoylated protein to increase its cytotoxicity through promoting its aberrant oligomerization. Moreover, copper is able to destabilize Fe–S cluster proteins, thereby enhancing proteotoxic stress. The above-mentioned two processes of copper-induced toxic gain eventually lead to cuproptosis.

Considering the critical roles of other patterns of cell death in cancers, such as apoptosis and ferroptosis, an increasing number of scholars move their attention on the

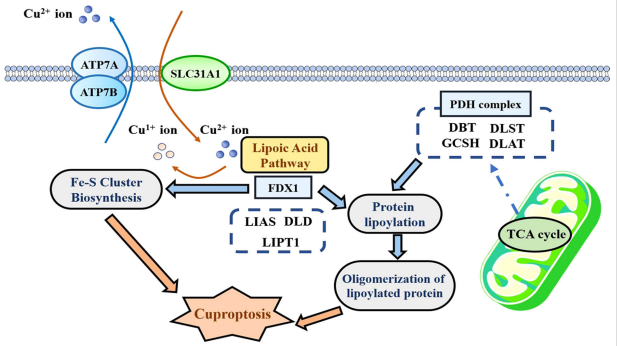

FIGURE 1
Mechanism diagram of cuproptosis.

associations of cuproptosis with human cancers. Recently, we focused on the research by X Wang et al. entitled "Copper and cuproptosis-related genes in hepatocellular carcinoma: Therapeutic biomarkers targeting tumor immune microenvironment and immune checkpoints", which was published in *Frontiers in Immunology* (2). In this study, the authors constructed a cuproptosis-related (CR) signature using Lasso regression analysis to evaluate tumor immune microenvironments (TIMs) and predict the prognosis of patients in hepatocellular carcinoma (HCC). Moreover, they found that some critical CR genes such as PRNP and COX17 were closely related with the expressions of immune checkpoints (ICs), which showed the potentials of the application of a CR model to predict the efficacy of immune checkpoint inhibitors (ICIs).

Despite the great inspiration of their findings to HCC clinical assessment, there is still a long way ahead the clinical application of cuproptosis in HCC. The first issue that needs to be urgently addressed is whether cuproptosis is the dominant pattern of cell death in a specific cancer compared to other PCD. If cuproptosis rarely occurred or is hardly induced in a specific cancer, the corresponding CR signature may be tedious. Moreover, how to detect the intensity of cuproptosis and how to assess the effects of genes on cuproptosis are the other critical issues needed to be addressed. Regretfully, several recent studies in *Frontiers in Immunology* have failed to eliminate the above-mentioned concerns well (3–5). Therefore, we performed the following discussion which aims to provide some insights into further CR research.

Roles of cuproptosis in cancer pathogenesis: leader or retinue?

As a novel type of PCD, the precise mechanisms of cuproptosis in the onset and progression of human cancers need to be further identified. A bibliometric research revealed that the majority of existing cuproptosis studies only exhibited the bioinformatic functional predictions or associations of cuproptosis in cancer (6). However, how big the roles of cuproptosis in cancer pathogenesis remain elusive. Compared with other PCD, cuproptosis is not characterized by the obvious alteration of cell microstructure—for instance, the abnormal changes in structure of the mitochondria observed through transmission electron microscopy can be the direct evidence supporting ferroptosis, but not for cuproptosis (7). Herein we provided some ideas for the above-mentioned issue.

It is now confirmed that cuproptosis is subjected to mitochondrial respiration due to the fact that inhibitors of the electron transport chain (ETC) as well as inhibitors of mitochondrial pyruvate uptake both hinder the copper ionophore-induced cell death (1). Not only that, the core link of cuproptosis, protein lipoylation, only occurs in four enzymes of the TCA cycle (8). Thus, it is not difficult to surmise that cuproptosis occurrence was tightly related to the activity of the TCA cycle. In the above-mentioned context, we speculate that the activity of the TCA cycle or mitochondrial respiration could act as the indicator to assess the cuproptosis level. At present, there have been reasonable and reliable approaches to detect the alterations of mitochondrial respiration, including the extracellular acidification rate (ECAR), the oxygen consumption rate (OCR), and the detection on the activity of key enzymes or products in the TCA cycle—for instance, X Pei et al. have applied ECAR and OCR assays to confirm the influence of MDH2 on mitochondrial respiration (9). FL Basei et al. have evaluated the changes in the protein expressions of respiratory complexes, such as NDUFB8, SDHB, MTCOI, and SDHB, thereby revealing the regulatory function of Nek4 in mitochondrial respiration (10).

Therefore, it is more reasonable to clarify the cuproptosis level in a certain tumor before constructing a CR signature for cancer clinical assessments. If there are no differences in the activity of mitochondrial respiration, especially the TCA cycle between normal and tumor cells or samples, the constructed CR signature is more like a purely mathematical model rather than an excellent assessment tool related to cuproptosis.

Paying more attention on the functions of research genes in cuproptosis

To date, a considerable proportion of cuproptosis bioinformatic studies have only investigated the oncogenic or inhibitory functions of CR genes in cancers from the biological perspective, without determining the impact of these genes on cuproptosis—for example, another cuproptosis research published on *Frontiers in Immunology* has established a CR model for predicting a metastatic event in melanoma, and the authors analyzed the effects of FDX1, the core gene in this model, on the proliferation and migration of melanoma cells (11). Similar research strategy is also observed in other studies (12). Nevertheless, the effects of CR genes on the cuproptosis process remain unanswered among these research, which inevitably raises a question on whether these genes actually regulate cancer development through cuproptosis. To resolve this issue, we suggest that researchers could determine the sensitivity of a tumor cell to cuproptosis agonists, such as elesclcomol under the deficiency or overexpression of the target gene. Alternatively, they could ascertain whether cuproptosis agonists are able to reverse the effects of genes on the malignant behaviors of tumor cells.

Conclusion

The discovery of cuproptosis extremely expands our understanding of cancer pathogenesis and inspires the work enthusiasm of researchers. Of note, conducting scientific functional analysis related to cuproptosis prior to initiating CR research, especially for CR bioinformatic research, is great of significance.

Author contributions

FX: Writing – original draft, Writing – review & editing. DC: Writing – original draft. ZY: Writing – original draft. JY: Writing – original draft. YS: Conceptualization, Project administration, Writing – review & editing.

Funding

The author(s) declare financial support was received for the research, authorship, and/or publication of this article.

Acknowledgments

All authors would like to thank Shaanxi Provincial People's Hospital for its support.

Conflict of interest

The authors declare that the research was conducted in the absence of any commercial or financial relationships that could be construed as a potential conflict of interest.

Publisher's note

References

1. Tsvetkov P, Coy S, Petrova B, Dreishpoon M, Verma A, Abdusamad M, et al. Copper induces cell death by targeting lipoylated TCA cycle proteins. *Science* (2022) 375:1254–61. doi: 10.1126/science.abf0529

2. Wang X, Chen D, Shi Y, Luo J, Zhang Y, Yuan X, et al. Copper and cuproptosis-related genes in hepatocellular carcinoma: Therapeutic biomarkers targeting tumor immune microenvironment and immune checkpoints. *Front Immunol* (2023) 14:1123231. doi: 10.3389/fimmu.2023.1123231

3. Lu D, Liao J, Cheng H, Ma Q, Wu F, Xie F, et al. Construction and systematic evaluation of a machine learning-based cuproptosis-related lncRNA score signature to predict the response to immunotherapy in hepatocellular carcinoma. *Front Immunol* (2023) 14:1097075. doi: 10.3389/fimmu.2023.1097075

4. Yang J, Liu K, Yang L, Ji J, Qin J, Deng H, et al. Identification and validation of a novel cuproptosis-related stemness signature to predict prognosis and immune landscape in lung adenocarcinoma by integrating single-cell and bulk RNA-sequencing. *Front Immunol* (2023) 14:1174762. doi: 10.3389/fimmu.2023.1174762

5. Yuan H, Xiu Y, Liu T, Fan Y, Xu D. The cuproptosis-associated 11 gene signature as a predictor for outcomes and response to Bacillus Calmette-Guerin and immune checkpoint inhibitor therapies in bladder carcinoma. *Front Immunol* (2023) 14:1126247. doi: 10.3389/fimmu.2023.1126247

6. Miao YD, Quan W, Dong X, Gan J, Ji CF, Wang JT, et al. A bibliometric analysis of ferroptosis, necroptosis, pyroptosis, and cuproptosis in cancer from 2012 to 2022. *Cell Death Discovery* (2023) 9:129. doi: 10.1038/s41420-023-01421-1

7. Stockwell BR. Ferroptosis turns 10: Emerging mechanisms, physiological functions, and therapeutic applications. *Cell* (2022) 185:2401–21. doi: 10.1016/j.cell.2022.06.003

8. Xie J, Yang Y, Gao Y, He J. Cuproptosis: Mechanisms and links with cancers. *Mol Cancer* (2023) 22:46. doi: 10.1186/s12943-023-01732-y

9. Pei X, Li KY, Shen Y, Li JT, Lei MZ, Fang CY, et al. Palmitoylation of MDH2 by ZDHHC18 activates mitochondrial respiration and accelerates ovarian cancer growth. *Sci China Life Sci* (2022) 65:2017–30. doi: 10.1007/s11427-021-2048-2

10. Basei FL, de Castro Ferezin C, Rodrigues de Oliveira AL, Muñoz JP, Zorzano A, Kobarg J. Nek4 regulates mitochondrial respiration and morphology. *FEBS J* (2022) 289:3262–79. doi: 10.1111/febs.16343

11. Liu JY, Liu LP, Li Z, Luo YW, Liang F. The role of cuproptosis-related gene in the classification and prognosis of melanoma. *Front Immunol* (2022) 13:986214. doi: 10.3389/fimmu.2022.986214

12. Shen J, Wang L, Bi J. Bioinformatics analysis and experimental validation of cuproptosis-related lncRNA LINC02154 in clear cell renal cell carcinoma. *BMC Cancer* (2023) 23:160. doi: 10.1186/s12885-023-10639-2

frontiers | Frontiers in Immunology

TYPE Original Research
PUBLISHED 27 April 2023
DOI 10.3389/fimmu.2023.1145080

OPEN ACCESS

EDITED BY
Chun Xu,
The University of Queensland, Australia

REVIEWED BY
Jia Li,
University of North Carolina at Charlotte, United States
Dipendra Khadka,
Wonkwang University School of Medicine, Republic of Korea

*CORRESPONDENCE
Mengxi Jiang
jmx@ccmu.edu.cn

†These authors have contributed equally to this work

RECEIVED 15 January 2023
ACCEPTED 10 April 2023
PUBLISHED 27 April 2023

CITATION
Liu Y, Wang J and Jiang M (2023) Copper-related genes predict prognosis and characteristics of breast cancer. *Front. Immunol.* 14:1145080. doi: 10.3389/fimmu.2023.1145080

Copper-related genes predict prognosis and characteristics of breast cancer

Yi Liu[1†], Jiandong Wang[2†] and Mengxi Jiang[1,3*]

[1]Department of Pharmacology, School of Basic Medical Sciences, Capital Medical University, Beijing, China, [2]Department of General Surgery, The First Medical Center, Chinese People's Liberation Army (PLA) General Hospital, Beijing, China, [3]Advanced Innovation Center for Human Brain Protection, Capital Medical University, Beijing, China

Background: The role of copper in cancer treatment is multifaceted, with copper homeostasis-related genes associated with both breast cancer prognosis and chemotherapy resistance. Interestingly, both elimination and overload of copper have been reported to have therapeutic potential in cancer treatment. Despite these findings, the exact relationship between copper homeostasis and cancer development remains unclear, and further investigation is needed to clarify this complexity.

Methods: The pan-cancer gene expression and immune infiltration analysis were performed using the Cancer Genome Atlas Program (TCGA) dataset. The R software packages were employed to analyze the expression and mutation status of breast cancer samples. After constructing a prognosis model to separate breast cancer samples by LASSO-Cox regression, we examined the immune statement, survival status, drug sensitivity and metabolic characteristics of the high- and low-copper related genes scoring groups. We also studied the expression of the constructed genes using the human protein atlas database and analyzed their related pathways. Finally, copper staining was performed with the clinical sample to investigate the distribution of copper in breast cancer tissue and paracancerous tissue.

Results: Pan-cancer analysis showed that copper-related genes are associated with breast cancer, and the immune infiltration profile of breast cancer samples is significantly different from that of other cancers. The essential copper-related genes of LASSO-Cox regression were ATP7B (ATPase Copper Transporting Beta) and DLAT (Dihydrolipoamide S-Acetyltransferase), whose associated genes were enriched in the cell cycle pathway. The low-copper related genes scoring group presented higher levels of immune activation, better probabilities of survival, enrichment in pathways related to pyruvate metabolism and apoptosis, and higher sensitivity to chemotherapy drugs. Immunohistochemistry staining showed high protein expression of ATP7B and DLAT in breast cancer samples. The copper staining showed copper distribution in breast cancer tissue.

Conclusion: This study displayed the potential impacts of copper-related genes on the overall survival, immune infiltration, drug sensitivity and metabolic profile of breast cancer, which could predict patients' survival and tumor statement. These findings may serve to support future research efforts aiming at improving the management of breast cancer.

KEYWORDS

breast cancer, copper metabolism, cuproptosis, prognosis, characteristics

Introduction

Breast cancer has become a significant worldwide health issue, with over two million emerging cases and six hundred thousand death records in 2020 (1, 2). Common treatment options, such as chemotherapy, endocrine therapy, immunotherapy and radiotherapy, do not always provide optimal therapeutic effects to breast cancer patients (3). Therefore, it is important to develop more accurate and effective prognostic models that can effectively characterize and classify the molecular subtypes of breast cancer in order to diagnose, treat and prevent breast cancer in a more precise manner.

Copper is a cofactor for various enzymes and plays a vital role in cellular metabolism and respiration, and disruption of copper homeostasis cause Wilson disease and Menkes disease (4, 5). Copper also contributes to cancer development by enhancing tumor cell proliferation and angiogenesis. Consequently, copper chelator has been applied to inhibit cancer metastasis in clinical trials (6–8). On the contrary, copper overload has been recently proposed to induce lipoylated protein aggregation and cancer cell death (9). Copper homeostasis-related genes have been implicated in breast cancer prognosis and chemotherapy resistance. Studies have shown that breast cancer patients with poor prognoses exhibit higher expression of the copper importer solute carrier family 31 member 1 (SLC31A1) and the copper binding protein ceruloplasmin, which could be utilized as potential prognosis factors (10–12). Decreased expression of the copper exporters ATPase copper transporting α (ATP7A) and ATPase copper transporting β (ATP7B) have been associated with decreased chemotherapy resistance in breast cancer cells (13, 14). It is currently not fully understood how copper metabolism may be involved in breast cancer or the potential mechanisms by which it may influence the development or progression of the disease. Therefore, a comprehensive analysis of the genetic alterations of copper-related genes in tumor tissue could identify molecular targets for future diagnosis and treatments for breast cancer.

Our pan-cancer analysis identified a differential expression pattern of copper-related genes and immune cell infiltration profile in breast cancer. We further investigated the expression and copy number variation (CNV) of copper-related genes in breast cancer and separated breast cancer samples based on the risk score. We then compared the survival status, immune status, drug sensitivity and metabolic pathways of the high- and low-copper related genes scoring groups. Specifically, we analyzed the protein expression, the related genes and the metabolic pathways of the essential copper-related genes, namely ATP7B and DLAT, in breast cancer samples. The clinical sample also confirmed that copper is distributed in breast cancer tissue. In summary, this study may offer valuable insights for identifying potential therapeutic interventions and biomarkers for breast cancer treatment.

Materials and methods

Acquisition of copper-related genes and data collection

We collected copper metabolism-related genes from MSigDB (15) and cuproptosis-related genes from literature (9). The 42 copper-related genes are listed in Table S1. The transcriptome data and medical information of breast cancer patients were obtained from the Cancer Genome Atlas (TCGA) database (https://www.cancer.gov/tcga). After excluding samples with incomplete transcriptomic and survival data, we obtained a final dataset with 1069 breast cancer samples and 113 paracancerous samples, which were used for the following analysis. The validating datasets were procured from Gene Expression Omnibus (GEO), including GSE96058 with 3273 breast cancer samples (16), GSE18229 with 82 samples of luminal A and HER2-enriched subtypes (17), and GSE58812 with 107 samples of triple-negative breast cancer (18). The data of Infiltration Estimation for all TCGA tumors were obtained from TIMER2.0 (19). Copy number variation landscape was presented by the R package "maftools" (20).

Heatmap, PPI network, and correlation network

The heatmap was presented by chiplot (https://www.chiplot.online/) and data were collected from TCGA database and Genotype-Tissue Expression (GTEx) based on UCSC XENA platform (21). The PPI network (Protein-Protein Interaction Networks) was created by the STRING database (22) and Cytoscape (23). The degree of cuproptosis and copper metabolism-related genes was calculated by CytoNCA (24). The correlation network was presented by the R package "corrr".

Construction and validation of the copper-related genes' prognostic index

Copper-related genes were analyzed by univariate Cox regression and genes with $p < 0.05$ were integrated into the LASSO-Cox regression *via* 10-fold cross-validation in order to narrow down candidate genes. A prognostic signature was built by multivariate Cox regression, whose predictive capability on overall survival (OS) was analyzed by time-dependent receptor operating characteristic (ROC) curves by using the R package "timeROC" and "ggplot2" (25). The univariate and multivariate Cox regression results were obtained from the online analysis platform ToPP (http://www.biostatistics.online/topp/index.php.) (26).

Survival analysis

The Kaplan–Meier curve was performed to compare the survival status of the high- and low-copper related genes scoring groups stratified by the risk score of copper-related genes using the R packages "survival", "survminer" and "ggplot2" (R version 4.1.3). Genes were considered statistically significant at the $p < 0.05$ level.

Immune profile analysis

In order to identify the immune states and prognostic features of the high- and low-copper related genes scoring groups, we

applied CIBERSORT (27) to evaluate and compare the immune composition between the two groups. By Tumor Immune Dysfunction and Exclusion (TIDE) (28), we obtained the MSI (microsatellite instability), Exclusion and Dysfunction to compare the potential of tumor immune escape between the two groups. We calculated the stromal score, immune score, tumor purity and estimated score through the ESTIMATE algorithm (29).

Immunohistochemical staining of ATP7B and DLAT by the human protein atlas (HPA) database

The gene expression data based on breast cancer clinical specimens were obtained from the HPA database (https://www.proteinatlas.org/). Visualizing data of HPA were presented using the R package "HPAanalyze".

GSEA

Gene set enrichment analysis (GSEA) of the high- and low-copper related genes scoring groups was created by the desktop application of GSEA 4.2.3. Pathways were considered statistically enriched at the cut-off point of $p< 0.05$ and $FDR < 0.25$ (15).

Drug sensitivity analysis

Based on the transcriptome data of breast cancer samples, the drug sensitivity was analyzed by the R package "oncoPredict" and the Genomics of Drug Sensitivity in Cancer (GDSC) database (30).

LinkedOmics analysis

The LinkFinder and LinkInterpreter modules of the LinkedOmics web application were employed to investigate the potential gene regulation network of the signature genes (31). These tools allowed for identifying and analyzing relevant attributes, providing insight into the functional relationships and regulatory mechanisms at play in the network.

Copper staining of breast cancer samples

Tissue sections were obtained from both cancerous and paracancerous areas of a patient with stage III/IV breast cancer that tested negative for both estrogen receptor (ER) and progesterone receptor (PR). The tissue sections were fixed with 4% formaldehyde (G1101; Servicebio, Wuhan, China) overnight. After dehydration, wax leaching, deparaffinization and rehydration with ethanol and xylene, the slides were stained following the kit manufacturer's instructions for copper stain (M094; Gefanbio, Shanghai, China) followed by hematoxylin stain (G1004-500ML; Servicebio, Wuhan, China). The histological images of the tissue sections were scanned by a digital slide scanner (Pannoramic scan, Hungary). This study was approved by the ethics committee of the Chinese People's Liberation Army (PLA) General Hospital (No. S2016-055).

Statistical analysis

The R version 4.1.3 was used to analyze data. The comparative methods of difference between the groups were applied, including Student's t-test, Wilcoxon test, Kruskal-Wallis, and Log-Rank test for survival analysis. The asterisks symbolized the statistical p value ($^{*}p < 0.05$; $^{**}p < 0.01$; $^{***}p < 0.001$, $^{****}p< 0.0001$).

Results

The pan-cancer expression patterns of the copper-related genes and the pan-cancer immune statement

Based on the Molecular Signatures Database (MsigDB) (15) and the recent cuproptosis literature (9), we selected 42 copper-related genes for analysis (Table S1). The expression of copper-related genes in 14 cancer types was examined and demonstrated by a heatmap (Figure 1A). The stacked bar chart showed differentially expressed copper-related genes in different cancer types (Figure 1B). The Sankey diagram showed the log2 fold change (tumor vs. non-tumor sample) of differentially expressed copper-related genes across different cancer types (Figure 1C). These results demonstrated the dysregulation of copper-related genes in breast cancer and other cancer types. To further identify the immune profile of different types of cancer, we generated the boxplot to compare the immune cells' infiltration profile in tumor samples and their paired non-tumor samples. The boxplot showed the different immune cells statement of tumor samples, demonstrating that the enrichment of naive B cells (Figure 1D), memory B cells (Figure 1E), $CD8^{+}$ T Cells (Figure 1F), activated memory $CD4^{+}$T Cells (Figure 1G), activated NK cells (Figure 1H), M0 macrophages (Figure 1I), M1 macrophages (Figure 1J) and M2 macrophages (Figure 1K) was significantly changed in many cancer types, especially in breast cancer samples.

The expression and genetic variation profile of copper-related genes in breast cancer samples

We analyzed the expression of copper-related genes in breast cancer and non-tumor samples, which verified that breast cancer samples had dysregulation of copper-related genes (Figures 2A, B). The PPI network (Figure 2C) and correlation analysis (Figure 2D) of copper-related genes in breast cancer samples showed the interactions between candidate genes. Genetic variation plays a crucial role in cancer origin and development. Therefore, we analyzed somatic mutations and CNV of copper-related genes in breast cancer samples (Figures 2E, F). According to the variant

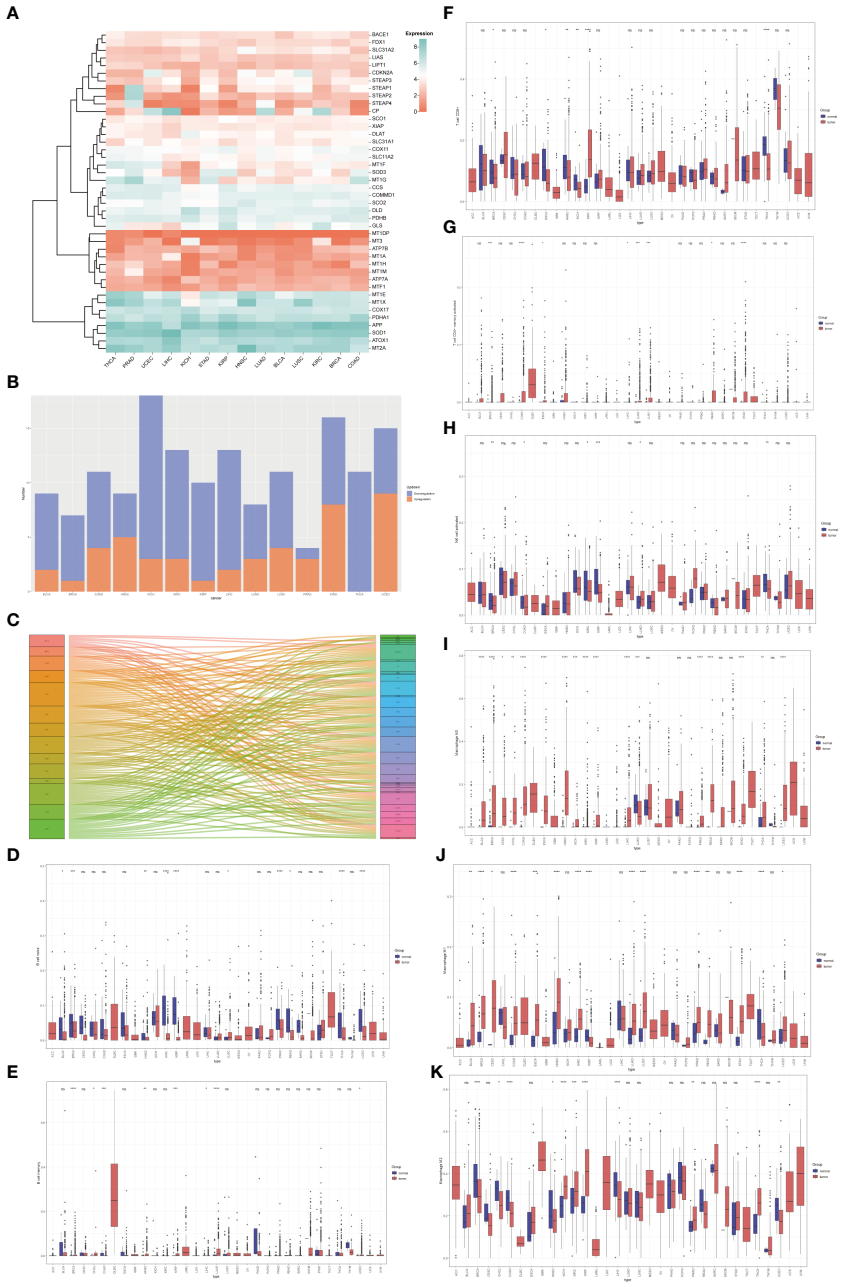

FIGURE 1
The pan-cancer analysis of copper-related genes. **(A)** Heatmap of copper-related genes showed different expression patterns across different types of cancers. **(B)** A stacked bar chart of copper-related genes in different types of cancer samples showed the number of differentially expressed genes. The red and blue colors represented upregulated and downregulated genes, respectively. **(C)** The Sankey diagram of differentially expressed copper-related genes across different cancer types. **(D–K)** Box plot comparison of the abundance of naive B cells **(D)**, memory B cells **(E)**, $CD8^+$ T Cells **(F)**, memory $CD4^+$ T cells **(G)**, activated NK cells **(H)**, M0 macrophages **(I)**, M1 macrophages **(J)**, and M2 macrophages **(K)** in different types of cancers compared with paired non-tumor samples. (*$p < 0.05$; **$p < 0.01$; ***$p < 0.001$, ****$p < 0.0001$,NS: no significance).

classification, the most prevalent variant, variant type and single nucleotide variant (SNV) were missense mutations, single-nucleotide polymorphisms (SNPs), and the C > T mutation, respectively. In breast cancer samples, ATP7A (18%), amyloid beta precursor protein (APP) (11%) and ATP7B (9%) were the more frequently mutated genes. Cuproptosis genes, such as dihydrolipoamide dehydrogenase (DLD) (2%) and dihydrolipoamide s-acetyltransferase (DLAT) (2%), were also among the top ten mutated genes.

Construction of the breast cancer's survival prediction model by copper-related genes

To predict the breast cancer survival pattern by a prognostic gene set, we utilized univariate and multivariate Cox regression analysis to plot the association between the expression of copper-related genes and the OS of breast cancer patients (Figures 3A, B and Table S2). Then, we built the LASSO-Cox model using univariate Cox regression

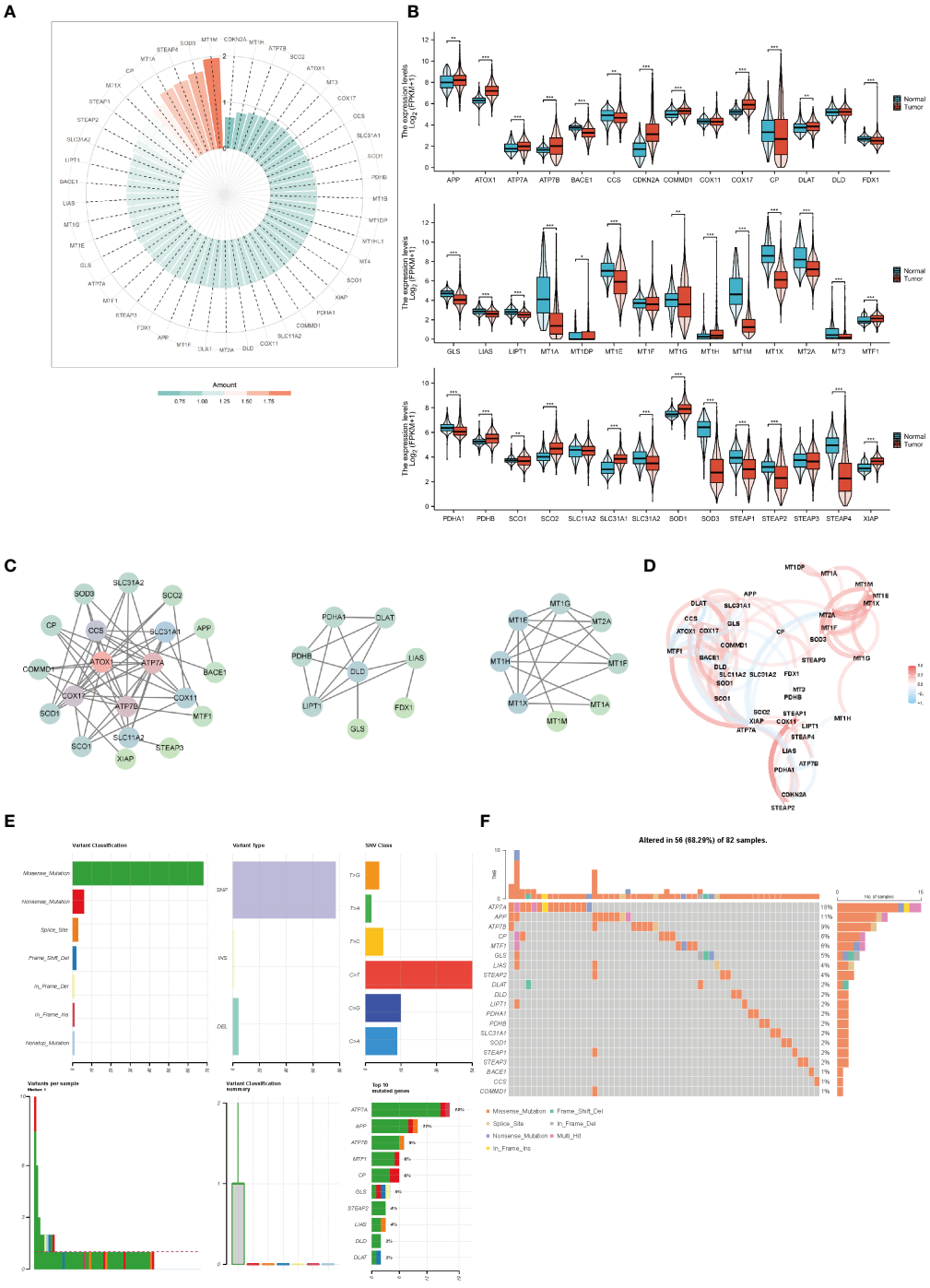

FIGURE 2
The expression and genetic variation of copper-related genes in breast cancer samples. Heatmap **(A)** and box plots **(B)** of differentially expressed copper-related genes in breast cancer samples. **(C)** PPI network of copper-related genes. **(D)** Correlation of copper-related genes in breast cancer samples. CNV, mutation frequency **(E)** and classification **(F)** of copper-related genes in breast cancer samples. (*$p < 0.05$; **$p < 0.01$; ***$p < 0.001$).

genes (p value <0.1) to select the best candidate genes for constructing a survival prediction model of breast cancer patients (Figure 3C). Eventually, 21 candidate gene signatures emerged with the optimal log λ value of the LASSO-Cox model. We selected DLAT and ATP7B as the signature genes to construct the prediction model based on OS outcomes using regression coefficients. Risk score= 0.6664 x DLAT - 0.1985 x ATP7B.

Prediction of breast cancer survival rates by gene expression of ATP7B and DLAT

We confirmed the predictive performance of the prognostic gene set using the TCGA-BRCA dataset (Figures 4A, C, E) and a validating dataset (Figures 4B, D, F). Figures 4A, B presented Kaplan-Meier plot of the two risk groups' OS in the training and validating dataset. We then further demonstrated the risk score distribution plot and expression of

ATP7B and DLAT in breast cancer samples (Figures 4C, D). The survival plots indicated that the high- copper related genes scoring group had poor survival. For ease of description, we define the high- and low-copper related genes scoring groups as high- and low-scoring groups. Time-dependent ROC curves were constructed to evaluate the predictive model's efficacy. At the 1-, 3-, and 5-year time points, the TCGA-BRCA dataset's area under curves (AUCs) were 0.617, 0.623, and 0.597, respectively (Figure 4E). As for the validating breast cancer dataset (GSE96058), the areas under the time-dependent ROC curve were 0.738, 0.623 and 0.595 at the 1-, 3- and 5-year time points (Figure 4F).

Comparison of the immune cells' infiltration profile of the high- and low-scoring groups

Immune infiltrates were increasingly considered responsible for influencing the prognosis and clinical outcome of breast cancer patients (32). Therefore, we compared the profile of tumor-infiltrating immune cells between the high- and low-scoring groups based on copper-related genes by heatmap (Figure 5A) and box plot (Figure 5B). The low-scoring group had more naive B cells, M2 macrophages, resting mast cells, monocytes, and $CD8^+$ T cells than the high-scoring group, while the high-scoring group had more activated dendritic cells, M0 macrophages, M1 macrophages and follicular helper T cells. The histogram (Figure 5C) and box plot (Figure 5D) displayed the composition of different immune cells in breast cancer samples. In order to further estimate the immune statement of the two subgroups, four immune state indicators, including the Immune score (Figure 5E), ESTIMATE score (Figure 5F), stromal score (Figure 5G) and tumor purity (Figure 5H) were plotted. The result showed that the low-scoring group had a higher ESTIMATE score and stromal score and lower tumor purity. To assess the likelihood of immune evasion in tumors, we used TIDE to compare the gene expression profiles of

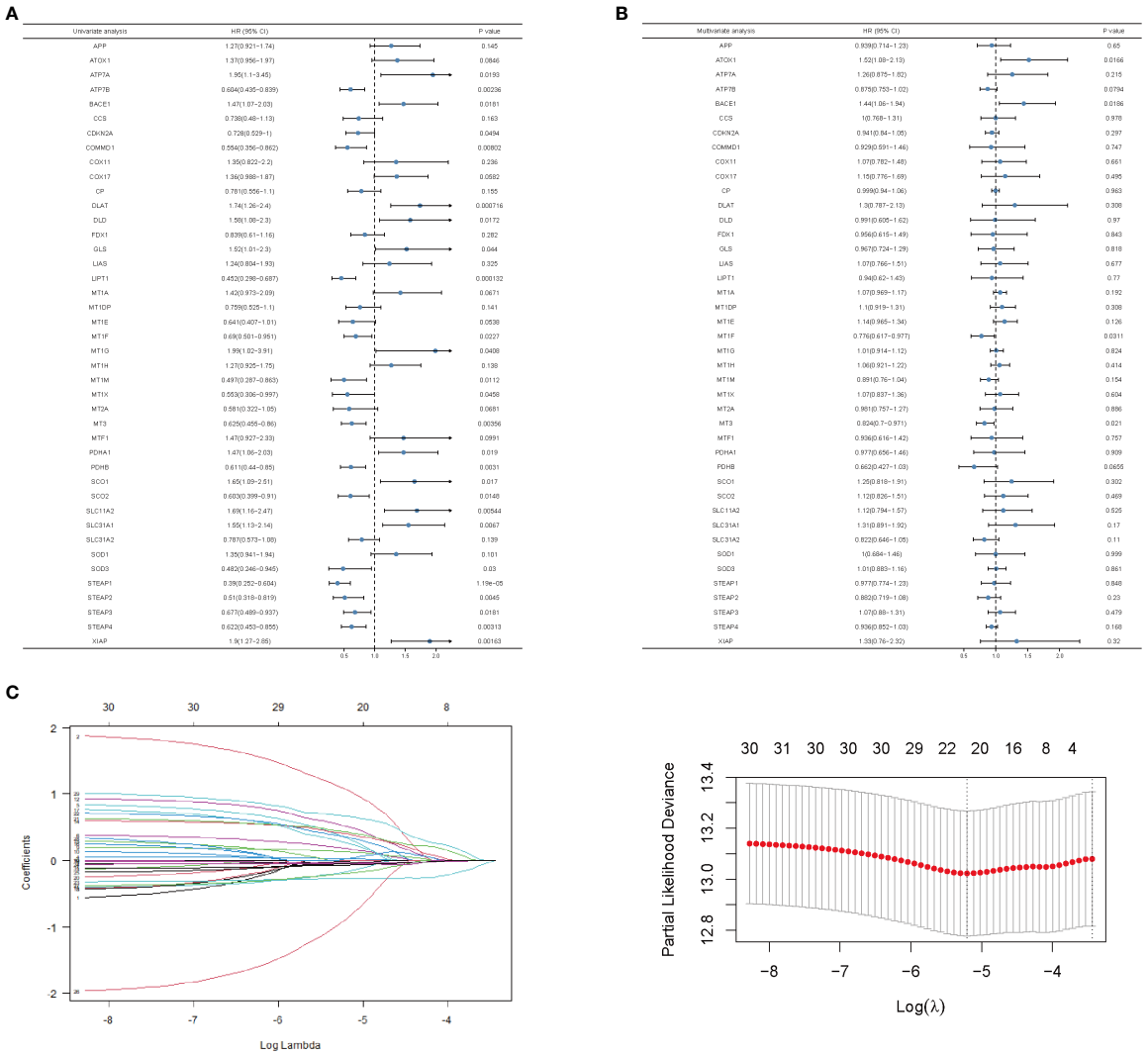

FIGURE 3
Univariate and multivariate analysis and LASSO-Cox regression of copper-related genes in breast cancer samples. Univariate **(A)**- and multivariate **(B)**-analysis of copper-related genes in breast cancer samples. **(C)** LASSO-Cox regression was built up from copper-related genes, based on which we selected optimal genes by the cross-validation method.

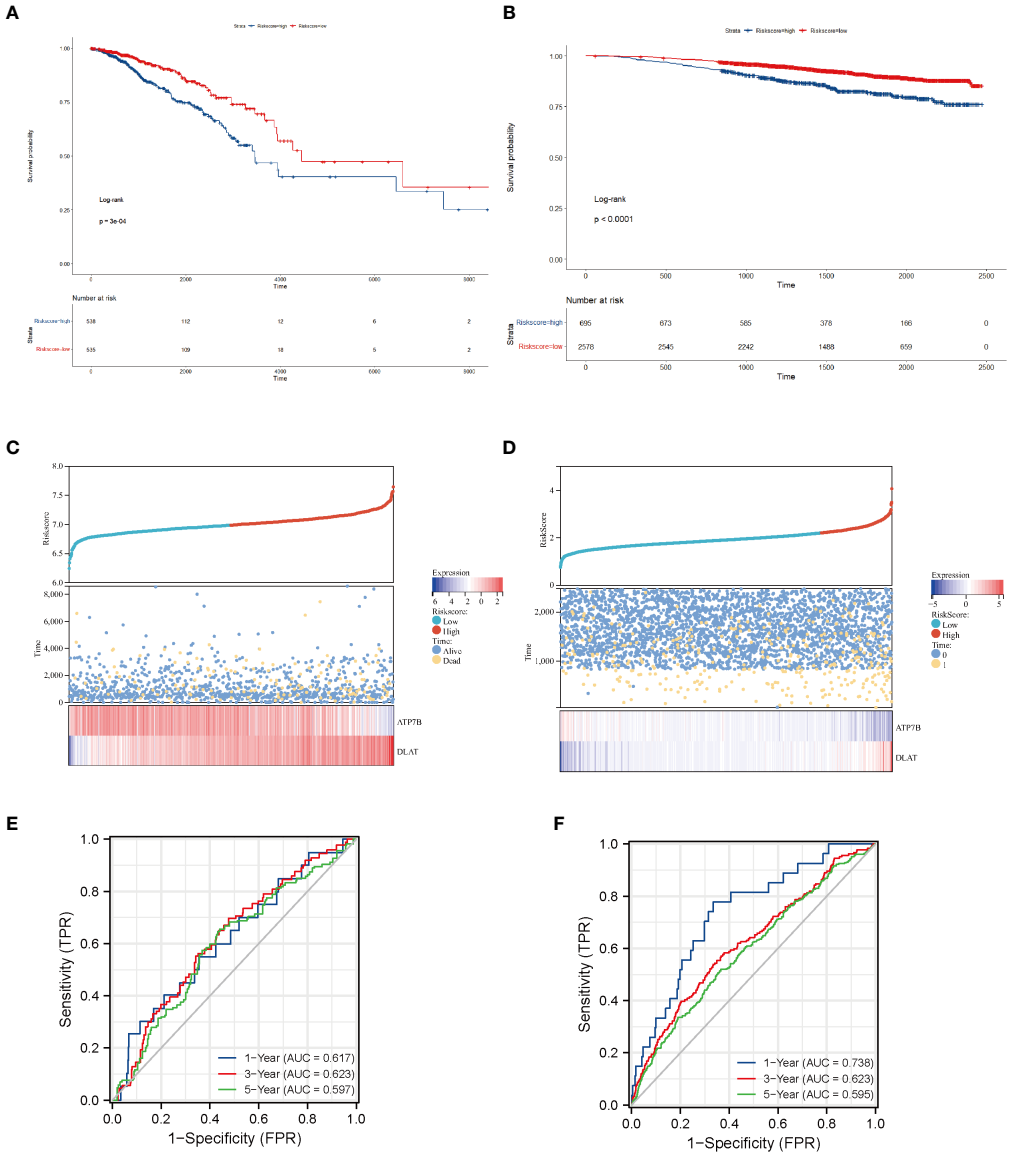

FIGURE 4
Survival analysis of breast cancer patients stratified by the risk score of copper-related genes. The Kaplan–Meier curves of TCGA-BRCA samples **(A)** and a validating dataset GSE96058 **(B)** grouped based on the risk score of copper-related genes at the best cut-off point. The statistical method is the Log-rank test. The low-scoring group had a better survival probability in both TCGA-BRCA samples and GSE96058 samples. The dot and line diagram of risk score, state of survival and expression of ATP7B and DLAT from TCGA-BRCA samples **(C)** and a validating dataset GSE96058 **(D)**. Time-dependent ROC curve of the constructed model of TCGA-BRCA samples **(E)** and the validating dataset **(F)**.

the high- and low-scoring groups (33). The box plot of Tide, MSI, Exclusion, and Dysfunction (Figures 5I–L) also demonstrated that the low-scoring group had lower TIDE, Exclusion and MSI than those of the high-scoring group.

Metabolic features of the high- and low-scoring groups

Cancer cells have a unique metabolic alteration known as aerobic glycolysis, in which glucose is preferentially converted to lactate even when oxygen is available (34). This phenomenon is in contrast to the typical cellular metabolism of non-malignant cells. GSEA demonstrated that breast cancer patients with lower scores for copper-related genes were more likely to have enrichment in pathways related to pyruvate metabolism and apoptosis (Figures 6A, B).

Tumor protein P53 (TP53), a crucial regulator of the Warburg effect, may influence glycolysis by reducing pyruvate dehydrogenase kinase-2 (Pdk2) expression, which results in the production of acetyl-CoA rather than lactate (35). We identified that the low-scoring group had a higher level of TP53 than the high-scoring group (Figure 6C). The pyruvate dehydrogenase (PDH) complex, which converts pyruvate

10.3389/fimmu.2023.1145080

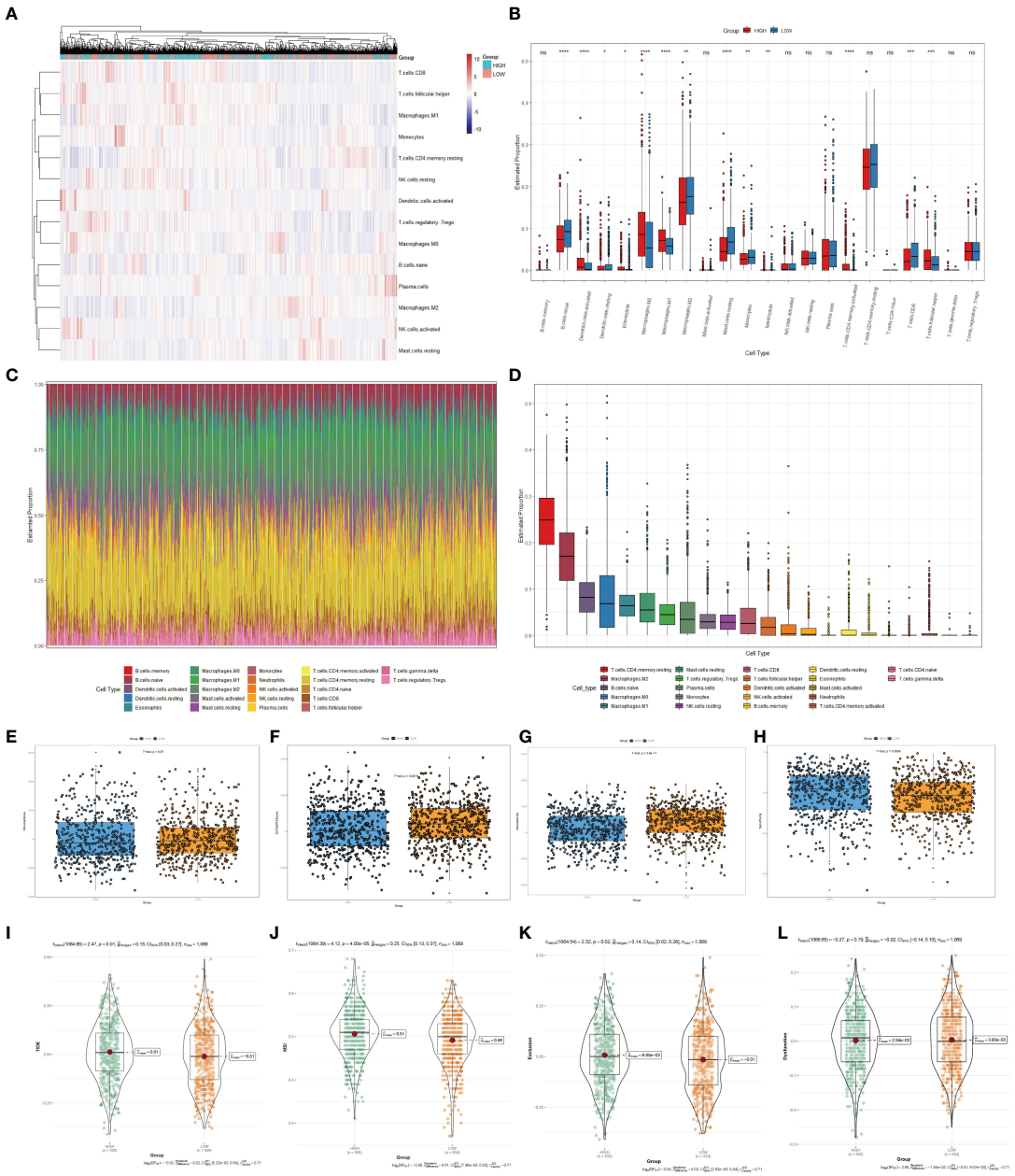

FIGURE 5
Immune cells infiltration analysis of the high- and low-scoring groups. Heatmap **(A)** and box plot **(B)** of immune cell abundance in breast cancer samples. **(C)** Histogram of the proportion of immune cells in each sample. **(D)** Box plot of the proportion of different immune cells (*$p < 0.05$; **$p < 0.01$; ***$p < 0.001$, ****$p < 0.0001$). Box plots of the immune score (p=0.67) **(E)**, ESTIMATE score ($p < 0.01$) **(F)**, stromal score (p<0.0001) **(G)** and tumor purity ($p < 0.01$) **(H)** of the high- and low-scoring groups were calculated by ESTIMATE algorithm. Violin plots of Tide (p=0.01) **(I)**, MSI (p <0.0001) **(J)**, Exclusion (p =0.02) **(K)**, and Dysfunction (p =0.79) **(L)** of the high- and low-scoring groups were calculated by TIDE algorithm. (NS: no significance).

to acetyl-CoA, controls pyruvate entering the citric acid cycle or participating in glycolysis. Pyruvate kinase M1/2 (PKM) converts phosphoenolpyruvate to pyruvate and can inhibit the expansion and metastasis of triple-negative breast cancer cells (36). We observed that the low-scoring group had a higher level of pyruvate dehydrogenase E1 subunit beta (PDHB) and PKM, which tends to produce pyruvate rather than lactate (Figure 6C). This result has revealed that the low-scoring group tended to rely on pyruvate metabolism for energy supply. Hypoxia inducible factor 1 subunit alpha (HIF1A) and the lactate transporter solute carrier family 16 member 1(SLC16A1) also regulate aerobic glycolysis in cancer metabolism, whose high expressions are correlated with poor clinical outcomes in breast cancer patients (37, 38). Pyruvate dehydrogenase kinase 1 (PDK1), a target of HIF1A, could prevent pyruvate from entering into the tricarboxylic acid cycle (TCA cycle) (39). The expression of

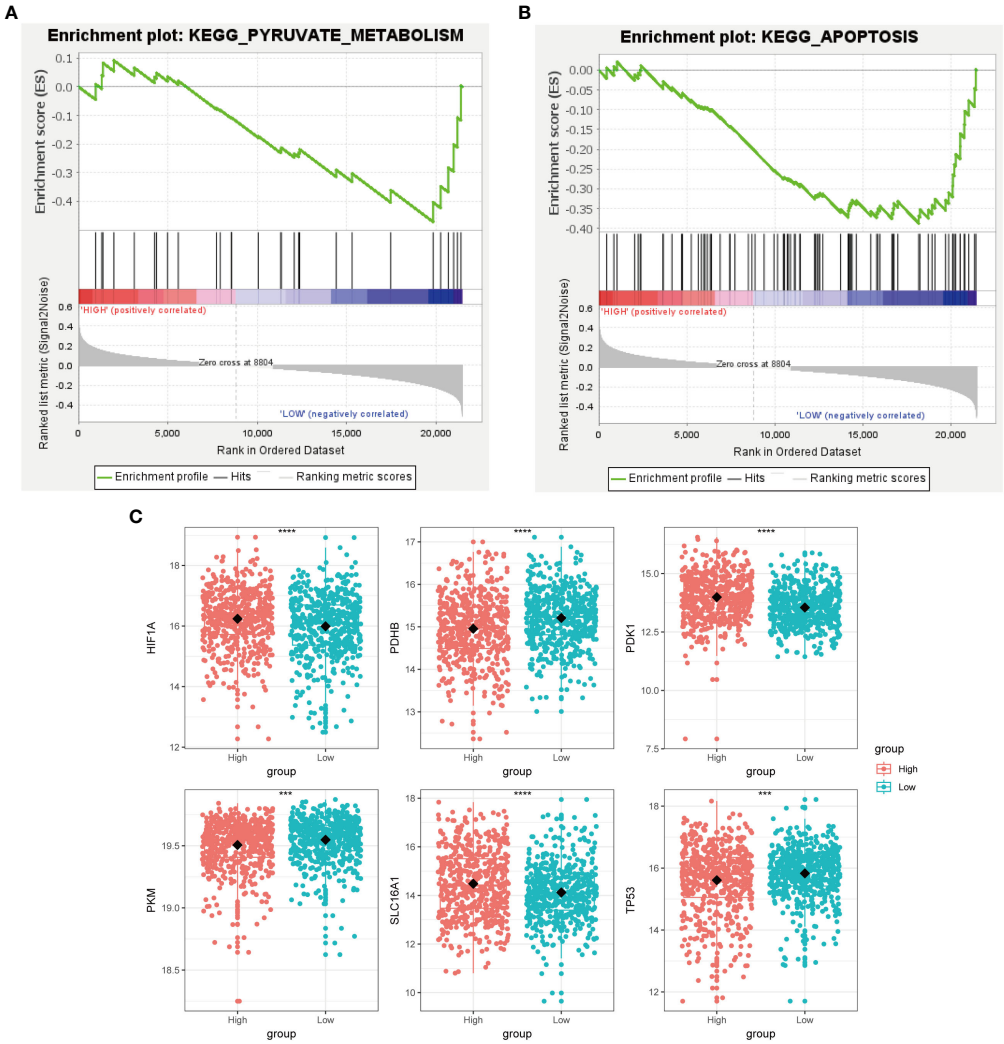

FIGURE 6
Metabolic characterization of breast cancer samples stratified by the high- and low-scoring groups. GSEA enrichment plot of regulation of autophagy **(A)** and pyruvate metabolism **(B)** of the low-scoring group. **(C)** Boxplot showed that glycolysis-related genes, including HIF1A, PDHB, PDK1, PKM, SLC16A1, and TP53, had a differential expression pattern among the high- and low-scoring groups. (****p < 0.001, ****p< 0.0001*).

HIF1A, SLC16A1 and PDK1 was increased in the high-scoring group (Figure 6C), suggesting its glycolysis metabolic feature.

Treatment prognosis of the high- and low-scoring groups

We predict breast cancer patients' drug response using "oncoPredict". The lower sensitivity score represented a more sensitive clinical response. Drugs with lower drug sensitivity scores in the low-scoring group were selected using the t-test ($p < 0.05$). These selected drugs are Nilotinib, Nutlin 3A, RO 3306, AZD8055, PF4708671, Niraparib, GSK269962A, Fulvestrant, Temozolomide, Ruxolitinib, LCL161, IWP_2, Ribociclib, Fludarabine, Nelarabine, GSK2578215A, MIM1, LJI30 and BMS_754807 (Figures 7A–S). The low-scoring group had lower drug sensitivity scores than the high-scoring group, indicating that individuals in the low-scoring group responded better to the above-indicated chemotherapy drugs.

ATP7B- and DLAT-related functional networks in breast cancer

To reveal additional links to the biological function of ATP7B and DLAT in breast cancer development, we utilized the functional module of LinkedOmics to analyze genes that were positively or negatively correlated with ATP7B and DLAT (Figures 8A–C, E–G). Additionally, we performed an enrichment analysis on the association results (Figures 8D, H). ATP7B and its associated genes were enriched in the cell cycle pathway (*FDR* ≤ 0.05). DLAT and its associated genes were enriched in the cell cycle, oxidative phosphorylation and DNA replication pathways (*FDR* ≤ 0.05). The result of this study suggested that the two feature genes may contribute to the development of breast

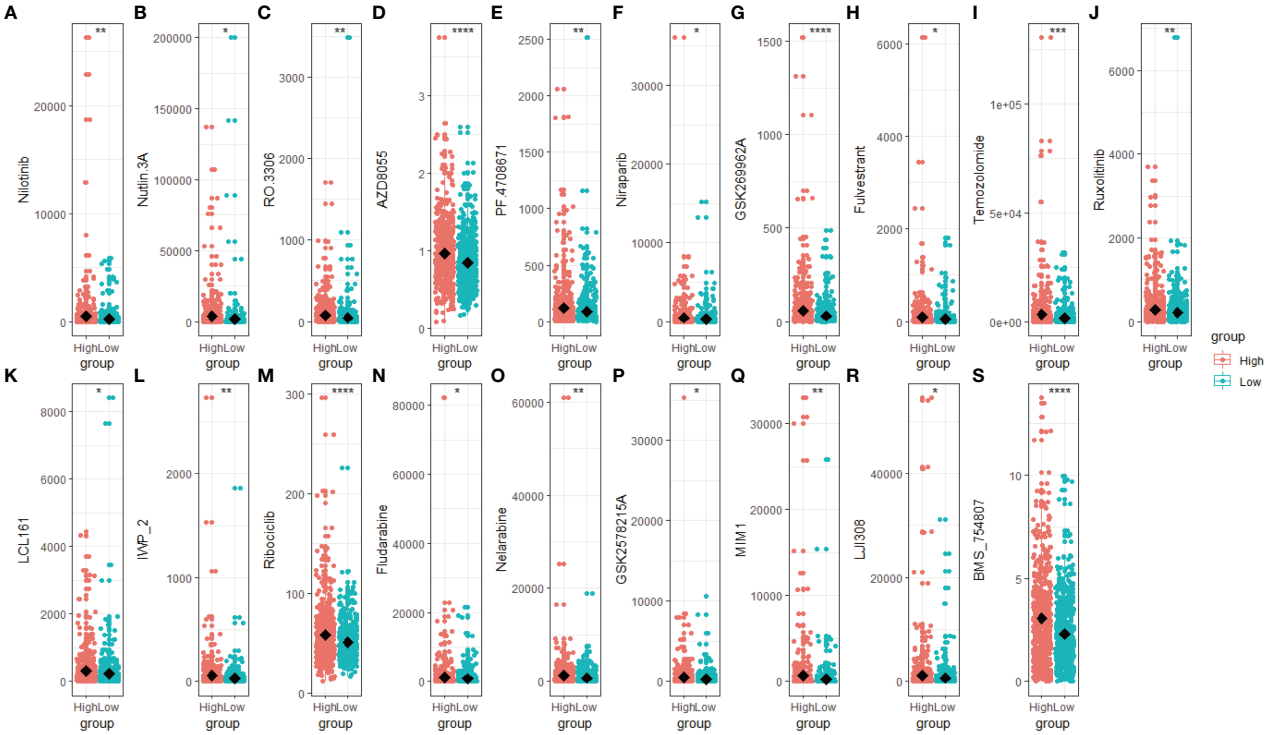

FIGURE 7
Drug sensitivity score of the high- and low-scoring groups. Box plot of the drug sensitivity score of Nilotinib **(A)**, Nutlin 3A **(B)**, RO 3306 **(C)**, AZD8055 **(D)**, PF4708671 **(E)**, Niraparib **(F)**, GSK269962A **(G)**, Fulvestrant **(H)**, Temozolomide **(I)**, Ruxolitinib **(J)**, LCL161 **(K)**, IWP_2 **(L)**, Ribociclib **(M)**, Fludarabine **(N)**, Nelarabine **(O)**, GSK2578215A **(P)**, MIM1 **(Q)**, LJI308 **(R)** and BMS_754807 **(S)**. The drug sensitivity score was predicted based on the R package "oncoPredict", with a lower score representing a better clinical response. (*$p < 0.05$; **$p < 0.01$; ***$p < 0.001$, ****$p < 0.0001$).

cancer by impacting cell growth and energy metabolism, potentially in collaboration with their co-expressed genes.

Dysregulation of ATP7B and DLAT proteins in breast cancer

According to the HPA database (http://www.proteinatlas.org) (40), the high staining intensity of ATP7B and DLAT in breast cancer tissues is in contrast to those lowly stained in normal tissues as indicated by the immunohistochemical analyses (Figures 9A, B). HPAanalyze, a visualization R package, presented the expression of ATP7B and DLAT proteins in myoepithelial and glandular cells in breast cancer tissue using a heatmap (41) (Figure 9C). The IHC staining intensity of ATP7B and DLAT is shown in Figure 9D, and the subcellular locations of ATP7B (Golgi apparatus) and DLAT (mitochondria) are also indicated (Figure 9E).

The expression profile and OS statement of different breast cancer subtypes

We obtained the subtype information of TCGA samples from XENA (42), based on which we grouped the primary breast cancers samples into five subtypes using the Prediction Analysis of Microarray 50 (PAM50) model, including luminal A, luminal B, normal-like, HER2-enriched and basal-like subtypes (43). The heatmap showed that copper-related genes had a differential expression pattern among breast cancer subtypes, indicating a potential role of copper in the heterogeneity of breast cancer (Figure 10A). Intriguingly, the expression of ATP7B and DLAT were decreased and increased respectively in the basal-like subtype compared with non-cancerous samples, which is opposite to those in other breast cancer subtypes. In addition to differences in copper-related gene expression, the survival status of breast cancer subtypes differed. The Kaplan–Meier curves of different breast cancer subtypes showed that the basal-like subtype had a worse survival probability than the luminal A- and luminal B-subtypes in the early stage (Figure 10B). We then used copper-related gene risk score to assess our predictive model in different subtypes. According to the survival curves, patients with basal-like subtype (Figure 10D) and triple-negative breast cancers (TNBC) (Figure 10G) present better survival in the high-scoring group and worse survival in the low-scoring group, in contrast to other subtypes (Figures 10C, E, F). This result suggests that the basal-like and TNBC patients had a unique copper-related genes profile among breast cancer subtypes.

Copper staining of clinicopathological sections of breast cancer

According to literature reports, breast cancer patients have higher tissue and serum copper levels than normal subjects (44,

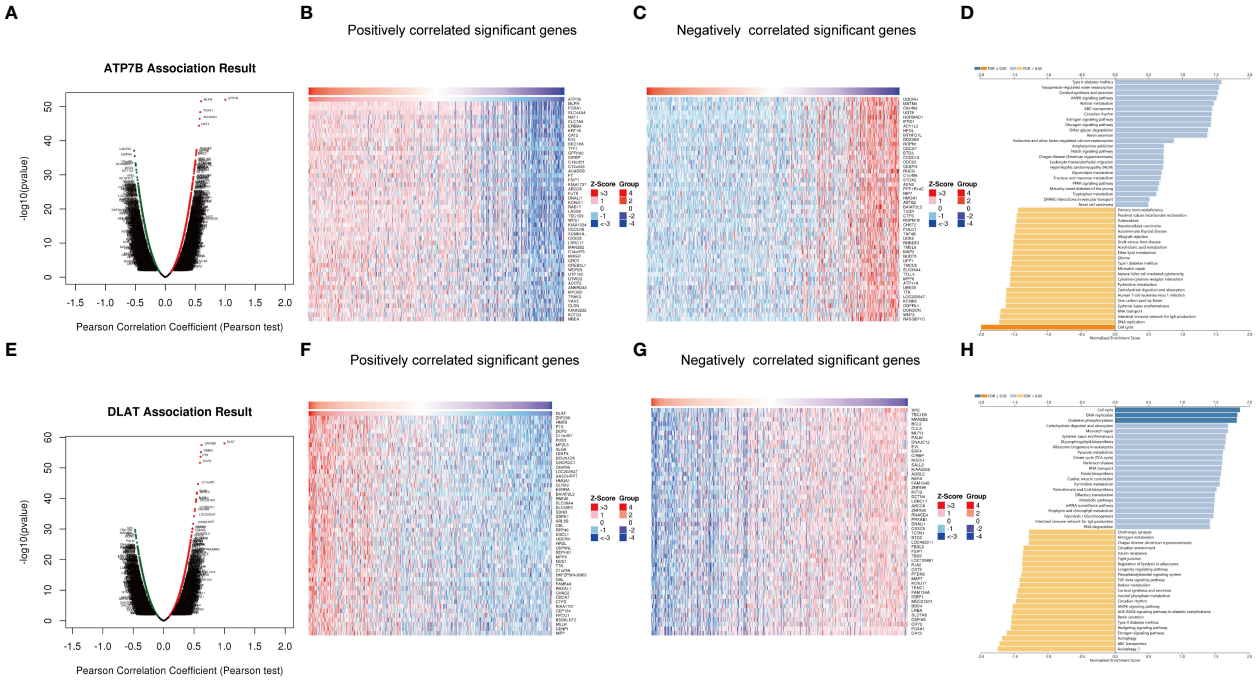

FIGURE 8
Genes co-expressed with ATP7B **(A–D)** and DLAT **(E–H)** in breast cancer. Volcano Plot showed genes associated with ATP7B **(A)** and DLAT **(E)** in breast cancer samples analyzed by LinkedOmics. Heatmap showed the positively correlated genes with ATP7B **(B)** and DLAT **(F)** and the negatively correlated genes with ATP7B **(C)** and DLAT **(G)** in breast cancer samples. The bar plot showed the GSEA results of genes associated with ATP7B **(D)** and DLAT **(H)**.

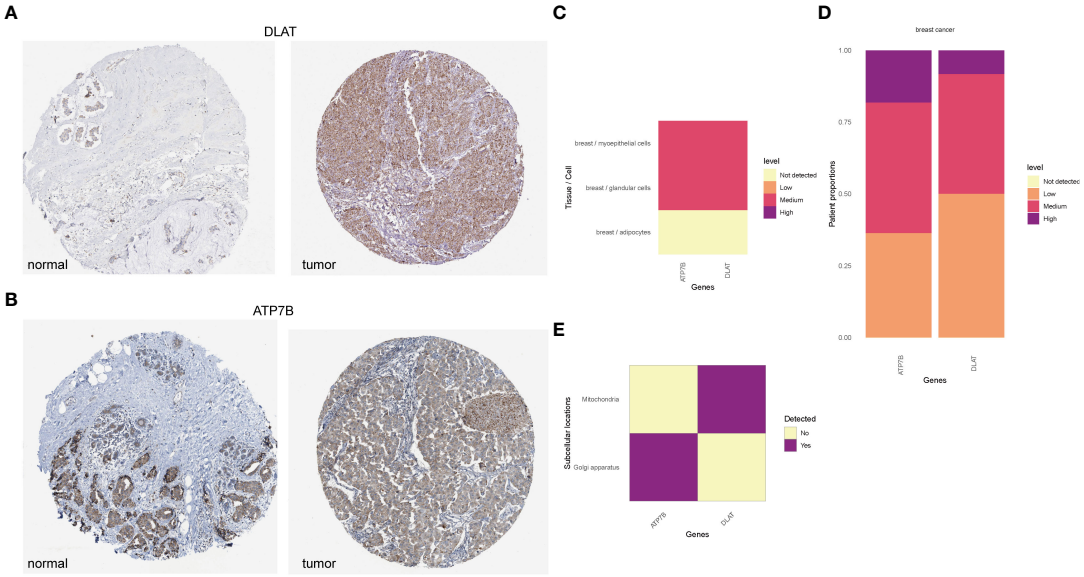

FIGURE 9
The protein expression of ATP7B and DLAT in BRCA tissues compared with non-tumor tissues in the HPA database. The protein expression of ATP7B **(A)** and DLAT **(B)** in breast cancer and normal tissues in the HPA database (http://www.proteinatlas.org) (40). **(C)** The expression of ATP7B and DLAT plotted according to cell types. **(D)** Column graphs showed the expression of ATP7B and DLAT in breast cancer samples. The subcellular localization of ATP7B and DLAT **(C–E)** was visualized by the R package "HPAanalyze" (41).

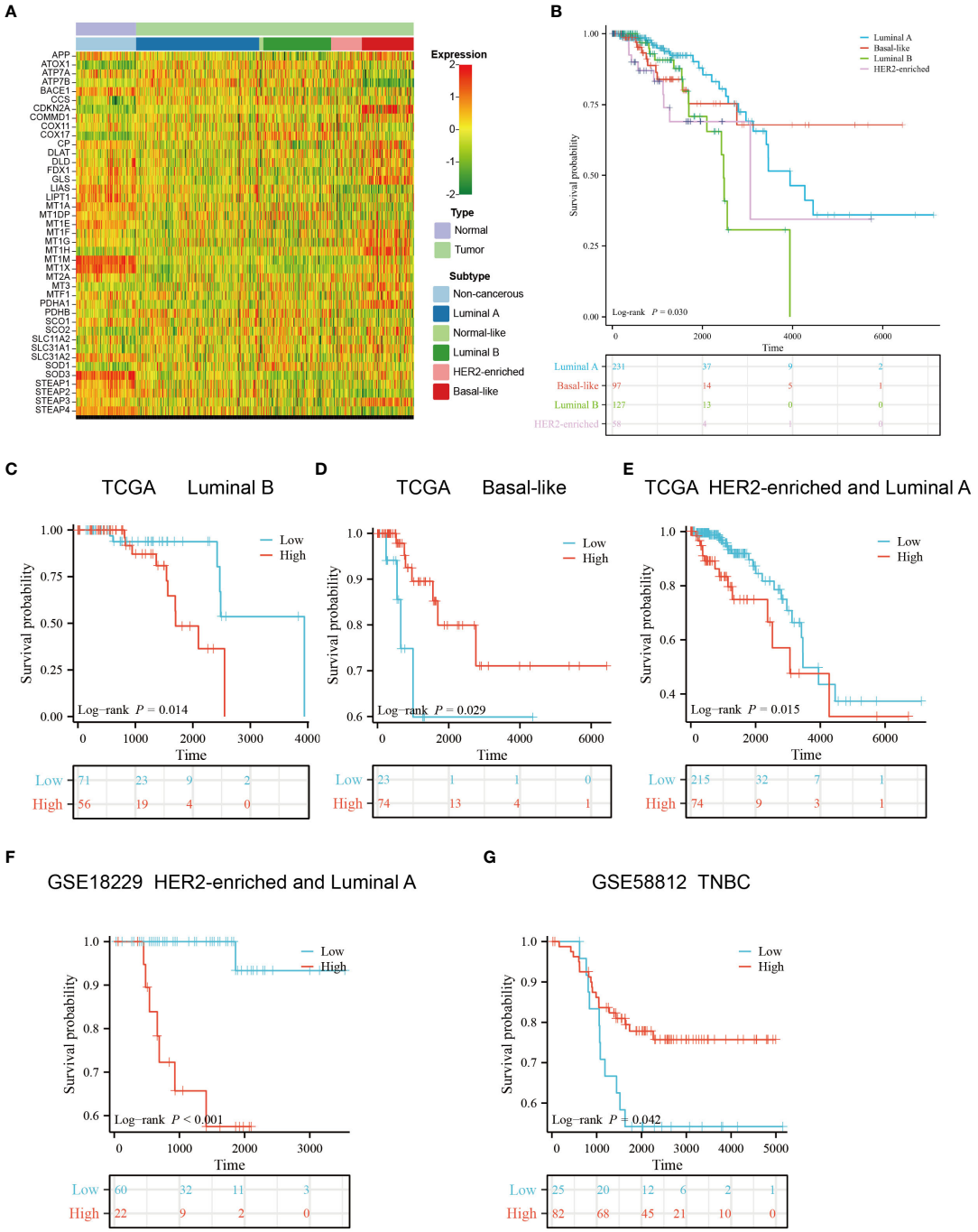

FIGURE 10
Gene expression profile and survival analysis of different subtypes of breast cancer stratified by the risk score of copper-related genes. **(A)** The gene expression heatmap of different subtypes of breast cancer. The subtype information was obtained from Xena. **(B)** The Kaplan–Meier curves of luminal A, luminal B, HER2-enriched and basal-like breast cancer patients. The Kaplan–Meier curves of luminal B **(C)**, basal-like **(D)**, luminal A and HER2-enriched patients **(E)** from TCGA. **(F)** The Kaplan–Meier curves of luminal A and HER2-enriched patients from GSE18229. **(G)** The Kaplan–Meier curves of Triple-negative breast cancers (TNBC) patients from GSE58812. The group was stratified based on the risk score of copper-related genes at the best cut-off point.

45). We performed Timms copper staining on the paraffin section of breast cancer patient to evaluate copper content and distribution in their tumor tissue. In the breast cancer sample, copper particles were found in the cytoplasm and nucleus of the breast cancer cells (Figures 11A, B). The paired paracancerous tissue did not yield a positive copper stain result (Figures 11C, D).

Discussion

Breast cancer patients have been reported to exhibit higher serum and tissue content of copper, with even higher serum copper levels observed in patients non-responsive to chemotherapy (46–48). The amount of copper-containing cells was positively

correlated with tumor growth rate (49). These results suggest that copper levels may indicate breast cancer progression and chemotherapy effectiveness in breast cancer patients. We found that copper particles in the clinical breast cancer sample were located in the cytoplasm and nucleus of the cancer cells (Figures 11A, B), which might be associated with the function of copper in promoting breast cancer metastasis. Several preclinical studies have found that reducing copper levels could inhibit tumor growth, angiogenesis and metastasis (50–52). Clinical trials using tetrathiomolybdate to deplete copper levels have enhanced event-free survival in breast cancer patients. Additionally, preclinical models have shown that tetrathiomolybdate could reduce breast cancer metastases to the lungs (53, 54). However, there is still a lack of elucidation on how copper content may influence breast cancer progression. Intriguingly, cuproptosis has been recently reported to mediate copper's effect on cell death and cancer development. In breast cancer models, overloading copper by copper ionophores could inhibit tumor growth (55–57). These seemingly opposite conclusions prompted us to investigate the exact function of copper homeostasis in breast cancer development.

We constructed a copper-related gene scoring system using LASSO-Cox regression based on cuproptosis and copper metabolism genes to recognize the essential copper-related genes (Figure 3C). Two essential copper-related genes, ATP7B and DLAT, were selected to construct the scoring model to predict breast cancer patient survival. The higher AUCs of this model indicated advanced predictive performance (Figure 4). ATP7B, a P-type ATPase involved in copper secretion, played a pivotal role as a copper transporter, whose mutation caused Wilson's disease due to excess copper accumulation-induced chronic liver diseases (58). DLAT, which is subjected to lipoylation modification, mediates the entry of carbon into the tricarboxylic acid cycle. Aggregation of lipoylated DLAT and reduction of iron-sulfur cluster proteins can be induced by copper ions, which results in proteotoxic stress and cell death (59). ATP7B and DLAT are both mutated in breast cancer samples, with the most common mutation being missense mutation (Figures 2E–F). Besides, we wonder what critical role ATP7B and DLAT played in breast cancer, given that these genes are essential for copper homeostasis and cuproptosis. The associated genes of ATP7B and DLAT genes are enriched in the cell cycle, oxidative phosphorylation, and DNA replication pathways (Figures 8A–H), suggesting that these two genes and their associated genes might influence breast cancer development by regulating the pathways mentioned above. Aerobic glycolysis, also known as the Warburg effect, is a characteristic metabolic process that is commonly observed in cancer cells (60). Many types of tumors limit the pyruvate oxidation process to meet the needs of the highly proliferative tumor cells (61). The low-scoring group is enriched in the pyruvate metabolism pathway (Figure 6A), suggesting that the low-scoring group might have an altered metabolic profile which is difficult to sustain the infinite growth of malignant cells. Breast cancer is heterogeneous in genetic and biological features (62). Generally, luminal A breast cancer had a better prognosis. Compared with the luminal A subtype, the luminal B-and HER2-enriched tumors present higher recurrence rates and worse survival (63, 64). The basal-like breast cancer is associated with poor prognosis, early relapses, and the highest locoregional recurrence among all subtypes (65, 66). Interestingly, basal-like patients had a unique expression and survival probability than other subtypes (Figure 10). The expression of ATP7B and SLC31A1 were decreased and increased, respectively, in the basal-like subtype patients (Figure 10A), suggesting that patients with the basal-like subtype of breast cancer may have different levels of copper in their tumor tissues compared with those with other breast cancer subtypes. This result might provide a comprehensive understanding of copper in different breast cancer subtypes.

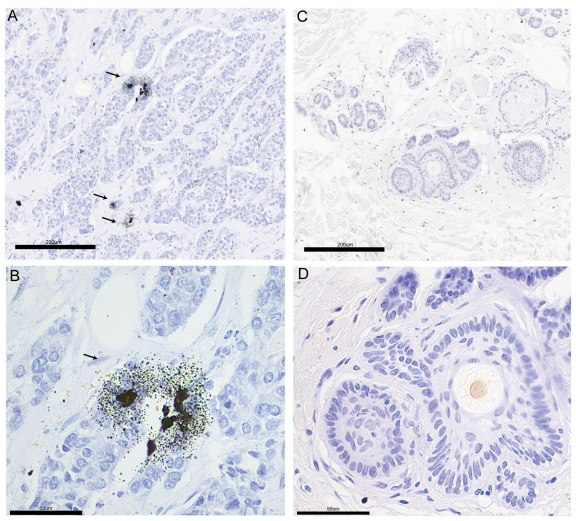

FIGURE 11
The copper stain of BRCA patients' paraffin section using Timm's method. Copper staining of the pathological section of breast cancer (**A**: 20x, **B**: 40x) and paired paracancerous (**C**: 20x, **D**: 40x) sample. The copper-positive areas contain small black granules. Coarse granules indicated intense copper deposition. The arrows indicate the distribution of copper in pathological sections.

Previous studies mainly focused on the relationship between cuproptosis-related genes and breast cancer (67, 68). Our study included not only cuproptosis-related genes but also copper metabolism-related genes to perform a comprehensive analysis of the role of copper-related genes in breast cancer development. Our results showed that the low-scoring group had lower expression of the copper importer SLC31A1 and higher expression of the copper exporter ATP7B (Figures S1A, B), which may altogether reduce intracellular copper content. The low-scoring group with less copper content appeared to have better survival outcomes and immune profiles. Combined with the evidence that copper chelators inhibited breast cancer metastasis, it is possible that reducing copper levels rather than increasing them is an effective way to improve breast cancer outcomes, which needs more experimental evidence for validation.

The composition of immune cells influences cancer progression. Evidence suggests that B cells are anti-tumor through various mechanisms, such as improving cytotoxic T cell activity and activating antibody dependence (69, 70). Activated $CD8^+$ T lymphocytes are anti-tumor with cytotoxic molecules and have been reported to correlate with favorable prognosis in triple-negative breast cancer patients (71). In our result, the low-scoring group had more naive B cells and $CD8^+$ T cells compared with the high-scoring group

(Figure 5B), indicating better immune response in the low-scoring group. Additionally, because the copper chelate could reprogram and enhance the anti-tumor reaction of T cells (72), eliminating copper might be helpful for the anti-tumor response of breast cancer.

Based on the R package "oncoPredict", we predict novel chemotherapy drugs which might be helpful for the low-scoring group's breast cancer treatment. The low-scoring group seemed to be more responsive to chemotherapy drugs (Figure 7) which have been reported to suppress the metastasis or growth of breast cancer cells and overcome tamoxifen resistance by targeting essential regulators such as discoidin domain receptor 1, mTORC1/2, PARP-1/2, JAK1/2, and CDK1 (73–82). In the future, utilizing these newly developed chemotherapy drugs to treat breast cancer may be possible after conducting appropriate screening and classification and providing clinical guidance.

In summary, our study provided a novel prognostic signature to predict breast cancer development, which revealed the association of copper-related gene expression with immune cell infiltration, cancer metabolic feature, and drug response. These results may assist in the clinical management of breast cancer.

Data availability statement

The original contributions presented in the study are included in the article/Supplementary Material. Further inquiries can be directed to the corresponding author.

Ethics statement

The studies involving human participants were reviewed and approved by the multicenter clinical study on screening genetic mutation hotspots in Chinese breast cancer patients, Chinese PLA General Hospital. The patients/participants provided their written informed consent to participate in this study.

Author contributions

MJ designed the study. YL and JW did data collection and analysis. YL and MJ wrote the manuscript. All authors contributed to the article and approved the submitted version.

Funding

This work was funded by the Beijing Municipal Natural Science Foundation Grant 7212148 (to MJ), the National Natural Science Foundation of China Grant 82000807 (to MJ), and the R&D Program of Beijing Municipal Education Commission Grant KM202110025023 (to MJ).

Conflict of interest

The authors declare that the research was conducted in the absence of any commercial or financial relationships that could be construed as a potential conflict of interest.

Publisher's note

Supplementary material

The Supplementary Material for this article can be found online at: https://www.frontiersin.org/articles/10.3389/fimmu.2023.1145080/full#supplementary-material

References

1. Lei S, Zheng R, Zhang S, Wang S, Chen R, Sun K, et al. Global patterns of breast cancer incidence and mortality: a population-based cancer registry data analysis from 2000 to 2020. *Cancer Commun* (2021) 41(11):1183–94. doi: 10.1002/cac2.12207

2. Cao W, Chen H-D, Yu Y-W, Li N, Chen W-Q, Ni J. Changing profiles of cancer burden worldwide and in China: a secondary analysis of the global cancer statistics 2020. *Chin Med J* (2021) 134(07):783–91. doi: 10.1097/CM9.0000000000001474

3. Trayes KP, Cokenakes SEH. Breast cancer treatment. *Am Fam Physician* (2021) 104(2):171–8.

4. Zischka H, Einer C. Mitochondrial copper homeostasis and its derailment in Wilson disease. *Int J Biochem Cell Biol* (2018) 102:71–5. doi: 10.1016/j.biocel.2018.07.001

5. Garza NM, Swaminathan AB, Maremanda KP, Zulkifli M, Gohil VM. Mitochondrial copper in human genetic disorders. *Trends Endocrinol Metab* (2023) 34(1):21–33. doi: 10.1016/j.tem.2022.11.001

6. Li Y. Copper homeostasis: emerging target for cancer treatment. *IUBMB Life* (2020) 72(9):1900–8. doi: 10.1002/iub.2341

7. Wang F, Jiao P, Qi M, Frezza M, Dou QP, Yan B. Turning tumor-promoting copper into an anti-cancer weapon *via* high-throughput chemistry. *Curr medicinal Chem* (2010) 17(25):2685–98. doi: 10.2174/092986710791859315

8. Liu YL, Bager CL, Willumsen N, Ramchandani D, Kornhauser N, Ling L, et al. Tetrathiomolybdate (TM)-associated copper depletion influences collagen remodeling and immune response in the pre-metastatic niche of breast cancer. *NPJ Breast Cancer* (2021) 7(1):108. doi: 10.1038/s41523-021-00313-w

9. Tsvetkov P, Coy S, Petrova B, Dreishpoon M, Verma A, Abdusamad M, et al. Copper induces cell death by targeting lipoylated TCA cycle proteins. *Science* (2022) 375(6586):1254–61. doi: 10.1126/science.abf0529

10. Li X, Ma Z, Mei L. Cuproptosis-related gene SLC31A1 is a potential predictor for diagnosis, prognosis and therapeutic response of breast cancer. *Am J Cancer Res* (2022) 12(8):3561–80.

11. Fan J, Wan Y, Wang Y, Wei H, Zhao G, Li S, et al. The relationship between serum level of copper and ceruloplasmin and pathologic and clinical characteristics in early breast cancer patients. *J Clin Oncol* (2018) 36(15_suppl):e13504–4. doi: 10.1200/JCO.2018.36.15_suppl.e13504

12. Chen F, Han B, Meng Y, Han Y, Liu B, Zhang B, et al. Ceruloplasmin correlates with immune infiltration and serves as a prognostic biomarker in breast cancer. *Aging (Albany NY)* (2021) 13(16):20438–67. doi: 10.18632/aging.203427

13. Chisholm CL, Wang H, Wong AH, Vazquez-Ortiz G, Chen W, Xu X, et al. Ammonium tetrathiomolybdate treatment targets the copper transporter ATP7A and enhances sensitivity of breast cancer to cisplatin. *Oncotarget* (2016) 7(51):84439–52. doi: 10.18632/oncotarget.12992

14. Janardhanan P, Somasundaran AK, Balakrishnan AJ, Pilankatta R. Sensitization of cancer cells towards cisplatin and carboplatin by protein kinase d inhibitors through modulation of ATP7A/B (copper transport ATPases). *Cancer Treat Res Commun* (2022) 32:100613. doi: 10.1016/j.ctarc.2022.100613

15. Subramanian A, Tamayo P, Mootha VK, Mukherjee S, Ebert BL, Gillette MA, et al. Gene set enrichment analysis: a knowledge-based approach for interpreting genome-wide expression profiles. *Proc Natl Acad Sci* (2005) 102(43):15545–50. doi: 10.1073/pnas.0506580102

16. Brueffer C, Vallon-Christersson J, Grabau D, Ehinger A, Häkkinen J, Hegardt C, et al. Clinical value of RNA sequencing-based classifiers for prediction of the five conventional breast cancer biomarkers: a report from the population-based multicenter Sweden cancerome analysis network-breast initiative. *JCO Precis Oncol* (2018) 2:1–18. doi: 10.1200/po.17.00135

17. Prat A, Parker JS, Karginova O, Fan C, Livasy C, Herschkowitz JI, et al. Phenotypic and molecular characterization of the claudin-low intrinsic subtype of breast cancer. *Breast Cancer Res* (2010) 12(5):R68. doi: 10.1186/bcr2635

18. Jézéquel P, Loussouarn D, Guérin-Charbonnel C, Campion L, Vanier A, Gouraud W, et al. Gene-expression molecular subtyping of triple-negative breast cancer tumours: importance of immune response. *Breast Cancer Res* (2015) 17:43. doi: 10.1186/s13058-015-0550-y

19. Li T, Fu J, Zeng Z, Cohen D, Li J, Chen Q, et al. TIMER2.0 for analysis of tumor-infiltrating immune cells. *Nucleic Acids Res* (2020) 48(W1):W509–w514. doi: 10.1093/nar/gkaa407

20. Mayakonda A, Lin DC, Assenov Y, Plass C, Koeffler HP. Maftools: efficient and comprehensive analysis of somatic variants in cancer. *Genome Res* (2018) 28(11):1747–56. doi: 10.1101/gr.239244.118

21. Goldman MJ, Craft B, Hastie M, Repečka K, Mcdade F, Kamath A, et al. Visualizing and interpreting cancer genomics data via the xena platform. *Nat Biotechnol* (2020) 38(6):675–8. doi: 10.1038/s41587-020-0546-8

22. Szklarczyk D, Franceschini A, Wyder S, Forslund K, Heller D, Huerta-Cepas J, et al. STRING v10: protein-protein interaction networks, integrated over the tree of life. *Nucleic Acids Res* (2015) 43(Database issue):D447–52. doi: 10.1093/nar/gku1003

23. Shannon P, Markiel A, Ozier O, Baliga NS, Wang JT, Ramage D, et al. Cytoscape: a software environment for integrated models of biomolecular interaction networks. *Genome Res* (2003) 13(11):2498–504. doi: 10.1101/gr.1239303

24. Tang Y, Li M, Wang J, Pan Y, Wu FX. CytoNCA: a cytoscape plugin for centrality analysis and evaluation of protein interaction networks. *Biosystems* (2015) 127:67–72. doi: 10.1016/j.biosystems.2014.11.005

25. Blanche P, Dartigues J-F, Jacqmin-Gadda H. Estimating and comparing time-dependent areas under receiver operating characteristic curves for censored event times with competing risks. *Stat Med* (2013) 32(30):5381–97. doi: 10.1002/sim.5958

26. Ouyang J, Qin G, Liu Z, Jian X, Shi T, Xie L. ToPP: tumor online prognostic analysis platform for prognostic feature selection and clinical patient subgroup selection. *iScience* (2022) 25(5):104190. doi: 10.1016/j.isci.2022.104190

27. Chen B, Khodadoust MS, Liu CL, Newman AM, Alizadeh AA. Profiling tumor infiltrating immune cells with CIBERSORT. *Methods Mol Biol* (2018) 1711:243–59. doi: 10.1007/978-1-4939-7493-1_12

28. Jiang P, Gu S, Pan D, Fu J, Sahu A, Hu X, et al. Signatures of T cell dysfunction and exclusion predict cancer immunotherapy response. *Nat Med* (2018) 24(10):1550–8. doi: 10.1038/s41591-018-0136-1

29. Yoshihara K, Shahmoradgoli M, Martínez E, Vegesna R, Kim H, Torres-Garcia W, et al. Inferring tumour purity and stromal and immune cell admixture from expression data. *Nat Commun* (2013) 4(1):2612. doi: 10.1038/ncomms3612

30. Maeser D, Gruener RF, Huang RS. oncoPredict: an r package for predicting in vivo or cancer patient drug response and biomarkers from cell line screening data. *Brief Bioinform* (2021) 22(6). doi: 10.1093/bib/bbab260

31. Vasaikar SV, Straub P, Wang J, Zhang B. LinkedOmics: analyzing multi-omics data within and across 32 cancer types. *Nucleic Acids Res* (2018) 46(D1):D956–d963. doi: 10.1093/nar/gkx1090

32. Dieci MV, Miglietta F, Guarneri V. Immune infiltrates in breast cancer: recent updates and clinical implications. *Cells* (2021) 10(2):223–50. doi: 10.3390/cells10020223

33. Fu J, Li K, Zhang W, Wan C, Zhang J, Jiang P, et al. Large-Scale public data reuse to model immunotherapy response and resistance. *Genome Med* (2020) 12(1):21. doi: 10.1186/s13073-020-0721-z

34. Jones W, Bianchi K. Aerobic glycolysis: beyond proliferation. *Front Immunol* (2015) 6:227. doi: 10.3389/fimmu.2015.00227

35. Contractor T, Harris CR. p53 negatively regulates transcription of the pyruvate dehydrogenase kinase Pdk2. *Cancer Res* (2012) 72(2):560–7. doi: 10.1158/0008-5472.Can-11-1215

36. Ma C, Zu X, Liu K, Bode AM, Dong Z, Liu Z, et al. Knockdown of pyruvate kinase m inhibits cell growth and migration by reducing NF-kB activity in triple-negative breast cancer cells. *Mol Cells* (2019) 42(9):628–36. doi: 10.14348/molcells.2019.0038

37. Generali D, Berruti A, Brizzi MP, Campo L, Bonardi S, Wigfield S, et al. Hypoxia-inducible factor-1alpha expression predicts a poor response to primary chemoendocrine therapy and disease-free survival in primary human breast cancer. *Clin Cancer Res* (2006) 12(15):4562–8. doi: 10.1158/1078-0432.Ccr-05-2690

38. Courtnay R, Ngo DC, Malik N, Ververis K, Tortorella SM, Karagiannis TC. Cancer metabolism and the warburg effect: the role of HIF-1 and PI3K. *Mol Biol Rep* (2015) 42(4):841–51. doi: 10.1007/s11033-015-3858-x

39. Kim JW, Tchernyshyov I, Semenza GL, Dang CV. HIF-1-mediated expression of pyruvate dehydrogenase kinase: a metabolic switch required for cellular adaptation to hypoxia. *Cell Metab* (2006) 3(3):177–85. doi: 10.1016/j.cmet.2006.02.002

40. Uhlen M, Zhang C, Lee S, Sjöstedt E, Fagerberg L, Bidkhori G, et al. A pathology atlas of the human cancer transcriptome. *Science* (2017) 357(6352):660–71. doi: 10.1126/science.aan2507

41. Tran AN, Dussaq AM, Kennell T, Willey CD, Hjelmeland AB. HPAanalyze: an r package that facilitates the retrieval and analysis of the human protein atlas data. *BMC Bioinf* (2019) 20(1):463. doi: 10.1186/s12859-019-3059-z

42. Koboldt DC, Fulton RS, Mclellan MD, Schmidt H, Kalicki-Veizer J, Mcmichael JF, et al. Comprehensive molecular portraits of human breast tumours. *Nature* (2012) 490(7418):61–70. doi: 10.1038/nature11412

43. Parker JS, Mullins M, Cheang MC, Leung S, Voduc D, Vickery T, et al. Supervised risk predictor of breast cancer based on intrinsic subtypes. *J Clin Oncol* (2009) 27(8):1160–7. doi: 10.1200/jco.2008.18.1370

44. Adeoti ML, Oguntola AS, Akanni EO, Agodirin OS, Oyeyemi GM. Trace elements; copper, zinc and selenium, in breast cancer afflicted female patients in LAUTECH osogbo, Nigeria. *Indian J Cancer* (2015) 52(1):106–9. doi: 10.4103/0019-509x.175573

45. Rizk SL, Sky-Peck HH. Comparison between concentrations of trace elements in normal and neoplastic human breast tissue. *Cancer Res* (1984) 44(11):5390–4.

46. Kuo HW, Chen SF, Wu CC, Chen DR, Lee JH. Serum and tissue trace elements in patients with breast cancer in Taiwan. *Biol Trace Elem Res* (2002) 89(1):1–11. doi: 10.1385/bter:89:1:1

47. Ding X, Jiang M, Jing H, Sheng W, Wang X, Han J, et al. Analysis of serum levels of 15 trace elements in breast cancer patients in Shandong, China. *Environ Sci pollut Res Int* (2015) 22(10):7930–5. doi: 10.1007/s11356-014-3970-9

48. Majumder S, Chatterjee S, Pal S, Biswas J, Efferth T, Choudhuri SK. The role of copper in drug-resistant murine and human tumors. *Biometals* (2009) 22(2):377–84. doi: 10.1007/s10534-008-9174-3

49. Fuchs AG, De Lustig ES. Copper histochemistry of 5 murine tumors and their respective metastases. *Tumour Biol J Int Soc Oncodevelopmental Biol Med* (1989) 10 (1):38–45. doi: 10.1159/000217592

50. Pass HI, Brewer GJ, Dick R, Carbone M, Merajver S. A phase II trial of tetrathiomolybdate after surgery for malignant mesothelioma: final results. *Ann Thorac Surg* (2008) 86(2):383–9;discussion 390. doi: 10.1016/j.athoracsur.2008.03.016

51. Brewer GJ, Dick RD, Grover DK, Leclaire V, Tseng M, Wicha M, et al. Treatment of metastatic cancer with tetrathiomolybdate, an anticopper, antiangiogenic agent: phase I study. *Clin Cancer Res* (2000) 6(1):1–10.

52. Ge EJ, Bush AI, Casini A, Cobine PA, Cross JR, Denicola GM, et al. Connecting copper and cancer: from transition metal signalling to metalloplasia. *Nat Rev Cancer* (2022) 22(2):102–13. doi: 10.1038/s41568-021-00417-2

53. Chan N, Willis A, Kornhauser N, Ward MM, Lee SB, Nackos E, et al. Influencing the tumor microenvironment: a phase II study of copper depletion using tetrathiomolybdate in patients with breast cancer at high risk for recurrence and in preclinical models of lung metastases. *Clin Cancer Res* (2017) 23(3):666–76. doi: 10.1158/1078-0432.Ccr-16-1326

54. Jain S, Cohen J, Ward MM, Kornhauser N, Chuang E, Cigler T, et al. Tetrathiomolybdate-associated copper depletion decreases circulating endothelial progenitor cells in women with breast cancer at high risk of relapse. *Ann Oncol* (2013) 24(6):1491–8. doi: 10.1093/annonc/mds654

55. Allensworth JL, Evans MK, Bertucci F, Aldrich AJ, Festa RA, Finetti P, et al. Disulfiram (DSF) acts as a copper ionophore to induce copper-dependent oxidative stress and mediate anti-tumor efficacy in inflammatory breast cancer. *Mol Oncol* (2015) 9(6):1155–68. doi: 10.1016/j.molonc.2015.02.007

56. Zhang H, Chen D, Ringler J, Chen W, Cui QC, Ethier SP, et al. Disulfiram treatment facilitates phosphoinositide 3-kinase inhibition in human breast cancer cells *in vitro* and in vivo. *Cancer Res* (2010) 70(10):3996–4004. doi: 10.1158/0008-5472.Can-09-3752

57. Chen D, Cui QC, Yang H, Dou QP. Disulfiram, a clinically used anti-alcoholism drug and copper-binding agent, induces apoptotic cell death in breast cancer cultures and xenografts *via* inhibition of the proteasome activity. *Cancer Res* (2006) 66 (21):10425–33. doi: 10.1158/0008-5472.Can-06-2126

58. Chen L, Min J, Wang F. Copper homeostasis and cuproptosis in health and disease. *Signal Transduction Targeted Ther* (2022) 7(1):378. doi: 10.1038/s41392-022-01229-y

59. Li S-R, Bu L-L, Cai L. Cuproptosis: lipoylated TCA cycle proteins-mediated novel cell death pathway. *Signal Transduction Targeted Ther* (2022) 7(1):158. doi: 10.1038/s41392-022-01014-x

60. Koltai T, Reshkin SJ, Harguindey S. Chapter 3 - the pH-centered paradigm in cancer. In: Koltai T, Reshkin SJ, Harguindey S, editors. *An innovative approach to understanding and treating cancer: targeting pH*. Academic Press (2020) 53–97. doi: 10.1016/B978-0-12-819059-3.00003-4

61. Woolbright BL, Rajendran G, Harris RA, Taylor JA. Iii: metabolic flexibility in cancer: targeting the pyruvate dehydrogenase Kinase:Pyruvate dehydrogenase axis. *Mol Cancer Ther* (2019) 18(10):1673–81. doi: 10.1158/1535-7163.Mct-19-0079

62. Dai X, Cheng H, Bai Z, Li J. Breast cancer cell line classification and its relevance with breast tumor subtyping. *J Cancer* (2017) 8(16):3131–41. doi: 10.7150/jca.18457

63. Yersal O, Barutca S. Biological subtypes of breast cancer: prognostic and therapeutic implications. *World J Clin Oncol* (2014) 5(3):412–24. doi: 10.5306/wjco.v5.i3.412

64. Haque R, Ahmed SA, Inzhakova G, Shi J, Avila C, Polikoff J, et al. Impact of breast cancer subtypes and treatment on survival: an analysis spanning two decades. *Cancer Epidemiology Biomarkers Prev* (2012) 21(10):1848–55. doi: 10.1158/1055-9965.Epi-12-0474

65. Bertucci F, Finetti P, Birnbaum D. Basal breast cancer: a complex and deadly molecular subtype. *Curr Mol Med* (2012) 12(1):96–110. doi: 10.2174/156652412798376134

66. Mcguire A, Lowery AJ, Kell MR, Kerin MJ, Sweeney KJ. Locoregional recurrence following breast cancer surgery in the trastuzumab era: a systematic review by subtype. *Ann Surg Oncol* (2017) 24(11):3124–32. doi: 10.1245/s10434-017-6021-1

67. Li J, Wu F, Li C, Sun S, Feng C, Wu H, et al. The cuproptosis-related signature predicts prognosis and indicates immune microenvironment in breast cancer. *Front Genet* (2022) 13:977322. doi: 10.3389/fgene.2022.977322

68. Song S, Zhang M, Xie P, Wang S, Wang Y. Comprehensive analysis of cuproptosis-related genes and tumor microenvironment infiltration characterization in breast cancer. *Front Immunol* (2022) 13:978909. doi: 10.3389/fimmu.2022.978909

69. Dilillo DJ, Yanaba K, Tedder TF. B cells are required for optimal CD4+ and CD8 + T cell tumor immunity: therapeutic b cell depletion enhances B16 melanoma growth in mice. *J Immunol* (2010) 184(7):4006–16. doi: 10.4049/jimmunol.0903009

70. Wu X-Z, Shi X-Y, Zhai K, Yi F-S, Wang Z, Wang W, et al. Activated naïve b cells promote development of malignant pleural effusion by differential regulation of TH1 and TH17 response. *Am J Physiology-Lung Cell Mol Physiol* (2018) 315(3):L443–55. doi: 10.1152/ajplung.00120.2018

71. Li X, Gruosso T, Zuo D, Omeroglu A, Meterissian S, Guiot M-C, et al. Infiltration of $CD8^+$ T cells into tumor cell clusters in triple-negative breast cancer. *Proc Natl Acad Sci* (2019) 116(9):3678–87. doi: 10.1073/pnas.1817652116

72. Chatterjee S, Mookerjee A, Mookerjee Basu J, Chakraborty P, Ganguly A, Adhikary A, et al. A novel copper chelate modulates tumor associated macrophages to promote anti-tumor response of T cells. *PloS One* (2009) 4(9):e7048. doi: 10.1371/journal.pone.0007048

73. Wang S, Xie Y, Bao A, Li J, Ye T, Yang C, et al. Nilotinib, a discoidin domain receptor 1 (DDR1) inhibitor, induces apoptosis and inhibits migration in breast cancer. *Neoplasma* (2021) 68(5):975–82. doi: 10.4149/neo_2021_201126N1282

74. Pedersen AM, Thrane S, Lykkesfeldt AE, Yde CW. Sorafenib and nilotinib resensitize tamoxifen resistant breast cancer cells to tamoxifen treatment via estrogen receptor α. *Int J Oncol* (2014) 45(5):2167–75. doi: 10.3892/ijo.2014.2619

75. Das M, Dilnawaz F, Sahoo SK. Targeted nutlin-3a loaded nanoparticles inhibiting p53–MDM2 interaction: novel strategy for breast cancer therapy. *Nanomedicine* (2011) 6(3):489–507. doi: 10.2217/nnm.10.102

76. Ni Z, Xu S, Yu Z, Ye Z, Li R, Chen C, et al. Comparison of dual mTORC1/2 inhibitor AZD8055 and mTORC1 inhibitor rapamycin on the metabolism of breast cancer cells using proton nuclear magnetic resonance spectroscopy metabolomics. *Investigational New Drugs* (2022) 40(6):1206–15. doi: 10.1007/s10637-022-01268-w

77. Shi J-J, Chen S-M, Guo C-L, Li Y-X, Ding J, Meng L-H. The mTOR inhibitor AZD8055 overcomes tamoxifen resistance in breast cancer cells by down-regulating HSPB8. *Acta Pharmacologica Sin* (2018) 39(8):1338–46. doi: 10.1038/aps.2017.181

78. Turner NC, Balmaña J, Poncet C, Goulioti T, Tryfonidis K, Honkoop AH, et al. Niraparib for advanced breast cancer with germline BRCA1 and BRCA2 mutations: the EORTC 1307-BCG/BIG5–13/TESARO PR-30–50–10-C BRAVO study. *Clin Cancer Res* (2021) 27(20):5482–91. doi: 10.1158/1078-0432.Ccr-21-0310

79. Zimmer AS, Steinberg SM, Smart DD, Gilbert MR, Armstrong TS, Burton E, et al. Temozolomide in secondary prevention of HER2-positive breast cancer brain metastases. *Future Oncol* (2020) 16(14):899–909. doi: 10.2217/fon-2020-0094

80. Lim ST, Jeon YW, Gwak H, Kim SY, Suh YJ. Synergistic anticancer effects of ruxolitinib and calcitriol in estrogen receptor–positive, human epidermal growth factor receptor 2–positive breast cancer cells. *Mol Med Rep* (2018) 17(4):5581–8. doi: 10.3892/mmr.2018.8580

81. Kim JW, Gautam J, Kim JE, Kim JA, Kang KW. Inhibition of tumor growth and angiogenesis of tamoxifen-resistant breast cancer cells by ruxolitinib, a selective JAK2 inhibitor. *Oncol Lett* (2019) 17(4):3981–9. doi: 10.3892/ol.2019.10059

82. Xia Q, Cai Y, Peng R, Wu G, Shi Y, Jiang W. The CDK1 inhibitor RO3306 improves the response of BRCA-proficient breast cancer cells to PARP inhibition. *Int J Oncol* (2014) 44(3):735–44. doi: 10.3892/ijo.2013.2240

frontiers | Frontiers in Oncology

TYPE Original Research
PUBLISHED 12 May 2023
DOI 10.3389/fonc.2023.1111480

OPEN ACCESS

EDITED BY
Chun Xu,
The University of Queensland, Australia

REVIEWED BY
Jia Li,
University of North Carolina at Charlotte, United States
Dipendra Khadka,
Wonkwang University School of Medicine, Republic of Korea

*CORRESPONDENCE
Hong Zheng
hzheng@scu.edu.cn

RECEIVED 07 December 2022
ACCEPTED 28 April 2023
PUBLISHED 12 May 2023

CITATION
Fan Y, Luo C, Wang Y, Wang Z, Wang C, Zhong X, Hu K, Wang Y, Lu D and Zheng H (2023) A nomogram based on cuproptosis-related genes predicts 7-year relapse-free survival in patients with estrogen receptor-positive early breast cancer.
Front. Oncol. 13:1111480.
doi: 10.3389/fonc.2023.1111480

A nomogram based on cuproptosis-related genes predicts 7-year relapse-free survival in patients with estrogen receptor-positive early breast cancer

Yu Fan[1], Chuanxu Luo[1], Yu Wang[1], Zhu Wang[1], Chengshi Wang[2], Xiaorong Zhong[1], Kejia Hu[2], Yanping Wang[1], Donghao Lu[2,3] and Hong Zheng[1*]

[1]Breast Center and Multi-omics Laboratory of Breast Diseases, West China Hospital, Sichuan University, Chengdu, China, [2]West China Biomedical Big Data Center, West China Hospital, Sichuan University, Chengdu, China, [3]Institute of Environmental Medicine, Karolinska Institutet, Stockholm, Sweden

Introduction: Excess copper induces cell death by binding to lipoylated components of the tricarboxylic acid cycle. Although a few studies have examined the relationship between cuproptosis-related genes (CRGs) and breast cancer prognosis, reports on estrogen receptor-positive (ER+) breast cancer are lacking. Herein, we aimed to analyze the relationship between CRGs and outcomes in patients with ER+ early breast cancer (EBC).

Methods: We conducted a case-control study among patients with ER+ EBC presenting poor and favorable invasive disease-free survival (iDFS) at West China Hospital. Logistic regression analysis was performed to establish the association between CRG expression and iDFS. A cohort study was performed using pooled data from three publicly available microarray datasets in the Gene Expression Omnibus database. Subsequently, we constructed a CRG score model and a nomogram to predict relapse-free survival (RFS). Finally, the prediction performance of the two models was verified using training and validation sets.

Results: In this case-control study, high expression of *LIAS*, *LIPT1*, and *ATP7B* and low *CDKN2A* expression were associated with favorable iDFS. In the cohort study, high expression of *FDX1*, *LIAS*, *LIPT1*, *DLD*, *PDHB*, and *ATP7B* and low *CDKN2A* expression were associated with favorable RFS. Using LASSO-Cox analysis, a CRG score was developed using the seven identified CRGs. Patients in the low CRG score group had a reduced risk of relapse in both training and validation sets. The nomogram included the CRG score, lymph node status, and age. The area under the receiver operating characteristic (ROC) curve (AUC) of the nomogram was significantly higher than the AUC of the CRG score at 7 years.

Conclusions: The CRG score, combined with other clinical features, could afford a practical long-term outcome predictor in patients with ER+ EBC.

KEYWORDS

breast cancer, cuproptosis-related genes, nomogram, ER positive, RFS

1 Introduction

In 2020, breast cancer (BC), for the first time, surpassed lung cancer as the most commonly diagnosed cancer. Overall, an estimated 2.3 million new cases of BC have been diagnosed (1). According to data on BC pathology among Asian women, 52–76% of patients with BC have estrogen receptor (ER)-positive (ER+) subtypes (2). Expression of ER has been associated with a favorable prognosis and can predict the efficacy of endocrine therapies, including aromatase inhibitors and tamoxifen (3). However, nearly one-quarter of patients with ER + early BC (EBC) experience relapse within 10 years (4). Approximately half of all relapses occur after five years of adjuvant endocrine therapy (5). Although the clinical stage, combined with other features like ki67 and differentiation grade, can afford a preliminary assessment of prognosis, additional molecular markers are needed to construct an exemplary long-term prognosis model. Furthermore, these molecular markers could help identify more effective therapeutic targets.

The copper-dependent regulation of cell death is distinct from known death mechanisms and depends on mitochondrial respiration in human cells (6). Copper directly binds to lipoylated components of the tricarboxylic acid (TCA) cycle, resulting in lipoylated protein aggregation (7) and subsequent iron-sulfur cluster protein loss, thereby inducing proteotoxic stress (8) and, ultimately, cell death (9). The regulators essential for cuproptosis include two components, the lipoic acid (LA) pathway (*FDX1*, *LIAS*, *LIPT1*, and *DLD*) and the pyruvate dehydrogenase (PDH) complex (*DLAT*, *PDHA1*, *PDHB*, *MTF1*, *GLS*, and *CDKN2A*) (9).

Research on cuproptosis and its relationship with cancer remains in its early stages of development. Correlations between cuproptosis-related genes (CRGs) and prognosis have been reported in patients with renal carcinoma (10), head and neck cancer (11), melanoma (12), glioma (13), and BC. However, data mining on BC and CRGs currently involves The Cancer Genome Atlas (TCGA) database with a relatively short follow-up period, and molecular subtype analysis is required. The relationship between CRGs and the long-term prognosis of ER+ EBC remains unclear.

Herein, we first suggested a correlation between the CRG profile and invasive disease-free survival (iDFS) or relapse-free survival (RFS) in patients with ER+ EBC by performing a case-control study at our hospital and a cohort study from publicly available datasets. In the case-control study performed at the West China Hospital (WCH), high expression of *LIAS*, *LIPT1*, and *ATP7B* and low expression of *CDKN2A* significantly reduced the odds ratio (OR) of iDFS in patients with ER+ EBC. For validation, we used pooled data from three publicly available microarray studies (GSE42568, GSE9195, and GSE20685). In this cohort, high expression of *LIAS*, *LIPT1*, and *ATP7B* and low expression of *CDKN2A* significantly reduced the hazard ratio (HR) of relapse of ER+ EBC. Moreover, high expression of *FDX1* and *DLD*, two molecules of the LA pathway, and *PDHB* of the PDH complex significantly reduced the HR for relapse. We then constructed a CRG score model in the training set, which confirmed that a high CRG score could significantly increase the risk of relapse in both training and validation datasets. The nomogram comprising CRG score, lymph node status, and age had an increased area under the receiver operating characteristics (ROC) curve (AUC) at 7 years when compared with that of the CRG score alone.

In brief, a novel nomogram comprising the CRG score and clinical features could predict the 3-, 5-, and 7-year relapse risks of ER+ EBC. Targeted enhancement of cuproptosis may be a potential therapeutic strategy for patients with ER+ BC.

2 Materials and methods

2.1 WCH patients

Since 1989, patients with BC have been enrolled in the Breast Cancer Management Information System of WCH, Sichuan University (14). Physicians collected medical records, pathological diagnoses, and treatment information. Between January 2008 and April 2018, 7,784 females diagnosed with non-metastatic invasive BC were prospectively followed up for clinical outcomes (15). Patients with freshly frozen tumor and germline samples, including blood or normal breast tissue, available during primary surgery were eligible for study inclusion (N = 1462)

2.2 Case-control study of WCH

A matched extreme case-control design was employed (16). Female patients diagnosed with EBC (stages I-III) who were assessed for any iDFS endpoint at 7 years after diagnosis were grouped into cases, and patients who survived without any iDFS endpoint for at least 7 years were grouped into controls. One control was randomly selected per case and individually matched to the case of molecular subtype classified according to the St. Gallen Consensus 2013, as previously described (15). Any local or

regional relapse, distant metastasis, new primary tumors from any site, cancer-specific death, or death from other causes were defined as iDFS endpoints. Subsequently, samples from 222 patients were RNA sequenced. Only ER+ samples were selected for further analysis, and ER- samples were excluded. Sixty-three patients were included in the case group and 62 in the control group. This study was approved by the Clinical Test and Biomedical Ethics Committee of the WCH, Sichuan University (No. 2019-16).

2.3 Pooled data from three mRNA expression datasets, GSE42568, GSE9195, and GSE20685

To verify the correlation between cuproptosis and patient outcomes, we selected three GSE datasets (GSE42568, GSE9195, and GSE20685) from the NCBI for Biotechnology Information Gene Expression Omnibus (GEO). The data met the following criteria: 1. Affymetrix Human Genome U133 Plus 2.0 Array; 2. provided ER status, tumor size, T stage, lymph node status, N stage, and age of patients with BC; 3. comprised at least 70 samples; 4. employed RFS as the endpoint; 5. at least 80% of the relapse-free patients were followed up for more than 5 years. In total, 508 samples from the three datasets were downloaded from "https://www.ncbi.nlm.nih.gov/geo/". We excluded 164 samples owing to metastasis at diagnosis or ER-. Overall, 344 patients were included in the subsequent analysis.

2.4 RNA sequencing data preparation

In the case-control study, RNA sequencing of frozen tumor tissues was performed using the Illumina NovaSeq S6000 platform. After quality control, reads were mapped to the reference genome using Hisat2 v2.0.5, as previously described (15). To calculate the fragments per kilobase of exons per million reads (FPKM) for gene i, the following formula was used:

$$\mathrm{FPKMi} = \frac{\mathrm{qi}}{\mathrm{li} * \Sigma \mathrm{jqj}} * 10^9$$

where qi is the raw read count, li is the gene length, and Σjqj corresponded to the total number of mapped reads (17). All FPKM data were then log2(x+1) transformed.

2.5 Microarray data preparation

The expression matrixes and clinical data for GSE42568, GSE9195, and GSE20685 were downloaded from "https://www.ncbi.nlm.nih.gov/geo". The R package limma (v3.48.1) was used to remove batch effects of these three GSE datasets, and principal component analysis (PCA) of each sample was performed before and after normalization. Each gene corresponded to a probe, except for *CDKN2A*, which corresponded to three probes. The probe with the highest normalized intensity averaged over all samples, was used to represent the expression level of *CDKN2A*. RFS endpoints were identical to iDFS endpoints, except for the occurrence of invasive contralateral BC, secondary primary invasive cancer, and contralateral ductal carcinoma *in situ* (18).

2.6 Association between CRGs and iDFS in the case-control study

We analyzed 13 CRGs from earlier studies: *FDX1*, *LIAS*, *LIPT1*, *DLD*, *DLAT*, *PDHA1*, *PDHB*, *MTF1*, *GLS*, *CDKN2A*, *SLC31A1*, *ATP7A*, and *ATP7B* (9, 19). Univariate and multivariate logistic regression analyses were performed to determine the association between individual CRG expression levels and iDFS endpoints. Pearson or Spearman correlation coefficient (r) was used for measuring the relationship between individual CRGs and clinicopathological features, including T stage, N stage, ki67, grade, and HER2 status in the WCH cohort.

2.7 Construction and validation of a prognostic CRG score in the cohort study

Univariate and multivariate Cox analyses of RFS were performed to screen for individual CRGs with prognostic values in the pooled GSE dataset. Kaplan-Meier survival analysis was used to estimate the RFS between the high- and low- CRGs expression groups. The "survminer" R package (V0.4.9) provided a cut-off for facilitating survival analysis. The 344 enrolled patients were randomly divided into two sets (7:3), with 241 and 103 patients in the training and validation sets, respectively. In the training set, CRGs with $P<0.05$ in the multivariate Cox regression were subjected to LASSO-penalized Cox regression analysis to construct a prognostic CRG score model using the "glmnet" R package (v4.1). The hyperparameter lambda (λ) was chosen based on tenfold cross-validation with the slightest mean squared error. Patient CRG scores were calculated according to the normalized expression levels of each gene and corresponding regression coefficients. The LASSO-penalized Cox regression formula is as follows:

$$\mathrm{CRGs.score} = \sum_{i=1}^{n} (\beta_i \times \exp\mathrm{ression}(\mathrm{gene_i}))\ (20)$$

β_i represented the corresponding coefficient of a specific gene, and the expression($\mathrm{gene_i}$) indicates the expression level of the corresponding gene. The CRGs score for each patient could be calculated according to the formula. ROC curve analysis was used to assess the performance of the CRG score using the R package "timeROC" (V0.4). Univariate and multivariate Cox analyses and Kaplan-Meier survival analysis were performed to verify the association between CRGs score and RFS in the training and validation sets.

2.8 Construction and validation of a prognostic nomogram based on CRGs score

A nomogram model predicting RFS was developed based on CRG scores and other clinical features, including lymph node status

and age, in the training set using the R package "rms" (V6.3). Univariate Cox and Kaplan-Meier survival analyses were performed to verify the relationship between the nomogram points and RFS. The ROC curve assessed the performance of the nomogram model using the "timeROC" package in both the training and validation sets. A comparison of ROCs was performed between the CRG score and nomogram points using the "compare" function in the "timeROC" package.

Statistical analyses were performed using R software (V4.1.0). Statistical significance was set at $P< 0.05$.

3 Results

3.1 Study design

Figure 1 presents the flow chart of the study. Our study used two datasets and two study designs to demonstrate the association between CRGs and iDFS or RFS in patients with ER+ EBC. The genes in dotted boxes represent overlapping genes associated with iDFS or RFS in both datasets.

3.2 Characteristics of patients in the case-control study

In the case-control study, 63 patients who experienced endpoint events within 7 years were grouped into cases, and the other 62 patients were grouped into controls. The two groups had no significant differences in menopause, age, T stage, N stage, grade, ki67, progesterone receptor status, or treatment, according to the chi-square test. The control group had a higher proportion of HER2-positive patients, given that the HER2 status of 8 patients was uncertain in the case group. The average iDFS and overall survival (OS) were 127.1 ± 15.2 and 127.1 ± 15.2 months in the control group and 31.4 ± 22.5 and 62.5 ± 35.2 months in the case group, respectively (Table 1).

3.3 CRG expression associated with iDFS in the case-control study

In the case-control study, the higher expression level of *LIAS* (OR = 0.14, 95% confidence interval [CI] 0.03–0.57, P = 0.008), *LITP1* (OR = 0.2, 95%CI 0.06–0.65, P = 0.01), and *ATP7B* (OR = 0.38, 95%CI 0.17–0.81, P = 0.016) was associated with a lower risk of iDFS endpoints. However, higher T stage (OR = 1.75, 95%CI 1.04–3.14, P = 0.045), N stage (OR = 2.32, 95%CI 1.12–4.88, P = 0.025), and *CDKN2A* expression (OR = 1.8, 95%CI 1.24–2.74, P = 0.003) were associated with a higher risk of iDFS endpoints (Figure 2A; Supplementary Table 1). Menopause, age, grade, ki67, HER2 status, chemotherapy, radiotherapy, trastuzumab, and other CRGs showed no association with iDFS endpoints (Figure 2A). Adjusted for T stage and N stage, *LIAS* (OR = 0.18, 95%CI 0.04–0.81, P = 0.025), *LIPT1* (OR = 0.26, 95%CI 0.07–0.9, P = 0.034), *CDKN2A* (OR = 1.73, 95%CI 1.16–2.59, P = 0.007), and *ATP7B* (OR = 0.42, 95%CI 0.19–0.94, P = 0.035) were still associated with iDFS endpoints (Figure 2B; Supplementary Table 2).

Furthermore, we noted the relationship between these four genes and other clinicopathological features. *LIAS* was negatively associated with N stage (R = -0.18, P = 0.041), tumor grade (R = -0.24, P = 0.012), ki67 (R = -0.2, P = 0.029), and HER2 expression (R = -0.35, P = 9E-5). *LITP1* was negatively associated with T stage

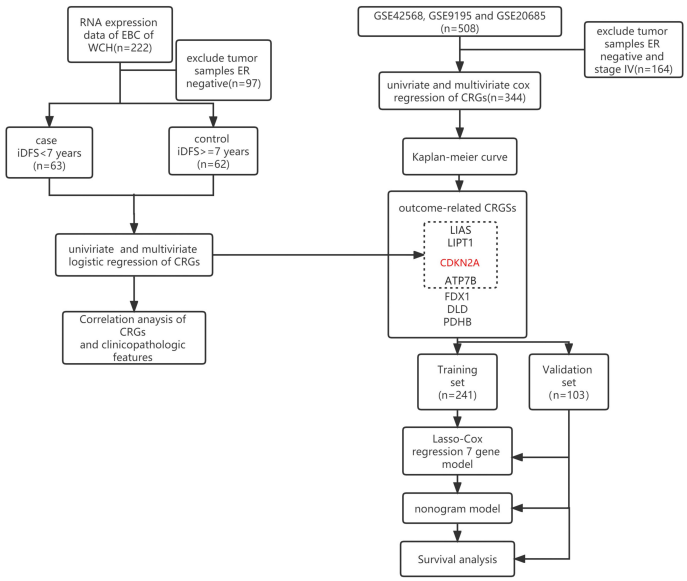

FIGURE 1
Flow diagram of the patient selection and study design. The red-marked gene represents the gene that negatively hit cuproptosis. Black-marked genes represent the genes that positively hit cuproptosis. WCH, West China Hospital; iDFS, invasive disease-free survival; ER, estrogen receptor; CRGs, cuproptosis-related genes.

TABLE 1 Clinical and pathological features of 125 estrogen receptor positive invasive breast cancer patients in West China Hospital.

Features	levels	Control (N = 62)	Case(N=63)	p
menopause	No	35 (56.5%)	32 (50.8%)	0.649
	Yes	27 (43.5%)	31 (49.2%)	
age	<40y	13 (21%)	8 (12.7%)	0.319
	≥40y	49 (79%)	55 (87.3%)	
T stage	1	23 (37.1%)	12 (19%)	0.252
	2	34 (54.8%)	43 (68.3%)	
	3	2 (3.2%)	3 (4.8%)	
	4	2 (3.2%)	4 (6.3%)	
	unknown	1 (1.6%)	1 (1.6%)	
N status	0	31 (50%)	20 (31.7%)	0.055
	1	19 (30.6%)	18 (28.6%)	
	2	8 (12.9%)	13 (20.6%)	
	3	4 (6.5%)	12 (19%)	
grade	1	0 (0%)	1 (1.6%)	0.114
	2	23 (37.1%)	15 (23.8%)	
	3	31 (50%)	43 (68.3%)	
	unknown	8 (12.9%)	4 (6.3%)	
ki67	≤10%	7 (11.3%)	4 (6.3%)	0.51
	>10%	55 (88.7%)	59 (93.7%)	
PR	negative	54 (87.1%)	49 (77.8%)	0.257
	positive	8 (12.9%)	14 (22.2%)	
HER2 status	negative	42 (67.7%)	36 (57.1%)	0.014*
	positive	20 (32.3%)	19 (30.2%)	
	uncertain	0 (0%)	8 (12.7%)	
chemotherapy	No	1 (1.6%)	4 (6.3%)	0.371
	Yes	61 (98.4%)	59 (93.7%)	
radiotherapy	No	36 (58.1%)	36 (57.1%)	1
	Yes	26 (41.9%)	27 (42.9%)	
Herceptin	No	57 (91.9%)	58 (92.1%)	1
	Yes	5 (8.1%)	5 (7.9%)	
OS_bin	0	62 (100%)	33 (52.4%)	<.001
	1	0 (0%)	30 (47.6%)	
iDFS_month	Mean ± SD	127.1 ± 15.2	31.4 ± 22.5	<.001
OS_month	Mean ± SD	127.1 ± 15.2	62.5 ± 35.2	<.001

(R = -0.2, P = 0.027), N stage (R = -0.16, P = 0.066, borderline significance), grade (R = -0.31, P = 0.001), ki67 (R = -0.28, P = 0.002), and HER2 levels (R = -0.32, P = 0.0004). *CDKN2A* expression was positively associated with N stage (R = 0.19, P = 0.034) and ki67 (R = 0.18, P = 0.047). *ATP7B* expression was negatively associated with T stage (R = -0.17, P = 0.06, borderline significance) (Figure 2C).

3.4 Expression of CRGs associated with RFS in the cohort study

In total, 344 patients were diagnosed with stage I-III ER-positive BC using the GSE42568, GSE9195, and GSE20685 databases. Supplemental Figure 1 shows the PCA of each sample before and

10.3389/fonc.2023.1111480

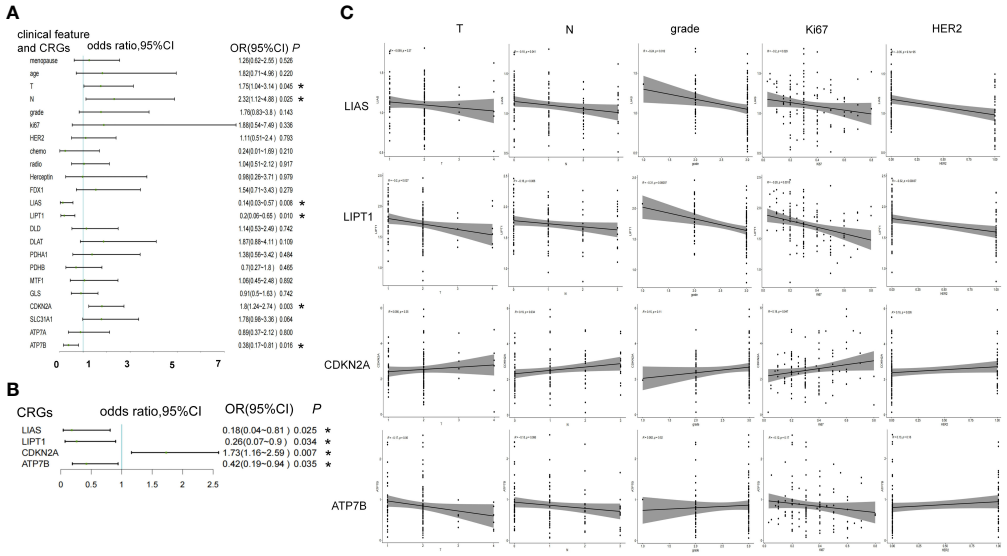

FIGURE 2
The association between CRGs and iDFS endpoints in WCH case-control study. **(A)** Univariate and **(B)** multivariate logistic regression analyses of clinical features and CRGs for association with iDFS in the WCH cohort. **(C)** The relation of CRGs and the T stage, N stage, grade, ki67 and HER2 status. *, a p -value less than 0.05.

after normalization using the R package "limma." Tumor size (HR = 1.6, 95%CI 1.1–2.2, P = 0.007) and lymph node status (HR = 3.8, 95%CI 2.3–6.3, P = 2.6E-07) were risk factors for relapse, and older age (HR = 0.48, 95%CI 0.29-0.81, P = 0.006) was a protective factor against relapse. Of identified CRGs, expression levels of *LIAS* (HR = 0.61,95%CI 0.41–0.9, P = 0.013), *LITP1* (HR = 0.44, 95%CI 0.29–0.66, P = 7.40E-05), *CDKN2A* (HR = 1.7, 95%CI 1.3–2.3, P = 0.0001), *ATP7B* (HR = 0.75, 95%CI 0.58–0.98, P = 0.032), *FDX1* (HR = 0.59, 95%CI 0.42–0.84, P = 0.003), *DLD* (HR = 0.59, 95%CI 0.42–0.83, P = 0.002), and *PDHB* (HR = 0.42, 95%CI 0.26-0.65, P = 0.0002) were associated with RFS (Figure 3A; Supplementary Table 3). After adjusting for tumor size, lymph node status, and age, these seven genes were still associated with the risk of relapse (Figure 3B; Supplementary Table 4). The high expression of *LIAS*,

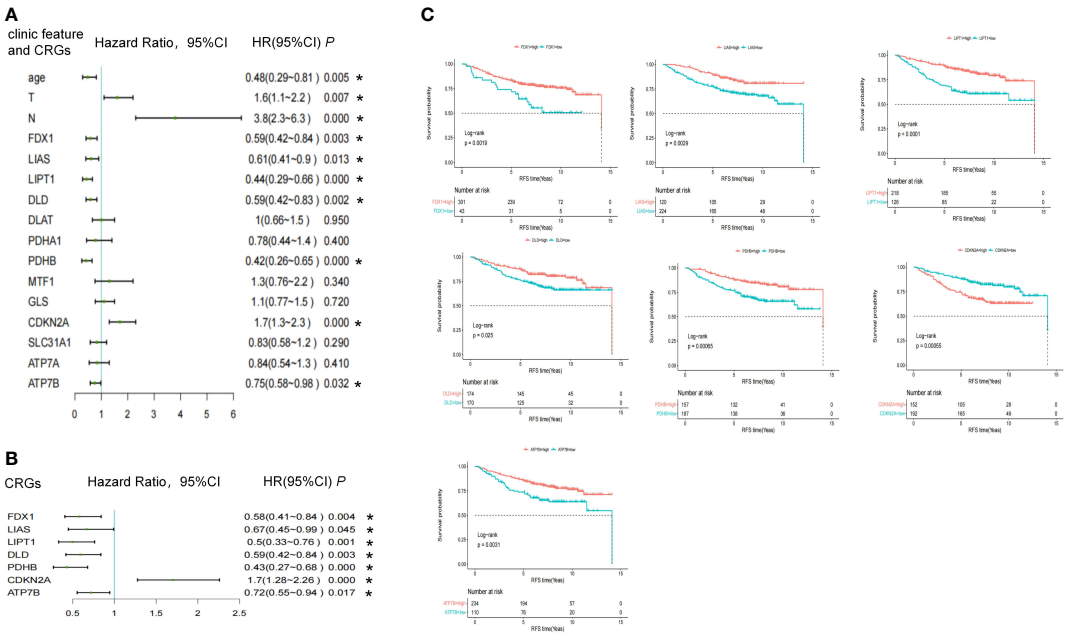

FIGURE 3
The association between CRGs and RFS endpoints in the pooled cohort study. **(A)** Univariate and **(B)** multivariate cox regression of clinical features and CRGs in pooled GSE data. **(C)** Kaplan-Meier survival analysis of CRGs. *, a p -value less than 0.05.

LITP1, *ATP7B*, *FDX1*, *DLD*, and *PDHB* and the low expression of *CDKN2A* were associated with longer RFS, as determined by the Kaplan-Meier curve (Figure 3C). Collectively, five genes positively affected cuproptosis, and one copper transporter gene decreased the risk of relapse. However, one gene negatively impacting cuproptosis may also increase the risk of relapse.

3.5 Construction CRGs score model in GSE dataset and validation

Enrolled patients (n = 344) were randomly divided into two sets (7:3): the training set (n = 241) and the validation set (n = 103). The training and validation sets showed no significant differences in clinical features or CRG expression (Supplementary Table 5). LASSO-Cox regression analysis was used to establish a prognostic model for the training set based on expression profiles of the seven genes (Figure 4A). Seven gene signatures were determined based on the optimal value (Figure 4B). The risk score was then calculated based on the coefficient of each gene as follows:

CRGs.score = -*FDX1**0.283 -*LIAS**0.314 -*LIPT1**0.428 -*DLD**0.139 -*PDHB**0.257 +*CDKN2A**0.635 -*ATP7B**0.275

According to the cut-off value of the CRG score calculated using the R package "survminer," patients were divided into the high CRG score group and the low CRG score group in the training and validation set. PCA revealed that patients in the different CRG score groups were distributed in two directions (Figure 4C). As shown in Figure 4D, the median survival time in the low and high CRG score groups was 14.1 and 5.73 years, respectively, in the training set. The HR of the low CRG score group was 0.21 (95%CI 0.13–0.35, P = 1.1E-9) when compared with that of the high CRG score group. After adjustment for tumor size, lymph node status and age, the HR of low CRG score was 0.24 (95%CI 0.14–0.41, P = 1.07E-07). The AUC value was used to evaluate the predictive performance of the CRG score over time. For the training set, the AUC was 0.74 at 3 years, 0.74 at 5 years, and 0.75 at 7 years (Figure 5C, left, solid line).

In the validation set, the median survival time was not reached (NR) and 6.59 years for the low and high CRG score groups, respectively. The HR of the low CRG score group was 0.29 (95%CI 0.13–0.64, P = 0.002), determined by univariate Cox regression analysis, and 0.23 (95%CI 0.1–0.52, P = 0.0005) by multivariate Cox regression analysis. For the validation set, the AUC was 0.77 at 3 years, 0.74 at 5 years, and 0.56 at 7 years (Figure 5C, right, solid line).

3.6 Development and validation of a predictive nomogram based on CRG score

Multivariate Cox analysis of the CRG score, age, tumor size, and lymph node status was performed. Tumor size (P = 0.52) was not an independent prognostic factor. The CRG score (P = 1.80E-09) and lymph node status (P = 3.03E-06) were independent prognostic factors, while age reached borderline significance as an independent prognostic factor (P = 0.055).

Based on the multivariate analysis results, we developed a nomogram model as an easy-to-use tool (Figure 5A). As shown in (Figures 5B, C), the median RFS time of patients with low and high nomogram points in the training set were 14.1 and 5.42 years, respectively. The HR of patients with low nomogram points was 0.14 (95%CI 0.085–0.24, P = 2.4E-13). The AUC was 0.79 at 3 years, 0.82 at 5 years, and 0.81 at 7 years (Figure 5C left, dotted line). Compared with the CRG score, the AUC values of the nomogram at 5 (P = 0.002) and 7 years (P = 0.02) were significantly improved.

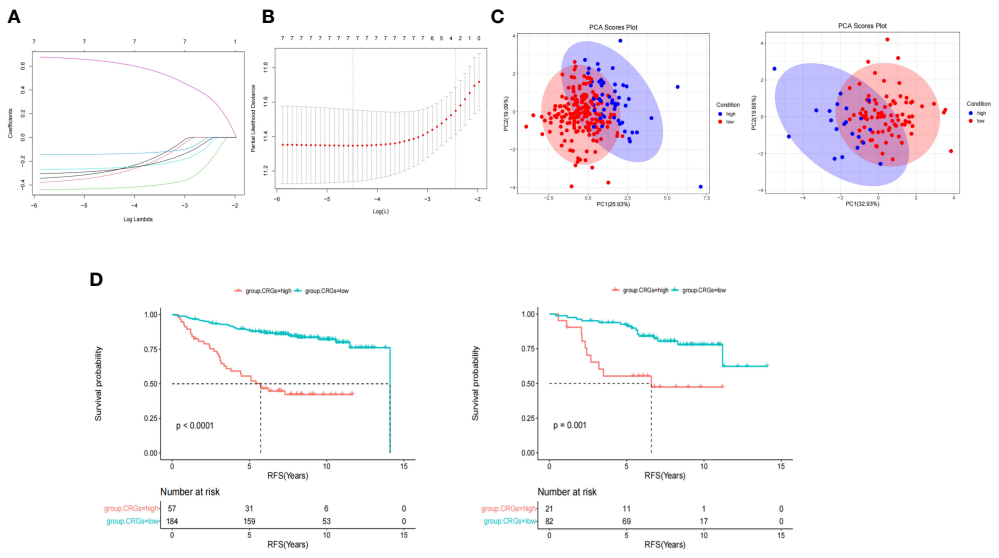

FIGURE 4
CRGs score model construction and survival analyses. **(A)** LASSO cox regression analysis was used to establish a prognostic model in the training group based on the expression profiles of 7 CRGs. **(B)** 7 gene signatures were determined based on the optimal value of λ. **(C)** Principal component analysis (PCA) showed patients in different CRGs score groups distribution. **(D)** Kaplan-Meier survival analysis of CRGs score in training (left) and validation set (right).

In the validation set, the median RFS time of patients with low and high nomogram points were NR and 3.5 years, respectively, and the HR of patients with low nomogram points was 0.17 (95%CI 0.079–0.38, P = 1.6E-05). The AUC was 0.82 at 3 years, 0.81 at 5 years, and 0.7 at 7 years, as shown in Figure 5C (right, dotted line). Compared with the CRG score, the AUC value of the nomogram points at 7 years (P = 0.03) significantly improved.

4 Discussion

In the present study, we employed two datasets and two study designs to demonstrate the association between CRGs and iDFS or RFS in patients with ER+ EBC. Considering patients from WCH and pooled GSE data, expression of *LIAS*, *LIPT1*, *CDKN2A*, and *ATP7B* correlated with patient endpoints, and the risk direction was consistent. In addition, three other CRGs, i.e., *FDX1*, *DLD*, and *PDHB*, were negatively associated with the risk of relapse in the GSE cohort. We then used pooled patients with GSEs to construct the CRG score model and a nomogram for RFS prediction. In the training and validation sets, the relapse risk of the high CRG score group, comprising the seven genes, was significantly higher than that of the low CRG score group. We used the CRG score combined with lymph node status and age to construct a nomogram and found that the RFS in the high-point group was significantly shorter than in the low-point group. The 7-year predicted AUC of the nomogram points was higher than that of the CRG score alone. The findings of the present study revealed the potential impact of CRGs on the clinicopathological features and prognosis of patients with ER+ EBC. Interestingly, five genes promoting cuproptosis were positively correlated with prognosis, and one gene inhibiting cuproptosis negatively correlated with prognosis, suggesting that cuproptosis may be a protective mechanism that reduces relapse in patients with ER+ EBC. Furthermore, high levels of LA pathway genes, including *FDX1*, *LIAS*, *LIPT1*, and *DLD*, correlated with prolonged RFS, suggesting that targeting the LA pathway in cuproptosis may be a potential therapeutic strategy in patients with ER+ BC.

Cu is a mineral nutrient, and a growing number of studies have confirmed the involvement of Cu in cell proliferation and death pathways (21). Given the intrinsic oxidized-reduced properties, Cu can be both beneficial and potentially toxic to cells. Cu is an essential cofactor for enzymes that mediate basic cellular functions, including mitochondrial respiration, antioxidant defense, and hormone and neurotransmitter biosynthesis. However, dysregulation of Cu storage can lead to oxidative stress and cytotoxicity (22, 23). First defined by Golub et al., cuproptosis is a new cell death pattern that reveals the critical mechanism through which CRGs regulate copper death (9). Copper ionophores, such as disulfide (24) and elesclomol (25) can induce oxidative stress by suppressing natural antioxidant systems, such as the mitochondria, thereby inducing copper death. However, research on cuproptosis remains in the early stages of development, and specific regulatory mechanisms in various cancers remain unexplored.

CRGs have been previously correlated with the prognosis of patients with renal carcinoma (10), head and neck cancer (11), melanoma (12), and glioma (13). Considering BC, Zhi et al. (26) analyzed the TCGA database and found that patients with high expression levels of *ATP7A*, *DBT*, *DLAT*, *DLD*, *GLS*, *PDHA1*, and *SLC31A1* had a poor prognosis. High expression levels of *ATP7B*, *LIPT1*, and *NLRP3* were associated with improved OS. Li et al. (27) found that expression of *SLC31A1*, *ATP7A*, *DLD*, *DLAT*, and *DBT* significantly increased the risk of death, as determined by analyzing the TCGA database. Li et al. (19) analyzed the TCGA database and found that DLAT, SLC31A1, ATP7A, and ATP7B expression levels were significantly related to the OS of patients

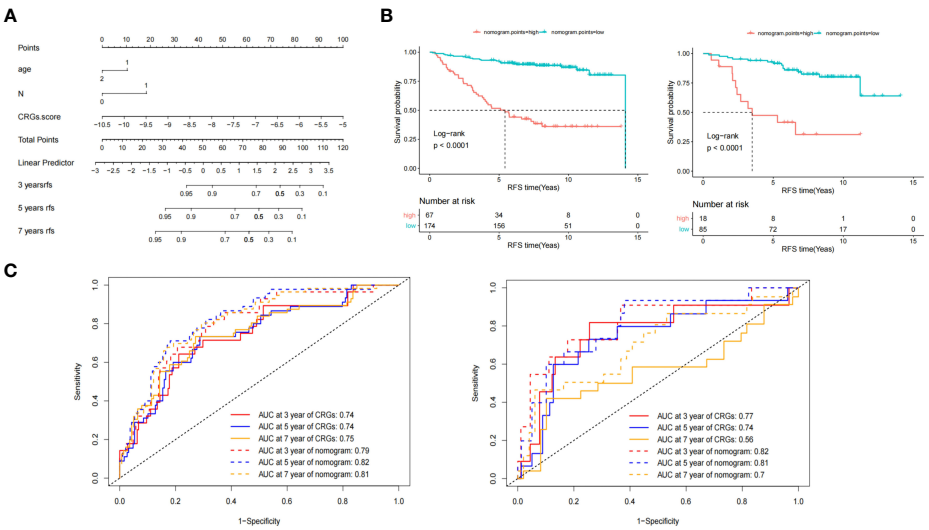

FIGURE 5
Nomogram model construction and survival analyses. **(A)** The Nomogram comprised the CRGs core, age, and lymph node status. **(B)** Kaplan-Meier survival analysis of nomogram points in training (left) and validation set (right). **(C)** The area under the curve (AUC) of receiver operating characteristics (ROC) of CRGs core and nomogram points model at 3-, 5- and 7- years in training (left) and validation (right) set.

with BC. Furthermore, Li et al. (28) found that SLC31A1 expression and its related pathway genes could potentially predict diagnosis, prognosis, and therapeutic response, as determined by analyzing the TCGA database. Sha et al. (29) analyzed a triple-negative subgroup of TCGA and found that high expression of *ATP7A*, *DLST*, and *LIAS* was associated with poor OS. Conversely, high expression levels of *LIPT1* and *PDHA1* indicated a good prognosis.

However, these studies have some limitations. First, the median follow-up time of patients without relapse in the TCGA database was 2.68 years for the ER+ subgroup. However, the relapse probability of ER+ patients within 5 years was the same as that after 5 years. Long-term follow-up of patients with ER+ BC is necessary. Second, analyses of BC subgroups, such as ER+ or HER2, are lacking in reported studies.

Herein, we used two independent long-term follow-up databases and two study designs to analyze the correlation between CRGs and outcomes in the ER+ subgroups and constructed a relapse prediction nomogram. Among patients enrolled at WCH, the control group had a median iDFS of 10.58 years. The median RFS of relapse-free patients was 7.3 years in the pooled GSE data. Considering the relationship between *DLD*, *LIAS*, and prognosis in TCGA, our findings contradict those reported in earlier studies, which may be attributed to the follow-up time and different molecular subgroups.

In our case-control study, the number of patients was limited. Therefore, we identified fewer prognostic genes than those in the pooled GSE data. In the cohort study, there were limited clinical features in public datasets that could be included in the model construction. Considering another limitation of our study, OS was not used as an endpoint.

In conclusion, our study indicates that high expression of positive hit genes (*FDX1, LIAS, LIPT1, DLD, PDH1*) and a copper-transporting gene (*ATP7B*) and low expression of negative hit genes (*CDKN2A*) related to cuproptosis can reduce the risk of iDFS or RFS in patients with ER+EBC. In addition, the constructed prognostic nomogram model had good predictive value for 7-year RFS of patients with ER+EBC.

Data availability statement

The raw data supporting the conclusions of this article will be made available by the authors, without undue reservation.

Ethics statement

The study involving human participants was conducted in accordance with the Declaration of Helsinki and was reviewed and approved by the Clinical Test and Biomedical Ethics Committee of West China Hospital, Sichuan University (No. 2019-16). The patients/participants provided their written informed consent to participate in this study

Author contributions

YF: Literature review, statistical analysis and interpretation of data, drafting of the manuscript, review of the manuscript for important intellectual content and final approval of the version to be submitted. YW, ZW, CW, CL and KH: Collection, preservation, sorting and delivery of frozen specimens for sequencing and approval of the version to be submitted. XZ: Clinical data collection and collation, revision and approval of the version to be submitted. HZ, DL and YPW: Study concept, review of the manuscript for important intellectual content and final approval of the version to be submitted. All authors contributed to the article and approved the submitted version.

Funding

This work was supported by the Key Program of Science & Technology Department of Sichuan Province (grant number: 2017SZ0005 to HZ) and the Key Research and Development Projects of the Science & Technology Department of Sichuan Province (grant number: 2019YFS0342 to YF).

Acknowledgments

The authors acknowledge the open access to the database from GEO.

Conflict of interest

The authors declare that the research was conducted in the absence of any commercial or financial relationships that could be construed as a potential conflict of interest.

Publisher's note

Supplementary material

The Supplementary Material for this article can be found online at: https://www.frontiersin.org/articles/10.3389/fonc.2023.1111480/full#supplementary-material

References

1. Sung H, Ferlay J, Siegel RL, Laversanne M, Soerjomataram I, Jemal A, et al. Global cancer statistics 2020: GLOBOCAN estimates of incidence and mortality worldwide for 36 cancers in 185 countries. *CA Cancer J Clin* (2021) 71:209–49. doi: 10.3322/caac.21660

2. Agarwal G, Pradeep PV, Aggarwal V, Yip CH, Cheung PS. Spectrum of breast cancer in Asian women. *World J Surg* (2007) 31:1031–40. doi: 10.1007/s00268-005-0585-9

3. Tang J, Cui Q, Zhang D, Liao X, Zhu J, Wu G. An estrogen receptor (ER)-related signature in predicting prognosis of ER-positive breast cancer following endocrine treatment. *J Cell Mol Med* (2019) 23:4980–90. doi: 10.1111/jcmm.14338

4. Early Breast Cancer Trialists' Collaborative G, Davies C, Godwin J, Gray R, Clarke M, Cutter D, et al. Relevance of breast cancer hormone receptors and other factors to the efficacy of adjuvant tamoxifen: patient-level meta-analysis of randomised trials. *Lancet* (2011) 378:771–84. doi: 10.1016/S0140-6736(11)60993-8

5. Cuzick J, Sestak I, Baum M, Buzdar A, Howell A, Dowsett M, et al. Effect of anastrozole and tamoxifen as adjuvant treatment for early-stage breast cancer: 10-year analysis of the ATAC trial. *Lancet Oncol* (2010) 11:1135–41. doi: 10.1016/S1470-2045(10)70257-6

6. Ruiz LM, Libedinsky A, Elorza AA. Role of copper on mitochondrial function and metabolism. *Front Mol Biosci* (2021) 8:711227. doi: 10.3389/fmolb.2021.711227

7. Li SR, Bu LL, Cai L. Cuproptosis: lipoylated TCA cycle proteins-mediated novel cell death pathway. *Signal Transduct Target Ther* (2022) 7:158. doi: 10.1038/s41392-022-01014-x

8. Zhao J, Guo S, Schrodi SJ, He D. Cuproptosis and cuproptosis-related genes in rheumatoid arthritis: implication, prospects, and perspectives. *Front Immunol* (2022) 13:930278. doi: 10.3389/fimmu.2022.930278

9. Tsvetkov P, Coy S, Petrova B, Dreishpoon M, Verma A, Abdusamad M, et al. Copper induces cell death by targeting lipoylated TCA cycle proteins. *Science* (2022) 375:1254–61. doi: 10.1126/science.abf0529

10. Long S, Wang Y, Chen Y, Fang T, Yao Y, Fu K. Pan-cancer analysis of cuproptosis regulation patterns and identification of mTOR-target responder in clear cell renal cell carcinoma. *Biol Direct* (2022) 17:28. doi: 10.1186/s13062-022-00340-y

11. Huang J, Xu Z, Yuan Z, Cheng L, Zhou C, Shen Y. Identification of cuproptosis-related subtypes and characterization of the tumor microenvironment landscape in head and neck squamous cell carcinoma. *J Clin Lab Anal* (2022) 36:e24638. doi: 10.1002/jcla.24638

12. Lv H, Liu X, Zeng X, Liu Y, Zhang C, Zhang Q, et al. Comprehensive analysis of cuproptosis-related genes in immune infiltration and prognosis in melanoma. *Front Pharmacol* (2022) 13:930041. doi: 10.3389/fphar.2022.930041

13. Wang W, Lu Z, Wang M, Liu Z, Wu B, Yang C, et al. The cuproptosis-related signature associated with the tumor environment and prognosis of patients with glioma. *Front Immunol* (2022) 13:998236. doi: 10.3389/fimmu.2022.998236

14. Fan Y, Xie G, Wang Z, Wang Y, Wang Y, Zheng H, et al. PTEN promoter methylation predicts 10-year prognosis in hormone receptor-positive early breast cancer patients who received adjuvant tamoxifen endocrine therapy. *Breast Cancer Res Treat* (2022) 192:33–42. doi: 10.1007/s10549-021-06463-6

15. Hu K, Wang C, Luo C, Zheng H, Song H, Bergstedt J, et al. Neuroendocrine pathways and breast cancer progression: a pooled analysis of somatic mutations and gene expression from two large breast cancer cohorts. *BMC Cancer* (2022) 22:680. doi: 10.1186/s12885-022-09779-8

16. Salim A, Ma X, Fall K, Andren O, Reilly M. Analysis of incidence and prognosis from 'extreme' case-control designs. *Stat Med* (2014) 33:5388–98. doi: 10.1002/sim.6245

17. Zhao Y, Li MC, Konate MM, Chen L, Das B, Karlovich C, et al. TPM, FPKM, or normalized counts? a comparative study of quantification measures for the analysis of RNA-seq data from the NCI patient-derived models repository. *J Transl Med* (2021) 19:269. doi: 10.1186/s12967-021-02936-w

18. Gourgou-Bourgade S, Cameron D, Poortmans P, Asselain B, Azria D, Cardoso F, et al. Guidelines for time-to-event end point definitions in breast cancer trials: results of the DATECAN initiative (Definition for the assessment of time-to-event endpoints in CANcer trials). *Ann Oncol Off J Eur Soc Med Oncol* (2015) 26:2505–6. doi: 10.1093/annonc/mdv478

19. Li L, Li L, Sun Q. High expression of cuproptosis-related SLC31A1 gene in relation to unfavorable outcome and deregulated immune cell infiltration in breast cancer: an analysis based on public databases. *BMC Bioinf* (2022) 23:350. doi: 10.1186/s12859-022-04894-6

20. Chu J, Sun N, Hu W, Chen X, Yi N, Shen Y. Bayesian Hierarchical lasso cox model: a 9-gene prognostic signature for overall survival in gastric cancer in an Asian population. *PloS One* (2022) 17:e0266805. doi: 10.1371/journal.pone.0266805

21. Ge EJ, Bush AI, Casini A, Cobine PA, Cross JR, DeNicola GM, et al. Connecting copper and cancer: from transition metal signalling to metalloplasia. *Nat Rev Cancer* (2022) 22:102–13. doi: 10.1038/s41568-021-00417-2

22. Kardos J, Heja L, Simon A, Jablonkai I, Kovacs R, Jemnitz K. Copper signalling: causes and consequences. *Cell Commun Signal* (2018) 16:71. doi: 10.1186/s12964-018-0277-3

23. Maung MT, Carlson A, Olea-Flores M, Elkhadragy L, Schachtschneider KM, Navarro-Tito N, et al. The molecular and cellular basis of copper dysregulation and its relationship with human pathologies. *FASEB J* (2021) 35:e21810. doi: 10.1096/fj.202100273RR

24. Allensworth JL, Evans MK, Bertucci F, Aldrich AJ, Festa RA, Finetti P, et al. Disulfiram (DSF) acts as a copper ionophore to induce copper-dependent oxidative stress and mediate anti-tumor efficacy in inflammatory breast cancer. *Mol Oncol* (2015) 9:1155–68. doi: 10.1016/j.molonc.2015.02.007

25. Zheng PJ, Zhou CT, Lu LY, Liu B, Ding YM. Elesclomol: a copper ionophore targeting mitochondrial metabolism for cancer therapy. *J Exp Clin Canc Res* (2022) 41:271. doi: 10.1186/s13046-022-02485-0

26. Li Z, Zhang H, Wang X, Wang Q, Xue J, Shi Y, et al. Identification of cuproptosis-related subtypes, characterization of tumor microenvironment infiltration, and development of a prognosis model in breast cancer. *Front Immunol* (2022) 13:996836. doi: 10.3389/fimmu.2022.996836

27. Li J, Wu F, Li C, Sun S, Feng C, Wu H, et al. The cuproptosis-related signature predicts prognosis and indicates immune microenvironment in breast cancer. *Front Genet* (2022) 13:977322. doi: 10.3389/fgene.2022.977322

28. Li X, Ma Z, Mei L. Cuproptosis-related gene SLC31A1 is a potential predictor for diagnosis, prognosis and therapeutic response of breast cancer. *Am J Cancer Res* (2022) 12:3561–80.

29. Sha S, Si L, Wu X, Chen Y, Xiong H, Xu Y, et al. Prognostic analysis of cuproptosis-related gene in triple-negative breast cancer. *Front Immunol* (2022) 13:922780. doi: 10.3389/fimmu.2022.922780

frontiers | Frontiers in Immunology

TYPE Original Research
PUBLISHED 23 May 2023
DOI 10.3389/fimmu.2023.1174762

OPEN ACCESS

EDITED BY
Guojun Chen,
McGill University, Canada

REVIEWED BY
Heidi Braumüller,
University of Freiburg Medical Center, Germany
Jiaxiang Ye,
Affiliated Tumor Hospital of Guangxi Medical University, China

*CORRESPONDENCE
Zhongqi Wang
lhyyzlekzr07@hotmail.com
Jia Yang
jiajiayy07@163.com

RECEIVED 27 February 2023
ACCEPTED 11 May 2023
PUBLISHED 23 May 2023

CITATION
Yang J, Liu K, Yang L, Ji J, Qin J, Deng H and Wang Z (2023) Identification and validation of a novel cuproptosis-related stemness signature to predict prognosis and immune landscape in lung adenocarcinoma by integrating single-cell and bulk RNA-sequencing.
Front. Immunol. 14:1174762.
doi: 10.3389/fimmu.2023.1174762

Identification and validation of a novel cuproptosis-related stemness signature to predict prognosis and immune landscape in lung adenocarcinoma by integrating single-cell and bulk RNA-sequencing

Jia Yang*, Kaile Liu, Lu Yang, Junqing Ji, Jingru Qin, Haibin Deng and Zhongqi Wang*

Department of Medical Oncology, Longhua Hospital Shanghai University of Traditional Chinese Medicine, Shanghai, China

Background: Cancer stem cells (CSCs) play vital roles in lung adenocarcinoma (LUAD) recurrence, metastasis, and drug resistance. Cuproptosis has provided a novel insight into the treatment of lung CSCs. However, there is a lack of knowledge regarding the cuproptosis-related genes combined with the stemness signature and their roles in the prognosis and immune landscape of LUAD.

Methods: Cuproptosis-related stemness genes (CRSGs) were identified by integrating single-cell and bulk RNA-sequencing data in LUAD patients. Subsequently, cuproptosis-related stemness subtypes were classified using consensus clustering analysis, and a prognostic signature was constructed by univariate and least absolute shrinkage operator (LASSO) Cox regression. The association between signature with immune infiltration, immunotherapy, and stemness features was also investigated. Finally, the expression of CRSGs and the functional roles of target gene were validated *in vitro*.

Results: We identified six CRSGs that were mainly expressed in epithelial and myeloid cells. Three distinct cuproptosis-related stemness subtypes were identified and associated with the immune infiltration and immunotherapy response. Furthermore, a prognostic signature was constructed to predict the overall survival (OS) of LUAD patients based on eight differently expressed genes (DEGs) with cuproptosis-related stemness signature (KLF4, SCGB3A1, COL1A1, SPP1, C4BPA, TSPAN7, CAV2, and CTHRC1) and confirmed in validation cohorts. We also developed an accurate nomogram to improve clinical applicability. Patients in the high-risk group showed worse OS with lower levels of immune cell infiltration and higher stemness features. Ultimately, further cellular experiments were performed to verify the expression of CRSGs and prognostic

DEGs and demonstrate that SPP1 could affect the proliferation, migration, and stemness of LUAD cells.

Conclusion: This study developed a novel cuproptosis-related stemness signature that can be used to predict the prognosis and immune landscape of LUAD patients, and provided potential therapeutic targets for lung CSCs in the future.

KEYWORDS

cuproptosis-related stemness genes (CRSGs), prognostic signature, immune landscape, single-cell sequencing, lung adenocarcinoma, cancer stem cells

Introduction

The most prevalent type of lung cancer, lung adenocarcinoma (LUAD), is the primary reason for cancer-related deaths worldwide (1). Although the advances of treatment in LUAD over the past 20 years, the 5-year overall survival (OS) is still below 20% due to its high recurrence and metastasis (2, 3). Increasing evidence indicates that lung cancer stem cells (CSCs) play a critical role in LUAD, and their self-renewal, unlimited proliferation, and immunosuppressive properties are responsible for generating tumor heterogeneity and radio-chemotherapy resistance (4, 5). Despite salinomycin and its derivatives have been identified that preferentially target breast CSCs (6, 7), more efforts are needed to identify novel therapeutic targets and develop effective prognostic models for LUAD patients to break the logjam of CSCs-mediated drug resistance and immune suppression.

Since the low levels of ROS in CSCs, new therapeutic strategies for generating intracellular reactive oxygen species (ROS) by exogenous metal chelators and ionophores have emerged (8). Copper (Cu), as an essential element for accumulating ROS, is closely related to the progression of cancer by promoting proliferation, angiogenesis, metastasis, and regulating immune responses (9, 10). A series of copper complexes have demonstrated encouraging anticancer potential by selectively suppressing lung, colorectal, and breast CSCs, including copper ionophore such as disulfiram, which has already entered phase I (11, 12). Recent studies have revealed this novel copper-dependent cell death that is triggered by copper ionophores, known as cuproptosis (13), which is associated with mitochondrial respiration and the tricarboxylic acid (TCA) cycle, resulting in proteotoxic stress that is distinct from oxidative stress-related cell death (14). Since Tsvetkov et al. first proposed that FDX1, LIAS, LIPT1, DLD, DLAT, PDHA1, and PDHB are positive cuproptosis-related genes, while MTF1, GLS, and CDKN2A are negative cuproptosis-related genes (13). More and more novel cuproptosis-related genes (CRGs) have been identified in various tumors (15, 16). Evidence shows that lung cancer cells, including LUAD, also require glutamine to fulfill metabolic needs, which is important for the TCA cycle (17, 18). Numerous studies have developed different cuproptosis-related risk models to predict prognosis and immune infiltration in LUAD using bioinformatics analyses (16, 19–21). However, no studies of CRGs combined with stemness signatures in LUAD have been reported to date, and their roles in prognosis and immune landscape remain unknown.

Compared to conventional bulk sequencing, single-cell RNA sequencing (scRNA-seq) is capable of uncovering specific cell populations and intratumoral heterogeneity at the single-cell level (22, 23). Therefore, we for the first time identified the cuproptosis-related stemness genes (CRSGs) in LUAD by integrating bulk and scRNA-seq and constructed a prognostic signature to predict the prognosis, immune infiltration, stemness features, immunotherapy response, and drug sensitivity. Lastly, *in vitro* experiments were performed to investigate the expression and biological function of CRSGs. These findings highlight the essential role of CRSGs in LUAD patients, which might provide new insights into elucidating heterogeneity and developing more effective therapeutic targets for CSCs.

Abbreviations: LUAD, lung adenocarcinoma; CSCs, Cancer stem cells; CRG, cuproptosis-related genes; CRSGs, cuproptosis-related stemness genes; DEGs, differentially expressed genes; scRNA-seq, Single-cell RNA sequencing; NK, natural killer; OS, overall survival; LASSO, least absolute shrinkage and selection operator; K-M, Kaplan–Meier; TCA, tricarboxylic acid cycle; ROS, reactive oxygen species; GEO, Gene Expression Omnibus; TCGA, The Cancer Genome Atlas; GO, Gene Ontology; KEGG, Kyoto Encyclopedia of Genes and Genomes; GDSC, Genomics of Drug Sensitivity in Cancer; TIDE: Tumor Immune Dysfunction and Exclusion; ROC, receiver operating characteristic; PCA, principal component analysis; UMAP, uniform manifold approximation and projection; AUC, area under curve; CDF, cumulative distribution function; DCA, decision curve analysis; ssGSEA, Single sample gene set enrichment analysis; GSVA, Gene Set Variation Analysis; CNV, copy-number variation; ICIs, immune checkpoints inhibitors.

Materials and methods

Data acquisition and preprocessing

The Gene Expression Omnibus (GEO) database (https://www.ncbi.nlm.nih.gov/geo/) was used to analyze the scRNA-seq data of 11 LUAD samples (GSE131907 (24)). The bulk RNA-seq data of 541 LUAD samples and 59 para-carcinoma samples were obtained from the Cancer Genome Atlas (TCGA) database, including 491 patients with clinicopathologic and survival information (Table S1). Additionally, transcriptomic data from 19

LUAD samples is included in GSE141569 (25) as the external validation set. All the datasets were normalized by the limma package (26) and the R package (27). Simultaneously, in total of 10 cuproptosis marker genes and 2916 cancer stemness genes were obtained by literature review (13, 28) and related databases (29, 30).

Single-cell data analysis and intercellular communication

The quality control of scRNA-seq data was performed using the Seurat R package (version 4.1.0) (31) to optimally eliminate potential doublets. Using Uniform Manifold Approximation and Projection (UMAP), the top 30 components from principal component analysis (PCA) on highly variable genes were chosen. Cells were clustered using the FindClusters function. The FindMarkers function was used to annotate cell types based on reported cell-specific marker genes (Table S2). The R package CellChat (version 1.1.3) (32) was used to evaluate cell–cell interactions based on the CellChatDB databases.

The scores of stemness and cuproptosis at the single-cell level

To obtain the stemness signature gene set of LUAD, we downloaded 2916 stemness-related genes from the literature and database, and aligned them with single-cell genes. The scores of stemness signature were divided by median values, which were calculated by the AddModuleScore function in Seurat. The scores of cuproptosis for each cell were obtained by calculating the Area Under the Curve (AUC) value of key CRGs using the AUCell R package (version 1.18.1) (31). The UMAP embedding is colored by the AUC scores. The scores of cuproptosis signature were divided by the activity of cell clusters in LUAD scRNA-seq.

Analysis of DEGs and cuproptosis-related molecular subtypes

DEGs were identified based on the TCGA-LUAD data by using the R package. DEGs were defined as $|\log2\ FC|>2$ with adjusted $p<0.05$ and visualized using heatmaps (33) and volcano plots from the R packages ggplot2 (34).

The consensus clustering analysis was used to identify different subtypes in LUAD based on cuproptosis-related DEGs by the "ConsensusClusterPlus" R package (35). To ascertain the K value, a cumulative distribution function (CDF) curve was employed, and the classification was verified by PCA in LUAD.

Functional enrichment and gene set variation analysis

Using the clusterProfiler (36) package, the Gene Ontology (GO) (37) and Kyoto Encyclopedia of Genes and Genomes (KEGG) (38) enrichment analyses of the DEGs were performed. The dataset of immune cells was downloaded from TISIDB (39) (http://cis.hku.hk/TISIDB/download.php) using the GSVA package (40). The stemness and immune scores based on the gene expression matrix were calculated using the single sample gene set enrichment analysis (ssGSEA).

Construction of the prognostic model and nomogram

Forest plots were drawn based on the results of univariate and multivariate Cox regression. By using univariate and least absolute shrinkage operator (LASSO) cox regression, a prognostic model based on differently expressed CRSGs was built. Cox regression coefficients using the formula:

$$\mathrm{RiskScore}' = \sum \exp_{\mathrm{Genei}} \times \mathrm{coef}_{\mathrm{Genei}}$$

Kaplan-Meier (K-M) analysis and the receiver operator characteristic (ROC) curve were performed to estimate the OS using the R 'survival' and 'timeROC' packages. A nomogram for predicting the OS was built by using the rms R package. To assess the clinical value of nomograms, decision curve analysis (DCA) and clinical impact curves were used.

Correlation analysis of immune infiltrating cells

The gene expression matrix of infiltrating immune cells was obtained by CIBERSORT (41) using the LM22 signature. The correlation of 22 immune cells was shown in a heatmap by the corrplot algorithm, and the correlation between immune infiltration and prognosis was calculated by the ggplot2 package. We also analyzed the correlation of prognostic genes with immune checkpoints.

Anticancer drug sensitivity analysis

The anticancer drug sensitivity and markers of drug response were collected from the Genomics of Drug Sensitivity in Cancer (GDSC) database (42). A ridge regression model was built using gene expression profiles by the pRRophetic algorithm (43). The sensitivity of an anticancer drug was classified by IC50 values.

Cell culture and transfection

The LUAD cell lines (A549 and SPC-A1) and human bronchial epithelial cells (BEAS-2B) were purchased from the Cell Bank of the Chinese Academy of Sciences (Shanghai, China). All cells were cultured in DMEM or RPMI-1640 medium (Hyclone, USA) supplemented with 10% fetal bovine serum (FBS; Gibco, USA).

The small interfering RNA of SPP1 (siSPP1) and control RNA (si-Ctrl) were synthesized by GenePharma Inc. (Shanghai, China). Lipofectamine 3000 (Invitrogen, USA) was used to transiently transfect the siRNA into cells. The sequence of siSPP1#1 is UAUUUUGGCCUUUAUUCUGUU, siSPP1#2 is GAGAA TTGCAGTGATTTGCTTTT, and siSPP1#3 is AGGAA AAGCAGCTTTACAAAA. After 48 hours of incubation, the interfering effect was confirmed by Western blotting. The following antibodies were used: anti-SPP1 (ab302942, 1:1000, Abcam, USA), β-actin (ab8226, 1:1000, Abcam, USA).

Quantitative real-time PCR

TRIzol reagent (Invitrogen, USA) was used to extract total RNA from the cells, and the cDNA synthesis kit (Takara, Japan) was used to reverse-transcribe the extracted total RNA into cDNA in accordance with the kit's instructions. SYBR Green RT-PCR Kits (Takara, Japan) were used for the qPCR, and $2^{-\Delta\Delta Ct}$ was used to determine the relative mRNA expression. β-actin provided internal control. Table 1 contained a list of the primers.

Cell proliferation and migration assay

Cell proliferation was evaluated using the CCK-8 assay. The transfected SPC-A1 cells were seeded onto 96-well plates with 2×10^3 cells/well and incubated for 5 days. Cell Counting Kit-8 (CCK-8) (Beyotime, China) was added and detected the absorbance of the solution at 490 nm. Transwell test was used to measure cell migration. Cells (2×10^5 cells/ml) were added to the upper 24-well plate chamber with FBS-free medium, while the lower chamber was

TABLE 1 Primer sequences used for qRT-PCR.

Gene	Primers	Sequence (5′–3′)
CDKN2A	Forward	GGAGGCCGATCCAGGTCAT
	Reverse	CACCAGCGTGTCCAGGAAG
GLS	Forward	CACTCAAATCAGGATTGCG
	Reverse	CCAGACTGCTTTTTAGCACTTT
FDX1	Forward	CCTGGCTTGTTCAACCTGTCA
	Reverse	CCAACCGTGATCTGTCTGTTAGTC
PDHA1	Forward	CAGACCATCTCATCACAGCCTACC
	Reverse	CCTCCTTTCCCTTTAGCACAACCT
PDHB	Forward	GACACTCCCATATCAGAGATGG
	Reverse	CTTGGCAGCTGAGTTTATAACC
DLD	Forward	GCCGACGACCCTTTACTAAGAAT
	Reverse	GGACCAGCAACTACATCACCAAT
KLF4	Forward	AACCTATACGAAGAGTTCTCAT
	Reverse	CCAGTCACAGTGGTAAGG
SCGB3A1	Forward	ATGTCCCCACAATCAGCAAG
	Reverse	CTCTGCAGCTGGAGCAAGG
COL1A1	Forward	GCTCCTCTTAGGGGCCACT
	Reverse	CCACGTCTCACCATTGGGG
SPP1	Forward	CAAATACCCAGATGCTGTGGC
	Reverse	TGGTCATGGCTTTCGTTGGA
C4BPA	Forward	CTACGCATACGGCTTTTCTGT
	Reverse	CCCATGTGAAACATCTGGCTTG
TSPAN7	Forward	CTCATCGGAACTGGCACCACTA
	Reverse	CCTGAAATGCCAGCTACGAGCT
CAV2	Forward	CGTGCCTAATGGTTCTGCCT

(Continued)

TABLE 1 Continued

Gene	Primers	Sequence (5′–3′)
	Reverse	CGCTCGTACACACAATGGAGCA
CTHRC1	Forward	ATAATGGAATGTGCTTACAAGG
	Reverse	TTCCCAAGATCTATGCCATAAT
β-actin	Forward	CTTCGCGGGCGACGAT
	Reverse	CCACATAGGAATCCTTCTGACC

contained with 20% FBS medium. After 24 hours, the cells in the lower chamber were stained and counted under the 200x microscope.

Tumorsphere formation assay

SPC-A1 cells (3×10^3/well) were plated into an ultralow attachment 6-well plate (Corning, USA) and incubated for 5-7 days. Serum-free DMEM/F12 (Gibco, USA) supplemented with 20 ng/mL epidermal growth factor (Sigma, USA), 20 ng/mL basic fibroblast growth factor (Sigma, USA), 20 μL/mL B27 (Invitrogen, USA), and 5 μg/mL insulin (Invitrogen, USA) was used to culture the cells. Morphology of CSC spheres was photographed under the 400x microscope.

Statistical analysis

Using R programming (version 4.1.0), all statistical analyses were carried out. T-tests or the Mann-Whitney U test were used to compare continuous variables between groups. All p values were two-sided, and significance was indicated by $p < 0.05$.

Results

Clustering and differential analysis of scRNA-seq data

The flow chat was shown in Figure 1. After quality control, we used scRNA-seq data (GSE131907) to obtain gene expression profiles for 45,149 cells from 11 primary LUAD samples. As shown in Figure 2A, these cells were classified into 27 clusters by the KNN algorithm. Subsequently, clusters were annotated into 8 major cell types (Figures 2B; S1A) based on the expression of marker genes (Table S2). They were epithelial cells (contain non-malignant cells and cancer cells), myeloid cells, T lymphocytes, natural killer (NK) cells, B lymphocytes, fibroblasts, mast cells, and endothelial cells (Figure 2C). There is a relatively high proportion of T lymphocytes and a low proportion of endothelial cells (Figure 2E). Then, we divided each cell into high- and low-stemness cells according to the median value of the stemness score (Figure 2D). Furthermore, a total of 6107 differentially expressed stemness genes were identified, and the top 20 genes were shown in the heatmap (Figure 2F).

Analysis of cuproptosis score based on stemness signature and functional enrichment

Through the intersection of the 6107 differentially expressed stemness genes and 10 cuproptosis-related genes, 6 CRSGs (CDKN2A, GLS, FDX1, PDHA1, PDHB, and DLD) were obtained (Figure 2G). We further explored that they were mainly expressed in epithelial (contain non-malignant cells and cancer cells), myeloid cells and T lymphocytes by scRNA-seq. (Figures 2H–M). Additionally, there was a positive correlation among these CRSGs, the expression of CDKN2A was positively correlated with GLS (cor = 0.394) (Figure 2N). These genes were significantly more active in epithelial and myeloid cells (Figure 3A). In total, 25802 cells with a high-cuproptosis score based on stemness signature were screened by the AUCell R package (AUC > 0.054) (Figure 3B).

We further explored the functional enrichment between the high- and low- cuproptosis score cells based on stemness signature by GO and KEGG analyses. They were most enriched in the metabolic microenvironments and cancer-related pathways, such as protein catabolism, DNA-binding proteins, and endocytosis (Figure 3C, D; Table S3-4).

Clustering subtypes of high-cuproptosis score with stemness signature in single-cell data

After obtaining the high-cuproptosis score stemness cells, we classified them into 30 clusters by the KNN algorithm (Figure 4A). Finally, cell types were recognized based on previous cell markers (Figures 4B; S1B): epithelial cells (contain non-malignant cells and cancer cells), myeloid cells, T lymphocytes, fibroblasts, B lymphocytes, mast cells, and endothelial cells (Figure 4C). Cell clusters were almost consistent with the distribution by stemness score above. Additionally, the expression of CRSGs in subtypes was similar to previous results from scRNA-seq (Figures 4D–I).

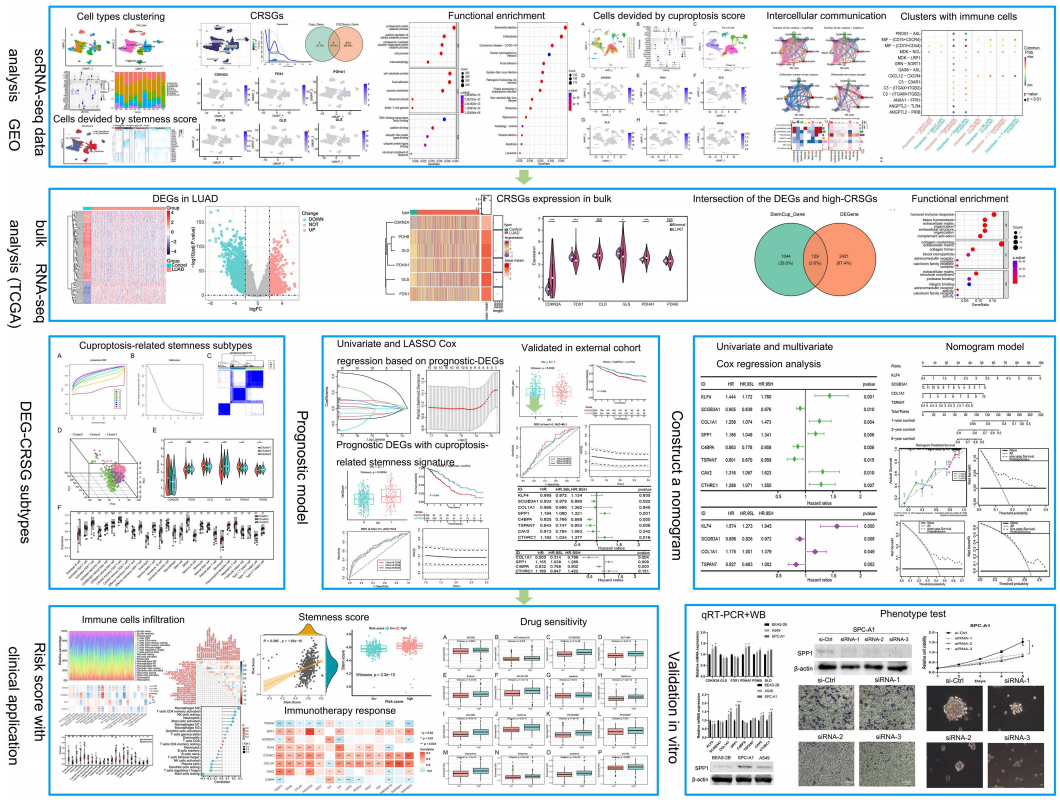

FIGURE 1
Flow chat in the study.

Intercellular communication between cuproptosis stemness cluster and others

CellChat was used to delineate intricate a cell-cell network from scRNA-seq. Figure 5A shows the intercellular communication of high- and low- cuproptosis score stemness cluster that mainly occurred in epithelial, endothelial, fibroblast, lymphocytes, and myeloid cells with differential interaction numbers and strengths. Further analysis suggested that high-cluster was more associated with immune cells, such as NK cells and lymphocytes, and less associated with epithelial cells, endothelial cells and myeloid cells (Figures 5B, C). Moreover, ligand-receptor pair analysis revealed that fibroblasts preferred to communicate with immunocytes through MIF-(CD74+CXCR4), MIF-(CD74+CD44) and MDK-NCL (Figure 5D).

Characteristics of CRSGs in the bulk RNA-seq of LUAD

Further, we examined 2550 DEGs in total, including 985 genes upregulated and 1565 genes downregulated in TCGA-LUAD (Figures S1C-D). The expression of CRSGs in bulk RNA-seq showed that CDKN2A and PDHA1 were higher in LUAD ($p < 0.001$), while FDX1 and GLS were lower in LUAD ($p < 0.05$), and with unaltered levels of DLD and PDHB ($p > 0.05$) (Figures 5E, F). Additionally, through the intersection of the DEGs and the marker genes in high-cuproptosis stemness cluster, a total of 129 genes were obtained (Figure 5G; Table S5). GO analysis showed they were mostly related to immune features and complement activation. (Figure 5H; Table S6).

Analysis of cuproptosis-related stemness subtypes and immune infiltration in LUAD

Three distinct cuproptosis-related stemness subtypes were identified (Cluster 1-3) based on 129 intersecting DEGs by unsupervised clustering. (Figures 6A–C). The clustering criteria were k=3, and the results were confirmed by PCA (Figure 6D, Figure S1E). Furthermore, most CRSGs except FDX1, were significantly differentially expressed among the three clusters ($p < 0.05$) (Figure 6E).

Next, the immune infiltration score of the 28 immune cell types was evaluated in the three subtypes by employing the ssGSEA analysis (Figure 6F). The results showed that most immune infiltrating cells like activated B cells, CD4+ T cells, CD8+ T cells, myeloid-derived suppressor cells (MDSCs), and NK cells were significantly lower in Cluster 1, indicating that patients in Cluster 1 would be more insensitive to immunotherapy.

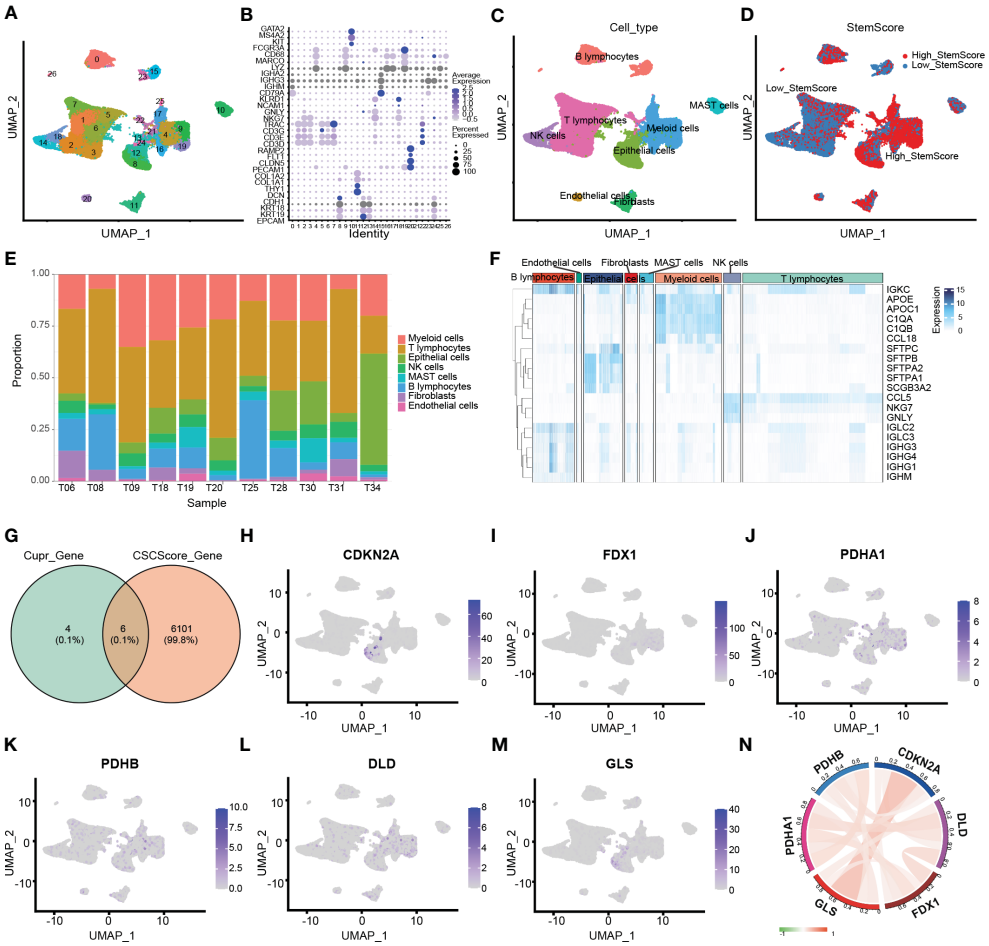

FIGURE 2
Clustering and differential analysis of scRNA-seq data. **(A)** Cells in scRNA-seq (GSE131907) were classified into 27 clusters by dimensional reduction and clustering analysis. **(B)** Marker gene expression in each cluster. **(C)** The UMAP diagram shows the distribution of the 8 major cell types in each sample. **(D)** The major cell types were divided into high- and low- stemness cells by the stemness score. **(E)** Histogram overlays display the proportion of cell types in each sample. **(F)** A heatmap showing the top 20 differentially expressed stemness genes in each cell type. **(G)** Venn diagram shows the intersection of differential stemness genes and cuproptosis-related genes. **(H-M)** Expression of CRSGs in different cell types: CDKN2A, FDX1, PDHA1, PDHB, DLD, and GLS. **(N)** The circle plot shows the correlation between CRSGs.

Construction and validation of the prognostic model with cuproptosis-related stemness signature

A prognostic signature was constructed by univariate and LASSO Cox regression to select the most significantly prognostic CRSGs among the 129 DEGs (Figures 7A, B). As a result, eight genes (KLF4, SCGB3A1, COL1A1, SPP1, C4BPA, TSPAN7, CAV2, and CTHRC1) with minimal lambda ($p = 0.01$) were finally screened out to construct the prognostic model. Internal validation cohort (TCGA-LUAD) shows patients with a high-risk score exhibited a worse OS (p=0.00004, Figure 7C). Similarly, K-M analysis showed that patients in the high-risk group had significantly lower survival rates ($p < 0.001$, Figure 7D). The ROC curves for 1-, 2- and 3- year OS were calculated, with AUCs of 0.7049, 0.7049, and 0.6836, respectively (Figures S2A, B). Additionally, we also validated in external cohort (GSE141569). Consistent with the above results, patients with higher risk scores showed higher mortality ($p = 0.0038$, Figure 7E). The K-M curve and AUC values also exhibited higher OS rates in the low-risk group ($p = 0.005$, Figurea 7F; S2C, D). All the results indicated that the risk score may be a trustworthy and accurate model to predict the prognosis of LUAD.

Construction of the nomogram for LUAD patients

To further apply the prognostic model, we performed the univariate and multivariate Cox regression analysis (Figure 8A-B; Table S7) based on the clinical information (Table S1) and CRSGs features from TCGA-LUAD. Similar results were validated in an external cohort (Figures S3A, B). The nomogram was constructed based on the results of multivariable Cox regression (Figure 8C). The accuracy of the nomogram's 1-, 3-, and 5-year survival predictions was demonstrated by calibration curves. (Figure 8D).

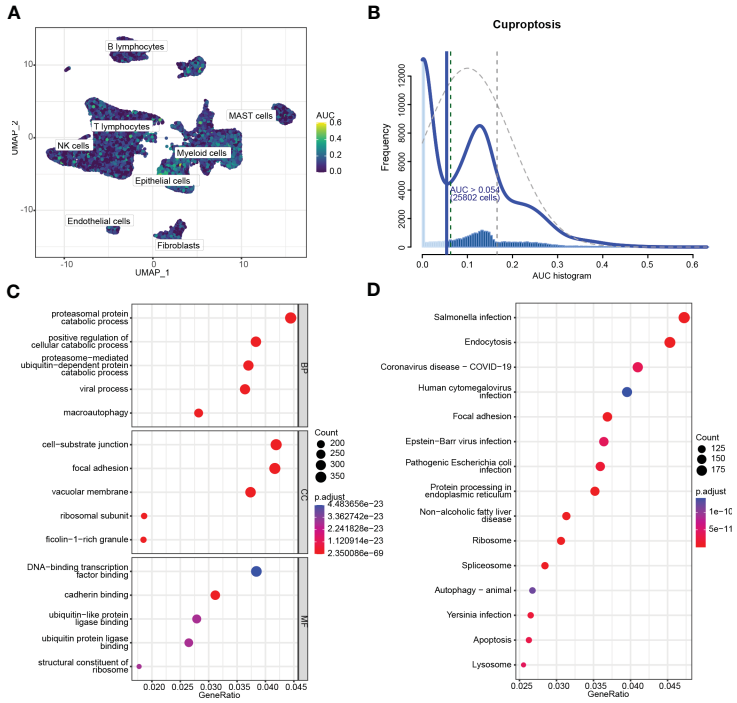

FIGURE 3
Analysis of cuproptosis score based on stemness signature and functional enrichment in scRNA-seq. **(A)** The UMAP plot shows the cuproptosis score based on stemness signature in each cell type. **(B)** The distribution graph of AUC. High-cuproptosis score cells were selected using AUCell function by AUC>0.054. **(C)** GO enrichment analysis of DEGs between the high- and low- cuproptosis score cells based on stemness signature. **(D)** KEGG pathway analysis of DEGs.

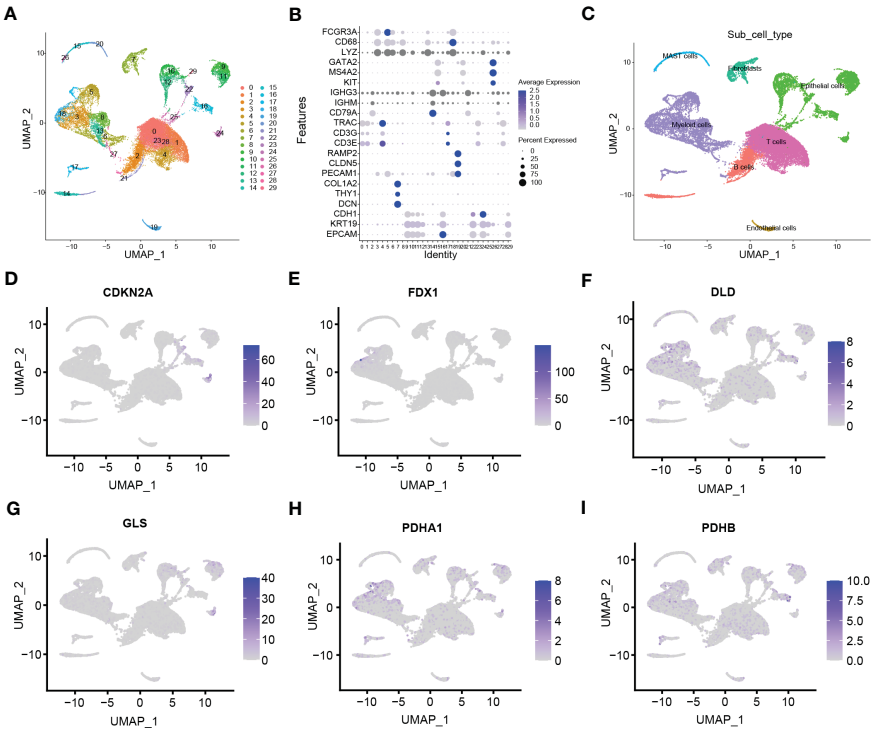

FIGURE 4
Clustering subtypes of high-cuproptosis score with stemness signatures in single-cell data. **(A)** The UMAP diagram shows the high-cuproptosis score stemness cells were classified into 30 clusters using dimensional reduction and clustering analysis. **(B)** Marker gene expression in each cluster. The bigger the dots, the higher the cell proportion. **(C)** Seven recognized cell types based on previous cell markers. **(D-I)** Expression of CRSGs in each cell type: CDKN2A **(D)**, FDX1 **(E)**, DLD **(F)**, GLS **(G)**, PDHA1 **(H)**, PDHB **(I)**.

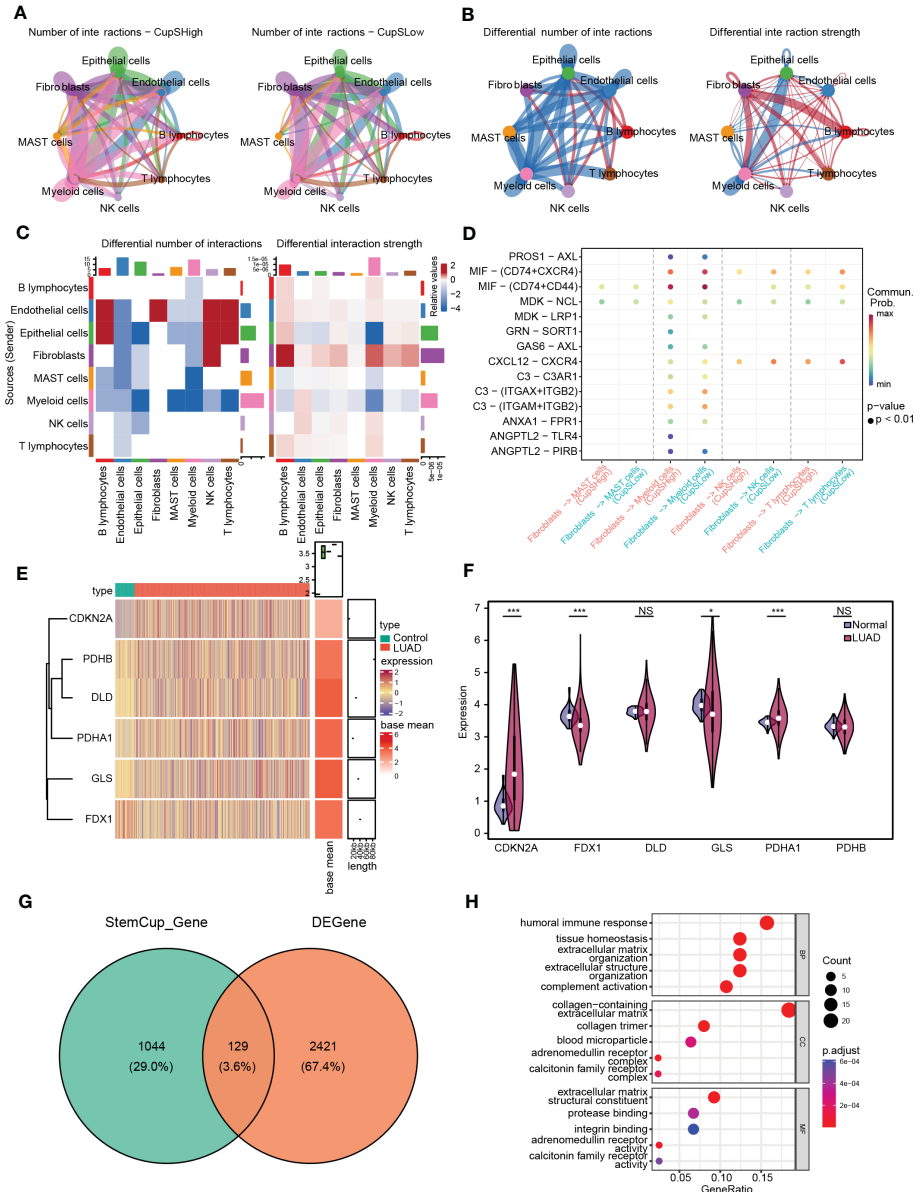

FIGURE 5
Intercellular communication between cuproptosis score stemness cluster and others. **(A)** Cell-cell communication network of high-(Left) and low-(Right) cuproptosis score stemness cluster with others by CellChat. **(B)** Differential interaction number (Left) and strength (Right) between the cuproptosis score stemness cluster with others. **(C)** The heatmap shows the differential interaction number and strength. **(D)** Ligand-receptor interactions plot. **(E)** The heatmap shows the differential expression of CRSGs in bulk RNA-seq. **(F)** Violin plots showing the expression of CRSGs between LUAD and para-carcinoma tissues in TCGA dataset. **(G)** Venn diagram shows the intersection of the DEGs and the marker genes in high-cuproptosis score stemness clusters. **(H)** GO analysis of the intersecting genes. *p* values were shown as: *, $p<0.05$; **, $p<0.01$; ***, $p<0.001$; NS, no significance.

Meanwhile, the DCA also indicated that LUAD patients were more likely to benefit from the nomogram model (Figures 8E–G).

Immune infiltration profiles and stemness score based on a prognostic signature

We further performed the CIBERSORT algorithm to assess the proportion and correlation of immune cells in each LUAD patient (Figures S3C, D). Correlation analyses found that CRSGs with prognostic signature were associated with most of the 22 immune cells (Figure 9A). Besides, there were significant immune cell differences between the high- and low-risk groups. (Figure 9B). Finally, a correlation analysis between risk score and immune infiltration was performed, which revealed that risk score was positively correlated with M0 macrophages, memory CD4+ T cells, and resting NK cells but negatively correlated with activated NK cells, resting mast cells and Tregs (Figure 9C)

Moreover, the stemness score was calculated using ssGSEA, and correlated with the risk score. A positive association was found between risk score and stemness score (r = 0.286, p = 1.95e-10, Figure 9E), which indicated that patients with a higher risk score

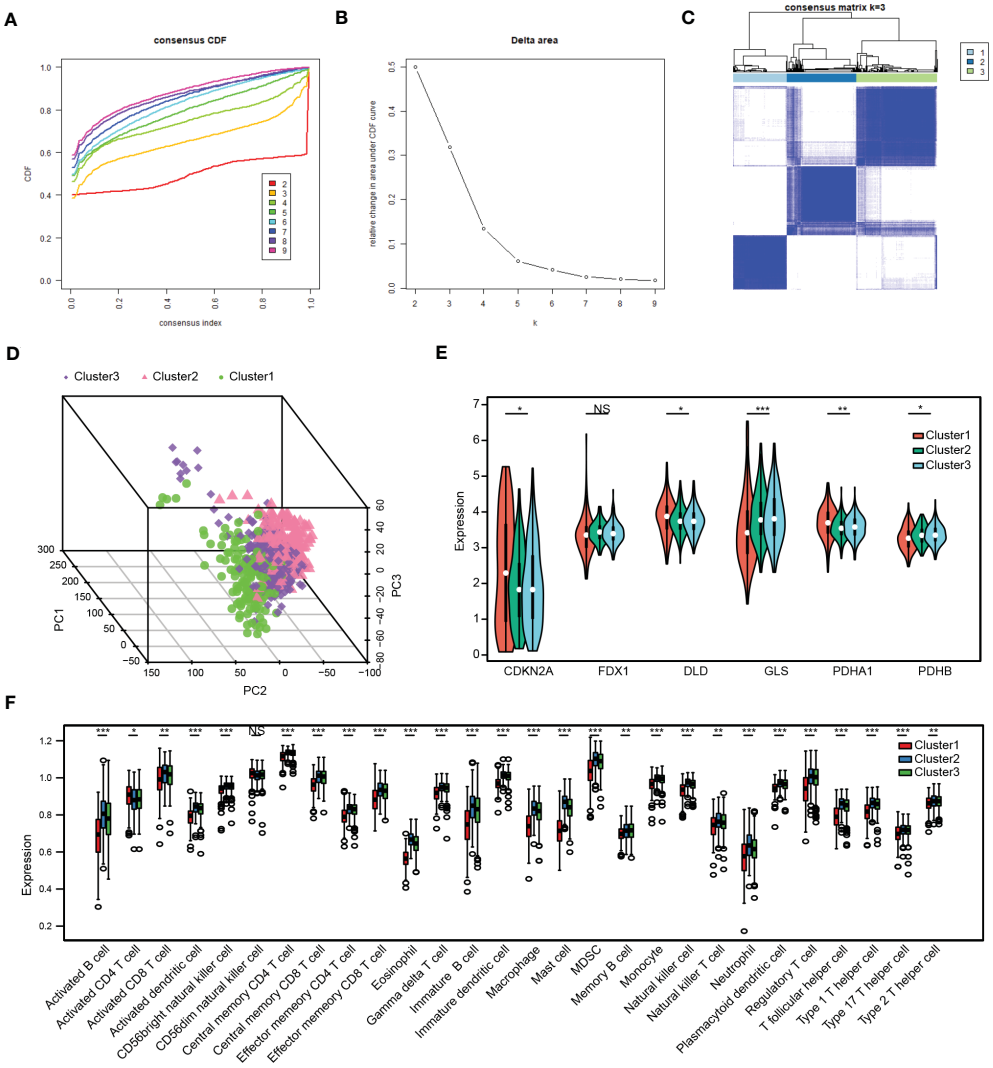

FIGURE 6
Analysis of cuproptosis-related stemness subtypes and immune infiltration in LUAD. **(A)** Plot of the Cumulative Distribution Function (CDF). **(B)** Delta area. **(C)** Unsupervised clustering heatmap when k=3. **(D)** Three distinct cuproptosis-related stemness subtypes were identified based on intersecting DEGs by principal component analysis (PCA). **(E)** Expression of CRSGs in the three clusters. **(F)** A box plot displaying the differences in immune cells that have infiltrated the three clusters by ssGSEA analysis. *, $p<0.05$, **, $p<0.01$, ***, $p<0.001$, NS, no significance.

also had a higher stemness score and more CSC features (p = 3.3e-13, Figure 9F).

Immunotherapy response and drug sensitivity

To further evaluate the immunotherapy response with CRSGs in LUAD, a correlation analysis between the prognostic CRSGs and the immune checkpoint genes was conducted. KLF4, COL1A1, SPP1, CAV2, and CTHRC1 were positively related to the top 14 immune checkpoint genes, of which CTHRC1 and COL1A1 had the highest correlation, while TSPAN7, C4BPA, and PSMB9 showed a negative correlation (Figure 9D). Taken together, these results indicated that the prognostic CRSGs could be a useful biomarker to predict LUAD patients who will benefit from immunotherapy.

We also evaluated potential anti-tumor drugs between high- and low- risk group based on drug sensitivity profiles from the GDSC database. The top 16 sensitivity drugs were selected by calculating IC50 values, such as AKT-VIII, EHT-1864, GW-441756, erlotinib, lapatinib, etc., implying that patients in the high-risk group were more sensitive to chemotherapy and targeted therapy (Figures S4A-P).

Validation of cuproptosis-related stemness signature in vitro

Finally, we further verified the mRNA expression of CRSGs and DEGs with prognostic signature in LUAD cells. Compared with normal bronchial epithelial BEAS-2B, the expression of CDKN2A, PDHA1, COL1A1, SPP1, CAV2, and CTHRC1 was significantly

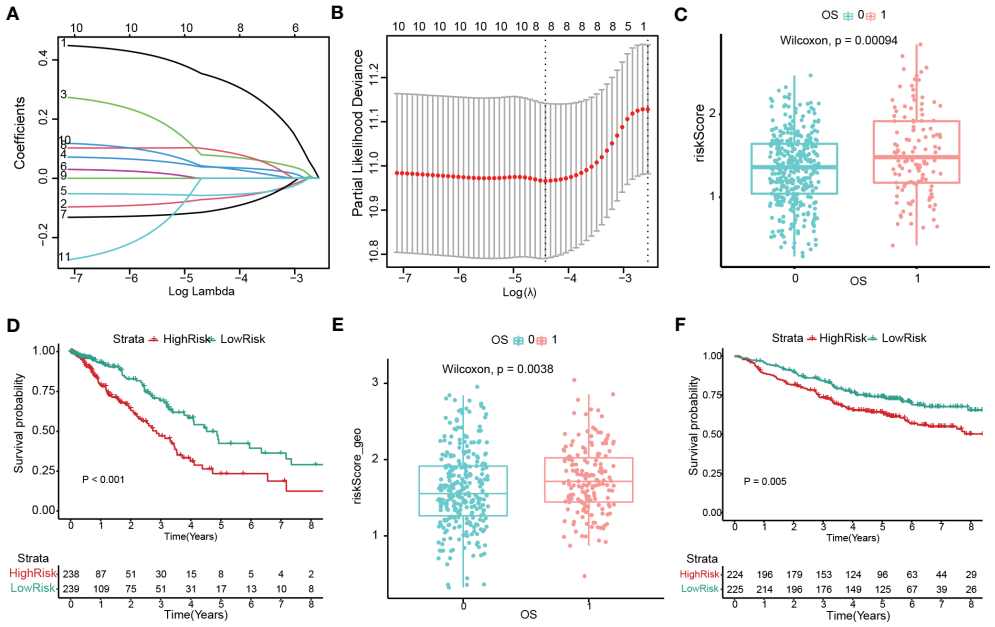

FIGURE 7
Construction and validation of the prognostic model with cuproptosis-related stemness signature. **(A, B)** Eight prognostic CRSGs were filtered to construct a prognostic model by LASSO-Cox regression. **(C)** The risk score for patients was validated in an internal cohort (TCGA-LUAD) and marked as low- (blue) and high-risk (red) (p=0.00004). **(D)** Kaplan-Meier survival analysis the survival probability between the low- and high-risk groups in TCGA-LUAD (p<0.001). **(E)** The risk score for patients was validated in an external cohort (GSE141569) and marked as low- and high-risk (p=0.0038). **(F)** K–M survival analysis of the risk score in an external cohort (p=0.005).

upregulated in A549 and SPC-A1 as expected with the above analyses ($p < 0.05$, Figure 10A, B). SPP1 in particular was found to be highly expressed at both the mRNA and protein levels ($p < 0.001$, Figure 10C). Thus, SPP1 was selected to further explore biological function *in vitro*. The effectiveness of SPP1 silencing was confirmed by western blot (Figure 10D). The CCK-8 and transwell assays revealed that the knockdown of SPP1 significantly suppressed the proliferation and migration of LUAD cells ($p < 0.01$, Figures 10E, F). Furthermore, tumorsphere numbers and sizes were markedly reduced in SPC-A1 after transfection with siRNA-2 and -3, indicating that SPP1 promoted cancer stemness and might be a potential target for CSCs (Figure 10G). Together, these results strongly support the reliability of our bioinformatics analysis.

Discussion

LUAD accounts for approximately 50% of all lung cancers, with a high morbidity and mortality rate due to its properties of high metastasis, radio-chemotherapy resistance, and immunotherapy insensitivity (1, 2). CSCs, only a small population of cancer cells possess the stemness abilities of tumor-initiation, self-renewal, and unlimited proliferation, which are considered the "root" of LUAD recurrence, metastasis, and resistance (4, 5). Thus, there is an urgent need to identify more effective therapeutic strategies for CSCs.

Low levels of ROS are essential to maintaining stemness in CSCs (44). A promising new approach for generating intracellular ROS and mitochondrial oxidative stress by copper ionophores has emerged, with an intrinsic selectivity for CSCs of the lung, colorectal, and breast (8, 11, 12). Copper acts as a "double-edged sword" and plays an essential role in cancer development, metastasis, and immunomodulatory (9, 10). In fact, a novel form of copper-dependent cell death that is triggered by copper ionophores, called cuproptosis, is accompanied by the accumulation of ROS and mitochondrial metabolism (13, 14). Previous studies have identified several genes and lncRNAs related to cuproptosis in LUAD (20, 21, 45–47), and developed a cuproptosis signature that correlates with the prognosis and tumor microenvironment of LUAD patients (16, 19, 48). Therefore, cuproptosis may play an important role in LUAD and provide new insights into the treatment of CSCs.

To the best of our knowledge, no studies of cuproptosis-related genes combined with the stemness signature in LUAD have been reported, and their roles in prognosis and the immune landscape remain unknown. Due to the high heterogeneity of CSCs (49, 50), we first systematically analyzed the CRSGs in LUAD by integrating bulk and single-cell RNA-seq. A total of 6 CRSGs were screened out, including CDKN2A, GLS, FDX1, PDHA1, PDHB, and DLD; most of them have been reported in the direct regulation of cuproptosis and cancer progression (13). In our study, the expression of CRSGs in bulk RNA-seq showed that CDKN2A and PDHA1 were significantly higher, while FDX1 and GLS were lower in LUAD patients, and with unaltered levels of DLD and PDHB. Although CDKN2A showed a high mutation frequency in various cancers, the expression of CDKN2A was overexpressed in many tumors and associated with immunosuppression and poor prognosis (51). CDKN2A genomic alterations were associated with urothelial carcinoma treated with immune checkpoint inhibitors (ICIs) (52).

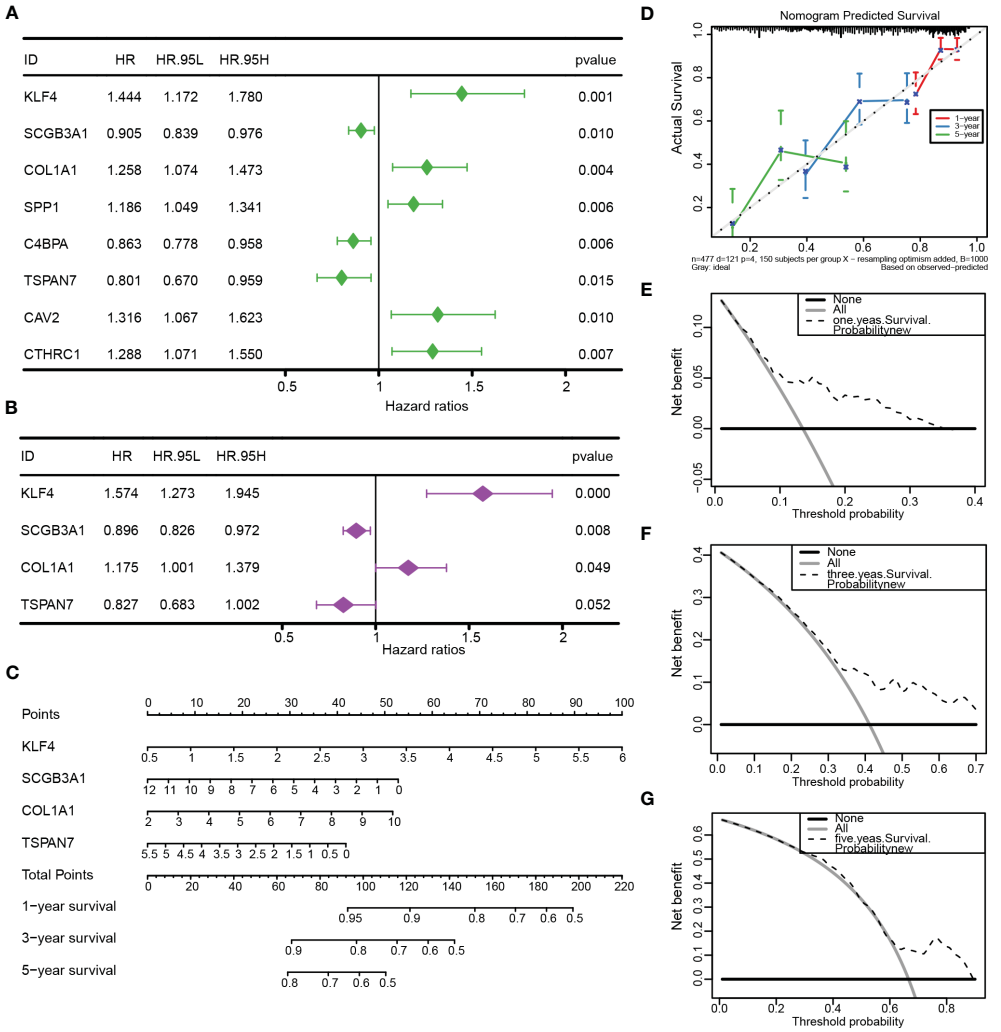

FIGURE 8
Construction and validation of the nomogram. **(A, B)** Univariate and multivariate Cox regression based on TCGA-LUAD. **(C)** The nomogram was constructed to predict OS. **(D)** The calibration curve demonstrated the validity and accuracy of the nomogram. **(E-G)** The decision curve analysis (DCA) for the nomogram at 1, 3, and 5 years.

PDHA1 is crucial to metabolic reprogramming and is often aberrantly expressed in various tumors (53). In LUAD, patients with high expression of PDHA1 had a significantly negative correlation with poor prognosis and immune infiltration (54). Our further qRT-PCR assay validated the expression trend in the datasets, with only CDKN2A and PDHA1 having statistically significant differences ($p < 0.05$), which may be attributed to the differences between tissues and cell lines.

Based on the expression of 129 intersecting DEGs in LUAD, cells were classified into three cuproptosis-related stemness subtypes (Cluster 1-3) by unsupervised clustering. Additionally, functional enrichment analysis showed that those subtypes were enriched in cancer and immune-related pathways. Thus, we further explored the association between the subtypes and immune infiltration. Notably, most of the immune infiltrating cells like activated B cells, CD4+ T cells, CD8+ T cells, MDSCs, and NK cells were significantly lower in Cluster 1, indicating that patients in Cluster 1 would be insensitive to immune treatment (55). Furthermore, we used CellChat to delineate intercellular communication at the single-cell level, and a high-cluster had more communication with immune cells such as fibroblasts, NK cells, T lymphocytes, and B lymphocytes than a low-cluster. Further potential ligand-receptor interactions including MIF-(CD74 +CXCR4), MIF-(CD74+CD44) and MDK-NCL have also been found (56). The persistent upregulation of CD74 could impair MHC class II antigen presentation, contributing to immune escape and promoting tumor metastasis (57). Overall, cuproptosis might bridge cancer stem cells and immunocyte infiltration to affect LUAD progression.

More importantly, to quantify the prognosis of cuproptosis-related stemness signature in each LUAD patient, we constructed a risk score based on the 129 intersecting DEGs by LASSO and univariate regression. Then, 8 prognostic genes with cuproptosis-related stemness signature (KLF4, SCGB3A1, COL1A1, SPP1, C4BPA, TSPAN7, CAV2, and CTHRC1) were involved in the novel prognostic model, which stratified LUAD patients into

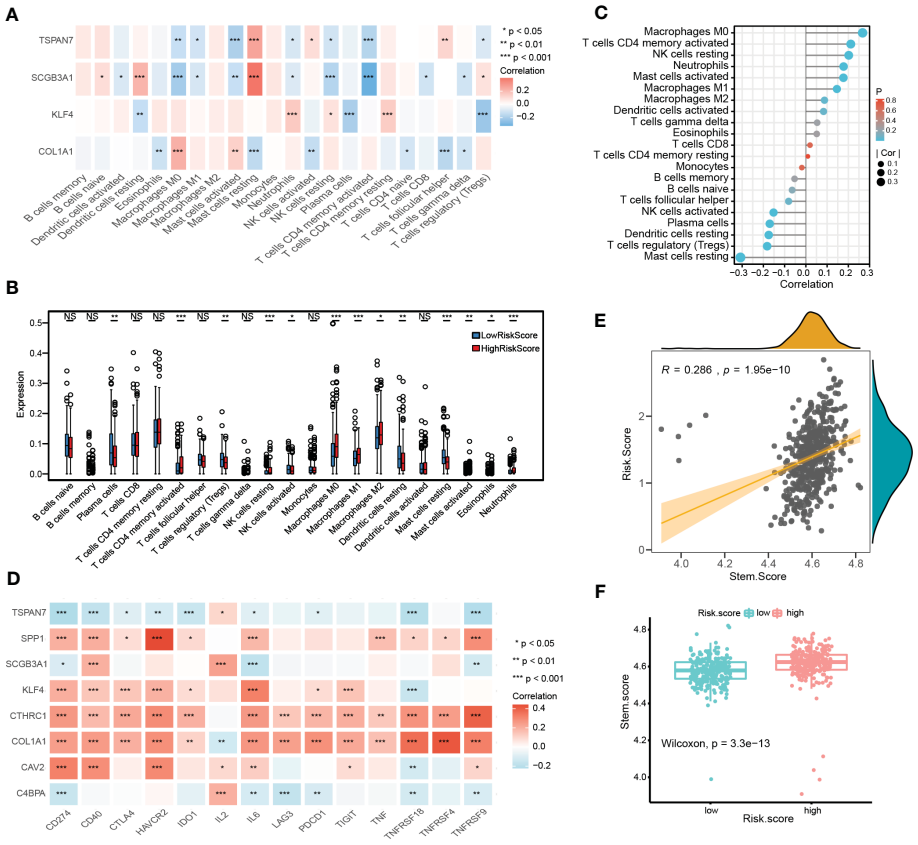

FIGURE 9
Immune landscape and stemness score based on prognostic signature. **(A)** The heatmap shows the correlation between CRSGs with prognostic signature and immune cells. **(B)** The differences in immune cells between high- and low- risk groups. **(C)** Lollipop plot showing the correlation between immune cells and the risk score. The size of the bubbles represents the strength of the correlation. **(D)** The correlation between prognostic CRSGs and immune checkpoint genes. Red, positive correlation; blue, negative correlation. **(E)** Correlation analysis between stemness score and the risk score (p=1.95e-10). **(F)** High- and low-risk groups' stemness score were compared (p=3.3e-13). *p* values were shown as: *$p<0.05$; **$p<0.01$; ***$p<0.001$.

high- and low-risk groups. The K-M survival and ROC curves, as expected, showed that patients in the high-risk group had a poor overall survival (OS), which was validated in both the TCGA internal cohort and the GSE 141569 external cohort. By combining the risk signature with clinical information, a more accurate nomogram was constructed to predict the OS of LUAD patients. All the results indicated that cuproptosis-related stemness signature could serve as a solid predictive model for LUAD.

Among the eight CRSGs with prognostic signature identified in this study, COL1A1, SPP1, CAV2 and CTHRC1 were significantly upregulated in A549 and SPC-A1, while KLF4 was downregulated in LUAD cells. SPP1 in particular was found to be highly expressed at both the mRNA and protein levels ($p < 0.001$). Secreted phosphoprotein 1 (SPP1), also called osteopontin, has been demonstrated overexpressed in many cancers including LUAD and was correlated with a poor OS (58). SPP1 can induces EMT through the PI3K/Akt and MAPK/ERK1/2 pathways in lung cancer (59). It can enhance EGFR-TKI resistance by up-regulating integrin αVβ3 (60) and promote colorectal cancer stem cell-like properties by PI3K/AKT/GSK3 (61). Knockdown of SPP1 greatly decreased stemness features in cancer-associated fibroblasts treated with pancreatic cancer cells (62). Moreover, SPP1 was also considered as a cuproptosis-related gene in similar research based on database and learning algorithm (63). Our further *in vitro* experiments revealed that the silencing of SPP1 inhibited the proliferation, migration, and stemness sphere-forming capacities of LUAD cells. Therefore, SPP1 might serve as a novel therapeutic target for lung CSCs. Nevertheless, more research is needed to unravel the underlying mechanism of SPP1 to regulate cuproptosis in LUAD.

Besides, we also analyzed the correlation between the prognostic signature and the immune landscape and stemness score in each LUAD patient. The results revealed that the risk score was significantly correlated with correlated with immune cell infiltration. The high-risk group has more resting NK cells and less activated NK cells. We did not observe a significant difference in CD8+ T cells between risk scores and prognosis may be related to the immune escape. A positive relationship was discovered between risk score and stemness score, indicating that patients with a higher risk score had more stemness features. Moreover, the predictive effect of the CRSGs with prognostic signature for immunotherapy was also evaluated. In our study, KLF4, COL1A1, SPP1, CAV2, and CTHRC1

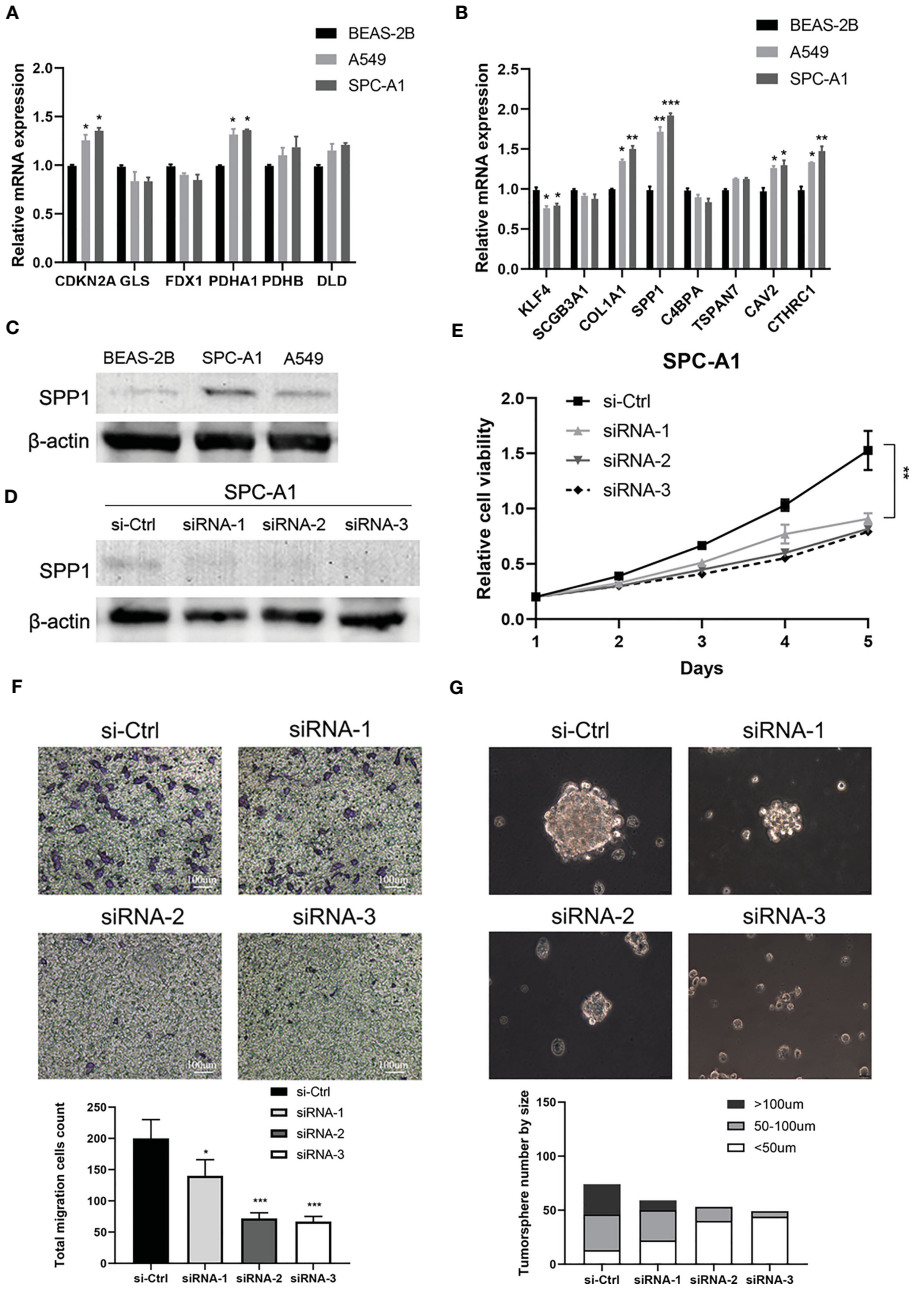

FIGURE 10
Validation of cuproptosis-related stemness signature in LUAD cells. **(A)** The mRNA expression of CRSGs in LUAD cells A549 and SPC-A1 and normal bronchial epithelial cells BEAS-2B was analyzed by qRT-PCR. **(B)** The mRNA expression level of DEGs with prognostic signature. **(C)** The protein expression of SPP1 in A549, SPC-A1, and BEAS-2B by Western blot. **(D)** Western blot assay verified the efficiency of SPP1 knockdown in SPC-A1. **(E)** CCK-8 assay was used to evaluate the effect of SPP1 on cell proliferation. **(F)** Transwell assay to assess the effect of SPP1 on the migration of SPC-A1 cells (scale bar, 100um). And the corresponding statistical plot was displayed. **(G)** Representative images show the effect of SPP1 knockdown on the tumorsphere formation ability of SPC-A1 cells, which were cultured in stemness medium for 7 days (scale bar, 100um). Quantitative analysis was counted by sphere diameters. *p* values were shown as: **p*<0.05; ***p*<0.01; ****p*<0.001.

had a high positive relationship with the immune checkpoint genes, while TSPAN7, C4BPA, and PSMB9 showed a negative correlation. Patients in the high-risk group were more susceptible to chemotherapy and targeted therapy based on drug sensitivity analysis. Taken together, we speculated that our model was capable of reflecting the immune infiltration and immunotherapy in LUAD.

Nowadays, increasing studies of CRGs, lncRNAs, and their prognostic value for lung cancer have been published. We for the first time identified the CRGs combined with stemness signature by integrating bulk and sc-RNAseq, and the prognosis and immune landscape in LUAD were also investigated. Inevitably, there were several limitations in this study. First, our research was mainly based on public databases and was retrospective, though we

have validated the prognostic signature in internal and external cohorts, and further validations using prospective multi-center studies are needed. Moreover, although we have verified the expression of CRSGs and the functional roles of target gene by cellular assays, the underlying cuproptosis mechanism of CRSGs in LUAD needs to be further investigated, and more studies directly connected to cuproptosis features of SPP1 (such as the elesclomol concentration in different LUAD cell lines and the intensity of intracellular cuproptosis at different expression levels of SPP1) *in vitro* are required.

Conclusion

Taken together, we comprehensively identified the CRSGs in LUAD and constructed a risk signature based on differentially expressed CRSGs, which was closely associated with the prognosis, immune infiltration, immunotherapy response, stemness features, and drug sensitivity. Additionally, the expression and biological function of CRSGs were also evaluated *in vitro*. These findings highlight the clinical significance of CRSGs in LUAD patients, and provide new insights for developing more effective therapeutic targets for lung CSCs in the future.

Data availability statement

The datasets presented in this study can be found in online repositories. The names of the repository/repositories and accession number(s) can be found in the article/Supplementary Material.

Author contributions

JY and ZW designed the study; HD and KL collected data; LY and JQ analyzed the data; JY and HD wrote the manuscript draft; JY and ZW revised the manuscript; JQ performed the experiments. All authors contributed to the article and approved the submitted version.

Funding

This study was supported by grants from the National Natural Science Foundation of China (No. 82274285), the Clinical Research Plan of SHDC (No. SHDC2020CR4050, No. SHDC12020123), Shanghai Science and Technology Innovation Plan (No. 20Y21902300), the Program of Shanghai university of TCM (No.2021LK045), and the Project of Longhua Hospital (No. KC2022007, No. YM2021023).

Acknowledgments

The authors gratefully thank the open-source provided by TCGA and GEO databases.

Conflict of interest

The authors declare that the research was conducted in the absence of any commercial or financial relationships that could be construed as a potential conflict of interest.

Publisher's note

Supplementary material

The Supplementary Material for this article can be found online at: https://www.frontiersin.org/articles/10.3389/fimmu.2023.1174762/full#supplementary-material

References

1. Siegel RL, Miller KD, Fuchs HE, Jemal A. Cancer statistics, 2022. *CA Cancer J Clin* (2022) 72(1):7–33. doi: 10.3322/caac.21708

2. Jhala H, Harling L, Rodrigo A, Nonaka D, McLean E, Ng W, et al. Clinicopathological predictors of survival in resected primary lung adenocarcinoma. *J Clin Pathol* (2022) 75(5):310–5. doi: 10.1136/jclinpath-2021-207388

3. Seguin L, Durandy M, Feral CC. Lung adenocarcinoma tumor origin: a guide for personalized medicine. *Cancers (Basel)* (2022) 14(7):1759. doi: 10.3390/cancers14071759

4. Raniszewska A, Kwiecień I, Rutkowska E, Rzepecki P, Domagała-Kulawik J. Lung cancer stem cells-origin, diagnostic techniques and perspective for therapies. *Cancers (Basel)* (2021) 13(12):2996. doi: 10.3390/cancers13122996

5. Rowbotham SP, Goruganthu MUL, Arasada RR, Wang WZ, Carbone DP, Kim CF. Lung cancer stem cells and their clinical implications. *Cold Spring Harb Perspect Med* (2022) 12(4):a041270. doi: 10.1101/cshperspect.a041270

6. Maiuthed A, Chantarawong W, Chanvorachote P. Lung cancer stem cells and cancer stem cell-targeting natural compounds. *Anticancer Res* (2018) 38(7):3797–809. doi: 10.21873/anticanres.12663

7. Versini A, Colombeau L, Hienzsch A, Gaillet C, Retailleau P, Debieu S, et al. Salinomycin derivatives kill breast cancer stem cells by lysosomal iron targeting. *Chemistry* (2020) 26(33):7416–24. doi: 10.1002/chem.202000335

8. Steinbrueck A, Sedgwick AC, Brewster JT2nd, Yan KC, Shang Y, Knoll DM, et al. Transition metal chelators, pro-chelators, and ionophores as small molecule cancer chemotherapeutic agents. *Chem Soc Rev* (2020) 49(12):3726–47. doi: 10.1039/c9cs00373h

9. Chen L, Min J, Wang F. Copper homeostasis and cuproptosis in health and disease. *Signal Transduct Target Ther* (2022) 7(1):378. doi: 10.1038/s41392-022-01229-y

10. Cheng F, Peng G, Lu Y, Wang K, Ju Q, Ju Y, et al. Relationship between copper and immunity: the potential role of copper in tumor immunity. *Front Oncol* (2022) 12:1019153. doi: 10.3389/fonc.2022.1019153

11. Boodram JN, McGregor IJ, Bruno PM, Cressey PB, Hemann MT, Suntharalingam K. Breast cancer stem cell potent Copper(II)-Non-Steroidal anti-inflammatory drug complexes. *Angew Chem Int Ed Engl* (2016) 55(8):2845–50. doi: 10.1002/anie.201510443

12. Oliveri V. Selective targeting of cancer cells by copper ionophores: an overview. *Front Mol Biosci* (2022) 9:841814. doi: 10.3389/fmolb.2022.841814

13. Tsvetkov P, Coy S, Petrova B, Dreishpoon M, Verma A, Abdusamad M, et al. Copper induces cell death by targeting lipoylated TCA cycle proteins. *Science* (2022) 375(6586):1254–61. doi: 10.1126/science.abf0529

14. Tang D, Chen X, Kroemer G. Cuproptosis: a copper-triggered modality of mitochondrial cell death. *Cell Res* (2022) 32(5):417–8. doi: 10.1038/s41422-022-00653-7

15. Wang S, Xing N, Meng X, Xiang L, Zhang Y. Comprehensive bioinformatics analysis to identify a novel cuproptosis-related prognostic signature and its ceRNA regulatory axis and candidate traditional Chinese medicine active ingredients in lung adenocarcinoma. *Front Pharmacol* (2022) 13:971867. doi: 10.3389/fphar.2022.971867

16. Chen Y, Tang L, Huang W, Zhang Y, Abisola FH, Li L. Identification and validation of a novel cuproptosis-related signature as a prognostic model for lung adenocarcinoma. *Front Endocrinol (Lausanne).* (2022) 13:963220. doi: 10.3389/fendo.2022.963220

17. Vanhove K, Derveaux E, Graulus GJ, Mesotten L, Thomeer M, Noben JP, et al. Glutamine addiction and therapeutic strategies in lung cancer. *Int J Mol Sci* (2019) 20 (2):252. doi: 10.3390/ijms20020252

18. Anderson NM, Mucka P, Kern JG, Feng H. The emerging role and targetability of the TCA cycle in cancer metabolism. *Protein Cell* (2018) 9(2):216–37. doi: 10.1007/s13238-017-0451-1

19. Pan S, Song C, Meng H, Li N, Li D, Hao B, et al. Identification of cuproptosis-related subtypes in lung adenocarcinoma and its potential significance. *Front Pharmacol* (2022) 13:934722. doi: 10.3389/fphar.2022.934722

20. Li K, Wu LL, Wang H, Cheng H, Zhuo HM, Hao Y, et al. The characterization of tumor microenvironment infiltration and the construction of predictive index based on cuproptosis-related gene in primary lung adenocarcinoma. *Front Oncol* (2022) 12:1011568. doi: 10.3389/fonc.2022.1011568

21. Liu Y, Lin W, Yang Y, Shao J, Zhao H, Wang G, et al. Role of cuproptosis-related gene in lung adenocarcinoma. *Front Oncol* (2022) 12:1080985. doi: 10.3389/fonc.2022.1080985

22. Sun D, Guan X, Moran AE, Wu LY, Qian DZ, Schedin P, et al. Identifying phenotype-associated subpopulations by integrating bulk and single-cell sequencing data. *Nat Biotechnol* (2022) 40(4):527–38. doi: 10.1038/s41587-021-01091-3

23. Kuksin M, Morel D, Aglave M, Danlos FX, Marabelle A, Zinovyev A, et al. Applications of single-cell and bulk RNA sequencing in onco-immunology. *Eur J Cancer.* (2021) 149:193–210. doi: 10.1016/j.ejca.2021.03.005

24. Kim N, Kim HK, Lee K, Hong Y, Cho JH, Choi JW, et al. Single-cell RNA sequencing demonstrates the molecular and cellular reprogramming of metastatic lung adenocarcinoma. *Nat Commun* (2020) 11(1):2285. doi: 10.1038/s41467-020-16164-1

25. Sugiyama E, Togashi Y, Takeuchi Y, Shinya S, Tada Y, Kataoka K, et al. Blockade of EGFR improves responsiveness to PD-1 blockade in EGFR-mutated non-small cell lung cancer. *Sci Immunol* (2020) 5(43):3937. doi: 10.1126/sciimmunol.aav3937

26. Ritchie ME, Phipson B, Wu D, Hu Y, Law CW, Shi W, et al. Limma powers differential expression analyses for RNA-sequencing and microarray studies. *Nucleic Acids Res* (2015) 43(7):e47. doi: 10.1093/nar/gkv007

27. Mounir M, Lucchetta M, Silva TC, Olsen C, Bontempi G, Chen X, et al. New functionalities in the TCGAbiolinks package for the study and integration of cancer data from GDC and GTEx. *PloS Comput Biol* (2019) 15(3):e1006701. doi: 10.1371/journal.pcbi.1006701

28. Song Q, Zhou R, Shu F, Fu W. Cuproptosis scoring system to predict the clinical outcome and immune response in bladder cancer. *Front Immunol* (2022) 13:958368. doi: 10.3389/fimmu.2022.958368

29. Pinto JP, Kalathur RK, Oliveira DV, Barata T, Machado RS, Machado S, et al. StemChecker: a web-based tool to discover and explore stemness signatures in gene sets. *Nucleic Acids Res* (2015) 43(W1):W72–7. doi: 10.1093/nar/gkv529

30. Hua Z, White J, Zhou J. Cancer stem cells in TNBC. *Semin Cancer Biol* (2022) 82:26–34. doi: 10.1016/j.semcancer.2021.06.015

31. Aibar S, González-Blas CB, Moerman T, Huynh-Thu VA, Imrichova H, Hulselmans G, et al. SCENIC: single-cell regulatory network inference and clustering. *Nat Methods* (2017) 14(11):1083–6. doi: 10.1038/nmeth.4463

32. Jin S, Guerrero-Juarez CF, Zhang L, Chang I, Ramos R, Kuan CH, et al. Inference and analysis of cell-cell communication using CellChat. *Nat Commun* (2021) 12(1):1088. doi: 10.1038/s41467-021-21246-9

33. Kolde R, Vilo J. GOsummaries: an r package for visual functional annotation of experimental data. *F1000Res* (2015) 4:574. doi: 10.12688/f1000research.6925.1

34. Gustavsson EK, Zhang D, Reynolds RH, Garca-Ruiz S, Ryten M. Ggtranscript: an r package for the visualization and interpretation of transcript isoforms using ggplot2. *Bioinformatics* (2022) 38(15):3844–6. doi: 10.1093/bioinformatics/btac409

35. Wilkerson MD, Hayes DN. ConsensusClusterPlus: a class discovery tool with confidence assessments and item tracking. *Bioinformatics* (2010) 26(12):1572–3. doi: 10.1093/bioinformatics/btq170

36. Yu G, Wang LG, Han Y, He QY. clusterProfiler: an r package for comparing biological themes among gene clusters. *Omics* (2012) 16(5):284–7. doi: 10.1089/omi.2011.0118

37. The Gene Ontology Consortium. Gene ontology consortium: going forward. *Nucleic Acids Res* (2015) 43(Database issue):D1049–56. doi: 10.1093/nar/gku1179

38. Kanehisa M, Furumichi M, Tanabe M, Sato Y, Morishima K. KEGG: new perspectives on genomes, pathways, diseases and drugs. *Nucleic Acids Res* (2017) 45 (D1):D353–d61. doi: 10.1093/nar/gkw1092

39. Ru B, Wong CN, Tong Y, Zhong JY, Zhong SSW, Wu WC, et al. TISIDB: an integrated repository portal for tumor-immune system interactions. *Bioinformatics* (2019) 35(20):4200–2. doi: 10.1093/bioinformatics/btz210

40. Hänzelmann S, Castelo R, Guinney J. GSVA: gene set variation analysis for microarray and RNA-seq data. *BMC Bioinf* (2013) 14:7. doi: 10.1186/1471-2105-14-7

41. Chen B, Khodadoust MS, Liu CL, Newman AM, Alizadeh AA. Profiling tumor infiltrating immune cells with CIBERSORT. *Methods Mol Biol* (2018) 1711:243–59. doi: 10.1007/978-1-4939-7493-1_12

42. Yang W, Soares J, Greninger P, Edelman EJ, Lightfoot H, Forbes S, et al. Genomics of drug sensitivity in cancer (GDSC): a resource for therapeutic biomarker discovery in cancer cells. *Nucleic Acids Res* (2013) 41(Database issue):D955–61. doi: 10.1093/nar/gks1111

43. Geeleher P, Cox N, Huang RS. pRRophetic: an r package for prediction of clinical chemotherapeutic response from tumor gene expression levels. *PloS One* (2014) 9(9):e107468. doi: 10.1371/journal.pone.0107468

44. Huang H, Zhang S, Li Y, Liu Z, Mi L, Cai Y, et al. Suppression of mitochondrial ROS by prohibitin drives glioblastoma progression and therapeutic resistance. *Nat Commun* (2021) 12(1):3720. doi: 10.1038/s41467-021-24108-6

45. Zhang P, Pei S, Liu J, Zhang X, Feng Y, Gong Z, et al. Cuproptosis-related lncRNA signatures: predicting prognosis and evaluating the tumor immune microenvironment in lung adenocarcinoma. *Front Oncol* (2022) 12:1088931. doi: 10.3389/fonc.2022.1088931

46. Wang F, Lin H, Su Q, Li C. Cuproptosis-related lncRNA predict prognosis and immune response of lung adenocarcinoma. *World J Surg Oncol* (2022) 20(1):275. doi: 10.1186/s12957-022-02727-7

47. Ma S, Zhu J, Wang M, Zhu J, Wang W, Xiong Y, et al. A cuproptosis-related long non-coding RNA signature to predict the prognosis and immune microenvironment characterization for lung adenocarcinoma. *Transl Lung Cancer Res* (2022) 11(10):2079–93. doi: 10.21037/tlcr-22-660

48. Shen Y, Li D, Liang Q, Yang M, Pan Y, Li H. Cross-talk between cuproptosis and ferroptosis regulators defines the tumor microenvironment for the prediction of prognosis and therapies in lung adenocarcinoma. *Front Immunol* (2022) 13:1029092. doi: 10.3389/fimmu.2022.1029092

49. Zheng H, Pomyen Y, Hernandez MO, Li C, Livak F, Tang W, et al. Single-cell analysis reveals cancer stem cell heterogeneity in hepatocellular carcinoma. *Hepatology* (2018) 68(1):127–40. doi: 10.1002/hep.29778

50. Prasetyanti PR, Medema JP. Intra-tumor heterogeneity from a cancer stem cell perspective. *Mol Cancer.* (2017) 16(1):41. doi: 10.1186/s12943-017-0600-4

51. Qin Y, Liu Y, Xiang X, Long X, Chen Z, Huang X, et al. Cuproptosis correlates with immunosuppressive tumor microenvironment based on pan-cancer multiomics and single-cell sequencing analysis. *Mol Cancer.* (2023) 22(1):59. doi: 10.1186/s12943-023-01752-8

52. Adib E, Nassar AH, Akl EW, Abou Alaiwi S, Nuzzo PV, Mouhieddine TH, et al. CDKN2A alterations and response to immunotherapy in solid tumors. *Clin Cancer Res* (2021) 27(14):4025–35. doi: 10.1158/1078-0432.Ccr-21-0575

53. Bian Z, Fan R, Xie L. A novel cuproptosis-related prognostic gene signature and validation of differential expression in clear cell renal cell carcinoma. *Genes (Basel)* (2022) 13(5):851. doi: 10.3390/genes13050851

54. Deng L, Jiang A, Zeng H, Peng X, Song L. Comprehensive analyses of PDHA1 that serves as a predictive biomarker for immunotherapy response in cancer. *Front Pharmacol* (2022) 13:947372. doi: 10.3389/fphar.2022.947372

55. Mao X, Xu J, Wang W, Liang C, Hua J, Liu J, et al. Crosstalk between cancer-associated fibroblasts and immune cells in the tumor microenvironment: new findings and future perspectives. *Mol Cancer.* (2021) 20(1):131. doi: 10.1186/s12943-021-01428-1

56. Chen Z, Yang X, Bi G, Liang J, Hu Z, Zhao M, et al. Ligand-receptor interaction atlas within and between tumor cells and T cells in lung adenocarcinoma. *Int J Biol Sci* (2020) 16(12):2205–19. doi: 10.7150/ijbs.42080

57. Schröder B. The multifaceted roles of the invariant chain CD74–more than just a chaperone. *Biochim Biophys Acta* (2016) 1863(6 Pt A):1269–81. doi: 10.1016/j.bbamcr.2016.03.026

58. Liu Y, Ye G, Dong B, Huang L, Zhang C, Sheng Y, et al. A pan-cancer analysis of the oncogenic role of secreted phosphoprotein 1 (SPP1) in human cancers. *Ann Transl Med* (2022) 10(6):279. doi: 10.21037/atm-22-829

59. Shi L, Hou J, Wang L, Fu H, Zhang Y, Song Y, et al. Regulatory roles of osteopontin in human lung cancer cell epithelial-to-mesenchymal transitions and responses. *Clin Transl Med* (2021) 11(7):e486. doi: 10.1002/ctm2.486

60. Fu Y, Zhang Y, Lei Z, Liu T, Cai T, Wang A, et al. Abnormally activated OPN/integrin αVβ3/FAK signalling is responsible for EGFR-TKI resistance in EGFR mutant non-small-cell lung cancer. *J Hematol Oncol* (2020) 13(1):169. doi: 10.1186/s13045-020-01009-7

61. Cheng Y, Wen G, Sun Y, Shen Y, Zeng Y, Du M, et al. Osteopontin promotes colorectal cancer cell invasion and the stem cell-like properties through the PI3K-AKT-GSK/3β-β/Catenin pathway. *Med Sci Monit* (2019) 25:3014–25. doi: 10.12659/msm.913185

62. Nallasamy P, Nimmakayala RK, Karmakar S, Leon F, Seshacharyulu P, Lakshmanan I, et al. Pancreatic tumor microenvironment factor promotes cancer stemness *via* SPP1-CD44 axis. *Gastroenterology* (2021) 161(6):1998–2013.e7. doi: 10.1053/j.gastro.2021.08.023

63. Li J, Chen S, Liao Y, Wang H, Zhou D, Zhang B. Arecoline is associated with inhibition of cuproptosis and proliferation of cancer-associated fibroblasts in oral squamous cell carcinoma: a potential mechanism for tumor metastasis. *Front Oncol* (2022) 12:925743. doi: 10.3389/fonc.2022.925743

frontiers | Frontiers in Oncology

TYPE Original Research
PUBLISHED 02 June 2023
DOI 10.3389/fonc.2023.1152681

OPEN ACCESS

EDITED BY
Chun Xu,
The University of Queensland, Australia

REVIEWED BY
Aitao Nai,
The First Affiliated Hospital of University of South China, China
Shaohua Chen,
Guangxi Medical University Cancer Hospital, China

*CORRESPONDENCE
Xichun Hu
huxichun2017@163.com

RECEIVED 28 January 2023
ACCEPTED 19 May 2023
PUBLISHED 02 June 2023

CITATION
Wang J, Tao Z, Wang B, Xie Y, Wang Y, Li B, Cao J, Qiao X, Qin D, Zhong S and Hu X (2023) Cuproptosis-related risk score predicts prognosis and characterizes the tumor microenvironment in colon adenocarcinoma.
Front. Oncol. 13:1152681.
doi: 10.3389/fonc.2023.1152681

Cuproptosis-related risk score predicts prognosis and characterizes the tumor microenvironment in colon adenocarcinoma

Jinyan Wang[1], Zhonghua Tao[1], Biyun Wang[1], Yizhao Xie[1], Ye Wang[1], Bin Li[1], Jianing Cao[1], Xiaosu Qiao[1], Dongmei Qin[2], Shanliang Zhong[3] and Xichun Hu[1]*

[1]Department of Breast and Urologic Medical Oncology, Shanghai Medical College, Fudan University Shanghai Cancer Center, Shanghai, China, [2]Department of Pathology, Nanjing Jiangning Hospital, The Affiliated Jiangning Hospital of Nanjing Medical University, Nanjing, China, [3]Center of Clinical Laboratory Science, The Affiliated Cancer Hospital of Nanjing Medical University & Jiangsu Cancer Hospital & Jiangsu Institute of Cancer Research, Nanjing, China

Introduction: Cuproptosis is a novel copper-dependent regulatory cell death (RCD), which is closely related to the occurrence and development of multiple cancers. However, the potential role of cuproptosis-related genes (CRGs) in the tumor microenvironment (TME) of colon adenocarcinoma (COAD) remains unclear.

Methods: Transcriptome, somatic mutation, somatic copy number alteration and the corresponding clinicopathological data of COAD were downloaded from The Cancer Genome Atlas (TCGA) and Gene Expression Omnibus database (GEO). Difference, survival and correlation analyses were conducted to evaluate the characteristics of CRGs in COAD patients. Consensus unsupervised clustering analysis of CRGs expression profile was used to classify patients into different cuproptosis molecular and gene subtypes. TME characteristics of different molecular subtypes were investigated by using Gene set variation analysis (GSVA) and single sample gene set enrichment analysis (ssGSEA). Next, CRG Risk scoring system was constructed by applying logistic least absolute shrinkage and selection operator (LASSO) cox regression analysis and multivariate cox analysis. Real-time quantitative polymerase chain reaction (RT-qPCR) and immunohistochemistry (IHC) were used to exam the expression of key Risk scoring genes.

Results: Our study indicated that CRGs had relatively common genetic and transcriptional variations in COAD tissues. We identified three cuproptosis molecular subtypes and three gene subtypes based on CRGs expression profile and prognostic differentially expressed genes (DEGs) expression profile, and found that changes in multilayer CRGs were closely related to the clinical characteristics, overall survival (OS), different signaling pathways, and immune cell infiltration of TME. CRG Risk scoring system was constructed according to the expression of 7 key cuproptosis-related risk genes (GLS, NOX1, HOXC6, TNNT1, GLS, HOXC6 and PLA2G12B). RT-qPCR and IHC indicated that the

expression of GLS, NOX1, HOXC6, TNNT1 and PLA2G12B were up-regulated in tumor tissues, compared with those in normal tissues, and all of GLS, HOXC6, NOX1 and PLA2G12B were closely related with patient survival. In addition, high CRG risk scores were significantly associated with high microsatellite instability (MSI-H), tumor mutation burden (TMB), cancer stem cell (CSC) indices, stromal and immune scores in TME, drug susceptibility, as well as patient survival. Finally, a highly accurate nomogram was constructed to promote the clinical application of the CRG Risk scoring system.

Discussion: Our comprehensive analysis showed that CRGs were greatly associated with TME, clinicopathological characteristics, and prognosis of patient with COAD. These findings may promote our understanding of CRGs in COAD, providing new insights for physicians to predict prognosis and develop more precise and individualized therapy strategies.

KEYWORDS

cuproptosis-related genes (CRGs), tumor microenvironment (TME), molecular subtypes, prognosis model, colon adenocarcinoma

1 Introduction

Colon adenocarcinoma (COAD) is presently considered as one of the most common malignancies and the leading cause for mortality worldwide, resulting in more than 500,000 deaths every year (1). Although surgery, adjuvant/neoadjuvant chemotherapy, targeted therapy and immunotherapy have achieved certain efficacy, some patients still have a poor prognosis due to high recurrence and mortality rate (2). In recent years, more and more studies have aimed to provide a more personalized and accurate assessment of patient prognosis through a comprehensive analysis of the genomic and clinicopathological characteristics of specific tumors, with a view to potentially improving patient prognosis (3). Nonetheless, present biomarkers or methods are far from satisfactory to accurately predict outcome of patients with COAD.

Copper (Cu) is known as the third most abundant trace element in human body (4). It is traditionally considered as a redox-active transition metal which participated in the process from cellular respiration to pigmentation, acting through cytochrome c oxidase and tyrosinase (5). However, in the last decade, metalloallostery, a new form of protein regulation and nutrient sensing, has appeared to extend the function of Cu beyond the catalytic proteins to dynamic signaling molecules, which are the basis of cell biology affecting pathophysiological processes (6). Blood concentrations of Cu were significantly increased in multiple cancers, such as thyroid cancer, lung cancer, breast cancer and pancreatic cancer (7–10). In addition, Cu concentration was elevated in tissues of large bowel and oesophageal cancer (11). However, the blood concentration of Cu was decreased in patients with endometrial cancer (12). As a result, researches started to pay attention to the specific underlying mechanisms of Cu dys-homeostasis in cancers. Increasing evidence indicated that Cu dys-homeostasis might induce cytotoxicity and affect proliferation, apoptosis, and metastasis of tumors, thus resulting in cancer progression, partly through regulating kinases activation, lipolysis, potassium channels, BRAF, NF-κB and TGF-β signaling pathways (13–18). Most importantly, Tsvetkov et al. (19) recently claimed that cuproptosis was a kind of copper-dependent death and different from all other known programmed cell death (PCD). In terms of mechanics, Cu directly bound to the fatty acylation component of the tricarboxylic acid (TCA) cycle, thus leading to the accumulation of fatty acylation proteins and the subsequent loss of iron-sulfur cluster proteins, which leaded to protein-toxic stress and ultimately to cell death. Additionally, a total of 10 cuproptosis-related genes (CRGs), including PDHB, MTF1, FDX1, DLAT, PDHA1, LIAS, LIPT1, DLD, GLS and CDKN2A, were identified in this study. Based on Tsvetkov et al.'s findings, a growing number of researches have begun to investigate the relationships between CRGs and typical cancers. For instance, Zhang, Z., et al. (20) demonstrated prognostic features associated with cuproptosis in patients with hepatocellular carcinoma (HCC). Wang, W., et al. (21), identified a cuproptosis-related prognostic signature (H19, CYTOR, IGFBP2, KLRC2, C5orf38 and CHI3L1) for patients with glioma.

Tumor microenvironment (TME), which contains different immune and stromal cells and their secreted factors, has been recognized to cultivate a chronic inflammatory, immunosuppressive, and pro-angiogenic intra-tumoral atmosphere and is closely associated with patient outcomes and treatment efficacy (22). Distinct cuproptosis-related signatures were also found to be significantly associated with TME of kidney renal clear cell carcinoma (KIRC) (23), triple-negative breast cancer (TNBC) (24) and lung adenocarcinoma (LUAD) (25). However, due to tumor and corresponding TME heterogeneity, CRGs characteristics vary across cancers. In addition, studies of CRGs in COAD are limited.

In our study, we aimed to comprehensively analyze the relationship between CRGs and TME in COAD and construct a

CRGs Risk scoring system to accurately predict COAD patient survival. The development of the scoring system provided physicians with new insights to design more effective and individualized treatment strategies.

2 Materials and methods

2.1 Data

Transcriptome and the corresponding clinicopathological data of COAD were downloaded from The Cancer Genome Atlas (TCGA) (https://portal.gdc.cancer.gov/) and Gene Expression Omnibus database (GEO) (https://www.ncbi.nlm.nih.gov/geo/). In detail, the TCGA cohort included 480 COAD tissues and 41 normal tissues. The GEO cohort containing GSE17536, GSE29623 and GSE39582, included 827 COAD samples. The detailed clinicopathological data of these COAD patients was presented in Table S1. The TCGA and GEO cohorts were combined by using "Combat" algorithm in R to eliminate batch effects before conducting subsequent analyses. Principal component analysis (PCA) was applied to validate the effect of batch effect removal by using the R package ggplot2. In order to verified the accuracy of model, we also downloaded transcriptome and the corresponding clinicopathological data of GSE40967 from GEO database, which contained 585 COAD sampes.

Additionally, we downloaded somatic mutation data of 454 tumor samples and copy number variation (CNV) data of 506 tumor samples from TCGA.

2.2 Difference analyses, survival analyses and correlation analyses of CRGs

A total of 10 CRGs (PDHA1, PDHB, FDX1, DLD, DLAT, MTF1, LIAS, LIPT1, GLS and CDKN2A) were obtained from the previous well-known publication of Tsvetkov et al. (19). Difference analyses of CRGs were conducted between tumor and normal tissues. Wilcoxon test was used to for statistical analysis. Survival and survminer R packages were used for survival analysis, the same as our previous study (26). Kaplan-Meier plot and cox regression analyze were further applied to evaluate the relationships between CRGs expression and patient overall survival (OS). Schoenfeld residuals were used to check the proportional assumption of COX model. Spearman correlation analyses were conducted to explore the interactions among CRGs

2.3 Consensus clustering analysis of CRGs

ConsensusClusterPlus R package was applied for consensus unsupervised clustering analysis. Patients were grouped into distinct molecular subtypes according to the expression of CRGs, and distinct gene subtypes according to the expression of prognostic differentially expressed genes (DEGs), derived from different molecular subtypes. The criteria included that the samples size in each set was relatively consistent and the cumulative distribution function (CDF) curve increased gradually and smoothly. After consensus clustering analysis, the intra-set association became stronger, while the inter-set association became weaker.

2.4 Associations among molecular subtypes, clinicopathological features and prognosis

We applied Kaplan-Meier plot and log-rank test to evaluate the associations between different molecular subtypes and patient survival. Correlation analyses between molecular subtypes and clinicopathological features were carried out to learn the clinical values of distinct molecular subtypes by using Chi-square test. The clinicopathological features contained age, gender, grade and tumor node metastasis (TNM) stage.

2.5 Relationships between molecular subtypes and TME

We downloaded the hallmark gene sets, including C2.CP.KEGG (186 gene sets) and C5.GO.Gene Ontology (10561 gene sets), from the Molecular Signatures Database (MSigDB) (https://www.gsea-msigdb.org/gsea/msigdb). Gene set variation analysis (GSVA) with the above two gene sets was conducted to explore the TME characteristics of different molecular subtypes. The adjusted P-value< 0.05 was considered statistically different. Additionally, the proportion of tumor-infiltrating immune cells (TICs) in tumor samples was calculated by using the deconvolution algorithm, which was also known as CIBERSORT (27). The gene expression signature matrix of TICs was downloaded from CIBERSORT platform (https://cibersortx.stanford.edu/). P-value for the deconvolution of each sample was obtained by using Monte Carlo sampling algorithm in R. A CIBERSORT P-value< 0.05 was considered suitable for further analysis. Single sample gene set enrichment analysis (ssGSEA) was used to evaluate the infiltration of TICs in different molecular subtypes.

2.6 Acquisition of DEGs from distinct molecular subtypes

DEGs of distinct molecular subtypes were acquired by applying limma package in R. The fold change of 1.5 and the adjusted P-value< 0.05 were considered qualified for searching DEGs. Gene Ontology (GO) and Kyoto Encylopedia of Genes and Genomes (KEGG) enrichment analysis of DEGs were carried out by using org.Hs.eg.db, ClusterProfiler, enrichplot, and ggplot2 packages in R. The adjusted P-value< 0.05 was deemed statistically significant.

2.7 Establishment of CRG Risk scoring system

Firstly, cox regression analyses of DEGs, achieved from different molecular subtypes, were carried out to seek those associated with

patients' prognosis. Secondly, patients were separated into different gene subtypes *via* consensus clustering analysis of prognostic DEGs expression. Thirdly, patients were randomly divided into the training (n=603) and testing (n=603) sets at a ratio of 1:1. Lastly, CRG Risk scoring system was established in the training set and verified in the testing set, GSE29263, GSE17536, GSE39582 and the combined set. Logistic least absolute shrinkage and selection operator (LASSO) cox regression analysis was carried out by applying Glmnet R package to decrease the risk of over-fitting. Next, we analyzed and cross-validated the varied trajectory of each independent variable. Multivariate Cox analysis was carried out to screen prognostic DEGs in the training group. The Risk score was calculated as follows:

$$\text{CRG Riskscore} = \Sigma(Expi * coefi)$$

In detail, Expi indicated key prognostic DEGs expression and coefi indicated the coefficient of Risk. Correlation analysis between CRG Risk score and distinct subtypes was also carried out. Survival analysis between high- and low-risk sets was conducted by Kaplan-Meier plot and log-rank test. Receiver operating characteristic (ROC) curves were utilized to learn the sensitivity and specificity of the scoring system. Similarly, all of the testing group, GSE29263, GSE17536, GSE39582 and the combined group were classified into high- and low-risk groups, respectively, and further analyzed by Kaplan-Meier survival curves and ROC curves.

2.8 Tissue samples acquisition, real-time quantitative polymerase chain reaction and immunohistochemistry

A total of 8 sets of COAD and paired normal tissues were harvested from COAD patients at Nanjing Jiangning Hospital. The study was permitted by the Ethics Committee of Nanjing Jiangning Hospital (2021-03-048-K01). Total RNA extraction and RT-qPCR were performed as our previous study (28). The primers used for RT-qPCR are shown in Table S2. Slides (4μm) of formalin-fixed paraffin-embedded tissue sections were incubated with GLS (1:200; Cell Signaling Technology), NOX1 (1:200; Proteintech), HOXC6 (1:50; Affinity Biosciences), TNNT1 antibody (1:100; Invitrogen). The expression level was scored semiquantitatively based on staining intensity and distribution using the immunoreactive score (IRS) as described (29) and as following: IRS = SI (staining intensity) x PP (percentage of positive cells). SI was determined as 0, negative; 1, weak; 2, moderate; and 3, strong. PP was defined as 0, negative; 1, 1-20% positive cells; 2, 21-50% positive cells; 3, 51-100% positive cells. Ten visual fields from different areas of each sample were selected randomly for the IRS evaluation and the average IRS was calculated as final value.

2.9 Relationships between TME and distinct Risk score groups

Difference analyses of CRGs expression levels were carried out between high- and low- Risk groups. Wilcoxon test was used for comparison. We further conducted correlation analyses not only between TICs and risk scores, but also TICs and key prognostic Risk genes. An ESTIMATE algorithm was used to analyze the ratio of immune/stromal components in TME. The Immune Score, Stromal Score and ESTIMATE Score presented the ratio of immune component, the stromal component and the sum of the both, respectively. Difference analyses of Immune/Stromal/ESTIMATE Score were conducted between high- and low- Risk score sets. Wilcoxon test was used for comparison.

2.10 Microsatellite instability cancer stem cell, tumor mutation burden and somatic mutations in different Risk score sets

Difference and correlation analyses of MSI, TMB and CSC in distinct CRG Risk score groups were conducted to study the underlying associations. Maftools package in R was applied for the comparison of mutation frequency in different Risk score sets.

2.11 Drug susceptibility analyses

In order to study effectiveness of drugs in different Risk groups, pRRophetic package in R was used to calculate the semi-inhibitory concentration (IC50) values of drugs.

2.12 Development of a nomogram

We applied Rms package in R to establish a nomogram, which combined clinicopathological characteristics, patient survival and CRG Risk score. In the nomogram, a variable matched a score and the scores for all variables were added together to get an overall score. Calibration maps of the nomogram were developed to evaluate the consistency between predicted 1, 3, and 5-year survival rates and actual outcomes. ROC curve was drawn to understand the sensitivity and specificity of the scoring system.

2.13 Statistical analyses

All statistical analyses were conducted by using R version 4.2.1. Statistical significance was set at P-value< 0.05.

3 Results

3.1 Identification of CRGs in COAD

We analyzed 10 CRGs in our study, including DLD, DLAT, PDHB, MTF1, PDHA1, FDX1, LIAS, LIPT1, GLS and CDKN2A. Difference analyses showed that 7 of 10 CRGs were dys-regulated in tumor samples compared with those in normal samples, among which LIPT1, PDHA1, GLS and CDKN2A were up-regulated, and FDX1, DLD and MTF1 were down-regulated (Figure 1A).

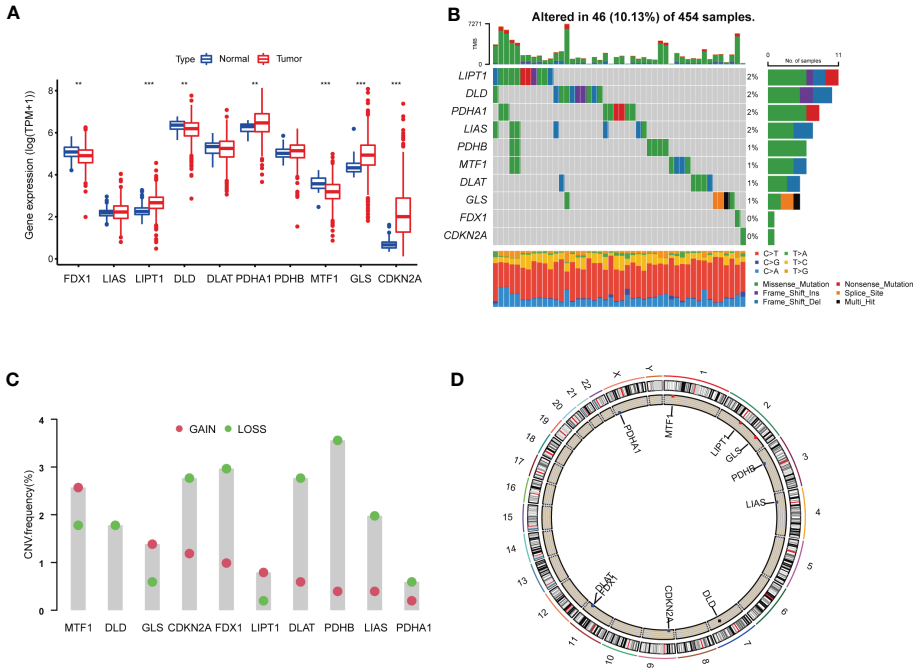

FIGURE 1
Genetic and transcriptional alterations of CRGs in colon adenocarcinoma. **(A)** The expression levels of 10 CRGs between 480 COAD samples and 41 normal samples. Wilcoxon test was used to compare two groups. **(B)** The maftool exhibited incidence of somatic mutations of CRGs in 454 COAD patients from TCGA database. **(C)** The CNV frequency of CRGs in 454 COAD samples from TCGA database. **(D)** Locations of CNV alterations on 23 chromosomes. P<0.05 was considered as significant importance. ** indicated P-value<0.01, *** indicated P-value<0.001.

In order to further study the genetic and transcriptional alterations of CRGs in COAD, we generally analyzed the somatic mutation frequency of CRGs and found 10.13% mutation frequency in tumor samples (Figure 1B). LIPT1, DLD, PDHA1 and LIAS shared the highest mutation frequency (2%), followed by PDHB, MTF1, DLAT and GLS (1%). Both FDX1 and CDKN2A had no mutations in tumor tissues. We further examined CNV frequency in CRGs, among which DLD, CDKN2A, FDX1, DLAT, PDHB and LIAS had elevated copy number loss (Figure 1C). The detailed locations of these CRGs on chromosomes were shown in Figure 1D. As a result, we noted that CRGs had relatively common genetic and transcriptional variations in COAD tissues, which might affect oncogenesis.

3.2 Identification of cuproptosis-related molecular subtypes

To learn the role of CRGs in oncogenesis of COAD, we combined expression patterns of CRGs and clinicopathological information of TCGA-COAD, GSE17536, GSE29623 and GSE39582 by using "Combat" algorithm to eliminate batch effects. PCA indicated that batch differences were well eliminated (Figure 2A). Kaplan-Meier plot revealed 3 of 10 CRGs were closely associated with patients' OS, among which GLS and CDKN2A were negatively related, while LIAS was positively related (Figures 2B–D). Multivariate Cox regression analyses of CRGs also indicated that both GLS and CDKN2A were closely related with the survival of COAD patients (Table 1). Cuproptosis network generally described the complex interrelations among CRGs and the prognosis of patients with COAD (Figure 2E; Table S3).

Considering the pervasive interrelations among CRGs, we used consensus clustering algorithm to divide patients into three groups based on the expression profile of CRGs. K=3 appeared to be an optimal choice for grouping samples into 3 sets, including molecular subtype A (n=511), B (n=444) and C (n=328) (Figures 3A, S1A–I, Tables S4, 5). Survival analysis revealed that patients in subtype C had the worst prognosis than those in subtype A or B (Figure 3B). The heat-map exhibited the expression profile of 10 CRGs in distinct molecular subtypes (Figure 3C). CDKN2A was obviously up-regulated in molecular subtype C, while PDHA1, FDX1, DLAT, DLD and GLS were greatly elevated in subtype A (Figure 3C). In addition, grade, N, M and stage were found to be significantly associated with cuproptosis molecular subtypes (Figure 3C).

3.3 Functional characteristics of TME in distinct molecular subtypes

We further performed GSVA enrichment analyses to explore the features of TME in different cuproptosis subtypes. GO GSVA enrichment analysis revealed that molecular subtype A was primarily enriched in messenger ribonucleoprotein complex, regulation of translational initiation by eif2 alpha phosphorylation and phosphatase activity, compared with subtype B (Figure 4A;

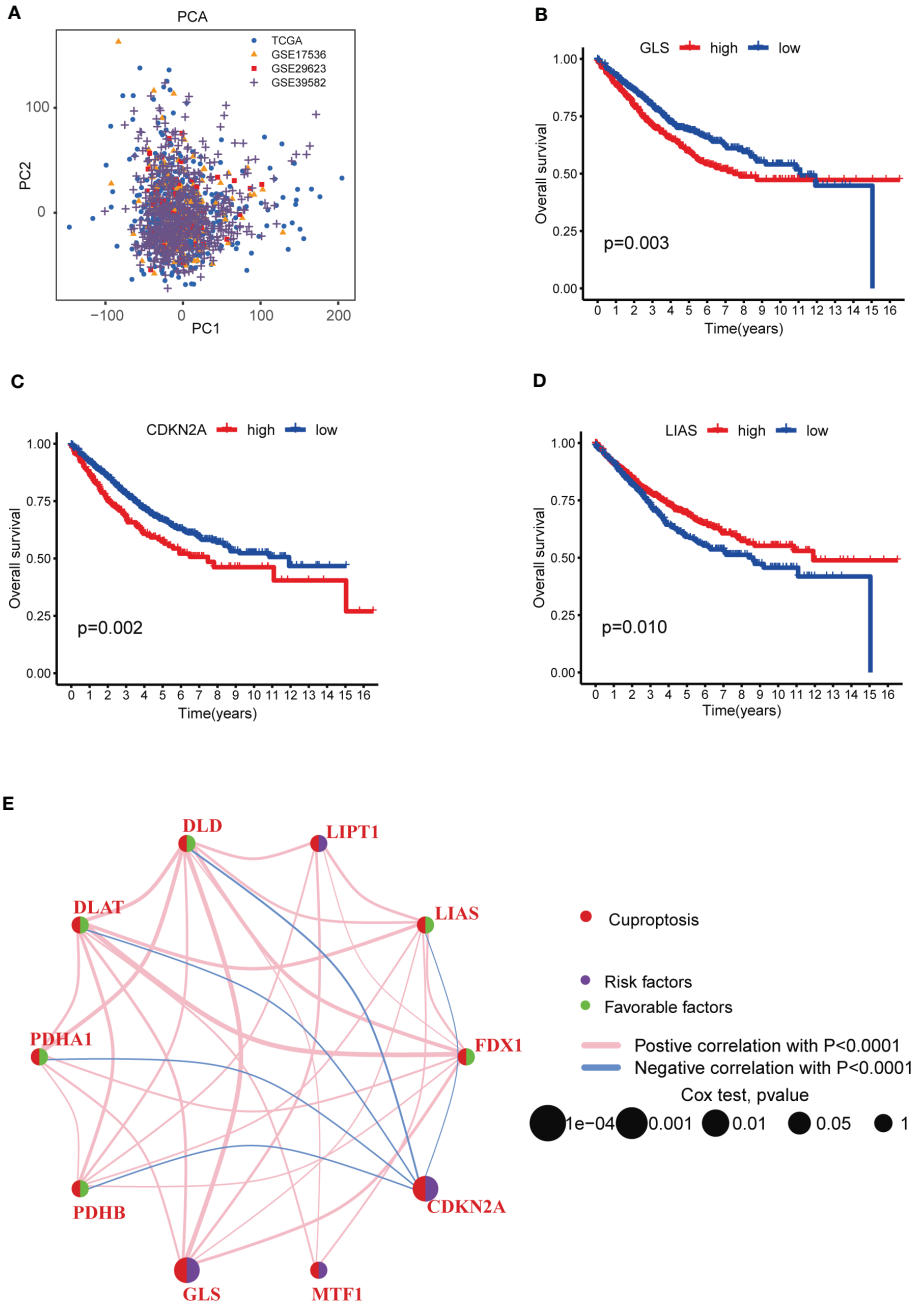

FIGURE 2
Survival analyses of CRGs and a comprehensive landscape of cuproptosis network in COAD patients from TCGA and GEO database. **(A)** PCA of TCGA, GSE17536, GSE29623 and GSE39582 after batch effect removal. **(B–D)** Survival analyses of CRGs (GLS, CDKN2A and LIAS) in COAD patients. Kaplan-Meier plot and log-rank tests were performed for survival analyses. Schoenfeld residuals was used to check the proportional assumption of COX model. **(E)** Mutual associations among CRGs in COAD samples. Spearman correlation analyses were used. The line between two CRGs indicated their interaction, and the stronger the correlation, the thicker the line. Pink line indicated positive correlation and blue line indicated negative correlation. P-value< 0.05 was considered to be statistically significant.

Table S6). Subtype B was enriched in acyl coa binding, fatty acid derivative binding and acylcoa dehydrogenase activity, compared with subtype C (Figure 4B; Table S6). Subtype C was significantly enriched in embryonic skeletal joint morphogenesis, gap junction and connexin complex, compared with subtype A (Figure 4C; Table S6). Several biological pathways, such as endoplasmic reticulum tubular network organization, cellular response to zinc ion and mrna methylation were recurrent in the comparisons of subtype A and B, A and C, and B and C (Table S7). KEGG GSVA enrichment analysis indicated subtype A mainly participated in TGF-β signaling pathway, riboflavin metabolism and RNA degradation, compared with subtype B (Figure 5A; Table S8). Subtype B was primarily enriched in metabolic related pathways, including fatty acid metabolism, butanoate metabolism, porphyrin and chlorophyll metabolism, compared with subtype C (Figure 5B; Table S8). Subtype C was mainly enriched in

TABLE 1 Multivariate Cox regression analyses of CRGs in COAD patients.

id	HR	HR.95L	HR.95H	P-value	km
CDKN2A	1.198237	1.0668866	1.3457599	0.002266	0.002461
GLS	1.302257	1.0853925	1.562451	0.004488	0.002666
LIAS	0.856896	0.718415	1.0220694	0.085936	0.009963
PDHB	0.792502	0.5976615	1.0508627	0.106232	0.002516
DLD	0.853752	0.6900535	1.0562847	0.145449	0.063517
PDHA1	0.887978	0.7283648	1.0825689	0.239915	0.066255
FDX1	0.884588	0.683168	1.1453929	0.352246	0.063822
DLAT	0.960967	0.7880859	1.1717723	0.693977	0.048397
LIPT1	1.02602	0.8300225	1.2682982	0.812277	0.112617
MTF1	1.027758	0.7957044	1.3274861	0.833903	0.10872

glycosphingolipid biosynthesis globo series, glycosaminoglycan biosynthesis chondroitin sulfate and glycosaminoglycan biosynthesis keratan sulfate, compared with subtype A (Figure 5C; Table S8).

Regarding the complex functions of different molecular subtypes in TME, we next conducted ssGSEA between TICs and different subtypes to further identify tumor immune microenvironment (TIME) characteristics of COAD. The ratio of

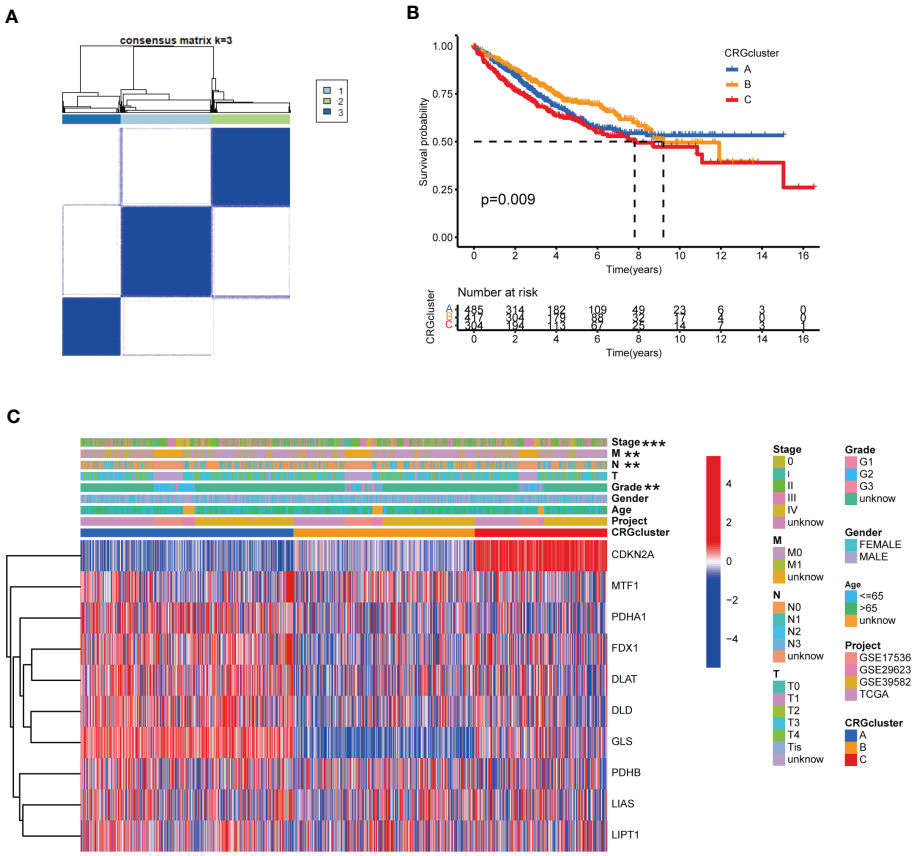

FIGURE 3
CRG molecular subtypes and their clinicopathological characteristics. **(A)** Identification of three molecular subtypes (k = 3) and their correlation area through consensus clustering analysis in COAD samples. **(B)** Survival analysis showed a significant difference in different molecular subtypes. Kaplan-Meier plot and log-rank tests were conducted for survival analyses. **(C)** The heat-map displayed the CRGs expression profile in distinct molecular subtypes, and the associations between clinicopathologic features and molecular subtypes. Chi-square test was used for the comparison. Red color indicated increased expression level and blue color indicated decreased expression level. P-value< 0.05 was considered to be statistically significant. ** indicated P-value<0.01, *** indicated P-value<0.001.

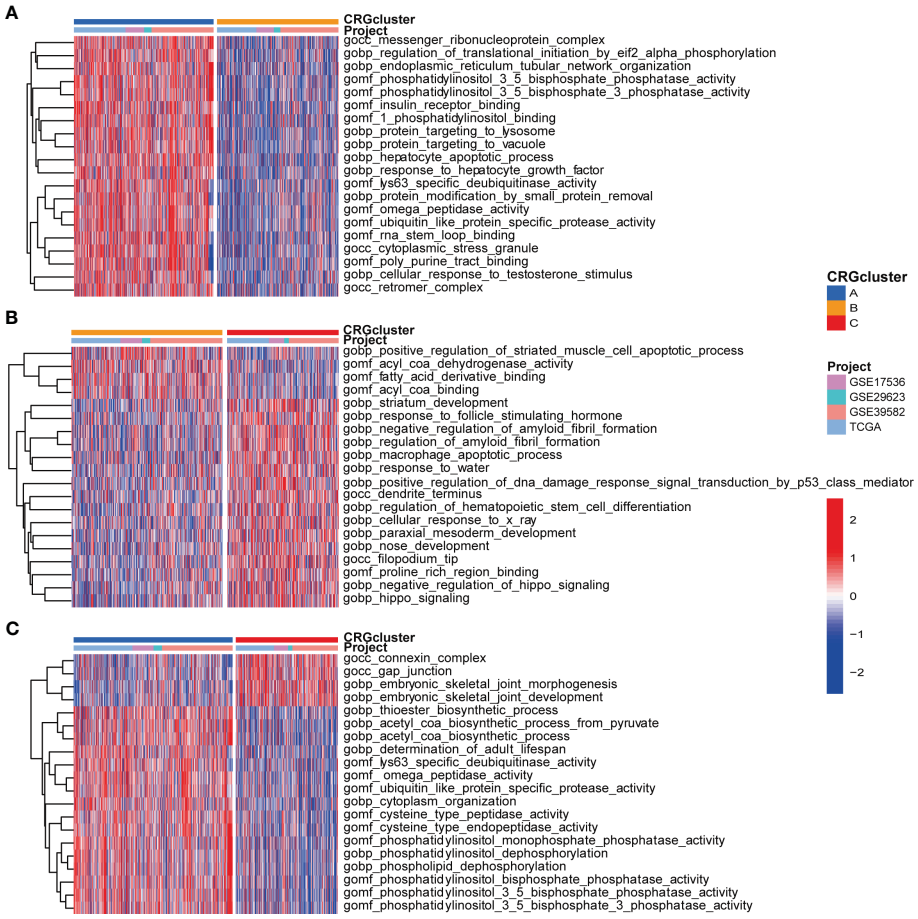

FIGURE 4
GO GSVA enrichment analyses indifferent molecular subtypes. **(A)** GO GSVA enrichment analyses between molecular subtype A and B **(B)** GO GSVA enrichment analyses between molecular subtype B and C **(C)** GO GSVA enrichment analyses between molecular subtype A and **(C)** Red color indicated more enriched in pathways and blue color indicated less enriched in pathways. Adjusted P-value<0.05 was considered to be statistically significant.

23 TICs in each tumor sample was presented in Table S9. The result of ssGSEA suggested great difference between the infiltration of 19 TICs and distinct subtypes. In detail, the infiltration levels of eosinophil and plasmacytoid dendritic cell were elevated in subtype A, activated B cell, activated CD8 T cell, activated dendritic cell, monocyte and neutrophil were up-regulated in subtype B, and another 12 TICs were obviously raised in subtype C (Figure 5D).

According to above analyses, we primarily speculated that different subtypes took a different part in TME, especially TIME of COAD.

3.4 Identification of cuproptosis-related gene subtypes

As the potential role of different molecular subtypes in TME of COAD, we further explore the underlying biological behavior of different subtypes through seeking for DEGs. We identified 114 DEGs derived from subtype A and B, 90 DEGs from subtype A and C, 49 DEGs from subtype B and C (Table S10). Finally, a total of 186 DEGs were obtained for further analyses through combination (Figure 6A; Table S11). GO enrichment analysis demonstrated that 186 DEGs mainly participated in signaling pathways associated with digestion, such as maintenance of gastrointestinal epithelium and digestive system process (Figures 6B, C; Table S12). Univariate Cox regression analysis was performed to seek DEGs of prognostic value and finally identified 86 DEGs associated with patients' OS, which were analyzed in the following section (Table S13). According to 86 prognostic DEGs expression, consensus clustering analysis was carried out to separate patients into 3 sets, namely gene subtype A (n=310), B (n=729) and C (n=244) (Figures 6D, S2A–I; Tables S14, 15). Distinct gene subtypes showed great differences in the expression levels of both prognostic DEGs and 8 CRGs (FDX1, LIPT1, DLD, PDHA1, PDHB, MTF1, GLS and CDKN2A) (Figures 6E, F; Tables S16, 17). In addition, cuproptosis gene subtypes were closely related with age, gender, grade, and T and N stage of COAD patients (Figure 6E). Survival analysis revealed that patients of gene subtype B had a better prognosis, compared with those of subtype A or C (Figure 6G).

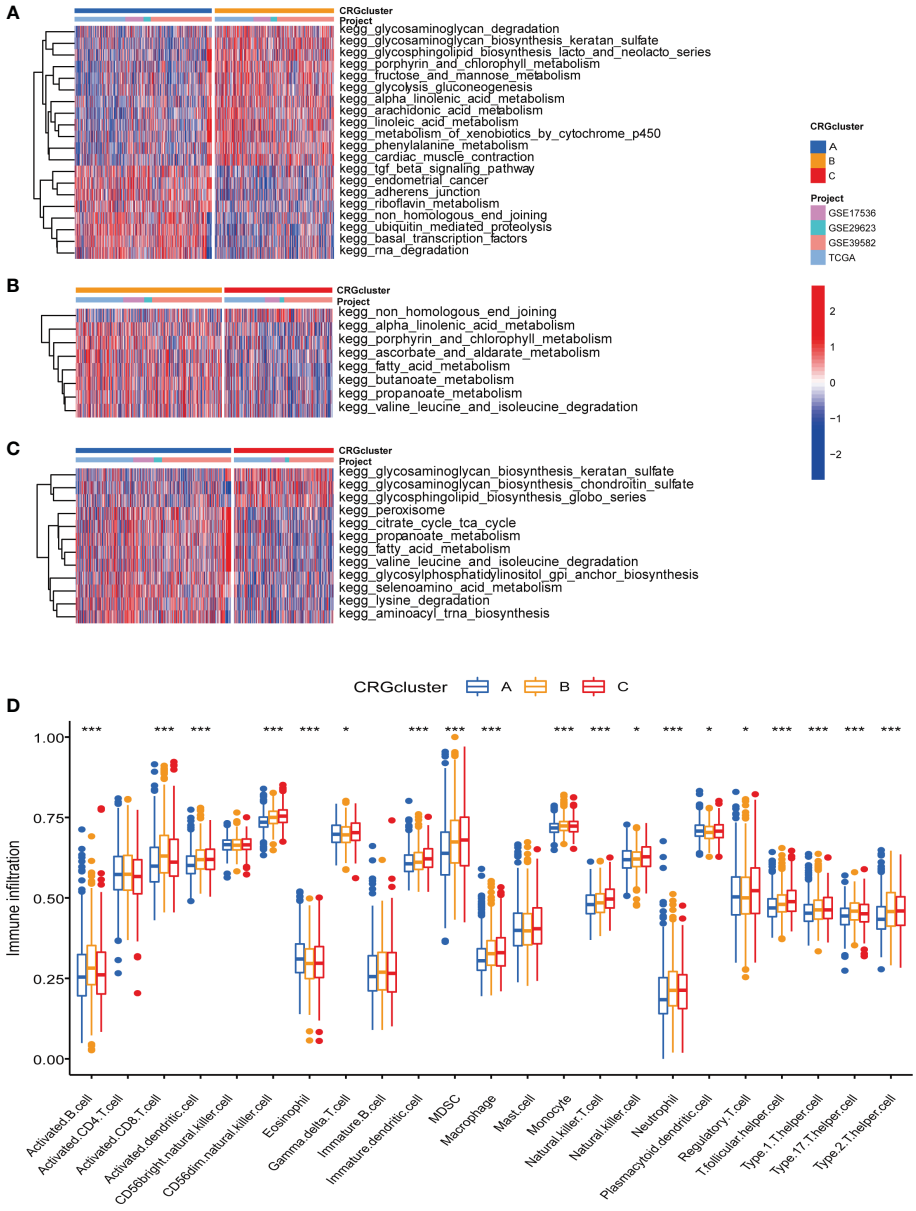

FIGURE 5
KEGG GSVA enrichment analyses and immune infiltration in different molecular subtypes. **(A)** KEGG GSVA enrichment analyses between molecular subtype A and B **(B)** KEGG GSVA enrichment analyses between molecular subtype B and C **(C)** KEGG GSVA enrichment analyses between molecular subtype A and C Red color indicated more enriched in pathways and blue color indicated less enriched in pathways. Adjusted P-value<0.05 was considered to be statistically significant. **(D)** ssGSEA indicated differences between the infiltration levels of TICs and distinct molecular subtypes. Pvalue<0.05 was considered to be statistically significant. * indicated P-value<0.05, *** indicated P-value<0.001.

3.5 Construction and validation of CRG Risk scoring system

To study the prognostic value of CRGs in COAD, we further constructed CRG Risk scoring system based on different molecular and gene subtypes. First, we applied "caret" package in R to randomly separate COAD patients into the training (n=603) and testing (n=603) groups at a ratio of 1:1. The clinicopathological characteristics of patients in the training and testing group were consistent (Table S18). Second, LASSO and multivariate Cox analyses were conducted to identify optimum prognostic signature based on 86 DEGs expression (Figure S3). Finally, CRG Risk scoring system was established through multivariate Cox regression analysis in the training set, the formula was as follow: Risk score = (0.30346935571892* expression of GLS) + (0.285346929484159 * expression of CAB39L) + (-0.171967289741126* expression of NOX1) + (0.149406405352724 * expression of HOXC6) + (0.128828618079011 * expression of TNNT1) + (-0.305462961248901* expression of ASRGL1) + (-0.142788274274145* expression of PLA2G12B). We classified patients into two groups, namely high- and low-Risk score sets, according to the calculation of Risk score in each tumor sample. Figure 7A presented the specific classifications of patients in the training set, including three cuproptosis molecular subtypes, three gene subtypes and two CRG Risk score sets. The detailed information of 7 key cuproptosis-related risk genes, Risk score and survival features in

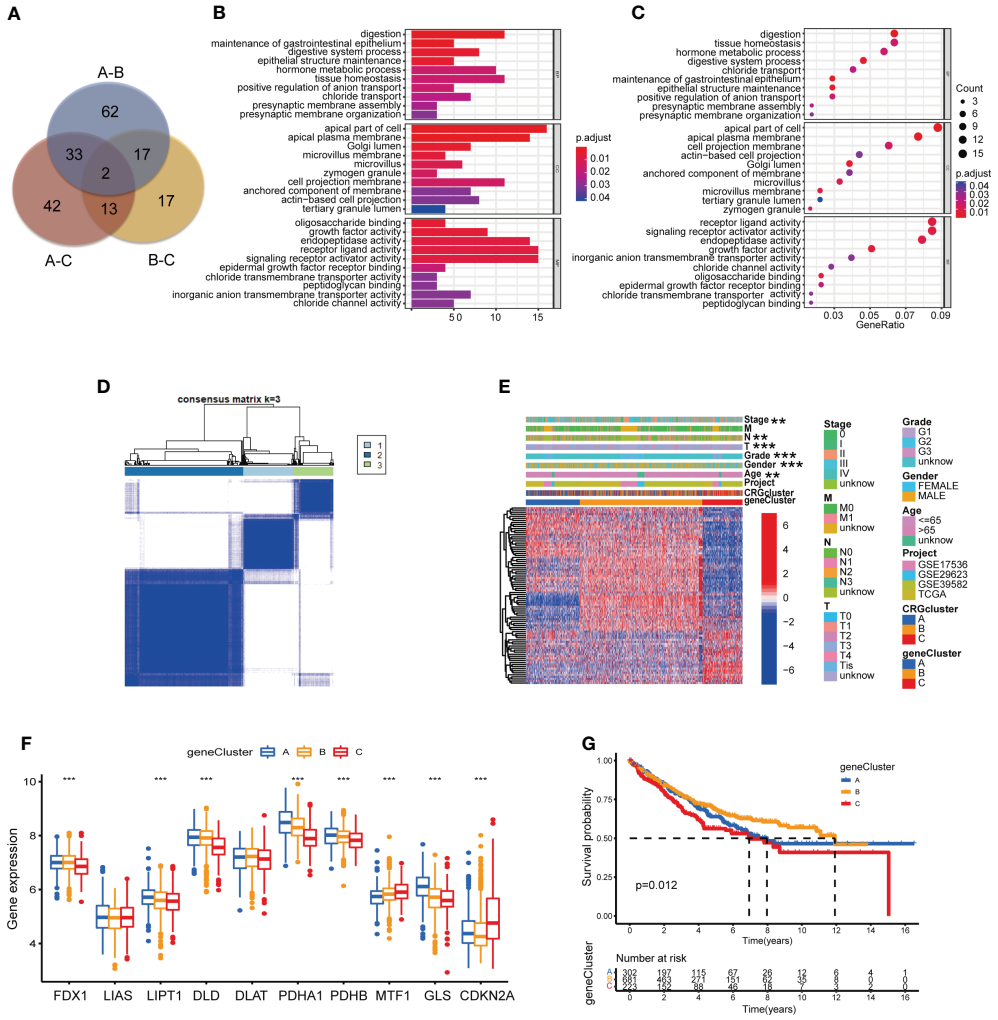

FIGURE 6
Identification of CRG gene subtypes based on 186 DEGs derived from different molecular subtypes. **(A)** The intersection of DEGs from the comparison between molecular subtype A and B, B and C, A and C **(B, C)** GO enrichment analyses of 186 DEGs from distinct molecular subtypes. Adjusted P-value<0.05 was considered to be statistically significant. **(D)** Identification of three gene subtypes (k = 3) and their correlation area through consensus clustering analysis according to the expression of 86 prognosis-related DEGs. **(E)** The heat-map presented the gene profiles in distinct gene subtypes, and the correlations between clinicopathologic characteristics and distinct gene subtypes. Chi-square test was used for the comparison. P-value< 0.05 was considered to be statistically significant. **(F)** Difference analyses of CRGs expression in different gene subtypes. Pvalue< 0.05 was considered to be statistically significant. **(G)** Survival analysis of three gene subtypes. Kaplan-Meier plot and log-rank tests were conducted for survival analyses. P-value< 0.05 was considered to be statistically significant. ** indicated P-value<0.01, *** indicated P-value<0.001.

training and testing groups was displayed in Tables S19, 20. The results of difference analyses indicated that all of the expression of GLS, NOX1, HOXC6, TNNT1 and PLA2G12B were increased in tumor tissues, compared with those in normal tissues (Figure S4). Among these five genes, GLS and HOXC6 were negatively associated with patients' survival, while NOX1 and PLA2G12B were positively related. RT-qPCR and IHC indicated the same result (Figures 7B–G). Difference analyses in the training set showed Risk score was extremely increased in both molecular subtype C and gene subtype C and decreased in both molecular subtype B and gene subtype B (Figures 7H, I). The heat-map presented a great difference of 7 key Risk score gene expression profile between high- and low-Risk score sets in the training group (Figure 7J). The scattergram of patients' survival in different Risk score groups revealed that COAD patients' survival got worse, while Risk score increased (Figure 7K), which was also proven by Kaplan-Meier survival curves (Figure 7L). In addition, area under the time-concentration curve (AUC) values of 1-, 3-, and 5-year survival rates of CRG Risk score in the training set were 0.693, 0.706, and 0.703, respectively, signifying both relative high sensitivity and specificity (Figure 6M).

To verify the accuracy of the scoring system, we further calculated Risk score according to the above Risk score formula, in the testing group, individual GSE17536, GSE29623, GSE39582, GSE40967, respectively (Tables S21–24). Patients were respectively divided into distinct cuproptosis molecular subtypes, gene subtypes and Risk score sets, the same as which in the training set (Figures S5–8A). Risk score showed a great difference in both molecular subtypes and gene subtypes of the testing group, individual GSE17536, GSE29623, GSE39582 (Figures S5–8B, C). The expressions of 7 key Risk scoring genes

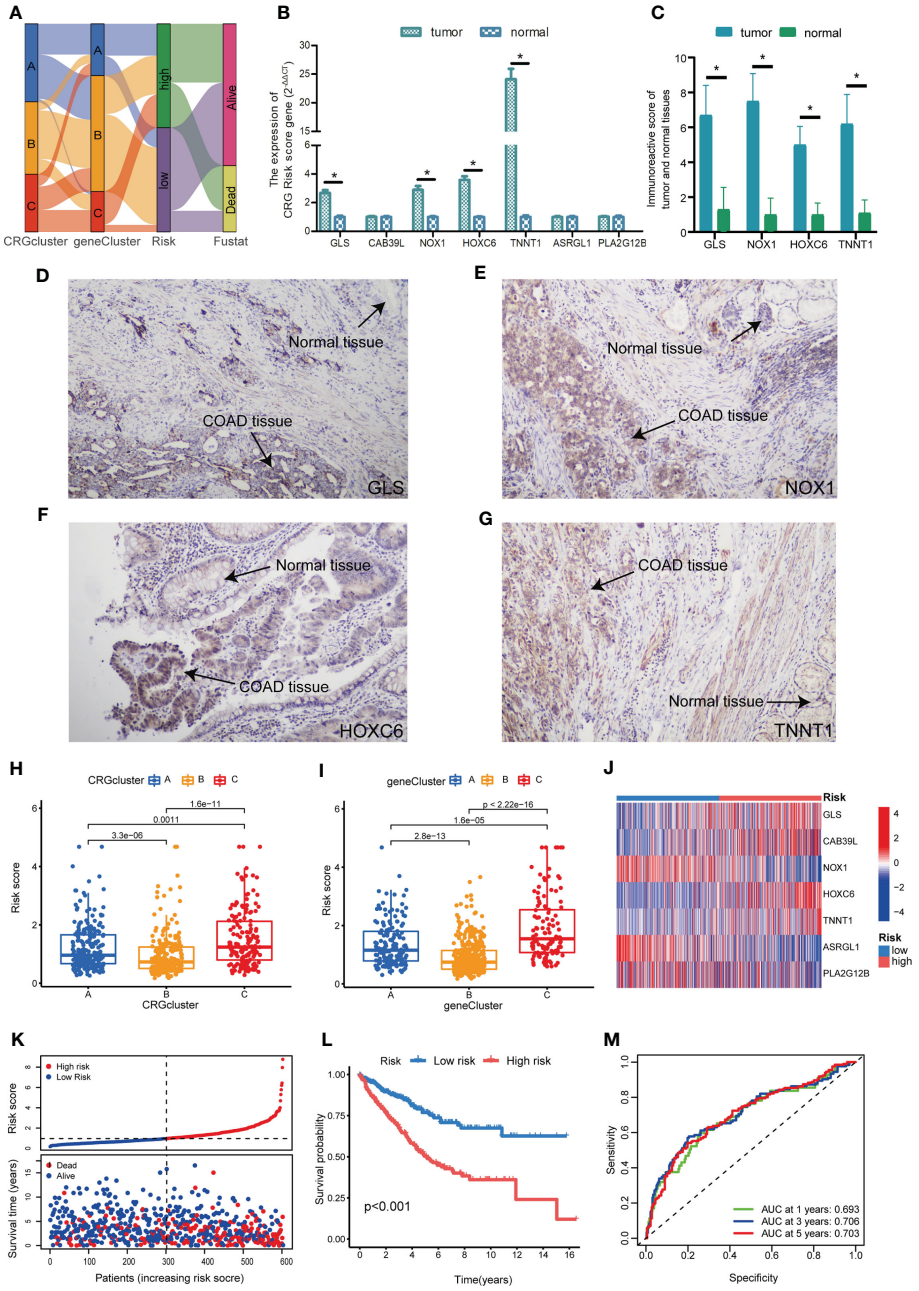

FIGURE 7
Construction of CRG Risk scoring system in the training group. **(A)** Alluvial diagram of patients' distributions in groups with different molecular subtypes, gene subtypes, Risk scores and survival outcomes. **(B)** The expression of 7 key genes between COAD and paired normal tissues. **(C)** Immunoreactive score of key genes between tumor and normal tissues. **(D)** The expression of GLS in COAD tissues and normal tissues. **(E)** The expression of NOX1 in COAD tissues and normal tissues. **(F)** The expression of HOXC6 in COAD tissues and normal tissues. **(G)** The expression of TNNT1 in COAD tissues and normal tissues. **(H)** Difference analysis of CRG Risk score in different molecular subtypes. **(I)** Difference analysis of CRG Risk score in different gene subtypes. **(J)** Heat-map displayed five scoring genes expression profile in different risk sets of the training group. **(K)** Ranked dot and scatter plot of CRG Risk score distribution and patient survival in the training group. **(L)** Survival analysis between high- and low-Risk score groups in the training set. Kaplan-Meier plot and log-rank tests were conducted for survival analyses. **(M)** ROC curve predicted the sensitivity and specificity of 1-, 3-, and 5-year survival according to CRG Risk score in the training group. P-value< 0.05 was considered to be statistically significant. * indicated P-value<0.05.

in different Risk group were shown in Figures S5–8 D; 9A, respectively. Both scattergram and Kaplan-Meier survival curves showed that high Risk score predicted poor survival in testing group, individual GSE17536, GSE39582 and GSE40967 (Figures S5E, F, S7–8E, F, S9B, C). However, in GSE29623, survival analysis revealed that Risk score was not associated with patients' survival, which might be related with the small sample size (Figure S6F). We further plot ROC curves to confirm the sensitivity and specificity of the scoring system and found relatively high AUC values in the cohorts of validation, indicating the system as an accurate predictor for patients' survival (Figures S5–8G, 9D).

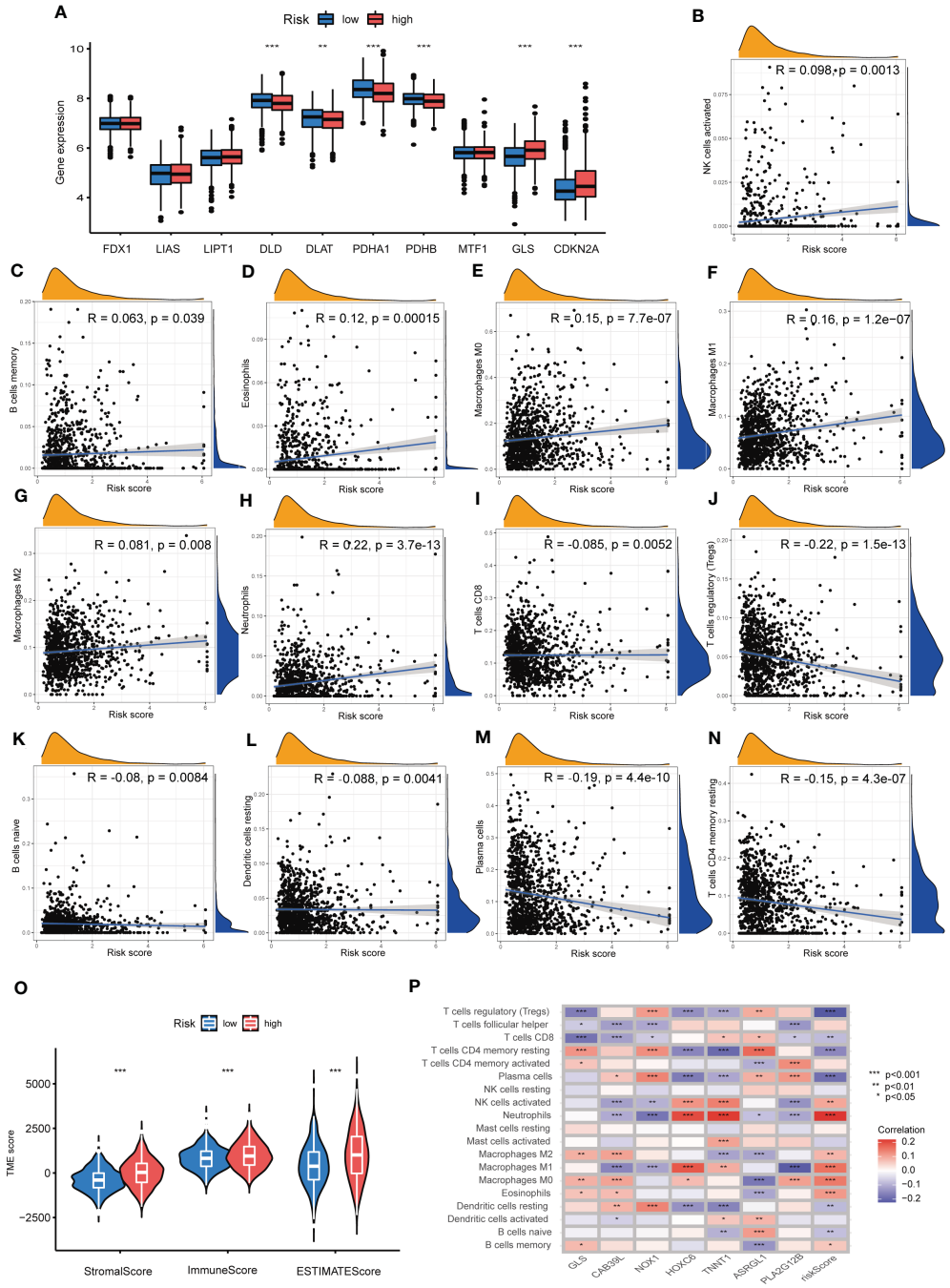

FIGURE 8
Associations between TME and CRG Risk score. **(A)** Difference analyses of CRGs expression in the high- and low-Risk score groups. **(B–N)** Correlation analyses between CRG Risk score and TICs. **(O)** Difference analyses between CRG Risk score and immune/stromal/estimate scores. **(P)** Correlation analyses between the abundance of TICs and seven key Risk scoring genes in the proposed model. P-value< 0.05 was considered to be statistically significant.

3.6 Associations between TME and the CRG Risk score

Difference analyses of CRGs indicated that 6 CRGs showed a great difference in distinct Risk score sets. To be specific, GLS and CDKN2A expression were increased, while DLD, DLAT, PDHA1 and PDHB expression were decreased in high-Risk score group, compared with those in low-Risk group (Figure 8A). In order to learn the relationships between CRG Risk score and TICs in TME of COAD, correlation analyses were carried out and suggested that CRG Risk score was positively associated with activated NK cells, memory B cells, eosinophils, M0 macrophages, M1 macrophages, M2 macrophages, and neutrophils, while negatively associated with CD8 T cells, regulatory T cells (Tregs), naïve B cells, resting dendritic cells, plasma cells and CD4 memory resting T cells (Figures 8B–N). Furthermore, all of immune, stromal and estimate score were higher in high-Risk score set than those in low-Risk score set (Figure 8O). Most immune cells were greatly associated with seven

prognostic genes (Figure 8P). Consequently, CRG Risk score might be associated with TME of COAD.

3.7 Associations among MSI, CSC, TMB, somatic mutations and CRG Risk score

Up to data, limited molecular markers are available to lead therapeutic decisions for patients with COAD, among which MSI, CSC, TMB and somatic mutations appeared to be the most promising. An increasing number of research revealed that patients with high microsatellite instability (MSI-H) tumor might benefit from immune checkpoint inhibitors (ICIs) in COAD (30, 31). As a result, we assessed the MSI status and found that in the low-risk group, 73% were MSS, 17% were low microsatellite instability (MSI-L), and 10% were MSI-H, while in the high-risk group, 59% were MSS, 20% were MSI-L, and 20% were MSI-H (Figure 9A). The results indicated that patients with high-risk shared a higher MSI-H frequency. Figure 9B suggested that patients bearing MSI-H tumors appeared to have a higher Risk score, compared with those with MSS. This might be related with better treatment outcomes of ICIs. Additionally, crosstalk between immune cells and CSCs, another important indicator of TIME, takes a great part in tumor progression (32). As presented in Figure 9C, CRG Risk score was negatively associated with CSC index, indicating COAD cells with high CRG Risk scores had less difference in stem cell properties and higher cell differentiation than those with low-risk scores. TMB, as an indicator of the number of tumor mutations, is known to be closely associated with patients' immunotherapy benefits (33). Differential analysis indicated that TMB in high-risk group was significantly higher than that in low-risk group (Figure 9D). Correlation analysis also suggested that TMB was positively associated CRG Risk score (Figure 9E). Maftools of somatic mutations showed that the top 10 mutant

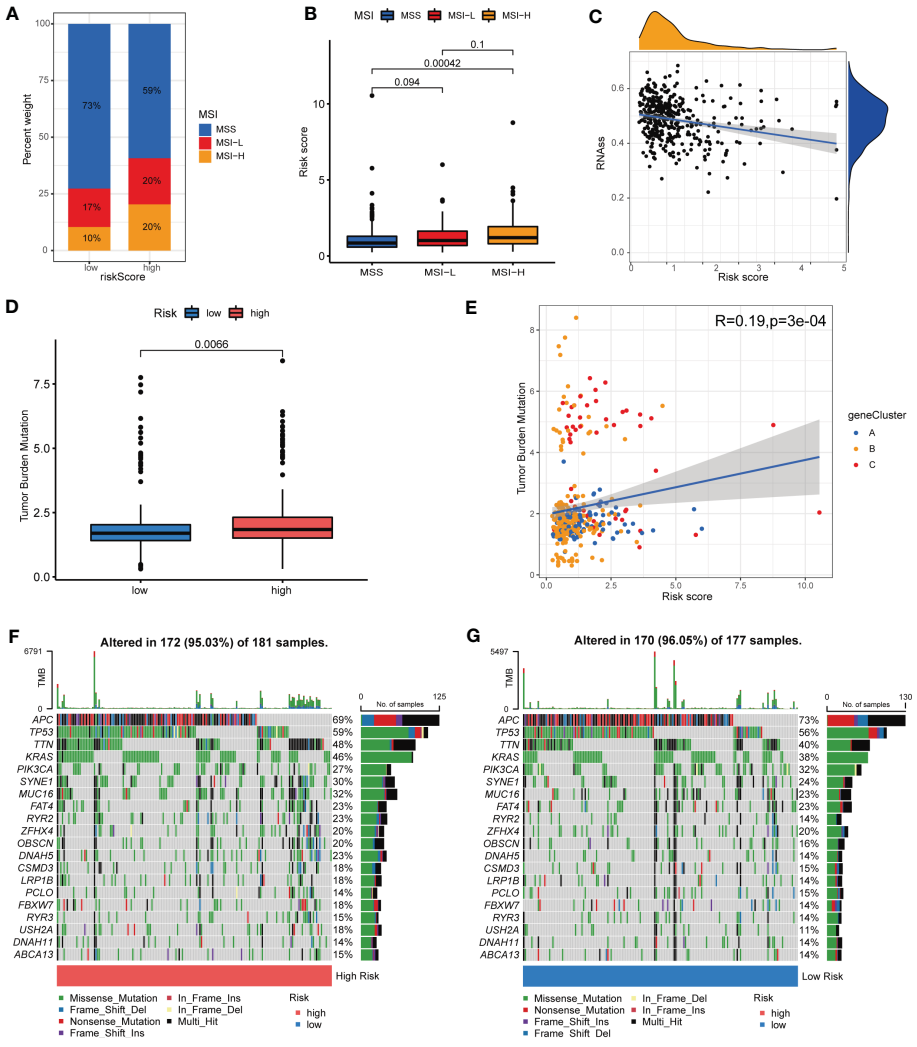

FIGURE 9
Associations among MSI, TMB, CSC and CRG Risk score. **(A)** The distribution of MSI in different Risk score groups. **(B)** Difference analysis between CRG Risk score and MSI. **(C)** Correlation analysis between CRG Risk score and CSC index. **(D)** Difference analysis of TMB in distinct CRG Risk score groups. **(E)** Correlation analysis between CRG Risk score and TMB. **(F-G)** The waterfall plot of somatic mutation characteristics in high- and low-Risk score groups. P-value< 0.05 was considered to be statistically significant.

genes in the high-risk and low-risk groups were APC, TP53, TTN, KRAS, PIK3CA, SYNE1, MUC16, FAT4, RYR2 and ZFHX4, respectively (Figures 9F, G).

3.8 Drugs susceptibility analysis in distinct Risk score groups

To investigate the predictive value of CRG Risk score in drug sensitivity, we used pRRophetic R package to calculate the IC50 values of various drugs (Figures S10, 11; Table 2). Both drugs under clinical use and clinical trials were included in our analyses. Various drugs were divided into different groups, such as AKT inhibitor, AMPK activator, Bcr-Abl inhibitor, BTK inhibitor, EGFR inhibitor, MAPK inhibitor, mTOR inhibitor, TrkA inhibitor, Topoisomerase inhibitor, Microtubule assosiated inhibitor, XIAP inhibitor, TNF inhibitor and so on. In particular, patients of low-Risk score set showed increased IC50 value for AMPK activator (AICAR), Bcl-2 inhibitor (TW.37, Obatoclax.Mesylate and ABT.263), BRAF inhibitor (PLX4720), c-Kit inhibitor (AMG.706), DNA Synthesis inhibitor (Cytarabine, Bleomycin and Gemcitabine), HSP90 inhibitor (AUY922), ITK inhibitor (BMS.509744), MEK inhibitor (CI.1040 and RDEA119), PARP inhibitor (AG.014699 and AZD.2281) and ROCK inhibitor (GSK269962A). In addition, patients of high-Risk score set showed increased IC50 value for AKT inhibitor (AKT.inhibitor.VIII and A.443654), CDK inhibitor (Roscovitine), Raf/VEGFR/c-Kit inhibitor (Sorafenib), Her-2 inhibitor (Lapatinib) and EGFR inhibitor (Erlotinib and BIBW2992).

However, drugs that target the same site may have opposite effects in different risk groups. For example, patients with low CRG risk scores had increased IC50 values for Aurora kinase inhibitors (ZM.447439) and decreased IC50 values for aurora kinase inhibitors (VX.680). HDAC inhibitors (Vorinostat) had increased IC50 values and HDAC inhibitors (MS.275) had decreased IC50 values in the low-risk score set. mTOR inhibitors (Temsirolimus, NVP.BEZ235 and AZD8055) presented better drug sensitivity in

TABLE 2 Drug susceptibility in patients of the low- and high-score groups.

Drugs		Low-score group	High-score group
AKT inhibitor	AKT.inhibitor.VIII		+
	A.443654		+
AMPK activator	AICAR	+	
Aurora Kinase inhibitor	ZM.447439	+	
	VX.680		+
Bcl-2 inhibitor	TW.37	+	
	Obatoclax.Mesylate	+	
	ABT.263	+	
Bcr-Abl inhibitor	Nilotinib	+	
	AP.24534	+	
	Dasatinib	+	
	Imatinib	+	
BRAF inhibitor	PLX4720	+	
BTK inhibitor	LFM.A13	+	
CDK inhibitor	Roscovitine		+
CHK inhibitor	AZD7762	+	
c-Kit inhibitor	AMG.706	+	
Raf/VEGFR/c-Kit inhibitor	Sorafenib		+
DNA Synthesis inhibitor	Cytarabine	+	
	Bleomycin	+	
	Gemcitabine	+	
DNA crosslinker/apoptosis inducer	Cisplatin	+	
EGFR inhibitor	Erlotinib		+
	BIBW2992		+

(Continued)

10.3389/fonc.2023.1152681

TABLE 2 Continued

Drugs		Low-score group	High-score group
FAK inhibitor	PF.562271	+	
FGFR inhibitor	PD.173074	+	
FTase inhibitor	FTI.277	+	
Proteosome inhibitor	Z.LLNle.CHO	+	
GSK-3 inhibitor	CHIR.99021	+	
	SB.216763	+	
HDAC inhibitor	Vorinostat	+	
	MS.275		+
Hedgehog inhibitor	GDC.0449	+	
Her-2 inhibitor	Lapatinib		+
HSP90 inhibitor	AUY922	+	
ITK inhibitor	BMS.509744	+	
JNK inhibitor	JNK.Inhibitor.VIII	+	
	JNK.9L	+	
	AS601245	+	
MAPK inhibitor	VX.702	+	
MDM2 inhibitor	JNJ.26854165	+	
MEK inhibitor	CI.1040	+	
	RDEA119	+	
mTOR inhibitor	Temsirolimus	+	
	Rapamycin		+
	NVP.BEZ235	+	
	AZD8055	+	
PAK inhibitor	IPA.3	+	
PARP inhibitor	AG.014699	+	
	AZD.2281	+	
TBK1 and PDK1 inhibitor	BX.795	+	
PI3K inhibitor	AZD6482	+	
	GDC0941	+	
	NVP.BEZ235	+	
PKC inhibitor	Midostaurin	+	
PLK inhibitor	BI.2536		+
	GW843682X		+
PPAR inhibitor	FH535	+	
Rac inhibitor	EHT.1864		+
Raf inhibitor	AZ628	+	
ROCK inhibitor	GSK269962A	+	
RPTK inhibitor	CEP.701	+	
RSK inhibitor	BI.D1870	+	

(Continued)

TABLE 2 Continued

Drugs		Low-score group	High-score group
	PF.4708671		+
	CMK	+	
RXR activator	Bexarotene	+	
Src inhibitor	A.770041	+	
	AZD.0530	+	
	Bosutinib	+	
Syk inhibitor	BAY.61.3606	+	
TNF inhibitor	Lenalidomide	+	
TrkA inhibitor	GW.441756		+
VEGFR inhibitor	Axitinib	+	
	Pazopanib	+	
PPM1D/Wip1 inhibitor	CCT007093	+	
XIAP inhibitor	Embelin	+	
Topoisomerase I inhibitor	Camptothecin	+	
Topoisomerase II inhibitor	Doxorubicin	+	
	Etoposide	+	
Microtubule Assosiated inhibitor	Docetaxel	+	
	Vinblastine	+	
Microtubule stabilizer	Paclitaxel		+
SER Ca2+-ATPase inhibitor	Thapsigargin	+	
	Metformin		+
Cuproptosis inducer	Elesclomol	+	
ARFGAP1 inhibitor	QS11	+	
Chloride Channel inhibitor	Shikonin	+	
eIF2α Dephosphorylation inhibitor	Salubrinal		+
SHP PTP inhibitor	NSC.87877	+	
DNA-PK inhibitor	NU.7441	+	

"+": Indicated up-regulated sensitivity.

low-risk score set, while mTOR inhibitor (rapamycin) had the opposite. RSK inhibitors (BI. D1870 and CMK) and PF.4708671. RSK inhibitor (BI.D1870 and CMK) and PF.4708671 also showed the opposite drug susceptibility between different risk score sets.

3.9 Construction of a nomogram for the prediction of COAD patient's survival

Regarding the important role of Risk score in patients' survival, we constructed a nomogram combining CRG Risk scores and clinicopathological characteristics to predict 1, 3, and 5-year survival rates of COAD patients (Figure 10A). The calibration graph showed that the nomogram functioned well in predicting patients' survival compared to an ideal model (Figure 10B). The AUC values of 1, 3, and 5-year survival rates of nomogram were 0.873, 0.798, and 0.804, respectively, suggesting both relatively high sensitivity and specificity (Figure 10C).

4 Discussion

COAD is a global health problem. Despite continuous improvement of early screening and treatment strategies, the survival of patients with advanced COAD remains poor (1). Previous research suggested genomic susceptibility contributed to the occurrence and development of COAD (34–37). For example, BRAF V600E and KRAS mutations were significantly related with poor prognosis of patients with microsatellite-stable COAD (38). However, risk factors affecting patients' survival varied and the

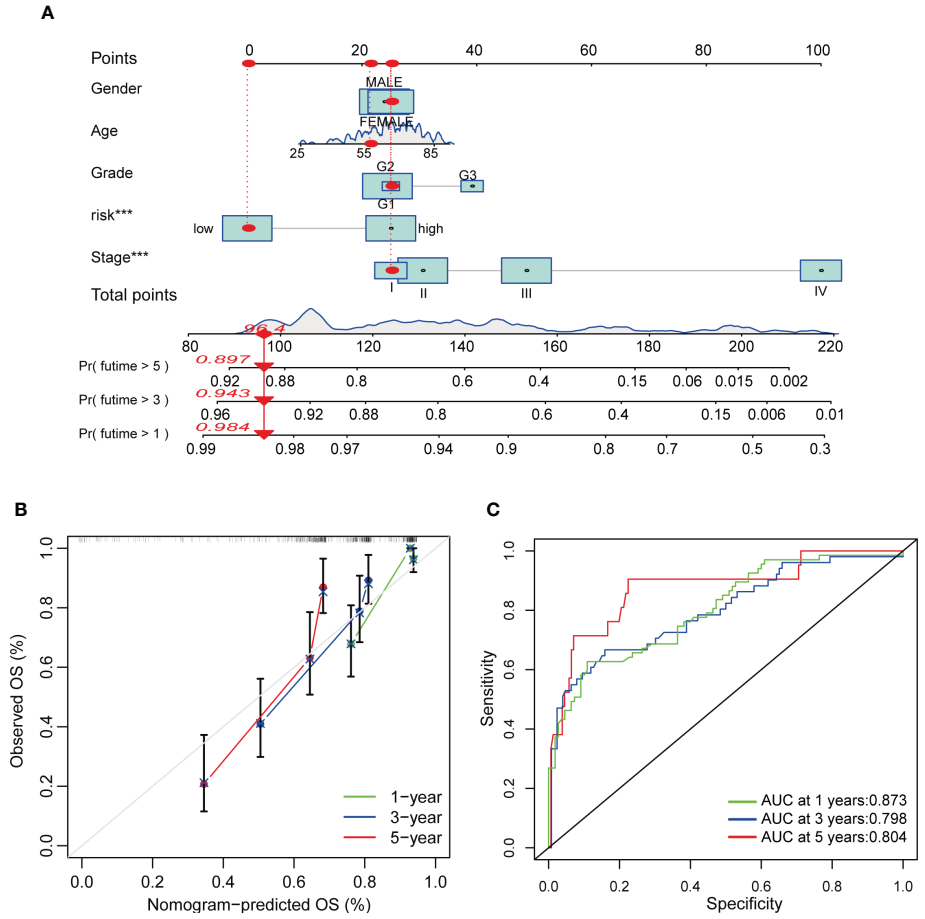

FIGURE 10
Construction and validation of a nomogram in COAD patients. **(A)** Nomogram for predicting the 1-, 3-, and 5-year OS of COAD patients. **(B)** Calibration curves of the nomogram. **(C)** ROC curves for predicting the 1-, 3-, and 5-year OS of COAD patients.

above risk factors predicting the prognosis of patients were not yet satisfactory.

TME is a highly complex ecosystem (39). The subtle interactions between tumor cells and co-existing immune cells in TME determine tumor's natural history. Based on pioneer studies on TME, the two most widely applied ICIs, blocking cytotoxic-T-lymphocyte-associated protein 4 (CTLA-4) and targeting programmed cell death 1 (PD-1) or programmed cell death ligand 1 (PD-L1), emerged as exciting treatment strategies across various malignancies in the last decade (40). ICIs showed impressive anti-tumor efficacy in COAD patients bearing tumors with the expression of PD-L1, deficient mismatch repair (dMMR), MSI-H, or high TMB (41, 42). Whereas the number of COAD patients who benefit from ICIs is limited due to primary and acquired resistance. Therefore, comprehensive knowledge of changes in genomic, transcriptome and somatic mutations in TME is of great significance for the prevention, treatment and prognosis assessment of COAD.

PCD, also termed as RCD, is a form of cell death that can be regulated by multiple biomacromolecules, thus leading to biochemical and morphological alterations which are depend on energy (43). Increasing evidence has indicated that RCD is the key features of tumorigenesis, which may ultimately affect therapeutic strategies in cancers (44). RCD subroutines containing apoptosis, necroptosis, autophagy, pyroptosis, ferroptosis, lysosome-dependent cell death (LCD), alkaliptosis and NETosis have been identified and are being extensively investigated in a variety of malignancies (45). For instance, interactions between specific pyroptosis-related subtypes and TME greatly influenced patients' prognosis (46). Dividing cancer patients into different subtypes according to their genomic features allows us to more accurately predict drug susceptibility and patient outcome, helping physicians design more precise and individualized treatment strategies (47–49).

Cu is an essential micronutrient participated in multiple fundamental biological processes (50). Aberrant Cu homeostasis (ACH) is associated with tumor growth, metastasis, and drug resistance due to its role in oxidative stress and chronic inflammation (51). A higher Cu level indicated a higher risk of colorectal cancer (52). In addition, Cu chelator exhibited great antitumor activity in various cancers, such as esophageal cancer, triple-negative breast cancer and COAD (53–57). For example, the disulfiram (DSF), a well-known antialcohol drug, combined with Cu triggered autophagic cell death and inhibited cell viability in colorectal cancer by targeting ULK1 (55). Tetrathiomolybdate (TM) and TPEN, specific Cu chelators, also showed obvious anti-tumor

activity in COAD (58–60). In addition, quite a few novel Cu compounds were developed to investigate their antitumor mechanisms and therapeutic effect in COAD. For instance, the copper-imidazo[1,2-a] pyridines induced COAD apoptosis (61). Cu $(dmp)_2(CH_3CN)]^{2+}$ exhibited anti-proliferative activity in human colorectal cancer cells (62). Cu(qmbn)(q)(Cl) triggered mitochondrion-mediated apoptotic cell death *via* activating the caspases-3 and 9 proteins (63). Moreover, nanoparticles combining Cu were designed to investigate the anticancer potential in COAD. Cu nanoparticles (CuNPs and Cu-Cy) shed a good insight for COAD treatment (64, 65). $Cu_2O@CaCO_3$ nanocomposites inhibited CRC distant metastasis and recurrence by immunotherapy through inducing an immunologically favorable TME and intensing the immune responses of anti-CD47 antibodies (66). The Bi : Cu_2O@HA nanoparticles exhibited excellent targeting ability and photothermal therapeutic effect (67). Cuproptosis, a novel RCD, was recently identified as copper-dependent death, which occurred through directly binding Cu to TCA cycle (19). However, the role of cuproptosis in COAD is unclear, and the prognostic value of CRGs has not been thoroughly evaluated.

Thanks to the large public database such as TCGA and GEO, we are able to access and analyze the transcriptome profiles of a variety of malignancies to gain a comprehensive understanding of genetic landscape, screen potential biomarkers, develop therapy strategies and predict patient outcome (68, 69). Several studies have described cuproptosis-related molecular patterns and the characterization of TME in colorectal cancer and found that cuproptosis patterns were closely associated with TME and served to predicted survival of patients with colorectal cancer (70–74). D. Hou, et al. (75) developed a risk model of 11-cuproptosis-related lncRNAs to predict clinical and therapeutic implications of CRC patients. However, colon and rectal cancer were quite different in their biological characteristics, surgical protocol, treatment strategy and prognosis (76). Previously, Luo, B., et al. (77) identified two clusters based on 30 differentially expressed CRGs of 963 COAD samples from TCGA-COAD and GSE39582 databases. However, the OS between the two clusters showed no statistical difference and the accuracy of risk model was not verified. Xu, C., et al. (78) classified COAD samples from TCGA-COAD and GSE39582 databases into two groups according to 9 cuproptosis-related DEGs and further constructed a risk model. Whereas, ROC curves of the model showed that AUC values for the 1-year, 2-year, and 3-year survival were 0.575, 0.577 and 0.571 respectively, signifying the moderate predictive power of the model. In addition, Yang, G., et al. (79) grouped 623 COAD patients from TCGA-COAD and GSE17536 databases into 2 sets based on 12 CRGs expression profiles and established nomogram pattern based on risk model to predict patient prognosis. However, the sensitivity and specificity of the nomogram was not verified. As a result, we aimed to establish a more accurate risk model to predict survival through comprehensively integrating CRGs expression patterns of 1307 COAD samples from TCGA-COAD, GSE17536, GSE29623 and GSE39582 databases. In our study, 7 of 10 CRGs were found to be dys-regulated in tumor samples compared with those in normal samples, and a relatively high mutation frequency and CNV of CRGs was observed in COAD samples. Survival analysis and univariate Cox regression analysis of patients from TCGA (TCGA-COAD) and GEO database (GSE17536, GSE29623 and GSE39582) suggested both GLS and CDKN2A were significantly related with patients' survival. The cuproptosis network demonstrated the complex interrelations among CRGs and prognosis of cancer patients. Considering the relatively common genetic and transcriptional variation and the potential prognostic value of CRGs in COAD, we speculated cuproptosis may be a new therapeutic target and that CRGs characteristics might play an important role in predicting therapeutic response and patient outcome, providing new insights into the role of Cu in COAD. We further categorized patients into three cuproptosis related molecular subtype, including subtype A, B and C, based on CRGs expression profile. Distinct molecular subtypes differed in both the CRGs expression profile, and the survival and clinicopathological features of COAD patients. GO and KEGG GSVA enrichment analyses suggested that different molecular subtypes enriched in different signaling pathways. Given the indispensable role of immunotherapy in colorectal adenocarcinoma, TIME-associated indicators such as TICs, MSI, CSC, TMB, somatic mutations, etc., were investigated to study the relationship between CRGs and TIME of colorectal adenocarcinoma. TICs profile revealed great difference in the infiltration of 19 TICs among distinct subtypes. GO enrichment analysis of 186 DEGs, obtained from the comparison between subtype A and B, A and C, and B and C, revealed that DEGs mainly enriched in signaling pathways associated with digestion. Univariate Cox regression analysis identified 86 prognostic DEGs from the above 186 genes. Based on 86 prognostic DEGs expression profile, we once again classified patients into 3 sets, namely gene subtype A, B and C, which were differed in the expressions of both prognostic DEGs and 8 CRGs. Additionally, cuproptosis gene subtypes were closely associated with the survival and clinicopathological characteristics (age, sex, grade, T and N stage) of COAD patients. In view of the important role of CRGs in COAD, the risk scoring system of CRG was further constructed in the training set according to prognostic DEGs expression, and verified in the testing set and the combined set. Risk scores of molecular subtype C and gene subtype C were significantly increased, while risk scores of molecular subtype B and gene subtype B were significantly decreased. The higher the risk score, the lower the survival rate. In addition, CRGs, TICs, CSC, TMB, MSI, somatic mutations, and drug sensitivity were closely associated with distinct risk score sets. Finally, a nomogram integrating risk scores and clinicopathological characteristics was established to predict OS rates of COAD patients. AUC values of 1-, 3-, and 5-year survival rates of nomogram were 0.873, 0.798, and 0.804, respectively, which was higher than previous nomogram established by Zhong, L., et al. (80). However, our study of the relationships between CRGs and TME in COAD were primarily based on the bioinformatics analysis. The specific mechanism of CRGs affecting TME needs to be further studied *in vitro* and *in vivo*, which may be crucial for the treatment of COAD.

5 Conclusion

CRGs were significantly correlated with clinicopathologic features, TME and immunoinfiltration of COAD. The higher the

Risk score, the higher the MSI and TMB, and the lower the CSC. In addition, the CRGs Risk scoring system showed good ability to predict patient survival and drug sensitivity.

Data availability statement

The original contributions presented in the study are included in the article/Supplementary Material. Further inquiries can be directed to the corresponding author.

Ethics statement

The studies involving human participants were reviewed and approved by the Ethics Committee of Nanjing Jiangning Hospital. The patients/participants provided their written informed consent to participate in this study.

Author contributions

(I) Conception and design: JW; ZT; (II) Administrative support: JW; ZT; BW; XH (III) Provision of study materials or patients: JW; XQ; DQ (IV) Collection and assembly of data: JW; YW; BL; DQ (V) Data analysis and interpretation: JW; YX; JC (VI) Manuscript writing: JW; (VII) All authors contributed to the article and approved the submitted version.

Funding

This research was funded by the National Nature Science Foundation of China, grant number 82103032, Medical Research Grant of Jiangsu Commission of Health, grant number M2020010, the Medical Science and Technology Development Foundation of Nanjing, grant number YKK21224.

Conflict of interest

The authors declare that the research was conducted in the absence of any commercial or financial relationships that could be construed as a potential conflict of interest.

Publisher's note

All claims expressed in this article are solely those of the authors and do not necessarily represent those of their affiliated organizations, or those of the publisher, the editors and the reviewers. Any product that may be evaluated in this article, or claim that may be made by its manufacturer, is not guaranteed or endorsed by the publisher.

Supplementary material

The Supplementary Material for this article can be found online at: https://www.frontiersin.org/articles/10.3389/fonc.2023.1152681/full#supplementary-material

SUPPLEMENTARY FIGURE 1
Unsupervised clustering of CRGs and consensus matrix heat-maps for k = 2, 4-9 through consensus clustering analysis in COAD samples from TCGA and GEO database.

SUPPLEMENTARY FIGURE 2
Unsupervised clustering of prognostic genes and consensus matrix heat-maps for k = 2, 4-9 through consensus clustering analysis in COAD samples from TCGA and GEO database.

SUPPLEMENTARY FIGURE 3
Identification of optimum prognostic genes in COAD samples. **(A, B)** The LASSO regression analysis and partial likelihood deviance analysis on 86 subtype-related prognostic DEGs.

SUPPLEMENTARY FIGURE 4
Difference, paired difference and survival analyses of 7 key Risk scoring genes (GLS, NOX1, HOXC6, TNNT1, PLA2G12B, CAB39L and ASRGL1) in COAD patients.

SUPPLEMENTARY FIGURE 5
Validation of CRG Risk score in the testing group. **(A)** Alluvial diagram of patients' distributions in testing groups with different molecular subtypes, gene subtypes, Risk scores and survival outcomes. **(B)** Differential analysis of CRG Risk score in different molecular subtypes of the testing group. **(C)** Differential analysis of CRG Risk score in different gene subtypes of the testing group. **(D)** The heat-map of seven scoring genes expression in different risk sets of the testing group. **(E)** Ranked dot and scatter plot of CRG Risk score distribution and patient survival in the testing group. **(F)** Survival analysis of high- and low- CRG Risk score in the testing group. Kaplan–Meier plot and log-rank tests were conducted for survival analyses. P-value < 0.05 was considered to be statistically significant. **(G)** ROC curve predicted the sensitivity and specificity of 1-, 3-, and 5-year survival according to CRG Risk score in the testing group.

SUPPLEMENTARY FIGURE 6
Validation of CRG Risk score in GSE29623. **(A)** Alluvial diagram of patients' distributions in testing groups with different molecular subtypes, gene subtypes, Risk scores and survival outcomes. **(B)** Differential analysis of CRG Risk score in different molecular subtypes of GSE29623. **(C)** Differential analysis of CRG Risk score in different gene subtypes of GSE29623. **(D)** The heat-map of seven scoring genes expression in different risk sets of GSE29623. **(E)** Ranked dot and scatter plot of CRG Risk score distribution and patient survival in GSE29623. **(F)** Survival analysis of high- and low- CRG Risk score in GSE29623. Kaplan–Meier plot and log-rank tests were conducted for survival analyses. P-value< 0.05 was considered to be statistically significant. **(G)** ROC curve predicted the sensitivity and specificity of 1-, 3-, and 5-year survival according to CRG Risk score in GSE29623.

SUPPLEMENTARY FIGURE 7
Validation of CRG Risk score in GSE17536. **(A)** Alluvial diagram of patients' distributions in testing groups with different molecular subtypes, gene subtypes, Risk scores and survival outcomes. **(B)** Differential analysis of CRG Risk score in different molecular subtypes of GSE17536. **(C)** Differential analysis of CRG Risk score in different gene subtypes of GSE17536. **(D)** The heat-map of seven scoring genes expression in different risk sets of GSE17536. **(E)** Ranked dot and scatter plot of CRG Risk score distribution and patient survival in GSE17536. **(F)** Survival analysis of high- and low- CRG Risk score in GSE17536. Kaplan–Meier plot and log-rank tests were conducted for survival analyses. P-value< 0.05 was considered to be statistically significant. **(G)** ROC curve predicted the sensitivity and

specificity of 1-, 3-, and 5-year survival according to CRG Risk score in GSE17536.

SUPPLEMENTARY FIGURE 8
Validation of CRG Risk score in GSE39582. **(A)** Alluvial diagram of patients' distributions in testing groups with different molecular subtypes, gene subtypes, Risk scores and survival outcomes. **(B)** Differential analysis of CRG Risk score in different molecular subtypes of GSE39582. **(C)** Differential analysis of CRG Risk score in different gene subtypes of GSE39582. **(D)** The heat-map of seven scoring genes expression in different risk sets of GSE39582. **(E)** Ranked dot and scatter plot of CRG Risk score distribution and patient survival in GSE39582. **(F)** Survival analysis of high- and low- CRG Risk score in GSE39582. Kaplan–Meier plot and log-rank tests were conducted for survival analyses. P-value< 0.05 was considered to be statistically significant. **(G)** ROC curve predicted the sensitivity and specificity of 1-, 3-, and 5-year survival according to CRG Risk score in GSE39582.

SUPPLEMENTARY FIGURE 9
Validation of CRG Risk score in GSE40967. **(A)** The heat-map of seven scoring genes expression in different risk sets of the combined group. **(B)** Ranked dot and scatter plot of CRG Risk score distribution and patient survival in the combined group. **(C)** Survival analysis of high- and low- CRG Risk score in the combined group. Kaplan–Meier plot and log-rank tests were conducted for survival analyses. P-value< 0.05 was considered to be statistically significant. **(D)** ROC curve predicted the sensitivity and specificity of 1-, 3-, and 5-year survival according to CRG Risk score in the combined group.

SUPPLEMENTARY FIGURE 10
Differential drugs susceptibility analyses in high- and low-Risk group. P-value< 0.05 was considered to be statistically significant.

SUPPLEMENTARY FIGURE 11
Differential drugs susceptibility analyses in high- and low-Risk group. P-value< 0.05 was considered to be statistically significant.

References

1. Sung H, Ferlay J, Siegel RL, Laversanne M, Soerjomataram I, Jemal A, et al. Global cancer statistics 2020: globocan estimates of incidence and mortality worldwide for 36 cancers in 185 countries. *CA Cancer J Clin* (2021) 71(3):209–49. doi: 10.3322/caac.21660

2. Formica V, Sera F, Cremolini C, Riondino S, Morelli C, Arkenau HT, et al. Kras and braf mutations in stage ii and iii colon cancer: a systematic review and meta-analysis. *J Natl Cancer Inst* (2022) 114(4):517–27. doi: 10.1093/jnci/djab190

3. Weiser MR, Hsu M, Bauer PS, Chapman WCJr., González IA, Chatterjee D, et al. Clinical calculator based on molecular and clinicopathologic characteristics predicts recurrence following resection of stage I-iii colon cancer. *J Clin Oncol* (2021) 39(8):911–9. doi: 10.1200/jco.20.02553

4. Barceloux DG. Copper. *J Toxicol Clin Toxicol* (1999) 37(2):217–30. doi: 10.1081/clt-100102421

5. Tsang T, Davis CI, Brady DC. Copper biology. *Curr Biol* (2021) 31(9):R421–r7. doi: 10.1016/j.cub.2021.03.054

6. Ge EJ, Bush AI, Casini A, Cobine PA, Cross JR, DeNicola GM, et al. Connecting copper and cancer: from transition metal signalling to metalloplasia. *Nat Rev Cancer* (2022) 22(2):102–13. doi: 10.1038/s41568-021-00417-2

7. Kazi Tani LS, Gourlan AT, Dennouni-Medjati N, Telouk P, Dali-Sahi M, Harek Y, et al. Copper isotopes and copper to zinc ratio as possible biomarkers for thyroid cancer. *Front Med (Lausanne)* (2021) 8:698167. doi: 10.3389/fmed.2021.698167

8. Wang W, Wang X, Luo J, Chen X, Ma K, He H, et al. Serum copper level and the copper-to-Zinc ratio could be useful in the prediction of lung cancer and its prognosis: a case-control study in northeast China. *Nutr Cancer* (2021) 73(10):1908–15. doi: 10.1080/01635581.2020.1817957

9. Yücel I, Arpaci F, Ozet A, Döner B, Karayilanoğlu T, Sayar A, et al. Serum copper and zinc levels and Copper/Zinc ratio in patients with breast cancer. *Biol Trace Elem Res* (1994) 40(1):31–8. doi: 10.1007/bf02916818

10. Fabris C, Farini R, Del Favero G, Gurrieri G, Piccoli A, Sturniolo GC, et al. Copper, zinc and Copper/Zinc ratio in chronic pancreatitis and pancreatic cancer. *Clin Biochem* (1985) 18(6):373–5. doi: 10.1016/s0009-9120(85)80078-3

11. Witkowski K, Kozłowski A, Pardela M, Piecuch J, Walichiewicz P. Level of copper in plasma and tissue of patients with esophageal and Large bowel cancer. *Wiad Lek* (1993) 46(15-16):586–8.

12. Atakul T, Altinkaya SO, Abas BI, Yenisey C. Serum copper and zinc levels in patients with endometrial cancer. *Biol Trace Elem Res* (2020) 195(1):46–54. doi: 10.1007/s12011-019-01844-x

13. Grasso M, Bond GJ, Kim YJ, Boyd S, Matson Dzebo M, Valenzuela S, et al. The copper chaperone ccs facilitates copper binding to Mek1/2 to promote kinase activation. *J Biol Chem* (2021) 297(6):101314. doi: 10.1016/j.jbc.2021.101314

14. Brady DC, Crowe MS, Turski ML, Hobbs GA, Yao X, Chaikuad A, et al. Copper is required for oncogenic braf signalling and tumorigenesis. *Nature* (2014) 509(7501):492–6. doi: 10.1038/nature13180

15. Krishnamoorthy L, Cotruvo JAJr., Chan J, Kaluarachchi H, Muchenditsi A, Pendyala VS, et al. Copper regulates cyclic-Amp-Dependent lipolysis. *Nat Chem Biol* (2016) 12(8):586–92. doi: 10.1038/nchembio.2098

16. Liu Q, Deng Y, Tang J, Chen D, Li X, Lin Q, et al. Potassium lignosulfonate as a washing agent for remediating lead and copper Co-contaminated soils. *Sci Total Environ* (2019) 658:836–42. doi: 10.1016/j.scitotenv.2018.12.228

17. Zhou Q, Zhang Y, Lu L, Zhang H, Zhao C, Pu Y, et al. Copper induces microglia-mediated neuroinflammation through Ros/Nf-κb pathway and mitophagy disorder. *Food Chem Toxicol* (2022) 168:113369. doi: 10.1016/j.fct.2022.113369

18. Li Y, Wang LH, Zhang HT, Wang YT, Liu S, Zhou WL, et al. Disulfiram combined with copper inhibits metastasis and epithelial-mesenchymal transition in hepatocellular carcinoma through the nf-κb and tgf-β pathways. *J Cell Mol Med* (2018) 22(1):439–51. doi: 10.1111/jcmm.13334

19. Tsvetkov P, Coy S, Petrova B, Dreishpoon M, Verma A, Abdusamad M, et al. Copper induces cell death by targeting lipoylated tca cycle proteins. *Science* (2022) 375(6586):1254–61. doi: 10.1126/science.abf0529

20. Zhang Z, Zeng X, Wu Y, Liu Y, Zhang X, Song Z. Cuproptosis-related risk score predicts prognosis and characterizes the tumor microenvironment in hepatocellular carcinoma. *Front Immunol* (2022) 13:925618. doi: 10.3389/fimmu.2022.925618

21. Wang W, Lu Z, Wang M, Liu Z, Wu B, Yang C, et al. The cuproptosis-related signature associated with the tumor environment and prognosis of patients with glioma. *Front Immunol* (2022) 13:998236. doi: 10.3389/fimmu.2022.998236

22. Cao R, Yuan L, Ma B, Wang G, Tian Y. Tumour microenvironment (Tme) characterization identified prognosis and immunotherapy response in muscle-invasive bladder cancer (Mibc). *Cancer Immunol Immunother* (2021) 70(1):1–18. doi: 10.1007/s00262-020-02649-x

23. Ji ZH, Ren WZ, Wang HQ, Gao W, Yuan B. Molecular subtyping based on cuproptosis-related genes and characterization of tumor microenvironment infiltration in kidney renal clear cell carcinoma. *Front Oncol* (2022) 12:919083. doi: 10.3389/fonc.2022.919083

24. Sha S, Si L, Wu X, Chen Y, Xiong H, Xu Y, et al. Prognostic analysis of cuproptosis-related gene in triple-negative breast cancer. *Front Immunol* (2022) 13:922780. doi: 10.3389/fimmu.2022.922780

25. Wang Y, Zhang C, Ji C, Jin W, He X, Yu S, et al. Molecular subtypes based on cuproptosis-related genes and immune profiles in lung adenocarcinoma. *Front Genet* (2022) 13:1006938. doi: 10.3389/fgene.2022.1006938

26. Wang J, Qin D, Ye L, Wan L, Wang F, Yang Y, et al. Ccl19 has potential to be a potential prognostic biomarker and a modulator of tumor immune microenvironment (Time) of breast cancer: a comprehensive analysis based on tcga database. *Aging (Albany NY)* (2022) 14(9):4158–75. doi: 10.18632/aging.204081

27. Wang J, Wang J, Gu Q, Yang Y, Ma Y, Zhang Q. Tgfβ1: an indicator for tumor immune microenvironment of colon cancer from a comprehensive analysis of tcga. *Front Genet* (2021) 12:612011. doi: 10.3389/fgene.2021.612011

28. Wang J, Zhang Q, Wang D, Yang S, Zhou S, Xu H, et al. Microenvironment-induced Timp2 loss by cancer-secreted exosomal mir-4443 promotes liver metastasis of breast cancer. *J Cell Physiol* (2020) 235(7-8):5722–35. doi: 10.1002/jcp.29507

29. Chui X, Egami H, Yamashita J, Kurizaki T, Ohmachi H, Yamamoto S, et al. Immunohistochemical expression of the c-kit proto-oncogene product in human malignant and non-malignant breast tissues. *Br J Cancer* (1996) 73(10):1233–6. doi: 10.1038/bjc.1996.236

30. Hindson J. Pd1 blockade for advanced msi-h crc. *Nat Rev Gastroenterol Hepatol* (2021) 18(2):82. doi: 10.1038/s41575-021-00415-7

31. Romero D. New first-line therapy for Dmmr/Msi-h crc. *Nat Rev Clin Oncol* (2021) 18(2):63. doi: 10.1038/s41571-020-00464-y

32. Bayik D, Lathia JD. Cancer stem cell-immune cell crosstalk in tumour progression. *Nat Rev Cancer* (2021) 21(8):526–36. doi: 10.1038/s41568-021-00366-w

33. High tmb predicts immunotherapy benefit. *Cancer Discov* (2018) 8(6):668. doi: 10.1158/2159-8290.Cd-nb2018-048

34. Giovannucci E, Ascherio A, Rimm EB, Colditz GA, Stampfer MJ, Willett WC. Physical activity, obesity, and risk for colon cancer and adenoma in men. *Ann Intern Med* (1995) 122(5):327–34. doi: 10.7326/0003-4819-122-5-199503010-00002

35. Giovannucci E, Willett WC. Dietary factors and risk of colon cancer. *Ann Med* (1994) 26(6):443–52. doi: 10.3109/07853899409148367

36. Ogino S, Shima K, Meyerhardt JA, McCleary NJ, Ng K, Hollis D, et al. Predictive and prognostic roles of braf mutation in stage iii colon cancer: results from intergroup trial calgb 89803. *Clin Cancer Res* (2012) 18(3):890–900. doi: 10.1158/1078-0432.Ccr-11-2246

37. Taieb J, Le Malicot K, Shi Q, Penault-Llorca F, Bouché O, Tabernero J, et al. Prognostic value of braf and kras mutations in msi and mss stage iii colon cancer. *J Natl Cancer Inst* (2017) 109(5). doi: 10.1093/jnci/djw272

38. Taieb J, Zaanan A, Le Malicot K, Julié C, Blons H, Mineur L, et al. Prognostic effect of braf and kras mutations in patients with stage iii colon cancer treated with leucovorin, fluorouracil, and oxaliplatin with or without cetuximab: a *Post hoc* analysis of the petacc-8 trial. *JAMA Oncol* (2016) 2(5):643–53. doi: 10.1001/jamaoncol.2015.5225

39. Giraldo NA, Sanchez-Salas R, Peske JD, Vano Y, Becht E, Petitprez F, et al. The clinical role of the tme in solid cancer. *Br J Cancer* (2019) 120(1):45–53. doi: 10.1038/s41416-018-0327-z

40. Naimi A, Mohammed RN, Raji A, Chupradit S, Yumashev AV, Suksatan W, et al. Tumor immunotherapies by immune checkpoint inhibitors (Icis); the pros and cons. *Cell Commun Signal* (2022) 20(1):44. doi: 10.1186/s12964-022-00854-y

41. Borelli B, Antoniotti C, Carullo M, Germani MM, Conca V, Masi G. Immune-checkpoint inhibitors (Icis) in metastatic colorectal cancer (Mcrc) patients beyond microsatellite instability. *Cancers (Basel)* (2022) 14(20). doi: 10.3390/cancers14204974

42. Xu Y, Fu Y, Zhu B, Wang J, Zhang B. Predictive biomarkers of immune checkpoint inhibitors-related toxicities. *Front Immunol* (2020) 11:2023. doi: 10.3389/fimmu.2020.02023

43. Peng F, Liao M, Qin R, Zhu S, Peng C, Fu L, et al. Regulated cell death (Rcd) in cancer: key pathways and targeted therapies. *Signal Transduct Target Ther* (2022) 7(1):286. doi: 10.1038/s41392-022-01110-y

44. Koren E, Fuchs Y. Modes of regulated cell death in cancer. *Cancer Discov* (2021) 11(2):245–65. doi: 10.1158/2159-8290.Cd-20-0789

45. Tang D, Kang R, Berghe TV, Vandenabeele P, Kroemer G. The molecular machinery of regulated cell death. *Cell Res* (2019) 29(5):347–64. doi: 10.1038/s41422-019-0164-5

46. Shao W, Yang Z, Fu Y, Zheng L, Liu F, Chai L, et al. The pyroptosis-related signature predicts prognosis and indicates immune microenvironment infiltration in gastric cancer. *Front Cell Dev Biol* (2021) 9:676485. doi: 10.3389/fcell.2021.676485

47. Fu XW, Song CQ. Identification and validation of pyroptosis-related gene signature to predict prognosis and reveal immune infiltration in hepatocellular carcinoma. *Front Cell Dev Biol* (2021) 9:748039. doi: 10.3389/fcell.2021.748039

48. Zheng S, Xie X, Guo X, Wu Y, Chen G, Chen X, et al. Identification of a pyroptosis-related gene signature for predicting overall survival and response to immunotherapy in hepatocellular carcinoma. *Front Genet* (2021) 12:789296. doi: 10.3389/fgene.2021.789296

49. Zhang Q, Tan Y, Zhang J, Shi Y, Qi J, Zou D, et al. Pyroptosis-related signature predicts prognosis and immunotherapy efficacy in muscle-invasive bladder cancer. *Front Immunol* (2022) 13:782982. doi: 10.3389/fimmu.2022.782982

50. Collins JF, Klevay LM. Copper. *Adv Nutr* (2011) 2(6):520–2. doi: 10.3945/an.111.001222

51. Michalczyk K, Cymbaluk-Płoska A. The role of zinc and copper in gynecological malignancies. *Nutrients* (2020) 12(12). doi: 10.3390/nu12123732

52. Stepien M, Jenab M, Freisling H, Becker NP, Czuban M, Tjønneland A, et al. Pre-diagnostic copper and zinc biomarkers and colorectal cancer risk in the European prospective investigation into cancer and nutrition cohort. *Carcinogenesis* (2017) 38(7):699–707. doi: 10.1093/carcin/bgx051

53. Xu R, Zhang K, Liang J, Gao F, Li J, Guan F. Hyaluronic Acid/Polyethyleneimine nanoparticles loaded with copper ion and disulfiram for esophageal cancer. *Carbohydr Polym* (2021) 261:117846. doi: 10.1016/j.carbpol.2021.117846

54. Chu M, An X, Zhang D, Li Q, Dai X, Yu H, et al. Combination of the 6-thioguanine and Disulfiram/Cu synergistically inhibits proliferation of triple-negative breast cancer cells by enhancing DNA damage and disrupting DNA damage checkpoint. *Biochim Biophys Acta Mol Cell Res* (2022) 1869(2):119169. doi: 10.1016/j.bbamcr.2021.119169

55. Hu Y, Qian Y, Wei J, Jin T, Kong X, Cao H, et al. The Disulfiram/Copper complex induces autophagic cell death in colorectal cancer by targeting Ulk1. *Front Pharmacol* (2021) 12:752825. doi: 10.3389/fphar.2021.752825

56. Huang X, Hou Y, Weng X, Pang W, Hou L, Liang Y, et al. Diethyldithiocarbamate-copper complex (Cuet) inhibits colorectal cancer progression *Via* mir-16-5p and 15b-5p/Aldh1a3/Pkm2 axis-mediated aerobic glycolysis pathway. *Oncogenesis* (2021) 10(1):4. doi: 10.1038/s41389-020-00295-7

57. Jiapaer Z, Zhang L, Ma W, Liu H, Li C, Huang W, et al. Disulfiram-loaded hollow copper sulfide nanoparticles show anti-tumor effects in preclinical models of colorectal cancer. *Biochem Biophys Res Commun* (2022) 635:291–8. doi: 10.1016/j.bbrc.2022.10.027

58. Baldari S, Di Rocco G, Heffern MC, Su TA, Chang CJ, Toietta G. Effects of copper chelation on Braf(V600e) positive colon carcinoma cells. *Cancers (Basel)* (2019) 11(5). doi: 10.3390/cancers11050659

59. Fatfat M, Merhi RA, Rahal O, Stoyanovsky DA, Zaki A, Haidar H, et al. Copper chelation selectively kills colon cancer cells through redox cycling and generation of reactive oxygen species. *BMC Cancer* (2014) 14:527. doi: 10.1186/1471-2407-14-527

60. Cui H, Zhang AJ, McKeage MJ, Nott LM, Geraghty D, Guven N, et al. Copper transporter 1 in human colorectal cancer cell lines: effects of endogenous and modified expression on oxaliplatin cytotoxicity. *J Inorg Biochem* (2017) 177:249–58. doi: 10.1016/j.jinorgbio.2017.04.022

61. Harmse L, Gangat N, Martins-Furness C, Dam J, de Koning CB. Copper-Imidazo[1,2-a]Pyridines induce intrinsic apoptosis and modulate the expression of mutated P53, haem-Oxygenase-1 and apoptotic inhibitory proteins in ht-29 colorectal cancer cells. *Apoptosis* (2019) 24(7-8):623–43. doi: 10.1007/s10495-019-01547-7

62. Ruiz MC, Perelmulter K, Levín P, Romo AIB, Lemus L, Fogolín MB, et al. Antiproliferative activity of two copper (Ii) complexes on colorectal cancer cell models: impact on ros production, apoptosis induction and nf-κb inhibition. *Eur J Pharm Sci* (2022) 169:106092. doi: 10.1016/j.ejps.2021.106092

63. Ali A, Mishra S, Kamaal S, Alarifi A, Afzal M, Saha KD, et al. Evaluation of catacholase mimicking activity and apoptosis in human colorectal carcinoma cell line by activating mitochondrial pathway of Copper(Ii) complex coupled with 2-(Quinolin-8-Yloxy)(Methyl)Benzonitrile and 8-hydroxyquinoline. *Bioorg Chem* (2021) 106:104479. doi: 10.1016/j.bioorg.2020.104479

64. Ghasemi P, Shafiee G, Ziamajidi N, Abbasalipourkabir R. Copper nanoparticles induce apoptosis and oxidative stress in Sw480 human colon cancer cell line. *Biol Trace Elem Res* (2022). doi: 10.1007/s12011-022-03458-2

65. Liu Z, Xiong L, Ouyang G, Ma L, Sahi S, Wang K, et al. Investigation of copper cysteamine nanoparticles as a new type of radiosensitiers for colorectal carcinoma treatment. *Sci Rep* (2017) 7(1):9290. doi: 10.1038/s41598-017-09375-y

66. Chang M, Hou Z, Jin D, Zhou J, Wang M, Wang M, et al. Colorectal tumor microenvironment-activated bio-decomposable and metabolizable Cu(2) O@Caco(3) nanocomposites for synergistic oncotherapy. *Adv Mater* (2020) 32(43):e2004647. doi: 10.1002/adma.202004647

67. Cheng Y, Bo H, Qin R, Chen F, Xue F, An L, et al. Hyaluronic acid-coated Bi:Cu(2)O: an H(2)S-responsive agent for colon cancer with targeted delivery and enhanced photothermal performance. *J Nanobiotechnol* (2022) 20(1):346. doi: 10.1186/s12951-022-01555-x

68. Tomczak K, Czerwińska P, Wiznerowicz M. The cancer genome atlas (Tcga): an immeasurable source of knowledge. *Contemp Oncol* (2015) 19(1a):A68–77. doi: 10.5114/wo.2014.47136

69. Barrett T, Troup DB, Wilhite SE, Ledoux P, Evangelista C, Kim IF, et al. Ncbi geo: archive for functional genomics data sets–10 years on. *Nucleic Acids Res* (2011) 39:D1005–10. doi: 10.1093/nar/gkq1184

70. Du Y, Lin Y, Wang B, Li Y, Xu D, Gan L, et al. Cuproptosis patterns and tumor immune infiltration characterization in colorectal cancer. *Front Genet* (2022) 13:976007. doi: 10.3389/fgene.2022.976007

71. Zhu Z, Zhao Q, Song W, Weng J, Li S, Guo T, et al. A novel cuproptosis-related molecular pattern and its tumor microenvironment characterization in colorectal cancer. *Front Immunol* (2022) 13:940774. doi: 10.3389/fimmu.2022.940774

72. Wu W, Dong J, Lv Y, Chang D. Cuproptosis-related genes in the prognosis of colorectal cancer and their correlation with the tumor microenvironment. *Front Genet* (2022) 13:984158. doi: 10.3389/fgene.2022.984158

73. Huang H, Long Z, Xie Y, Qin P, Kuang L, Li X, et al. Molecular subtypes based on cuproptosis-related genes and tumor microenvironment infiltration characterization in colorectal cancer. *J Oncol* (2022) 2022:5034092. doi: 10.1155/2022/5034092

74. Huang Y, Yin D, Wu L. Identification of cuproptosis-related subtypes and development of a prognostic signature in colorectal cancer. *Sci Rep* (2022) 12(1):17348. doi: 10.1038/s41598-022-22300-2

75. Hou D, Tan JN, Zhou SN, Yang X, Zhang ZH, Zhong GY, et al. A novel prognostic signature based on cuproptosis-related lncrna mining in colorectal cancer. *Front Genet* (2022) 13:969845. doi: 10.3389/fgene.2022.969845

76. Dekker E, Tanis PJ, Vleugels JLA, Kasi PM, Wallace MB. Colorectal cancer. *Lancet* (2019) 394(10207):1467–80. doi: 10.1016/s0140-6736(19)32319-0

77. Luo B, Lin J, Ni A, Cai W, Yu X, Wang M. A novel defined cuproptosis-related gene signature for predicting the prognosis of colon adenocarcinoma. *Front Oncol* (2022) 12:927028. doi: 10.3389/fonc.2022.927028

78. Xu C, Liu Y, Zhang Y, Gao L. The role of a cuproptosis-related prognostic signature in colon cancer tumor microenvironment and immune responses. *Front Genet* (2022) 13:928105. doi: 10.3389/fgene.2022.928105

79. Yang G, Wang H, Sun B. Construction of Cuproptosis–Associated prognostic signature in colon adenocarcinoma based on bioinformatics and Rt–Qpcr analysis. *Oncol Lett* (2023) 25(3):91. doi: 10.3892/ol.2023.13677

80. Zhong L, Zhu J, Shu Q, Xu G, He C, Fang L. A prognostic cuproptosis-related lncrna signature for colon adenocarcinoma. *J Oncol* (2023) 2023:5925935. doi: 10.1155/2023/5925935

frontiers | Frontiers in Oncology

TYPE Original Research
PUBLISHED 13 June 2023
DOI 10.3389/fonc.2023.1083956

OPEN ACCESS

EDITED BY
Chun Xu,
The University of Queensland, Australia

REVIEWED BY
Eleonora Lai,
University of Cagliari, Italy
Samantha Sharma,
Indiana University Bloomington,
United States

*CORRESPONDENCE
Xiangyu Kong
xiangyukong185@hotmail.com
Yiqi Du
duyiqi@hotmail.com
Feng Liu
drliuffeng@hotmail.com

†These authors have contributed equally to this work and share first authorship

RECEIVED 04 November 2022
ACCEPTED 21 April 2023
PUBLISHED 13 June 2023

CITATION
Li L, Sun F, Kong F, Feng Y, Song Y, Du Y, Liu F and Kong X (2023) Characterization of a cuproptosis-related signature to evaluate immune features and predict prognosis in colorectal cancer.
Front. Oncol. 13:1083956.
doi: 10.3389/fonc.2023.1083956

Characterization of a cuproptosis-related signature to evaluate immune features and predict prognosis in colorectal cancer

Lei Li[1,2†], Fengyuan Sun[3†], Fanyang Kong[3†], Yongpu Feng[3†], Yingxiao Song[3†], Yiqi Du[3*], Feng Liu[1*] and Xiangyu Kong[3,4*]

[1]Digestive Endoscopy Center, Shanghai Tenth People's Hospital, Shanghai, China, [2]Department of Gastroenterology, Shanghai Tenth People's Hospital, Tongji University School of Medicine, Shanghai, China, [3]Department of Gastroenterology, Changhai Hospital, Naval Medical University, Shanghai, China, [4]Clinical Research Unit, Changhai Hospital, Naval Medical University, Shanghai, China

Purpose: Cuproptosis is a newly discovered type of cell death. Little is known about the roles that cuproptosis related genes (CRGs) play in colorectal cancer (CRC). The aim of this study is to evaluate the prognostic value of CRGs and their relationship with tumor immune microenvironment.

Methods: TCGA-COAD dataset was used as the training cohort. Pearson correlation was employed to identify CRGs and paired tumor-normal samples were used to identify those CRGs with differential expression pattern. A risk score signature was constructed using LASSO regression and multivariate Cox stepwise regression methods. Two GEO datasets were used as validation cohorts for confirming predictive power and clinical significance of this model. Expression patterns of seven CRGs were evaluated in COAD tissues. *In vitro* experiments were conducted to validate the expression of the CRGs during cuproptosis.

Results: A total of 771 differentially expressed CRGs were identified in the training cohort. A predictive model termed riskScore was constructed consisting of 7 CRGs and two clinical parameters (age and stage). Survival analysis suggested that patients with higher riskScore showed shorter OS than those with lower ($P<0.0001$). ROC analysis revealed that AUC values of cases in the training cohort for 1-, 2-, and 3-year survival were 0.82, 0.80, 0.86 respectively, indicating its good predictive efficacy. Correlations with clinical features showed that higher riskScore was significantly associated with advanced TNM stages, which were further confirmed in two validation cohorts. Single sample gene set enrichment analysis (ssGSEA) showed that high-risk group presented with an immune-cold phenotype. Consistently, ESTIMATE algorithm analysis showed lower immune scores in riskScore-high group. Expressions of key molecules in riskScore model are strongly associated with TME infiltrating cells and immune checkpoint molecules. Patients with a lower riskScore exhibited a higher complete remission rate in CRCs. Finally, seven CRGs involved in riskScore were significantly altered between cancerous and paracancerous normal tissues.

Elesclomol, a potent copper ionophore, significantly altered expressions of seven CRGs in CRCs, indicating their relationship with cuproptosis.

Conclusions: The cuproptosis-related gene signature could serve as a potential prognostic predictor for colorectal cancer patients and may offer novel insights into clinical cancer therapeutics.

KEYWORDS

cuproptosis, prognosis, immune infiltration, elesclomol, colorectal cancer

Introduction

Colorectal cancer (CRC) is the third most common cancer and the second leading cause of cancer-related deaths worldwide, with more than 1.85 million cases and 850,000 deaths annually occurred (1). Among people diagnosed with CRC, 20% have metastatic CRC, and 40% patients with localized disease will have a relapsing metastasis after curative surgical resection. The 5-year survival rate for those diagnosed with metastatic CRC is less than 20% (1, 2). To improve the prognosis of patients with CRC, there is an urgent need to develop more efficient prognostic models and targeted therapy against CRC.

Regulated cell death (RCD) is generally regulated by signaling molecules and has unique biochemical, morphological, and immunological characteristics (3). Different forms of RCD, including apoptosis, necroptosis, autophagy, ferroptosis, pyroptosis, alkaliptosis, and etc., have been identified to be involved in diverse pathological processes, including tumorigenesis (4). Certain RCD forms are regarded as targets of almost all treatment strategies. Resistance to these RCDs are common causes for failure of cancer treatment. Different forms of RCDs can be alternative therapeutics to each other to conquer treatment resistance (5). Therefore, finding new forms of RCD will bring novel therapeutics for refractory cancer cases.

Copper is an essential cofactor for all organisms, and yet it becomes toxic if concentrations exceed a threshold maintained by evolutionally conserved mechanisms (6). Accumulating evidence suggests that organic chelators of copper, e.g., elesclomol, can induce cellular copper overload and restrain malignant behaviors across various cancer types, including CRC (7). However, detained mechanisms underlying copper-related anticancer effects remain poorly understood. Different publications raised contradictory opinions, including either induction of ferroptosis (7), autophagy (8), apoptosis (9), or inhibition of the aerobic glycolysis pathway (10). Recently, Tsvetkov et al. established that copper induced death, namely cuproptosis, was a totally distinct RCD form from previous identified ones, e.g., apoptosis, ferroptosis, and necroptosis. They also showed that cuproptosis occurs by means of direct binding of copper to lipoylated components of the tricarboxylic acid cycle. Ten pivotal genes were identified involved in cuproptosis through whole-genome CRISPR-Cas9 selection screen, including seven genes (FDX1, LIAS, LIPT1, DLD, DLAT, PDHA1 and PDHB) conferred resistance to cuproptosis, while three genes (MTF1, GLS and CDKN2A) sensitized the cells to cuproptosis. Mounting evidence showed that those cuproptosis associated molecules, including noncoding genes, exhibited strong association with prognosis and immune infiltration levels.

In current study, we defined a list of cuproptosis associated genes (CRGs) as candidate molecules, and further developed a predictive model through LASSO regression and multivariate Cox stepwise regression in TCGA dataset. We further evaluated its associations with a list of clinical parameters, e.g., TNM stages, overall survival, treatment response, immune infiltration levels, and etc., to test its predictive efficacy and relationship with immune microenvironment features. An overview of the research design was presented in Figure 1.

Material and methods

Data collection and preprocessing

Gene expression data and clinical feature of colon cancer samples were collected from publicly available datasets of the NCBI GEO database and TCGA. A total of three colon cancer expression profile cohorts were included in our study, including GSE17536, GSE39582 and TCGA-COAD cohorts. We downloaded the normalized matrix files of each GEO cohort for further analyses (https://www.ncbi.nlm.nih.gov/geo/). For RNA sequencing data from TCGA, we downloaded the read counts of gene expression from the Xena Genomic Data Commons (http://xena.ucsc.edu/), including 471 tumor and 41 normal samples. Study participants with incomplete clinical information were excluded for further survival analysis.

Identification of differentially expressed genes

Differential expression analysis was carried out using R package DESeq2 (11) on the 41 paired samples. Genes that showed significantly differential expression ($P<0.05$ and $|\log_2$ fold-change$| > 1$) between

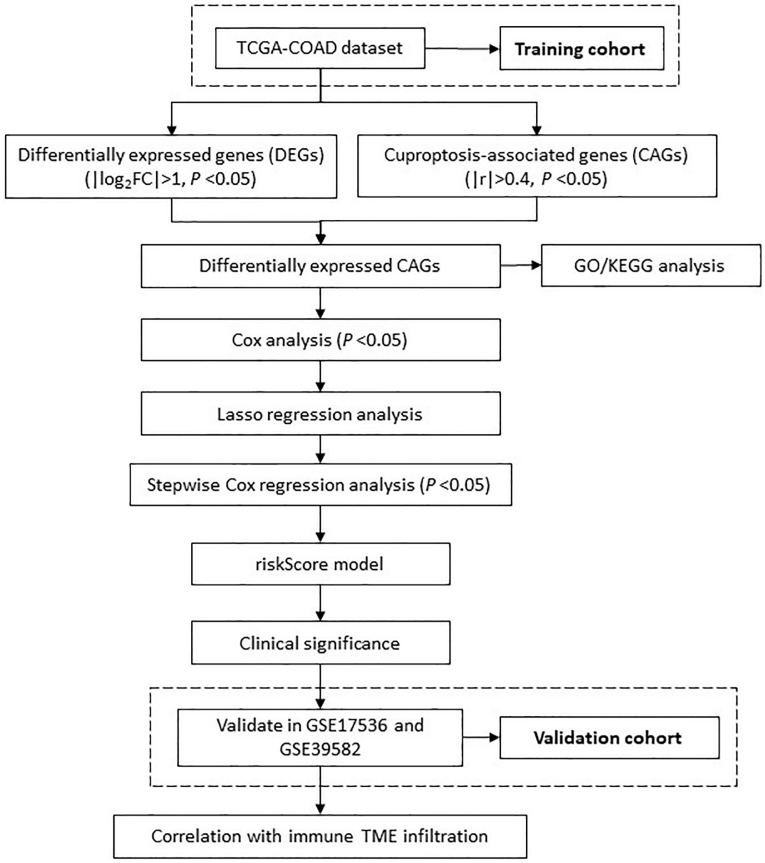

FIGURE 1
The flowchart shows the overall analytical process of this study.

paired tumor and normal samples were selected for downstream analysis.

Identification of cuproptosis-related genes

We then assessed the correlation of DEGs with 10 key cuproptosis regulators (CDKN2A, DLAT, DLD, FDX1, GLS, LIAS, LIPT1, MTF1, PDHA1 and PDHB) by Pearson's correlation analysis. In order to identify cuproptosis-related genes, absolute Pearson's correlation coefficients higher than 0.4 and *P* values less than 0.05 were required.

Functional annotation and gene set enrichment analysis

To explore potential biological processes related to the obtained cuproptosis-related DEGs, we performed gene ontology (GO) and KEGG enrichment analysis using the ClusterProfiler R package (12). The GO enrichment analysis was conducted based on three aspects including biological process (BP), molecular functions (MF) and cellular components (CC). We also identified the activated or inactivated biological pathways among patients with low- and high-riskScore by running the gene set enrichment analysis (GSEA) of the adjusted expression data for all transcripts. The used gene sets were downloaded from MSigDB database, and the "c5.go.bp.v7.5 .1.symbols" gene sets were used to quantify the activity of biological pathways, which was represented by the enrichment score.

Survival analysis

Survival analysis was performed using univariate and multivariate Cox regression hazard analysis and survival curves derived from Kaplan–Meier survival analysis by using the packages survival and survminer. The receiver operating characteristic curve (ROC) were performed with the timeROC packages.

CRG-related risk signature construction and validation

TCGA-COAD dataset was set as the training cohort to screen for those survival-related genes in COAD. Univariate Cox regression analysis was performed to screen out OS-related DEGs. LASSO regression analysis was further applied to refine DEGs, and multivariate Cox regression hazard analysis (backward stepwise) was eventually used to establish a predictive model, performance of which was ultimately validated in two independent GEO datasets.

Risk score was computed with the following equation:

$$riskScore = \sum_{i=1}^{n}(Coef_i \times x_i)$$

Establishment and validation of a nomogram scoring system

We later created a hybrid nomogram using the regplot R package that incorporates the mRNA signature and clinicopathological features of COAD patients to predict their OS (1-, 3-, and 5-year). For determining the predictive power of a nomogram, calibration curves and consistency indices (C-index) were used.

Evaluation of intratumoral immune cell infiltration

ssGSEA was used to quantify the abundance of each TME cell infiltration based on the gene sets obtained from the study of Charoentong (13). To control the bias resulted by the tumor purity, we adjusted the enrichment scores of each TME cell subtype by calculating the tumor purity using ESTIMATE algorithm. The adjusted enrichment scores calculated by ssGSEA analyses were used to represent the abundance of each TME infiltration cell.

Mutation analysis

Somatic mutation data of COAD from whole exome/genome sequencing (WXS/WGS) were downloaded from the GDC TCGA-COAD project on the UCSC Xena server. Oncoplot was drawn according to the descending order of mutations using the R package " maftools" (14).

Cell culture

HCT116 and SW480 were cultured in Dulbecco's modified Eagle medium which was supplemented with 100 U*mL-1 penicillin and streptomycin as well as 10% fetal bovine serum in a humidified atmosphere of 5% CO_2 at 37°C.

Reagents and drug treatment *in vitro*

Elesclomol was purchased from Master of Bioactive Molecules (MCE). When cells were adherent and had morphologically spread, Colon cancer cell lines (HCT116 and SW480) were treated with 2μM copper chloride and/or 40nM elesclomol for 24 hours, respectively. Cells were harvested after treatment and RNA was collected *via* the following extraction method.

RNA extraction and quantitative real-time polymerase chain reaction

Total cellular RNA was extracted using a total RNA extraction kit (220010, Shanghai Feijie) according to standard protocol. The RNA was used to synthesize complementary DNA (cDNA) with a cDNA Synthesis SuperMix (RR036A, TaKaRa). The cDNA was used as a template and the seven cuproptosis related genes (GRGs) expression was quantified with the Roche LightCycler 480 using TB Green Premix Ex Taq II (RR820A, TaKaRa). GAPDH was used as an endogenous control. Primers were synthesized by Sangon Biotech (Sangon, Shanghai). The primer sequences are shown in Table 1.

Statistical analyses

The data were analyzed with R software version 4.2.0. For comparisons, data conforming to normal and nonnormal distributions were assessed using the unpaired/paired Student's t-test and the Wilcoxon test, respectively. The difference significance test for three or more groups was performed using One-way ANOVA and Kruskal-Wallis tests. All statistical P value were two-side, with $P< 0.05$ as statistically significance.

Results

Identification of CRGs in TCGA-COAD cohort

As the sample size of normal cases is relatively small (41 out of 512 cases), we employed paired tumor vs. normal samples to improve detection rate for differentially expressed genes (DEGs). Principal component analysis (PCA) of the full transcriptomes identified differential grouping between two cohorts (Figure 2A). Differential expression analysis identified 4319 significantly upregulated and 4398 significantly downregulated transcripts in CRC tissues compared with paired normal tissues (Figures 2B, C) at

10.3389/fonc.2023.1083956

TABLE 1 PCR primer sequences of target genes.

Primer	Sequence (5' to 3')
DPP7-F	GGACCACTTCAACTTCGAGC
DPP7-R	GCCCTCGTTCCCAGTGTAG
GPRASP1-F	AGGAGGAGACCAATATGGGGT
GPRASP1-R	GGACCTAGACATGGTATTAGCCT
UNC5C-F	TGGGACTGGGATACTTGCTG
UNC5C-R	ACAGTACAGGTTCACAGGCTTAT
CDR2L-F	TGGGCTGACGGAGACCATT
CDR2L-R	TGTAGGCGGAAAGCATCCTTG
RAB3B-F	CCGCTATGCTGATGACACGTT
RAB3B-R	ACGGTAGACTGTCTTCACCTTG
PCDH9-F	CTGCTCTGATTGCCTGTTTAAGG
PCDH9-R	ACCAGTCTGTAGACAAGGCTG
SLC18A2-F	CGGAAGCTCATCCTGTTCATC
SLC18A2-R	CCTGGCCGTCTGGATTTCTG
GAPDH-F	GGAGCGAGATCCCTCCAAAAT
GAPDH-R	GGCTGTTGTCATACTTCTCATGG

a $P<0.05$ and a |log2 fold-change| >1. Of note, seven out of ten pivotal CRGs, which were identified in *Science* article (6), showed significantly altered expression patterns, with CDKN2A exhibited higher and DLAT, DLD, FDX1, LIAS, MTF1, PDHB exhibited lower expression in tumor tissues (Supplementary Figure 1A, $P<0.05$). Correlations across these seven molecules in CRCs were shown in Figure 2D. Survival analysis showed that five out of seven molecules were significantly associated with overall survival ($P<0.05$, Supplementary Figure 1B).

As the concept of Cuproptosis has just recently been proposed (6) and no database are available to download the full picture of CRGs, here we used coexpression strategy (15) to define mRNAs with 7 reported CRGs absolute coefficients values >0.4 and P values<0.05 as the standard of CRGs. A total of 7946 genes were identified CRGs. Further Venn diagram showed 771 overlapping genes in DEGs and CRGs (Figure 3A), which we select as candidates for constructing a prognosis predictive signature. Functional annotations of GO enrichment indicated these genes were significantly associated with TME immune related biological processes such as B cell receptor signaling pathway, humoral immune response, production of molecular mediator of immune response, positive regulation of B cell activation, leukocyte migration, suggesting these CRGs could be significantly correlated with TME immune cell infiltration (Figures 3B-D). Consistently,

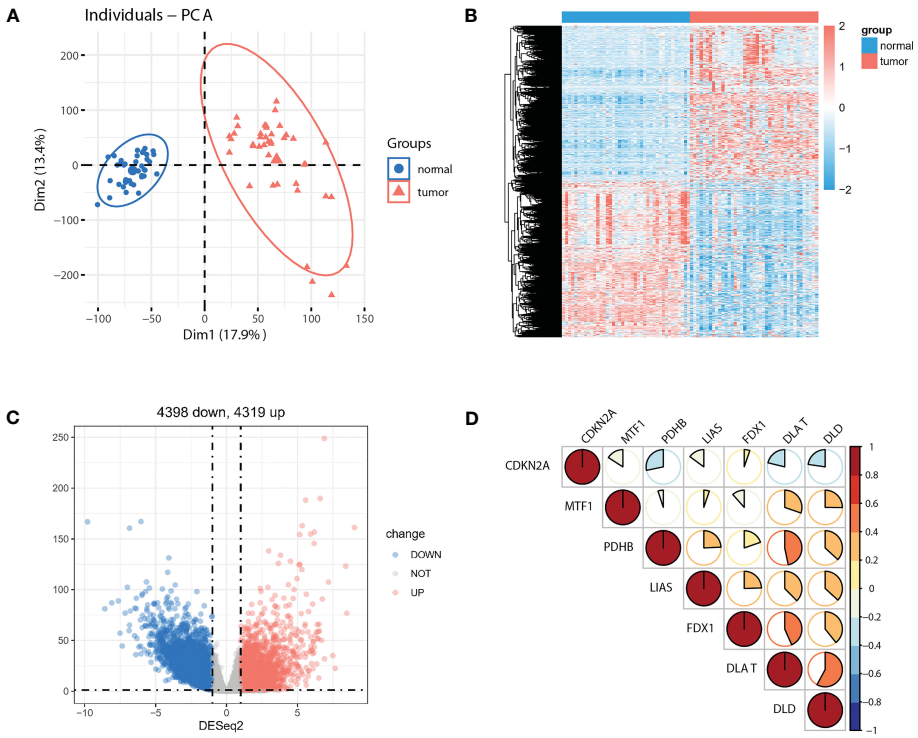

FIGURE 2
Identification of DEGs between paired normal and tumor cases in TCGA-COAD cohort. **(A)** PCA of the global transcriptome in tumor (red) and paired normal (blue) cases. A heatmap **(B)** and volcano plot **(C)** of significantly ($P<0.05$) upregulated (log2 fold-change >1, red) and downregulated (log2 fold-change<–1, blue) genes in tumor vs. normal cases. **(D)** Seven out of ten reported CRGs were differentially expressed between tumor and paired normal cases ($P<0.05$).

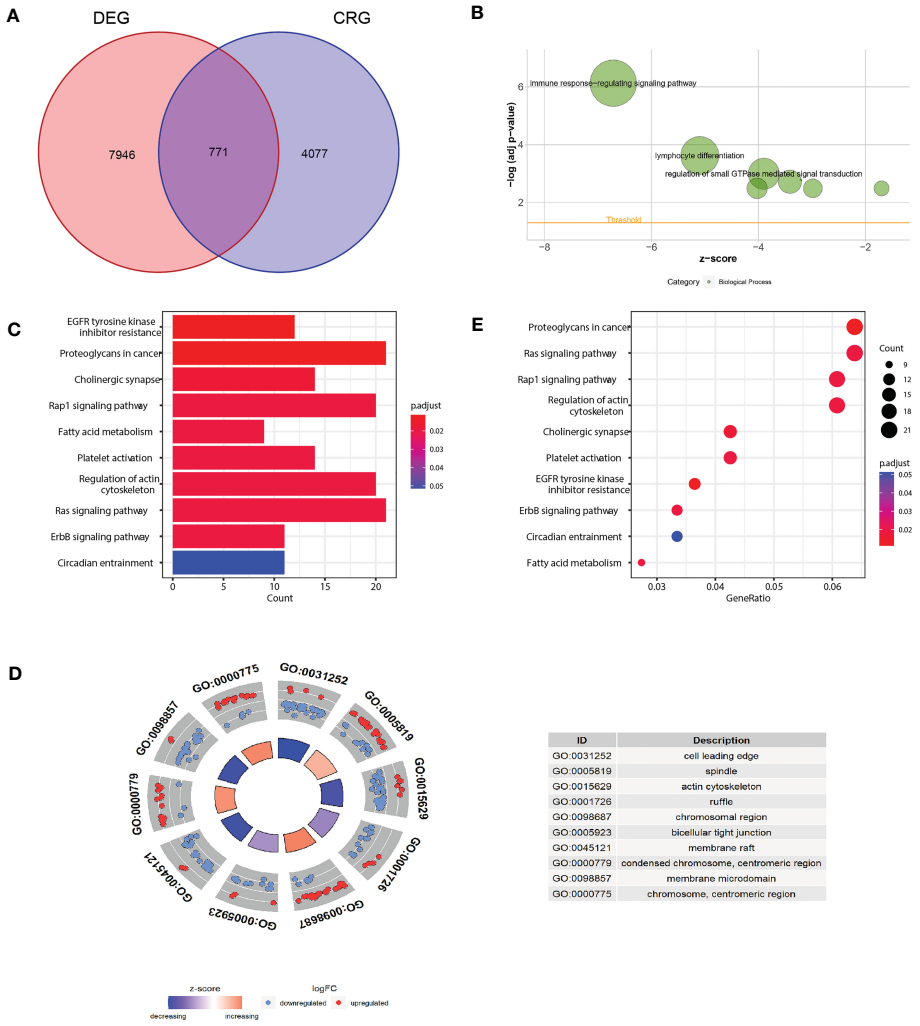

ID	Description
GO:0031252	cell leading edge
GO:0005819	spindle
GO:0015629	actin cytoskeleton
GO:0001726	ruffle
GO:0098687	chromosomal region
GO:0005923	bicellular tight junction
GO:0045121	membrane raft
GO:0000779	condensed chromosome, centromeric region
GO:0098857	membrane microdomain
GO:0000775	chromosome, centromeric region

FIGURE 3
Functional annotation of differentially expressed CRGs. **(A)** Venn diagram analysis demonstrated genes appeared both in DEGs and CRGs. **(B-D)** Gene Ontology functional enrichment analyses for differentially expressed genes. **(B)** Biological processes enrichment. **(C)** Cellular component enrichment. **(D)** Molecular function enrichment. **(E)** KEGG pathway enrichment analyses for differentially expressed CRGs. All enriched pathways were significant. The color depth represented enriched adjusted *P* value.

KEGG pathway analysis also demonstrated that these genes were correlated with immune related signaling pathways (Figure 3E).

Establishment of risk model for prognosis prediction based on CRGs

Considering the markedly differential expression patterns of these CRGs, we set TCGA-COAD dataset as the training cohort to screen for those survival-related genes (n = 44, $P<0.05$ both in log-rank test and in univariate Cox regression analysis). We used LASSO Cox regression to distinguish those most informative prognostic mRNA biomarkers for prognosis. Regression coefficients of the 44 DEGs were evaluated (Figure 4A; Supplementary Table 1). It was finally verified through cross-validation that 20 (Supplementary Table 1) DEGs could achieve a better effect in the model (Figure 4B). Eventually, multivariate Cox stepwise regression method was used to establish several multivariate regression models. A risk model consisting of 7 DEGs (DPP7, GPRASP1, UNC5C, CDR2L, RAB3B, PCDH9, SLC18A2), as well as two clinical parameters (age and stage), was at last identified (Figure 4C). DPP7, CDR2L exhibited higher and UNC5C, RAB3B, SLC18A2, GPRASP1, PCDH9 exhibited lower expression in tumor tissues (Supplementary Figure 2A, $P<0.05$). Survival analysis showed that UNC5C, RAB3B, SLC18A2 were low-risk genes, while DPP7, GPRASP1, CDR2L, PCDH9, were high-risk genes ($P<0.05$, Supplementary Figure 2B). The correlation analysis was performed to investigate the similarities among seven key molecules, and the results are visually displayed in Figure 4D.

Somatic mutation profiles of 7 key genes for 406 CRC patients were retrieved from the TCGA dataset. The waterfall plot was used to present the mutation data for each gene in every sample

10.3389/fonc.2023.1083956

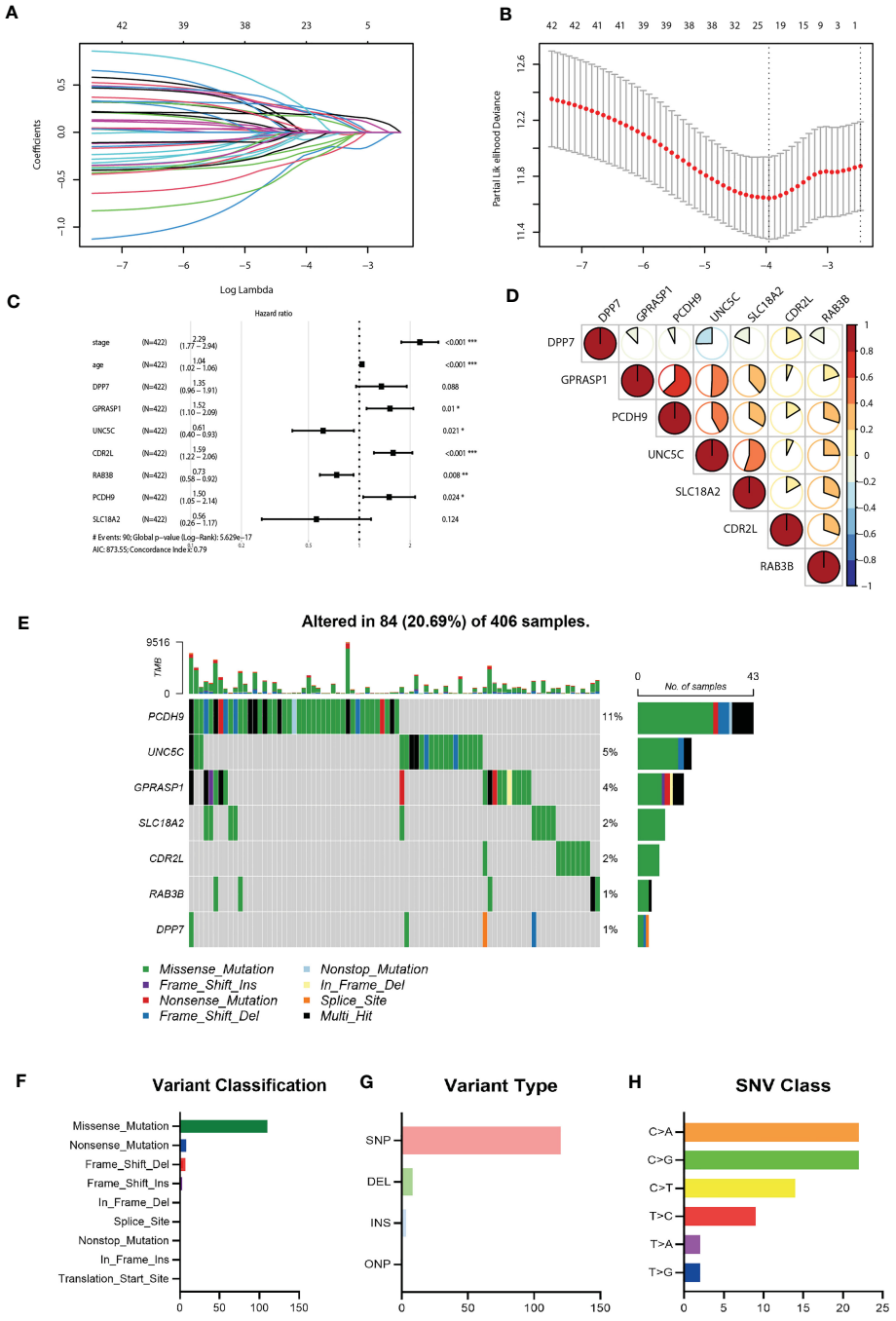

FIGURE 4
Construction of the riskScore signature and mutation analysis of seven riskScore-associated molecules. **(A)** Least absolute shrinkage and selection operator (LASSO) coefficient profiles of the 45 key molecules. **(B)** Tuning parameter selection by tenfold cross-validation in the LASSO model. The partial likelihood deviance was plotted against log(Lambda/λ), and λ was the tuning parameter. The partial likelihood deviance values were shown and error bars represented s.e. The dotted vertical lines showing the optimal values through minimum criteria and 1 -s.e. criteria. **(C)** Multivariate Cox regression analysis of seven CRGs and two clinical parameters **(D)** Correlation between seven riskScore-associated molecules. Blue, negative correlation; Red, positive correlation. **(E)** The mutation landscape of key molecules in 406 samples of TCGA-COAD cohort. **(F-H)** the CNV and mutation frequency and classification of seven prognosis-related CRGs in Colorectal cancer. *P<0.05, **P<0.01, ***P<0.001.

(Figure 4E), Further, mutations were grouped based on various categories. In the grouping, missense mutation was the most common (Figure 4F), while single nucleotide polymorphisms (SNP) is more common than other kinds of mutations (Figure 4G). Regarding single nucleotide variants, C>A and C>G are two most common kinds (Figure 4H).

Evaluation of the predictive efficacy of the riskScore for prognosis in TCGA-COAD

We further evaluated the predictive efficacy of riskScore for prognosis. Based on the model, cases in the training cohort were scored and divided into high- and low- risk group with the median

riskScore as the cutoff. Survival analysis showed that cases with higher riskScore had a significant shorter OS compared with those with lower riskScore ($P< 0.0001$) (Figure 5A). ROC analysis revealed that AUC values of cases in the training cohort for 1-, 2-, and 3-year survival were 0.82, 0.80, 0.86 respectively, indicating good predictive efficacy of this model (Figure 5B). As the values of riskScore increased, mortality of those cases correspondingly increased (Figure 5C). Hierarchical clustering showed distinct expression patterns of seven key molecules between two groups (Figure 5C). Furthermore, levels of riskScore progressively increased with TNM stages of cases in the training cohort, which further consolidate its strong association with malignant phenotype (Figure 6A; Supplementary Figure 3A).

Gene set enrichment analysis (GSEA) reveals two immune related pathways, including humoral immune response and B cell receptor signaling pathway, were significantly attenuated, indicating that TME immune cells may be involved in high malignant phenotype of the high-risk cases (Figure 5D). To develop a clinically related quantitative method for predicting probability of patient mortality, we established the nomogram integrating all

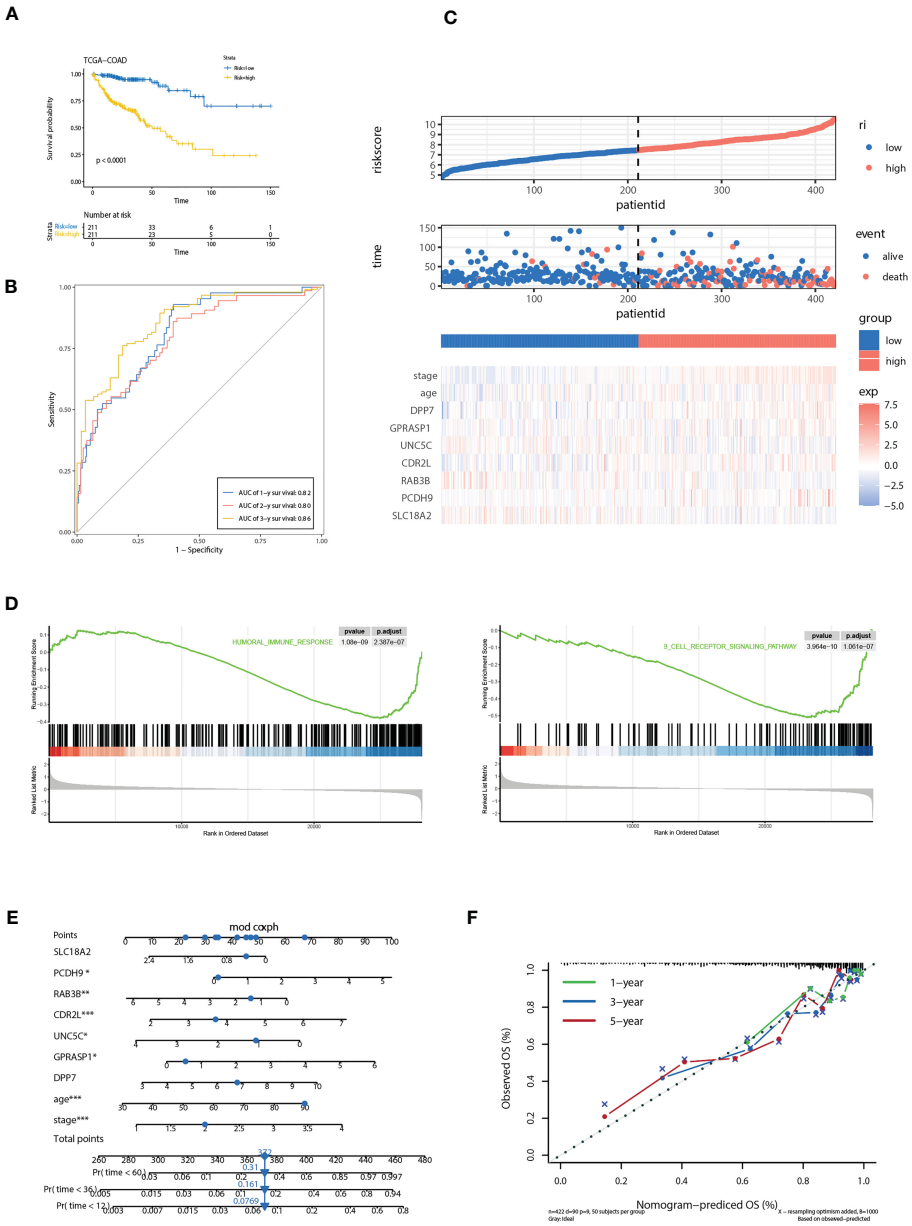

FIGURE 5
Correlation of the riskScore with clinicopathological features. **(A)** Kaplan-Meier plot of the riskScore signature in the TCGA cohort (log-rank test). **(B)** ROC curves for one-year, three-year and five-year overall survival prediction of the riskScore signature in the TCGA cohort. **(C)** Distribution of riskScore, survival status and the expression of prognostic CRGs. **(D)** Gene set enrichment analysis (GSEA) reveals two significantly activated signaling pathways including angiogenesis pathway and epithelial to mesenchymal transition pathway. **(E)** The nomogram to predict the probability of patient mortality using seven key molecules, age, and stage. **(F)** The calibration plot of nomograms between predicted and observed 1-year, 2-year, and 3-year outcomes. The 45-degree line represented the ideal prediction. *P<0.05, **P<0.01, ***P<0.001.

10.3389/fonc.2023.1083956

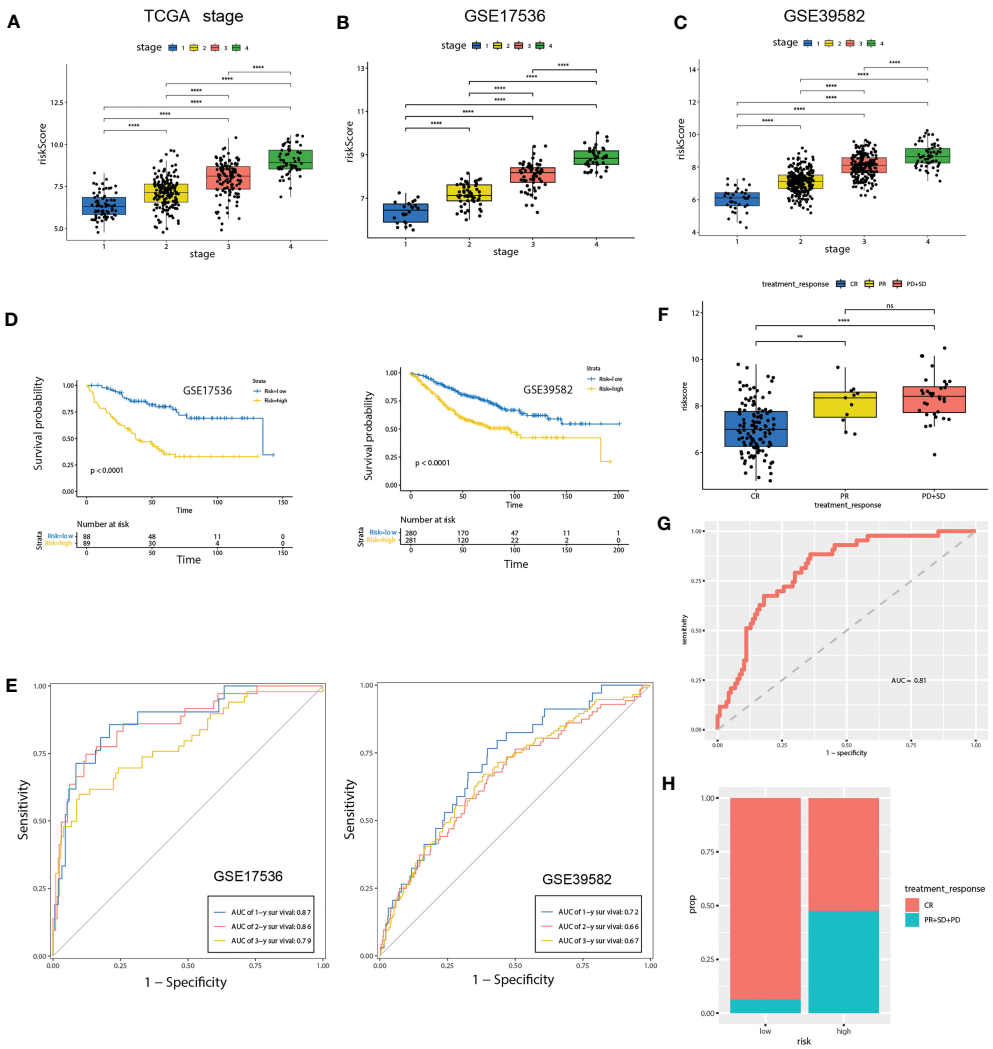

FIGURE 6
Validation of the prognostic prediction value of the riskScore in TCGA-COAD cohort, GSE17536 and GSE39582 dataset. **(A-C)** Differential levels of the riskScore between various TNM stages in TCGA-COAD cohort **(A)**, GSE17536 **(B)**and GSE39582 dataset **(C)**. **(D)** Kaplan-Meier plot of the riskScore signature in the GSE17536 and GSE39582 datasets (log-rank test). **(E)** ROC curves for one-year, three-year and five-year overall survival prediction of the riskScore signature in the GSE17536 and GSE 39582 datasets. **(F)** Differential levels of the riskScore between various treatment response in TCGA-COAD cohort. **(G)** ROC curves of the riskScore signature for complete remission prediction in the TCGA cohort. **(H)** The proportion of patients with response to chemical therapy in high or low riskScore groups. ns, not significant; **P<0.01, ****P<0.0001.

factors involved in the riskScore model (Figure 5E). The calibration plots demonstrated that the derived nomogram performed well compared to the ideal model (Figure 5F).

Validation of the riskScore in two independent GEO datasets

To further confirm the prognosis predictive efficacy of the riskScore signature, we used GSE17536 and GSE39582 datasets as validation cohorts (n=177 and 561, respectively). Among different stages of COAD, cases with advanced TNM stages exhibited higher riskScore than in early TNM stages (Figures 6B, C). Higher riskScore was associated with advanced stages of T, N, M, stages in GSE39582 dataset, which is consistent with results in training cohort (Supplementary Figure 3B). Survival analysis showed OS of the high-risk group was significantly shorter than that of low-risk group (both $P< 0.001$) (Figure 6D). ROC analysis revealed that AUC value of the cases in the validation cohort for 1-, 2-, and 3-year survival were 0.87, 0.86, 0.79 for GSE17536, and 0.72, 0.66, 0.67 for GSE39582, respectively, indicating good predictive efficacy of the model (Figure 6E). We further evaluated association of riskScore with treatment response. Patients with complete remission (CR) exhibited a lower riskScore (Figure 6F). ROC analysis revealed that AUC value reached 0.81, indicating this model has excellent discriminant ability for CR (Figure 6G). CR rate was significantly enhanced in patients with low risk than those with high risk (93.75% vs 52.5%, Figure 6H).

Evaluation of TME immune infiltration and checkpoints between the high- and low-risk groups

The diverse range of immune responses are largely attributed to the differential composition of immune cell population. It is uncertain whether those key molecules and riskScore signature are associated with TME immune infiltration, which may account for their association with prognosis. In this study, ssGSEA was used to determine the immune heterogeneity between riskScore-high group and -low group. We generated a heatmap to visualize the relative abundance of 28 infiltrating immune cells in each group. Of note, samples with low riskScore present with a high degree of immune cell infiltration, suggesting that they adopt an immune-hot phenotype, whereas those samples with high riskScore did the opposite (Figure 7A). We further evaluated proportion of immunoreactive and immunosuppressive cells in each of these populations. Consistent with the immune-hot phenotype of riskScore-low samples, the infiltrating cells were largely associated with immune activation (e.g., activated B cell, activated CD4 T cell, activated CD8 T cell, activated dendritic cell, etc.) (Figure 7B). An analysis based on the Tumor Immune Estimation Resource (TIMER; cistrome.shinyapps.io/timer) (16) further confirmed the relationship between seven key CRGs and the abundance of six immune cells (B cells, CD8+ T cells, CD4+ T cells, macrophages, neutrophils and dendritic cells) (Supplementary Figure 4). ESTIMATE algorithm analysis showed that immune scores, but not stromal scores, were significantly lower in riskScore-high group than in -low group (Figure 7C). We further used pearson correlation analysis to correlate key molecules with TME infiltrating cells, and multiple strong correlations were identified among them (Figure 7D). We also found that patients with lower riskScore is associated with elevated expression of PD-L1, CTLA4 and PD-L2, which is consistent with their immune-hot phenotype and suggested their potential vulnerability to Immune checkpoint inhibitors (ICI) treatments (Figure 7E). Expressions of seven key molecules were significantly correlated with immune checkpoint molecules (Figure 7F), of these, PD-1 and PD-L2 were consistently associated with seven key molecules. Correlations between SLC18A2 and PD-L2, PCDH9 and PD-L2, SLC18A2 and CTLA4 were particularly significant (Figures 7G-I).

Validation of expression patterns of seven CRGs included in the riskScore

We further evaluated the expressions of the seven cuproptosis-related genes involved in our riskScore signature. Ten paired cancer and paracancerous normal colon tissues were retrieved from COAD patients in our hospital. Consistent with results obtained from the TCGA-COAD cohort (Supplementary Figure 1A), six CRGs, including DPP7, GPRASP1, UNC5C, RAB3B, PCDH9, SLC18A2, were significantly downregulated, whereas CDR2L was upregulated in cancer tissues in comparison with paracancerous normal tissues (Figure 8). These results indicated that seven CRGs involved in our newly developed riskScore signature, may have regulatory effects in colon carcinogenesis, and may be explored as therapeutic targets against COAD.

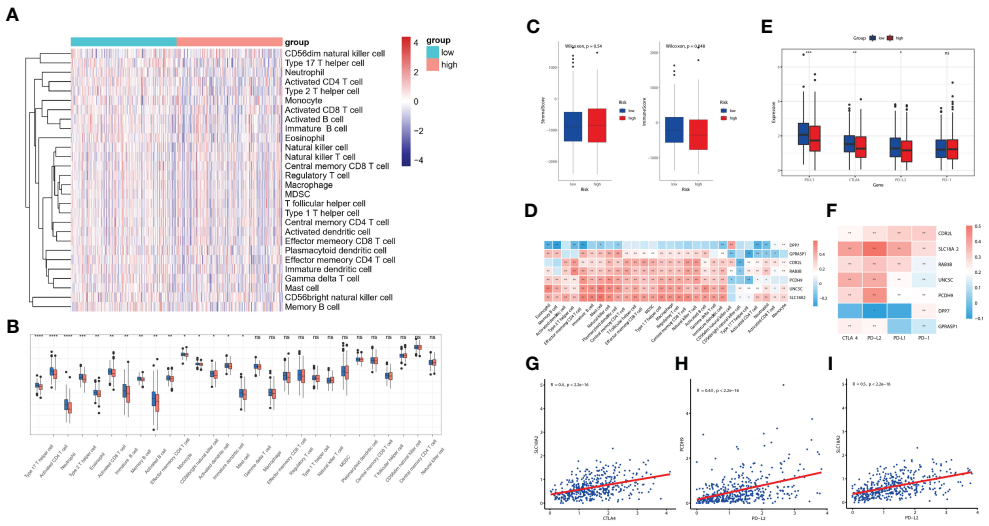

FIGURE 7
Evaluation of TME immune infiltration and checkpoints between the high- and low-risk groups. **(A)** Heatmap visualization of the relative abundance of 28 infiltrating immune cell types in the TCGA database data. Each small grid represents each immune cell, and the shade of color represents the infiltration level of this immune cell. The larger infiltration level is, the darker color will be (red is upregulated, and blue is downregulated). **(B)** Differences in 28 TME infiltration cells between high- and low-risk tissues (*P< 0.05; **P< 0.01; ***P< 0.001; **** P< 0.0001) **(C)** The difference of overall immune and stromal activity between high- and low-risk tissues using ESTIMATE algorithm. **(D)** The different expression levels of immune checkpoint molecules between high- and low-risk tissues **(E)** The correlation between each key molecule and each TME infiltration cell type. Red, positive; Blue, negative. **(F)** The correlation between the seven key molecules and immune checkpoint molecules. Red, positive; Blue, negative. **(G-I)** The correlations between SLC18A2 and CTLA4 **(G)**, PCDH9 and PD-L2 **(H)**, SLC18A2 and PD-L2 expression levels **(I)**. ns, not significant.

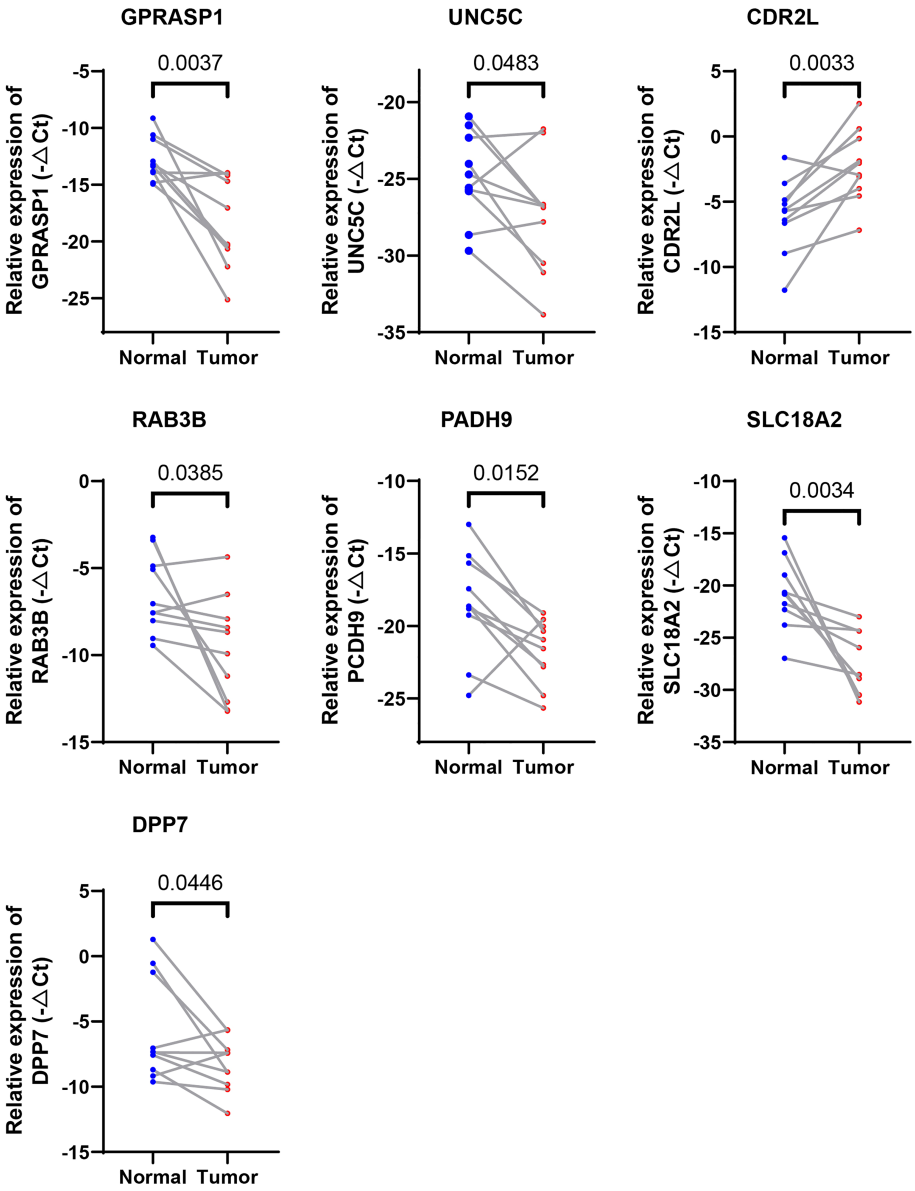

FIGURE 8
Validation of the expression levels of the seven cuproptosis-related genes in human tissues. Expression analysis of DPP7, GPRASP1, UNC5C, RAB3B, PCDH9, SLC18A2 and CDR2L were quantitated using qPCR in 10 pairs of cancer and paracancerous normal colon tissues.

The seven CRGs involved in riskScore are regulated by copper

We next examined whether expressions of these 7 CRGs are altered in the setting of cuproptosis. Elesclomol is a copper ionophore that could shuttle copper into CRC cells and induce its overload, thus cuproptosis. We treated HCT116 and SW480 with copper chloride (2μM) in combination with different concentrations of elesclomol (10μM and 40μM) for 24 hours. RT-PCR analysis showed that expressions of all 7 CRGs were significantly altered (Figure 9). These results showed that these CRGs may be involved in the process of cuproptosis in COAD.

Discussion

Cuproptosis is a newly discovered cell death form with emerging potential as a silver bullet in treatment against cancer. As apoptosis is the most common mechanism that mediates resistance to chemotherapy, identification of new cell death types, e.g., cuproptosis, will shed light on alternative treatment strategies for conquering drug resistance in refractory cancer cases.

Copper is an indispensable mineral nutrient for all organisms, homeostasis of which play critical roles in different physiological and pathological processes. Though previous publications established that copper overload was detrimental to cancer cells, a

10.3389/fonc.2023.1083956

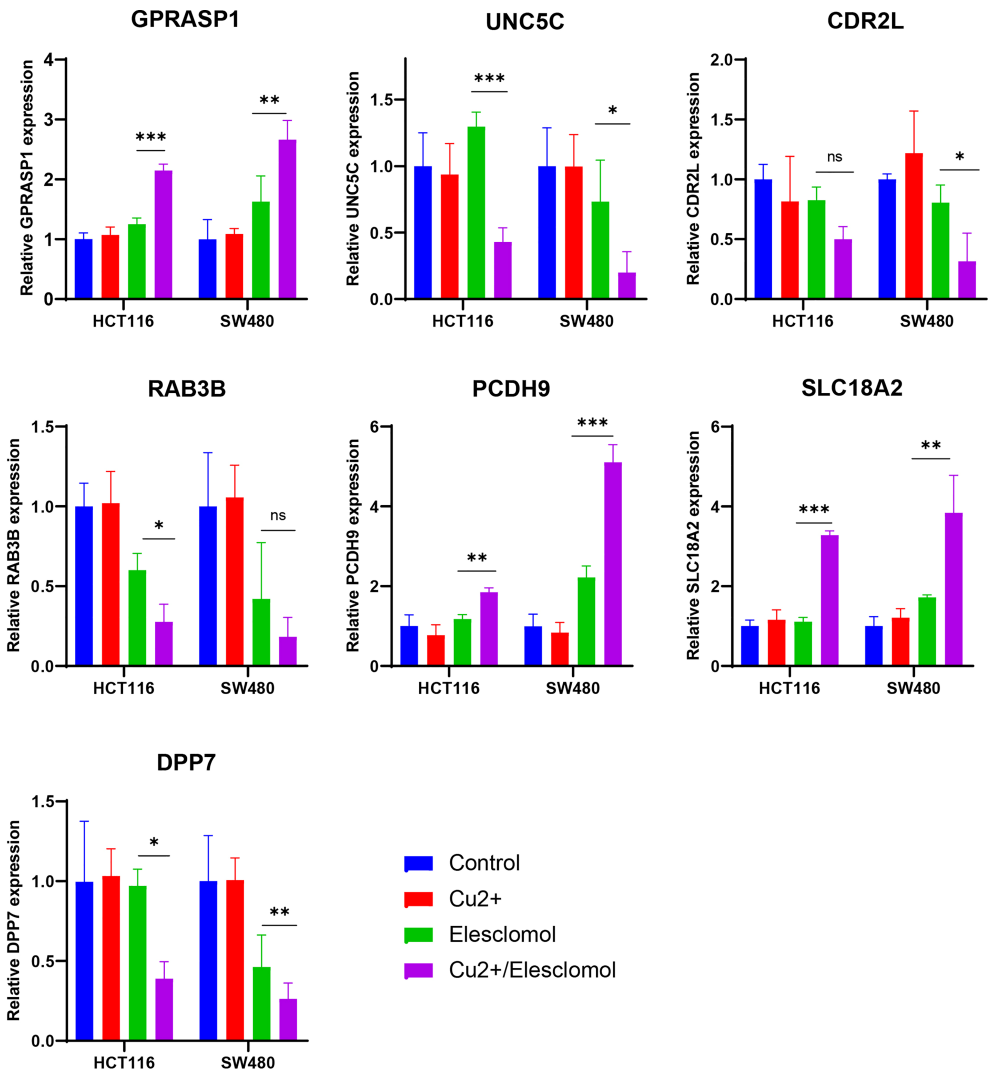

FIGURE 9
Regulation of cuproptosis on seven CRGs involved in riskScore. qPCR showed CRGs expression in HCT116 and SW480 cells treated with indicated drugs for 24 h (n=3). Drugs included $CuCl_2$ (2mM), elesclomol (40 nM) alone or in combination. *P<0.05, **P<0.01, ***P<0.001. ns, not significant.

clear picture of the mechanisms underlying copper-induced toxicity has not yet emerged. Take CRC as an example, though numerous studies validated the anti-tumor effects of copper, distinct but contradictory death forms were suggested for underlying mechanisms, including ferroptosis (7, 17), autophagy (8), paraptosis (18), and etc. Recently, Tsvetkov et al. established a new death form named Cuproptosis, in which excess intracellular copper directly binds to lipoylated components of the tricarboxylic acid (TCA) Cycle. Ten genes, including FDX1, LIAS, LIPT1, DLD, DLAT, PDHA1, PDHB, MTF1, GLS and CDKN2A, were identified playing pivotal roles in cuproptosis.

A growing number of studies showed that prognostic models constructed based on RCD associated genes, including both coding and non-coding genes, may contribute greatly to the evaluation of patient prognosis, molecular characteristics and treatment modalities, and could be further translated into clinical applications (15, 19). Correspondingly, various prognostic models based on cuproptosis-regulated genes have recently been constructed in diverse tumors, including soft tissue sarcoma (20), melanoma (21), clear cell renal cell carcinoma (22), liver cancer (23), and so on. However, no research regarding the role that cuproptosis played in CRC has been reported. As studies regarding the field of cuproptosis are still in its infancy, those molecules constitute the complicated network are severely understudied. Our study first systematically investigates CRGs by calculating a coexpression correlation matrix in CRC, and established a riskScore model consisting of seven key CRGs and two clinical parameters (stage and age). Survival analysis suggested that patients with higher riskScore showed longer OS than those with lower riskScore. ROC analysis revealed that AUC values of cases in the training cohort for 1-, 2-, and 3-year survival were 0.82, 0.80, 0.86 respectively, indicating the good predictive efficacy of this model. Correlations with clinical features showed that higher riskScore was significantly associated with advanced stages of T, N, M, and TNM stages. Consistent results were further validated in two independent

GEO datasets. Regarding associations with treatment response, CR rate was significantly enhanced in patients with low risk than those with high risk. Through integrating those factors involved in riskScore, we established a quantitative nomogram, which improved the performance and facilitated clinical use of the riskScore.

Numerous studies revealed the essential roles of RCDs in innate immunity and antitumor effects (15, 19); however, few studies reported the potential role of CRGs in immunotherapy, with none regarding CRC. Several lines of evidence support the potential involvement of our riskScore model in CRC TME immunity. First, cases in the TCGA cohort were scored and divided into high- and low- risk group with the median riskScore as the cutoff, and Gene set enrichment analysis (ssGSEA) showed that high-risk group presents with an immune-cold phenotype. Second, Gene set enrichment analysis (GSEA) reveals that certain immune-related pathways were significantly associated with riskScore levels. Third, ESTIMATE algorithm analysis showed that immune scores varied widely in different riskScore groups. Therefore, we quantified the proportions of tumor infiltrating immune cells in the low- and high-risk groups to evaluate their associations. Emerging evidence supported the potential role of B cells in cancer immune response (24, 25). In soft-tissue sarcomas, B cell infiltration was an independent and the strongest prognostic factor for good prognosis and correlated with improved response to PD-1 blockade (26). Consistently, favorable prognosis was also identified in CRC patients with enhanced tumor-infiltrating B cells (27), which is the case in metastatic CRC, that increased B cells infiltration was associated with lower risk of recurrence and improved survival (28). These data established B cells as a novel target for immunotherapy and could be a strong weapon against cancer. In our study, patients with lower riskScore, showed higher infiltration of B cells, suggesting that they play an anti-tumor role in CRC development. Cytotoxic T cells which corresponds to our finding of more activated CD8+ T cells in patients with lower riskScore compared with those in the high-risk group. ICIs based immunotherapy has provided a new direction for tumor treatment in various cancer types (29, 30), including CRC (31). In the present study, higher levels of ICIs, including PDL1, CTLA4, and PDL2, were observed in patients with lower riskScore group, indicating their potential good response to immune checkpoint blockade.

Recently, several papers have been published on the use of a model based on cuproptosis-associated genes for predicting prognosis (32–35). However, these papers suffer from several limitations, including a small number of genes in their signature, relatively low prognostic power, and illogical combination with other cell death types like ferroptosis. Additionally, no experiments on colorectal cancer cells have been conducted regarding CRGs. Our work is unique in that we evaluate the association between our predictive score and treatment response. Our results show excellent discriminant ability for complete remission, providing valuable information to clinicians for therapeutic selection.

There are several strengths in our study. First, our study is the first to systematically investigate CRGs by calculating a coexpression correlation matrix in CRC. A riskScore model was constructed with good predictive efficacy for survival and TME immune infiltration. Second, clinical significance of our model was validated in two independent GEO datasets, indicating stability and universality of our model. Third, we established a nomogram involving all factors of this model, which further improved clinical applicability of the riskScore. Last but not least, we examined expressions of these CRGs and validated that their levels were significantly altered in cancer tissues in comparison with paracancerous normal tissues. *In vitro* studies also showed that these CRGs may be altered in the setting of copper overload. All these findings expand our knowledge regarding the potential roles of seven key CRGs in the process of cuproptosis. Certainly, there are some limitations of current study. All analysis were conducted based on data extracted from retrospective public databases with possible selection bias, large-scale prospective studies are needed to confirm our results.

In conclusion, this study is the first that constructed a riskScore based on CRGs that exhibited good predictive performance for OS in CRC. Future studies are warranted to dissect the underlying mechanisms by which these CRGs get involved in the process of cuproptosis and explore their potential roles as therapeutic targets against CRC. We hope that this riskScore can be validated and used in future clinic to guide therapeutics selection.

Data availability statement

The datasets presented in this study can be found in online repositories. The names of the repository/repositories and accession number(s) can be found in the article/Supplementary Material.

Ethics statement

The studies involving human participants were reviewed and approved by Shanghai Changhai Hospital Ethics Committee. The patients/participants provided their written informed consent to participate in this study.

Author contributions

This research was conducted in collaboration with all authors. LL, FS and FK performed the data curation and analysis. YS and YF analyzed and interpreted the results. YD and FL drafted the manuscript. XK finally reviewed the manuscript. All authors contributed to the article and approved the submitted version.

Funding

This work is supported in part by National Key R&D Program of China No. 2019YFC1315900 and 2019YFC1315802; grant 81872043 and 82172572 (LL) from the National Natural Science Foundation of China; grant 82072760 and 81772640 (XYK) from the National Natural Science Foundation of China.

Acknowledgments

We thank Shanghai Zhi Bei Biotechnology Co., Ltd. for bioinformatics analysis and data processing. We also thank Dr. Jianming Zeng (University of Macau), and all the members of his bioinformatics team, biotrainee, for generously sharing their experience and codes.

Conflict of interest

The authors declare that the research was conducted in the absence of any commercial or financial relationships that could be construed as a potential conflict of interest.

Publisher's note

All claims expressed in this article are solely those of the authors and do not necessarily represent those of their affiliated organizations, or those of the publisher, the editors and the reviewers. Any product that may be evaluated in this article, or claim that may be made by its manufacturer, is not guaranteed or endorsed by the publisher.

Supplementary material

The Supplementary Material for this article can be found online at: https://www.frontiersin.org/articles/10.3389/fonc.2023.1083956/full#supplementary-material

SUPPLEMENTARY FIGURE 1
The expression level and survival of 7 pivotal CRGs. **(A)** Seven out of ten reported CRGs were differentially expressed between tumor and paired normal cases ($P<0.05$). **(B)** Kaplan-Meier plot of seven genes in TCGA-COAD (log-rank test).

SUPPLEMENTARY FIGURE 2
The expression level and survival of seven prognosis-related CRGs. **(A)** Seven prognosis-related CRGs were differentially expressed between tumor and paired normal cases ($P<0.05$). **(B)** Kaplan-Meier plot of seven prognosis-related CRGs in TCGA-COAD (log-rank test).

SUPPLEMENTARY FIGURE 3
The relationship between the riskScore and TNM stage. **(A)** Differential levels of the riskScore between various T, N, M stage in TCGA-COAD cohort. **(B)** Differential levels of the riskScore between various T, N, M stage in GSE39582 dataset.

SUPPLEMENTARY FIGURE 4
(A-G) Correlation between each key molecule expression and immune infiltration in TCGA-COAD in the TIMER database.

References

1. Siegel RL, Miller KD, Goding Sauer A, Fedewa SA, Butterly LF, Anderson JC, et al. Colorectal cancer statistics, 2020. *CA Cancer J Clin* (2020) 70(3):145–64. doi: 10.3322/caac.21601

2. Biller LH, Schrag D. Diagnosis and treatment of metastatic colorectal cancer: a review. *JAMA* (2021) 325(7):669–85. doi: 10.1001/jama.2021.0106

3. Del Re DP, Amgalan D, Linkermann A, Liu Q, Kitsis RN. Fundamental mechanisms of regulated cell death and implications for heart disease. *Physiol Rev* (2019) 99(4):1765–817. doi: 10.1152/physrev.00022.2018

4. Tang D, Kang R, Berghe TV, Vandenabeele P, Kroemer G. The molecular machinery of regulated cell death. *Cell Res* (2019) 29(5):347–64. doi: 10.1038/s41422-019-0164-5

5. Gong Y, Fan Z, Luo G, Yang C, Huang Q, Fan K, et al. The role of necroptosis in cancer biology and therapy. *Mol Cancer* (2019) 18(1):100. doi: 10.1186/s12943-019-1029-8

6. Tsvetkov P, Coy S, Petrova B, Dreishpoon M, Verma A, Abdusamad M, et al. Copper induces cell death by targeting lipoylated TCA cycle proteins. *Science* (2022) 375(6586):1254–61. doi: 10.1126/science.abf0529

7. Gao W, Huang Z, Duan J, Nice EC, Lin J, Huang C. Elesclomol induces copper-dependent ferroptosis in colorectal cancer cells *via* degradation of ATP7A. *Mol Oncol* (2021) 15(12):3527–44. doi: 10.1002/1878-0261.13079

8. Hu Y, Qian Y, Wei J, Jin T, Kong X, Cao H, et al. The Disulfiram/Copper complex induces autophagic cell death in colorectal cancer by targeting ULK1. *Front Pharmacol* (2021) 12:752825. doi: 10.3389/fphar.2021.752825

9. Harmse L, Gangat N, Martins-Furness C, Dam J, de Koning CB. Copper-imidazo [1,2-a]pyridines induce intrinsic apoptosis and modulate the expression of mutated p53, haem-oxygenase-1 and apoptotic inhibitory proteins in HT-29 colorectal cancer cells. *Apoptosis* (2019) 24(7-8):623–43. doi: 10.1007/s10495-019-01547-7

10. Huang X, Hou Y, Weng X, Pang W, Hou L, Liang Y, et al. Diethyldithiocarbamate-copper complex (CuET) inhibits colorectal cancer progression *via* miR-16-5p and 15b-5p/ALDH1A3/PKM2 axis-mediated aerobic glycolysis pathway. *Oncogenesis* (2021) 10(1):4. doi: 10.1038/s41389-020-00295-7

11. Love MI, Huber W, Anders S. Moderated estimation of fold change and dispersion for RNA-seq data with DESeq2. *Genome Biol* (2014) 15(12):550. doi: 10.1186/s13059-014-0550-8

12. Yu G, Wang LG, Han Y, He QY. clusterProfiler: an r package for comparing biological themes among gene clusters. *OMICS* (2012) 16(5):284–7. doi: 10.1089/omi.2011.0118

13. Charoentong P, Finotello F, Angelova M, Mayer C, Efremova M, Rieder D, et al. Pan-cancer immunogenomic analyses reveal genotype-immunophenotype relationships and predictors of response to checkpoint blockade. *Cell Rep* (2017) 18(1):248–62. doi: 10.1016/j.celrep.2016.12.019

14. Mayakonda A, Lin DC, Assenov Y, Plass C, Koeffler HP. Maftools: efficient and comprehensive analysis of somatic variants in cancer. *Genome Res* (2018) 28(11):1747–56. doi: 10.1101/gr.239244.118

15. Tang R, Wu Z, Rong Z, Xu J, Wang W, Zhang B, et al. Ferroptosis-related lncRNA pairs to predict the clinical outcome and molecular characteristics of pancreatic ductal adenocarcinoma. *Brief Bioinform* (2022) 23(1). doi: 10.1093/bib/bbab388

16. Li T, Fan J, Wang B, Traugh N, Chen Q, Liu JS, et al. TIMER: a web server for comprehensive analysis of tumor-infiltrating immune cells. *Cancer Res* (2017) 77(21):e108–e10. doi: 10.1158/0008-5472.CAN-17-0307

17. You SY, Rui W, Chen ST, Chen HC, Liu XW, Huang J, et al. Process of immunogenic cell death caused by disulfiram as the anti-colorectal cancer candidate. *Biochem Biophys Res Commun* (2019) 513(4):891–7. doi: 10.1016/j.bbrc.2019.03.192

18. Gandin V, Pellei M, Tisato F, Porchia M, Santini C, Marzano C. A novel copper complex induces paraptosis in colon cancer cells *via* the activation of ER stress signalling. *J Cell Mol Med* (2012) 16(1):142–51. doi: 10.1111/j.1582-4934.2011.01292.x

19. Song W, Ren J, Xiang R, Kong C, Fu T. Identification of pyroptosis-related subtypes, the development of a prognosis model, and characterization of tumor microenvironment infiltration in colorectal cancer. *Oncoimmunology* (2021) 10(1):1987636. doi: 10.1080/2162402X.2021.1987636

20. Han J, Hu Y, Liu S, Jiang J, Wang H. A newly established cuproptosis-associated long non-coding RNA signature for predicting prognosis and indicating immune microenvironment features in soft tissue sarcoma. *J Oncol* (2022) 2022:8489387. doi: 10.1155/2022/8489387

21. Lv H, Liu X, Zeng X, Liu Y, Zhang C, Zhang Q, et al. Comprehensive analysis of cuproptosis-related genes in immune infiltration and prognosis in melanoma. *Front Pharmacol* (2022) 13:930041. doi: 10.3389/fphar.2022.930041

22. Bian Z, Fan R, Xie L. A novel cuproptosis-related prognostic gene signature and validation of differential expression in clear cell renal cell carcinoma. *Genes* (2022) 13(5):851–66. doi: 10.3390/genes13050851

23. Zhang G, Sun J, Zhang X. A novel cuproptosis-related LncRNA signature to predict prognosis in hepatocellular carcinoma. *Sci Rep* (2022) 12(1):11325. doi: 10.1038/s41598-022-15251-1

24. Cabrita R, Lauss M, Sanna A, Donia M, Skaarup Larsen M, Mitra S, et al. Tertiary lymphoid structures improve immunotherapy and survival in melanoma. *Nature* (2020) 577(7791):561–5. doi: 10.1038/s41586-019-1914-8

25. Helmink BA, Reddy SM, Gao J, Zhang S, Basar R, Thakur R, et al. B cells and tertiary lymphoid structures promote immunotherapy response. *Nature* (2020) 577 (7791):549–55. doi: 10.1038/s41586-019-1922-8

26. Petitprez F, de Reynies A, Keung EZ, Chen TW, Sun CM, Calderaro J, et al. B cells are associated with survival and immunotherapy response in sarcoma. *Nature* (2020) 577(7791):556–60. doi: 10.1038/s41586-019-1906-8

27. Berntsson J, Nodin B, Eberhard J, Micke P, Jirstrom K. Prognostic impact of tumour-infiltrating b cells and plasma cells in colorectal cancer. *Int J Cancer* (2016) 139 (5):1129–39. doi: 10.1002/ijc.30138

28. Meshcheryakova A, Tamandl D, Bajna E, Stift J, Mittlboeck M, Svoboda M, et al. B cells and ectopic follicular structures: novel players in anti-tumor programming with prognostic power for patients with metastatic colorectal cancer. *PloS One* (2014) 9(6): e99008. doi: 10.1371/journal.pone.0099008

29. Yaghoubi N, Soltani A, Ghazvini K, Hassanian SM, Hashemy SI. PD-1/PD-L1 blockade as a novel treatment for colorectal cancer. *BioMed Pharmacother* (2019) 110:312–8. doi: 10.1016/j.biopha.2018.11.105

30. Rotte A. Combination of CTLA-4 and PD-1 blockers for treatment of cancer. *J Exp Clin Cancer Res* (2019) 38(1):255. doi: 10.1186/s13046-019-1259-z

31. Marin-Acevedo JA, Dholaria B, Soyano AE, Knutson KL, Chumsri S, Lou Y. Next generation of immune checkpoint therapy in cancer: new developments and challenges. *J Hematol Oncol* (2018) 11(1):39. doi: 10.1186/s13045-018-0582-8

32. Li Y, Wang RY, Deng YJ, Wu SH, Sun X, Mu H. Molecular characteristics, clinical significance, and cancer immune interactions of cuproptosis and ferroptosis-associated genes in colorectal cancer. *Front Oncol* (2022) 12:975859. doi: 10.3389/fonc.2022.975859

33. Huang Y, Yin D, Wu L. Identification of cuproptosis-related subtypes and development of a prognostic signature in colorectal cancer. *Sci Rep* (2022) 12(1):17348. doi: 10.1038/s41598-022-22300-2

34. Du Y, Lin Y, Wang B, Li Y, Xu D, Gan L, et al. Cuproptosis patterns and tumor immune infiltration characterization in colorectal cancer. *Front Genet* (2022) 13:976007. doi: 10.3389/fgene.2022.976007

35. Wu W, Dong J, Lv Y, Chang D. Cuproptosis-related genes in the prognosis of colorectal cancer and their correlation with the tumor microenvironment. *Front Genet* (2022) 13:984158. doi: 10.3389/fgene.2022.984158

frontiers | Frontiers in Cell and Developmental Biology

TYPE Original Research
PUBLISHED 18 July 2023
DOI 10.3389/fcell.2023.1157841

OPEN ACCESS

EDITED BY
Lin-Lin Bu,
Wuhan University, China

REVIEWED BY
Zhi-Ping Liu,
Shandong University, China
Antonio Giovanni Solimando,
University of Bari Aldo Moro, Italy
Antonella Argentiero,
National Cancer Institute Foundation (IRCCS), Italy

*CORRESPONDENCE
Gang Ren,
rengang@xinhuamed.com.cn
Yufei Wang,
yufei8828@gmail.com
Fang Guo,
guof0818@hku.hk

†These authors have contributed equally to this work

RECEIVED 03 February 2023
ACCEPTED 03 July 2023
PUBLISHED 18 July 2023

CITATION
Shi H, Huang J, Wang X, Li R, Shen Y, Jiang B, Ran J, Cai R, Guo F, Wang Y and Ren G (2023), Development and validation of a copper-related gene prognostic signature in hepatocellular carcinoma.
Front. Cell Dev. Biol. 11:1157841.
doi: 10.3389/fcell.2023.1157841

Development and validation of a copper-related gene prognostic signature in hepatocellular carcinoma

Haoting Shi[1†], Jingxuan Huang[2†], Xue Wang[3†], Runchuan Li[2], Yiqing Shen[4], Bowen Jiang[5], Jinjun Ran[6], Rong Cai[1], Fang Guo[7]*, Yufei Wang[2]* and Gang Ren[8]*

[1]Department of Radiation Therapy, Ruijin Hospital, Shanghai Jiao Tong University School of Medicine, Shanghai, China, [2]Department of Clinical Medicine, Shanghai Jiao Tong University School of Medicine, Shanghai, China, [3]Department of Pathology, Ruijin Hospital, Shanghai Jiao Tong University School of Medicine, Shanghai, China, [4]Department of Computer Science, Johns Hopkins University, Baltimore, MD, United States, [5]College of Biophotonics, South China Normal University, Guangzhou, China, [6]School of Public Health, Shanghai Jiao Tong University School of Medicine, Shanghai, China, [7]School of Public Health, Li Ka Shing Faculty of Medicine, The University of Hong Kong, Hong Kong, Hong Kong SAR, China, [8]Department of Radiology, Xinhua Hospital, Shanghai Jiao Tong University School of Medicine, Shanghai, China

Introduction: Reliable biomarkers are in need to predict the prognosis of hepatocellular carcinoma (HCC). Whilst recent evidence has established the critical role of copper homeostasis in tumor growth and progression, no previous studies have dealt with the copper-related genes (CRGs) signature with prognostic potential in HCC.

Methods: To develop and validate a CRGs prognostic signature for HCC, we retrospectively included 353 and 142 patients as the development and validation cohort, respectively. Copper-related Prognostic Signature (Copper-PSHC) was developed using differentially expressed CRGs with prognostic value. The hazard ratio (HR) and the area under the time-dependent receiver operating characteristic curve (AUC) during 3-year follow-up were utilized to evaluate the performance. Additionally, the Copper-PSHC was combined with age, sex, and cancer stage to construct a Copper-clinical-related Prognostic Signature (Copper-CPSHC), by multivariate Cox regression. We further explored the underlying mechanism of Copper-PSHC by analyzing the somatic mutation, functional enrichment, and tumor microenvironment. Potential drugs for the high-risk group were screened.

Results: The Copper-PSHC was constructed with nine CRGs. Patients in the high-risk group demonstrated a significantly reduced overall survival (OS) (adjusted HR, 2.65 [95% CI, 1.83–3.84] and 3.30, [95% CI, 1.27–8.60] in the development and validation cohort, respectively). The Copper-PSHC achieved a 3-year AUC of 0.74 [95% CI, 0.67–0.82] and 0.71 [95% CI, 0.56–0.86] for OS in the development and validation cohort, respectively. Copper-CPSHC yield a 3-year AUC of 0.73 [95% CI, 0.66–0.80] and 0.72 [95% CI, 0.56–0.87] for OS in the development and validation cohort, respectively. Higher tumor mutation burden, downregulated metabolic processes, hypoxia status and infiltrated stroma cells were found for the high-risk group. Six small molecular drugs were screened for the treatment of the high-risk group.

Conclusion: Copper-PSHC services as a promising tool to identify HCC with poor prognosis and to improve disease outcomes by providing potential clinical decision support in treatment.

KEYWORDS
liver cancer, cuproptosis, hepatocellular carcinoma, copper, gene

Introduction

Liver cancer is the second leading cause of cancer-related death and the seventh most common cancer worldwide (Sung et al., 2021). Hepatocellular carcinoma (HCC) is unequivocally the most dominant type of liver cancer, accounting for 90% of all cases (Llovet et al., 2021). The disease burden of HCC has been rising, with over 1 million new cases per year being estimated during the next decade globally (Llovet et al., 2018). Despite recent advances in the clinical management of HCC including both local and systemic therapies, there remain large and growing unmet medical needs (Villanueva, 2019). Due to occult onset and limited treatment efficacy, HCC is generally subject to poor prognosis (Golabi et al., 2017), with the 5-year survival rate as low as 18% in the United States (Jemal et al., 2017). The conventional clinical decisions for HCC treatment depend substantially on the tumor stage employing the Barcelona Clinic Liver Cancer (BCLC) staging system (EASL Clinical Practice Guidelines, 2018) and Tumor Node Metastasis (TNM) staging system. However, these staging systems, which take primarily tumor size and metastasis into account, have failed to benefit a considerable proportion of patients, owing to their insensitivity to the molecular features in HCC (Yang et al., 2019). Thus, it is crucial to formulate a more precise and Supplementary Model to identify the segments of HCC patients who are at high risk of unfavorable prognosis necessitating additional treatment or targeted therapy (Solimando et al., 2022), so as to improve the survival rate and terminal life quality of patients with better clinical decision making. With the insight into the biology of HCC updated, several biomarkers and gene expression-based signatures have been proposed (Mann et al., 2007; van Malenstein et al., 2011; Wu et al., 2020; Dai et al., 2021); yet, they were rarely incorporated into clinical practice due to less-than-satisfactory performance and insufficient validation (Liu et al., 2019), which warrants a high demand for novel and robust prognostic models.

Elevated levels of copper have been previously observed in the malignant neoplasms of breast, lung, and gastrointestinal tract (Jin et al., 2011; Adeoti et al., 2015; Stepien et al., 2017), indicating an essential role of copper in the genesis of carcinoma. Specifically, increased cellular copper concentrations might contribute to cancer progression by enhancing blood vessel formation which is critical for tumor initiation, growth and metastasis (Blockhuys et al., 2017). With the concept of "Cuproplasia" (i.e., copper-dependent cell growth and proliferation) being proposed, the diverse mechanisms of copper sensing involved in the cancer have been further unveiled (Ishida et al., 2013). Meanwhile, cuproptosis, a newly proposed form of cell death triggered by copper overloads (Tsvetkov et al., 2022), was found to be closely linked to cancer such as clear cell renal cell carcinoma (Bian et al., 2022). Notably, as the central regulatory organ of copper homeostasis, the liver is particularly susceptible to copper-related carcinogenesis (Kim et al., 2008). Patients with Wilson's disease, characterized by a progressively increased copper load in the liver, are more likely to develop liver cancer than the general population (Bandmann et al., 2015). This finding indicates that elevated intracellular copper levels would impair the liver physiological functions and increase the risk of developing HCC (McGlynn et al., 2021). Additionally, serum copper concentrations were demonstrated to be correlated with the BCLC stage (Tamai et al., 2020). The alterations in copper transporter genes, such as *ATP7A*, *ATP7B*, *SLC31A1*, and *SLC31A2*, were also found to be associated with poor prognosis in HCC patients (Davis et al., 2020). Those findings collectively highlight an important role of copper in the HCC, suggesting that copper-related biomarkers might provide valuable information for the treatment and prognosis of HCC.

Copper-related genes (CRGs) which regulate copper metabolisms including copper homeostasis, cuproptosis and copper binding (Ge et al., 2022) serve as a valid channel for us to examine the copper-HCC link. Hence, in this study, we used publicly available gene dataset to develop a prognostic stratification model, Copper-related Prognostic Signature (Copper-PSHC), for HCC patients based on CRGs. We then incorporated Copper-PSHC with clinical factors to establish an integrative prognostic model for pragmatic application. Beyond that, we also explored the potential underlying mechanism of Copper-PSHC.

Materials and method

Study design and patients

To construct a CRG-based prognostic signature (i.e., Copper-PSHC), we retrospectively analyzed the RNA sequencing data from two public HCC cohorts. The overall study design was depicted in Figure 1. HCC patients from The Cancer Genome Atlas (TCGA) liver and intrahepatic carcinoma dataset were utilized as the development cohort (Grossman et al., 2016) and those from Liver Cancer—RIKEN, JP (LIRI-JP) dataset were adopted as an independent validation cohort (The International Cancer Genome Consortium Data Portal, 2019). We excluded patients who had received systemic pharmaceutical therapy or radiotherapy prior to sample collection since such treatment may influence gene expression (Nakamura et al., 2013). Similarly, patients with multiple samples were also excluded to minimize the bias from tumor heterogeneity (Pe'er et al., 2021). Totally, we included 495 patients (351 men [70.9%], 304 aged ≥60 years [86.1%] and 355 at the cancer stage I/II [71.7%]), with 353 in the development cohort and 142 in the independent validation cohort (Supplementary Figure S1). Variables with less than 20% missing observations were imputed using multiple imputations by Chained Equations (White et al., 2011). Characteristics of participants following imputation were displayed in Supplementary Table S1. Details of case identification and imputation can be found in the Supplementary Method S1. The study was exempted from ethical review due to its use of de-identified, publicly available data.

Construction of the Copper-PSHC and Copper-CPSHC

In accordance with the previous literature, ninety-six genes relevant to copper homeostasis, cuproptosis, and copper binding were screened (Supplementary Table S2) to construct the Copper-related Prognostic Signature (Copper-PSHC). First, the

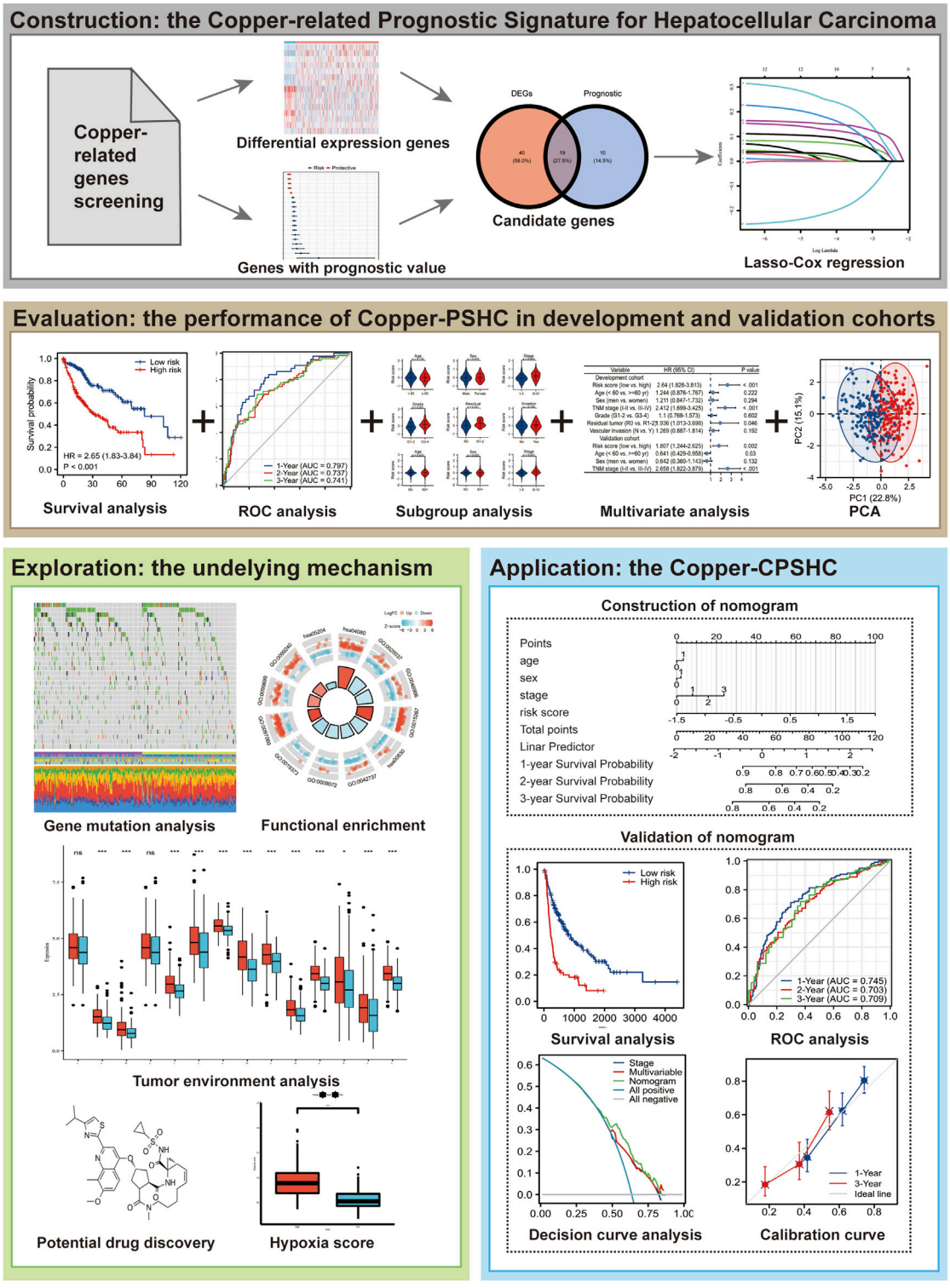

FIGURE 1
Flowchart of this study.

differentially expressed genes (DEGs) between tumor and adjacent non-tumor tissues with a false discovery rate (FDR) < 0.05 were identified in the development cohort. Then, univariable Cox analysis of overall survival (OS) was performed, with $p < 0.05$ chosen as the significance threshold, to determine the DEGs having prognostic value. Those prognostic DEGs measured in both cohorts were included to build the Copper-PSHC. Thereafter, we used the String Interaction Network to demonstrate the association between these genes (Szklarczyk et al., 2021) and estimated the correlation of gene expression. To minimize the risk of overfitting, a

LASSO-Cox regression was applied to select the most contributing prognostic genes and to construct Copper-PSHC (Engebretsen and Bohlin, 2019). To calculate the risk score of each patient in the development and validation cohort, the normalized expression level of each gene and the corresponding regression coefficients generated from the development cohort were used. Then, patients were stratified into low-risk and high-risk groups based on the median risk score determined by the development cohort. Details of gene screening and Copper-PSHC construction can be found in Supplementary Method S2.

We further applied multivariable Cox regression, which integrated age, sex, cancer stage and Copper-PSHC risk score, to construct a composite prognostic model, Copper-CPSHC, in the development cohort. Age, sex, and cancer stage were treated as continuous variables. We also presented a nomogram of Copper-CPSHC to facilitate its use in clinical settings. The optimal cut-off value for classifying the patients into low- or high-risk groups was determined using a time-dependent ROC curve at 3 years of follow-up by Youden index (Fluss et al., 2005) in the development cohort. Details of Copper-CPSHC construction can be found in Supplementary Method S2.

Validation of the Copper-PSHC and Copper-CPSHC

The primary endpoint was overall survival (OS), and the secondary endpoint was disease-free survival (DFS) which was not evaluated in the validation cohort owing to a lack of information on tumor recurrence. Proportional hazard assumption was not violated (Supplementary Table S3). The prognosis value of Copper-PSHC was first assessed as binary variables (high vs. low risk) in both cohorts by the univariable Cox proportional hazard model and represented with the Kaplan-Meier curve. Restricted mean survival time (RMST) was estimated for the high- and low-risk groups to quantify the life expectancy at 3 years of follow-up, while the difference between the two risk groups was determined by their disparity. Stratified analyses by age, sex, cancer stage were conducted for both cohorts, and the hazard ratio (HR) was merged using a fixed model. Then, we combined Copper-PSHC with age, sex and cancer stage in multivariable Cox proportional hazard regression to justify the prognostic value of Copper-PSHC. Adjusted HR (controlling for age, sex and cancer stage) was used to assess the performance of Copper-PSHC as a binary variable. We additionally performed time-dependent ROC analysis for OS and DFS to evaluate the predictive power of the model over time. The performance of Copper-PSHC continuous risk score was assessed by the area under the curve (AUC) of the time-dependent ROC curve at 3 years of follow-up. The concordance index (c-index) was also estimated to quantify the prognostic accuracy of the Copper-PSHC. Details of Copper-PSHC validation can be found in Supplementary Method S3.

Similarly, we performed univariable analysis for Copper-CPSHC using Kaplan-Meier curve and compared the RMSTs of two risk groups. The performance of Copper-CPSHC was also evaluated by HR (in binary scenario) and AUC of time-dependent ROC curve at 3 years of follow-up (in continuous form). The c-index was calculated. Additionally, calibration curves were depicted to characterize the discrimination of Copper-CPSHC. Decision curve analysis (DCA) was applied to measure the net benefits, which was compared with tumor stage and the clinical model. Details of Copper-CPSHC validation can be found in Supplementary Method S3.

Annotation of Copper-PSHC

Somatic mutation analysis

In an attempt to explore the somatic mutations in high- and low-risk groups determined by Copper-PSHC in the development cohort, gene mutation data (available at cBioprotal, in ".maf" format) (Cerami et al., 2012) were analyzed. The 20 most commonly mutated genes were listed for each risk group and measured as frequency. Meanwhile, the total mutation frequency and tumor mutation burden (TMB) were also estimated. The waterfall plots were depicted to manifest the mutation landscape for the high- and low-risk groups by the "maftool" R package (Mayakonda et al., 2018).

Functional enrichment analysis

We performed the functional enrichment analysis in both the development and validation cohorts. Biological function and pathways regarding Copper-PSHC were analyzed based on Gene Ontology (GO) (The Gene Ontology Consortium, 2019) and the Kyoto Encyclopedia of Genes and Genomes (KEGG) database (Kanehisa et al., 2021) using the DEGs between high- and low-risk groups. Further, Gene Set Enrichment Analysis (GSEA) was conducted to determine the upregulated and downregulated cellular pathways in high-risk group compared with low-risk group, with an FDR <0.01 as the screening criteria (Kos et al., 2021). The function enrichment analysis was conducted by the "clusterProfiler" R package (Yu et al., 2012). We also estimated the HCC hypoxia score proposed by Hu et al. (2020) (Supplementary Method S4.1) for two risk groups.

Tumor microenvironment analysis

The correlation between Copper-PSHC and the tumor microenvironment (TME), which is comprised primarily of immune cells and stromal cells, was investigated in both the development and validation cohorts. We first applied ESTIMATE (Yoshihara et al., 2013) algorithm to depict the presence of immune cells, stromal cells, and tumor purity in two risk groups. Then, we adopted CIBERSORT (Newman et al., 2015), ssGESA (Barbie et al., 2009) and xCell (Aran et al., 2017) for the comparison of TME cells infiltration in two groups (Supplementary Method S4.2). Moreover, we also analyzed the expression of multiple cell markers related to immune checkpoint blockade (ICB) and exhausted T-cells (Kos et al., 2021) between high- and low-risk groups. These markers could represent the cell progressively losing function due to long-term exposure to persistent antigens or chronic inflammation (Wherry and Kurachi, 2015).

Exploration of potential therapy for HCC

We explored potential therapy for HCC patients in different risk groups via the CLUE (Subramanian et al., 2017) based on the DEGs between the high- and low-risk groups (Lamb et al., 2006). CLUE was developed based on the concept of CMap (connectivity map), where genes, drugs and disease states are connected. Hence, the potential drug to reverse the current disease status for the high-risk group can be

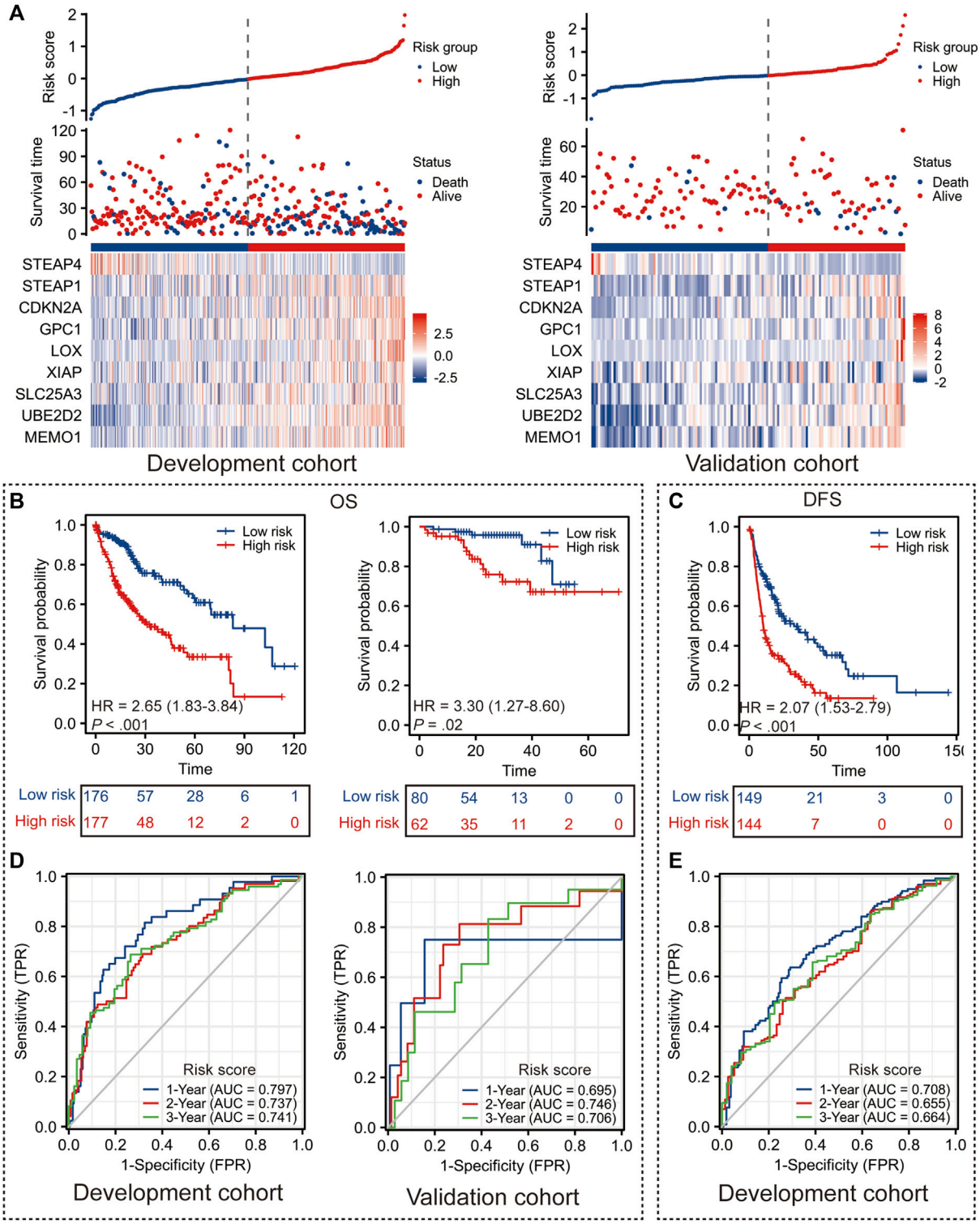

FIGURE 2
Performance of Copper-PSHC. **(A)** The distribution of Copper-PSHC risk score, survival time and the expression of each gene in Copper-PSCH in the development and validation cohort. **(B)** Kaplan-Meier survival curves showing the difference of overall survival (OS) and disease-free survival (DFS) between high- and low-risk groups in the development cohort. **(C)** Kaplan-Meier survival curves showing the difference of OS between high- and low-risk groups in the validation cohort. **(D)** Time-dependent ROC curves of 1-year, 2-year and 3-year OS and DFS for Copper-PSHC in the development cohort. **(E)** Time-dependent ROC curves and AUC in 1-year, 2-year and 3-year OS for Copper-PSHC in the validation cohort.

identified by DEGs. See Supplementary Method S4.3 for detail. The potential drugs were selected with the criteria of enrichment score < −0.60 with $p < 0.005$ as the significance level (Yue et al., 2022).

Statistical analysis

All statistical analyses were carried out using R software (version 4.1.0). To compare the difference in proportions, Chi-square test was implemented. Student's **t**-test was used for the comparison of continuous variables between two groups when the assumption of normal distribution was met; otherwise, its non-parametric counterpart Mann-Whitney *U* test was adopted. The correlation between gene expressions was examined by Spearman's correlation coefficient. RMST was estimated by the "survRM2" package (survRM2, 2022) and c-index was calculated by the "survminer" package. A two-tailed $p < 0.05$ was deemed as statistically significant, unless otherwise specified.

Results

Construction of the Copper-PSHC

A total of 59 CRGs selected from 96 CRGs in previous literature were screened as DEGs between tumor and adjacent non-tumor tissues. By assessing the association of 59 DEGs with OS in the development cohort, 19 DEGS with prognostic value were determined as candidate genes (All $p < 0.05$, Supplementary Figures S2A–C). The correlation between these genes was shown in Supplementary Figure S2D and Supplementary Table S4, where *ALB* and *LOX* were identified as hub genes (Supplementary Figure S2E).

Thirteen DEGs out of the 19 candidate genes were measured in both cohorts and were included for further analysis. Finally, nine genes were selected by LASSO-Cox regression to construct the Copper-PSHC index, i.e., *CDKN2A*, *GPC1*, *LOX*, *MEMO1*, *SLC25A3*, *STEAP1*, *STEAP4*, *UBE2D2*, and *XIAP* (Supplementary Figure S3), where high expression of those genes portended a poor prognosis, with an exception for *STEAP4*. The associations of the nine genes with OS were presented in Supplementary Figure S4. According to the normalized expression level of each gene and the corresponding Cox regression coefficients, the Copper-PSHC risk score was generated for each individual as follows:

Copper-PSHC risk score = 0.069*expression level of *CDKN2A*+ 0.228*expression level of *GPC1* + 0.119*expression level of *LOX* + 0.089*expression level of *MEMO1* + 0.007*expression level of *SLC25A3* + 0.150* expression level of *STEAP1* −0.187*expression level of *STEAP4* + 0.147*expression level of *UBE2D2* + 0.017*expression level of *XIAP*.

Taking the median risk score in the development cohort as the optimal cut-off value, the patients in the development cohort and the validation cohort were dichotomized into the low-risk (risk score < −0.021) and high-risk (risk score ≥ −0.021) groups (Figure 2A).

Validation of the prognostic value of Copper-PSHC

Copper-PSHC demonstrated outstanding prognostic value. In terms of the primary endpoint, patients from the high-risk group demonstrated a significantly reduced OS (Figure 2B; HR: 2.65 [95% CI, 1.83–3.84] and 3.30 [95% CI, 1.27–8.60] in the development and validation cohorts, respectively) compared with those from the low-risk group. The 3-year RMSTs were significantly prolonged for the low-risk group in both the development (RMST difference: −7.4 [95% CI, −10.0 to −4.8] months) and validation cohorts (RMST difference: −4.1 [95% CI, −6.8 to −1.4] months) (Supplementary Table S5). After adjusting for age, sex and cancer stage, Copper-PSHC remained as an independent prognostic factor in the development cohort (HR: 2.33 [95% CI, 1.60–3.39]) as well as the validation cohort (HR: 3.11 [95% CI, 1.15–8.42]), as shown in Supplementary Table S6. Stratified analysis indicated that the Copper-PSHC maintained a prognostic factor for all subgroups, except for females (Supplementary Figure S5; Supplementary Table S7). Concerning the secondary endpoint, patients in the high-risk group had a significantly worse DFS than the low-risk group with (Figure 2C; HR: 2.07 [95%CI, 1.53–2.79]) or without adjusting for age, sex, vascular invasion and cancer stage (HR: 1.86 [95% CI, 1.36–2.52]) in the development cohort (Supplementary Table S8).

Time-dependent ROC curves for OS and DFS exhibited an excellent discriminative power of Copper-PSHC at 3 years of follow-up (Figure 2D). In development cohort, the AUC of OS achieved 0.80 [95% CI, 0.73–0.87], 0.74 [95% CI, 0.66–0.81] and 0.74 [95% CI, 0.67–0.82] at 1-, 2- and 3-year time points, respectively (Figure 3F). In validation cohort, the AUC value of OS remained 0.70 [95% CI, 0.30–1.10], 0.75 [95% CI, 0.60–0.89] and 0.71 [95% CI, 0.56–0.86] at 1-, 2- and 3-year time points, respectively (Figure 2D). For DFS, AUC yielded 0.71 [95% CI, 0.65–0.77], 0.66 [95% CI, 0.58–0.73] and 0.66 [95% CI, 0.58–0.75] at 1-, 2- and 3-year of follow-up, respectively (Figure 2E). Copper-PSHC also demonstrated accurate prediction for OS in both cohorts (c-index: 0.64 [95% CI, 0.60–0.68] and 0.68 [95% CI, 0.58–0.78] for development and validation cohorts, respectively; Supplementary Table S5).

A higher risk score was observed in patients with undesirable biological behaviors or processes, including more advanced TMN stage (III-IV, $p < 0.001$), margin residual ($p = 0.021$) and higher tumor grade (G3/G4, $p < 0.001$), as shown in Supplementary Figures S6A–I. Additionally, PCA analysis also divided patients into two directions, which was consistent with the classification pattern generated by Copper-PSHC (Supplementary Figures S6J, K).

Construction and validation of the Copper-CPSHC

The Copper-CPSHC was derived after combining Copper-PSHC risk score with age, sex and TNM stage, leveraging the complementary value of molecular and clinical characteristics:

Copper-CPSHC risk score = [1.07292* Copper-PSHC risk score] + [0.12480* age] + [0.07879* sex] + [0.29818* stage].

Then, patients were classified into the high- (≥0.677) and low-risk (<0.677) groups according to the optimal cut-off determined by *Youden* index of the time-dependent ROC curve at 3-year follow-up in the development cohort.

The significant prolonged OS was observed among the low-risk group in the development cohort (HR: 4.27 [95% CI, 3.00–6.08]) and validation cohort (HR: 2.63 [95%CI, 1.09–6.32]) (Supplementary Figures S7A, C), with the difference of 3-year RMST of −11.8 (95%

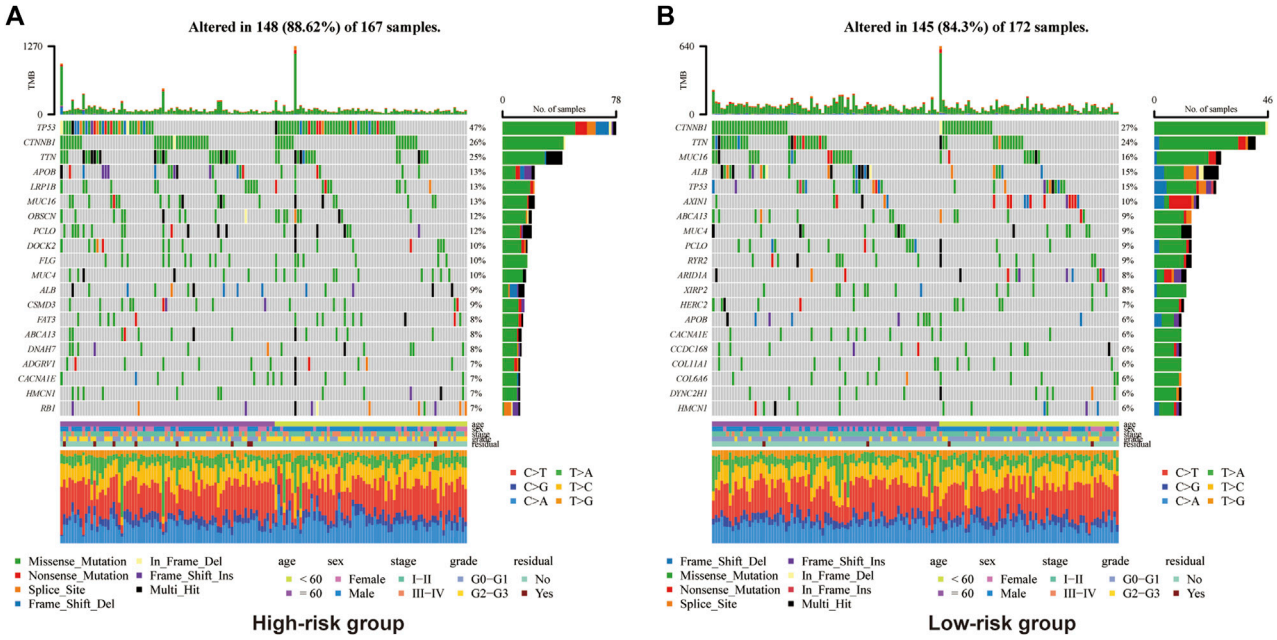

FIGURE 3
Somatic genes mutation analysis in the development cohort for high-risk group **(A)** and **(B)** low-risk group.

CI, −14.9 to −8.7) months and −4.0 (95% CI, −7.5 to −0.5) months for the development and validation cohorts, respectively (Supplementary Table S9). In development cohort, the AUC of the time-dependent ROC for OS reached 0.78 [95% CI, 0.72–0.84], 0.70 [95% CI, 0.63–0.78] and 0.73 [95% CI, 0.66–0.80] at 1-, 2- and 3-year time points, respectively (Supplementary Figure S7B). The AUC for OS in validation cohort yielded 0.72 [95% CI, 0.31–1.13], 0.75 [95% CI, 0.62–0.89] and 0.72 [95% CI, 0.56–0.87] at 1-, 2- and 3-year of follow-up, respectively (Supplementary Figure S7D). The c-index also demonstrated the validity of Copper-CPSHC on prognostic prediction in the development cohort (0.68 [95% CI, 0.63–0.72]) as well as the validation cohort (0.65 [95% CI, 0.53–0.77]), as shown in Supplementary Table S9.

We then constructed a nomogram to provide a handy quantitative instrument for clinical use (Supplementary Figure S7E). The calibration curves for 1-year and 3-year follow-up confirmed that the nomogram's predicted probabilities were close to the observed probabilities (Supplementary Figures S7F, G), indicating the consistency between the prediction and the actual observation in both development and validation cohorts. Meanwhile, DCA demonstrated that the nomogram prediction possessed more area than the TNM stage and a clinical model including age, sex and cancer stage (Supplementary Figures S7H–K). Similar results were obtained for DFS in the development cohort (Supplementary Figure S8).

Annotation of Copper-PSHC

Somatic mutation analysis

In view of the causal role of somatic mutation in cancer, we depicted the somatic mutation spectrum of the high- and low-risk groups determined by Copper-PSHC in the development cohort. In general, high-risk group was characterized by a higher mutation frequency (high-vs. low-risk: 88.6% vs. 84.3%, $p < 0.01$). The TMB was significantly higher for patients in the high-risk group (high-vs. low-risk:1.98 vs. 1.54, $p < 0.05$, Supplementary Figure S9). We exhibited the 20 most frequently mutated genes in two risk groups, respectively (Figure 3). The mutation related to undesirable biological behavior was enriched in high-risk group when compared to low-risk group, such as *TP53* (47% vs. 15%; OR: 5.15 [95% CI, 4.80–5.53]), a well-known carcinogenic gene of P53 pathway, and *DOCK2* (10% vs. 2%; OR: 4.76 [95% CI, 3.45–6.56]), an intercellular regulator of the Rho family GTPase, RAC1 (Sanui et al., 2003). The overview of mutations was also presented in Supplementary Figure S10 for both cohorts, revealing that missense mutation, SNP and C>T mutation were more common.

Functional enrichment analysis

The functional enrichment analysis highlighted the role of metabolic and biosynthesis pathways in the molecular mechanism regarding Copper-PSHC. GO enrichment revealed that the DEGs between high- and low-risk groups were related to metabolic processes, such as those regarding alpha-amino acid, hormone, and fatty acid (Figures 4A, B). Likewise, KEGG analysis demonstrated an enrichment of carbon metabolism and biosynthesis of amino acids in both cohorts (Figures 4C, D). Generally, most gene pathways were downregulated in the high-risk group when compared to the low-risk group, except for cell cycle and DNA replication pathways (Figure 4E). Considering that several pathways related to oxidation (e.g., pyruvate metabolism) were downregulated in the high-risk group, we additionally estimated the

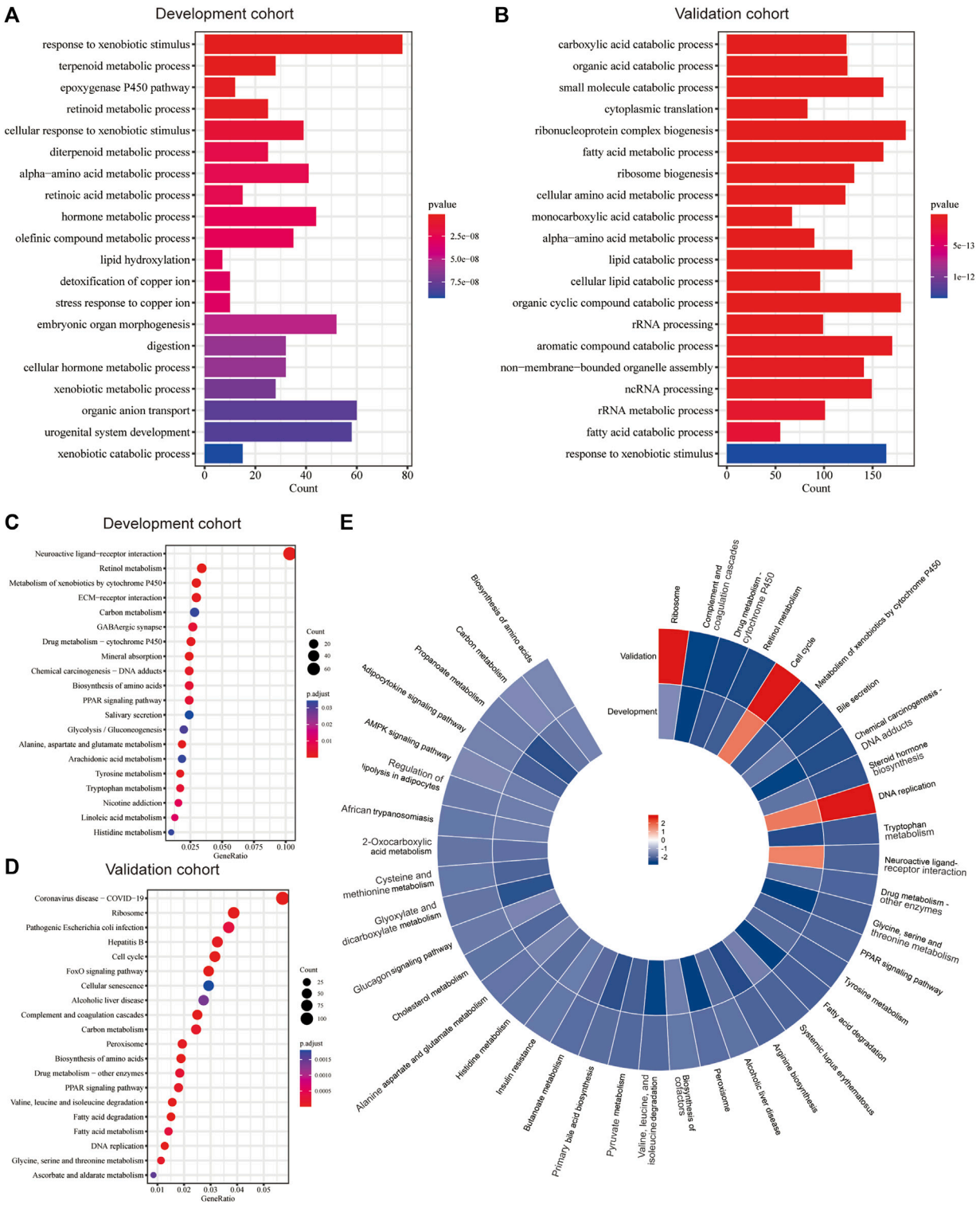

FIGURE 4
Functional enrichment analysis. The significant GO enrichment in the **(A)** development and **(B)** validation cohorts. The significant KEGG pathways in the **(C)** development and **(D)** validation cohorts. **(E)** The significantly upregulated and downregulated KEGG pathways in both cohorts according to GSEA.

hypoxia score in two risk groups. The high-risk group was associated with a significantly increased hypoxia score than the low-risk group (1.39 vs. 1.08, $p < 0.001$; Supplementary Figure S11), suggesting a low oxygen status in HCC patients from the high-risk group.

Tumor microenvironment analysis

The association between Copper-PSHC and tumor microenvironment was shown in Figure 5 and Supplementary

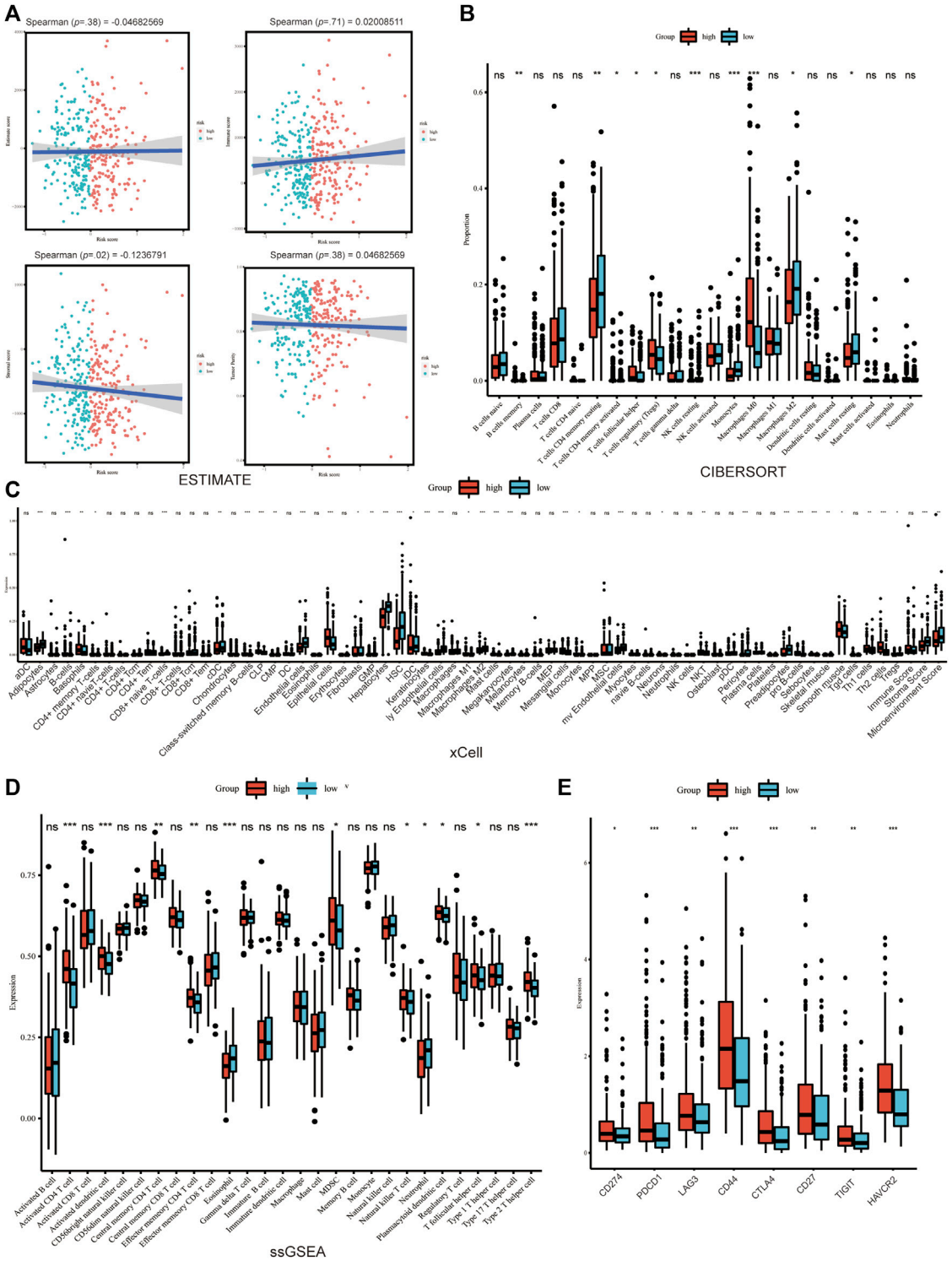

FIGURE 5
Tumor microenvironment analysis in development cohort. **(A)** The immune, stroma and Estimate score according to ESTIMATE algorithm. The differences of TME cells infiltration between high- and low-risk groups according to **(B)** Cibersort, **(C)** xCELL and **(D)** ssGSEA. **(E)** The significant difference of the expression of the cell marker related to ICB between groups. (where *$p < 0.05$, **$p < 0.01$, ***$p < 0.001$).

Figures S12, S13. Overall, a significantly negative correlation was demonstrated between stroma score and Copper-PSHC risk score in both development and validation cohorts, with Spearman correlation coefficient estimated as −0.12 ($p = 0.02$) and −0.56 ($p < 0.001$), respectively. That echoed the observation of high stroma cell infiltration in the low-risk group (both $p < 0.001$).

TABLE 1 Potential small molecules drug for high-risk HCC treatment.

CMap name	MOA	Target	Enrichment[a]
Flavokavain-b	Carcinogen	IKBKB	−0.6015
Simeprevir	HCV inhibitor	CYP2C19, CYP2C8, SLCO1B3, CYP1A2, CYP3A4	−0.6017
BRD-K88741031	Tyrosine kinase inhibitor, EGFR inhibitor	EGFR	−0.6018
RAF-265	RAF inhibitor, VEGFR inhibitor	BRAF, KDR, KIT, PDGFRB, RAF1	−0.6116
Butein	EGFR inhibitor, Src inhibitor	ACE, CXCL8, IL6, SIRT1, SRD5A1, SRD5A2, TNF	−0.6118
ASC-J9	Androgen receptor agonist	AR	−0.6487

Abbreviations: HCC, hepatocellular carcinoma; CMap, Connectivity map.
[a]The enrichment score represents the similarity between drugs and current biological process or disease status. A negative score indicates that the drug could reverse the disease status and have potential therapeutic value.

The enrichment of stroma cells in low-risk group is primarily driven by (pre-) adipocytes, pericytes, lymphatic endothelial cells, and skeletal muscle cells (Figure 5C; Supplementary Figure S12C).

The immune score was neither significantly correlated with Copper-PSHC risk score nor differed between the two risk groups. However, between-group differences were observed for certain immune cell infiltration, despite disagreement using different algorithms. For example, CD4+T cells memory resting and conventional dendritic cell (cDC) were highly infiltrated among the low-risk group, while CD4+T cells memory activated, natural killer T cell (NKT), type 2T helper cell (Th2) were enriched among the high-risk group (All $p < 0.05$; Figures 5B–D; Supplementary Figures S12B–D).

Additionally, the expression of markers related to ICB and T cell exhaustion was significantly elevated for the high-risk group in the development cohort, including CD274, PDCD1, LAG3, CD44, CTLA4, CD27, TIGHT and HAVCR2 (All $p < 0.05$; Figure 5E; Supplementary Figure S13A, B). This result hinted that immunotherapy might benefit the high-risk group.

Identification of potential drugs

Potential treatments were explored via CLUE based on the DEGs between high- and low-risk groups. Under our screening criteria, flavokavain-b, simeprevir, BRD-K88741031, RAF-265 butein and ASC-J9 were discovered as potential drugs for the high-risk group (Table 1). EGFR inhibitor was the primary mode of action for the drugs above. Also, carcinogens, HCV inhibitors, tyrosine kinase inhibitors, RAF inhibitors, Src inhibitors and androgen receptor agonists were the potential targets for treating the high-risk group as well.

Discussion

In this study, we developed and validated a 9-CRG prognostic signature, Copper-PSHC, for HCC patients. We also combined clinical features including age, sex and cancer stage with Copper-PSHC to build a composite prediction model, Copper-CPSHC, for clinical prognostic stratification. Both Copper-PSHC and Copper-CPSHC were demonstrated as reliable tools with excellent prognostic value in the development and validation cohorts. Beyond that, extensive work has been carried out for the annotation of Copper-PSHC.

An increasing number of prognostic models for HCC have been proposed. For example, Liang et al. (2020) developed a ferroptosis-related gene signature for OS prediction. Tang et al. (2022) constructed an immunological phenotype-related gene signature for predicting prognosis. Xu et al. (2021) fitted a ferroptosis-related nine-lncRNA signature for predicting prognosis and immune response. Compared to those models, Copper-PSHC had an exceptional advantage in predicting OS and DFS in both the development and validation cohorts. We also provided a nomogram combining clinical variables and risk score for ready clinical application. Additional advantage of our study includes examining the potential of immunotherapy in the management of HCC. On balance, we developed a reliable copper-related model to predict prognosis which is of high significance in clinical decision-making.

Our study confirmed previous findings on the association between 9 genes in Copper-PSHC with cancer. It is collectively speculated that these genes could play crucial roles in tumor development and/or progression, and therefore own considerable prognostic value for HCC. Previous research on network-based prioritization of HCC markers by module detection and ranking has demonstrated the diagnostic value of CDKN2A (Shang and Liu, 2021). Besides, Luo et al. (2021) found that *CDKN2A* was highly expressed in HCC and associated with a decreased OS via facilitating the proliferation of cancer cells and inhibiting apoptosis. *LOX* was the mediator of remodeling of the extracellular matrix cross-linking, thereby contributing to the angiogenesis (Sun et al., 2022). *XIAP* could induce the resistance to apoptosis, providing survival advantage to the metastatic tumor cells (Shi et al., 2008). As a cell surface heparan sulfate proteoglycan, *GPC1* was found to exhibit a mitogenic response to multiple heparin-binding growth factors and lead to progression in breast cancer (Matsuda et al., 2001). *GPC1* was also used as a potent predictive biomarker for the general prognosis of HCC (Wang JY. et al., 2021). Analogously, *SLC25* protein family, *MEMO* and *STEAP* were identified as potential biomarkers for prognosis (Gomes et al., 2012; MacDonald et al., 2014; Rochette et al., 2020). However, much uncertainty still exists about the opposite roles of *STEAP1* and *STEAP4* in HCC.

To our knowledge, Copper-PSHC was the first prognostic prediction model related to copper binding, copper homeostasis and cuproptosis. Recently, the association between cuproptosis and HCC has been elucidated. As a mineral nutrient, the significance of

copper for various physiological processes has been well recognized across the animal kingdom to human (Ge et al., 2022). Copper functions as a crucial cofactor for enzymes that mediate a range of cellular activities including mitochondrial respiration and antioxidant defense (Luo et al., 2021); therefore, copper homeostasis was critical for cellular growth and maintenance. Of note, increasing evidence demonstrated that copper and the disruption of copper homeostasis were involved in oncogenesis (Brady et al., 2014; Shanbhag et al., 2019; Llovet et al., 2021). This supports the argument that copper may activate several proangiogenic factors such as vascular endothelial growth factor, fibroblast growth factor 2, tumor necrosis factor and interleukin-1 (Gérard et al., 2010; Das et al., 2022; Ge et al., 2022). Meanwhile, emerging cancer therapeutics targeting copper and copper-dependent signaling pathways exhibit significant promise, including copper chelators to inhibit cuproplasia and copper supplementation to promote cuproptosis. Taken together, it is of great importance to assess the copper status and characterize the landscape of copper in HCC patients. Regarding this, our study might provide valuable insights for understanding HCC and the management of HCC patients through the lens of copper homeostasis.

Our findings of correlation between high expression of CDKN2A and poor prognosis in HCC further evidenced the antitumor effect of cuproptosis, a distinct form of cell death dependent on intracellular copper accumulation, where FDX1 and protein lipoylation serve as the hub regulators and CDKN2A serve as a negative regulator (Tsvetkov et al., 2022). Besides, we found that pyruvate metabolism related to the TCA cycle, which is a necessary condition for copper-induced cell death, was downregulated in the high-risk group. This finding again echoes the currently available evidence that cuproptosis may contribute to the inhibition of tumor growth and recurrence and thus a favorable prognosis by killing cancer cells modulated by the tumor microenvironment. It was reported that copper-dependent cell death was attenuated under the hypoxic condition, leading to an increased risk of tumor growth and progression. In support of this, we analyzed the hypoxic level in high- and low-risk groups and found that tumor cells in high-risk group were prone to be in hypoxic environments. Our results reveal that evaluation of the hypoxia level may help guide HCC treatment, especially the copper-targeted therapeutic strategies. Patients at high-risk are warranted for more intensive or personalized treatment strategies. For example, regorafenib and cabozantinib should be additionally used as systemic therapy for those high-risk patients (Solimando et al., 2022). Also, more targeted clinical studies need to be conducted in the high-risk populations we identified. Elesclomol, in combination with paclitaxel for melanoma, was a good example where statistically significant improvement was observed for patients with normal baseline levels of lactate dehydrogenase (LDX) (O'Day et al., 2013).

Additionally, we found that the high-risk group held a higher mutation frequency and TMB. *TP53*, as the most common mutation in the high-risk group, has been reported to be associated with undesirable biological behaviors including high AFP, advanced tumor stage, vascular invasion, poor tumor differentiation, and poor Child-Pugh class (Long et al., 2019). Other undesirable mutations were also enriched in the high-risk group, such as DOCK2 which regulates Rac activation and cytoskeletal reorganization (survRM2, 2022), accounting partly for poor prognosis in the high-risk group as well.

Functional enrichment analysis suggested that the metabolic and biosynthetic processes were instrumental in Copper-PSHC. The downregulated pathways related to amino acid and lipid metabolism implied that the high-risk group featured low metabolic activity. According to the metabolism-associated molecular classification of HCC, high metabolic activity was related to α-fetoprotein (AFP) expression and good prognosis (Yang et al., 2020). Another model proposed by Désert et al. classified HCC as "ECM-type," "STEM-type," "PV-type" and "PP-type." Among them, "PP-type" characterized by high lipid and bile salt metabolism has displayed low proliferation and favorable prognosis (Ng et al., 2017). Given that liver is the primary handler of amino acid and lipid metabolism, we supposed that maintenance of high metabolic activity in the low-risk group conferred high chances of preserving normal liver phenotype, which may lead to less aggressive clinical and biological behaviors (Phillips, 2022).

Importantly, we explored the association between Copper-PSHC and tumor microenvironment. Overall, more infiltration of stromal cells was found in the low-risk group, suggesting their low degree of tumor purity and well differentiation. Although no significant difference in overall immune cell infiltration was observed between high- and low-risk groups, great disparities exist for certain types of immune cells. Patients in the high-risk group were prone to possess more activated cells and T helper cells. Generally, the infiltration of immune cells including T cells, macrophages, and B cells would conduct to the desirable prognosis (Galluzzi et al., 2020), especially in colorectal cancer (Picard et al., 2020) and breast cancer (Wang S. et al., 2021). Such inconsistency led us to further explore the expression of receptors in immune cells. As a result, high expression of immune regulators including CTLA-4 and PD-L1 was found in the high-risk group, which suggested that the infiltrated T cells in the high-risk group were mainly exhausted T cells. T cell exhaustion characterized by a loss of effector functions and memory T cell properties would hamper optimal control of tumors (Blank et al., 2019) and thereby account for poor prognosis of the high-risk group. Notably, the enrichment of cell markers related to ICB lent credence to the availability of immunotherapy for the high-risk subpopulation. This implication was also supported by the finding that higher TMB was shown in the high-risk group. Tumors with high TMB were more likely to respond to ICB agents (Chan et al., 2019) because greater tumor load could enhance the likelihood of being recognized by T cells (Litchfield et al., 2021).

Apart from the advantages and implications of this study as discussed above, several limitations also require due consideration. Firstly, restricted to the retrospective study, we may introduce the selection bias such as the exclusion of some patients who lacked data or were ineligible for sequencing, particularly those patients who are unable to undertake surgery treatment due to comorbidities or tumor metastasis. Secondly, the sample size was not considered large enough owing to the limited number of HCC patients in advanced stage. Further optimization of the

Copper-PSHC index taking the stages of patient population into account is warranted for future studies. Thirdly, due to the unavailability of other clinical data including treatment history, comorbidities and laboratory values, and radiomic data, we were unable to incorporate more variables into our composite model. Notwithstanding, the index Copper-CPSHC developed in this study already owns satisfactory prognostic prediction value. Fourthly, with an aim of ensuring the robustness of results in tumor microenvironmental analysis, most immune cells were analyzed by two or more algorithms. However, certain cells, stromal cells for instance, were exclusively analyzed by xCell. Fifthly, the screening of potential drugs in this study is explorative and more efforts are warranted to further validate these finding in future studies. Lastly, the validation was performed using the public cohorts and we only provided a brief discussion of the potential mechanism of the genes in the model. More prospective studies and further exploration of the biological mechanism in the context of copper and HCC was in warranted.

In conclusion, this study constructed a copper-related signature, Copper-PSHC, based on nine CRGs, which has been subsequently demonstrated to be a reliable biomarker for prognostic prediction. We then move forward to examine the hypothesis of metabolic process and tumor immunity being the mechanisms of this signature, illuminating the potential of certain small molecular drugs and immunotherapy for better management of HCC patients. It is envisaged that further investigation using different research tools will help to elucidate the underlying mechanism and verify its clinical utility in the real world.

Data availability statement

The original contributions presented in the study are included in the article/Supplementary Material, further inquiries can be directed to the corresponding authors.

Ethics statement

Ethical review and approval was not required for the study on human participants in accordance with the local legislation and institutional requirements. Written informed consent for participation was not required for this study in accordance with the national legislation and the institutional requirements.

Author contributions

HS: Conceptualization, data curation, formal analysis, investigation, methodology, project administration, software, writing—original draft, visualization. JH: Conceptualization, data curation, formal analysis, methodology, writing—original draft, visualization. XW: Conceptualization, investigation, writing–original draft. RL: Writing–review and editing. YS: Methodology, software, writing—review and editing. BJ: Writing—review and editing. JR: Writing—review and editing. RC: Funding acquisition, writing—review and editing. FG: Writing–review and editing, supervision. YW: Conceptualization, data curation, formal analysis, methodology, software, writing—review and editing, visualization, supervision. GR: Conceptualization, writing—review and editing, supervision. All authors contributed to the article and approved the submitted version.

Funding

This work was supported by Shanghai Health Bureau Fund, grant number: 2010057 (RC).

Conflict of interest

The authors declare that the research was conducted in the absence of any commercial or financial relationships that could be construed as a potential conflict of interest.

Publisher's note

Supplementary material

The Supplementary Material for this article can be found online at: https://www.frontiersin.org/articles/10.3389/fcell.2023.1157841/full#supplementary-material

References

Adeoti, M. L., Oguntola, A. S., Akanni, E. O., Agodirin, O. S., and Oyeyemi, G. M. (2015). Trace elements; copper, zinc and selenium, in breast cancer afflicted female patients in LAUTECH Osogbo, Nigeria. *Indian J. Cancer* 52 (1), 106–109. doi:10.4103/0019-509x.175573

Aran, D., Hu, Z., and Butte, A. J. (2017). xCell: digitally portraying the tissue cellular heterogeneity landscape. *Genome Biol.* 18 (1), 220. doi:10.1186/s13059-017-1349-1

Bandmann, O., Weiss, K. H., and Kaler, S. G. (2015). Wilson's disease and other neurological copper disorders. *Lancet Neurol.* 14 (1), 103–113. doi:10.1016/s1474-4422(14)70190-5

Barbie, D. A., Tamayo, P., Boehm, J. S., Kim, S. Y., Moody, S. E., Dunn, I. F., et al. (2009). Systematic RNA interference reveals that oncogenic KRAS-driven cancers require TBK1. *Nature* 462 (7269), 108–112. doi:10.1038/nature08460

Bian, Z., Fan, R., and Xie, L. (2022). A novel cuproptosis-related prognostic gene signature and validation of differential expression in clear cell renal cell carcinoma. *Genes (Basel).* 13 (5), 851. doi:10.3390/genes13050851

Blank, C. U., Haining, W. N., Held, W., Hogan, P. G., Kallies, A., Lugli, E., et al. (2019). Defining 'T cell exhaustion. *Nat. Rev. Immunol.* 19 (11), 665–674. doi:10.1038/s41577-019-0221-9

Blockhuys, S., Celauro, E., Hildesjö, C., Feizi, A., Stål, O., Fierro-González, J. C., et al. (2017). Defining the human copper proteome and analysis of its expression variation in cancers. *Metallomics* 9 (2), 112–123. Epub 2016/12/13. doi:10.1039/c6mt00202a

Brady, D. C., Crowe, M. S., Turski, M. L., Hobbs, G. A., Yao, X., Chaikuad, A., et al. (2014). Copper is required for oncogenic BRAF signalling and tumorigenesis. *Nature* 509 (7501), 492–496. doi:10.1038/nature13180

Cerami, E., Gao, J., Dogrusoz, U., Gross, B. E., Sumer, S. O., Aksoy, B. A., et al. (2012). The cBio cancer genomics portal: An open platform for exploring multidimensional cancer genomics data. *Cancer Discov.* 2 (5), 401–404. doi:10.1158/2159-8290.CD-12-0095

Chan, T. A., Yarchoan, M., Jaffee, E., Swanton, C., Quezada, S. A., Stenzinger, A., et al. (2019). Development of tumor mutation burden as an immunotherapy biomarker: Utility for the oncology clinic. *Ann. Oncol.* 30 (1), 44–56. doi:10.1093/annonc/mdy495

Dai, Y., Qiang, W., Lin, K., Gui, Y., Lan, X., and Wang, D. (2021). An immune-related gene signature for predicting survival and immunotherapy efficacy in hepatocellular carcinoma. *Cancer Immunol. Immunother.* 70 (4), 967–979. doi:10.1007/s00262-020-02743-0

Das, A., Ash, D., Fouda, A. Y., Sudhahar, V., Kim, Y. M., Hou, Y., et al. (2022). Cysteine oxidation of copper transporter CTR1 drives VEGFR2 signalling and angiogenesis. *Nat. Cell Biol.* 24 (1), 35–50. doi:10.1038/s41556-021-00822-7

Davis, C. I., Gu, X., Kiefer, R. M., Ralle, M., Gade, T. P., and Brady, D. C. (2020). Altered copper homeostasis underlies sensitivity of hepatocellular carcinoma to copper chelation. *Metallomics* 12 (12), 1995–2008. doi:10.1039/d0mt00156b

EASL Clinical Practice Guidelines (2018). European association for the study of the liver EASL clinical practice Guidelines: Management of hepatocellular carcinoma. *J. Hepatol.* 69 (1), 182–236. doi:10.1016/j.jhep.2018.03.019

Engebretsen, S., and Bohlin, J. (2019). Statistical predictions with glmnet. *Clin. Epigenetics* 11 (1), 123. doi:10.1186/s13148-019-0730-1

Fluss, R., Faraggi, D., and Reiser, B. (2005). Estimation of the Youden Index and its associated cutoff point. *Biom J.* 47 (4), 458–472. doi:10.1002/bimj.200410135

Galluzzi, L., Humeau, J., Buqué, A., Zitvogel, L., and Kroemer, G. (2020). Immunostimulation with chemotherapy in the era of immune checkpoint inhibitors. *Nat. Rev. Clin. Oncol.* 17 (12), 725–741. doi:10.1038/s41571-020-0413-z

Ge, E. J., Bush, A. I., Casini, A., Cobine, P. A., Cross, J. R., DeNicola, G. M., et al. (2022). Connecting copper and cancer: From transition metal signalling to metalloplasia. *Nat. Rev. Cancer* 22 (2), 102–113. doi:10.1038/s41568-021-00417-2

Gérard, C., Bordeleau, L. J., Barralet, J., and Doillon, C. J. (2010). The stimulation of angiogenesis and collagen deposition by copper. *Biomaterials* 31 (5), 824–831. doi:10.1016/j.biomaterials.2009.10.009

Golabi, P., Fazel, S., Otgonsuren, M., Sayiner, M., Locklear, C. T., and Younossi, Z. M. (2017). Mortality assessment of patients with hepatocellular carcinoma according to underlying disease and treatment modalities. *Med. Baltim.* 96 (9), e5904. doi:10.1097/md.0000000000005904

Gomes, I. M., Maia, C. J., and Santos, C. R. (2012). STEAP proteins: From structure to applications in cancer therapy. *Mol. Cancer Res.* 10 (5), 573–587. doi:10.1158/1541-7786.Mcr-11-0281

Grossman, R. L., Heath, A. P., Ferretti, V., Varmus, H. E., Lowy, D. R., Kibbe, W. A., et al. (2016). Toward a shared vision for cancer genomic data. *N. Engl. J. Med.* 375 (12), 1109–1112. doi:10.1056/NEJMp1607591

Hu, B., Yang, X. B., and Sang, X. T. (2020). Development and verification of the hypoxia-related and immune-associated prognosis signature for hepatocellular carcinoma. *J. Hepatocell. Carcinoma* 7, 315–330. doi:10.2147/jhc.S272109

Ishida, S., Andreux, P., Poitry-Yamate, C., Auwerx, J., and Hanahan, D. (2013). Bioavailable copper modulates oxidative phosphorylation and growth of tumors. *Proc. Natl. Acad. Sci. U. S. A.* 110 (48), 19507–19512. doi:10.1073/pnas.1318431110

Jemal, A., Ward, E. M., Johnson, C. J., Cronin, K. A., Ma, J., Ryerson, B., et al. (2017). Annual report to the nation on the status of cancer, 1975-2014, featuring survival. *J. Natl. Cancer Inst.* 109 (9), djx030. doi:10.1093/jnci/djx030

Jin, Y., Zhang, C., Xu, H., Xue, S., Wang, Y., Hou, Y., et al. (2011). Combined effects of serum trace metals and polymorphisms of CYP1A1 or GSTM1 on non-small cell lung cancer: A hospital based case-control study in China. *Cancer Epidemiol.* 35 (2), 182–187. doi:10.1016/j.canep.2010.06.004

Kanehisa, M., Furumichi, M., Sato, Y., Ishiguro-Watanabe, M., and Tanabe, M. (2021). Kegg: Integrating viruses and cellular organisms. *Nucleic Acids Res.* 49 (D1), D545–D551. doi:10.1093/nar/gkaa970

Kim, B. E., Nevitt, T., and Thiele, D. J. (2008). Mechanisms for copper acquisition, distribution and regulation. *Nat. Chem. Biol.* 4 (3), 176–185. doi:10.1038/nchembio.72

Kos, M. Z., Carless, M. A., Blondell, L., Leland, M. M., Knape, K. D., Göring, H. H. H., et al. (2021). Whole Genome sequence data from captive baboons implicate RBFOX1 in epileptic seizure risk. *Front. Genet.* 12, 714282. doi:10.3389/fgene.2021.714282

Lamb, J., Crawford, E. D., Peck, D., Modell, J. W., Blat, I. C., Wrobel, M. J., et al. (2006). The connectivity map: Using gene-expression signatures to connect small molecules, genes, and disease. *Science* 313 (5795), 1929–1935. doi:10.1126/science.1132939

Liang, J. Y., Wang, D. S., Lin, H. C., Chen, X. X., Yang, H., Zheng, Y., et al. (2020). A novel ferroptosis-related gene signature for overall survival prediction in patients with hepatocellular carcinoma. *Int. J. Biol. Sci.* 16 (13), 2430–2441. doi:10.7150/ijbs.45050

Litchfield, K., Reading, J. L., Puttick, C., Thakkar, K., Abbosh, C., Bentham, R., et al. (2021). Meta-analysis of tumor- and T cell-intrinsic mechanisms of sensitization to checkpoint inhibition. *Cell* 184 (3), 596–614.e14. doi:10.1016/j.cell.2021.01.002

Liu, X. N., Cui, D. N., Li, Y. F., Liu, Y. H., Liu, G., and Liu, L. (2019). Multiple "Omics" data-based biomarker screening for hepatocellular carcinoma diagnosis. *World J. Gastroenterol.* 25 (30), 4199–4212. doi:10.3748/wjg.v25.i30.4199

Llovet, J. M., Kelley, R. K., Villanueva, A., Singal, A. G., Pikarsky, E., Roayaie, S., et al. (2021). Hepatocellular carcinoma. *Nat. Rev. Dis. Prim.* 7 (1), 6. doi:10.1038/s41572-020-00240-3

Llovet, J. M., Montal, R., Sia, D., and Finn, R. S. (2018). Molecular therapies and precision medicine for hepatocellular carcinoma. *Nat. Rev. Clin. Oncol.* 15 (10), 599–616. doi:10.1038/s41571-018-0073-4

Long, J., Wang, A., Bai, Y., Lin, J., Yang, X., Wang, D., et al. (2019). Development and validation of a TP53-associated immune prognostic model for hepatocellular carcinoma. *EBioMedicine* 42, 363–374. doi:10.1016/j.ebiom.2019.03.022

Luo, J. P., Wang, J., and Huang, J. H. (2021). CDKN2A is a prognostic biomarker and correlated with immune infiltrates in hepatocellular carcinoma. *Biosci. Rep.* 41 (10). doi:10.1042/bsr20211103

MacDonald, G., Nalvarte, I., Smirnova, T., Vecchi, M., Aceto, N., Dolemeyer, A., et al. (2014). Memo is a copper-dependent redox protein with an essential role in migration and metastasis. *Sci. Signal* 7 (329), ra56. doi:10.1126/scisignal.2004870

Mann, C. D., Neal, C. P., Garcea, G., Manson, M. M., Dennison, A. R., and Berry, D. P. (2007). Prognostic molecular markers in hepatocellular carcinoma: A systematic review. *Eur. J. Cancer* 43 (6), 979–992. doi:10.1016/j.ejca.2007.01.004

Matsuda, K., Maruyama, H., Guo, F., Kleeff, J., Itakura, J., Matsumoto, Y., et al. (2001). Glypican-1 is overexpressed in human breast cancer and modulates the mitogenic effects of multiple heparin-binding growth factors in breast cancer cells. *Cancer Res.* 61 (14), 5562–5569.

Mayakonda, A., Lin, D. C., Assenov, Y., Plass, C., and Koeffler, H. P. (2018). Maftools: Efficient and comprehensive analysis of somatic variants in cancer. *Genome Res.* 28 (11), 1747–1756. doi:10.1101/gr.239244.118

McGlynn, K. A., Petrick, J. L., and El-Serag, H. B. (2021). Epidemiology of hepatocellular carcinoma. *Hepatology* 73 (1), 4–13. doi:10.1002/hep.31288

Nakamura, N., Suyama, A., Noda, A., and Kodama, Y. (2013). Radiation effects on human heredity. *Annu. Rev. Genet.* 47, 33–50. doi:10.1146/annurev-genet-111212-133501

Newman, A. M., Liu, C. L., Green, M. R., Gentles, A. J., Feng, W., Xu, Y., et al. (2015). Robust enumeration of cell subsets from tissue expression profiles. *Nat. Methods* 12 (5), 453–457. doi:10.1038/nmeth.3337

Ng, C. K. Y., Piscuoglio, S., and Terracciano, L. M. (2017). Molecular classification of hepatocellular carcinoma: The view from metabolic zonation. *Hepatology* 66 (5), 1377–1380. doi:10.1002/hep.29311

O'Day, S. J., Eggermont, A. M., Chiarion-Sileni, V., Kefford, R., Grob, J. J., Mortier, L., et al. (2013). Final results of phase III SYMMETRY study: Randomized, double-blind trial of elesclomol plus paclitaxel versus paclitaxel alone as treatment for chemotherapy-naive patients with advanced melanoma. *J. Clin. Oncol.* 31 (9), 1211–1218. doi:10.1200/jco.2012.44.5585

Pe'er, D., Ogawa, S., Elhanani, O., Keren, L., Oliver, T. G., and Wedge, D. (2021). Tumor heterogeneity. *Cancer Cell* 39 (8), 1015–1017. doi:10.1016/j.ccell.2021.07.009

Phillips, M. C. (2022). Metabolic strategies in healthcare: a new era. *Aging Dis.* 13 (3), 655–672. doi:10.14336/AD.2021.1018

Picard, E., Verschoor, C. P., Ma, G. W., and Pawelec, G. (2020). Relationships between immune landscapes, genetic subtypes and responses to immunotherapy in colorectal cancer. *Front. Immunol.* 11, 369. doi:10.3389/fimmu.2020.00369

Rochette, L., Meloux, A., Zeller, M., Malka, G., Cottin, Y., and Vergely, C. (2020). Mitochondrial SLC25 carriers: Novel targets for cancer therapy. *Molecules* 25 (10), 2417. doi:10.3390/molecules25102417

Sanui, T., Inayoshi, A., Noda, M., Iwata, E., Stein, J. V., Sasazuki, T., et al. (2003). DOCK2 regulates Rac activation and cytoskeletal reorganization through interaction with ELMO1. *Blood* 102 (8), 2948–2950. doi:10.1182/blood-2003-01-0173

Shanbhag, V., Jasmer-McDonald, K., Zhu, S., Martin, A. L., Gudekar, N., Khan, A., et al. (2019). ATP7A delivers copper to the lysyl oxidase family of enzymes and promotes tumorigenesis and metastasis. *Proc. Natl. Acad. Sci. U. S. A.* 116 (14), 6836–6841. doi:10.1073/pnas.1817473116

Shang, H., and Liu, Z. P. (2021). Network-based prioritization of cancer biomarkers by phenotype-driven module detection and ranking. *Comput. Struct. Biotechnol. J.* 8, 206–217. doi:10.1016/j.csbj.2021.12.005

Shi, Y. H., Ding, W. X., Zhou, J., He, J. Y., Xu, Y., Gambotto, A. A., et al. (2008). Expression of X-linked inhibitor-of-apoptosis protein in hepatocellular carcinoma promotes metastasis and tumor recurrence. *Hepatology* 48 (2), 497–507. doi:10.1002/hep.22393

Solimando, A. G., Susca, N., Argentiero, A., Brunetti, O., Leone, P., De Re, V., et al. (2022). Second-line treatments for advanced hepatocellular carcinoma: A systematic review and bayesian network meta-analysis. *Clin. Exp. Med.* 22 (1), 65–74. doi:10.1007/s10238-021-00727-7

Stepien, M., Jenab, M., Freisling, H., Becker, N. P., Czuban, M., Tjønneland, A., et al. (2017). Pre-diagnostic copper and zinc biomarkers and colorectal cancer risk in the European Prospective Investigation into Cancer and Nutrition cohort. *Carcinogenesis* 38 (7), 699–707. doi:10.1093/carcin/bgx051

Subramanian, A., Narayan, R., and Corsello, S. M. (2017). A next generation connectivity map: L1000 platform and the first 1,000,000 profiles. *Cell* 171 (6), 1437–1452.e17. doi:10.1016/j.cell.2017.10.049

Sun, C., Ma, S., Chen, Y., Kim, N. H., Kailas, S., Wang, Y., et al. (2022). Diagnostic value, prognostic value, and immune infiltration of LOX family members in liver cancer: Bioinformatic analysis. *Front. Oncol.* 12, 843880. doi:10.3389/fonc.2022.843880

Sung, H., Ferlay, J., Siegel, R. L., Laversanne, M., Soerjomataram, I., Jemal, A., et al. (2021). Global cancer statistics 2020: GLOBOCAN estimates of incidence and mortality worldwide for 36 cancers in 185 countries. *CA Cancer J. Clin.* 71 (3), 209–249. doi:10.3322/caac.21660

survRM2 (2022). Comparing restricted mean survival time R package version 1.0-4. Available at: https://CRAN.R-project.org/package=survRM2.

Szklarczyk, D., Gable, A. L., Nastou, K. C., Lyon, D., Kirsch, R., Pyysalo, S., et al. (2021). The STRING database in 2021: Customizable protein-protein networks, and functional characterization of user-uploaded gene/measurement sets. *Nucleic Acids Res.* 49 (D1), D605–D612. doi:10.1093/nar/gkaa1074

Tamai, Y., Iwasa, M., Eguchi, A., Shigefuku, R., Sugimoto, K., Hasegawa, H., et al. (2020). Serum copper, zinc and metallothionein serve as potential biomarkers for hepatocellular carcinoma. *PLoS One* 15 (8), e0237370. doi:10.1371/journal.pone.0237370

Tang, Y., Guo, C., Yang, Z., Wang, Y., Zhang, Y., and Wang, D. (2022). Identification of a tumor immunological phenotype-related gene signature for predicting prognosis, immunotherapy efficacy, and drug candidates in hepatocellular carcinoma. *Front. Immunol.* 13, 862527. doi:10.3389/fimmu.2022.862527

The Gene Ontology Consortium (2019). The gene Ontology resource: 20 years and still GOing strong. *Nucleic Acids Res.* 47 (D1), D330–D338. doi:10.1093/nar/gky1055

The International Cancer Genome Consortium Data Portal (2019). The international cancer Genome Consortium data portal. Available from: https://dcc.icgc.org/.

Tsvetkov, P., Coy, S., Petrova, B., Dreishpoon, M., Verma, A., Abdusamad, M., et al. (2022). Copper induces cell death by targeting lipoylated TCA cycle proteins. *Science* 375 (6586), 1254–1261. doi:10.1126/science.abf0529

van Malenstein, H., van Pelt, J., and Verslype, C. (2011). Molecular classification of hepatocellular carcinoma anno 2011. *Eur. J. Cancer* 47 (12), 1789–1797. doi:10.1016/j.ejca.2011.04.027

Villanueva, A. (2019). Hepatocellular carcinoma. *N. Engl. J. Med.* 380 (15), 1450–1462. doi:10.1056/NEJMra1713263

Wang, J. Y., Wang, X. K., Zhu, G. Z., Zhou, X., Yao, J., Ma, X. P., et al. (2021a). Distinct diagnostic and prognostic values of Glypicans gene expression in patients with hepatocellular carcinoma. *BMC Cancer* 21 (1), 462. doi:10.1186/s12885-021-08104-z

Wang, S., Xiong, Y., Zhang, Q., Su, D., Yu, C., Cao, Y., et al. (2021b). Clinical significance and immunogenomic landscape analyses of the immune cell signature based prognostic model for patients with breast cancer. *Brief. Bioinform* 22 (4), bbaa311. doi:10.1093/bib/bbaa311

Wherry, E. J., and Kurachi, M. (2015). Molecular and cellular insights into T cell exhaustion. *Nat. Rev. Immunol.* 15 (8), 486–499. doi:10.1038/nri3862

White, I. R., Royston, P., and Wood, A. M. (2011). Multiple imputation using chained equations: Issues and guidance for practice. *Stat. Med.* 30 (4), 377–399. doi:10.1002/sim.4067

Wu, C., Lin, J., Weng, Y., Zeng, D. N., Xu, J., Luo, S., et al. (2020). Myeloid signature reveals immune contexture and predicts the prognosis of hepatocellular carcinoma. *J. Clin. Invest.* 130 (9), 4679–4693. doi:10.1172/jci135048

Xu, Z., Peng, B., Liang, Q., Chen, X., Cai, Y., Zeng, S., et al. (2021). Construction of a ferroptosis-related nine-lncRNA signature for predicting prognosis and immune response in hepatocellular carcinoma. *Front. Immunol.* 12, 719175. doi:10.3389/fimmu.2021.719175

Yang, C., Huang, X., Liu, Z., Qin, W., and Wang, C. (2020). Metabolism-associated molecular classification of hepatocellular carcinoma. *Mol. Oncol.* 14 (4), 896–913. PubMed PMID: 31955511;. doi:10.1002/1878-0261.12639

Yang, J. D., Hainaut, P., Gores, G. J., Amadou, A., Plymoth, A., and Roberts, L. R. (2019). A global view of hepatocellular carcinoma: Trends, risk, prevention and management. *Nat. Rev. Gastroenterol. Hepatol.* 16 (10), 589–604. doi:10.1038/s41575-019-0186-y

Yoshihara, K., Shahmoradgoli, M., Martínez, E., et al. (2013). Inferring tumour purity and stromal and immune cell admixture from expression data. *Nat. Commun.* 4, 2612. doi:10.1038/ncomms3612

Yu, G., Wang, L. G., Han, Y., and He, Q. Y. (2012). clusterProfiler: an R package for comparing biological themes among gene clusters. *Omics* 16 (5), 284–287. doi:10.1089/omi.2011.0118

Yue, Z., Sun, J., and Shi, L. (2022). Construction and validation of a 6-ferroptosis related gene signature for prognosis and immune landscape prediction in melanoma. *Front. Genet.* 13, 887542. doi:10.3389/fgene.2022.887542

frontiers | Frontiers in Immunology

TYPE Original Research
PUBLISHED 02 August 2023
DOI 10.3389/fimmu.2023.1181370

OPEN ACCESS

EDITED BY
Lin-Lin Bu,
Wuhan University, China

REVIEWED BY
Jamshid Hadjati,
Tehran University of Medical Sciences, Iran
Jinghang Li,
The University of Chicago, United States

*CORRESPONDENCE
Zhihui Zhang
zhangzhihuidev@126.com
Dongdong Xie
xiedd_urology@163.com

†These authors have contributed equally to this work

RECEIVED 07 March 2023
ACCEPTED 17 July 2023
PUBLISHED 02 August 2023

CITATION
Yao K, Zhang R, Li L, Liu M, Feng S, Yan H, Zhang Z and Xie D (2023) The signature of cuproptosis-related immune genes predicts the tumor microenvironment and prognosis of prostate adenocarcinoma. *Front. Immunol.* 14:1181370. doi: 10.3389/fimmu.2023.1181370

The signature of cuproptosis-related immune genes predicts the tumor microenvironment and prognosis of prostate adenocarcinoma

Kai Yao[1†], Rumeng Zhang[2†], Liang Li[1], Mingdong Liu[1], Shiyao Feng[1], Haixin Yan[1], Zhihui Zhang[1*] and Dongdong Xie[1,3*]

[1]Department of Urology, The Second Affiliated Hospital of Anhui Medical University, Hefei, China, [2]Department of Pathology, School of Basic Medicine, Anhui Medical University, Hefei, Anhui, China, [3]Department of Urology, Affiliated Fuyang Hospital of Anhui Medical University, Fuyang, Anhui, China

Background: Cuproptosis plays a crucial role in cancer, and different subtypes of cuproptosis have different immune profiles in prostate adenocarcinoma (PRAD). This study aimed to investigate immune genes associated with cuproptosis and develop a risk model to predict prognostic characteristics and chemotherapy/immunotherapy responses of patients with PRAD.

Methods: The CIBERSORT algorithm was used to evaluate the immune and stromal scores of patients with PRAD in The Cancer Genome Atlas (TCGA) cohort. Validation of differentially expressed genes DLAT and DLD in benign and malignant tissues by immunohistochemistry, and the immune-related genes of DLAT and DLD were further screened. Univariable Cox regression were performed to select key genes. Least absolute shrinkage and selection operator (LASSO)–Cox regression analyse was used to develop a risk model based on the selected genes. The model was validated in the TCGA, Memorial Sloan-Kettering Cancer Center (MSKCC) and Gene Expression Omnibus (GEO) datasets, as well as in this study unit cohort. The genes were examined *via* functional enrichment analysis, and the tumor immune features, tumor mutation features and copy number variations (CNVs) of patients with different risk scores were analysed. The response of patients to multiple chemotherapeutic/targeted drugs was assessed using the pRRophetic algorithm, and immunotherapy was inferred by the Tumor Immune Dysfunction and Exclusion (TIDE) and immunophenoscore (IPS).

Results: Cuproptosis-related immune risk scores (CRIRSs) were developed based on PRLR, DES and LECT2. High CRIRSs indicated poor overall survival (OS), disease-free survival (DFS) in the TCGA-PRAD, MSKCC and GEO datasets and higher T stage and Gleason scores in TCGA-PRAD. Similarly, in the sample collected by the study unit, patients with high CRIRS had higher T-stage and Gleason scores. Additionally, higher CRIRSs were negatively correlated with the abundance of activated B cells, activated $CD8^+$ T cells and other stromal or immune cells. The expression of some immune checkpoints was negatively correlated with CRIRSs. Tumor mutational burden (TMB), mutant-allele tumor

heterogeneity (MATH) and copy number variation (CNV) scores were all higher in the high-CRIRS group. Multiple chemotherapeutic/targeted drugs and immunotherapy had better responsiveness in the low-CRIRS group.

Conclusion: Overall, lower CRIRS indicated better response to treatment strategies and better prognostic outcomes.

KEYWORDS

cuproptosis, PrlR, des, LECT2, prostate cancer

1 Introduction

Prostate adenocarcinoma (PRAD) is a major disease affecting the health of men worldwide and is the second most common malignancy among men (1). In 2020, more than 1.4 million new cases of PRAD were reported worldwide (2). Recent changes in acquired risk factors have led to an increase in the incidence of PRAD in Asian countries (3). Radical prostatectomy (RP) or radiotherapy is the standard treatment for most patients with local PRAD (4). However, biochemical relapse occurs in 30%–50% of patients after treatment (5). Approximately 20% of intermediate-risk patients experience biochemical failure within 18 months of initial local treatment (6, 7). The oncogenic mechanisms underlying PRAD remain unclear, and targeted therapy, especially for high-risk PRAD and castration-resistant prostate cancer (CRPC), remains challenging (8, 9). Therefore, an in-depth understanding of the multiple characteristics of PRAD and the identification of effective prognostic indicators can help to develop more effective treatment strategies for PRAD.

Copper is an indispensable trace element involved in biological processes in eukaryotes, including iron transport, oxygen free radical detoxification and mitochondrial respiration (10). The intracellular copper concentration is in a dynamic gradient-based equilibrium and various cellular processes such as lipolysis, proliferation and autophagy are regulated by this dynamic signal (11–15). Owing to the dysregulation of copper transmembrane transport, intracellular copper accumulation leads to cytotoxicity and cell death (16). Excess copper increases intracellular reactive oxygen species (ROS) levels, induces endoplasmic reticulum stress, enhances damage-related molecular patterns and promotes macrophage phagocytosis (17). Peter et al. identified a novel mechanism by which copper induces cell death: copper directly binds to the lipoacylated components of the tricarboxylic acid (TCA) cycle, leading to toxic protein stress and, eventually, cell death (18). They also identified seven genes positively associated with cupviaroptosis, including FDX1, LIAS, LIPT1, DLD, DLAT, PDHA1 and PDHB. Cuproptosis is a new cell death mechanism that is different from necrosis (19), apoptosis (20), necroptosis (21), autophagy (22), pyroptosis (23), oxeiptosis (24), parthanatos (25) and ferroptosis (26). Copper importers (SCL31A1) and exporters (ATP7A and ATP7B) are key genes that regulate and maintain intracellular copper concentration (18). Mutations in the ATP7A and ATP7B genes can lead to deficiency and accumulation of copper, leading to Menkes and Wilson diseases, respectively. Supplementation or removal of copper represents a novel therapeutic strategy for neurodegenerative diseases (27).

Copper may also play a role in the pathogenesis and progression of cancer (28, 29). Elevated serum copper levels are associated with tumor stage and disease progression in patients with colorectal, lung and breast cancers (30–32). Daily administration of copper sulfate (CuSO4) has been shown to increase tumor growth in a rat model of chemically induced mammary tumors (33). The cuproenzyme LOX is involved in the invasion and metastasis of tumor cells (34). In a mouse model of breast cancer, knockdown of ATP7A reduced LOX activity, decreased the recruitment of bone marrow cells to the lung, and inhibited tumor growth and metastasis (35). Further, it has been reported that patients with high expression of FDX1, SDHB, DLAT and DLST in colorectal cancer tissues have a better prognosis (36). In hepatocellular carcinoma, characteristics based on cuproptosis patterns are important for predicting the tumor microenvironment (TME) and immunotherapy responses (37). Cuproptosis features can also help to predict the prognosis and immune microenvironment of patients with breast cancer (38). Copper chelators can be used as

Abbreviations: AUC, area under the curve; CI, confidence interval; CR-DEG, cuproptosis-related differentially expressed gene; CRIRS, cuproptosis-related immune risk score; CRPC, castration-resistant prostate cancer; CNV, copy number variation; DEG, differentially expressed gene; DFS, disease-free survival; ER, endoplasmic reticulum; FC, fold change; GDSC, Genomics of Drug Sensitivity in Cancer; GEO, Gene Expression Omnibus; GO, Gene Ontology; GSEA, gene set enrichment analysis; HLA, human leukocyte antigens; HR, hazard ratio; ICB, immune checkpoint blockade; IHC, Immunohistochemistry; IRG, immune-related gene; IR-DEG, immune-related differentially expressed gene; IPS, immunophenoscore; KEGG, Kyoto Encyclopedia of Genes and Genomes; LASSO, least absolute shrinkage and selection operator; MAF, mutation annotation format; MATH, mutant-allele tumor heterogeneity; MHC, major histocompatibility complex; MSKCC, Memorial Sloan Kettering Cancer Center; OR, odds ratio; OS, overall survival; PRAD, prostate adenocarcinoma; ROC, receiver operating characteristic; ROS, reactive oxygen species; RT-qPCR, quantitative real-time PCR; ssGSEA, single-sample gene set enrichment analysis; TCA, tricarboxylic acid; TCGA, The Cancer Genome Atlas; TIDE, Tumor Immune Dysfunction and Exclusion; TIP, Tracking Tumor Immunophenotype; TMB, tumor mutation burden; TME, tumor microenvironment; TNM, tumor node metastasis.

antiangiogenic agents to alter the TME (39) and enhance antitumor immunity (40) in various cancers (39). However, the role of cuproptosis in prostate adenocarcinoma (PRAD) remains unclear. An in-depth study on the impact of cuproptosis on the immune landscape of PRAD may help to elucidate the role of cuproptosis in PRAD and identify novel therapeutic targets.

In this study, we clustered and analysed alterations in immune-related genes associated with two subtypes of cuproptosis with different prognostic features. We developed a new metric named 'cuproptosis-related immune risk score' (CRIRS) based on cuproptosis- and immune-related genes to assess the immune characteristics and prognosis of patients with PRAD. Additionally, immune-related components, metabolic characteristics, and gene mutation profiles were analysed in different risk groups, and the results showed significant differences in these aspects between the high- and low-risk groups. The predictive staging model showed great potential to guide the classification of patients with PRAD and predict the chemotherapy and immunotherapy responses of risk-stratified patients. Overall, the model exhibited potential clinical value.

2 Materials and methods

2.1 Data collection

Survival data, clinical information and mRNA expression data, CNV and somatic mutation data for PRAD in the TCGA dataset downloaded from the UCSC-Xena database (https://xenabrowser.net/datapages/). The Memorial Sloan Ketterring Cancer Center (MSKCC)-PRAD database (Cancer Cell 2010, https://www.cbioportal.org/) and Gene Expression Omnibus (GEO) database (GSE70770, https://www.ncbi.nlm.nih.gov/geo/query/acc.cgi?acc=GSE70770) were used as validation sets (Supplementary Table S1). Samples without important clinical or survival data were excluded from further analysis. Immune-related genes were extracted from ImmPort Shared Data (http://www.immport.org). Raw reads were post-processed and normalized using the 'DESeq2' (version 1.38.3) package in the R (version 4.2.0) software.

2.2 Estimation of stromal and immune cells

The CIBERSORT algorithm was used to assess the proportion of immune cell subpopulations in each PRAD sample (41). The single-sample gene set enrichment analysis (ssGSEA) algorithm was used to assess the levels of human leukocyte antigens (HLAs), immune cell infiltration and immune cell function (42). In addition, the proportion of 64 cell types in the TME of patients in TCGA-PRAD cohort was assessed using the xCell algorithm, and elements of TME, including immune, stromal and microenvironment scores, were estimated (43).

2.3 Consensus clustering

To examine the effects of cuproptosis on the immune function of patients with PRAD, the correlation between the expression of cuproptosis-related positive regulators and CIBERSORT results was examined *via* Spearman analysis. The R package 'ConsensusClusterPlus' was used for consensus clustering of tumor samples based on the expression of DLAT and DLD and for visualisation of the results (44). The Kaplan–Meier method and log-rank test were used to compare OS between two clusters.

2.4 Analysis and validation of scRNA data

IMMUcan Database (https://immucanscdb.vital-it.ch/) is a comprehensive tumor microenvironment database platform that mines the single cell characteristics of tumor immune microenvironment based on a large collection and integrated analysis of single cell data (45). To validate the expression of DLAT and DLD in prostate cancer immune cells, the prostate cancer single-cell sequencing dataset GSE141445 was analyzed using the UMAP algorithm in the IMMUcan Database.

2.5 Differentially expressed genes and cuproptosis-related immune scores

Differentially expressed genes (DEGs) in cancerous and paraneoplastic tissues were identified using the 'DESeq2' package in R in TCGA-PRAD cohort, with the threshold set as log2 foldchange (FC) values of ≥1 and FDR < 0.05. Pearson correlation analysis was performed to select DEGs associated with DLAT and DLD (cor > 0.3, $P < 0.05$), named cuproptosis-related DEGs (CR-DEGs). On the other hand, crossover between immune-related genes and DEGs was performed to obtain immune-related DEGs (IR-DEGs); the latter immune-related genes (n = 2,483) were extracted from the Immunology Database and Analysis Portal (ImmPort, https://www.immport.org/) database. The cuproptosis- and immune-related genes are the intersecting genes of CR-DEGs and IR-DEGs (CR-IRGs). The screening process of CR-IRGs is shown in Figure 1. The potential function of these CR-DEGs and CR-IRGs was then determined by Gene Ontology (GO) annotation and Kyoto Encyclopedia of Genes and Genomes (KEGG) enrichment pathway analysis using the "clusterProfiler" package in R. Univariable Cox regression analysis was performed to screen for CR-IRGs related to the prognosis of PRAD ($P < 0.05$). Subsequently, a CR-IRGs signature was constructed *via* least absolute shrinkage and selection operator (LASSO)–Cox regression analysis. The risk score was calculated as follows: Risk score = $\sum Coefi * Expi$, where Coefi represents the coefficients and Expi represents the expression levels of the three key genes.

2.6 Functional enrichment analysis

The 'GSVA' (version 1.30.0) package was used to identify the different pathways associated with cuproptosis-related genes and analyse the relationship between CRIRSs and HALLMARK pathways. Heatmaps were drawn using the 'heatmap' package in R to visualise the results. GSEA was performed for CRIRS-based

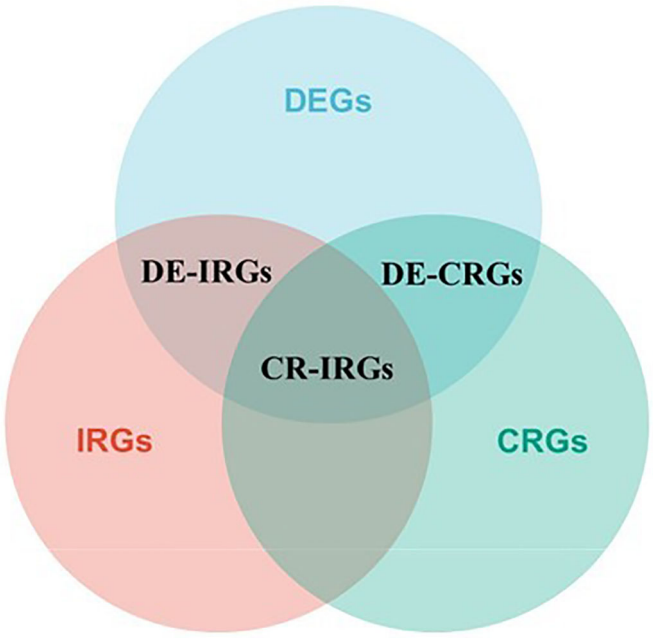

FIGURE 1
Venn diagram of the CR-IRGs screening process.

classification of patients with PRAD. Line plots were drawn using the 'ggplot2' package in R.

2.7 Survival analysis

FPKM method was used to normalize the raw data. Based on the best survival cut-off grouping, we classified patients into high- or low-CRIRS groups. For Kaplan–Meier curves, *P*-values and hazard ratios (HRs) with 95% confidence intervals (CIs) were calculated *via* the log-rank test. HRs of > 1 indicated risk factors, whereas HRs of < 1 indicated protective factors. The R packages 'survival', 'survminer' and 'timeROC' were used for survival analysis. *P*-values of < 0.05 were considered statistically significant. More importantly, 1-year, 3-year and 5-year prognostic values for OS and DFS, survival-dependent subject operating characteristic (ROC) curves and calibration curves were used to evaluate the CRIRS model in the TCGA training set and robustly validated in the MSKCC and GSE70770 cohorts.

2.8 Correlations between CRIRS model and clinical characteristics

A subgroup analysis of the three signature genes in the prognostic profile associated with cuproptosis was performed according to the clinical characteristics of the patients. Next, univariable and multivariable Cox regression analyses were performed to determine the prognostic role of the CRIRS model. The 'forestplot' R package was used to draw a forest plot to demonstrate *P*-values, HRs and 95% CIs for each variable. Then, the association between CRIRSs and each clinical parameter was further analyzed and presented by boxplots and pieTable.

2.9 Quantitative real-time PCR

Total RNA was extracted from paraffin-embedded tissues using a reliable RNA-isolation kit from Thermo Fisher Scientific, USA. The mRNA levels of specific genes, PRLR, DES and LECT2, were measured by qRT-PCR using SYBR green Master MIX from Applied Biosystems, which fluoresces when it binds to double-stranded DNA during the PCR reaction. GAPDH was used as an endogenous control. The primer sequences are presented below: GAPDH: 5'- TGGCCATTATAGGACCGAGACTT -3' (forward) and 5'- CACCCTGTTGCTGTAGCCAAA -3' (reverse); PRLR: 5'- TCTCCACCTACCCTGATTGAC -3' (forward) and 5'- CGAACC TGGACAAGGTATTTCTG -3' (reverse); DES: 5'- TCGGCTCTA AGGGCTCCTC -3' (forward) and 5'- CGTGGTCAGAAACTCCT GGTT -3' (reverse); LECT2: 5'- TGGGCCAGGAGAAACCTTATC -3' (forward) and 5'- CAAGGGCAATAGAGTTCCAAGTT -3' (reverse).

2.10 Immunohistochemistry

Immunohistochemistry (IHC) was utilized to evaluate the protein expression of DLD and DLAT in paraffin sections obtained from patients diagnosed with prostate cancer and benign prostatic hyperplasia. Mouse monoclonal antibodies (Proteintech Group, Inc, Chicago, USA) for DLAT (1: 1000) and DLD (1:500) were used, respectively. All tissue information on the

sections was captured using the Panoramic MIDI (manufacturer: 3D HISTECH).

2.11 Frequency of somatic mutations and copy number variations

The somatic mutation data of TCGA-PRAD cohort were extracted in the varscan file format. CNV data were downloaded from UCSC Xena (https://xenabrowser.net/datapages/). To determine the somatic mutation patterns of patients with PRAD in the high- and low-CRIRS groups, the data were converted into the mutation annotation format (MAF) using the 'maftools' R package. Tumor mutation burden (TMB) and mutant-allele tumor heterogeneity (MATH) scores were also evaluated in both groups.

2.12 Chemotherapy and immunotherapy drug sensitivity

The Genomics of Drug Sensitivity in Cancer (GDSC; https://www.cancerrxgene.org/) database was used to assess the sensitivity of each patient to several chemotherapeutic agents, and the half-maximal inhibitory concentration (IC50) was quantified using the 'pRRophetic' package in R. The response to immune checkpoint blockade therapy (ICB) was predicted using the TIDE score (http://tide.dfci.harvard.edu/login/) and immunophenoscore (IPS) (TCIA, https://tcia.at/patients).

2.13 Statistical analysis

Survival analysis was performed using the R survival package, and the survival rate of each group was evaluated using the log-rank test. Student T test and Wilcoxon test were used to compare data between groups. The Kaplan–Meier method was used to generate survival curves. The chi-square test was used to analyse the association of CRIRS subgroups and clinicopathological parameters. Pearson and Spearman methods were used for correlation analysis. All statistical analyses were performed using the R software. In the analysis of differences between cancerous and paraneoplastic tissues in PRAD, the screening condition was FDR < 0.05 and |log2 FC| > 1. A *P*-value of < 0.05 indicated significant differences in other analyses.

3 Results

3.1 Consensus clustering of patients with PRAD based on cuproptosis-related genes

The analysis flow chart of this study is shown in Figure 2. After excluding primary tumor samples without sufficient survival information, 499 samples were selected for follow-up analysis. To assess whether the expression of cuproptosis regulators affects the immune status of patients with PRAD, the expression of seven cuproptosis regulators, including FDX1, LIAS, LIPT1, DLD, DLAT, PDHA1 and PDHB, was compared among patients, and the immune cell infiltration levels of patients were calculated using the CIBERSORT algorithm. The results were ordered by absolute value of correlation with the ImmuneScore, and the expression of the seven cuproptosis regulators was significantly correlated with the infiltration of immune cells (Figure 3A). The expressions of the three highest correlated regulators with ImmuneScore, PDHB, DLAT and DLD, were compared among 550 samples. PDHB expression was not significantly different in cancerous and paracancerous tissues, and DLAT and DLD were significantly downregulated in cancerous tissues (Figure 3B). To further assess the expression of DLAT and DLD in prostate cancer tissues, we conducted IHC assays. Consistent with the aforementioned findings, our results indicated that DLAT and DLD expression was higher in benign prostatic hyperplasia tissues compared to prostate cancer tissues (Figure 3C). Next, the scRNA data were analyzed using the IMMUcan database to explore the expression of DLAT and DLD in the immune microenvironment of prostate cancer. Figure 4A shows the results of annotating prostate cancer cell types at the immune level. DLAT and DLD are expressed in both tumor cells and different types of stromal and immune cell subsets (Figures 4B, C). In stromal cell subpopulations, DLAT expression was mainly in fibroblasts, pericytes and myofibroblasts (Figure 4D), whereas DLD was mainly expressed in mast cells, NK cells and macrophages (Figure 4E). Subsequently, we selected DLAT and DLD to construct a risk profile and consensus clustering was performed to obtain two cuproptosis-associated clusters (Figures 4F, G). The survival of patients in the two clusters was analysed based on Kaplan–Meier curves. As shown in Figure 4H, patients in Cluster 2 had significantly better OS than patients in Cluster 1 ($P = 0.034$).

3.2 Identification and annotation cuproptosis- related and immune- related PRAD DEGs

To determine the correlation between cuproptosis subtypes and immune function, 2483 IRGs were obtained from the ImmPort database. The 'DESeq2' package was used to identify differentially expressed genes (DEGs) in cancerous and paraneoplastic tissues (FDR < 0.05, |log2 FC| > 1). Further investigation of the relationship between PRAD DEGs and cuproptosis-related genes by Pearson correlation analysis showed 603 cuproptosis-related DEGs (CR-DEGs) (Figure 5A) (Supplementary Table S2). As shown in Figure 5B, 223 immune-related DEGs were screened in PRAD (IR-DEGs) (Supplementary Table S3). By taking the intersection of CR-DEGs and DE-IRGs, we identified 50 cuproptosis- related immune-related DEGs and were therefore referred to as CR-IRGs (Supplementary Table S4). Analysis of the GO and KEGG pathways of CR-DEGs and IR-DEGs showed intriguing results. Some of the pathways most enriched by CR-DEGs are overlapping with pathways associated with the most enriched by IR-DEGs, including Ras signaling pathway, Neuroactive ligand-receptor

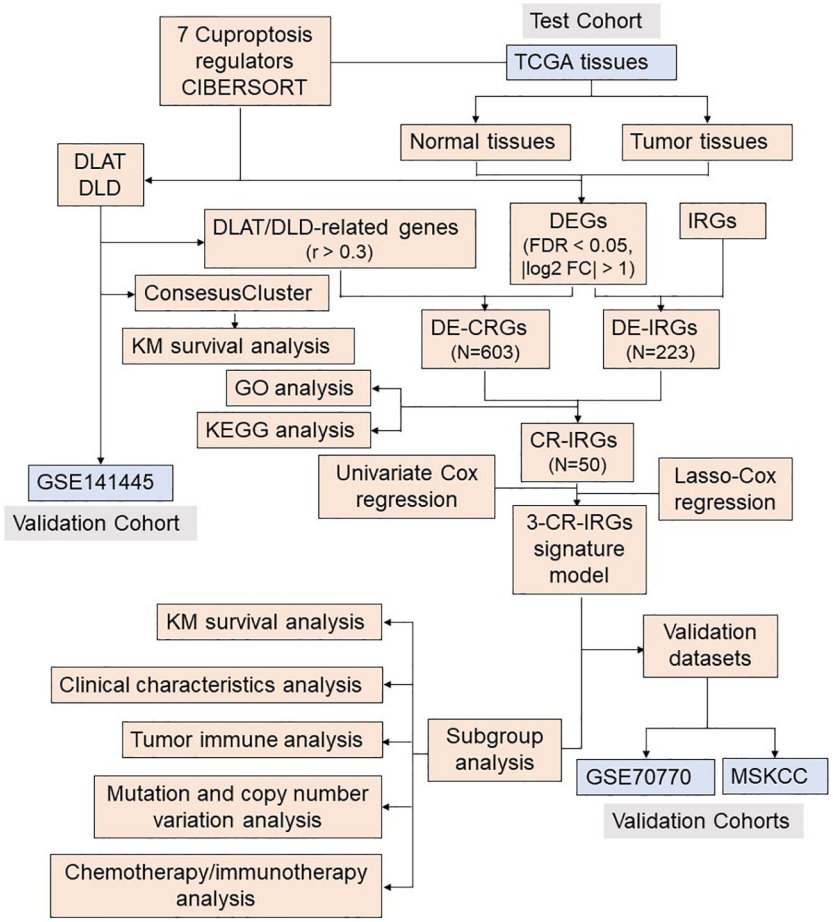

FIGURE 2
Flow chart of the analysis process.

interaction, Regulation of actin cytoskeleton, Calcium signaling pathway and Axon guidance (Figures 5C–F), suggesting that the different cuproptosis states affecting PRAD prognosis may be associated with activation of immune pathways.

3.3 Construction of a prognostic model based on cuproptosis-related immune-related genes in TCGA-PRAD cohort

Based on the expression profiles of the 50 CR-IRGs, 3 significant CR-IRGs were initially screened *via* univariable Cox regression analysis (Supplementary Table S5). Subsequently, a prognostic model based on these genes was established *via* LASSO–Cox regression analysis (Figures 6A–C). Of the 499 patients, 311 patients (about 62%) were included in the high-risk group and 188 patients (about 38%) were included in the low-risk group (Figure 6D). Consistently, Kaplan–Meier curves showed that OS (P = 0.022) and DFS (P = 0.0028) were significantly worse in the high-CRIRS group than in the low-CRIRS group (Figures 6E, H). The OS and DFS predictive performance of the CRIRSs was assessed based on time-dependent ROC curves, and the area under the curve (AUC) values at 1, 3 and 5 years were 1.000, 0.666 and 0.698, and 0.631, 0.619 and 0.594, respectively (Figures 6F, I). The calibration curve shows that CRIRSs may accurately estimate the OS and DFS (Figures 6G, J). CRIRSs are calculated in the MSKCC and GSE70770 cohorts and validated by taking the same grouping approach as the TCGA-PRAD cohort (Figures 6K, O). Patients with lower CRIRSs had longer DFS in both MSKCC (P = 0.029) and GSE70770 (P = 0.035) cohorts (Figures 6L, P). Therefore, CRIRS was identified as a strong predictor of DFS, with AUC values of 0.687, 0.646 and 0.642 in MSKCC cohort and 0.573, 0.547 and 0.512 in the GSE70770 cohort at 1, 3 and 5 years, respectively (Figures 6M, Q). The calibration curves further validate the accurate predictive performance of CRIRSs for DFS (Figures 6N, R). These results illustrate the strong efficacy of the CRIRS model to predict the prognosis of prostate cancer.

3.4 Validation of the independent prognostic value of the 3-immune-gene signature

Figure 7A illustrates the expression of PRLR and LECT2 was higher and that of DES was lower in the high-CRIRS group. Univariable and multivariable Cox regression analyses based on

10.3389/fimmu.2023.1181370

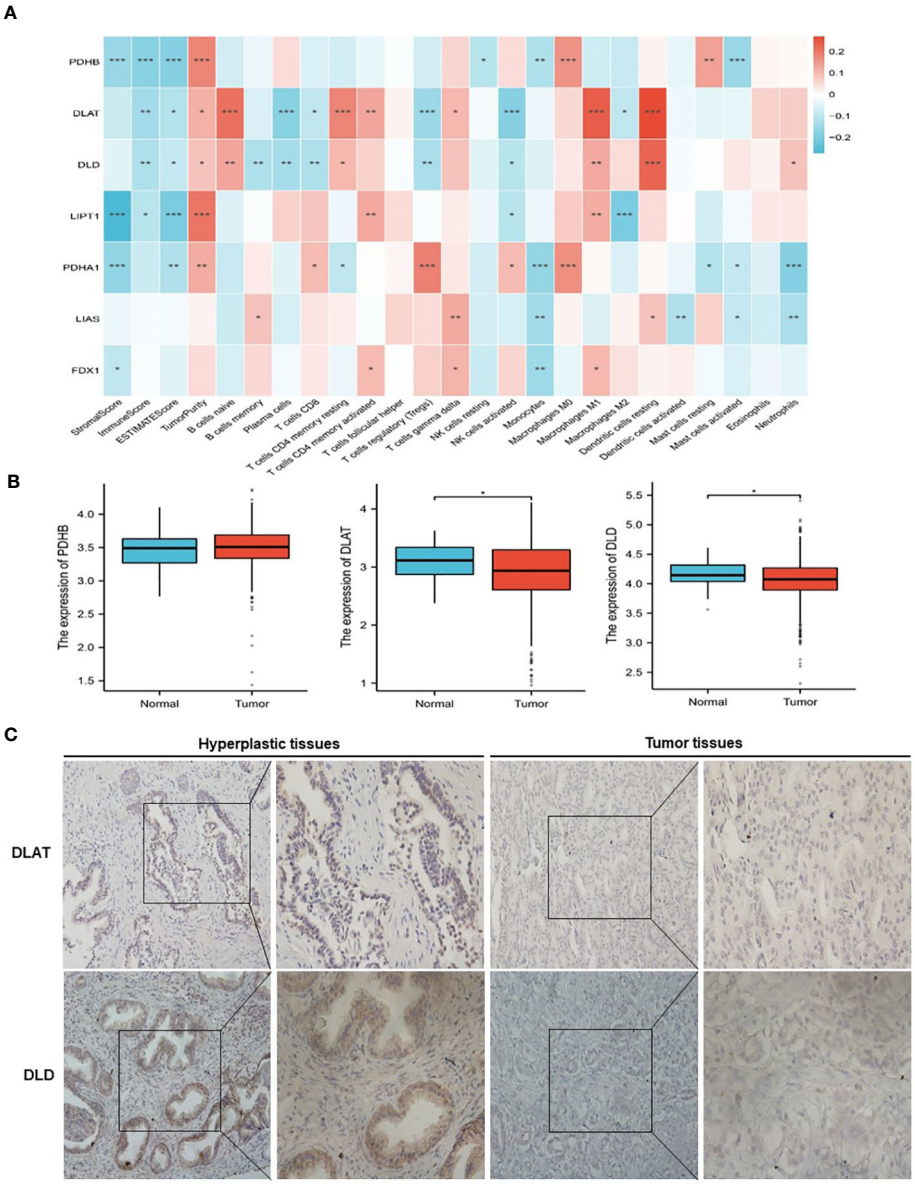

FIGURE 3
Classification of patients with PRAD in TCGA cohort according to the expression of DLAT and DLD. **(A)** Association of cuproptosis-related genes with the results of CIBERSORT. **(B)** Comparison of the expression of PDHB, DLAT and DLD between normal and PRAD tissues. **(C)** The protein levels of DLAT and DLD in prostate hyperplasia and prostate cancer clinical tissues were examined by immunohistochemistry. *$P < 0.05$, **$P < 0.01$, ***$P < 0.001$.

age, TNM stage, Gleason scores and CRIRSs revealed that the CRIRS was an independent prognostic factor for OS (Figure 7B). Additionally, To investigate whether CRIRS model correlated with the clinical characteristics of PRAD, we performed the Wilcoxon test and found that the high-CRIRS group had a later T stage (P = 0.0058) (Figure 7D), N stage (P = 0.014) (Figure 7E) and higher Gleason scores (P = 5.2e-05) (Figure 7G). However, age (Figure 7C) and M stage (Figure 7F) did not significantly differ between the two groups. The pieTable further demonstrates the significant correlation of CRIRSs with T stage (P = 0.0064) and Gleason scores (P = 0.0024) (Figure 7H). Additionally, we obtained 32 prostate cancer tissue samples to conduct correlation analysis between CRIRS and clinical parameters. The mRNA levels of PRLR, DES, and LECT2 were determined by qRT-PCR, while CRIRS was calculated using a specific formula. Results showed that in prostate cancer patients, CRIRS was positively correlated with their T stage (P = 0.033) and Gleason score (P = 0.025). However, no significant correlation was found between CRIRS and patients' age and clinical stage ($P > 0.05$) (Table 1).

3.5 Metabolic characteristics of patients classified based on CRIRSs

Cuproptosis is associated with multiple cancer pathways (46). HALLMARK enrichment analysis showed that pathways related to

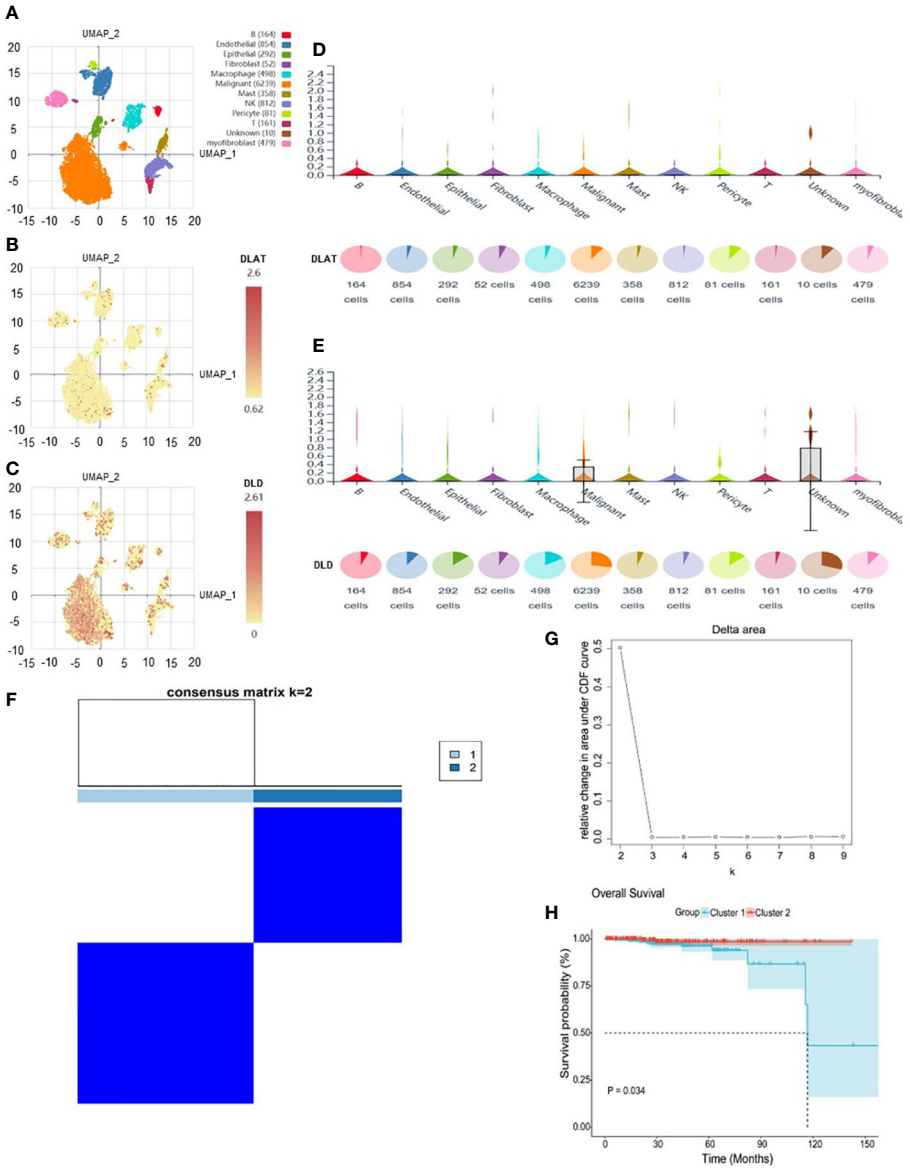

FIGURE 4
The expression of DLAT and DLD in immune cells in the GSE141445 dataset. **(A)** UMAP diagram of 13 samples. **(B, C)** UMAP distribution diagram showed the relative expression of DLAT and DLD in each cell. **(D, E)** Violin diagram showed the relative expression of DLAT and DLD in 8 types of cells. **(F, G)** Consensus matrix heat map defining two clusters (k = 2) and their correlation area. **(H)** Kaplan–Meier curves of overall survival in the two clusters.

tumor growth and invasion, such as mTORC1 signaling (47), PI3K/Akt/mTOR signaling (47), G2M checkpoint and Myc signaling (48) were significantly enriched in the high-CRIRS group (Figure 8A). Additionally, various immune activities, including complement, IL2/STAT5 signaling and IL6/Jak/STAT3 signaling, as well as metabolic pathways, such as spermatogenesis, myogenesis, and xenobiotic metabolism, were significantly enriched in the low-CRIRS group (Figure 8A). These findings explain, to some extent, the better prognosis of the low group. Subsequently, to further validate the function of the CRIRS model in terms of immunity, we performed GSEA pathway enrichment analysis and found six immune-related gene sets enriched in the high-CRIRS group, including Early T Lymphocyte Up, Large To Small Pre Bii Lymphocyte Up, IL6 Deprivation Dn, Immunature B Lymphocyte Dn and Pre Bii Lymphocyte Up. Three other immune-related pathways Innate Immune System, Blebbishield To Immune Cell Fusion Pbshms Dn and Silenced By Tumor Microenvironment were enriched in the low-CRIRS group (Figure 8B). Due to the complexity of enrichment of immune-related gene sets between the two CRIRS groups, we need further in-depth assessment of the immune status of the CRIRS model.

3.6 Correlation Between CRIRSs and the Tumor Microenvironment of PRAD

Several studies have shown that patients with higher immune scores and lower stromal scores have a better prognosis (49, 50).

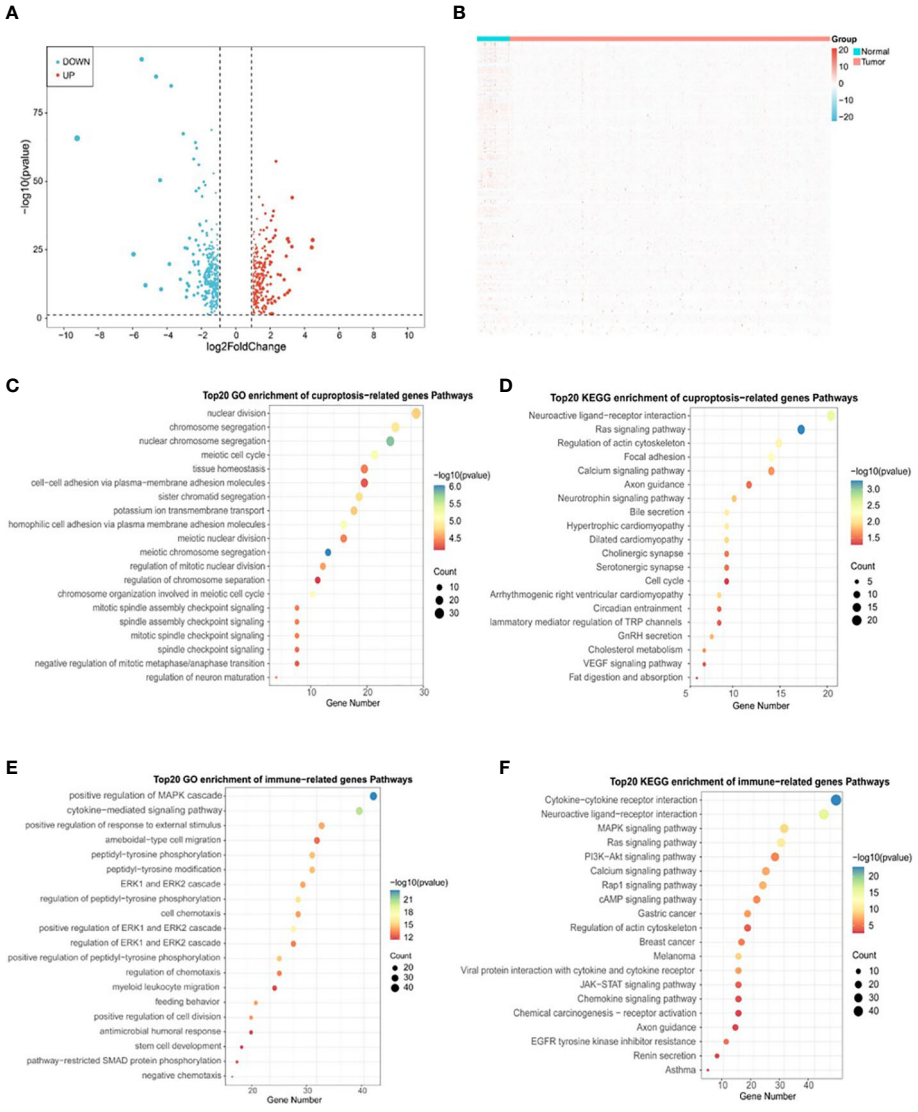

FIGURE 5
Identification of DLAT and DLD-related immune genes in TCGA-PRAD cohort. **(A)** Volcano plot of cuproptosis-related DEGs between normal and tumor tissues in TCGA-PRAD cohort. **(B)** Heatmap plot of immune-related DEGs between normal and tumor tissues in TCGA-PRAD cohort. **(C)** Top 20 terms for GO analysis of cuproptosis genes DLAT and DLD-related DEGs. **(D)** Top 20 pathways for KEGG analysis of cuproptosis genes DLAT and DLD-related DEGs. **(E)** Top 20 terms for GO analysis of immune-related DEGs. **(F)** Top 20 pathways for KEGG analysis of immune-related DEGs.

However, the low-CRIRS group with a better prognosis had higher stromal scores and lower immune scores, and no significant differences in immune microenvironment scores were observed between the low and high CRIRS groups in our study (Figures 9A–C). It has been showed that the density of infiltration of different immune cells in the center and invasive margins of tumors has different predictive significance for tumor prognosis and outcome due to the different immune structures of different tumors (51). This was also demonstrated in a study by Sun et al., kidney renal clear cell carcinoma patients who had a worse prognosis had higher immune scores and stromal scores (52). The relationship between CRIRSs and 64 types of adaptive and congenital immune cells, haematopoietic progenitor cells, epithelial cells and extracellular stromal cells was examined using the xCell algorithm. The proportion of multiple cell types was significantly different between the high- and low-CRIRS groups (Figure 9D). The proportion of multiple stromal cells including adipocytes, fibroblasts, lymphatic (ly) endothelial cells, and microvascular (mv) endothelial cells was high in the low-CRIRS group, whereas that of stem cells, such as hematopoietic stem cells (HSCs), megakaryocytes and megakaryocyte-erythroid progenitors (MEPs), and lymphoids NKT cells were also in higher proportions in the low-CRIRS group. Additionally, the proportion of a variety of lymphoids, such as B cells, CD4+ memory T cells, CD8+ Tcm, Th2 cells and Tregs, and some myeloids including Basophils and Mast cells, were highly represented in the high-CRIRS group. The ssGSEA analysis further demonstrates the infiltration of immune cells in two CRIRS groups. As shown in Figure 9E, activated B cells, activated CD8 T cells, CD56bright natural killer cells, CD56dim natural killer cells and natural killer cells was high in

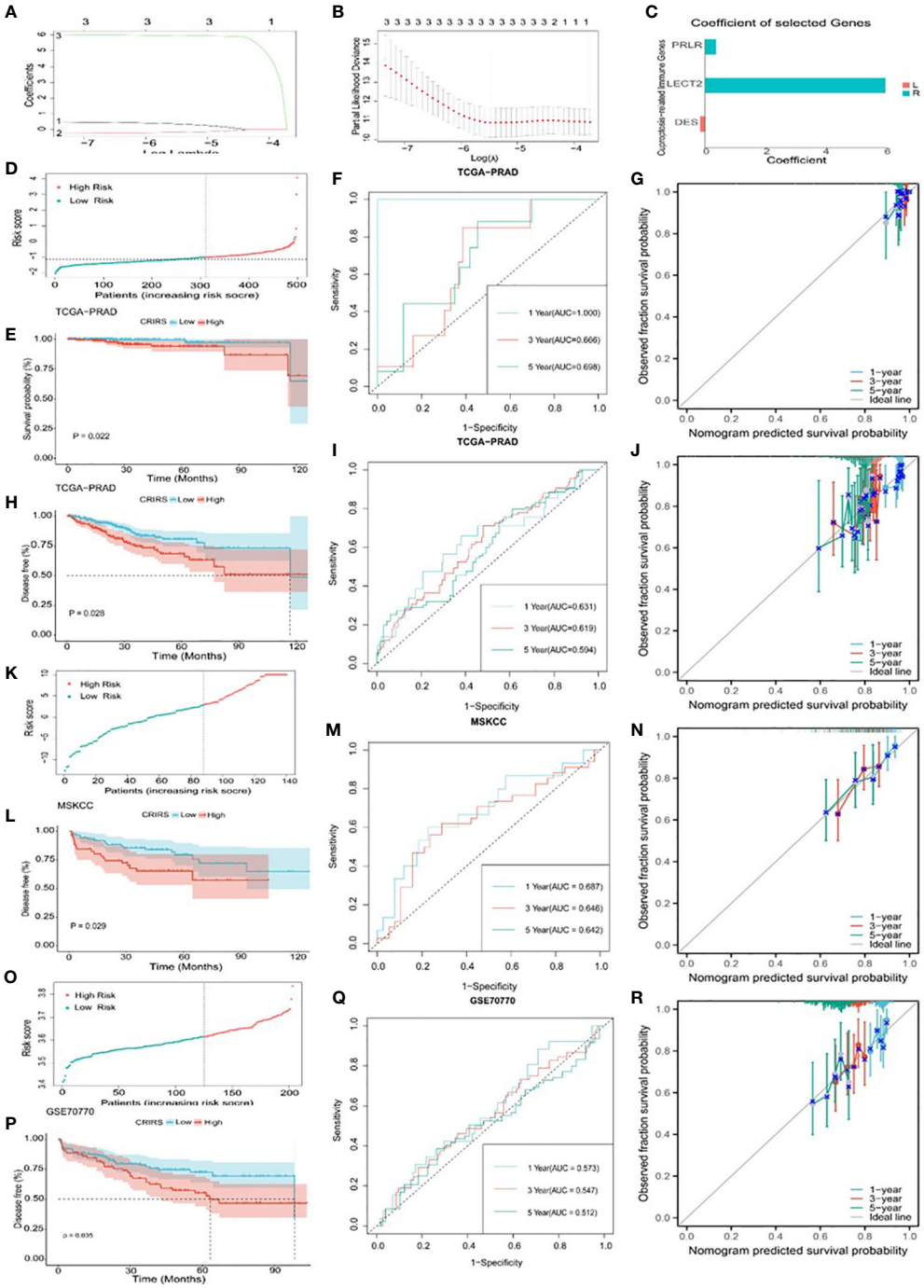

FIGURE 6
Construction and validation of a cuproptosis-related-IRG-based prognostic signature in TCGA-PRAD cohort. **(A, B)** DE-IRGs screened using a LASSO−Cox regression model. **(C)** Coefficients of three selected genes PRLR, LECT2, DES. **(D-J)** Construction of TCGA-PRAD training cohort. **(D)** Distribution and cut-off values of CRIRSs of TCGA training cohort. **(E)** OS of two CRIRS groups of TCGA-PRAD cohort. **(F)** ROC curves demonstrating the prognostic value of the CRIRS model in predicting 1-, 3- and 5-year OS in TCGA. **(G)** Calibration curves for CRIRS model of TCGA-PRAD cohort. y-axis: actual OS; x-axis: nomogram-predicted OS. **(H)** DFS of two CRIRS groups of TCGA-PRAD cohort. **(I)** ROC curves demonstrating the prognostic value of the CRIRS model in predicting 1-, 3- and 5-year DFS in TCGA. **(J)** Calibration curves for CRIRS model of TCGA-PRAD cohort. y-axis: actual DFS; x-axis: nomogram-predicted DFS. **(K-N)** Construction of MSKCC validation cohort. **(K)** Distribution and cut-off values of CRIRSs of MSKCC validation cohort. **(L)** DFS of two CRIRS groups of MSKCC cohort. **(M)** ROC curves demonstrating the prognostic value of the CRIRS model in predicting 1-, 3- and 5-year DFS in MSKCC. **(N)** Calibration curves for CRIRS model of MSKCC cohort. y-axis: actual DFS; x-axis: nomogram-predicted DFS. **(O-R)** Construction of GSE70770 validation cohort. **(O)** Distribution and cut-off values of CRIRSs of GSE70770 validation cohort. **(P)** DFS of two CRIRS groups of GSE70770 cohort. **(Q)** ROC curves demonstrating the prognostic value of the CRIRS model in predicting 1-, 3- and 5-year DFS in GSE70770. **(R)** Calibration curves for CRIRS model of GSE70770 cohort. y-axis: actual DFS; x-axis: nomogram-predicted DFS.

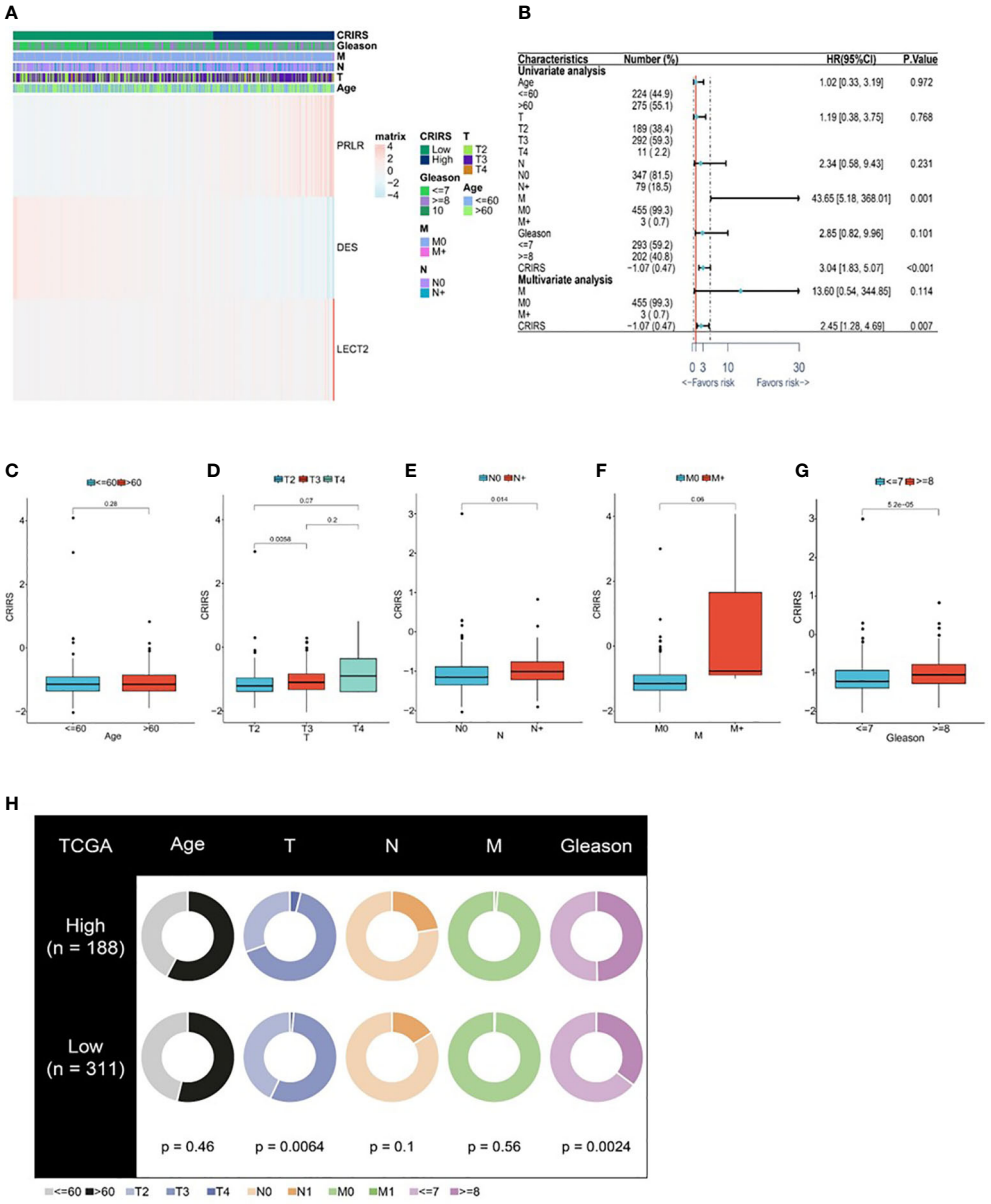

FIGURE 7
Correlation between CRIRS model and clinical characteristics based on TCGA-PRAD cohort. **(A)** Differences in clinicopathological features and expression levels of PRLR, LECT2 and DES between the low- and high-CRIRS groups. **(B)** Results of univariable and multivariable Cox regression analyses for predicting OS. Differences in CRIRS levels by age **(C)**, T stage **(D)**, N stage **(E)**, M stage **(F)**, and Gleason score **(G)** grouping. **(H)** Clinical characteristics of the high- and low-CRIRS groups.

the low-CRIRS group, whereas that of activated CD4 T cells, memory B cells, neutrophils, regulatory T cells and type 2 T helper cells was high in the high-CRIRS group. The activity status of the seven-step tumor–immunity cycle of patients with PRAD was determined using the Tracking Tumor Immunophenotype (TIP) (http://biocc.hrbmu.edu.cn/TIP/) and visualised on a thermogram. Consistent with the above results, CRIRSs were negatively correlated with multiple step tumor–immunity cycle, especially in Step 4 (trafficking of immune cells to tumors) (Figure 9F). All three types of immune checkpoints, major histocompatibility complex (MHC), immunoinhibitors and immunostimulators, were highly expressed in the low-CRIRS group, especially HLA-A, HLA-B, LAG3, LGALS9, CD40 and CTLA (Figures 9G–I). These results reveal the reasons for the better prognosis in the low-CRIRS group.

3.7 Mutation landscape of patients classified based on CRIRSs

TMB and CNV in tumor patients correlate with prognosis (53). The mutation profile of patients stratified based on CRIRSs was examined. Higher TMB and MATH scores were observed in the high-CRIRS group (Figures 10A, B). The mutation profiles of patients were different between the two groups. As shown in Figures 10C, D,

TABLE 1 Association of CRIRS with clinicopathological parameters in prostate cancer patients.

Characteristics	CRIRS (Low)(%)	CRIRS (High) (%)	*P*
n	20	12	
Age			0.399
≤ 60	3(15.0)	3(25.0)	
> 60	17(85.0)	9(75.0)	
T stage			**0.033**
T2	13(65.0)	3(25.0)	
T3	7(35.0)	9(75.0)	
Stage			0.227
II	9(45.0)	5(41.7)	
III-V	11(55.0)	7(58.3)	
Gleason Score			**0.025**
≤ 7	15(75.0)	4(33.3)	
≥ 8	5(25.0)	8(66.7)	

Bold values means $P < 0.05$.

the top 5 genes with the highest mutation frequency were tumor protein P53 (TP53; 9%); titin (TTN; 8%); speckle-type BTB/POZ protein (SPOP; 7%); mucin 16, cell surface associated (MUC16; 7%) and titin-interacting RhoGEF (OBSCN; 6%) in the low-CRIRS group and TTN (18%); SPOP (17%); TP53 (11%); MUC16 (8%) and spectrin repeat containing nuclear envelope protein 1 (SYNE1; 8%) in the high-CRIRS group. TTN mutations were found in 34 patients in the high-CRIRS group and 24 patients in the low-CRIRS group (odds ratio [OR] = 0.374, $P < 0.01$, Figure 10E). The mutation frequency of HTR1E was high in the low-CRIRS group ($P < 0.05$), whereas mutation frequencies in 53 genes including SPOP, ADGRE2 and KIRREL were higher in the high-CRIRS group ($P < 0.05$, Figure 10E). Co-mutation relationships were observed between multiple genes and the five genes with the highest mutation frequencies: TTN mutations were related to FAT4, FLG, OBSCN and SYNE1 mutations; SPOP mutations were related to USH2A and FOXA1 mutations, TP53 mutations were related to FOXA1 mutations; MUC16 mutations were related to FOXA1 and HMCN1 mutations; and SYNE1 mutations were related to FLG, FOXA1, ABCA13 and FAT3 (Figure 10F). Given that CNVs may lead to chromosomal alterations, we further investigated the relationship between CRIRSs and CNVs. The frequency of CNV amplification and deletion was significantly high in the high-CRIRS group (Figures 11A–C). Figure 11D shows the topography of CNVs in the high- and low-risk groups. More genes had CNV amplification and deletion in the high-CRIRS group than in the low-CRIRS group.

3.8 Predicting the sensitivity of patients to antitumor therapy

The IC50 values of several chemotherapeutic agents commonly used in the treatment of PRAD were evaluated to predict the response of patients with different CRIRSs to antitumor therapy. The IC50 values of Camptothecin ($P = 0.00623$) (Figure 12A), Dactolisib ($P = 1.8e-07$) (Figure 12B), Epirubicin ($P = 0.0016$) (Figure 12C), Gemcitabine ($P = 6.4e-05$) (Figure 12D), Irinotecan ($P = 3.8e-05$) (Figure 12E), Mitoxantrone ($P = 3.5e-06$) (Figure 12F), Niraparib ($P = 0.0013$) (Figure 12G) and Oxaliplatin ($P = 0.027$) (Figure 12H) were significantly higher in the high-CRIRS group than in the low-CRIRS group. In addition, TIDE analysis showed that CRIRS was significantly and negatively correlated with TIDE, Dysfunction and Exclusion scores (Figure 12I). However, IPS scores were higher in the low-CRIRS group, indicating a better response to immunotherapy in the low-CRIRS group (Figure 12J).

4 Discussion

Unbalanced copper homeostasis can affect tumor growth and induce tumor cell death (54). Copper also plays an integral role in tumor immunity and antitumor therapy (55, 56). Cuproptosis plays a complex regulatory role in the TME of various cancers such as endometrial and colorectal cancers. However, its role in the development of TME and its potential therapeutic value in PRAD remain unclear. Multiple risk models based on cuproptosis-associated genes can accurately predict prognosis and assess the tumor microenvironment (57, 58). Zhu et al. reported that the three cuproptosis patterns they constructed in colorectal cancer were consistent with the results of immune infiltration characteristics (59).

In this study, we proposed a cuproptosis-related immune scoring system to assess individual immune profiles. Immune regulation was analyzed based on transcriptional changes and the expression of cuproptosis-related genes in TCGA-PRAD cohort. The cuproptosis genes DLAT and DLD were found to be closely

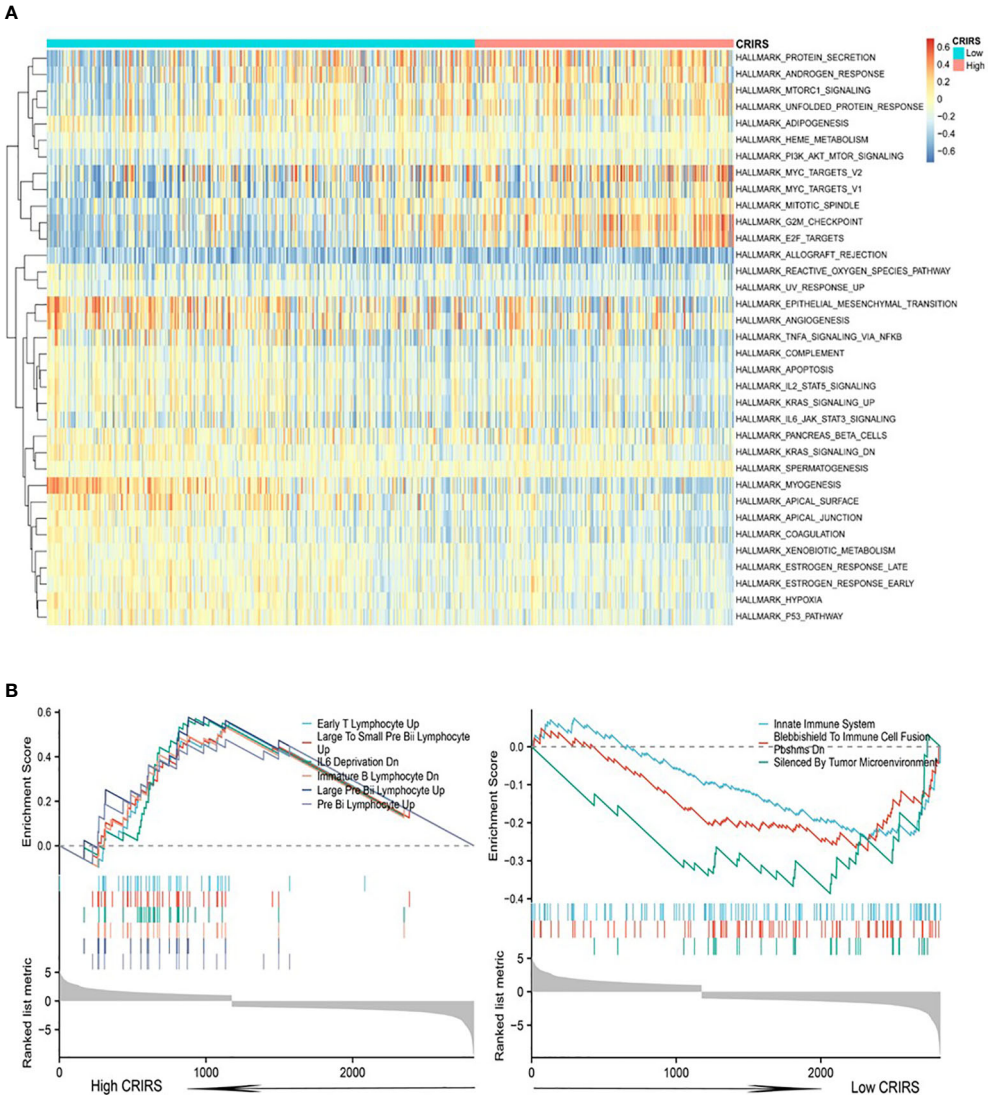

FIGURE 8
Enrichment analysis in the two CRIRS groups. **(A)** Analysis of multiple HALLMARK pathways *via* GSVA in the two CRIRS groups. **(B)** Immune-related pathways for GSEA enrichment analysis in two CRIRS groups.

associated with PRAD. An unsupervised clustering approach was used to divide TCGA-PRAD cohort into two differentially characterized cuproptosis clusters based on the expression of DLAT and DLD. Prognosis was significantly different between the two groups. Based on cuproptosis-related IRGs, three genes associated with different clinical outcomes, immune activity and immune function were identified, namely, PRLR, DES and LECT2. These three genes play an important role in tumor immunity. It has been reported that PRLR might affect the prognosis of breast cancer by inhibiting the expression of immune checkpoints (60). Liu et al. demonstrated that TP53-associated immune prognostic model (TIPM) including PRLR predicts overall survival and treatment response in pancreatic cancer (61). Absence of Reed-Sternberg cell DES and cytokeratin expression in Hodgkin's disease with Ki-1 antigen expression may be associated with dysregulation of the immune system and the observed immunological abnormalities (62). Pouyanfard et al. demonstrated that treatment of liver fibrosis with a population of human iPSC-derived M2 subtype macrophages in an immunodeficient Rag2 γc mouse model significantly reduced the expression of fibrotic genes, including DES (63). LECT2 deficiency fosters the accumulation of pejorative inflammatory monocytes harboring immunosuppressive properties and strong tumor-promoting potential in hepatocellular carcinoma (64). Qin et al. reported that LECT2 expression was low in hepatocellular carcinoma and negatively correlated with the infiltration of immune cells such as B cells, neutrophils and monocytes and positively correlated with naïve CD8 T cells, endothelial cells and hematopoietic stem cells (65).

The CRIRS system was established *via* LOSSO–Cox regression analysis. High CRIRSs were associated with shorter OS and DFS.

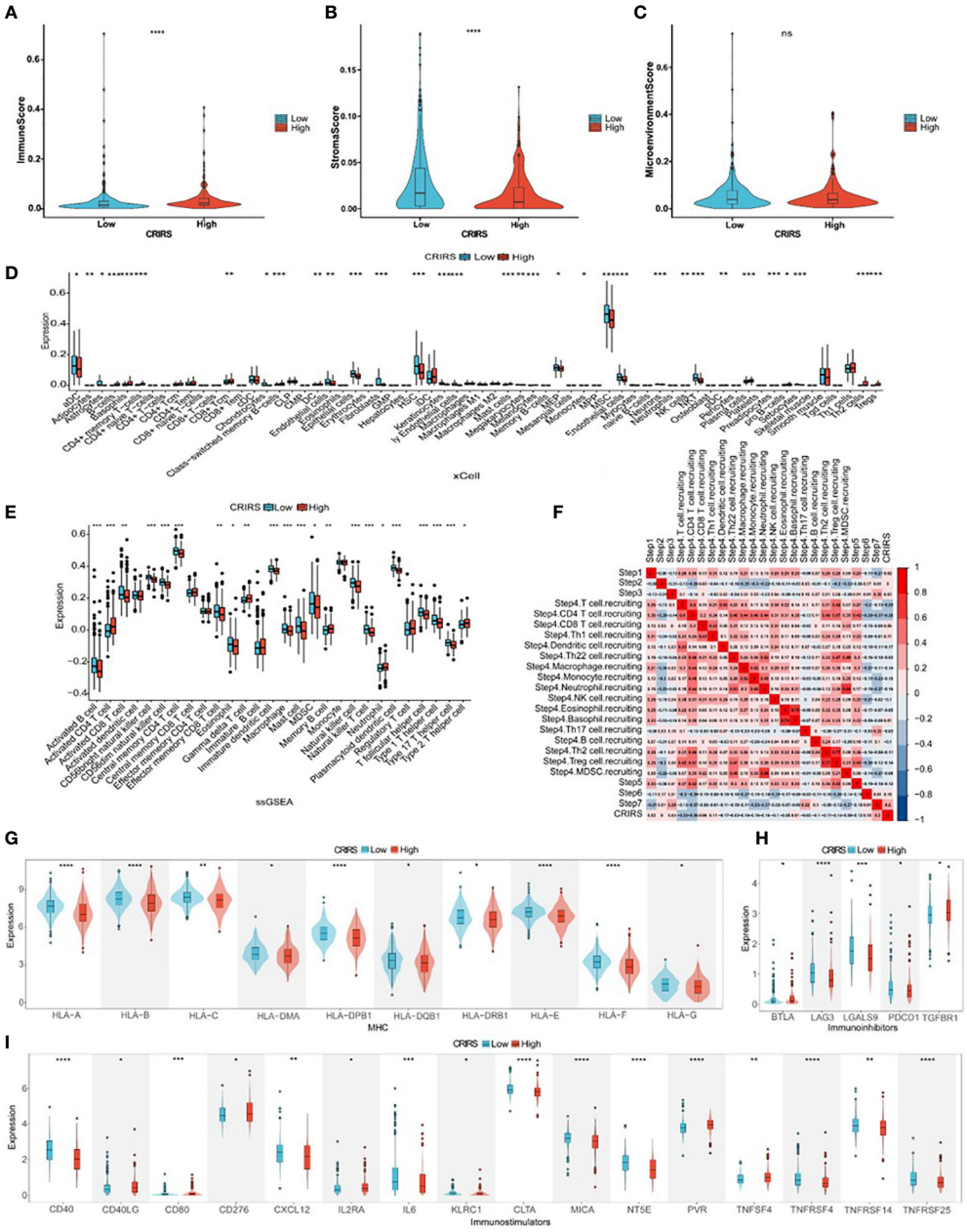

FIGURE 9
Comparison of immune activity in the two CRIRS groups. **(A-C)** Immune, stromal and microenvironment scores in the two CRIRS subtypes. **(D)** Different infiltration levels of 64 immune and stromal cells in the two CRIRS groups analysed using the xCell algorithm. **(E)** ssGSEA showed differences in the infiltration of immune cells between the two CRIRS groups. **(F)** Heatmap demonstrating correlation between seven key steps in the tumor immune cycle and CRIRSs. Differential expression of different types of immunomodulatory molecules MHC **(G)**, immunoinhibitors **(H)** and immunostimulators **(I)** in the two CRIRS groups. *$P < 0.05$, **$P < 0.01$, ***$P < 0.001$, ****$P < 0.0001$.

GSEA revealed that multiple cancer-related pathways were significantly enriched in the high-CRIRS group, suggesting that the three cuproptosis-associated IRGs are involved in tumor development. CRIRSs were significantly correlated with the clinicopathological features of PRAD, such as T stage and Gleason scores. After controlling for confounding factors, CRIRS was identified as an independent predictor of survival outcomes in PRAD. ROC curves and Calibration curves demonstrated that CRIRSs had good accuracy in predicting OS and DFS at 1, 3 and 5 years. Therefore, CRIRSs may serve as an effective tool to predict the prognosis of PRAD. Significant differences were observed in the frequency of gene mutations between the high- and low-CRIRS groups. Multiple genes had higher mutation frequencies in the high-CRIRS group. CNVs are one of the most important somatic

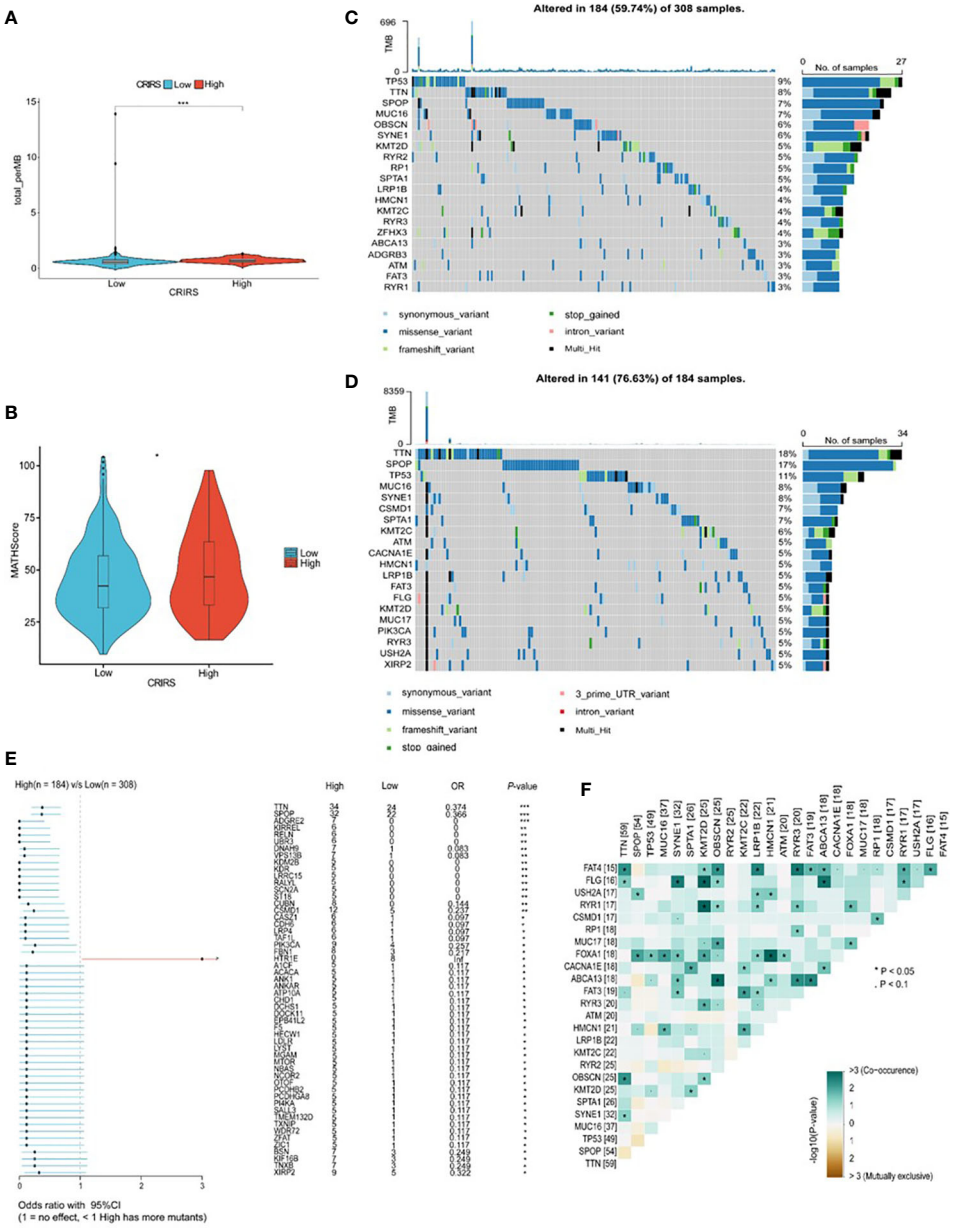

FIGURE 10
Genetic characteristics in the two CRIRS groups. **(A)** The distribution of TMB scores in the two CRIRS groups. **(B)** The distribution of MATH scores in the two CRIRS groups. **(C, D)** Waterfall plot of mutations in the top 20 genes in the low-CRIRS group top and high-CRIRS group bottom. **(E)** Forest plots demonstrating the frequency of 54 mutations that differed significantly between the two CRIRS groups. Higher mutation frequencies were found in the high-CRIRS group. **(F)** Heatmap demonstrating the commonality of mutations in the top 25 genes in PRAD. $^{*}P < 0.05$, $^{***}P < 0.001$.

aberrations in cancer, which contribute to the pathogenesis of many disease phenotypes. In this study, the frequency of CNV amplification and deletion was high in the high-CRIRS group.

The immune response plays a dominant role in tumorigenesis and can often serve as the target of tumor therapy. Immune and stromal cells are major components of TME (66). Our study found that the CIBERSORT algorithm showed zero abundance of T cell CD4 naive infiltration, probably because CIBERSORT calculated the relative proportions of immune cell subpopulations in tumor tissues instead of the actual values (67). Immune cell infiltration is associated with the prognosis of PRAD, and high infiltration levels of $CD8^+$ T cells and NK cells may indicate a good prognosis, which is consistent with the results of this study (68–70). Therefore, cuproptosis may be involved in regulating TME, especially $CD8^+$ T cells and NK cells, thereby promoting tumor growth and progression. Previous studies have reported that reactivation of

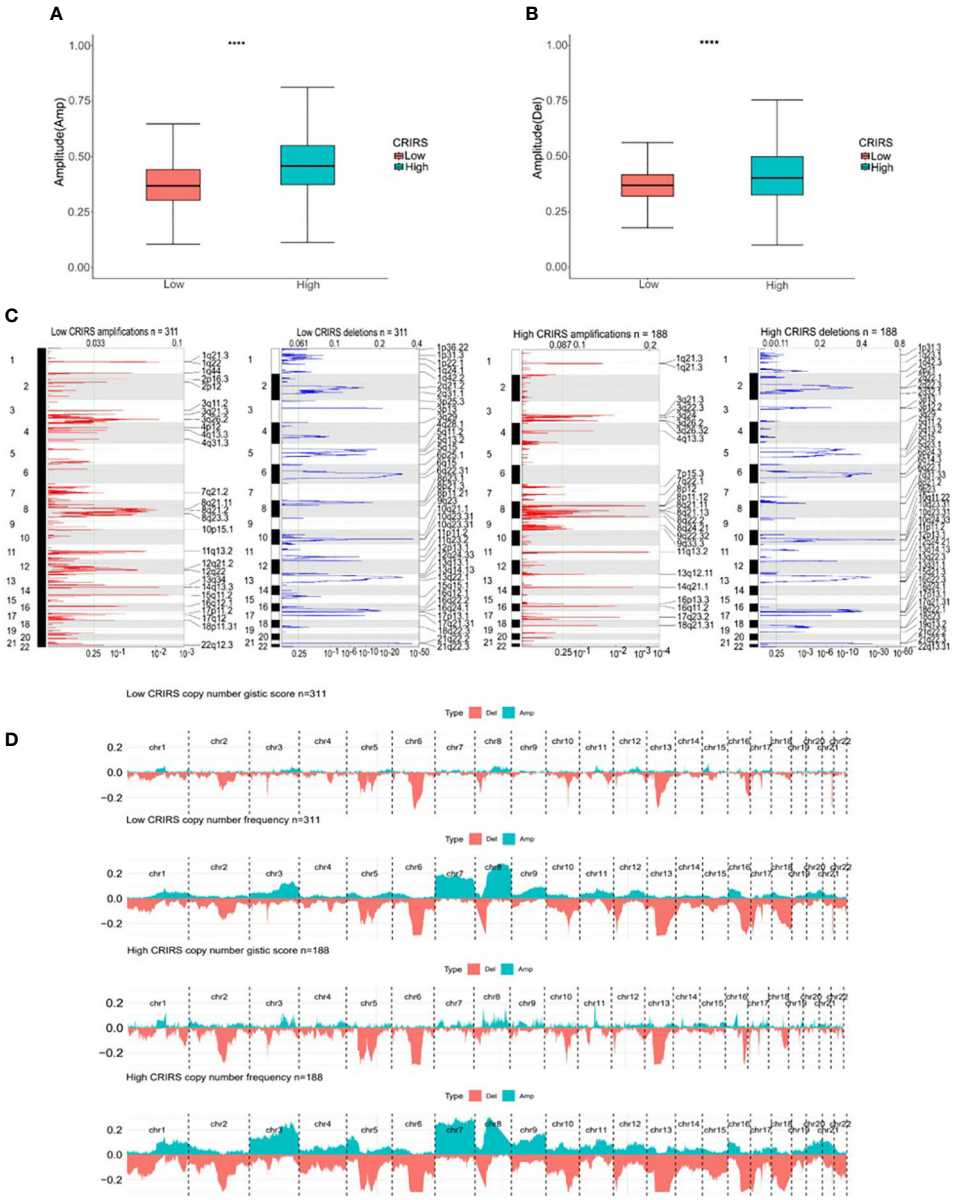

FIGURE 11
Genomic mutation profiles in the two CRIRS groups. **(A, B)** Box plot demonstrating the amplitudes of all chromosome amplifications/deletions in the two CRIRS groups. **(C)** Focal amplification/deletion of different chromosomal regions in the two CRIRS groups. **(D)** CNVs in the two CRIRS groups, including the logistic scores and mutation frequencies corresponding to different CNVs. ****$P < 0.0001$.

CD8+ T cells can indicate the efficacy of immunotherapy. Therefore, targeting cuproptosis-related IRGs may be an effective and novel therapeutic strategy for the treatment of PRAD.

Chemotherapy and androgen deprivation therapy may limit tumor progression and improve the prognosis of patients with PRAD (71, 72). At present, the decreasing sensitivity of PRAD to chemotherapy is a major concern worldwide (73). The 'cold' tumor characteristics of PRAD inhibit the development of immunotherapeutic strategies that can optimize treatment by driving T cells into the tumor and transforming the 'cold' TME into an immune 'hot' TME (74). In this study, patients in low-CRIRS groups were potentially sensitive to several therapeutic drugs, which may help to mitigate resistance mechanisms and improve clinical outcomes. To investigate whether CRIRSs can help to predict the efficiency of immunotherapy in PRAD, the correlation between CRIRSs and 31 immune checkpoint genes was examined. The vast majority of these genes were highly expressed in the low-CRIRS group. The TIDE algorithm and IPS scores

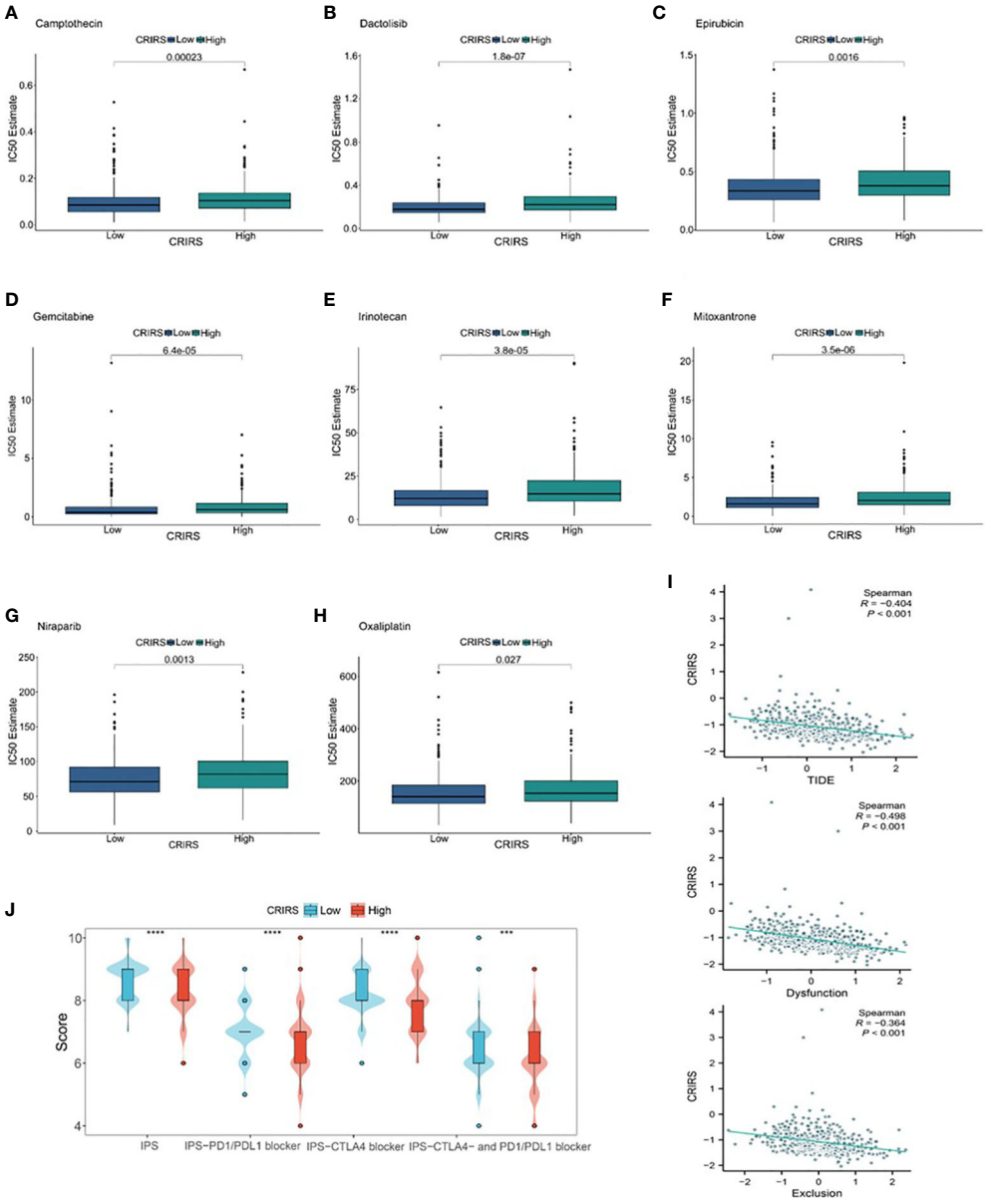

FIGURE 12
Assessment of chemotherapy and immunotherapy responses in the two CRIRS groups. **(A–H)** The response of patients to eight common chemotherapeutic drugs in the high- and low-CRIRS groups. **(I–J)** Immunotherapy response prediction in the two CRIRS groups. ***$P < 0.001$, ****$P < 0.0001$.

were used to predict the ICB responses of patients with the low-CRIRS group with higher IPS predicted a better response to immunotherapy.

This study has some limitations. First, individual differences among patients with PRAD might have affected the cuproptosis-associated IRG-based prognostic signature, and more external and practical validation is required to determine whether the signature can be used in clinical practice. In addition, we have only limited knowledge of the signalling pathways related to the three cuproptosis-associated IRGs identified in this study, and the specific molecular mechanisms of these genes in PRAD and their relationship with TME and cuproptosis remain unknown. The role of these genes in PRAD should be examined *in vivo* and *in vitro* in future studies using the results of GSEA as a reference.

Data availability statement

The datasets used in this study TCGA-PRAD (https://portal.gdc.cancer.gov/) were accessed online on September 30, 2022, MSKCC (https://www.cbioportal.org/) GSE70770 (https://www.ncbi.nlm.nih.gov/geo/query/acc.cgi?acc=GSE70770) and GSE141445 (https://www.ncbi.nlm.nih.gov/geo/query/acc.cgi) were accessed online on December 17, 2022.

Author contributions

KY participated in the study conception, data analysis and visualization. RZ performed data collection and visualization. LL and ML participated in data analysis, SF and HY analyzed the data and prepared the manuscript. ZZ participated in data analysis and manuscript revision. DX contributed to study design and writing. All authors contributed to the article and approved the submitted version.

Funding

This work was supported in part by grants from the Anhui Medical University Translational Medicine Program (2021zhyxC58), Anhui Provincial Natural Science Foundation (2108085MH261), University Natural Science Research Project of Anhui Province (KJ2021A0318).

Acknowledgments

We thank Bullet Edits Limited for the linguistic editing and proofreading of the manuscript.

Conflict of interest

The authors declare that the research was conducted in the absence of any commercial or financial relationships that could be construed as a potential conflict of interest.

Publisher's note

Supplementary material

The Supplementary Material for this article can be found online at: https://www.frontiersin.org/articles/10.3389/fimmu.2023.1181370/full#supplementary-material

References

1. Nguyen-Nielsen M, Borre M. Diagnostic and therapeutic strategies for prostate cancer. *Semin Nucl Med* (2016) 46(6):484–90. doi: 10.1053/j.semnuclmed.2016.07.002

2. Gandaglia G, Leni R, Bray F, Fleshner N, Freedland SJ, Kibel A, et al. Epidemiology and prevention of prostate cancer. *Eur Urol Oncol* (2021) 4(6):877–92. doi: 10.1016/j.euo.2021.09.006

3. Kimura T, Egawa S. Epidemiology of prostate cancer in Asian countries. *Int J Urol* (2018) 25(6):524–31. doi: 10.1111/iju.13593

4. Siegel RL, Miller KD, Jemal A. Cancer statistics, 2017. *CA Cancer J Clin* (2017) 67 (1):7–30. doi: 10.3322/caac.21387

5. Lalonde E, Ishkanian AS, Sykes J, Fraser M, Ross-Adams H, Erho N, et al. Tumour genomic and microenvironmental heterogeneity for integrated prediction of 5-year biochemical recurrence of prostate cancer: a retrospective cohort study. *Lancet Oncol* (2014) 15(13):1521–32. doi: 10.1016/S1470-2045(14)71021-6

6. Shao YH, Demissie K, Shih W, Mehta AR, Stein MN, Roberts CB, et al. Contemporary risk profile of prostate cancer in the United States. *J Natl Cancer Inst* (2009) 101(18):1280–3. doi: 10.1093/jnci/djp262

7. Nichol AM, Warde P, Bristow RG. Optimal treatment of intermediate-risk prostate carcinoma with radiotherapy: clinical and translational issues. *Cancer* (2005) 104(5):891–905. doi: 10.1002/cncr.21257

8. Xie L, Li J, Wang X. Updates in prostate cancer detections and treatments - Messages from 2017 EAU and AUA. *Asian J Urol* (2018) 5(1):3–7. doi: 10.1016/j.ajur.2017.11.004

9. Li J, Xie H, Ying Y, Chen H, Yan H, He L, et al. YTHDF2 mediates the mRNA degradation of the tumor suppressors to induce AKT phosphorylation in N6-methyladenosine-dependent way in prostate cancer. *Mol Cancer* (2020) 19(1):152. doi: 10.1186/s12943-020-01267-6

10. Ruiz LM, Libedinsky A, Elorza AA. Role of copper on mitochondrial function and metabolism. *Front Mol Biosci* (2021) 8:711227. doi: 10.3389/fmolb.2021.711227

11. Krishnamoorthy L, Cotruvo JA Jr., Chan J, Kaluarachchi H, Muchenditsi A, Pendyala VS, et al. Copper regulates cyclic-AMP-dependent lipolysis. *Nat Chem Biol* (2016) 12(8):586–92. doi: 10.1038/nchembio.2098

12. Brady DC, Crowe MS, Turski ML, Hobbs GA, Yao X, Chaikuad A, et al. Copper is required for oncogenic BRAF signalling and tumorigenesis. *Nature* (2014) 509 (7501):492–6. doi: 10.1038/nature13180

13. Dodani SC, Firl A, Chan J, Nam CI, Aron AT, Onak CS, et al. Copper is an endogenous modulator of neural circuit spontaneous activity. *Proc Natl Acad Sci USA* (2014) 111(46):16280–5. doi: 10.1073/pnas.1409796111

14. Turski ML, Brady DC, Kim HJ, Kim BE, Nose Y, Counter CM, et al. A novel role for copper in Ras/mitogen-activated protein kinase signaling. *Mol Cell Biol* (2012) 32 (7):1284–95. doi: 10.1128/MCB.05722-11

15. Tsang T, Posimo JM, Gudiel AA, Cicchini M, Feldser DM, Brady DC. Copper is an essential regulator of the autophagic kinases ULK1/2 to drive lung adenocarcinoma. *Nat Cell Biol* (2020) 22(4):412–24. doi: 10.1038/s41556-020-0481-4

16. Gul NS, Khan TM, Chen M, Huang KB, Hou C, Choudhary MI, et al. New copper complexes inducing bimodal death through apoptosis and autophagy in A549 cancer cells. *J Inorg Biochem* (2020) 213:111260. doi: 10.1016/j.jinorgbio.2020.111260

17. Kaur P, Johnson A, Northcote-Smith J, Lu C, Suntharalingam K. Immunogenic cell death of breast cancer stem cells induced by an endoplasmic reticulum-targeting copper(II) complex. *Chembiochem* (2020) 21(24):3618–24. doi: 10.1002/cbic.202000553

18. Tsvetkov P, Coy S, Petrova B, Dreishpoon M, Verma A, Abdusamad M, et al. Copper induces cell death by targeting lipoylated TCA cycle proteins. *Science* (2022) 375(6586):1254–61. doi: 10.1126/science.abf0529

19. Ning L, Zhao W, Gao H, Wu Y. Hesperidin induces anticancer effects on human prostate cancer cells *via* ROS-mediated necrosis like cell death. *J BUON* (2020) 25 (6):2629–34.

20. Torrealba N, Rodriguez-Berriguete G, Vera R, Fraile B, Olmedilla G, Martinez-Onsurbe P, et al. Homeostasis: apoptosis and cell cycle in normal and pathological prostate. *Aging Male* (2020) 23(5):335–45. doi: 10.1080/13685538.2018.1470233

21. Beretta GL, Zaffaroni N. Necroptosis and prostate cancer: molecular mechanisms and therapeutic potential. *Cells* (2022) 11(7):1221. doi: 10.3390/cells11071221

22. Lin JZ, Wang WW, Hu TT, Zhu GY, Li LN, Zhang CY, et al. FOXM1 contributes to docetaxel resistance in castration-resistant prostate cancer by inducing AMPK/mTOR-mediated autophagy. *Cancer Lett* (2020) 469:481–89. doi: 10.1016/j.canlet.2019.11.014

23. Xi H, Zhang Y, Xu Y, Yang WY, Jiang X, Sha X, et al. Caspase-1 inflammasome activation mediates homocysteine-induced pyrop-apoptosis in endothelial cells. *Circ Res* (2016) 118(10):1525–39. doi: 10.1161/CIRCRESAHA.116.308501

24. Zhang J, Gao RF, Li J, Yu KD, Bi KX. Alloimperatorin activates apoptosis, ferroptosis, and oxeiptosis to inhibit the growth and invasion of breast cancer cells in vitro. *Biochem Cell Biol* (2022) 100(3):213–22. doi: 10.1139/bcb-2021-0399

25. Robinson N, Ganesan R, Hegedus C, Kovacs K, Kufer TA, Virag L. Programmed necrotic cell death of macrophages: Focus on pyroptosis, necroptosis, and parthanatos. *Redox Biol* (2019) 26:101239. doi: 10.1016/j.redox.2019.101239

26. Zaffaroni N, Beretta GL. Ferroptosis inducers for prostate cancer therapy. *Curr Med Chem* (2022) 29(24):4185–201. doi: 10.2174/0929867329666220111120924

27. Gromadzka G, Tarnacka B, Flaga A, Adamczyk A. Copper dyshomeostasis in neurodegenerative diseases-therapeutic implications. *Int J Mol Sci* (2020) 21(23):9259. doi: 10.3390/ijms21239259

28. Babak MV, Ahn D. Modulation of intracellular copper levels as the mechanism of action of anticancer copper complexes: clinical relevance. *Biomedicines* (2021) 9 (8):852. doi: 10.3390/biomedicines9080852

29. Shanbhag VC, Gudekar N, Jasmer K, Papageorgiou C, Singh K, Petris MJ. Copper metabolism as a unique vulnerability in cancer. *Biochim Biophys Acta Mol Cell Res* (2021) 1868(2):118893. doi: 10.1016/j.bbamcr.2020.118893

30. Gupta SK, Shukla VK, Vaidya MP, Roy SK, Gupta S. Serum and tissue trace elements in colorectal cancer. *J Surg Oncol* (1993) 52(3):172–5. doi: 10.1002/jso.2930520311

31. Diez M, Arroyo M, Cerdan FJ, Munoz M, Martin MA, Balibrea JL. Serum and tissue trace metal levels in lung cancer. *Oncology* (1989) 46(4):230–4. doi: 10.1159/000226722

32. Sharma K, Mittal DK, Kesarwani RC, Kamboj VP, Chowdhery. Diagnostic and prognostic significance of serum and tissue trace elements in breast malignancy. *Indian J Med Sci* (1994) 48(10):227–32.

33. Skrajnowska D, Bobrowska-Korczak B, Tokarz A, Bialek S, Jezierska E, Makowska J. Copper and resveratrol attenuates serum catalase, glutathione peroxidase, and element values in rats with DMBA-induced mammary carcinogenesis. *Biol Trace Elem Res* (2013) 156(1-3):271–8. doi: 10.1007/s12011-013-9854-x

34. Erler JT, Bennewith KL, Cox TR, Lang G, Bird D, Koong A, et al. Hypoxia-induced lysyl oxidase is a critical mediator of bone marrow cell recruitment to form the premetastatic niche. *Cancer Cell* (2009) 15(1):35–44. doi: 10.1016/j.ccr.2008.11.012

35. Shanbhag V, Jasmer-McDonald K, Zhu S, Martin AL, Gudekar N, Khan A, et al. ATP7A delivers copper to the lysyl oxidase family of enzymes and promotes tumorigenesis and metastasis. *Proc Natl Acad Sci USA* (2019) 116(14):6836–41. doi: 10.1073/pnas.1817473116

36. Yang W, Wang Y, Huang Y, Yu J, Wang T, Li C, et al. 4-Octyl itaconate inhibits aerobic glycolysis by targeting GAPDH to promote cuproptosis in colorectal cancer. *BioMed Pharmacother* (2023) 159:114301. doi: 10.1016/j.biopha.2023.114301

37. Zhang Z, Zeng X, Wu Y, Liu Y, Zhang X, Song Z. Cuproptosis-related risk score predicts prognosis and characterizes the tumor microenvironment in hepatocellular carcinoma. *Front Immunol* (2022) 13:925618. doi: 10.3389/fimmu.2022.925618

38. Li J, Wu F, Li C, Sun S, Feng C, Wu H, et al. The cuproptosis-related signature predicts prognosis and indicates immune microenvironment in breast cancer. *Front Genet* (2022) 13:977322. doi: 10.3389/fgene.2022.977322

39. Chan N, Willis A, Kornhauser N, Ward MM, Lee SB, Nackos E, et al. Influencing the tumor microenvironment: A phase II study of copper depletion using tetrathiomolybdate in patients with breast cancer at high risk for recurrence and in preclinical models of lung metastases. *Clin Cancer Res* (2017) 23(3):666–76. doi: 10.1158/1078-0432.CCR-16-1326

40. Voli F, Valli E, Lerra L, Kimpton K, Saletta F, Giorgi FM, et al. Intratumoral copper modulates PD-L1 expression and influences tumor immune evasion. *Cancer Res* (2020) 80(19):4129–44. doi: 10.1158/0008-5472.CAN-20-0471

41. Newman AM, Liu CL, Green MR, Gentles AJ, Feng W, Xu Y, et al. Robust enumeration of cell subsets from tissue expression profiles. *Nat Methods* (2015) 12 (5):453–7. doi: 10.1038/nmeth.3337

42. Rooney MS, Shukla SA, Wu CJ, Getz G, Hacohen N. Molecular and genetic properties of tumors associated with local immune cytolytic activity. *Cell* (2015) 160(1-2):48–61. doi: 10.1016/j.cell.2014.12.033

43. Aran D, Hu Z, Butte AJ. xCell: digitally portraying the tissue cellular heterogeneity landscape. *Genome Biol* (2017) 18(1):220. doi: 10.1186/s13059-017-1349-1

44. Wilkerson MD, Hayes DN. ConsensusClusterPlus: a class discovery tool with confidence assessments and item tracking. *Bioinformatics* (2010) 26(12):1572–3. doi: 10.1093/bioinformatics/btq170

45. Camps J, Noel F, Liechti R, Massenet-Regad L, Rigade S, Gotz L, et al. Meta-analysis of human cancer single-cell RNA-seq datasets using the IMMUcan database. *Cancer Res* (2023) 83(3):363–73. doi: 10.1158/0008-5472.CAN-22-0074

46. Zhang C, Zeng Y, Guo X, Shen H, Zhang J, Wang K, et al. Pan-cancer analyses confirmed the cuproptosis-related gene FDX1 as an immunotherapy predictor and prognostic biomarker. *Front Genet* (2022) 13:923737. doi: 10.3389/fgene.2022.923737

47. Yi J, Zhu J, Wu J, Thompson CB, Jiang X. Oncogenic activation of PI3K-AKT-mTOR signaling suppresses ferroptosis *via* SREBP-mediated lipogenesis. *Proc Natl Acad Sci USA* (2020) 117(49):31189–97. doi: 10.1073/pnas.2017152117

48. Wu MJ, Chen CJ, Lin TY, Liu YY, Tseng LL, Cheng ML, et al. Targeting KDM4B that coactivates c-Myc-regulated metabolism to suppress tumor growth in castration-resistant prostate cancer. *Theranostics* (2021) 11(16):7779–96. doi: 10.7150/thno.58729

49. Song Q, Zhou R, Shu F, Fu W. Cuproptosis scoring system to predict the clinical outcome and immune response in bladder cancer. *Front Immunol* (2022) 13:958368. doi: 10.3389/fimmu.2022.958368

50. Lyu F, Li Y, Yan Z, He Q, Cheng L, Zhang P, et al. Identification of ISG15 and ZFP36 as novel hypoxia- and immune-related gene signatures contributing to a new perspective for the treatment of prostate cancer by bioinformatics and experimental verification. *J Transl Med* (2022) 20(1):202. doi: 10.1186/s12967-022-03398-4

51. Li Y, Ding J, Wang H, Xu J. Research progress of immunoscore in prediction of tumor prognosis and efficacy to treatment. *Cancer Res Prev Treat* (2021) 48 (8):809–13.

52. Sun Z, Tao W, Guo X, Jing C, Zhang M, Wang Z, et al. Construction of a lactate-related prognostic signature for predicting prognosis, tumor microenvironment, and immune response in kidney renal clear cell carcinoma. *Front Immunol* (2022) 13:818984. doi: 10.3389/fimmu.2022.818984

53. Zhou H, Hu Y, Luo R, Zhao Y, Pan H, Ji L, et al. Multi-region exome sequencing reveals the intratumoral heterogeneity of surgically resected small cell lung cancer. *Nat Commun* (2021) 12(1):5431. doi: 10.1038/s41467-021-25787-x

54. Jiang Y, Huo Z, Qi X, Zuo T, Wu Z. Copper-induced tumor cell death mechanisms and antitumor theragnostic applications of copper complexes. *Nanomedicine (Lond)* (2022) 17(5):303–24. doi: 10.2217/nnm-2021-0374

55. Percival SS. Copper and immunity. *Am J Clin Nutr* (1998) 67(5 Suppl):1064S–68S. doi: 10.1093/ajcn/67.5.1064S

56. Prajapati N, Karan A, Khezerlou E, DeCoster MA. The immunomodulatory potential of copper and silver based self-assembled metal organic biohybrids nanomaterials in cancer theranostics. *Front Chem* (2020) 8:629835. doi: 10.3389/fchem.2020.629835

57. Chen J, Wang G, Luo X, Zhang J, Zhang Y. Cuproptosis patterns and tumor microenvironment in endometrial cancer. *Front Genet* (2022) 13:1001374. doi: 10.3389/fgene.2022.1001374

58. Shan J, Geng R, Zhang Y, Wei J, Liu J, Bai J. Identification of cuproptosis-related subtypes, establishment of a prognostic model and tumor immune landscape in endometrial carcinoma. *Comput Biol Med* (2022) 149:105988. doi: 10.1016/j.compbiomed.2022.105988

59. Zhu ZL, Zhao QY, Song W, Weng JY, Li SB, Guo TA, et al. A novel cuproptosis-related molecular pattern and its tumor microenvironment characterization in colorectal cancer. *Front Immunol* (2022) 13:940774. doi: 10.3389/fimmu.2022.940774

60. Qin J, Sun W, Zhang H, Wu Z, Shen J, Wang W, et al. Prognostic value of LECT2 and relevance to immune infiltration in hepatocellular carcinoma. *Front Genet* (2022) 13:951077. doi: 10.3389/fgene.2022.951077

61. Schneider AK, Chevalier MF, Derre L. The multifaceted immune regulation of bladder cancer. *Nat Rev Urol* (2019) 16(10):613–30. doi: 10.1038/s41585-019-0226-y

62. Liang J, Deng Y, Zhang Y, Wu B, Zhou J. PRLR and CACNA2D1 impact the prognosis of breast cancer by regulating tumor immunity. *J Pers Med* (2022) 12 (12):2086. doi: 10.3390/jpm12122086

63. Liu Y, Cheng L, Song X, Li C, Zhang J, Wang L. A TP53-associated immune prognostic signature for the prediction of the overall survival and therapeutic responses in pancreatic cancer. *Math Biosci Eng* (2022) 19(1):191–208. doi: 10.3934/mbe.2022010

64. Zoltowska A. Immunohistochemical comparative investigations of lymphatic tissue in reactive processes, myasthenic thymuses and Hodgkin's disease. *Arch Immunol Ther Exp (Warsz)* (1995) 43(1):15–22.

65. Pouyanfard S, Meshgin N, Cruz LS, Diggle K, Hashemi H, Pham TV, et al. Human induced pluripotent stem cell-derived macrophages ameliorate liver fibrosis. *Stem Cells* (2021) 39(12):1701–17. doi: 10.1002/stem.3449

66. L'Hermitte A, Pham S, Cadoux M, Couchy G, Caruso S, Anson M, et al. Lect2 controls inflammatory monocytes to constrain the growth and progression of hepatocellular carcinoma. *Hepatology* (2019) 69(1):160–78. doi: 10.1002/hep.30140

67. Hu P, Gao Y, Huang Y, Zhao Y, Yan H, Zhang J, et al. Gene expression-based immune cell infiltration analyses of prostate cancer and their associations with survival outcome. *DNA Cell Biol* (2020) 39(7):1194–204. doi: 10.1089/dna.2020.5371

68. Wang L, Saci A, Szabo PM, Chasalow SD, Castillo-Martin M, Domingo-Domenech J, et al. EMT- and stroma-related gene expression and resistance to PD-1 blockade in urothelial cancer. *Nat Commun* (2018) 9(1):3503. doi: 10.1038/s41467-018-05992-x

69. Han HS, Jeong S, Kim H, Kim HD, Kim AR, Kwon M, et al. TOX-expressing terminally exhausted tumor-infiltrating CD8(+) T cells are reinvigorated by co-blockade of PD-1 and TIGIT in bladder cancer. *Cancer Lett* (2021) 499:137–47. doi: 10.1016/j.canlet.2020.11.035

70. Shimasaki N, Jain A, Campana D. NK cells for cancer immunotherapy. *Nat Rev Drug Discovery* (2020) 19(3):200–18. doi: 10.1038/s41573-019-0052-1

71. Nader R, El Amm J, Aragon-Ching JB. Role of chemotherapy in prostate cancer. *Asian J Androl* (2018) 20(3):221–29. doi: 10.4103/aja.aja_40_17

72. Desai K, McManus JM, Sharifi N. Hormonal therapy for prostate cancer. *Endocr Rev* (2021) 42(3):354–73. doi: 10.1210/endrev/bnab002

73. Galletti G, Leach BI, Lam L, Tagawa ST. Mechanisms of resistance to systemic therapy in metastatic castration-resistant prostate cancer. *Cancer Treat Rev* (2017) 57:16–27. doi: 10.1016/j.ctrv.2017.04.008

74. Bilusic M, Madan RA, Gulley JL. Immunotherapy of prostate cancer: facts and hopes. *Clin Cancer Res* (2017) 23(22):6764–70. doi: 10.1158/1078

frontiers | Frontiers in Cell and Developmental Biology

TYPE Original Research
PUBLISHED 07 August 2023
DOI 10.3389/fcell.2023.1180625

OPEN ACCESS

EDITED BY
Lin-Lin Bu,
Wuhan University, China

REVIEWED BY
Chih-Yang Wang,
Taipei Medical University, Taiwan
Jinghang Li,
The University of Chicago, United States

*CORRESPONDENCE
Yu-Jun Dai,
daiyj@sysucc.org.cn

†These authors have contributed equally to this work

RECEIVED 06 March 2023
ACCEPTED 28 July 2023
PUBLISHED 07 August 2023

CITATION
Shao R-N, Bai K-H, Huang Q-Q, Chen S-L, Huang X and Dai Y-J (2023), A novel prognostic prediction model of cuprotosis-related genes signature in hepatocellular carcinoma.
Front. Cell Dev. Biol. 11:1180625.
doi: 10.3389/fcell.2023.1180625

A novel prognostic prediction model of cuprotosis-related genes signature in hepatocellular carcinoma

Ruo-Nan Shao[1,2†], Kun-Hao Bai[1,3†], Qian-Qian Huang[1,2†], Si-Liang Chen[4†], Xin Huang[1,5] and Yu-Jun Dai[1,2*]

[1]State Key Laboratory of Oncology in South China, Collaborative Innovation Center for Cancer Medicine, Guangzhou, China, [2]Department of Hematologic Oncology, Sun Yat-sen University Cancer Center, Guangzhou, China, [3]Department of Endoscopy, Sun Yat-sen University Cancer Center, Guangzhou, China, [4]Department of Hematology, Peking University Shenzhen Hospital, Shenzhen, China, [5]Department of Pancreatobiliary Surgery, Sun Yat-sen University Cancer Center, Guangzhou, China

Background: Cuprotosis is a recently discovered copper-dependent cell death mechanism that relies on mitochondrial respiration. However, the role of cuprotosis-related genes (**CRGs**) in hepatocellular carcinoma (**HCC**) and their prognostic significances remain unknown.

Methods: Based on the recently published **CRGs**, the LASSO Cox regression analysis was applied to construct a **CRGs** risk model using the gene expression data from the International Cancer Genome Consortium as a training set, followed by validation with datasets from The Cancer Genome Atlas and the Gene Expression Omnibus (GSE14520). Functional enrichment analysis of the **CRGs** was performed by single-sample gene set enrichment analysis.

Results: Five of the 13 previously published **CRGs** were identified to be associated with prognosis in HCC. Kaplan-Meier analysis suggested that patients with high-risk scores have a shorter overall survival time than patients with low-risk scores. ROC curves indicated that the average **AUC** was more than 0.7, even at 4 years, and at least 0.5 at 5 years. Moreover, addition of this **CRG** risk score can significantly improve the efficiency of predicting overall survival compared to using traditional factors alone. Functional analysis demonstrated increased presence of Treg cells in patients with high-risk scores, suggesting a suppressed immune state in these patients. Finally, we point to the possibility that novel immunotherapies such as inhibitors of *PDCD1, TIGIT, IDO1, CD274, CTLA4,* and *LAG3* may have potential benefits in high-risk patients.

Conclusion: We constructed a better prognostic model for liver cancer by using **CRGs**. The **CRG** risk score established in this study can serve as a potentially valuable tool for predicting clinical outcome of patients with **HCC**.

KEYWORDS

cuprotosis (CRGs), prognostic model, hepatocellular carcinoma (HCC), treg cells, immunotherapy

Background

Multicellular organisms have a variety of predetermined and precisely programmed cell death pathways, such as apoptosis, necroptosis (programmed necrosis), pyroptosis (inflammation mediated), and ferroptosis (iron regulated cell death) (Yan et al., 2022). Recent research reported a novel mechanism known as cuprotosis where cell death is regulated by copper. This mechanisms can be triggered by copper ions even when other common cell death pathways are blocked (Tang et al., 2022). Copper ions directly bind to fatty acylated components of the tricarboxylic acid (**TCA**) cycle within the mitochondria, leading to aggregation of fatty acylated proteins and downregulation of iron-sulfur cluster proteins, which induces proteotoxic stress and cell death (Tsvetkov et al., 2022). This novel pathway may have significant implications for understanding cancer biology and treatment.

Copper concentrations are elevated in the tumor tissues and serum samples of animals and patients with cancers (Jiang et al., 2022). The level of copper is associated with liver cirrhosis, acute hepatitis, and liver cancer. Serum copper may be useful as a marker for liver cancer detection (Jaafarzadeh et al., 2021). In patients with hepatocellular carcinoma (**HCC**), excessive copper concentrations can enhance tumor development, chemoresistance, and poor prognosis (Fang et al., 2019). All the above studies indicate that copper may be related to the occurrence of liver tumors, providing a new perspective for the treatment of this malignancy (Ge et al., 2022).

Here, we comprehensively explored the clinical relevance of the expression of cuproptosis-related genes (**CRGs**), their molecular alterations, and the tumor immune microenvironment in **HCC**. Moreover, our study also constructed a new prognostic model for **HCC** with **CRGs** and laid a foundation for potential therapeutic development utilizing cuproptosis regulators for **HCC** targeting and immunotherapy.

Methods

Data acquisition

Gene expression information and related clinicopathologic data of 817 HCC patients were retrieved from The Cancer Genome Atlas (https://portal.gdc.cancer.gov/repository) (**TCGA**, 231 samples), International Cancer Genome Consortium (https://dcc.icgc.org) (**ICGC**, 231 samples) and Gene Expression Omnibus (http://www.ncbi.nlm.nih.gov/geo/) (**GEO**, GSE14520, 365 samples). Log2 transformation was performed to normalize the expression profiles of the gene sets. A total of 370 samples with copy number variation (**CNV**) and single nucleotide variant (**SNV**) relevant to HCC were downloaded from the **TCGA-LIHC** site (University of California Santa Cruz Xena database). Moreover, 13 **CRGs** were collected from a previous literature (Tsvetkov et al., 2022) and are shown in Supplementary Table S1.

Cuproptosis-related prognostic signature model

The LIRI-JP cohort from the **ICGC** database was employed as the training cohort. Overall survival (**OS**)—related **CRGs** were screened via the univariate Cox analysis ($p < 0.1$). The prognostic **CRG** signature was constructed using the LASSO regression analysis based on 10-fold cross-validation penalized maximum likelihood estimators. The minimum criteria were used to choose the optimal penalty parameter (λ) values. The GSE14520 and **TCGA-LIHC** datasets were selected as the external validation cohorts. We calculated the **CRG** risk score (**RS**) for each **HCC** patient using the following formula: RS = (β * *ATP7A* expression level) + (β * *DLAT* expression level) + (β * *DLD* expression level) + (β * *FDX1* expression level) + (β * *PDHB* expression level), where β is the coefficient for each gene. Patients were further assigned into the high- and low-risk sets in accordance with the median RS. Kaplan-Meier and time-dependent receptor operating characteristic (**ROC**) curves were employed to assess the predictability of the **CRG** signature. The design of the study is shown in Figure 1.

Cell lines

The liver cancer cell lines including HEG2, MHCC97-H, HUH-7, SNU449, PLC-PRF-5, LM3, and LM9, and normal liver cell lines such as HL7702, WRL68, QSG-7701, and MIHA cells were obtained from Sun Yat-sen University Cancer Center. The expression data of these **CRGs** were obtained from Cancer Cell Line Encyclopedia (**CCLE**).

Quantitative reverse transcription polymerase chain reaction (qRT-PCR)

Total RNA was extracted from cells using TRIzol reagent (Takara Bio, Carlsbad, United States) and reverse transcribed using a cDNA reverse transcription kit (Takara Bio, Carlsbad, United States) in accordance with the manufacturer's instructions, and the obtained cDNA was amplified using TB Green® Premix Ex Taq (Takara Bio, Carlsbad, United States). qRT-PCR was performed to detect expression levels of the genes of interest. Each experiment was repeated three times. The $2^{-\Delta\Delta CT}$ methodology was adopted to calculate the relative expression of genes. The primers used are listed in Supplementary Table S2.

Functional enrichment analysis

The GSEA_4.2.3 software was applied to examine the physiological pathways that genes in the low- and high-risk datasets are involved in according to the KEGG and GO analyses, "c2. cp.kegg.v7.5.1. symbols" and "c5. go.bp.v7.5.1. symbols", respectively. Normalized p-value <0.05 was considered statistically significant. In addition, we calculated the activity of 13 immune-linked networks and 16 immune cell types through the single-sample gene set enrichment analysis (**ssGSEA**) (Rooney et al., 2015). Protein interactions between model-related proteins were constructed with the STRING algorithm (https://cn.string-db.org). Genetic variation information in the cancer cell lines was from the cBioPortal Genomics database. DNA methylation analysis was performed by methsurv (https://biit.cs.ut.ee/methsurv/) (Modhukur et al., 2018; Anuraga et al., 2021; Xing et al., 2021).

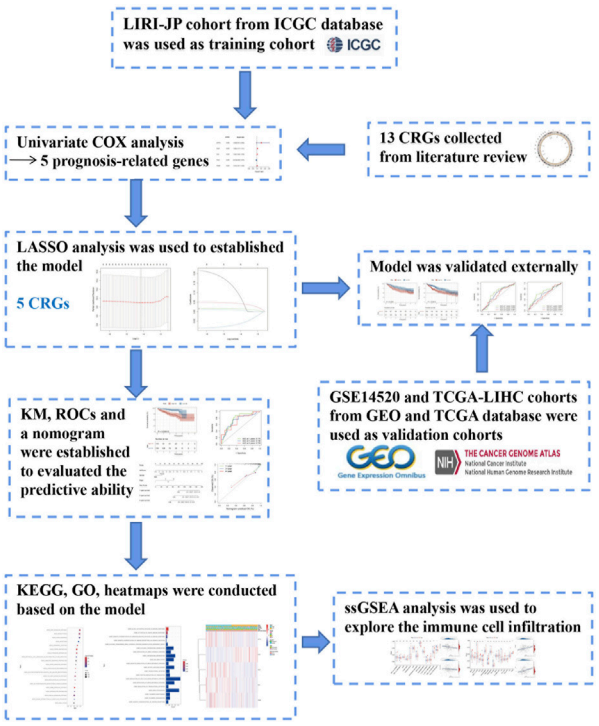

FIGURE 1
Flow chart of data collection and analysis, LIRI-JP cohort OCHC database was used as training cohort.

Statistical analysis

The Student's t-test or Wilcoxon test was employed to analyze continuous data. **OS** comparisons between two sets were completed by the log-rank test. The time-**ROC** package was applied to complete the ROC curves and estimate the values of the area under the curve (**AUC**). The independent prognosis index was estimated by the uni- and multivariate COX analyses. All statistical analyses were performed using the R software (Version 4.0.4) or SPSS (Version 25.0). A two-sided p-value <0.05 indicated statistical significance.

Results

Genetic landscape of cuprotosis related genes

A recent study reported 13 genes related to the cuproptosis pathway, including *ATP7A*, *ATP7B*, *DBT*, *DLA*, *DLD*, *DLAT*, *DLST*, *FDX1*, *GCSH*, *LIAS*, *LIPT1*, *PDHA1*, and *PDHB* (Tsvetkov et al., 2022). To determine whether these cuproptosis-related genes (**CRGs**) are involved in **HCC**, we extracted their expression levels from 817 **HCC** patient samples from three databases (**TCGA**, **ICGC** and **GEO**) for further analysis (Supplementary Figure S1A; Supplementary Table S1). Many of these **CRGs** are mutated in **HCC** samples and the top 10 mutated genes with the highest frequencies are showed in the Supplementary Figure S1A. Among them, the gene with the highest mutation frequency is *ATP7A*, accounting for about 10%, followed by *DLST*, *DLD*, and *DBT* accounting for about 7%. The major mutation type is missense mutation (43.33%, 13/33), with C>T being the most common (Figure 2A). The expression levels of most CRGs, except for *FDX1*, showed a positive correlation to **HCC** samples (Supplementary Figure S1B). In addition, the **CRGs**, *DLAT*, *DLD*, *PDHB*, *ATP7A*, *PDHA1*, *DLST*, *LIPT1*, and *LIAS*, are also expressed at significantly higher levels in liver cancer cells than in normal tissues (Figure 2B). On the other hand, the heatmaps suggested that expression of *ATP7A*, *DBT*, and *LIPT1* are lower than other genes, and lower in tumors compared to controls (Supplementary Figure S1C). Twelve of the **CRGs** are significantly differentially expressed in the **TCGA** database and analysis also indicated that *FDX1* has the lowest expression (Supplementary Figure S1D). In addition, except for *ATP7A* and *PDHA1*, which are located on the X chromosome, all other genes are located in the autosomes (Supplementary Figure S1E). Copy number variation (**CNV**) analysis showed that most of the 13 genes have copy number losses, with *GCSH* and *ATP7B* being the most obvious, while *DLD* showed a copy number gain (Figure 2C). We further validated the expressions of the **CRGs** in liver cancer cell lines and related normal cells and found that the expression of *DLAT* and *DLA* are much higher and *FDX1* lower in cancer cell lines compared to normal cells (Supplementary Figure S2A). We also validated the same results of CRGs expressions in **HCC** cancer cell lines through Cancer Cell Line Encyclopedia (**CCLE**) project (Supplementary Figure S2B).

Establishment and validation of a prognostic model for HCC

Next, we used the **ICGC** databset to explore the prognostic value of these 13 **CRGs** in liver cancer. The forest plot results indicated that the expressions of five genes (*ATP7A*, *DLAT*, *DLD*, *FDX1*, and *PDHB*) are associated with prognosis. Except for *FDX1*, expressions of the other four genes are closely related to poor prognosis (Figure 2D). The gene correlation results also pointed out that in addition to *FDX1*, the other **CRGs** are associated with at least three or more other genes (Supplementary Figure S3A). Protein interaction analysis showed that FDX1 is weakly associated with the other proteins, while DLD, PDHB, and DLAT have stronger interactions among these five proteins (Supplementary Figure S3B). Moreover, the mutational landscape of these five **CRGs** in different cancer cell lines indicated that they also have different frequencies of mutations in tumor cells (Supplementary Figure S3C). Further, LASSO-Cox regression analysis of these five prognosis-related **CRGs** in the **ICGC LIRI-JP** training dataset showed that they can be used as a cuprotosis signature (Supplementary Figures S3D, E).

To further examine the prognostic significance of this five-gene cuprotosis signature in **HCC**, we validated this signature in the GSE14520 and **TCGA** datasets. A **CRG** risk score was established using the expression levels of the five **CRGs** and the **HCC** patients were divided into two groups based on the median **CRG** risk score. Patients in different risk categories are scattered in two directions (Supplementary Figures S4A–C). The scatter charts demonstrated that patients with high-risk scores have shorter survival time than patients with low-risk scores (Supplementary Figures S4D–F). This can also be seen in the Kaplan-Meier analysis showing that high-risk

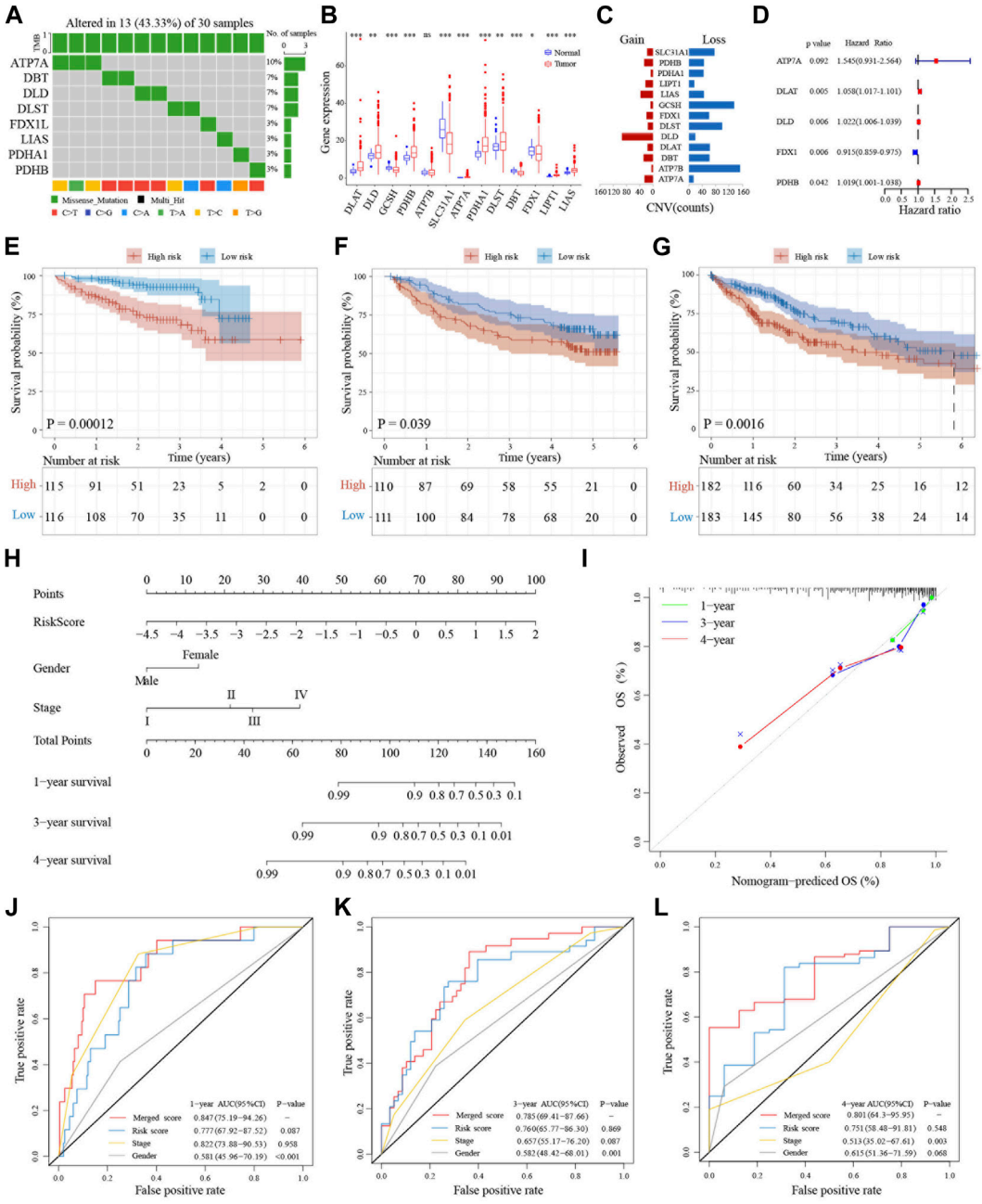

FIGURE 2
Genetic landscape and prognostic significance of CRGs in HCC. **(A)** Mutation status of 13 CRGs in the TCGA database. **(B)** Tumor-normal expression difference of CRGs in TCGA database. **(C)** CNV situation of CRGs in TCGA database. **(D)** Forest plot of five prognosis-related CRGs in ICGC database. **(E–G)** Kaplan-Meier curves for the OS of patients in the high-risk group and low-risk group in ICGC, GSE14520 and TCGA cohort. **(H)** Nomogram model built on the ICGC dataset. **(I)** Calibration curves for nomogram models. **(J–L)** AUC of time-dependent ROC curves verified the prognostic performance of merged risk score in 1-year, 3-years or 4 years of ICGC, GSE14520 and TCGA cohort.

patients have shorter overall survival than low-risk patients in both the training and validation datasets (Figures 2E–G). To further validate the survival prediction of this prognostic CRG signature, we utilized the time-dependent **ROC** curves to analyze the **AUC** between the specificity and sensitivity of these risk factors in liver cancer patients. In the training set, the **AUC** was more than 0.7, even at 4 years, and it was also at least 0.5 at 5 years in the validation datasets (Supplementary Figures S4G–I).

Implications of the CRG risk score for clinical features and prognosis

To further validate the importance of the **CRG** risk score in clinical features and prognosis, univariate and multivariate analyses were applied to examine whether the **CRG** risk score can be an independent prognostic marker for **OS** in **HCC** patients. Univariate Cox analysis showed that a high-risk score is a poor prognostic indicator of OS in liver

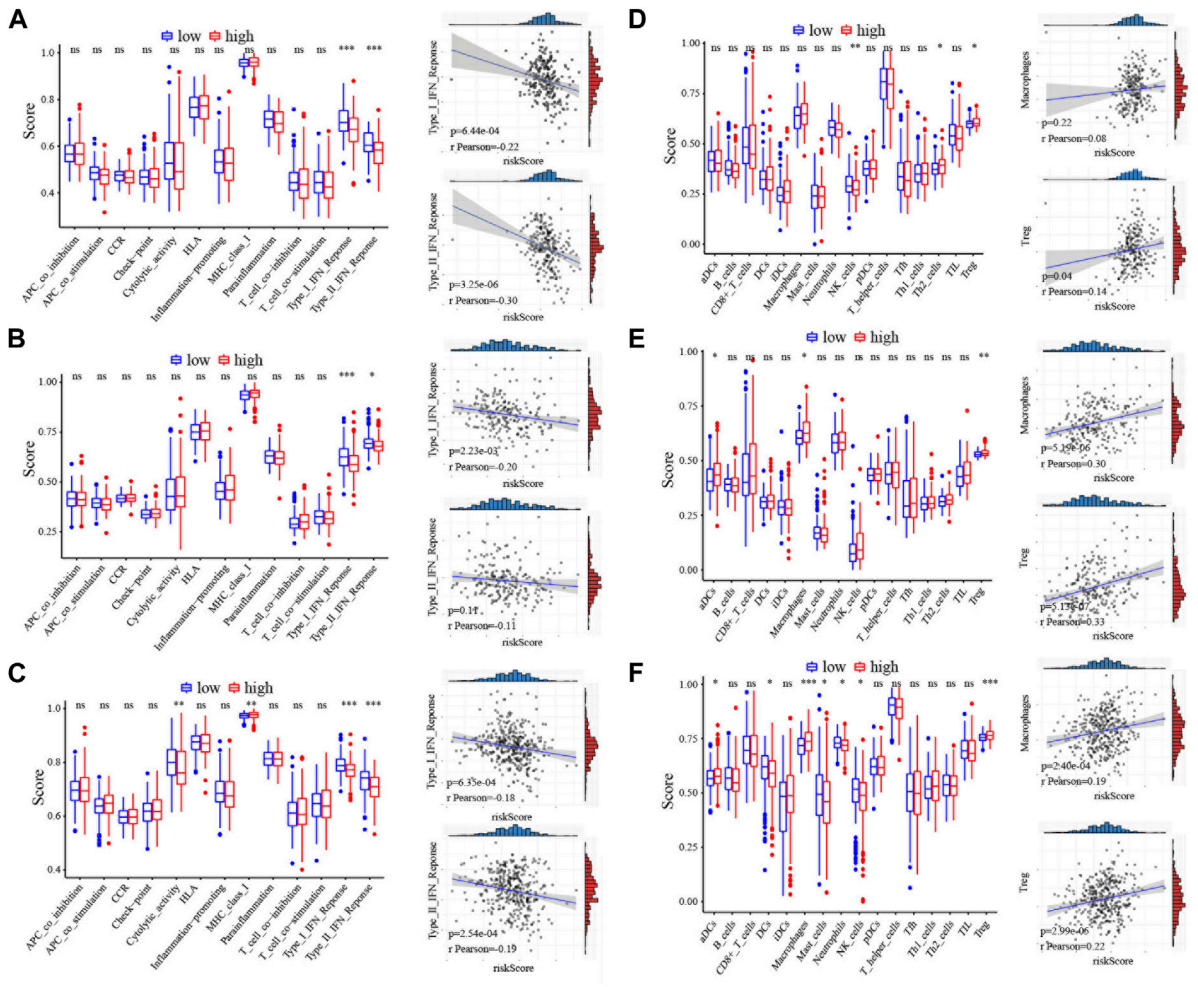

FIGURE 3
Immunoassay correlation analysis of CRGs in HCC. **(A–C)** Immune-related functions between different risk groups in ICGC, GSE14520 and TCGA cohort. The correlation of the type I IFN response or type II IFN response with risk score was displayed on the right panel. The relation value was calculated by pearson analysis. **(D–F)** The scores of immune cells between different risk groups in ICGC, GSE14520 and TCGA cohort. The correlation of the macrophages or Treg cells with risk score was displayed on the right panel. The relation value was calculated by pearson analysis. *, $p < 0.05$; **, $p < 0.01$; ***, $p < 0.001$.

cancers (Supplementary Figures S5A–C). Moreover, when combining with other well-known prognostic factors, multivariate Cox analysis suggested that the **CRG** risk score can also be a significant predictor of **OS** in liver cancer (Supplementary Figures S5D–F). Further, heatmap of clinical features including grade, TNM staging, AFP levels, BCLC staging, ALT levels, HBV status, and so on indicated that some of these biomarkers distributed differently in the high- and low-risk groups (Supplementary Figures S5G–I).

To further expand the clinical applicability of the five-**CRG** signature, a nomogram of clinical variables and the **CRG** risk score was created as shown in Figure 2H. A total score was obtained for each patient by combining the scores for each prognostic criterion. The results suggested that patients with higher total scores have poorer clinical outcomes. Furthermore, the nomogram calibration plots are highly consistent with the operating modes of the ideal model and predicted the 1-, 3- and 4-year survival time (Figure 2I). The **AUC** for 1-year overall survival of the merged score group is 0.847 [95% CI: 0.75–0.94], the **CRG** risk score group is 0.777 [95% CI: 0.68–0.88], the stage is 0.822 [95% CI: 0.74–0.91], and the gender is 0.581 [95% CI: 0.46–0.70]. In addition, the **AUC** for 3-year survival of the merged score group is 0.785 [95% CI: 0.69–0.88], the **CRG** risk score group is 0.760 [95% CI: 0.66–0.86], the stage is 0.657 [95% CI: 0.55–0.76], and the gender is 0.582 [95% CI: 0.48–0.68]. Further, the **AUC** for 4-year OS of merged score group is 0.801 [95% CI: 0.64–0.96], the **CRG** risk score group is 0.751 [95% CI: 0.58–0.92], the stage is 0.513 [95% CI: 0.35–0.68], and the gender is 0.615 [95% CI: 0.51–0.72]. All these results suggested that the addition of this five-**CRG** risk score can significantly improve the **OS** prediction efficiency compared to traditional factors alone (Figures 2J–L).

Functional analyses of the CRG risk model

Since the five-**CRG** signature described above can distinguish between high- and low-risk patients, we look wider to asked which

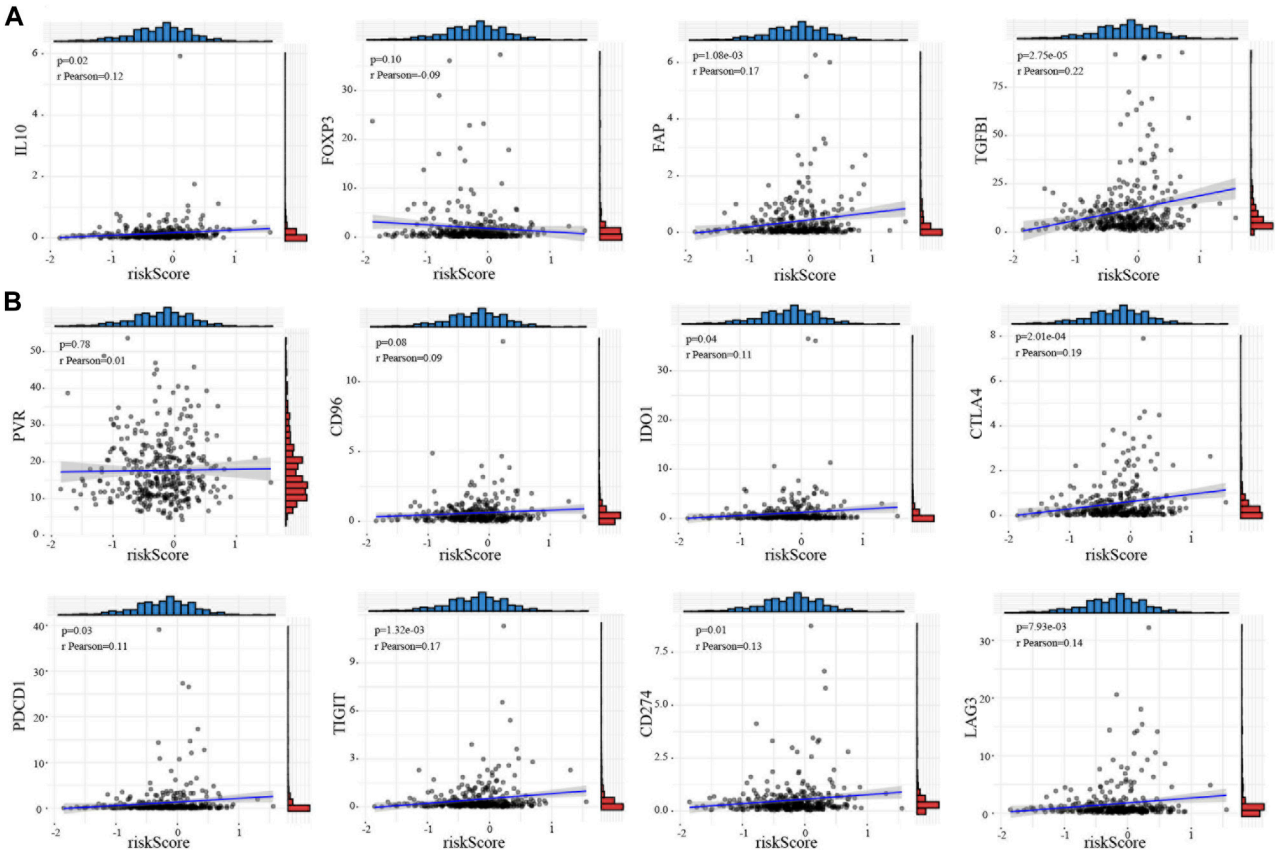

FIGURE 4
Immune checkpoint target correlation analysis of CRGs in HCC **(A)** Relationship between the risk score and immunosuppressive marker molecules including *IL-10*, *FOXP3*, *FAP*, *TGFB1*, and *IL-6*. **(B)** The correlation between the risk score and the targets of immunotherapy such as *PVR*, *PDCD1*, *CD96*, *TIGHT*, *IDO1*, *CD274*, *CTLA4*, and *LAG3*. The relation value was calculated by pearson analysis.

genes are differentially expressed between these patient subgroups. We applied "limma" to identify the differentially expressed genes with the criterion ($|\log_2 FC| \geq 1$ and FDR <0.05) in the **ICGC**, GSE14520 and **TCGA** datasets. Functional pathway analysis of these differentially expressed genes using Go terms showed that immune response pathways of different types of immune cells are more enriched in the high-risk score group. Moreover, single sample gene set enrichment analysis (**ssGSEA**) functional results further indicated that several different immune-related pathways are closely associated with the **CRG** risk score (Supplementary Figures S6A–C). What caught our attention was that the results of the refined immunophenotyping analysis suggested that the type I and II interferon (**IFN**) response pathway is the only pathway significantly more enriched in the low-risk score group in all three datasets (Figures 3A–C). To further determine the correlation between immune cell infiltration and the **CRG** risk score, we quantified and analyzed the enriched fractions of different immune cell subsets using ssGSEA. We found that NK cells, Th2, and Treg cells have significant differences between the high- and low-risk groups in the **ICGC** dataset. In the GSE14520 dataset, activated dendritic cells (**aDCs**), macrophages, and Treg cells are more enriched in the high-risk group. While in the **TCGA** dataset, aDCs, DCs, macrophages, neutrophils, masts, NK cells, and Treg cells have significant enrichment differences (Figures 3D–F). Interestingly, Treg cells are the only immune cell subtype, that is, more enriched in the high-risk score group, with significant differences in all three datasets.

CRG-related immune microenvironment and therapeutic targets

Cancer immunotherapy has made great breakthroughs and significantly improved the survival rate of cancer patients (Riley et al., 2019). Our results showed that the high-risk score is closely associated with Treg cells, indicating that cuprotosis may affect the prognosis of **HCC** patients by regulating the tumor immune microenvironment. We explored the relationship between the **CRG** risk score and immunosuppressive marker molecules including *IL-10*, *FOXP3*, *FAP*, *TGFB1*, and *IL-6* and found that the **CRG** risk score is positively correlated with *IL-10* (t = 2.36, p = 0.02), *FAP* (t = 3.3, p = 1.08e-03), and *TGFB1* (t = 4.25, p = 2.75e-05) (Figure 4A; Supplementary Figure S5D). Therefore, we wondered whether the current immunotherapy-related drugs can improve the prognosis of patients in the high-risk group. We investigated the correlation between the **CRG** risk score and the known targets genes of immunotherapy, including *PVR*, *PDCD1*, *CD96*, *TIGIT*, *IDO1*, *CD274*, *CTLA4*, and *LAG3*. Consistent with our predictions, the

CRG risk score is positively correlated with *PDCD1* (t = 2.2, p = 0.03), *TIGIT* (t = 3.24, p = 1.32e-03), *IDO1* (t = 2.11, p = 0.04), *CD274* (t = 2.51, p = 0.01), *CTLA4* (t = 3.76, p = 2.01e-04), and *LAG3* (t = 2.67, p = 7.93e-03) (Figure 4B; Supplementary Figure S6D). The DNA methylation of these genes showed no significant changes among these genes in **HCC** (Supplementary Table S3).

Discussion

Copper is an essential nutrient with redox properties that can be both beneficial and harmful to cells. The role of copper in tumor biology is gradually being recognized and the understanding of cuprotosis in tumors is continuously being improved (Riley et al., 2019). Numerous observations had shown that tumor tissue requires higher levels of copper than healthy tissue (Shanbhag et al., 2021). Gene analysis in clear cell renal cell carcinoma suggested that **CRGs** play a key role in clinical outcomes of this disease (Xia et al., 2017).

For liver cancer, there are currently insufficient studies supporting a role for **CRGs** in this disease. Our study found that the **CRGs** are significantly overexpressed in liver cancer. Among the 13 published **CRGs**, we found that the expression levels of five genes are correlated with the prognosis of liver cancer patients. Except for the high expression of *FDX1*, which indicated a lower risk of poor prognosis, the other genes, *ATP7A*, *DLAT*, *DLD*, and *PDHB*, all correlated with poor prognosis. We constructed a prognostic score model composed of these five genes and found that patients with high **CRG** risk scores tend to have the worse prognosis in all three datasets. FDX1 and fatty acylation of proteins are key factors in copper ionophore-induced cell death (Dorsam and Fahrer, 2016). Deletion of FDX1 blocks the progress of the **TCA** cycle, triggering the accumulation of pyruvate and α-ketoglutarate in cells and promotes tumor development (Rayess et al., 2012). DLAT is one of the components of the pyruvate dehydrogenase (PDH) complex, which catalyzes the decarboxylation of pyruvate in the **TCA** cycle to form acetyl-CoA (Tsvetkov et al., 2022). The expression of ATP7A in breast cancer tissues is significantly higher than that in normal tissues, and inhibiting the expression of ATP7A can improve the sensitivity of breast cancer to cisplatin (Yu et al., 2020). A spectrum of diverse genomic alterations in PDHB has been found in non-clear cell renal carcinoma (Durinck et al., 2015). These research support the significance of our **CRG** model in the prognostic prediction of **HCC**.

The tumor microenvironment is intimately involved the occurrence and development of tumors, and affects the therapeutic effect of any treatments that targets the tumor (Kennedy and Salama, 2020). Several studies have shown that pyroptosis is closely associated with tumor immunity (Gao et al., 2022). In this study, we emphasized the relationship between the immune microenvironment and **CRGs**, and found that in the high-risk group with high expression of **CRGs**, the expression of the type I and II IFN response pathways are significantly lower than that in the low-risk group, indicating that the overall immunity of the patients in the high-risk group is in a suppressed state. In addition, we also found that immunosuppressive Treg cells are significantly increased in the high-risk score group. This suggested that the high expression of **CRGs** can induce immune disorders to promote the development of tumors. The novel immunotherapy agents such as inhibitors of PDCD1, TIGHT, IDO1, CD274, CTLA4 and LAG3 were considered had potential survival benefit in several cancers. The CD274 and PDCD1 immune checkpoint interaction could accelerate cancer progression in the colorectal cancer microenvironment and elderly non-small cell lung cancer patients (Elomaa et al., 2023; Tanaka et al., 2023). The SNP of PDCD1, including rs11568821 and rs2227981 was a prognostic marker in a triple-negative breast cancer (Boguszewska-Byczkiewicz et al., 2023). Moreover, TIGHT regulated TWIST1and promoted vasculature remodeling in bladder cancer (Liu et al., 2022). It also affected autophagy in leukemia and esophageal squamous cell carcinoma (Gschwind et al., 2022; Huang et al., 2023). LAG3 was identified as an important therapeutic target in pancreatic cancer, liver, brain, breast cancer and melanoma (Gulhati et al., 2023; Huuhtanen et al., 2023; Ulase et al., 2023; Zou et al., 2023). In this study, we found that these inhibitors of PDCD1, TIGHT, IDO1, CD274, CTLA4 and LAG3 had potential benefit in high-risk patients.

Conclusion

With increasing knowledge of the mechanism of copper-driven cell death in tumors, we demonstrated here that this mechanism is also likely to be applicable for **HCC**. Using copper death-related genes, we constructed a prognostic model that will help to better understand the relationship between cuprotosis and liver cancer. The CRG risk score is related to the overall immune status of patients, particularly the presence of Treg cells. This suggested that immune checkpoint inhibitor therapies may have better effects in **HCC** patients with high **CRG** risk scores.

Data availability statement

The original contributions presented in the study are included in the article/Supplementary Material, further inquiries can be directed to the corresponding author.

Ethics statement

This work has been approved by the Ethics Committee of Sun Yat-sen University Cancer Center and Ruijin Hospital affiliated to Shanghai Jiao Tong University School of Medicine.

Author contributions

R-NS, K-HB, and Q-QH performed bioinformatics analyses; XH and S-LC. interpreted data, created a graphical summary; Y-JD. conceived and oversaw the study, interpreted data, and wrote the paper. All authors contributed to the article and approved the submitted version.

Funding

This work was supported by the National Natural Science Foundation of China (81800140), the Fundamental Research Funds for the Central Universities, Sun Yat-sen University

(22qntd4001). GuangDong Basic and Applied Basic Research Foundation (KY037906 and KY030709).

Acknowledgments

We especially thank Si-Yuan He (The University of Texas MD Anderson Cancer Center) for helping perform analysis of samples.

Conflict of interest

The authors declare that the research was conducted in the absence of any commercial or financial relationships that could be construed as a potential conflict of interest.

Publisher's note

Supplementary material

The Supplementary Material for this article can be found online at: https://www.frontiersin.org/articles/10.3389/fcell.2023.1180625/full#supplementary-material

References

Anuraga, G., Wang, W. J., Phan, N. N., An Ton, N. T., Ta, H. D. K., Berenice Prayugo, F., et al. (2021). Potential prognostic biomarkers of NIMA (never in mitosis, gene A)-Related kinase (NEK) family members in breast cancer. *J. Pers. Med.* 11 (11), 1089. doi:10.3390/jpm11111089

Boguszewska-Byczkiewicz, K., Wow, T., Szymańska, B., Kosny, M., and Kolacinska-Wow, A. (2023). The PD-1 single-nucleotide polymorphism rs11568821 and rs2227981 as a novel prognosis model in a triple-negative breast cancer patient. *Mol. Biol. Rep.* 50 (7), 6279–6285. doi:10.1007/s11033-023-08423-3

Dorsam, B., and Fahrer, J. (2016). The disulfide compound alpha-lipoic acid and its derivatives: A novel class of anticancer agents targeting mitochondria. *Cancer Lett.* 371 (1), 12–19. doi:10.1016/j.canlet.2015.11.019

Durinck, S., Stawiski, E. W., Pavía-Jiménez, A., Modrusan, Z., Kapur, P., Jaiswal, B. S., et al. (2015). Spectrum of diverse genomic alterations define non-clear cell renal carcinoma subtypes. *Nat. Genet.* 47 (1), 13–21. doi:10.1038/ng.3146

Elomaa, H., Ahtiainen, M., Väyrynen, S. A., Ogino, S., Nowak, J. A., Lau, M. C., et al. (2023). Spatially resolved multimarker evaluation of CD274 (PD-L1)/PDCD1 (PD-1) immune checkpoint expression and macrophage polarisation in colorectal cancer. *Br. J. Cancer* 128 (11), 2104–2115. doi:10.1038/s41416-023-02238-6

Fang, A. P., Chen, P. Y., Wang, X. Y., Liu, Z. Y., Zhang, D. M., Luo, Y., et al. (2019). Serum copper and zinc levels at diagnosis and hepatocellular carcinoma survival in the Guangdong Liver Cancer Cohort. *Int. J. Cancer* 144 (11), 2823–2832. doi:10.1002/ijc.31991

Gao, W., Wang, X., Zhou, Y., Wang, X., and Yu, Y. (2022). Autophagy, ferroptosis, pyroptosis, and necroptosis in tumor immunotherapy. *Signal Transduct. Target Ther.* 7 (1), 196. doi:10.1038/s41392-022-01046-3

Ge, E. J., Bush, A. I., Casini, A., Cobine, P. A., Cross, J. R., DeNicola, G. M., et al. (2022). Connecting copper and cancer: From transition metal signalling to metalloplasia. *Nat. Rev. Cancer* 22 (2), 102–113. doi:10.1038/s41568-021-00417-2

Gschwind, A., Marx, C., Just, M. D., Severin, P., Behring, H., Marx-Blümel, L., et al. (2022). Tight association of autophagy and cell cycle in leukemia cells. *Cell Mol. Biol. Lett.* 27 (1), 32. doi:10.1186/s11658-022-00334-8

Gulhati, P., Schalck, A., Jiang, S., Shang, X., Wu, C. J., Hou, P., et al. (2023). Targeting T cell checkpoints 41BB and LAG3 and myeloid cell CXCR1/CXCR2 results in antitumor immunity and durable response in pancreatic cancer. *Nat. Cancer* 4 (1), 62–80. doi:10.1038/s43018-022-00500-z

Huang, S., Zhang, J., Li, Y., Xu, Y., Jia, H., An, L., et al. (2023). Downregulation of Claudin5 promotes malignant progression and radioresistance through Beclin1-mediated autophagy in esophageal squamous cell carcinoma. *J. Transl. Med.* 21 (1), 379. doi:10.1186/s12967-023-04248-7

Huuhtanen, J., Kasanen, H., Peltola, K., Lönnberg, T., Glumoff, V., Brück, O., et al. (2023). Single-cell characterization of anti-LAG-3 and anti-PD-1 combination treatment in patients with melanoma. *J. Clin. Invest.* 133 (6), e164809. doi:10.1172/JCI164809

Jaafarzadeh, M. M., Ranji, N., and Aboutaleb, E. (2021). The effect of N-acetylcysteine on the levels of copper, zinc and expression of matrix metalloproteinases in the liver. *Pol. J. Vet. Sci.* 24 (2), 191–199. doi:10.24425/pjvs.2020.135816

Jiang, Y., Huo, Z., Qi, X., Zuo, T., and Wu, Z. (2022). Copper-induced tumor cell death mechanisms and antitumor theragnostic applications of copper complexes. *Nanomedicine (Lond)* 17 (5), 303–324. doi:10.2217/nnm-2021-0374

Kennedy, L. B., and Salama, A. K. S. (2020). A review of cancer immunotherapy toxicity. *CA Cancer J. Clin.* 70 (2), 86–104. doi:10.3322/caac.21596

Liu, X. Q., Shao, X. R., Liu, Y., Dong, Z. X., Chan, S. H., Shi, Y. Y., et al. (2022). Tight junction protein 1 promotes vasculature remodeling via regulating USP2/TWIST1 in bladder cancer. *Oncogene* 41 (4), 502–514. doi:10.1038/s41388-021-02112-w

Modhukur, V., Iljasenko, T., Metsalu, T., Lokk, K., Laisk-Podar, T., and Vilo, J. (2018). MethSurv: A web tool to perform multivariable survival analysis using DNA methylation data. *Epigenomics* 10 (3), 277–288. doi:10.2217/epi-2017-0118

Rayess, H., Wang, M. B., and Srivatsan, E. S. (2012). Cellular senescence and tumor suppressor gene p16. *Int. J. Cancer* 130 (8), 1715–1725. doi:10.1002/ijc.27316

Riley, R. S., June, C. H., Langer, R., and Mitchell, M. J. (2019). Delivery technologies for cancer immunotherapy. *Nat. Rev. Drug Discov.* 18 (3), 175–196. doi:10.1038/s41573-018-0006-z

Rooney, M. S., Shukla, S. A., Wu, C. J., Getz, G., and Hacohen, N. (2015). Molecular and genetic properties of tumors associated with local immune cytolytic activity. *Cell* 160 (1-2), 48–61. doi:10.1016/j.cell.2014.12.033

Shanbhag, V. C., Gudekar, N., Jasmer, K., Papageorgiou, C., Singh, K., and Petris, M. J. (2021). Copper metabolism as a unique vulnerability in cancer. *Biochim. Biophys. Acta Mol. Cell Res.* 1868 (2), 118893. doi:10.1016/j.bbamcr.2020.118893

Tanaka, T., Yoshida, T., Masuda, K., Takeyasu, Y., Shinno, Y., Matsumoto, Y., et al. (2023). Prognostic role of modified Glasgow Prognostic score in elderly non-small cell lung cancer patients treated with anti-PD-1 antibodies. *Respir. Investig.* 61 (1), 74–81. doi:10.1016/j.resinv.2022.10.003

Tang, D., Chen, X., and Kroemer, G. (2022). Cuproptosis: A copper-triggered modality of mitochondrial cell death. *Cell Res.* 32 (5), 417–418. doi:10.1038/s41422-022-00653-7

Tsvetkov, P., Coy, S., Petrova, B., Dreishpoon, M., Verma, A., Abdusamad, M., et al. (2022). Copper induces cell death by targeting lipoylated TCA cycle proteins. *Science* 375 (6586), 1254–1261. doi:10.1126/science.abf0529

Ulase, D., Behrens, H. M., Krüger, S., Heckl, S. M., Ebert, U., Becker, T., et al. (2023). LAG3 in gastric cancer: it's complicated. *J. Cancer Res. Clin. Oncol.* doi:10.1007/s00432-023-04954-1

Xia, Y., Liu, L., Bai, Q., Long, Q., Wang, J., Xi, W., et al. (2017). Prognostic value of copper transporter 1 expression in patients with clear cell renal cell carcinoma. *Oncol. Lett.* 14 (5), 5791–5800. doi:10.3892/ol.2017.6942

Xing, C., Wang, Z., Zhu, Y., Zhang, C., Liu, M., Hu, X., et al. (2021). Integrate analysis of the promote function of Cell division cycle-associated protein family to pancreatic adenocarcinoma. *Int. J. Med. Sci.* 18 (3), 672–684. doi:10.7150/ijms.53243

Yan, J., Wan, P., Choksi, S., and Liu, Z. G. (2022). Necroptosis and tumor progression. *Trends Cancer* 8 (1), 21–27. doi:10.1016/j.trecan.2021.09.003

Yu, Z., Cao, W., Ren, Y., Zhang, Q., and Liu, J. (2020). ATPase copper transporter A, negatively regulated by miR-148a-3p, contributes to cisplatin resistance in breast cancer cells. *Clin. Transl. Med.* 10 (1), 57–73. doi:10.1002/ctm2.19

Zou, Y., Ye, F., Kong, Y., Hu, X., Deng, X., Xie, J., et al. (2023). The single-cell landscape of intratumoral heterogeneity and the immunosuppressive microenvironment in liver and brain metastases of breast cancer. *Adv. Sci. (Weinh)* 10 (5), e2203699. doi:10.1002/advs.202203699

Glossary

TCA	Tricarboxylic acid cycle
CRG	Cuproptosis related genes
HCC	Hepatocellular carcinoma
TCGA	The cancer genome Atlas
ICGC	International cancer genome consortium
GEO	Gene expression omnibus
CNV	Copy number variation
SNV	Single nucleotide variant
OS	Overall survival
LASSO	Least absolute shrinkage and selection operator
RS	Risk score
ROC	Receptor operating characteristic
ssGSEA	Single-sample gene set enrichment analysis
AUC	Area under the curve
HR	Hazard ratio
CI	Confidence interval
TNM	Tumor node metastasis
AFP	Alpha fetoprotein
BCLC	Barcelona clinic liver cancer
ALT	Alanine amiotransferase
HBV	Hepatitis B virus
aDC	Activated dendritic cell
APC	Antigen presenting cell
CCR	Cytokine-cytokine receptor
HLA	Human leukocyte antigen
iDC	Immature dendritic cell
pDC	Plasmacytoid dendritic cell
Tfh	T follicular helper cell
TIL	Tumor infiltrating lymphocyte
Treg	Regulatory T cells
NK	Natural killer

frontiers | Frontiers in Cell and Developmental Biology

TYPE Original Research
PUBLISHED 08 September 2023
DOI 10.3389/fcell.2023.1240390

OPEN ACCESS

EDITED BY
Lin-Lin Bu,
Wuhan University, China

REVIEWED BY
Kaichao Song,
Chinese Academy of Medical Sciences and Peking Union Medical College, China
Peng Chen,
Zhejiang University, China

*CORRESPONDENCE
Xutong Li,
18661390557@163.com
Chuang Yang,
chuang.yang@medizin.uni-leipzig.de

†These authors have contributed equally to this work and share first authorship

RECEIVED 14 June 2023
ACCEPTED 24 August 2023
PUBLISHED 08 September 2023

CITATION
Cao F, Qi Y, Wu W, Li X and Yang C (2023), Single-cell and genetic multi-omics analysis combined with experiments confirmed the signature and potential targets of cuproptosis in hepatocellular carcinoma.
Front. Cell Dev. Biol. 11:1240390.
doi: 10.3389/fcell.2023.1240390

Single-cell and genetic multi-omics analysis combined with experiments confirmed the signature and potential targets of cuproptosis in hepatocellular carcinoma

Feng Cao[1†], Yong Qi[2†], Wenyong Wu[2], Xutong Li[3*] and Chuang Yang[4*]

[1]Department of General, Visceral and Transplantation Surgery, University Hospital RWTH Aachen, Aachen, Germany, [2]Department of General Surgery, The First Hospital of Anhui Medical University, Hefei, China, [3]Department of Infectious Diseases, The First Affiliated Hospital of Anhui Medical University, Hefei, China, [4]Department of Visceral, Transplant, Thoracic and Vascular Surgery, University Hospital of Leipzig, Leipzig, Germany

Background: Cuproptosis, as a recently discovered type of programmed cell death, occupies a very important role in hepatocellular carcinoma (HCC) and provides new methods for immunotherapy; however, the functions of cuproptosis in HCC are still unclear.

Methods: We first analyzed the transcriptome data and clinical information of 526 HCC patients using multiple algorithms in R language and extensively described the copy number variation, prognostic and immune infiltration characteristics of cuproptosis related genes (CRGs). Then, the hub CRG related genes associated with prognosis through LASSO and Cox regression analyses and constructed a prognostic prediction model including multiple molecular markers and clinicopathological parameters through training cohorts, then this model was verified by test cohorts. On the basis of the model, the clinicopathological indicators, immune infiltration and tumor microenvironment characteristics of HCC patients were further explored via bioinformation analysis. Then, We further explored the key gene biological function by single-cell analysis, cell viability and transwell experiments. Meantime, we also explored the molecular docking of the hub genes.

Results: We have screened 5 hub genes associated with HCC prognosis and constructed a prognosis prediction scoring model. And the model results showed that patients in the high-risk group had poor prognosis and the expression levels of multiple immune markers, including PD-L1, CD276 and CTLA4, were higher than those patients in the low-risk group. We found a significant correlation between risk score and M0 macrophages and memory $CD4^+$ T cells. And the single-cell analysis and molecular experiments showed that BEX1 were higher expressed in HCC tissues and deletion inhibited the proliferation, invasion and migration and EMT pathway of HCC cells. Finally, it was observed that BEX1 could bind to sorafenib to form a stable conformation.

Conclusion: The study not only revealed the multiomics characteristics of CRGs in HCC but also constructed a new high-accuracy prognostic prediction model.

Meanwhile, BEX1 were also identified as hub genes that can mediate the cuproptosis of hepatocytes as potential therapeutic targets for HCC.

KEYWORDS

hepatocellular carcinoma, cuproptosis, programmed cell death, immune microenvironment, single-cell RNA-sequencing, molecular docking

1 Introduction

The latest global cancer statistics indicate that there are more than 900,000 new cases of liver cancer and 800,000 deaths per year, and its morbidity and mortality rank seventh and third among all cancers, respectively (Sung et al., 2021), which pose a serious threat to human health and safety (Llovet et al., 2021). Among them, nearly 90% of the cases are hepatocellular carcinoma (HCC) and it is also the most common type of pathology (Llovet et al., 2016). HCC progresses rapidly and stealthily, with a high degree of malignancy, the prognosis of HCC is very poor and the 5-year survival rate is below 20% (Craig et al., 2020). Although alpha-fetoprotein (AFP) is currently widely used in early HCC screening and prognosis assessment, it is affected not only by many non-hepatic carcinoma-related factors, but its expression level is also significantly increased in other diseases, such as acute viral hepatitis (AHA), resulting in low sensitivity and specificity (Huo et al., 2018; Cai et al., 2019). For lack of effective biomarkers, most patients are in the advanced stages when they are diagnosed with HCC. Although a variety of modalities including surgical resection, radiofrequency ablation, trans-arterial chemoembolization, systemic chemotherapy and liver transplantation have been significantly developed, the clinical effect is still very limited. In addition, the complex pathogenesis of HCC is also an important factor in its high mortality, which involves multiple molecular mechanisms, such as cell death regulation, genetic mutation, tumor heterogeneity, immune regulation, and dysregulation of the tumor microenvironment (Kurebayashi et al., 2018; Demirtas and Gunduz, 2021; Torrens et al., 2021). Thus, it is vital to identify new HCC-specific biomarkers, extensively study the pathogenesis of HCC and explore new precise therapeutic targets.

In recent years, with the in-depth understanding of cell death, a growing number of studies have confirmed that a serious of programmed cell death (PCD) programs, such as autophagy, ferroptosis and pyroptosis, play an indispensable role in tumorigenesis and progression (Mou et al., 2019; Li et al., 2020; Hou et al., 2020). Cuproptosis, as a new PCD program, has the characteristics of copper dependence and copper regulation. The mechanism is mainly through copper binding directly to lipoylated components in the tricarboxylic acid (TCA) cycle to mediate lipoylated protein aggregation and iron-sulfur cluster protein loss, which ultimately leads to proteotoxic stress and cell death (Tsvetkov et al., 2022). Copper has the functions as a metabolic cofactor at the active site as well as a dynamic signaling metal and metalloallosteric regulator, which is connected with various clinical diseases, especially cancer, because the growth and metastasis of tumors have higher requirements for this metal nutrient (Ge et al., 2022). As the Mortada study found, the copper levels in the plasma and bladder tissue were significantly higher in patients with bladder cancer than in those non-bladder cancer patients (Mortada et al., 2020). Interestingly, Atakul et al. (2020) found that the serum copper level of patients with endometrial cancer was significantly lower than that of normal people, and it was negatively correlated with the degree of tumor invasion. Relevant studies have shown that unbalanced copper homeostasis can induce many forms of cell death including apoptosis, autophagy and ferroptosis, through various mechanisms, such as reactive oxygen species accumulation, proteasome inhibition and mitochondrial dysfunction (Jiang et al., 2022). However, the specific mechanism of copper ion-induced PCD is still unclear. In addition, with the role of copper in tumor proliferation, invasion and metastasis, its antitumor potential has also been highlighted. Li et al. (2020) showed that the combination of disulfiram with copper can greatly improve its antitumor efficacy. Similarly, Mariani et al. (2021) also demonstrated that the combined use of copper complexes and cisplatin enhanced the antitumor effect against melanoma, lung cancer and breast cancer. Therefore, this could be a new strategy for cancer treatment by using copper ion metal carriers to eliminate cancer cells. However, the role of copper-induced cuoproptosis in HCC has not been reported. Therefore, this study aimed to explore the possible molecular markers and drug targets of copper death in HCC, comprehensively analyze the multiomics characteristics of cuproptosis related genes (CRGs), including genomics, transcriptomics and tumor microenvironment (TME), and extensively investigate the latent function of cuproptosis in the TME, clinical characteristics and prognosis of HCC to provide a new strategy and prediction model for clinical diagnosis, treatment and prognosis evaluation.

2 Methods and materials

2.1 Data sources

The workflow chart of this study is shown in Supplementary Figure S1. We downloaded 424 HCC patients with ribonucleotide (RNA) sequences, clinical information and GSE76427, GSE52018, GSE149614 datasets from the Cancer Genome Atlas (TCGA) (https://portal.gdc.cancer.gov/) databases and Gene Expression Omnibus (GEO) (https://www.ncbi.nlm.nih.gov/geo/). All raw files were normalized and annotated by using "limma" package in R, and the RNA sequences of fragments per kilobase million (FPKM) in TCGA were converted to transcripts per kilobase million (TPM) sequences. Then, batch effects of the three datasets were eliminated by the "Combat" algorithm. After integrating all datasets and excluding patients lacking overall survival (OS) data, the clinical data of 526 HCC patients were saved for succeeding analysis.

2.2 Difference analysis and cluster analysis of CRGs

We obtained 10 CRGs from previous publications [13]. According to the expression levels of CRGs in the HCC genomic dataset, the R language "reshape2" and "ggpubr" packages were used to analyze and plot the expression differences of CRGs in tumor and normal samples. Then, Kaplan–Meier survival curves and interaction networks were analyzed and plotted using the HCC clinical dataset. Finally, according to the gene expression levels of CRGs, consensus unsupervised clustering (CUC) analysis was performed using the k-means method in the "ConensusClusterPlus" package to classify all HCC patients into different molecular subtypes. The principal component analysis (PCA) graph was drawn by analyzing the expression levels of CRGs and typing results by the "ggplot2" software package.

2.3 Difference analysis between CRG-related subtypes

We compared the prognosis and clinical characteristics of CRGS-related subtypes according to the clinical information files and classification results of HCC patients and drew Kaplan–Meier survival curves and clinical characteristic heatmaps using R language for visualization. Then, we used the R language "GSVA" package to complete the gene set variation analysis (GSVA) enrichment analysis. At the same time, the ssGSEA algorithm in the "GSVA" package was used to quantitatively analyze the immune cells to compare the immune infiltration fraction between different subtypes.

2.4 Difference analysis between DEG-related subtypes and functional annotation

At first, we used R language "limma" package with parameters set to fold-change of 1.5 and adjusted p-value of <0.05 to extract CRG-related genes. Gene ontology (GO) and Kyoto encyclopedia of genes and genomes enrichment (KEGG) functional enrichment analyses were performed. Then, univariate cox regression analysis was performed on CRG-related genes to screen for prognosis-related differentially expressed genes (DEGs). The prognostic and clinical features between DEG-related subtypes were compared using the R "survival" package and the "PheATmap" package and visualized using Kaplan–Meier survival curves and heatmaps. In addition, the differences in the expression of CRGs among the related types of CRG-related genes were compared again using the R packages "Reshape2" and "GGPubR."

2.5 Prognosis model construction and validation

First, 526 HCC patients were randomly divided into training and test cohorts with 263 cases each according to the 1:1 ratio. The R package "Glmnet" was used to include prognosis-related DEGs in the Least Absolute shrinkage and Selection Operator (LASSO) and multivariate Cox regression analyses. Then, risk scores (RSs) were calculated for genes with nonzero regression coefficients. The RS was calculated as follows: RS = $\sum_{j=1}^{n} Xj * Coefj$, (n represent number of prognosis-related DEGs, Xj and $Coefj$ represent the DEGs expression level and risk coefficient). According to the median value of RS, two cohorts were divided into low-risk and high-risk groups, respectively. "ggalluvial" and "dplyr" are used to draw an alluvial diagram to visualize the model building process. Based on the typing results, RS differences were compared in CRG-related subtypes and gene-related subtypes using the "limma" and "ggpubr" packages, respectively. In addition, boxplots of the differential expression of CRGs and immune checkpoints were constructed by the "GGPLOT2" and "GGPUBR" packages. In addition, the survival differences and the receiver operating characteristic (ROC) curves were analyzed and plotted in the training and test cohorts.

2.6 Establishment of a nomogram scoring system

Based on the clinical data and grouping results, the "pheatmap" package was used to visualize the correlation of RS with survival status and the difference in expression of prognosis-related DEGs. Then, the "rms" package was used to construct a nomogram scoring system for predicting prognosis, and the "calibrate" function was used to draw a calibration curve for evaluating the accuracy of the prognostic prediction model.

2.7 Analysis of immune cell infiltration, TME and CSCs

The 22 immune cell infiltration degrees of each sample were evaluated by the "preprocessCore" and "e1071" packages, and then the "CiberSort" algorithm was used to calculate the correlation between immune cell infiltration degree and RS- and prognosis-related DEGs. Next, we used the "estimate" package to calculate the stromal score, immune score and estimation score and further evaluated tumor purity. In addition, we evaluated the relationship between CSCs and RSs using cancer stem cell (CSC) score files.

2.8 Somatic mutation and drug susceptibility analysis

Differences in somatic mutations of HCC patients were analyzed using the "maftools" package and displayed in a waterfall diagram. We continued to use the "pRophetic" software package and the genomics of drug sensitivity in cancer (GDSC) database (https://cancerrxgene.org) to calculate the semi-inhibitory concentration (IC50) value of commonly used chemotherapy drugs in tumors, and the Wilcoxon signed rank test was used to compare the difference in IC50 values between the risk group and the low-risk group. The filter condition was set to $p < 0.001$.

2.9 Western blotting

We randomly collected tumor tissues and paracancerous tissues from 3 HCC patients treated at the First Affiliated Hospital of Anhui Medical University from March to April 2022. Tissue and normal LO2 hepatocytes and Hep3b, Huh7 and LM3 HCC cells were extracted with RIPA (Beyotime, Shanghai, China) after grinding and filtration. Then, the tissue was lysed on ice and centrifuged. We collected the supernatant and then the protein concentration was determined by a BCA kit (Beyotime). After gel preparation, electrophoresis, and transfer, the membrane was incubated with primary (BEX1, 1:5000, 12390-1-AP, Proteintech), (G6PC, 1:5000, 66860-1-Ig, Proteintech), (NEIL3, 1:5000, 11621-1-AP, Proteintech), (GCLM, 1:5000, 66808-1-Ig, Proteintech), (NT5DC2, 1:5000, YLS-K0806, Yilisa) and secondary antibodies (Anti-rabbit IgG, HRP-linked Antibody, 7074S, CST). For Western blotting analysis, the proteins underwent separation by SDS–PAGE, nitrocellulose membrane transfer, quick blocker kit (Beyotime) blocking. After that, the bands were detected by ECL Plus (EMD Millipore, Billerica, MA, United States).

2.10 Single-cell analysis

GSE149614 raw data were processed in R using the "Seurat" package, and cells within the tissue were filtered and visualized with parameters of 500–6,000 expressed genes and mitochondrial ratio >10%. After performing quality control (QC) and selecting cells using the "CreateSeuratObject" algorithm. Then, we used the Seurat function of FindIntegrateionAnchors to merge sample files with common anchors among variables (dims = 1:20). We performed PCA on the scaled data using the "JackStraw" algorithm and ranked the PCA using the "ElbowPlot" function. The FindClusters function was used to perform T-distributed stochastic neighbor embedding (tSNE) dimensionality reduction clustering (resolution = 0.2) on the first 20 PC data. The FindMarkers function of Seurat and the CIBERSORT algorithm were used to determine the expression of marker genes in each cluster.

2.11 Cell viability, migration and invasion assays

LM3 cells were purchased from. Then cells were cultured with RPMI-1640 supplemented with 10% FBS (Beyotime, Shanghai, China). Subsequently, two siRNAs were used to knock out the expression of BEX1. Specifically, the sequences of siRNAs for BEX1 were listed. Then, LM3 cells were cultured until the density reached about 60%–70%, and plasmids, shRNA and Lipofectamine™ 2000 diluents were prepared by serum-free Opti-MEM medium to prepare transfection complexes. The transfection complex was added to LM3 cells and cultured for 48 h. Then 5,000 cells with BEX1 siRNAs were cultured in 96-well plate and incubated for 48 h at 37°C. Then the cell viability was measured using CCK-8 kit. In addition, 24-well inserts were used to perform cell migration and invasion assays. Briefly, LM3 cells were infected with BEX1 siRNAs for 48 h. Then 5,000 cells were seeded in the upper chamber with (migration assay) or without Matrigel (invasion assay). Meanwhile, 500 μl fresh medium were transferred to the low chamber and incubated for 24 h. After that, cells were fixed by 3.7% paraformaldehyde and stained with crystal violet. Cell images were obtained by fluorescence microscope and counted using ImageJ.

2.12 Molecular docking

We used AutoDock Vina software for molecular docking (Trott and Olson, 2010). Sorafenib was used as a ligand, and the key genes BEX1, NEIL3, GCLM, G6PC and NT5DC2 were used as receptors. The PDB format files were downloaded from the RSCB PDB database (http://www.rcsb.org/). Convert the Suolafeini PDB format to MOL2 format using Chem3D. Then, AutoDockTools 1.5.6 (https://autodock.scripps.edu/) was used to process receptor proteins and small molecule ligands and saved as PDBQT format files. During the molecular docking process, the Lamarckian algorithm was used to identify the most binding mode. The search space volume was > 27,000 A^3, the exhaustiveness was set to 8 and the maximum number of conformations output was set to 15.

2.13 Statistical analyses

The study was carried out under the R version 4.1.3, Strawberry Perl version 5.32.1.1, GraphPad Prism 7 and ImageJ. *, **, *** indicated $p < 0.05$, $p < 0.01$, $p < 0.001$, respectively. A $p < 0.05$ was considered statistically significant.

3 Results

3.1 Differential expression of CRGs and identification of cuproptosis-related subtypes

A total of 10 CRGs were obtained in this study for subsequent analysis. First, the results of copy number variation (CNV) analysis showed that there were clear CNVs in all genes except MIF1. CDKN2A had the highest gene mutation frequency and was mainly amplified on chromosome 9. The remaining CRGs also had different degrees of deletion and amplification variation, and their positions on the chromosome were also shown (Figures 1A, B). In addition, we obtained results showed that the remaining CRGs, except FDX1 and MIF1, were significantly highly expressed in tumor tissues. Interestingly, CDKN2A, which had the highest frequency of CNVs, also had the most significant differences in expression (Figure 1C). This suggests that the expression levels of genes in tumor tissues may be regulated by their CNVs. The results of the interaction network showed that CDKN2A and FDX1 were negatively correlated and were not found to be associated with other CRGs, while other genes interacted closely. Among them, FDX1, DLD and LIAS may be anticancer factors (Figure 1D). Further survival analysis found that CDKN2A, DLAT, FDX1, PDHA1, GLS and LIPT1 were associated with HCC prognosis

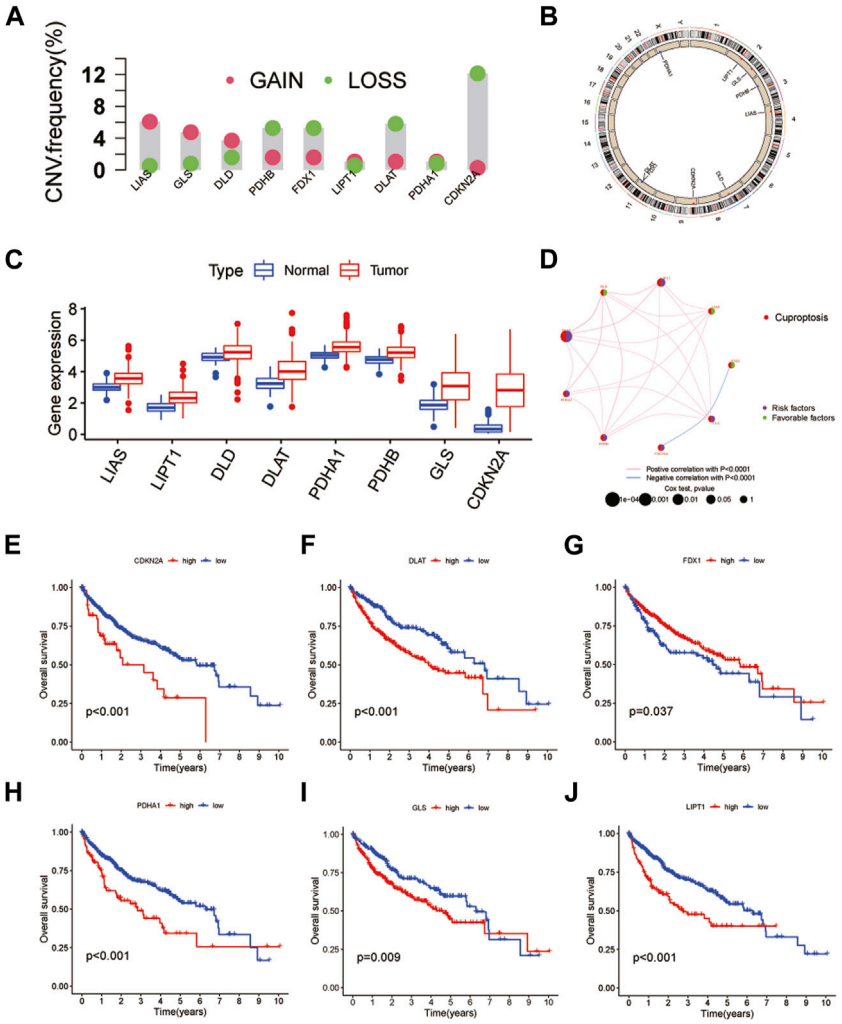

FIGURE 1
Genetic and transcriptional alterations of CRGs in HCC. **(A)** CNV of CRGs in 424 samples in TCGA. **(B)** Chromosomal localization of CRGs with CNV. **(C)** Expression of CRGs. **(D)** CRGs interaction network. **(E–J)** Kaplan-Meier survival analysis of 6 CRGs associated with HCC prognosis.

(Figures 1E–J). Patients with highly-expressed FDX1 had a better prognosis, which further verified the anticancer effect of FDX1. The remaining five genes are the opposite. In addition, HCC patients were classified by CUC analysis of CRGs. The obtained results showed that k = 2 was the best choice, and the correlation between samples in subtypes A and B was the highest (Supplementary Figure S2). Besides, HCC samples can be separated into subtype A and subtype B, which was also verified by PCA (Supplementary Figure S3).

3.2 Differences in clinical features and functional annotations of CRG-related genes across subtypes

Kaplan–Meier survival curves between different subtypes showed that patients with subtype A had a longer OS time than patients with subtype B (Figure 2A). Compared with subtype B, patients with subtype A had lower TNM stage and clinical stage than those with subtype B, the expression of FDX1 was relatively high, while the other genes were highly expressed in subtype B (Figure 2B). Moreover, GSVA suggested that subtype A was primarily enriched in fatty acid, bile acid and amino acid metabolism pathways, while cell cycle regulation, nucleic acid repair, nucleic acid synthesis and metabolism pathways were more likely to be found in subtype B (Figure 2C). The dysregulation of these pathways can cause gene mutation which can lead to abnormal cell metabolism or cell death. In the differences of immune cell infiltration. We found that activated B cell, activated CD8 T cell, eosinophilna, macrophagena, etc., degree was significantly higher in subtype A than in subtype B, whereas those of activated CD4 T cells and type 2 T helper cells were lower than those of subtype B (Figure 2D). To explore the underlying molecular behaviors of cuproptosis pattern, we identified 614 CRG-related DEGs and performed functional annotation analysis. These CRG-related DEGs were mainly enriched in biological processes such as cell cycle regulation and DNA replication (Supplementary Figure S4A). KEGG analysis

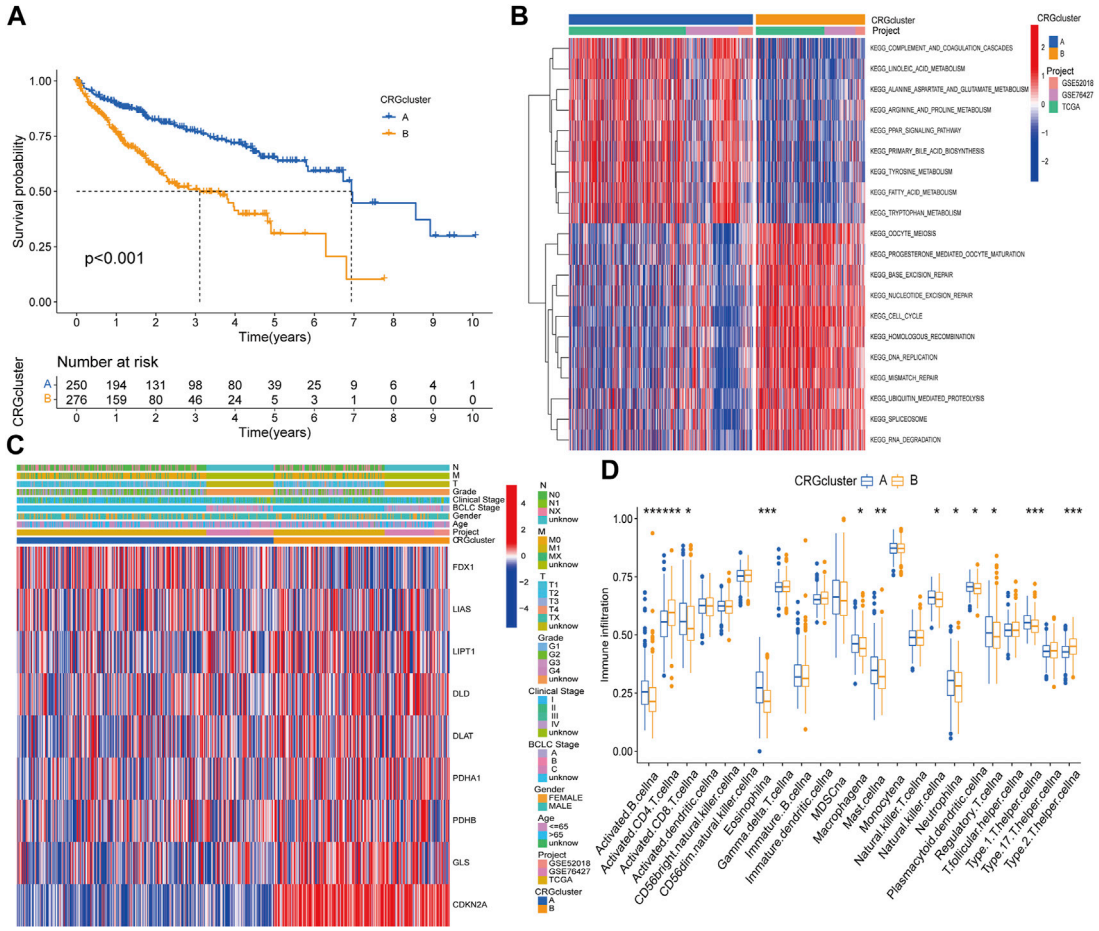

FIGURE 2
Difference analysis in distinct subtypes and functional annotations of CRGs related genes. **(A)** Survival curves between CRGs subtypes. **(B)** Clinical characteristics of CRGs subtypes. **(C)** GSVA enrichment analysis. **(D)** Differences in immune cell infiltration.

showed that these genes were mainly enriched in cell cycling and DNA replication signaling pathways (Supplementary Figure S4B).

3.3 Identification of gene subtypes and construction of a prognostic model

First, we obtained 382 DEGs that were associated with prognosis. We divided HCC patients into two subtypes, A and B, by CUC analysis (Supplementary Figure S5). Kaplan–Meier survival curves showed that patients of subtype A survived longer than those of subtype B (Figure 3A). Combined with clinical characteristics, a positive correlation was found between B subtype pattern and advanced TNM staging, BCLC staging, and high expression of prognosis-related genes (Figure 3B). In addition, FDX1, DLD, CDKN2A, DLAT, PDHB, PDHA1, GLS and LIPT1 also showed significant differences in expression between the two subtypes. Among them, only FDX1 was highly expressed in subtype A, which further verified the role of FDX1 as an anticancer factor (Figure 3C). We then constructed a predictive model based on CRG-related genes. LASSO regression analysis was performed on CRG-related DEGs with prognostic value, and the risk coefficient of each CRG-related DEGs was evaluated. Thirteen prognostic CRG-related DEGs were retained according to the minimum partial likelihood deviance (Figures 3D, E). Then, we performed multivariate Cox regression analysis on 13 genes related to prognosis and finally found that BEX1, G6PC, GCLM, NEIL3 and NT5DC2 CRG-related genes are independent influencing factors of HCC. The Sankey diagram shows the distribution and correlation of patients with different prognoses in distinct subtypes and RS subgroups (Figure 3F). Among the different gene subtypes, the RS of subtype B was higher than that of subtype A (Figure 3G). Interestingly, the difference in CRG expression between the two groups was consistent with the difference between gene subtypes. Only FDX1 was highly expressed in the low-risk group, while DLD, CDKN2A, DLAT, PDHB, PDHA1, GLS and LIPT1 were all highly expressed in the high-risk group (Figure 3H). This further demonstrates the anticancer effect of FDX1. In addition, there was also a clear correlation between RS and immune checkpoints, including programmed cell death protein 1 (PD-1), programmed cell death 1 ligand 1 (PD-L1), cytotoxic T-lymphocyte-associated protein 4 (CTLA4) and cluster of differentiation 44 (CD44), which were highly expressed in the high-risk group (Figure 3I).

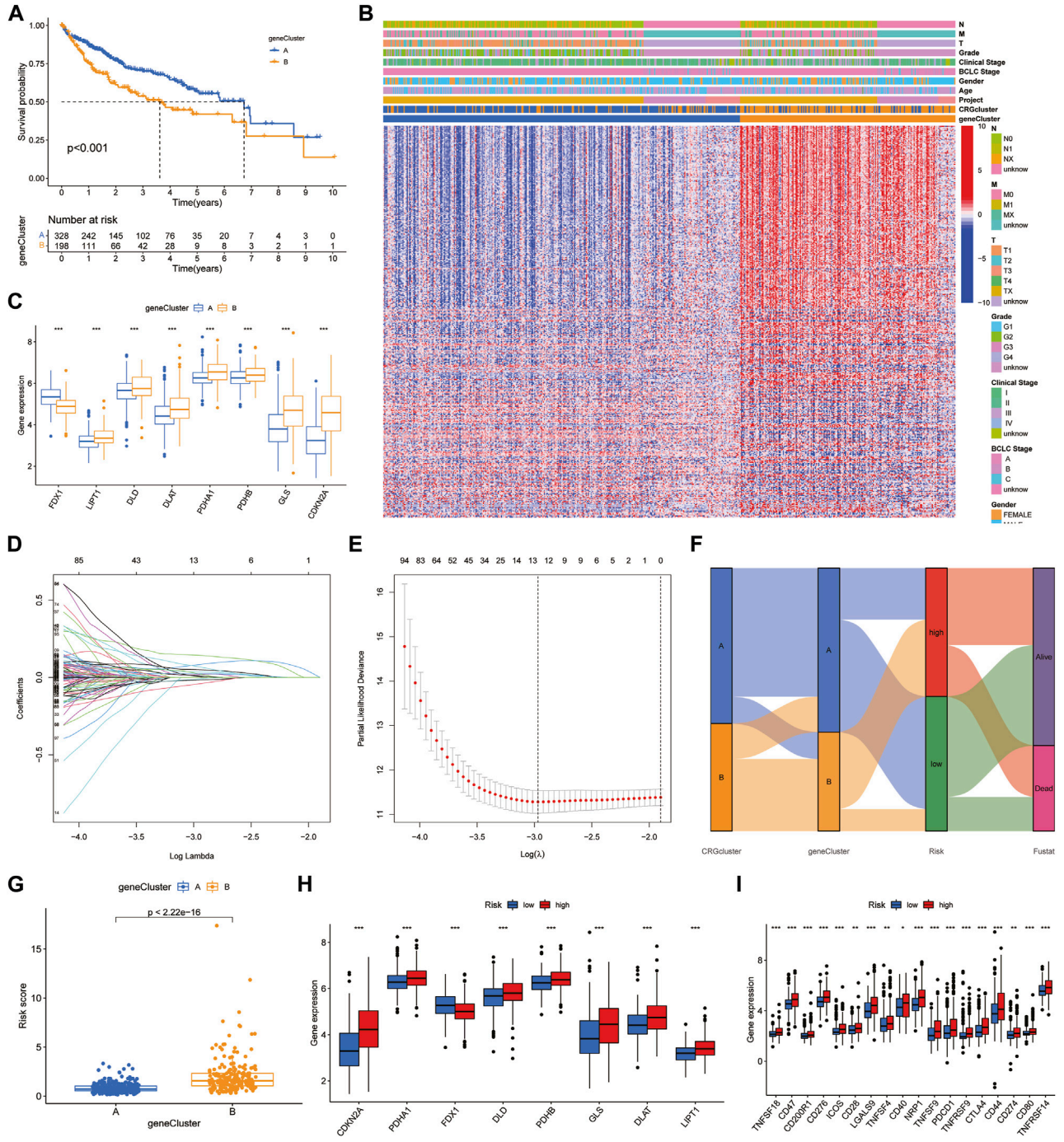

FIGURE 3
Identification of hub genes and construction of the prognostic model. **(A)** Survival curves between the hub genes subtypes. **(B)** Clinical characteristics of DEGs. **(C)** Expression of CRGs between DEGs subtypes. **(D,E)** LASSO regression analysis and partial likelihood deviance. **(F)** Alluvial diagram of subtype and RS distributions. **(G)** Differences of RS in DEGs clusters. **(H,I)** Expression of CRGs and immune checkpoints.

3.4 Validation of the prognostic model and development of a nomogram

Based on the median RS, the patients in the training and test groups were sorted according to the RS (Figures 4A, B). Survival status showed that patients in high-risk group of training group had a worse outcome than those in the low-risk group. We also found the similar results in the test group (Figures 4C, D). The heatmaps showed that NEIL3, GCLM and NT5DC2 had a higher expression level in the high-risk group, and G6PC and BEX1 were expressed at low levels (Figures 4E, F). Furthermore, in both the training and test groups, Kaplan–Meier survival curves showed

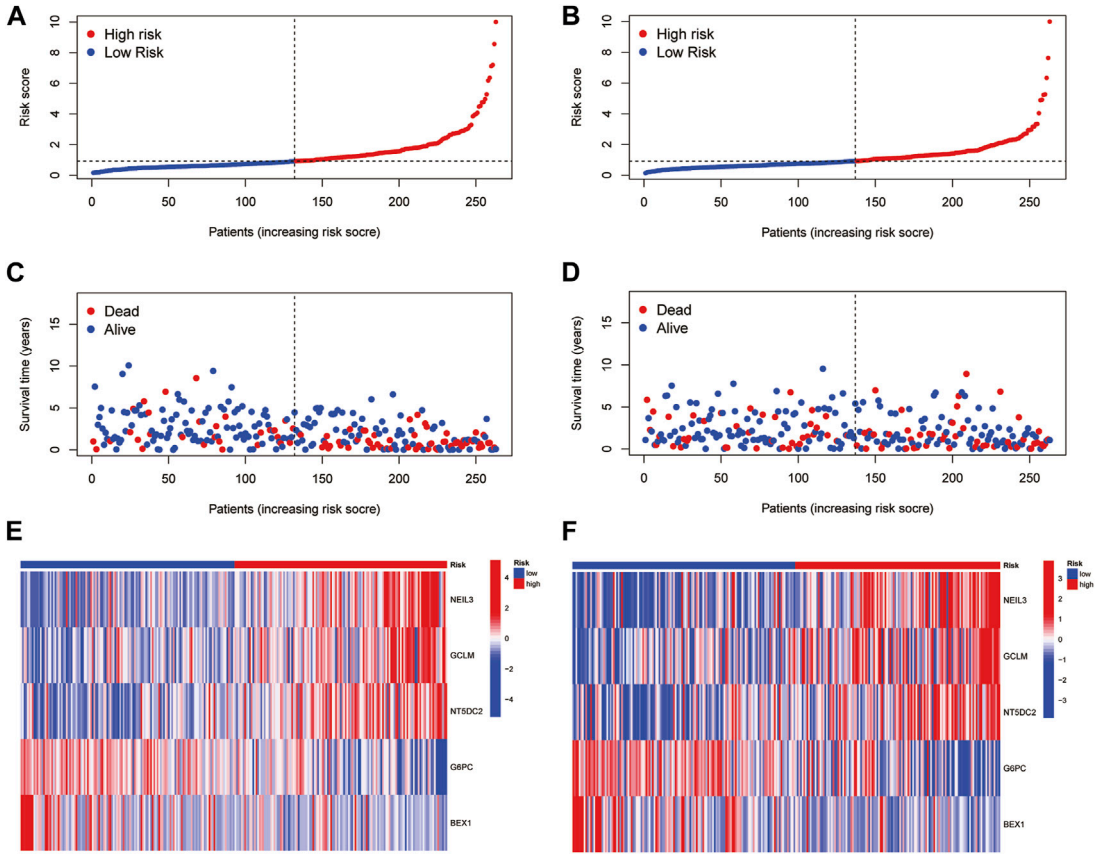

FIGURE 4
Prognostic value of the CRGs signature. **(A,B)** RS distribution. **(C,D)** Survival status. **(E,F)** Expression of the 5 hub genes.

that the survival rate in the high-risk group was significantly lower than that in the low-risk group (Figures 5A, B). This may be related to the high expression of BEX1 and G6PC in the low-risk group, indicating that BEX1 and G6PC may have a synergistic effect with FDX1. In addition, to assess the efficacy of the prognostic model, the areas under the curve (AUCs) of the training group at 1, 3, and 5 years were 0.792, 0.756, and 0.740, respectively. Likewise, the test group also had the similar performance, with AUCs of 0.720, 0.688, and 0.641 at 1, 3, and 5 years, respectively (Figures 5C, D). Therefore, this study created a nomogram that integrated multiple molecular markers and clinicopathological parameters to predict the prognosis (Figure 5E). Meanwhile, the calibration diagram also demonstrated that the model had a perfect reliability (Figure 5F).

3.5 Correlation of RS with immune cells, TME score and somatic mutation and drug susceptibility analysis

The protein interaction network between CRG-related DEGs showed that five key prognosis-related genes in the prognostic model were negatively correlated with FDX1. Among them, NEIL3 and NT5DC2 were positively correlated with CDKN2A, and the correlation was the highest (Figure 6A). In addition, we found RS was positively correlated with M0 macrophages and negatively correlated with resting memory CD4$^+$ T cells (Figures 6B, C). Among the five key prognosis-related genes, G6PC, GCLM, NEIL3 and NT5DC2 were significantly associated with a variety of immune cells, among which G6PC was positively associated with M1 macrophages, and NEIL3 was positively correlated with activated memory CD4$^+$ T cells and negatively correlated with resting memory CD4$^+$ T cells (Figure 6D). TME difference analysis found that the stromal score in the low-risk group was significantly higher than that in the high-risk group (Figure 6E). Our study also assessed the correlation between CSC and RS and concluded that RS was positively correlated with CSC (Figure 6F). Furthermore, we analyzed the somatic mutation profile. The obtained results showed that the top 10 mutated genes in the two groups were TP53, CTNNB1, TTN, MUC16, ALB, PCLO, APOB, RYR2, MUC4 and FLG. Among them, the PCLO mutation frequency was higher in the low-risk group, while other genes were lower than those in the high-risk group (Figures 6G, H). Finally, we evaluated the association between RS and drug sensitivity. We found that the IC50 values of various chemotherapeutics were significantly different between the high- and low-risk groups, including axitinib, gefitinib and erlotinib, sorafenib, vinorelbine, gemcitabine, nilotinib and tipifarnib (Supplementary Figures S6A–H).

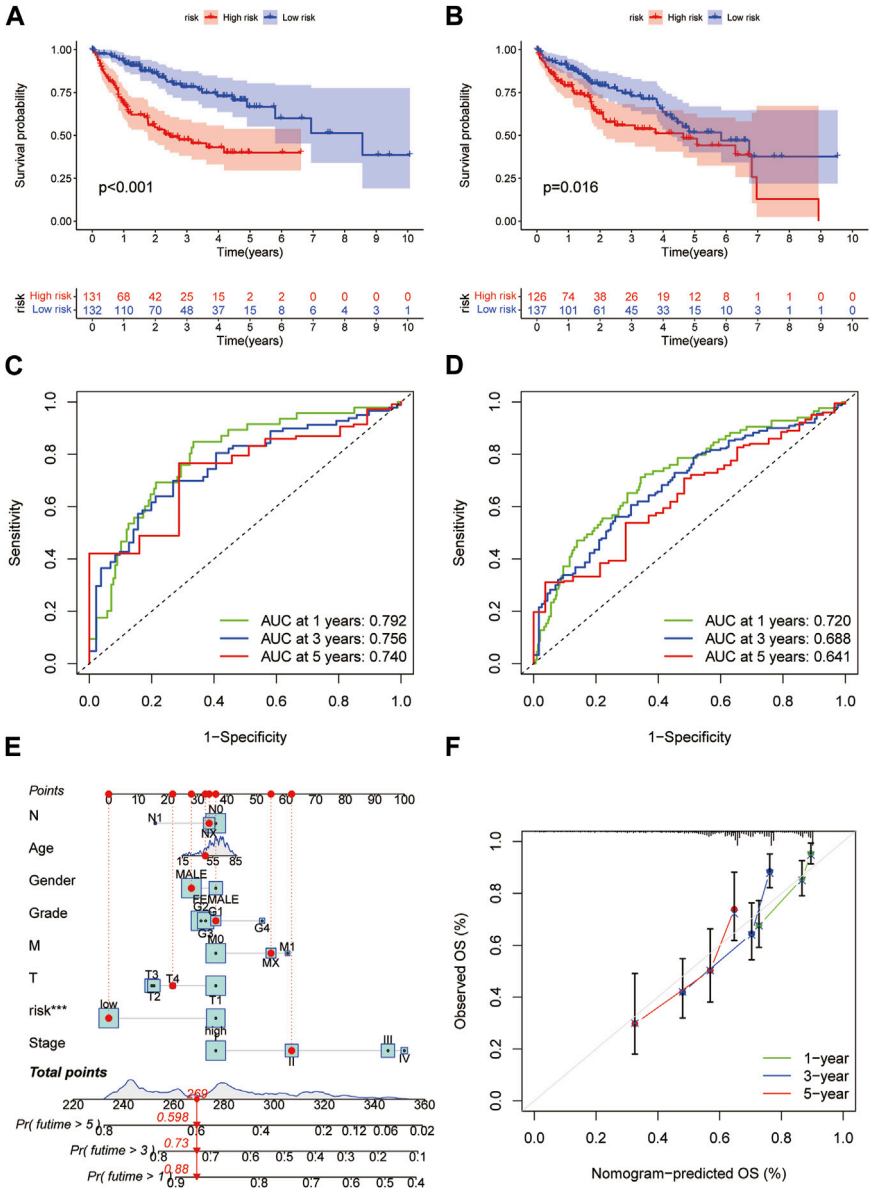

FIGURE 5
Prediction model and nomogram. **(A,B)** Kaplan-Meier curves in the training and test cohorts. **(C,D)** ROC curves estimate prognosis value. **(E)** Nomogram for predicting the OS of HCC patients. **(F)** Calibration curves of the nomogram.

3.6 BEX1 are differentially expressed in hepatocytes

Detecting protein expression in HCC cells found that these five key genes were abnormally expressed to varying degrees in different HCC cells, especially BEX1 (Figure 7A). Compared with normal tissues, the expression levels of BEX1 in tumor tissues were significantly different, while the GCLM, G6PC, NEIL3 and NT5DC2 protein bands were unclear, which may be related to their low expression levels (Figure 7B). This was confirmed by single-cell analysis, which showed that there was no significant expression in hepatocytes (Figures 7K, L). To further explore the cellular expression of BEX1 in HCC tumors, 18 HCC samples in the GSE149614 dataset were analyzed. First, we controlled the effects of low-quality cells, mitochondrial genes, ribosomal genes, and hemoglobin. The correlations between the total number of unique molecular identifiers (UMIs) in each cell and the mitochondrial ratio, the total number of genes, and the hemoglobin ratio were 0.11, 0.91, and −0.01, respectively (Supplementary Figures S7A, B). No significant separation trend of HCC cells was observed when PCA was used to reduce the dimension, and we finally selected the top 20 PCs for further analysis based on the elbow plots (Supplementary Figures S5C, D). tSNE analysis classified HCC cells into 30 clusters (Figure 7C). The cells were annotated and divided into immune cell clusters and non-immune cell clusters (Figure 7D). We then proceeded to annotate eight subclusters using single-cell markers, including B cells, endothelial cells, hepatocytes, macrophages, monocytes, NK cells, smooth muscle cells and T cells (Figure 7E). In addition, normal and tumor tissues were similarly clustered and annotated by tSNE (Figures 7F, G). Finally, we tested

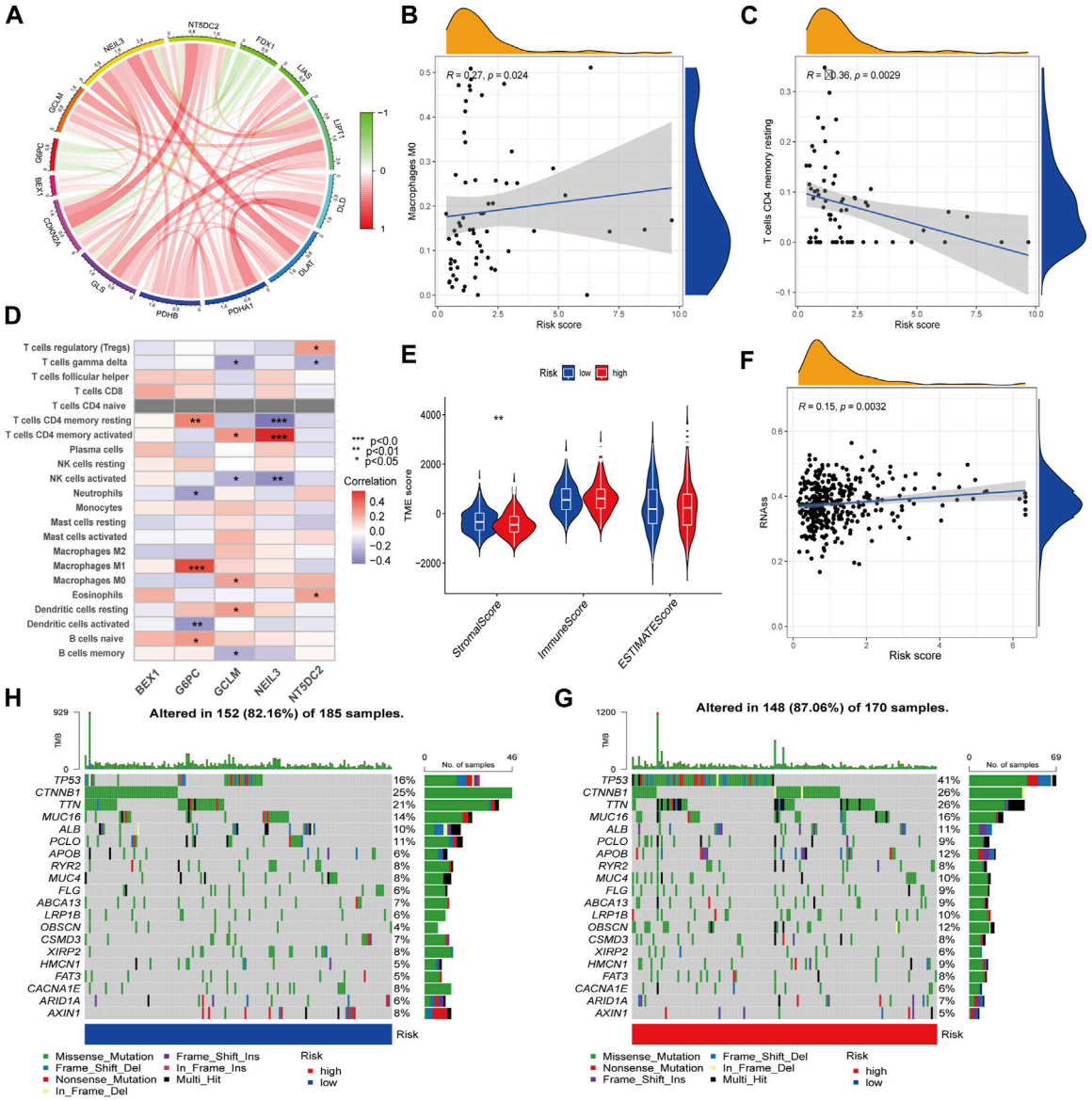

FIGURE 6
TME characteristics and drug susceptibility. **(A)**The interaction network of CRGs and hub genes. **(B,C)** Correlation between immune cells and RS. **(D)** Correlations between the immune cells and 5 hub genes. **(E)** Differences in the StromalScore and ImmuneScore. **(F)** Correlation of RS with CSCs. **(G,H)** Mutation of genes in distinct RS group.

the expression patterns of target genes in HCC cell clusters. The obtained results showed that the expression levels of BEX1 were the same as Western blotting, and they were only expressed in hepatocytes (Figures 7H–J). This finding indicates that BEX1 may be the key genes mediating cuproptosis in HCC cells.

3.7 Knockdown of BEX1 inhibited HCC cell proliferation, invasion and migration

We found that BEX1 had the most significant differences in the five hub genes after detection of liver cancer cells, tissues and single-cell analysis. In order to further explore the biological function of BEX1, we used two methods to knockdown BEX1, both of which could effectively silence the expression of BEX1 (Figure 8C). The results of cell viability experiment showed that the viabilities of liver cancer cells decreased significantly after 48 h of BEX1 knockdown compared with the control group (Figure 8A). In addition, transwell results showed that the invasion and migration of LM3 cells with low BEX1 were significantly reduced (Figure 8B). Finally, we also detected the expression of epithelial mesenchymal transition (EMT) markers including E-cadherin, N-cadherin and Vimentin. The results indicated that BEX1 knockdown promoted E-cadherin expression and decreased the expression of N-cadherin and Vimentin. Which demonstrated that inhibition of BEX1 suppressed liver cancer cells EMT pathway (Figure 8C). Those results indicated that BEX1 deletion inhibited the proliferation, invasion and migration and EMT pathway of HCC cells.

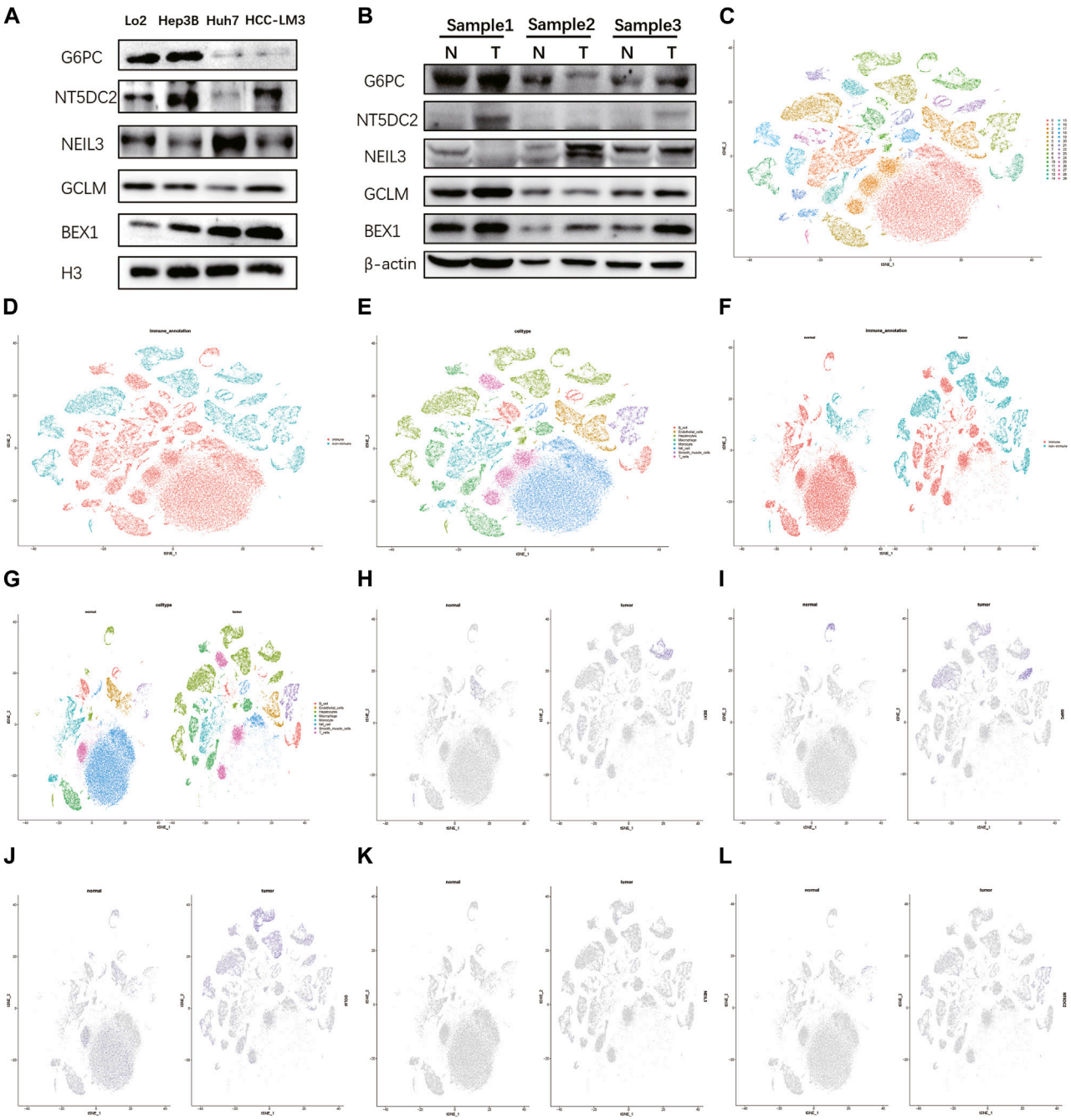

FIGURE 7
Western blotting and single cell analysis of the 5 hub genes. **(A,B)** Western blotting in HCC cell and tumor tissue. **(C–G)** Cell clusters and annotates for GSE149614 of HCC patients. **(H–L)** Expression pattern of 5 hub genes at the single-cell level in normal and tumor cell clusters through t-SNE analysis.

3.8 Sorafenib specifically binds to key genes

To further explore whether the target gene may be a potential target of HCC immunotherapy, we used sorafenib as the ligand and the hub gene as the receptor for molecular docking analysis. The obtained results showed that the binding energies of sorafenib to G6PC, GCLM, BEX1, NT5DC2 and NEIL3 were −9.6, −8.5, −6.7, −8.3, and −8.0 kcal/mol, respectively. These hub genes can bind to sorafenib and form a stable conformation (Figure 8D). This finding suggests that the high expression of BEX1 in hepatocytes may be a potential therapeutic target to mediate cuproptosis in HCC.

4 Discussion

Numerous studies have indicated that PCD plays a key role in tumorigenesis and progression of HCC and antitumor response, with the powerful immunotherapeutic potential (Demirtas and Gunduz, 2021). However, the specific function in anti-tumor

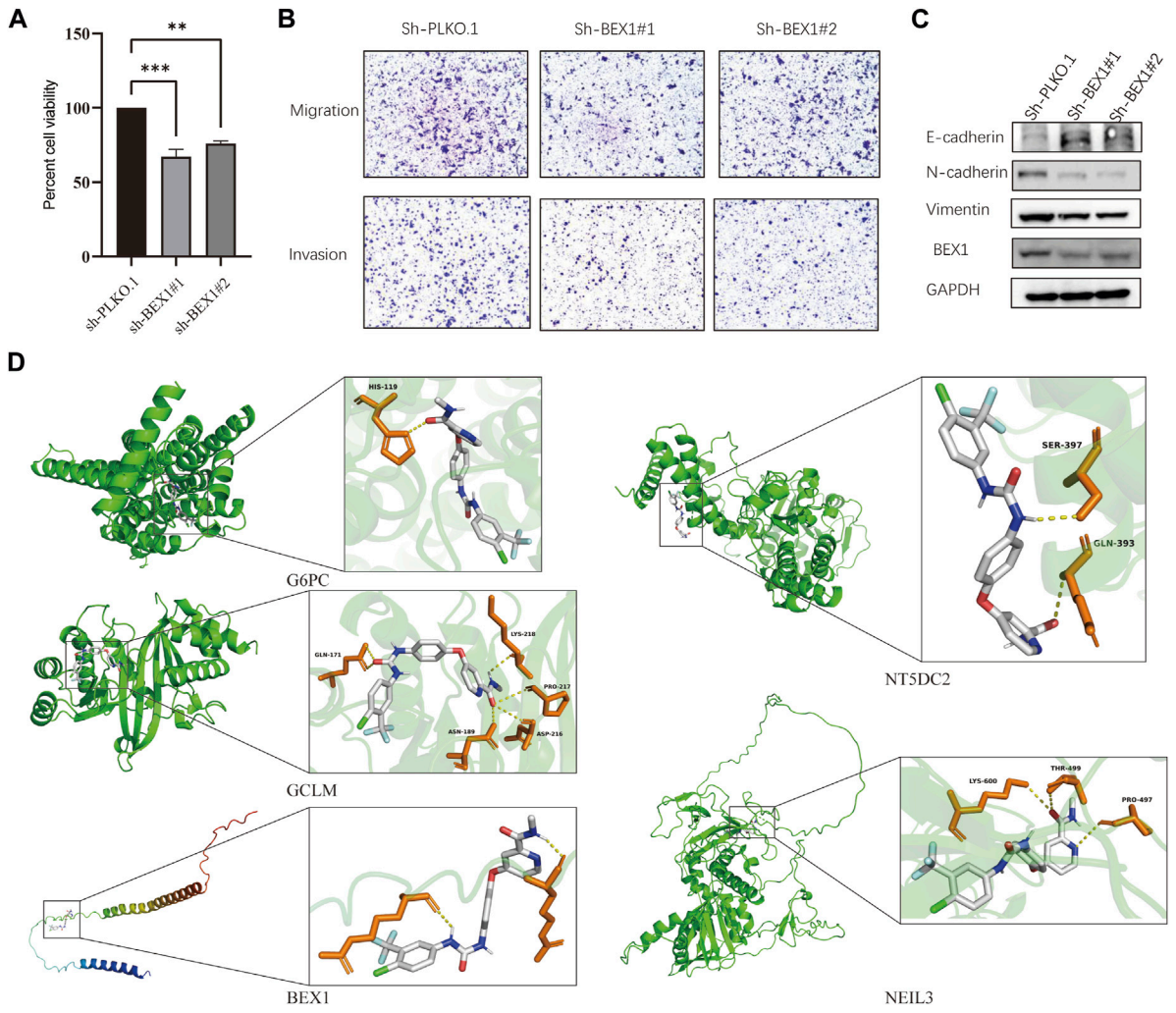

FIGURE 8
BEX1 biological function and molecular docking. **(A)** Cell viability experiment of BEX1 knockdown. **(B,C)** Transwell results and cadherin proteins expression in HCC cell with sh-BEX1. **(D)** Molecular docking of sorafenib and the 5 hub genes.

remains unknown, and research on cuproptosis is even scarcer. Therefore, this study extensively explored the copy number variation, clinical feature relationship, TME and immune infiltration of CRGs in HCC at the transcriptome level, single-cell level and network pharmacology level and revealed that GCLM and BEX1 may be potential therapeutic targets mediating cuproptosis in HCC.

CNV is a characteristic change in neoplastic diseases that has been gradually recognized in the postgenomic era. The human genome contains numerous repetitive sequences of varying frequencies and intensities, and CNV is defined as a type of alteration involving deletion, insertion, replication and multilocus variation of gene segments ranging from 1 Kb to 3 Mb (Kinross et al., 2012; Shi et al., 2021). Current studies suggest that CNV is not only the basis of individual genetic differences but also plays an essential role in tumorigenesis, invasion and metastasis. CNV-related indicators may become ideal tumor diagnostic markers (Behroozi et al., 2020; Pariyar et al., 2021). Huang et al. (2021) found that estrogen-related receptor alpha (ESRRA) CNV was significantly correlated with the histological grade of ovarian cancer (OC). The results indicated that CNV has the function in affecting biological phenotype and heterogeneity of tumors and promoting tumor progression. However, the above mentioned study evaluated only the CNV of genes alone and lacked a comprehensive study combining CNV and gene expression. In this study, we analyzed them together, and the characteristics of cuproptosis genes in HCC were more accurately identified. We found clear CNVs in all CRGs except MIF1. Among them, CDKN2A had the highest mutation frequency and expression difference, while FDX1 had no difference in expression between normal tissue and tumor tissue, although there was a higher amplification mutation. Similarly, previous studies by Ghaffari et al. (2016) showed that the CNV of the baculoviral inhibitor of apoptosis repeat-containing 5 gene is highly increased in tumor tissue and may become a marker for early cancer detection and prognosis. Therefore, this study suggests that CNV detection of these highly expressed CRGs may contribute to the diagnosis of HCC. Of note, CNVs can also activate proto-oncogenes and reduce the activity of tumor suppressor genes,

thereby mediating the pathogenesis and prognostic mechanisms of various tumors, including liver cancer (Diskin et al., 2009; Nik-Zainal et al., 2016). In the analysis of prognosis and clinical features in this study, it was found that CNV genes were closely related to OS, disease progression and immune invasion in HCC patients. This finding indicates that CNV genes, such as CDKN2A, plays a key role in the escape from immune surveillance.

Furthermore, this study also screened CRG-related genes to construct an HCC risk model for predicting prognosis, searching for immunotherapy strategies and drug targets. The obtained results indicated that five CRG-related genes were independent prognostic factors of HCC. We further constructed a new prognostic model based on these genes. Compared with traditional TNM staging, this model integrates multiple molecular markers, clinicopathological parameters and other multilevel prognostic indicators, which can not only identify HCC patients with different risks but also more accurately and dynamically monitor tumor progression and prognosis. Similar studies have been conducted in previous studies, such as by Song et al. (2021), who screened pyroptosis-related genes and constructed a colorectal cancer (CRC) risk model. Based on these model results, Liao et al. (2022) found that FOXP2 promotes CRC pyroptosis by interacting with caspase-1. In addition, several studies have reported the role of cuproptosis in HCC. Zhao et al. (2022) explored cuproptosis related genes (CRGs) related to HCC survival and clinical features. And they found 20 CRGs were correlated to HCC outcomes and might be used as a prognostic biomarker for HCC. Besides, Zhang et al. (2022) investigated the association between FDX1 expression and cancer stages and outcomes in HCC. They constructed the model based on FDX1 and its related genes. And the AUC values of cuproptosis-related risk score (CRRS) in predicting the OS were 0.72 and 0.68 at 1 and 3 years respectively. Similarly, Yan et al. (2022) developed a predictive model (GCSH, LIPT1 and CDKN2A) based on CRGs in HCC. The AUC values of ROC analysis for 1 year OS were from 0.614 to 0.683. And they found LIPT1 might be a target in the treatment of HCC. In our study, a predictive model was constructed consists of five genes (BEX1, NEIL3, GCLM, G6PC and NT5DC2) through comprehensive bioinformatics analysis. The model was validated by an internal dataset with an AUC was 0.720–0.792 for 1 year, 0.688–0.756 for 3 years and 0.641–0.740 for 5 years, respectively, which showed a robust performance than previous models. Besides, molecular docking and experiments indicated that BEX1 may mediate the cuproptosis of hepatocytes as potential therapeutic targets for HCC. Therefore, the five key genes and risk models screened in this study play an extremely vital role in the diagnosis and treatment of HCC. On the other hand, the accuracy of quantitative analysis of these genes is not less than that of whole transcriptome sequencing, and it is more economical and clinically feasible.

With the great breakthrough in immunotherapy, an increasing number of researchers have realized that tumor cells do not exist in isolation, and the TME in which they are located plays an indispensable role in tumor progression. The TME is mainly composed of immune cells including lymphocytes, macrophages and granulocytes in the center and fibroblasts, inflammatory cells and various signaling molecules in the surroundings (Turley et al., 2015; Seager et al., 2017). Numerous evidence have shown that the cellular components in the TME are strongly linked to the progression, metastasis and efficacy of HCC (Chew et al., 2017; Satilmis et al., 2021). For example, Mano et al. (2019) found that bone morphogenetic protein 4 (BNP-4) could enhance the aggressiveness of HCC by activating fibroblasts (CAFs) to secrete cytokines in the TME. Besides, tumor-associated macrophages (TAMs) also exhibited different activation states in the TME depending on the different stimulus. Previous studies have shown that TAMs in HCC tumor stroma produce various proinflammatory cytokines, including TNF-α, IL-β, IL-6 and IL-23, which induce the expansion of $CD4^+$ Th17 cells, according to the overexpression of PD-L1, CTLA4 to inhibit antitumor immunity (Kuang et al., 2010). Previous studies have mainly concentrated on the innate T cell immune response. However, in the ongoing exploration of advanced HCC and other cancers, immunotherapy methods increasingly focus on immune checkpoint inhibitors (ICIs), such as CTLA-4, PD-1 and PD-L1, which lock the immune checkpoint inhibition pathways (Kudo, 2019a). These results indicate that ICIs based on TME changes will be a new therapeutic strategy for HCC.

However, in this research, we found that multiple immune markers, such as PD-L1, CD276, CD80 and CTLA4, were significantly higher in the high-risk group with worse prognosis than in the low-risk group, and RS was significantly correlated with M0 macrophages and memory $CD4^+$ T cells. This suggests that HCC hepatocytes may achieve immune resistance or immune escape by overexpressing PD-L1 and binding to PD-1 on the surface of specific cytotoxic T cells. Of course, this mechanism is more complicated in practice. For example, Kudo (2019b) found that activated $CD8^+$ T cells released interferon gamma (IFN-γ) during the process of initial cellular immunity, which not only attacked tumor cells but also engaged with receptors on the surface of cancer cells to upregulate PD-L1 and inhibit antitumor effects. Currently, research on PD-1 and PD-L1 inhibitors is in full swing and has become an important part of the systemic treatment of HCC in clinical practice. Numerous studies demonstrated that nivolumab and pembrolizumab have shown efficacy in the treatment of HCC especially as an alternative strategy after sorafenib failure or unacceptable toxicity (El-Khoueiry et al., 2017; Zhu et al., 2018). In addition, as a transmembrane receptor on the surface of activated T cells, the expression of CTLA4 is strictly regulated. In resting or naive T cells, CTLA4 is mainly located in intracellular vesicles (Valk et al., 2008). However, on activated T cells, CTLA4 directly competes with CD28 for B7 ligands to mediate tumor immune responses (Hathcock et al., 1993). In addition, CTLA4 activation also supported the transformation of $CD4^+$ T cells into regulatory T cells by increasing transforming growth factor-β (TGFβ) secretion and forkhead box protein 3 (FOXP3) expression (Zheng et al., 2006). In fact, many mechanisms are involved in the tumor immune response in the TME, but the specific effects are still controversial.

In addition, we detected the protein level of five important genes and found that the expression of BEX1 in tumor cells and tissues was higher than that in normal liver cells and tissues. To further explore the biological function of BEX1, cell viability experiment and transwell results showed that BEX1 deletion inhibited the proliferation, invasion and migration of HCC cells. These results suggest that BEX1 may play a key role in HCC tumorigenesis and development. However, only few studies described the role of BEX1 in HCC. BEX1 (brain-expressed X-linked protein 1), attached to the BEX family and consists of five proteins with unclear functions (Kazi et al., 2015). BEX1 was initially thought

to be associated with retinoic acid differentiation in teratomas (Faria et al., 1998). Later, multiple research teams successively reported its expression changes in many cancers (Quentmeier et al., 2005; Foltz et al., 2006; Kazi et al., 2015). Current research suggests that in addition to being involved in the regeneration of neuronal axons and regulating the cell cycle, BEX1 is also involved in the proliferation and invasion (Vilar et al., 2006; Khazaei et al., 2010; Doi et al., 2020; Lee et al., 2021) showed that BEX1 and BEX4 can improve the tumor formation and radio resistance of glioblastoma multiforme cells. In breast cancer, overexpression of BEX1 and BEX2 can inhibit the apoptosis of tumor cells (Naderi et al., 2007). Deficiency of Bex1 expression led to the decrease of cell proliferation, colony and tumor formation, and the increase of cell apoptosis in acute myeloid leukemia (Lindblad et al., 2015). These studies all suggest that BEX1 may be an oncogene, but there is still a lack of studies on the gene, especially in HCC. Sagawa et al. (2015) showed that BEX1 was upregulated in Cx32ΔTg rat liver, and knockdown of BEX1 could significantly inhibit the growth of rat hepatoma cell lines. In human HCC studies, Wang et al. (2021) discovered that BEX1 is an oncofetal protein that interacts with RUNX family transcription factor 3 (RUNX3) in hepatoblastoma (HB) and CSC-HCC to block β-catenin transcription and activate the Wnt/β-catenin signaling pathway, thereby regulating the self-renewal of hepatic CSCs. These results indicate that BEX1 is a promising therapeutic target forHB and CSC-HCC, and targeting the BeX1-mediated Wnt/β-catenin signaling pathway may help to resolve the heterogeneity and high recurrence rate of HCC.

Previous studies also explored the potential targets of cuproptosis in HCC. For example, FDX1, LIPT1, DLAT, CDKN2A and GLS were reported to have potential value as cuproptosis targets in HCC. Zhang et al. (2022) found FDX1 was downregulated in HCC, and higher expression of FDX1 was related to a better outcome. Beside, FDX1 inhibited the proliferation and colony formation of tumor cells in the presence of copper ions and this inhibitory effect was diminished by using tetrathiomolybdate (TTM) to chelate copper ions, which indicated that FDX1 exerted anti-tumor effects through cuproptosis (Li et al., 2022). And Yan et al. (2022) revealed that LIPT1 was higher expressed in HCC and patients with low LIPT1 expression had longer OS than those high LIPT1 expression. Cell proliferation assay showed that LIPT1 depletion inhibited cancer viability in HCC cells. Besides, LIPT1 knock down significantly suppressed cell migration and invasion capacity in HCC cells. Similar results were found in DLAT (Yang et al., 2023), CDKN2A and GLS (Ma et al., 2023). In our study, we found BEX1 deletion inhibited the proliferation, invasion and migration and EMT pathway of HCC cells. Besides, BEX1 can bind to sorafenib and form a stable conformation which further suggests that the BEX1 in hepatocytes may be a potential therapeutic target to mediate cuproptosis in HCC.

Furthermore, we detected the protein level of five important genes and found that the expression of the other genes except BEX1 in tumor cells and tissues was higher than that in normal liver cells and tissues. To further explore the specific cellular expression patterns of these genes in HCC, we conducted scRNA-seq data to identify the distribution of G6PC, GCLM NEIL3 and NT5DC2 in different cell subclusters in HCC tissues including HCC tumor cells and non-tumor cells. And the results clearly revealed that GCLM and G6PC were only highly expressed in HCC cells, while lowly expressed in non-tumor cells. The expression of NEIL3 and NT5DC2 was not obvious in hepatocellular carcinoma cells. These results suggest that GCLM and G6PC regulate HCC development directly on the target of hepatocytes rather than other cells, which provides potential therapeutic targets.

Glucose-6-phosphatase (G6PC) is a component critical for catalyzing glycogenolysis, and the downregulated of G6PC enhances glucose storage in premalignant cells (Franco et al., 2005; Resaz et al., 2014), and glycogen accumulation is a key carcinogenic event in the malignant transformation of the liver (Liu et al., 2021). Bioinformatics analysis demonstrated that low expression of G6PC was related to poor outcomes in HCC (Tian and Liao, 2022). However, there still is an empty in studies related to the regulation of copper by BEX1 and GP6C.

GCLM is a glutamate cysteine ligase modifier subunit that is the main component of glutathione (GSH) synthetase and participates in the synthesis and metabolism of GSH on multiple levels, and increasing evidence has shown that GSH metabolic dysregulation is involved in the pathophysiological mechanisms of various diseases, including diabetes, liver fibrosis, alcoholic liver disease, and malignant tumors (Liu and Gaston, 2010; Lv et al., 2019; Shen and Wang, 2021). Previous studies have shown that HCC patients showed higher levels of oxidative stress markers and low levels of GSH and GSH-related antioxidant enzymes in plasma compared with nonalcoholic steatohepatitis patients (Shimomura et al., 2017). The imbalance between high oxidative stress and low antioxidant capacity may be an important reason for the occurrence and development of HCC. Therefore, regulating the expression of GCLM may indirectly play an essential function in the development of HCC. In addition, studies have shown that GCLM expression is mainly regulated by transcription factors, including activator protein-1 (AP-1), nuclear factor kappa B (NFκB) and nuclear factor erythroid 2 related factor 2 (Nrf2) (Jaiswal, 2004; Yang et al., 2005; Roos et al., 2020) confirmed that treatment of human hepatocellular carcinoma (HepG2) cells with the receptor tyrosine kinase inhibitor lapatinib activates the Kelch-like ECH-associated protein 1 (Keap1)-Nrf2 signaling pathway, thereby upregulating GCLM levels and inducing GSH synthesis. Most interestingly, Thai et al. (2021) found that copper nanoparticles (Cu NPs) have the most significant effect on NrF2-mediated cytotoxicity, and upregulated GCLM can be used as a biomarker for Cu NP exposure in HCC cells. This is similar to our study, indicating that GCLM is more sensitive to copper damage and may be a key target in mediating cuproptosis in hepatocytes.

Finally, we verified the potential role of these hub genes as therapeutic targets in HCC. We performed drug-target network and molecular docking analyses with sorafenib as the ligand and the hub gene as the receptor, and the obtained results showed that BEX1, G6PC and GCLM could bind to sorafenib and form stable conformations. Sorafenib, as a multiple-target tyrosine kinase inhibitor (TKI), has the functions of anti-angiogenesis and anti-proliferation, besides it can also prolong the overall median survival time of patients with advanced HCC (Llovet et al., 2008). Two important clinical trials, the Asia-Pacific and Sorafenib HCC Assessment Randomized Protocol (SHARP), also showed that sorafenib has a powerful function in improving the prognosis of patients with HCC (Cheng et al., 2009; Vogel and Saborowski, 2020). In addition, Sorafenib is an effective first-line treatment in patients with advanced HCC (Xing et al., 2021). *In vitro* experiments revealed that sorafenib inhibits tumor cell viability,

promotes cell apoptosis in HCC cells (Xie et al., 2018). Therefore, we used sorafenib as the ligand and the hub gene as the receptor for molecular docking analysis.

Although current ICIs have opened up a new strategy in treating malignant tumors, sorafenib is still the first-line drug for HCC chemotherapy (Benson et al., 2021). In recent years, studies on the discovery of new efficacy and potential therapeutic targets for known drugs are not uncommon; Pushpakom et al. (2019) found that Raloxifene was initially used to treat osteoporosis and was later approved for the treatment of breast cancer. Additionally, a study by Pang et al. (2019) is similar to ours; they confirmed that C3 and ANXN1 can stably bind to Vorinostat, which can be used as potential therapeutic targets for papillary renal cell carcinoma through genetic screening and molecular docking. Therefore, it is reasonable to speculate that BEX1, G6PC and GCLM can be used as potential therapeutic targets of HCC to mediate the mechanism of cuproptosis in hepatocytes.

Nevertheless, there are still several limitations in this study. First, this is a prospective study, outcomes can be affected by the introduction of unknown variables during follow-up, or changes in known variables including treatment modality disease and surgery-related complications. Second, our prognostic model was obtained based on TCGA and GEO data but lacked validation with external datasets, limited the breadth of its use. Third, we investigated the cellular molecular function of BEX1 in HCC but did not explore the interaction between BEX1 and copper ions in hepatic tumor cells, therefore, we could not clarify whether the BEX1-regulated cellular activity was related to copper ions. Finally, the specific mechanism by which BEX1 regulates HCC progression remains unclear. In the future studies, external datasets or one's own data to assess the stability of the model is needed. Furthermore, *in vivo* and *in vitro* experiments are needed to investigate the exact mechanism by which BEX1 regulates cuproptosis especially in the presence of copper ions or when activity is inhibited.

5 Conclusion

This study extensively explored the multi-omics features of CRGs in HCC, including CNV, clinicopathological indicators, prognosis, immune infiltration, and TME, and constructed a prognostic prediction model integrating multiple molecular markers and clinicopathological parameters, which offers a new method for clinical diagnosis and prognosis evaluation. Meanwhile, GCLM and BEX1 were identified as hub genes, which are potential therapeutic targets to mediate the cuproptosis program in HCC cells.

Data availability statement

The raw data supporting the conclusion of this article will be made available by the authors, without undue reservation.

Ethics statement

The study was carried out under the permission of the Ethics Committee of the First Affiliated Hospital of Anhui Medical University. Patients or their relatives signed written informed consent. All the studies were performed in accordance with the Declaration of Helsinki.

Author contributions

FC: Data curation, Writing–Original draft preparation. YQ: Software, Writing–Reviewing and Editing. WW: Visualization, Investigation. XL and CY: Methodology, Software and Revision. All authors contributed to the article and approved the submitted version.

Funding

This work was supported by the China Scholarship Council under No. 202008340087 and No. 202108340033. We acknowledge support from the German Research Foundation (DFG) and Leipzig University within the program of Open Access Publishing.

Acknowledgments

We thank the investigators who participated and provided data unselfishly in TCGA and GEO databases.

Conflict of interest

The authors declare that the research was conducted in the absence of any commercial or financial relationships that could be construed as a potential conflict of interest.

Publisher's note

Supplementary material

The Supplementary Material for this article can be found online at: https://www.frontiersin.org/articles/10.3389/fcell.2023.1240390/full#supplementary-material

References

Atakul, T., Altinkaya, S. O., Abas, B. I., and Yenisey, C. (2020). Serum copper and zinc levels in patients with endometrial cancer. *Biol. TRACE Elem. Res.* 195 (1), 46–54. doi:10.1007/s12011-019-01844-x

Behroozi, J., Shahbazi, S., Bakhtiarizadeh, M. R., and Mahmoodzadeh, H. (2020). ADAR expression and copy number variation in patients with advanced gastric cancer. *BMC Gastroenterol.* 20 (1), 152. doi:10.1186/s12876-020-01299-8

Benson, A. B., D'Angelica, M. I., Abbott, D. E., Anaya, D. A., Anders, R., Are, C., et al. (2021). Hepatobiliary cancers, version 2.2021, NCCN clinical practice guidelines in oncology. *J. Natl. Compr. CANC NE* 19 (5), 541–565. doi:10.6004/jnccn.2021.0022

Cai, J., Chen, L., Zhang, Z., Zhang, X., Lu, X., Liu, W., et al. (2019). Genome-wide mapping of 5-hydroxymethylcytosines in circulating cell-free DNA as a non-invasive approach for early detection of hepatocellular carcinoma. *Multicent. Study* 68 (12), 2195–2205. doi:10.1136/gutjnl-2019-318882

Cheng, A. L., Kang, Y. K., Chen, Z., Tsao, C. J., Qin, S., Kim, J. S., et al. (2009). Efficacy and safety of sorafenib in patients in the asia-pacific region with advanced hepatocellular carcinoma: A phase III randomised, double-blind, placebo-controlled trial. *LANCET Oncol.* 10 (1), 25–34. doi:10.1016/S1470-2045(08)70285-7

Chew, V., Lai, L., Pan, L., Lim, C. J., Li, J., Ong, R., et al. (2017). Delineation of an immunosuppressive gradient in hepatocellular carcinoma using high-dimensional proteomic and transcriptomic analyses. *P Natl. Acad. Sci. U. S. A.* 114 (29), E5900-E5909–9. doi:10.1073/pnas.1706559114

Craig, A. J., von Felden, J., Garcia-Lezana, T., Sarcognato, S., and Villanueva, A. (2020). Tumour evolution in hepatocellular carcinoma. *Nat. Rev. GASTRO Hepat.* 17 (3), 139–152. doi:10.1038/s41575-019-0229-4

Demirtas, C. O., and Gunduz, F. (2021). Programmed cell death 1 and hepatocellular carcinoma: an epochal story. *J. Gastrointest. CANC* 52 (4), 1217–1222. doi:10.1007/s12029-021-00758-z

Diskin, S. J., Hou, C., Glessner, J. T., Attiyeh, E. F., Laudenslager, M., Bosse, K., et al. (2009). Copy number variation at 1q21.1 associated with neuroblastoma. *NATURE* 459 (7249), 987–991. doi:10.1038/nature08035

Doi, T., Ogawa, H., Tanaka, Y., Hayashi, Y., and Maniwa, Y. (2020). Bex1 significantly contributes to the proliferation and invasiveness of malignant tumor cells. *Oncol. Lett.* 20 (6), 362. doi:10.3892/ol.2020.12226

El-Khoueiry, A. B., Sangro, B., Yau, T., Crocenzi, T. S., Kudo, M., Hsu, C., et al. (2017). Nivolumab in patients with advanced hepatocellular carcinoma (CheckMate 040): an open-label, non-comparative, phase 1/2 dose escalation and expansion trial. *LANCET* 389 (10088), 2492–2502. doi:10.1016/S0140-6736(17)31046-2

Faria, T. N., LaRosa, G. J., Wilen, E., Liao, J., and Gudas, L. J. (1998). Characterization of genes which exhibit reduced expression during the retinoic acid-induced differentiation of F9 teratocarcinoma cells: involvement of cyclin D3 in RA-mediated growth arrest. *Mol. Cell Endocrinol.* 143 (1-2), 155–166. doi:10.1016/s0303-7207(98)00127-0

Foltz, G., Ryu, G. Y., Yoon, J. G., Nelson, T., Fahey, J., Frakes, A., et al. (2006). Genome-wide analysis of epigenetic silencing identifies BEX1 and BEX2 as candidate tumor suppressor genes in malignant glioma. *CANCER Res.* 66 (13), 6665–6674. doi:10.1158/0008-5472.CAN-05-4453

Franco, L. M., Krishnamurthy, V., Bali, D., Weinstein, D. A., Arn, P., Clary, B., et al. (2005). Hepatocellular carcinoma in glycogen storage disease type ia: A case series. *J. Inherit. Metab. Dis.* 28 (2), 153–162. doi:10.1007/s10545-005-7500-2

Ge, E. J., Bush, A. I., Casini, A., Cobine, P. A., Cross, J. R., DeNicola, G. M., et al. (2022). Connecting copper and cancer: from transition metal signalling to metalloplasia. *Nat. Rev. CANCER* 22 (2), 102–113. doi:10.1038/s41568-021-00417-2

Ghaffari, K., Hashemi, M., Ebrahimi, E., and Shirkoohi, R. (2016). BIRC5 genomic copy number variation in early-onset breast cancer. *Iran. Biomed. J.* 20 (4), 241–245. doi:10.7508/ibj.2016.04.009

Hathcock, K. S., Laszlo, G., Dickler, H. B., Bradshaw, J., Linsley, P., and Hodes, R. J. (1993). Identification of an alternative CTLA-4 ligand costimulatory for T cell activation. *SCIENCE* 262 (5135), 905–907. doi:10.1126/science.7694361

Hou, J., Zhao, R., Xia, W., Chang, C. W., You, Y., Hsu, J. M., et al. (2020). PD-L1-mediated gasdermin C expression switches apoptosis to pyroptosis in cancer cells and facilitates tumour necrosis. *Nat. Cell Biol.* 22 (10), 1264–1275. doi:10.1038/s41556-020-0575-z

Huang, X., Ruan, G., and Sun, P. (2021). Estrogen-related receptor alpha copy number variation is associated with ovarian cancer histological grade. *J. Obstet. Gynaecol. Re.* 47 (5), 1878–1883. doi:10.1111/jog.14741

Huo, T. I., Hsu, C. Y., and Liu, P. H. (2018). Magic mirror on the wall: which is the best biomarker for hepatocellular carcinoma? *HEPATOLOGY* 67 (6), 2482–2483. doi:10.1002/hep.29869

Jaiswal, A. K. (2004). Nrf2 signaling in coordinated activation of antioxidant gene expression. *FREE Radic. BIO Med.* 36 (10), 1199–1207. doi:10.1016/j.freeradbiomed.2004.02.074

Jiang, Y., Huo, Z., Qi, X., Zuo, T., and Wu, Z. (2022). Copper-induced tumor cell death mechanisms and antitumor theragnostic applications of copper complexes. *NANOMEDICINE-UK* 17 (5), 303–324. doi:10.2217/nnm-2021-0374

Kazi, J. U., Kabir, N. N., and Ronnstrand, L. (2015). Brain-Expressed X-linked (BEX) proteins in human cancers. *Biochim. Biophys. Acta.* 1856 (2), 226–233. doi:10.1016/j.bbcan.2015.09.001

Khazaei, M. R., Halfter, H., Karimzadeh, F., Koo, J. H., Margolis, F. L., and Young, P. (2010). Bex1 is involved in the regeneration of axons after injury. *J. Neurochem.* 115 (4), 910–920. doi:10.1111/j.1471-4159.2010.06960.x

Kinross, K. M., Montgomery, K. G., Kleinschmidt, M., Waring, P., Ivetac, I., Tikoo, A., et al. (2012). An activating Pik3ca mutation coupled with Pten loss is sufficient to initiate ovarian tumorigenesis in mice. *J. Clin. Invest.* 122 (2), 553–557. doi:10.1172/JCI59309

Kuang, D. M., Peng, C., Zhao, Q., Wu, Y., Chen, M. S., and Zheng, L. (2010). Activated monocytes in peritumoral stroma of hepatocellular carcinoma promote expansion of memory T helper 17 cells. *HEPATOLOGY* 51 (1), 154–164. doi:10.1002/hep.23291

Kudo, M. (2019b). Combination cancer immunotherapy with molecular targeted agents/anti-CTLA-4 antibody for hepatocellular carcinoma. *LIVER CANCER* 8 (1), 1–11. doi:10.1159/000496277

Kudo, M. (2019a). Immuno-oncology therapy for hepatocellular carcinoma: current status and ongoing trials. *LIVER CANCER* 8 (4), 221–238. doi:10.1159/000501501

Kurebayashi, Y., Ojima, H., Tsujikawa, H., Kubota, N., Maehara, J., Abe, Y., et al. (2018). Landscape of immune microenvironment in hepatocellular carcinoma and its additional impact on histological and molecular classification. *HEPATOLOGY* 68 (3), 1025–1041. doi:10.1002/hep.29904

Lee, S., Kang, H., Shin, E., Jeon, J., Youn, H., and Youn, B. (2021). BEX1 and BEX4 induce GBM progression through regulation of actin polymerization and activation of YAP/TAZ signaling. *Int. J. Mol. Sci.* 22 (18), 9845. doi:10.3390/ijms22189845

Li, H., Wang, J., Wu, C., Wang, L., Chen, Z. S., and Cui, W. (2020b). The combination of disulfiram and copper for cancer treatment. *DRUG Discov. TODAY* 25 (6), 1099–1108. doi:10.1016/j.drudis.2020.04.003

Li, X., Dai, Z., Liu, J., Sun, Z., Li, N., Jiao, G., et al. (2022). Characterization of the functional effects of ferredoxin 1 as a cuproptosis biomarker in cancer. *Front. Genet.* 13, 969856. doi:10.3389/fgene.2022.969856

Li, X., He, S., and Ma, B. (2020a). Autophagy and autophagy-related proteins in cancer. *Mol. CANCER* 19 (1), 12. doi:10.1186/s12943-020-1138-4

Liao, P., Huang, W. H., Cao, L., Wang, T., and Chen, L. M. (2022). Low expression of FOXP2 predicts poor survival and targets caspase-1 to inhibit cell pyroptosis in colorectal cancer. *J. CANCER* 13 (4), 1181–1192. doi:10.7150/jca.62433

Lindblad, O., Li, T., Su, X., Sun, J., Kabir, N. N., Levander, F., et al. (2015). BEX1 acts as a tumor suppressor in acute myeloid leukemia. *Oncotarget* 6 (25), 21395–21405. doi:10.18632/oncotarget.4095

Liu, Q., Li, J., Zhang, W., Xiao, C., Zhang, S., Nian, C., et al. (2021). Glycogen accumulation and phase separation drives liver tumor initiation. *Cell* 184 (22), 5559–5576.e19. doi:10.1016/j.cell.2021.10.001

Liu, R. M., and Gaston, P. K. (2010). Oxidative stress and glutathione in TGF-beta-mediated fibrogenesis. *FREE Radic. BIO Med.* 48 (1), 1–15. doi:10.1016/j.freeradbiomed.2009.09.026

Llovet, J. M., Kelley, R. K., Villanueva, A., Singal, A. G., Pikarsky, E., Roayaie, S., et al. (2021). Hepatocellular carcinoma. *Nat. Rev. Dis. Prim.* 7 (1), 6. doi:10.1038/s41572-020-00240-3

Llovet, J. M., Ricci, S., Mazzaferro, V., Hilgard, P., Gane, E., Blanc, J. F., et al. (2008). Sorafenib in advanced hepatocellular carcinoma. *NEW Engl. J. Med.* 359 (4), 378–390. doi:10.1056/NEJMoa0708857

Llovet, J. M., Zucman-Rossi, J., Pikarsky, E., Sangro, B., Schwartz, M., Sherman, M., et al. (2016). Hepatocellular carcinoma. *Nat. Rev. Dis. Prim.* 2, 16018. doi:10.1038/nrdp.2016.18

Lv, H., Zhen, C., Liu, J., Yang, P., Hu, L., and Shang, P. (2019). Unraveling the potential role of glutathione in multiple forms of cell death in cancer therapy. *Oxid. Med. Cell Longev.* 2019, 3150145. doi:10.1155/2019/3150145

Ma, Y. L., Yang, Y. F., Wang, H. C., Yang, C. C., Yan, L. J., Ding, Z. N., et al. (2023). A novel prognostic scoring model based on copper homeostasis and cuproptosis which indicates changes in tumor microenvironment and affects treatment response. *Front. Pharmacol.* 14, 1101749. doi:10.3389/fphar.2023.1101749

Mano, Y., Yoshio, S., Shoji, H., Tomonari, S., Aoki, Y., Aoyanagi, N., et al. (2019). Bone morphogenetic protein 4 provides cancer-supportive phenotypes to liver fibroblasts in patients with hepatocellular carcinoma. *J. Gastroenterol.* 54 (11), 1007–1018. doi:10.1007/s00535-019-01579-5

Mariani, D., Ghasemishahrestani, Z., Freitas, W., Pezzuto, P., Costa-da-Silva, A. C., Tanuri, A., et al. (2021). Antitumoral synergism between a copper(II) complex and cisplatin improves *in vitro* and *in vivo* anticancer activity against melanoma, lung and

breast cancer cells. *BBA-GEN Subj.* 1865 (10), 129963. doi:10.1016/j.bbagen.2021.129963

Mortada, W. I., Awadalla, A., Khater, S., Ahmed, A., Hamam, E. T., El-Zayat, M., et al. (2020). Copper and zinc levels in plasma and cancerous tissues and their relation with expression of VEGF and HIF-1 in the pathogenesis of muscle invasive urothelial bladder cancer: A case-controlled clinical study. *Environ. Sci. Pollut. R.* 27 (13), 15835–15841. doi:10.1007/s11356-020-08113-8

Mou, Y., Wang, J., Wu, J., He, D., Zhang, C., Duan, C., et al. (2019). Ferroptosis, a new form of cell death: opportunities and challenges in cancer. *J. Hematol. Oncol.* 12 (1), 34. doi:10.1186/s13045-019-0720-y

Naderi, A., Teschendorff, A. E., Beigel, J., Cariati, M., Ellis, I. O., Brenton, J. D., et al. (2007). BEX2 is overexpressed in a subset of primary breast cancers and mediates nerve growth factor/nuclear factor-kappaB inhibition of apoptosis in breast cancer cell lines. *CANCER Res.* 67 (14), 6725–6736. doi:10.1158/0008-5472.CAN-06-4394

Nik-Zainal, S., Davies, H., Staaf, J., Ramakrishna, M., Glodzik, D., Zou, X., et al. (2016). Landscape of somatic mutations in 560 breast cancer whole-genome sequences. *NATURE* 534 (7605), 47–54. doi:10.1038/nature17676

Pang, J. S., Li, Z. K., Lin, P., Wang, X. D., Chen, G., Yan, H. B., et al. (2019). The underlying molecular mechanism and potential drugs for treatment in papillary renal cell carcinoma: A study based on TCGA and cmap datasets. *Oncol. Rep.* 41 (4), 2089–2102. doi:10.3892/or.2019.7014

Pariyar, M., Johns, A., Thorne, R. F., Scott, R. J., and Avery-Kiejda, K. A. (2021). Copy number variation in triple negative breast cancer samples associated with lymph node metastasis. *NEOPLASIA* 23 (8), 743–753. doi:10.1016/j.neo.2021.05.016

Pushpakom, S., Iorio, F., Eyers, P. A., Escott, K. J., Hopper, S., Wells, A., et al. (2019). Drug repurposing: progress, challenges and recommendations. *Nat. Rev. DRUG Discov.* 18 (1), 41–58. doi:10.1038/nrd.2018.168

Quentmeier, H., Tonelli, R., Geffers, R., Pession, A., Uphoff, C. C., and Drexler, H. G. (2005). Expression of BEX1 in acute myeloid leukemia with MLL rearrangements. *LEUKEMIA* 19 (8), 1488–1489. doi:10.1038/sj.leu.2403820

Resaz, R., Vanni, C., Segalerba, D., Sementa, A. R., Mastracci, L., Grillo, F., et al. (2014). Development of hepatocellular adenomas and carcinomas in mice with liver-specific G6Pase-alpha deficiency. *Dis. Model Mech.* 7 (9), 1083–1091. doi:10.1242/dmm.014878

Roos, N. J., Aliu, D., Bouitbir, J., and Krahenbuhl, S. (2020). Lapatinib activates the kelch-like ECH-associated protein 1-nuclear factor erythroid 2-related factor 2 pathway in HepG2 cells. *Front. Pharmacol.* 11, 944. doi:10.3389/fphar.2020.00944

Sagawa, H., Naiki-Ito, A., Kato, H., Naiki, T., Yamashita, Y., Suzuki, S., et al. (2015). Connexin 32 and luteolin play protective roles in non-alcoholic steatohepatitis development and its related hepatocarcinogenesis in rats. *CARCINOGENESIS* 36 (12), 1539–1549. doi:10.1093/carcin/bgv143

Satilmis, B., Sahin, T. T., Cicek, E., Akbulut, S., and Yilmaz, S. (2021). Hepatocellular carcinoma tumor microenvironment and its implications in terms of anti-tumor immunity: future perspectives for new therapeutics. *J. Gastrointest. CANC* 52 (4), 1198–1205. doi:10.1007/s12029-021-00725-8

Seager, R. J., Hajal, C., Spill, F., Kamm, R. D., and Zaman, M. H. (2017). Dynamic interplay between tumour, stroma and immune system can drive or prevent tumour progression. *Converg. Sci. Phys. Oncol.* 3, 034002. doi:10.1088/2057-1739/aa7e86

Shen, H., and Wang, W. (2021). Effect of glutathione liposomes on diabetic nephropathy based on oxidative stress and polyol pathway mechanism. *J. LIPOSOME Res.* 31 (4), 317–325. doi:10.1080/08982104.2020.1780607

Shi, X., Qu, M., Jin, X., Liu, L., Meng, F., and Shen, H. (2021). Relationship between TSHR, BRAF and PIK3CA gene copy number variations and thyroid nodules. *ENDOCRINE* 73 (1), 116–124. doi:10.1007/s12020-020-02587-9

Shimomura, Y., Takaki, A., Wada, N., Yasunaka, T., Ikeda, F., Maruyama, T., et al. (2017). The serum oxidative/anti-oxidative stress balance becomes dysregulated in patients with non-alcoholic steatohepatitis associated with hepatocellular carcinoma. *Intern. Med.* 56 (3), 243–251. doi:10.2169/internalmedicine.56.7002

Song, W., Ren, J., Xiang, R., Kong, C., and Fu, T. (2021). Identification of pyroptosis-related subtypes, the development of a prognosis model, and characterization of tumor microenvironment infiltration in colorectal cancer. *ONCOIMMUNOLOGY* 10 (1), 1987636. doi:10.1080/2162402X.2021.1987636

Sung, H., Ferlay, J., Siegel, R. L., Laversanne, M., Soerjomataram, I., Jemal, A., et al. (2021). Global cancer statistics 2020: GLOBOCAN estimates of incidence and mortality worldwide for 36 cancers in 185 countries. *CA-CANCER J. Clin.* 71 (3), 209–249. doi:10.3322/caac.21660

Thai, S. F., Jones, C. P., Robinette, B. L., Ren, H., Vallant, B., Fisher, A., et al. (2021). Effects of copper nanoparticles on mRNA and small RNA expression in human hepatocellular carcinoma (HepG2) cells. *J. Nanosci. Nanotechnol.* 21 (10), 5083–5098. doi:10.1166/jnn.2021.19328

Tian, L., and Liao, Y. (2022). Identification of G6PC as a potential prognostic biomarker in hepatocellular carcinoma based on bioinformatics analysis. *MEDICINE* 101 (33), e29548. doi:10.1097/MD.0000000000029548

Torrens, L., Montironi, C., Puigvehi, M., Mesropian, A., Leslie, J., Haber, P. K., et al. (2021). Immunomodulatory effects of lenvatinib Plus anti-programmed cell death protein 1 in mice and rationale for patient enrichment in hepatocellular carcinoma. *HEPATOLOGY* 74 (5), 2652–2669. doi:10.1002/hep.32023

Trott, O., and Olson, A. J. (2010). AutoDock Vina: improving the speed and accuracy of docking with a new scoring function, efficient optimization, and multithreading. *J. Comput. Chem.* 31 (2), 455–461. doi:10.1002/jcc.21334

Tsvetkov, P., Coy, S., Petrova, B., Dreishpoon, M., Verma, A., Abdusamad, M., et al. (2022). Copper induces cell death by targeting lipoylated TCA cycle proteins. *SCIENCE* 375 (6586), 1254–1261. doi:10.1126/science.abf0529

Turley, S. J., Cremasco, V., and Astarita, J. L. (2015). Immunological hallmarks of stromal cells in the tumour microenvironment. *Nat. Rev. Immunol.* 15 (11), 669–682. doi:10.1038/nri3902

Valk, E., Rudd, C. E., and Schneider, H. (2008). CTLA-4 trafficking and surface expression. *TRENDS Immunol.* 29 (6), 272–279. doi:10.1016/j.it.2008.02.011

Vilar, M., Murillo-Carretero, M., Mira, H., Magnusson, K., Besset, V., and Ibanez, C. F. (2006). Bex1, a novel interactor of the p75 neurotrophin receptor, links neurotrophin signaling to the cell cycle. *EMBO J.* 25 (6), 1219–1230. doi:10.1038/sj.emboj.7601017

Vogel, A., and Saborowski, A. (2020). Current strategies for the treatment of intermediate and advanced hepatocellular carcinoma. *CANCER Treat. Rev.* 82, 101946. doi:10.1016/j.ctrv.2019.101946

Wang, Q., Liang, N., Yang, T., Li, Y., Li, J., Huang, Q., et al. (2021). DNMT1-mediated methylation of BEX1 regulates stemness and tumorigenicity in liver cancer. *J. Hepatol.* 75 (5), 1142–1153. doi:10.1016/j.jhep.2021.06.025

Xie, L., Zeng, Y., Dai, Z., He, W., Ke, H., Lin, Q., et al. (2018). Chemical and genetic inhibition of STAT3 sensitizes hepatocellular carcinoma cells to sorafenib induced cell death. *Int. J. Biol. Sci.* 14 (5), 577–585. doi:10.7150/ijbs.22220

Xing, R., Gao, J., Cui, Q., and Wang, Q. (2021). Strategies to improve the antitumor effect of immunotherapy for hepatocellular carcinoma. *Front. Immunol.* 12, 783236. doi:10.3389/fimmu.2021.783236

Yan, C., Niu, Y., Ma, L., Tian, L., and Ma, J. (2022). System analysis based on the cuproptosis-related genes identifies LIPT1 as a novel therapy target for liver hepatocellular carcinoma. *J. Transl. Med.* 20 (1), 452. doi:10.1186/s12967-022-03630-1

Yang, H., Magilnick, N., Ou, X., and Lu, S. C. (2005). Tumour necrosis factor alpha induces co-ordinated activation of rat GSH synthetic enzymes via nuclear factor kappaB and activator protein-1. *Biochem. J.* 391 (2), 399–408. doi:10.1042/BJ20050795

Yang, Q., Zeng, S., and Liu, W. (2023). Roles of cuproptosis-related gene DLAT in various cancers: A bioinformatic analysis and preliminary verification on pro-survival autophagy. *PEERJ* 11, e15019. doi:10.7717/peerj.15019

Zhang, Z., Zeng, X., Wu, Y., Liu, Y., Zhang, X., and Song, Z. (2022). Cuproptosis-related risk score predicts prognosis and characterizes the tumor microenvironment in hepatocellular carcinoma. *Front. Immunol.* 13, 925618. doi:10.3389/fimmu.2022.925618

Zhao, X., Chen, J., Yin, S., Shi, J., Zheng, M., He, C., et al. (2022). The expression of cuproptosis-related genes in hepatocellular carcinoma and their relationships with prognosis. *Front. Oncol.* 12, 992468. doi:10.3389/fonc.2022.992468

Zheng, S. G., Wang, J. H., Stohl, W., Kim, K. S., Gray, J. D., and Horwitz, D. A. (2006). TGF-beta requires CTLA-4 early after T cell activation to induce FoxP3 and generate adaptive CD4+CD25+ regulatory cells. *J. Immunol.* 176 (6), 3321–3329. doi:10.4049/jimmunol.176.6.3321

Zhu, A. X., Finn, R. S., Edeline, J., Cattan, S., Ogasawara, S., Palmer, D., et al. (2018). Pembrolizumab in patients with advanced hepatocellular carcinoma previously treated with sorafenib (KEYNOTE-224): A non-randomised, open-label phase 2 trial. *LANCET Oncol.* 19 (7), 940–952. doi:10.1016/S1470-2045(18)30351-6

Frontiers in Immunology

Explores novel approaches and diagnoses to treat immune disorders.

The official journal of the International Union of Immunological Societies (IUIS) and the most cited in its field, leading the way for research across basic, translational and clinical immunology.

Discover the latest Research Topics

See more →

Frontiers

Avenue du Tribunal-Fédéral 34
1005 Lausanne, Switzerland
frontiersin.org

Contact us

+41 (0)21 510 17 00
frontiersin.org/about/contact